Analysis and Design of Buried Pipelines

by

Rashid Bashir

A Thesis Presented to the

FACULTY OF THE COLLEGE OF GRADUATE STUDIES

KING FAHD UNIVERSITY OF PETROLEUM & MINERALS

DHAHRAN, SAUDI ARABIA

In Partial Fulfillment of the
Requirements for the Degree of

MASTER OF SCIENCE

In

CIVIL ENGINEERING

July, 2000

INFORMATION TO USERS

This manuscript has been reproduced from the microfilm master. UMI films the text directly from the original or copy submitted. Thus, some thesis and dissertation copies are in typewriter face, while others may be from any type of computer printer.

The quality of this reproduction is dependent upon the quality of the copy submitted. Broken or indistinct print, colored or poor quality illustrations and photographs, print bleedthrough, substandard margins, and improper alignment can adversely affect reproduction.

In the unlikely event that the author did not send UMI a complete manuscript and there are missing pages, these will be noted. Also, if unauthorized copyright material had to be removed, a note will indicate the deletion.

Oversize materials (e.g., maps, drawings, charts) are reproduced by sectioning the original, beginning at the upper left-hand corner and continuing from left to right in equal sections with small overlaps.

Photographs included in the original manuscript have been reproduced xerographically in this copy. Higher quality 6" x 9" black and white photographic prints are available for any photographs or illustrations appearing in this copy for an additional charge. Contact UMI directly to order.

Bell & Howell Information and Learning
300 North Zeeb Road, Ann Arbor, MI 48106-1346 USA
800-521-0600

UMI®

ANALYSIS AND DESIGN OF BURIED PIPELINES

BY

RASHID BASHIR

A Thesis Presented to the

DEANSHIP OF GRADUATE STUDIES

KING FAHD UNIVERSITY OF PETROLEUM & MINERALS

DHAHRAN, SAUDI ARABIA

In Partial Fulfillment of the
Requirements for the Degree of

MASTER OF SCIENCE

In

CIVIL ENGINEERING

JULY 2000

KING FAHD UNIVERSITY OF PETROLEUM AND MINERALS
DHAHRAN 31261, SAUDI ARABIA

DEANSHIP OF GRADUATE STUDIES

This thesis, written by

RASHID BASHIR

under the direction of his Thesis Advisor and approved by his Thesis Committee, has been presented to and accepted by the Dean of Graduate Studies, in partial fulfillment of the requirements for the degree of

MASTER OF SCIENCE IN CIVIL ENGINEERING.

THESIS COMMITTEE:

Prof. Sahel N. Abduljauwad, Chairman

Dr. Hamdan N. Al-Ghamedy, Member

Dr. Naser A. Al-Shayea, Member

Dr. Ibrahim M. K. Asi, Member

Chairman, Civil Engineering Department

Dean of Graduate Studies

Date: 28 August, 2000

To my **MOTHER &FATHER**

ACKNOWLEDGEMENTS

All praises are for **ALLAH** the Almighty and his prophet **Mohammad** (peace be upon him) for giving me the strength to complete this work

Acknowledgements are also due to King Fahd University of Petroleum and Minerals for providing support for this research. Thanks are also due to Civil Engineering department and Saudi Arabian Oil Company (Saudi Aramco) for sponsoring this research.

I am very thankful to my thesis advisor Prof. Sahel Abduljauwad who is the mastermind behind this research. Thanks are also due to Dr. Hamdan Al-Ghamdey with whom I did all my numerical work. My deep appreciation is for my committee member Dr. Nasir Al-Shayea; under whose supervision I did the experimental part of this work. My profound gratitude is for Dr. Ibrahim Asi who has major contribution in the development of the regression models. I am greatly indebted to Junaid Abdulwahid Siddique who contributed a lot in my thesis and is always there when I need him. I am also thankful to Dr. Mohmed Balah for his help in problems related to engineering mechanics.

I would like to express my profound gratitude to my parents for their love, affection, and sacrifices, which made me what I am today. I am also thankful to my family members for a remarkable level of understanding and patience. My thanks are also due to my sister, brother in law, and nephew for their love and support during my stay in KFUPM.

My appreciation is also for Asad-ur-Rehman for introducing me LaTeX and so many other things. My deep appreciation is for my friends Mazhar, Noman Ali Tassduq, Naved, and Leyah who were always there for the moral support. I am also indebted to my friends Ayaz

and Nadir back home and my friends Bilal and Shafaqat in the U.S. for their continuous support during my stay in the Kingdom of Saudi Arabia.

I would also like to thank Mr. Hasan Zikria of the soil laboratory for help in carrying out the experimental part of this research and Mr. Mumtaz secretary civil engineering department for his cooperation during my stay with the department

TABLE OF CONTENTS

LIST OF FIGURES

LIST OF TABLES

THESIS ABSTRACT

Name : Rashid Bashir

Thesis Title : Analysis and Design of Buried Pipelines

Major Field : Civil Engineering

Date of Degree : July 2000

The analysis and design of buried pipelines is a problem of soil-structure interaction. Compared with previous work in this area, this study utilizes a more realistic and comprehensive non-linear finite element method to analyze pipes subjected to sand overburden and crossing highways. Soils associated with local pipe network are characterized, and soil properties for Duncan and Selig model, which are to be used in the non-linear finite element analyses, are determined. A parametric study is carried out for pipes of various diameters and thicknesses under sand overburden up to 60 feet and subjected to various other loadings such as live load, internal pressure, and temperature. The results of the parametric study are used to develop regression models using the multiple linear regression method. The regression models are capable of predicting stresses and diameter changes in the pipes under sand overburden and crossing highways.

MASTER OF SCIENCE DEGREE

KING FAHD UNIVERSITY OF PETROLEUM AND MINERALS

Dhahran, Saudi Arabia

ملخص الرسالة

الاسم : راشد بشير

عنوان الرسالة : **تحليل وتصميم الأنابيب المدفونة**

التخصص : **هندسة مدنية**

تاريخ التخرج : **يوليو ٢٠٠٠**

ان تصميم وتحليل الأنابيب المدفونة يتطلب مراعاة التفاعل بين الانابيب والتربة. مقارنة بالدراسات السابقة في هذا المجال ، تستعمل الدراسة الحالية طريقة العناصر المحدودة الغير خطية الأكثر واقعية وشمولاً لتحليل الأنابيب تحت تأثير الأكوام الرملية والطرق العابرة .

لقد تم تصنيف التربة المحيطة بشبكة الأنابيب المحلية وتم إيجاد خواص كل تربة لنموذج دنكن وسليق. وقد استعمل هذا النموذج لمحاكاة تصرف التربة بطريقة العناصر المحدودة الغير خطية .

لقد أجريت دراسة العوامل المؤثرة على الأنابيب بمختلف أقطارها تحت تأثير الأكوام الرملية التي يصل علوها في بعض الأحيان إلى ٦٠ قدماً كما تتعرض هذه الأنابيب لضغوط عديدة نتيجة التحميل المتحرك والضغط الداخلي وكذا التحميل الناتج عن تغير الحرارة . و قد أستخدمت نتائج هذه الدراسة لتطوير نماذج احصائية ترتكز على طريقة التراجع الخطي ذات المتغيرات المتعددة . ولقد بينت النماذج المطورة قدرتها على التنبؤ بالإجهادات والتغييرات القطرية التي تحدث في الأنابيب تحت تأثير الأكوام الرملية والطرق العابرة .

درجة الماجستير في العلوم

جامعة الملك فهد للبترول والمعادن

CHAPTER 1

INTRODUCTION

1.1 General

Underground pipes constructed of various materials in a wide variety of sizes and shapes have served mankind throughout the ages. Remnants of this type of structure have been found among the earliest examples of the practice of engineering art. They serve civilization today as sewers, drains, water distribution mains, highway and railway culverts, pedestrian and stock passes, gas and liquid-petroleum transmission lines, and numerous other special functions.

Although the use of underground pipelines can be traced to the beginning of civilization, it is only within the early decades of the previous century that rational methods of the structural design of buried pipelines based upon sound principles of mechanics have become available as the result of engineering research.

1.2 Mechanics of Buried Pipes

The procedure employed in the design of buried pipelines is basically the same as in the design of any other structure. First, it is necessary to determine the loads to which the pipe will be subjected in service, such as the overburden earth load plus any traffic and impact load. Also in case of pressure pipelines, the magnitude of the internal pressure must be determined.

The second step in the structural design of a buried pipe is the determination of its supporting strength, that is, its ability to carry the load to which it will be subjected, with an appropriate margin of safety. The supporting strength of the pipe primarily depends on three factors: the inherent strength of the pipe which depend upon modulus of elasticity, diameter, thickness, and material; the distribution of the vertical load and the bottom reaction; and the magnitude and distribution of the lateral earth pressure which may act against the sides of the structure.

1.3 Problem Statement

The analysis and design of buried pipelines have a great practical importance for pipeline engineers. Buried pipelines are subjected to the dead load of the overfill soil or combination of dead and live loads wherever they cross under highways and railways. In addition to the external loads just mentioned pipelines are also subjected to an internal load due to the internal pressure if they are pressurized. Methods of analysis and design based on classical theories and empirical equations have low level of confidence and lead to a very

conservative design. Some procedures based on the finite element analysis are available but these are usually site-specific and are not capable of modeling all the combinations of design parameters. Numerous attempts have been made to model the pipe-soil interaction using numerical methods. There are a number of finite element software available which can be used as a black box to model various geotechnical problems. In this study, a more realistic non-linear finite element method will be used to study the interaction between the buried pipelines and the soil surrounding them. The main focus of this research will be on pipelines under very high overfills and pipelines crossings under highways. An attempt will be made to simulate the local soil conditions and field installation procedures. Several parameters will be considered.

1.4 Objective

The primary goal of this research is to study buried pipeline behavior using suitable non-linear finite element software and to develop a procedure that can assist in the analysis and design of pipelines under deep fills and crossing highways. Material characterization will be carried out in order to make realistic simulations of the local conditions. Moreover this research is also aimed at developing a design procedure that can handle among other parameters, diameters up to 60 inch and D/t ratios up to 150, which are not usually covered by most design procedures.

The specific objectives of this research are enumerated below.

1. Selection and validation of a non-linear finite element software capable of modeling

pipeline-soil interaction problem for deep fills and pipelines crossing highways.

2. Characterization and determination of model parameters for local soils at various densities to be used in the non-linear finite element analysis.
3. Finite element simulations of pipelines under deep fills and crossing highways.
4. Determination of allowable sand dune accumulation on existing pipelines and calculation of stresses and strains as a function of sand overburden.
5. Parametric study of the buried pipelines for the various possible combinations of parameters that influence the behavior of pipelines subjected to sand overburden and highway loads.
6. Development of regression models, using the finite element results that are capable of analysis and design of pipelines under deep fills and crossings under highways.

1.5 Thesis Organization

The thesis comprises of 9 Chapters. Chapter 1 gives an introduction to the thesis. The chapter starts with the mechanics of the buried pipelines followed by the problem statement and research objectives.

Chapter 2 presents the review of the literature on buried pipelines. The conventional methods for the design of buried pipelines are reviewed at the beginning of the chapter. Works regarding the strength of the pipe ring is presented next in the chapter. Literature related to pipelines crossing railroads and highways is also presented in this chapter. The chapter is concluded by a comprehensive literature review of the numerical methods for

the analysis and design of buried pipelines.

The third chapter of the thesis gives a technical background on the analysis and design of buried pipelines. This chapter can be distinguished in to three different sections. The first section comprises of basic pipe definitions and various components of the pipe-soil system. Theory of arching and differences between rigid and flexible pipes are also outlined in this section. The second section of the chapter gives the necessary background in the soil modeling. In this section various material models for the geologic media are discussed followed by a detailed discussion of the soil models mostly used in the finite element simulations of the buried pipelines. The same section is concluded by the reasons for selecting a specific model to be used in this research. The third section of the chapter reviews the existing methods of analysis and design for the buried pipelines. This section aims at providing enough background to the reader to understand the comparison between the existing methods of design and the results of this research.

The experimental program and the determination of soil properties are explained in Chapter 4. The various experimental tests that are performed on the soils associated with the local pipe network are reported in this chapter. The determinations of soil properties from the test results, which are used in the finite element simulations for this research. are also presented in this chapter.

Chapter 5 deals with the numerical modeling of the buried pipelines. Criteria for the analysis and design of pipelines and the selection of suitable non-linear finite element software are outlined in this chapter. Various VBA (Visual Basic for Applications) programs developed to aid in the data file preparation and post processing are also mentioned in this

chapter. The last part of the chapter deals with the validation and comparison of the finite element software used in this study with the other finite element programs.

The results of the initial parametric study are presented in Chapter 6 of the thesis. The initial parametric study identifies the various parameters that influence the buried pipelines. Effects of various parameters are presented in this chapter. This chapter serves as a prologue to the detailed parametric study that has been carried out in the next chapter. A more detailed parametric study for pipelines subjected to sand overburden and highway load is presented in the next chapter.

Chapter 7 presents the results of the parametric study carried out for pipelines subjected to sand overburden and highway loads. The various parameters that are varied in the parametric study are identified at the beginning of the chapter followed by the results of the parametric study. Following the results of the parametric study is the analysis of the results to check the authenticity of the results. A detailed comparison of the results with the existing design procedures is also an important part of this chapter.

The development of regression models for the analysis and design of pipelines subjected to sand overburden and highway live loads is presented in Chapter 8 of the thesis. Making use of the results presented in Chapter 7 and applying the principle of multiple linear regression design equations to predict the absolute maximum stress and diameter change are presented in this chapter. Testing and validation of the regression models are also part of this chapter.

Chapter 9 consists of a summary of the work followed by conclusions from this research and recommendations for future research.

CHAPTER 2

LITERATURE REVIEW

2.1 Introduction

The first attempts to structurally design buried circular conduits were limited to rigid ones such as clay and concrete pipes. The analysis started with the conduit ring as a free body diagram as shown in Fig. 2.1 [1].The vertical soil load was calculated and kept less than the three-edge bearing load which developed a 0.01 inch crack in a laboratory sample of the same conduit. The procedure was only approximate but adequate. For the flexible pipe, again the analysis started with the free-body diagram of the conduit ring with soil loads acting on it, but the horizontal support of the soil which resists the lateral deflection of the conduit was also considered. These basic principles are still in use.

2.2 Conventional Methods of Design

Most codes of practice for the design and laying of pipes have made use of extensive experimental and analytical studies carried out originally by Marston, who began work on

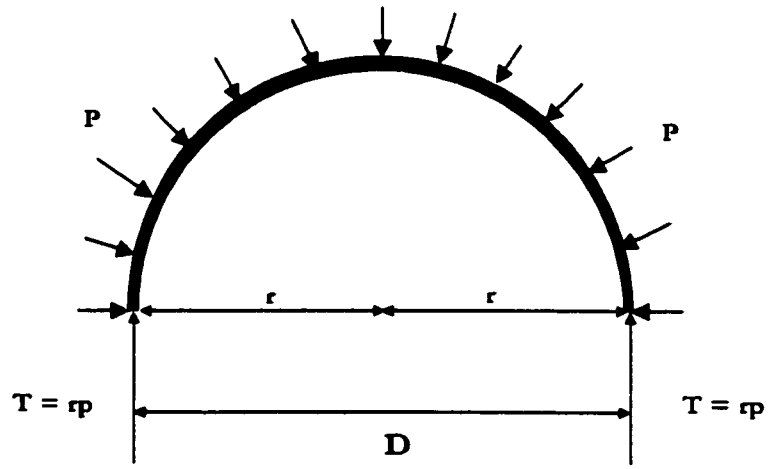

T = compression thrust in conduit wall,
D = mean diameter of conduit,
E = modulus of elasticity of conduit,
p = soil pressure on the conduit,
r = radius of curvature at the thrust point.

Fig. 2.1: Ring Compression stress for a buried circular conduit

the problem of design of buried pipes at Iowa State University, Ames, USA, in the early years of the previous century. He published an authoritative paper on the theory of loads on pipes in ditches and tests on cement, clay, and sewer pipes in 1913 [2]. A series of bulletins was issued from then on, but perhaps the most useful one was a review of theories of external loads on buried conduits, published in 1930 [3]. Marston discussed the loads on rigid conduits in terms of the shearing forces developed in the prism of soil above the structure as shown in Fig. 2.2. His theory clearly took into account the relative deflection of the pipe and the settlement of the soil.

The work was carried forward by Spangler, a former student of Marston. Following some of the earlier work at Iowa State College in 1920's and 30's, Spangler observed that flexible pipes of relatively light weight and low strength can support back fills of considerable height by using the passive pressure induced in the surrounding soil as the sides try to move outward against the soil. So, high deformation characteristic of thin-walled pipes can be of great advantage by mobilizing the passive pressure at the springline. He rationalized that structural analysis of flexible pipe should include a method of determining pipe deflection under specified conditions of load and installation. Spangler presented the IOWA formula [4] for the calculation of deflection in buried pipes making use of the field measurements made on conduits of widely varying flexibility, by American Railway Engineering Association [5]. Based on the rationale of passive resistance at the pipe springline and elastic ring bending theory, the IOWA formula predicts the change in the vertical pipe diameter due to the external dead and live loads. Spangler wrote the most comprehensive review in 1948 [6].

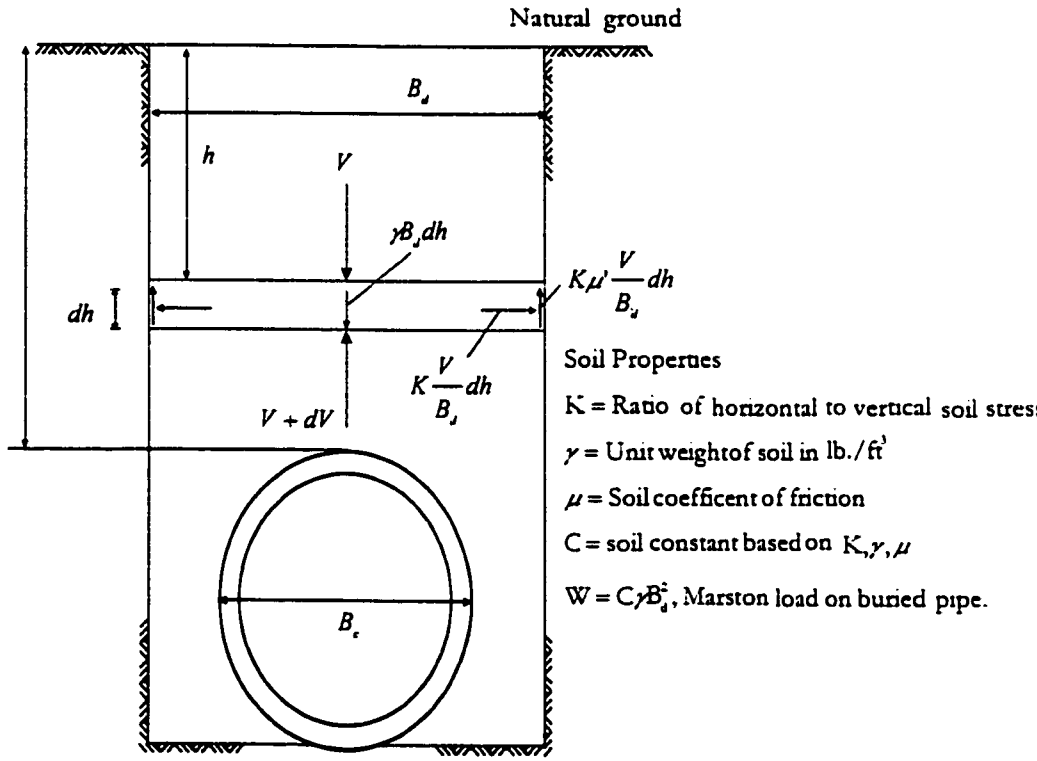

Fig. 2.2: Marston theory of soil loads on rigid buried pipes

2.3 Strength of the Pipe Ring

A ring compression theory for the design of buried flexible pipes was presented by White and Layer in 1960 [7]. This theory is based on the assumption that ring deflection of the structure is negligible and the pipe fails by wall crushing. Luscher [8] was the first one to look into the elastic buckling of the flexible pipe and used the concept of a thin cylindrical tube surrounded by an annular ring of soil and presented expressions for the buckling strength. Dar and Bates [9] presented some equations, based on classical theory of elasticity, that closely predict the behavior of cylinders in materials like sand. Allgood [10] examined various aspects of arching phenomenon in relation to flexible and rigid culverts. Burns et al. [11], and Höeg [12] approached the problem partly on the basis of thin shell theory and partly on the elasticity theory and further narrowed the solution of the soil-structure interaction problem. However, their emphasis has been mainly on the stress distribution in the surrounding soil. Their assumption of thin sheet theory provided limited information regarding the stress distribution in the structure as compared to the approach based entirely on elasticity.

Gerbault [13] and ATV [14] proposed improved assumptions for the lateral soil distribution at the sides of the pipe. They proposed a sum of parabolic distribution corresponding to 0.2 and 0.3 of the geo-static load as shown in Fig. 2.3. Gerbault [15] proposed a model where the soil interaction was modeled by distributed springs placed around the pipe. Assuming the rigidity of these springs as constant, a linear analysis can be carried out by hand calculations. Moreover, by using elastoplastic constitutive laws for springs to simu-

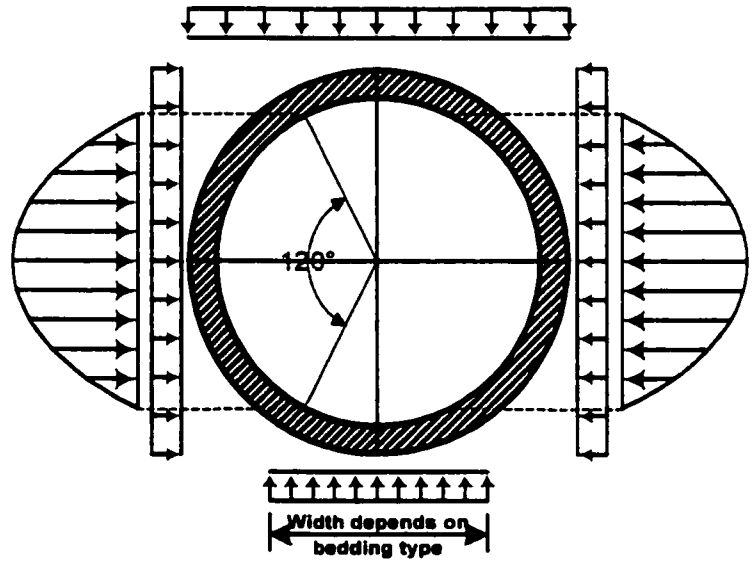

Fig. 2.3: ATV's earth pressure distribution

late the surrounding soil, an analytic process using transfer matrix technique was used to model other situations. The model is capable of taking into account the 2nd order effects of buckling and pressure re-rounding.

With the increase in the usage of flexible pipes in the 1970's, a lot of work was carried out on the analysis or design of buried flexible pipes. Einstein and Shwartz [16] proposed a linear model while Duncan [17] and Moore and Booker [18] presented rigorous non-linear models for the buried pipe system.

Moore [19] and Jeyapalan [20] reported that despite of the fact that Spangler [6] and Luscher [8] have received much criticism over the time their equations are heavily relied upon for design of flexible pipes.

2.4 Design of Pipelines Crossing Railroads and Highways

The problem of structural design of pipelines crossing railroads and highways is of considerable interest to those responsible for right of way as well as pipeline users. The problem is compounded when the pipeline crosses various highways and railroads controlled by different management each with different ideas and policies relative to the design specifications. Casing of pipelines under railroads and highways was a common practice in the past. Technological improvements in the manufacturing process, construction, and protection of pipelines have reduced the need of casing. The development of design criteria for uncased pipelines crossing railroads and highways is an extension of the work by Spangler and contained many of the original assumptions and design parameters of the IOWA formula. The main differences are the inclusion of the internal pressure and the consideration

of the maximum stress in pipe wall as the design criterion.

In 1964, Spangler [21] proposed a procedure for defining the combined circumferential stress in the pipe wall due to the soil, rail loads, and the operating internal pressure. The method combines the Barlow formula [22] for calculating the circumferential or hoop stress due to the internal pressure and the Spangler formula [21] for estimating the circumferential stress due to the external dead and live loads. Despite the statements by Spangler [21] regarding the possibility of over conservative results, the procedure was adopted as a design method for buried-in-place pipeline crossings by the American Petroleum Institute (API) [23].

Bakht [24] studied the effect of soil-steel structures by the live loads. He reviewed the methods of determining live load analysis, described the live load tests on three in-service soil-steel pipes, and presented an improved simplified method for determining the load responses. Pierce et al. [25] presented a design procedure for natural gas pipeline crossings railroads and highways. The procedure is based on the proposal by Spangler [21] and included suggested values for some of the experimental parameters.

Öey et al. [26] made recommendations for the design of pipeline crossings under railroads and highways using Spangler's method [21]. They proposed the use of Direct earth-load method by the American National Standard (ANSI A21-50 1976) for the thickness design of ductile iron pipes for calculating dead load on pipes instead of Marston's formula. They compared the different methods for calculating live loads on pipes and recommend the use of Timoshenko method [27] in preference to Spangler's single load and Boussinesq's point load methods [28].

Daines [29] made the recommendation of Marston's formula for the dead load calculations for use in the formula for stress calculations by Spangler. He also recommended the use of Spangler's single load method for the calculations of the live loads on pipes beneath flexible pavements and Portland Cement Association (PCA) method [30] for pipes under rigid pavements.

O'Rourke, et. al. [31] presented a model based on the collapse, or caving mechanism. whereby loads are transferred to the top of the pipe in a manner consistent with the vertical load transfer likely to occur at many auger bored pipeline crossings at railroads and highways. The proposed model is shown in Fig. 2.4. This model provides an analytical basis for computing the soil load per pipe unit length that results from the construction process of auger boring the pipes at crossings. This model is conservative in that it neglects the arching stresses which may develop in the soil masses. This model applies specifically to auger-boring methods.

Stewart and O'Rourke [32] characterized live loads and gave recommendations on the selection of impact factors to be used in pipeline stress analysis for transportation crossings. They reviewed impact factors for both railroads and highways and made their recommendations based on a large-scale field study. Various configurations of truck traffic were evaluated for the selection of a maximum loading scenario for pipelines at highway crossings. A computer program based on a layered elastic system model with the ability to perform non-linear analysis was used to find the three dimensional stress distributions for different vehicles under flexible pavement at varying depths.

Inegreffea et al. [33]. proposed an entirely new empirical method for the design of

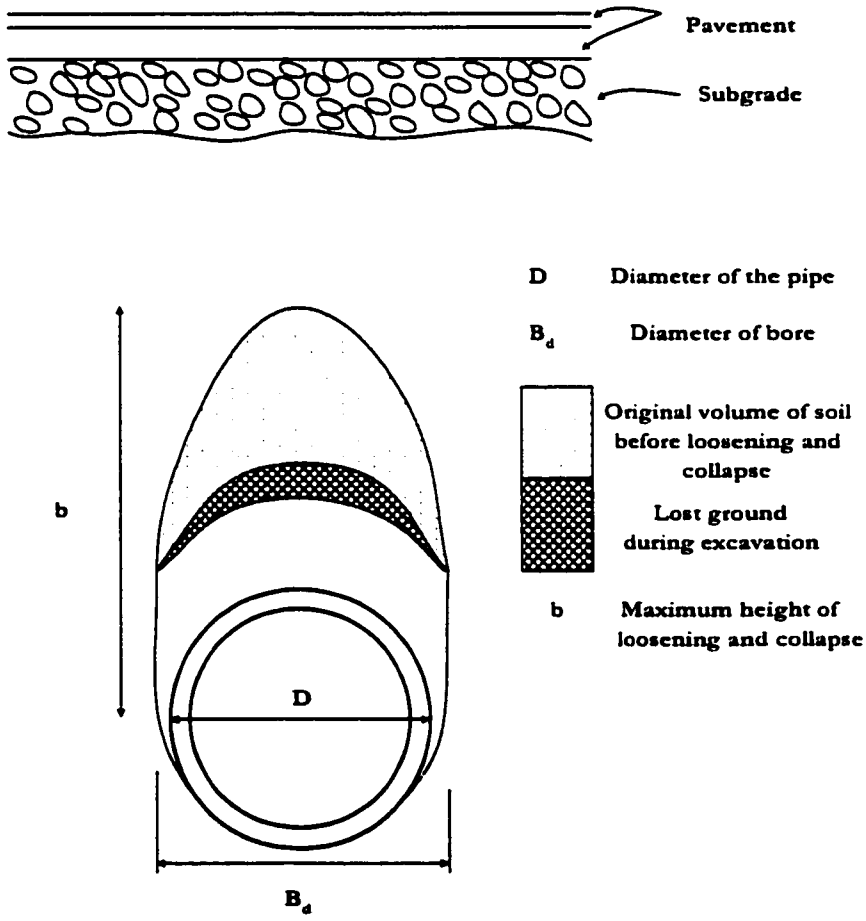

Fig. 2.4: Pipe within a bored excavation beneath a highway

pipeline crossings under railroads and highways. The proposed method is incorporated into API recommendation practice 1102 in 1993 [34]. This method is for the analysis and design of steel pipelines installed by auger boring. The dead load stresses on the pipeline crossing are predicted by the collapse model [31] and the live load stresses from highway and railroad are calculated from graphs developed from some 200, three dimensional linear elastic finite element simulations.

2.4.1 Impact Factor

Since the vehicular load is not really static, the dynamic effect has to be taken into account. This dynamic load, which is imposed by the railroad or highway vehicle, is generally evaluated by an impact factor; it is the ratio of the dynamic to static load applied by the vehicle. The total live load conveyed to an underlying pipeline is determined by multiplying the static load by this impact factor. The impact factors vary depending on vehicle speed, axle load, surface conditions, vehicle dynamic characteristics and type of measurement [35].

Duncan [17] considered the live load approximation using Boussinesq's theory as too conservative; however, he mentioned that if additional conservation in design is desired, the loads calculated by Boussinesq's theory should be increased using impact factors recommended by American Association of State Highways and Transportation Official (AASHTO). These amount up to a 30% increase in live load for less than 1 ft. of cover, 20% for 1-2 ft. of cover and 10% for 2-3 ft. of cover.

Bakht [24] reported that contrary to usual belief the dynamic load allowance (impact

factor) is not equal to one in soil-steel structures with depths of cover in excess of 3 ft.

Potter [36] reported that for normal modes of vehicle operations (e.g. high-speed travel, stopping, and accelerating), the impact factors are less than or equal to 1.3. In fact, impact factors less than 1.0 are not uncommon. For moving vehicles, load duration is too short to allow the mobilization of full static deflections. He also suggested an impact factor of 5 as an upper bound for tracked vehicle.

Stewart and O'Rourke [35] tried to replicate upper bound conditions as closely as possible by carrying out a series of special impact tests. The tests were conducted to investigate live load response for changes in track quality consistent with Federal Railroad Administration (FRA) class standards. They found out that the distribution of the impact factors is roughly from 0.8 to 1.6. Factors of less than unity are possible due to wheel bounce, load transfer between inside and outside rails, and the dynamic interaction effect of the train passing through the irregular test sections. They also carried out field impact measurements for pipelines at a depth of approximately 5.75 ft. under railroad loads to find an impact factor of 1.6 which is larger than that recommended by American Society of Civil Engineers (ASCE) for similar depths, but which falls within the envelope of maximum impact factor proposed by American Petroleum Institute (API).

API Recommended Practice 1102 [34] recommends that the line load be increased by an impact factor, F_i, which is a function of the depth of burial, H, of the carrier pipeline at crossing. The impact factors for both railroad and highway crossings are shown graphically in Fig. 2.5. The impact factors are 1.75 for railroads and 1.5 for highways, each decreasing by 0.03 per foot for depths of 5 feet and higher until the impact factor becomes 1.0.

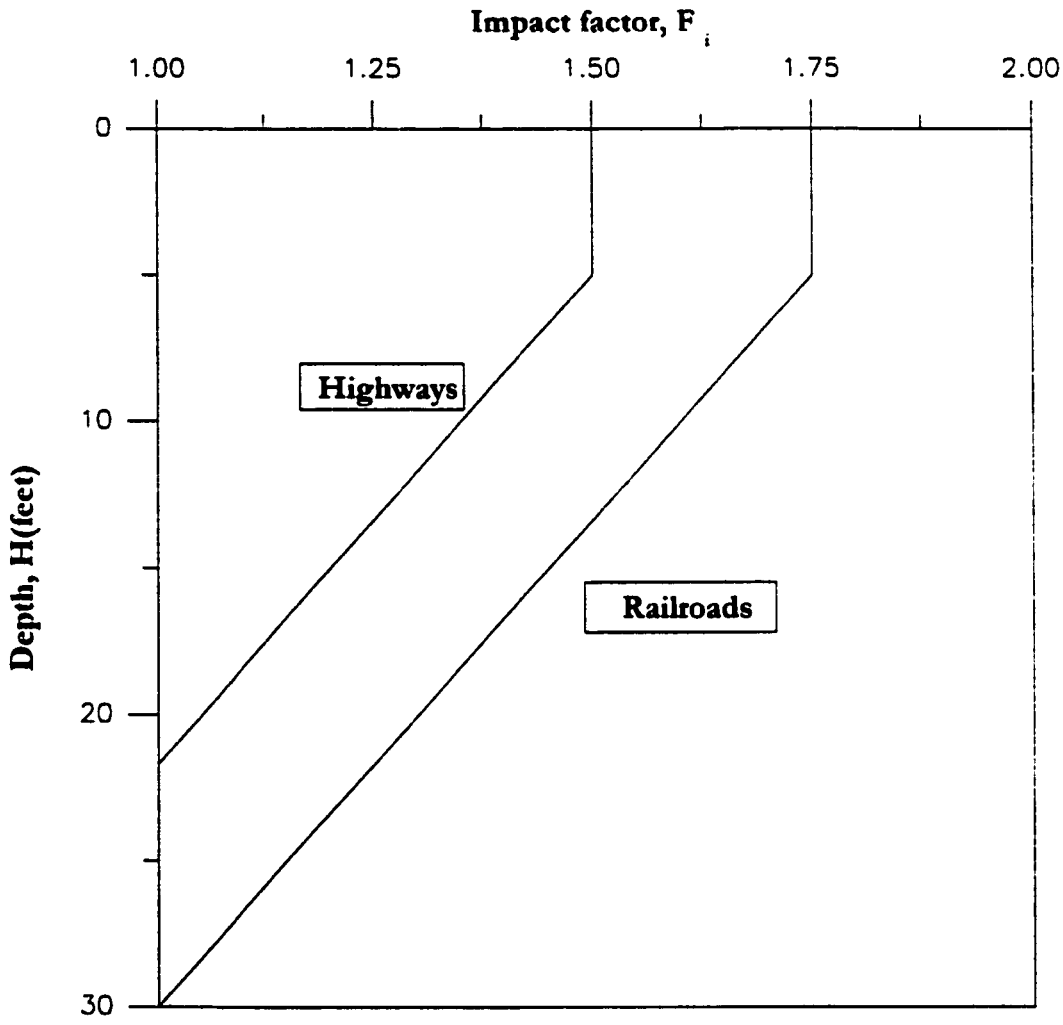

Fig. 2.5: Impact factors for highways and railroads by API RP 1102

The equations used to represent the impact factors are:

For railroad,

$$F_i = 1.75 \qquad \text{for } H \leq 5 \text{ ft}$$

$$F_i = 1.75 - .03\,(H - 5) \qquad \text{for } 5 \text{ ft} \leq H \leq 30 \text{ ft}$$

For highway,

$$F_i = 1.5 \qquad \text{for } H \leq 5 \text{ ft}$$

$$F_i = 1.5 - .03\,(H - 5) \qquad \text{for } 5 \text{ ft} \leq H \leq 21 \text{ ft}$$

Saudi Aramco Engineering Standard SAES-L-046 Section 7.3.2 recommends that the impact factor shall be applied to design wheel loads as shown in Table 2.1. For depth of cover larger than 1.5 m, the impact factors mentioned should be reduced by not more than 0.03 per meter of extra cover and shall not be less than 1.

Antaki [37] in his review report on methods for analysis of buried pressure-piping mentioned that the impact factor varies with the speed and stiffness of the surface vehicles, the roughness of the road and the burial depth. For a static load the impact factor is 1, and it ranges from 1.5 to 2.0 for unpaved surfaces.

2.5 Numerical Methods for Analysis and Design of Buried Pipelines

The development of a valid design procedure for the complicated soil-structure interaction problem associated with describing the response of buried pipe systems requires (a) the formulation of a mathematical model, (b) the specification of material properties, and

TABLE 2.1: Impact factors recommended by Aramco

Traffic Load Classification*	Impact Factor
AR-2, AR-10, AR-20, AR-40	1.5
AR-300	1.0
B-737	1.0
E-73	1.75

*Note: See Saudi Aramco Engineering Standard SAES-L-046 for Traffic Load Classifications

(c) field verification. The finite element method provides a very versatile and powerful analytical tool for solving problems with a wide variety of boundary and loading conditions and for handling material properties in a relatively realistic manner., A number of finite element programs based on small and large strain continuum theory with varying degrees of complexity have been developed to describe soil-pipe system.

Duncan [17] analyzed the behavior and design of long span metal culverts subjected to live loads using two different finite element codes. His live load representation was based on Boussinesq's solution of homogenous half space. The results from the finite element simulations were compared with field measurements and an approximate criterion was recommended. Chua [38] developed a viscoelastic solution to predict time-dependent deflections and strain levels of large diameter pipes buried in trenches. The solution was obtained by developing regression equations from a database of finite element simulations by Culvert Analysis and DEsign (CANDE) [39].

Seed and Duncan [40] used non linear finite element analysis to investigate the effect of earth pressure and surface loads on buried pipelines. In the finite element analysis, they used the hyperbolic soil model [41] and simulated the compaction loads on pipelines during the backfilling.

Frank et al. [42] used the finite element code CANDE to study the influence of the depth of cover on pipe-soil interaction. They modeled soil non-homogeneity, (linear) anisotropy and non-linearity and they compared the results with actual field data. However, they concluded that favorable comparisons can be obtained for the deep burial situations, but the results for shallow burial covers did not reflect the observed lateral compression.

Singh et al. [43] utilized the finite element software Finite Element Analysis Program (FEAP) [44] to analyze two pipes adjacent to each other having different sizes and asymmetrical layout. Leonards et al. [45] investigated the fundamental response characteristic of buried metal pipes using the finite element program CANDE. They carefully studied the effect of different soil models, effect of different soil-pipe interface conditions and the importance of the sequence on the placement of soil layers.

Sherma, et al. [46] used CANDE to study the stability of rib reinforced, low profile, long span steel arch culverts located at Hayden Creek, Hyder Lake, North Idaho. The main object was to investigate the unexpected deformations (sag) during the first few months after installation.

Leonard et al. [47] also utilized CANDE to predict the performance of buried metal pipe arches. The effect of the state of compaction of soil backfill and of inclusions around the haunches on the fundamental response characteristics of closed pipe arches were summarized. Their results were compared with some design recommendations from the American Iron and Steel Institute handbook.

Sharp et al. [48] analyzed a fiber reinforced plastic pipe under various installation conditions taking into account the geometric and material non-linearities. The results from the analysis were compared with the measured response from a soil-box test. Selig et al. [49] evaluated the performance of rib-reinforced long-span culverts using CANDE.

Jeyapalan et al. [50] proposed a design procedure based on the finite element analysis of a pipe-soil system at the microscopic level and composite laminate analysis at the individual laminate level for fiber reinforced mortar plastic pipes. Conventional ways of assess-

ing the effects of soil arching over buried pipes were examined by utilizing finite element analyses by Tzong et al. [51] using CANDE. A recommendation was made which stated that design procedures utilizing the soil arching concepts whether explicitly or implicitly, should be used with caution beyond the empirical database from which they were derived.

The behavior of a soil-pipe system was assessed by Yoshiyuki et al. [52] using non-linear elasto-plastic finite element analysis. They used a model which was based on critical state mechanics in the elastic region and cap-type model in the plastic region and interpreted the actual performance of a buried flexible pipeline in a field investigation.

Various general purpose finite element codes were used by Duane et al. [53] to model pipeline-soil interaction system. They demonstrated the capability of several general purpose finite element codes to model pipe-soil systems by comparing their results with the semi-empirical formulations of White and Layer [7] and the closed form solutions of culvert models obtained by Burns and Richard [11].

Fernando et al. [54] used Fourier transform to model the 3-D behavior of buried pipes under centrally located vertical patch loads applied to the surface of a layered soil and conventional finite element analyses to approximate the field quantities in the 2-D transform plane.

Syed and Bakht [55] analyzed the effect of the live loads in soil-steel structure. They compared the homogeneous isotropic half-space, homogeneous isotropic finite layer, non-homogeneous half-space, and cross-anisotropic half-space solutions to calculate the stress distribution in the soil due to concentrated point or live loads. Moreover, they also considered the load dispersion in the soil by plain strain and in the span direction. The load

dispersion in the span direction was analyzed by isolating a longitudinal unit-width slice of the soil above the crown and using uniformly spaced linear springs, as shown in Fig. 2.6.

The mechanical effects of selected types of military traffic on buried high pressure steel pipes were examined by Potter [36]. Traffic loads were applied with both wheeled and tracked vehicles. Vehicles and payloads were selected to simulate the severest vehicle loading configurations anticipated at Fort Carson's Pinion Canyon Maneuver site. Experimental test results were compared with the Spangler methods [21] of design for flexible and rigid pipes.

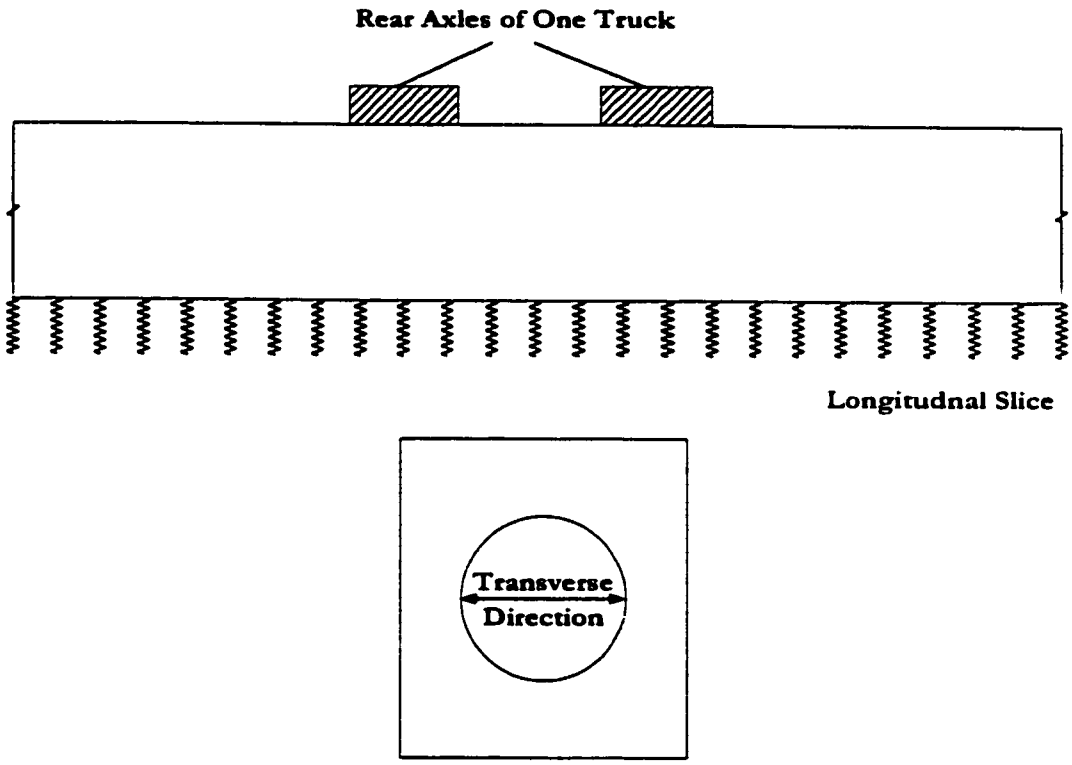

Fig. 2.6: Idealization of load dispersion along conduit axis [55]

CHAPTER 3

TECHNICAL BACKGROUND

3.1 Introduction

This chapter reviews the fundamentals of the soil-pipe system and its various components followed by the essentials of soil modeling for the realistic nonlinear finite element simulations. Criteria for the selection of suitable soil models and current design practices in underground pipeline engineering are presented at the end of the chapter. This will help in the appreciation of the development of the new design procedure for pipelines crossing highways and under sand overburden.

3.2 Pipe Definition

Although the plain strain cylindrical conduit (or pipe) is a well studied structural configuration, it is worthwhile to review some basic definitions. Fig. 3.1(a) shows a typical circular pipe cross section with commonly defined areas identified. The crown and invert (regardless of the pipe shape) are the top and bottom of the pipe, respectively and the

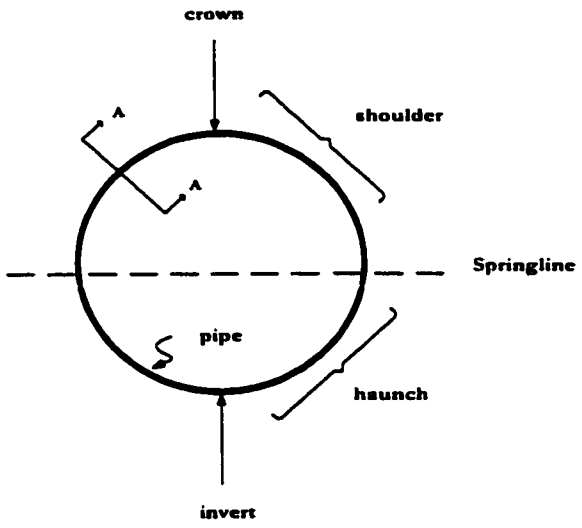

(a)

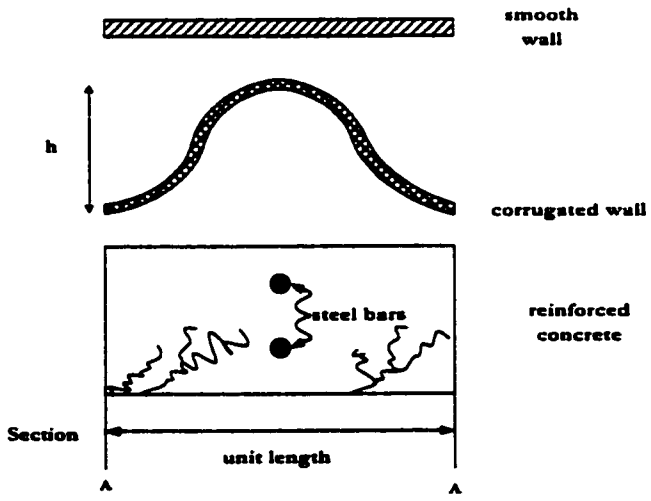

(b)

Fig. 3.1: (a)Pipe definition, (b) wall types

springline is an imaginary line connecting the left and right extremities. The zone between the crown and the springline is called the shoulder, while zone between the springline and the invert is called the haunch.

A cross section of a pipe wall is shown in Fig. 3.1(b) is described by following four properties

E = Young's modulus,

υ = Poisson's ratio,

I = Moment of inertia of wall per unit length

A = thrust area of wall per unit length

For a pipe of radius R, two useful measures of stiffness are given as: hoop stiffness. $(\frac{EA}{R})$. and bending stiffness, $(\frac{EI}{R^2})$. Naturally, the type of material and wall construction greatly influences these stiffness, as does the pipe radius. For example, if the wall is homogenous and of uniform thickness, t, (see Fig. 3.1(b)), then $A = t$ and $I = t^3/12$, and if $t << 1.0\,inch$, the bending stiffness becomes very small. However, by corrugating the pipe wall the bending stiffness is increased by the order of $(h/t)^2$, where h is the height of corrugation.

As a general rule for most culverts (including thick-walled reinforced concrete), bending stiffness is substantially less than the hoop stiffness because of the radius influence. Consequently, visible deformations are primarily in the bending mode as opposed to hoop compression.

3.3 Loads on Buried Pipes

Buried pipelines are generally designed to withstand dead loads due to any surrounding fill material plus the weight of the structure itself and any traffic loadings that may be imposed upon it during its life time. In addition to the above-mentioned loads, internal pressure is also an important loading in the case of pressurized pipelines. Dead load on cross-country pipelines usually comes 2 to 4 feet of the overfill soil. However for pipelines crossing railroads or highways the dead load acting on the pipeline is not only due to the overfill soil but also the embankment and the pavement material. Moreover at crossings the pipelines may be buried at greater depth to reduce the effect of live load, but will result in higher dead load on the pipe. Although the dead load on cross-country pipelines is usually due to a shallow cover of soil, sometimes if the pipeline is passing through an area of active sand dune movement the dead load on the pipe can be due to a 30 feet or more high sand dune [56].

The live load acting on the pipeline crossing railroads and highways result from vehicular weight and impact. It is well known that despite of the high volumes, light vehicles have a negligible effect on pavement and pavement foundation. Therefore, the stresses of primary concern are those generated by the heaviest vehicle passing over the crossing.

3.4 Behavior of Buried Pipes Under Various Loadings

A pipe subjected to two extreme loading conditions is shown in Fig. 3.2. Basic notions of structural behavior of pipes can be understood by these two extreme load distributions

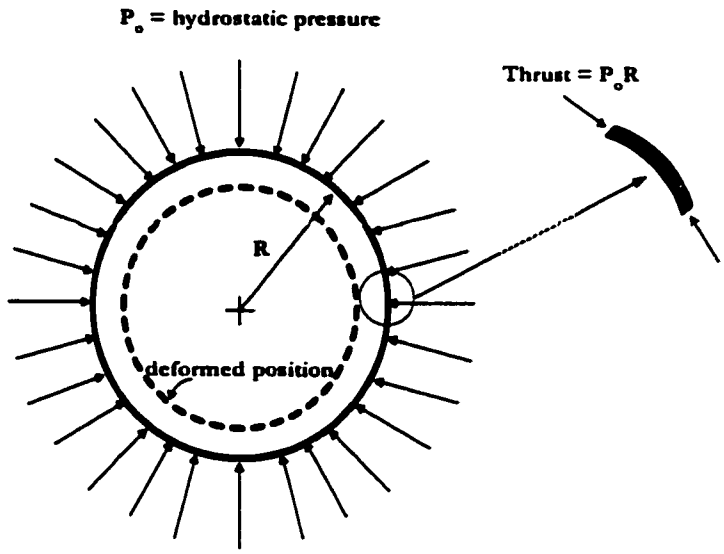

(a)

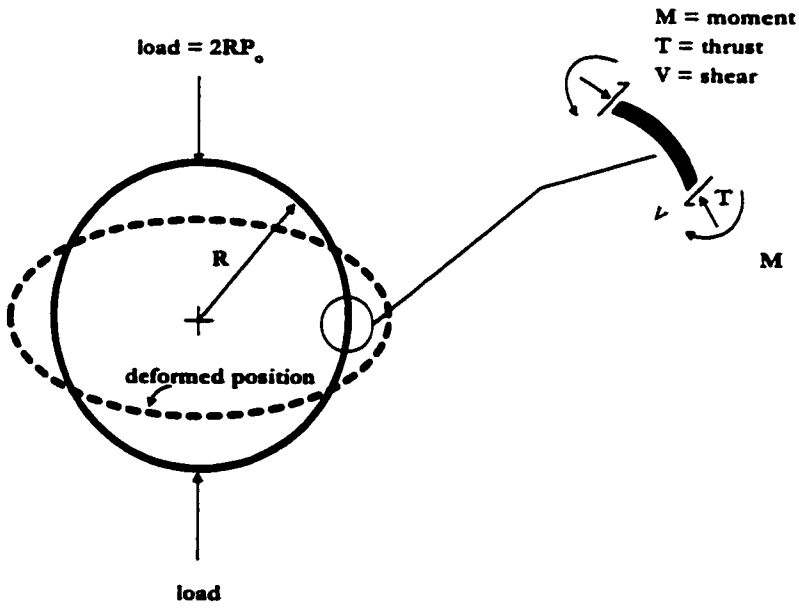

(b)

Fig. 3.2: Comparison of two extreme loading conditions

of hydrostatic and concentrated loads. In the hydrostatic case (Fig. 3.2(a)). only hoop or thrust force exists in the pipe wall, and the deformation is radially inward and inversely proportional to the hoop stiffness. This hydrostatic case of loading exactly represents the application of internal pressure in the pipe but in the reverse direction. In the second case, if the same load is applied to the pipe, but is concentrated at the crown and invert, it results in moment, thrust, and shear force in the pipe wall as shown in the Fig. 3.2(b). The pipe takes an oval shape, which is inversely proportional to the bending stiffness.

Comparison of the two load cases dramatizes the importance of properly assessing the load distribution on the pipeline. In the first case, the pipe material is fully utilized both through the cross-section and around the pipe. However. in the second case large bending deformations occur that produce large tensile stresses at the crown and invert. This fact clearly indicates the correct assumptions about the distribution of load along the pipe periphery. One of the most important load distribution models, still used widely. was originally proposed by Spangler [4]. In the Spangler model, it is assumed that the vertical load is distributed in an approximately uniform pattern over a horizontal plane at the pipe crown as shown in Fig. 3.3. The width of the horizontal plane at the top of the pipe is equal to the diameter of the pipe while the width through which the pipe receives the bottom reaction is generally narrower than the pipe diameter and is a function of the bedding conditions. The factors which define the bedding conditions are the bedding shape and the relative flexibility of the soil and the pipe. Moreover, at the sides of the pipe, the magnitude of the horizontal soil pressure mobilized at each point is a a function of the amount of outward movement of the pipe.

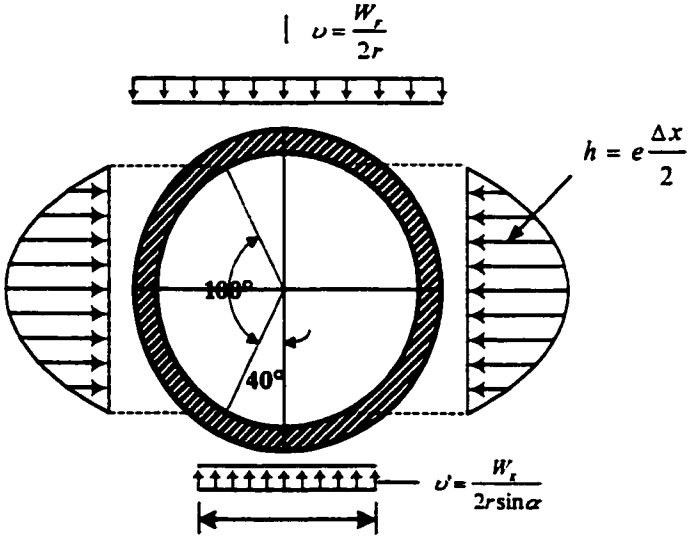

Fig. 3.3: Earth pressure distribution by Spangler[4]

3.5 Pipe Soil System

Pipe buried in soil is a soil-structure interaction problem, as the pipe and the soil working in tandem and it is one of the most remarkably synergistic systems in engineering. If the soil is properly compacted around the pipe, the load carrying capacity of the pipe-soil system will far exceeds the individual capacity of each component. In order to understand the behavior of the pipe-soil system, it is essential to identify whether the pipe is rigid or flexible. Moreover, the design approach is also affected by the nature of the pipe, being rigid or flexible; rigid pipes support loads by the virtue of the resistance of the pipe, as a ring, to bending or moment, whereas flexible pipes rely on horizontal thrust from the soil at the sides to enable them to resist vertical loads without excessive deformation. A rigid pipe is analogous to a beam, and a flexible pipe is analogous to an arch. Schematic diagrams of the deflections usually associated with rigid and flexible pipes are shown in Fig. 3.4. The difference in the deformation pattern suggests that the stresses and strains in the soil mass will be different, hence the mechanism of interaction in the two soil-pipe systems will also be different.

3.6 Rigid Versus Flexible Pipe

Separate design procedures exist for rigid and flexible pipes, so it is essential to identify whether the pipe will be acting as rigid or flexible. A rigid pipe may be defined as one which under the maximum load doesn't deform sufficiently to produce a significant amount of passive resistance at the sides from the soil in which it is laid. Clay pipes and

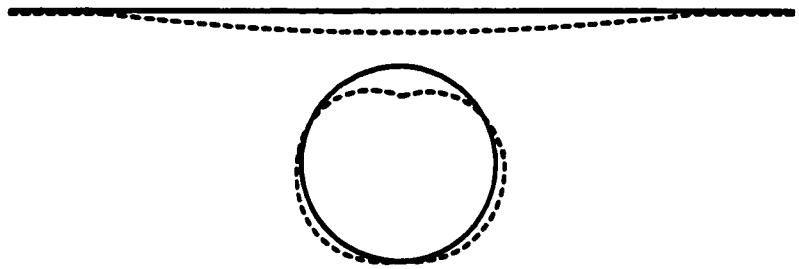

(a) Flexible pipe

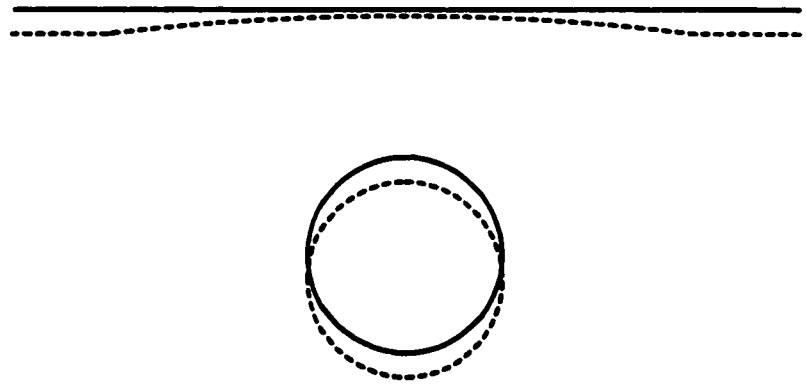

(b) Rigid pipe

Fig. 3.4: Schematic diagrams of the deformation of (a) a flexible pipe and (b) a rigid pipe

un-reinforced concrete pipes are typical examples. To perform as a 'flexible' pipe, a pipe must be capable of becoming appreciably oval in cross-section, with a decrease in the vertical diameter and an increase in the horizontal diameter without fracture. The deformation is usually expressed as a percentage of the diameter by which the vertical diameter decreases, and a 10% may be considered the very least that a 'flexible' pipe should be capable of sustaining without any risk of damage to the pipe material. For the flexibility to be of substantial use the vertical load needed to produce say about 5 – 10% deformation in the absence of a horizontal restraint needs to be small relative to the actual vertical load on the ground. Pipes that are to a large extent rigid, but are also capable of carrying a significant amount of extra load by virtue of their 'flexibility' are often referred to as 'semi flexible' or 'intermediate' pipe. A thin-walled steel pipe is a typical example of a flexible pipe. Although pre-stressed concrete and asbestos cement pipes are in general classified as rigid, they can, with very large diameters, behave as semi flexible pipes.

3.7 Soil Arching

An inclusion, in the form of an underground structure, in a soil medium will cause a redistribution of the 'free field' stresses and deflections. The nature of this redistribution influences the load that reaches the structure, whether it is due to the weight of the soil above the structure (the overburden) or to the surface loading. The proportion of the superimposed load that reaches the structure is governed by the characteristic of the soil, the geometry and stiffness of the structure, and whether the load is static or dynamic.

Because this redistribution in many practical cases results in a decrease in loading over

the deflection or 'yielding' areas of a structure, and an increase over adjoining rigid and stationary parts, the transfer of pressure has become known as 'arching'. It is particularly applicable to structures that deflect enough under the action of the super imposed load to mobilize the shearing resistance of the soil immediately adjoining the deflecting part it effects the buried pipe behavior to a large extent.

Positive arching is a favorable condition for buried pipelines because a portion of the overburden load is directed around the pipe in a compression arch of the soil, i.e., the pipe 'ducks' the load. The concept is illustrated in Fig. 3.5(a). On the other extreme, negative arching is unfavorable and implies that the pipe is drawing loads in excess of the soil column weight above it. The transition case, neutral arching is the one in which the pipe is drawing the same load as that of the soil column above it. The concept of neutral and negative arching are shown in Fig. 3.5(b) and (c) respectively.

The extent of soil arching can be expressed as (1) the ratio of the normal soil pressure at the crown, P_c, to the free-field normal stress at the crown, γh, in which γ is the unit weight of the soil and H is the soil height above the crown, or (2) the ratio of the maximum thrust in the conduit wall, which often occurs near the springline, to $w = \gamma HR$, where R is the pipe radius (Fig. 3.6).

In either measurements, if the ratio is less than one, positive arching is said to occur. The smaller the ratio the greater the positive arching. When positive arching occurs, the loads over the pipe are transferred to the soil around the two sides of the pipe. In the case of negative arching, the reverse is true: in other words, when negative arching occurs the loads are concentrated on the pipe and correspondingly reduced in the surrounding soil. If,

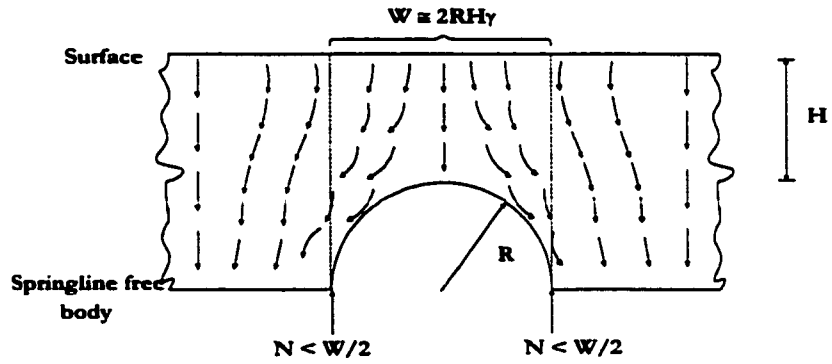

(a) positive arching

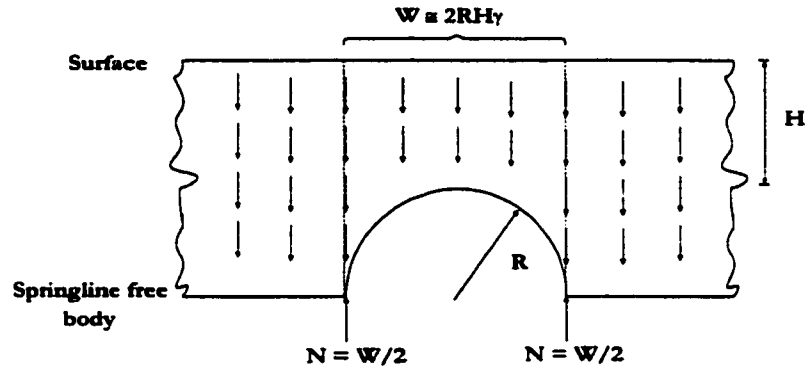

(b) Neutral arching

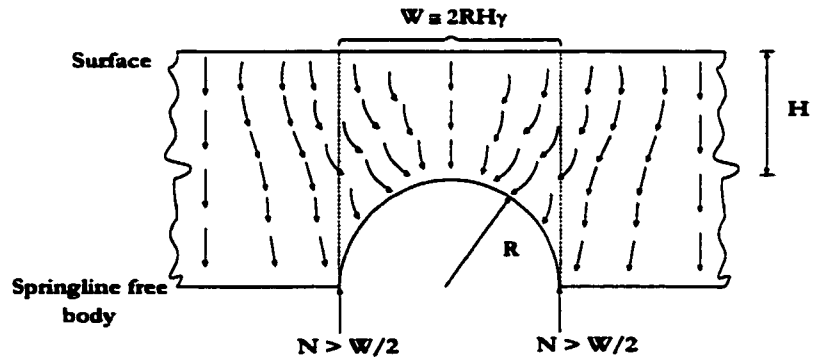

(c) Negative arching

Fig. 3.5: Arching, (a) Positive , (b) Neutral, (c) Negative arching

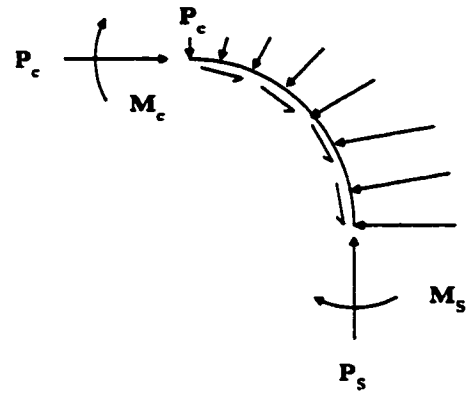

Positive arching: $P_c/\gamma H < 1$
Negative arching: $P_c/\gamma H > 1$

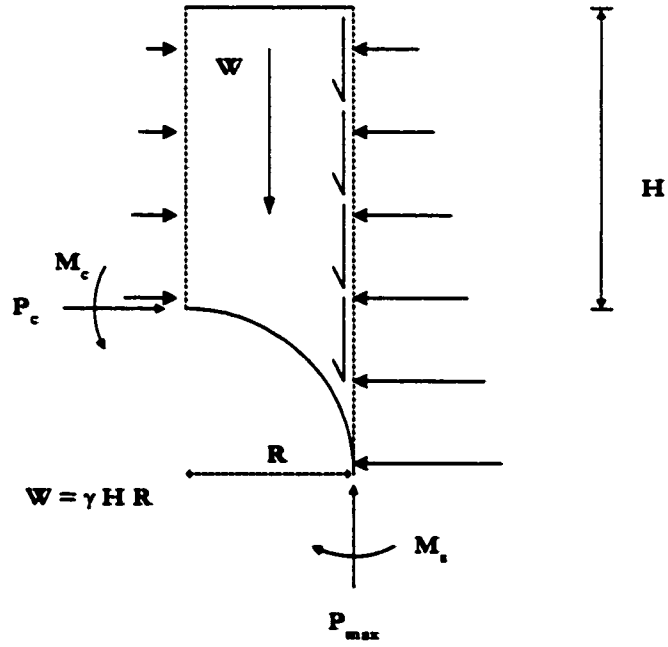

Positive arching: $P_{max}/W < 1$
Negative arching: $P_{max}/W > 1$

Fig. 3.6: Two measurements of soil arching

however, ratio is equal to one, neutral arching is said to occur. Qualitatively, it can be said that positive arching is enhanced as the soil stiffness increases relative to the pipe stiffness and the reverse is true for negative arching.

3.8 Plain Strain Approximation of Live Load

Computer-based analyses of pipe-soil structures using two-dimensional plain strain analysis use a unit width slice of the structure. The inherent assumption in this analysis is that there is no variation of force in the longitudinal direction of the pipe. This assumption, while being quite realistic under dead loads, may not be so under live loads which disperses through the fill both longitudinally and transversely.

Two different analogies are possible to convert vehicular loads to equivalent line loads; they are based on elasticity solutions for a homogeneous half space domain. One is based on a concentrated load assumption, while the other one utilizes the tire pressure. Both analyses are discussed below.

Katona, et al. [57] utilized Boussinesq's theory to idealize the concentrated load as an equivalent line load running parallel to the pipe axis. They used the elasticity solution to find the maximum vertical pressure σ_z along a horizontal line due to a concentrated load P, as shown in Fig. 3.7. Using the symbols in that Fig. 3.7 (c), the equation for (σ_z) is given by:

$$\sigma_z = \frac{3Pz^3}{2\pi R^5} \tag{3.1}$$

The corresponding maximum stress due to a line load with intensity Q (per unit length) as

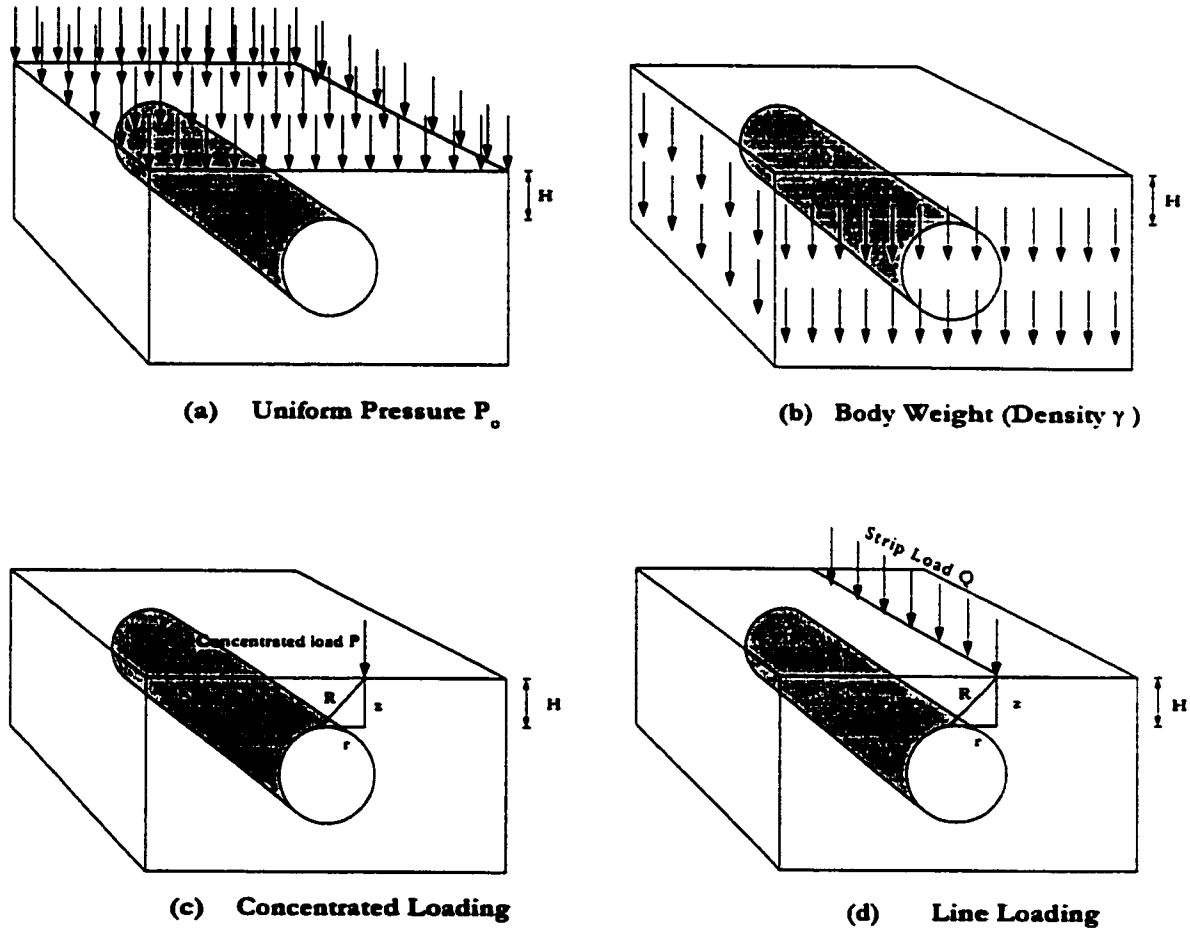

(a) Uniform Pressure P_o

(b) Body Weight (Density γ)

(c) Concentrated Loading

(d) Line Loading

Fig. 3.7: Fundamental load distributions for pipe soil system

shown in Fig. 3.7 (d) is given by

$$\sigma_z = \frac{2Qz^3}{\pi R^4} \tag{3.2}$$

Equating Eqn.(3.1) and Eqn.(3.2) yields

$$Q = \frac{3P}{4R} \tag{3.3}$$

Thus Eqn.(3.3) is used to calculate the intensity of the line load which is equivalent (and replaces) the concentrated load.

Another method is proposed by Duncan [17], cited by Bakht [24], and also reported by Seed and Duncan [58]. This theory utilizes the same technique as the first one by Katona, but instead of determining an equivalent strip load for a single load, an equivalent line load, which produces the same peak vertical stress (based on Boussinesq's theory) as do two HS-20 vehicle, is calculated. Table 3.1 gives such equivalent line loads for different cover depths.

Since the tire load is not really a concentrated one as it is applied over the contact area between the tire and the road, Katona [59] proposed a method to convert such pressure to an equivalent strip (plain strain) one as shown in Fig. 3.8. In this second analogy, he argued that the tire contact area on the surface must be known in addition to the tire load to determine the minimum soil cover requirements for culverts. For any given tire loading, the air pressure in the tire is a close approximation to the average contact pressure between the tire and roadway surface. Accordingly, the tire contact area (or tire footprint) may be computed by dividing the tire loading by the tire air pressure. A high-pressure tire induces more structural distress in a shallow buried culvert than the equally loaded low-pressure

TABLE 3.1: Equivalent line loads for HS-20 Vehicles

Cover depth, H, in ft	Line Load*, LL, in kips per foot
1	6.1
2	4.7
3	3.6
5	2.6
7	2.4
10	2.0
15	1.6
20	1.3
30	0.9
50	0.6
100	0.3
150	0.2
200	0.2

*produces same peak stress at depth H as do two HS-20 truck trailers with single rear axle side by side

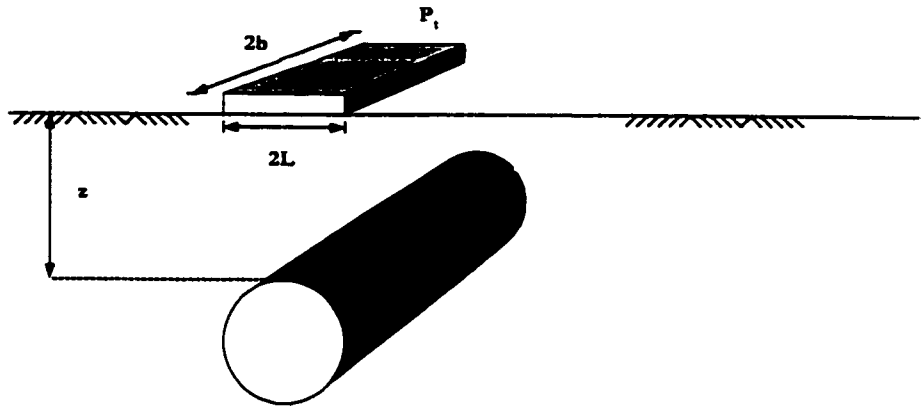

(a) Actual pressure distribution for tire

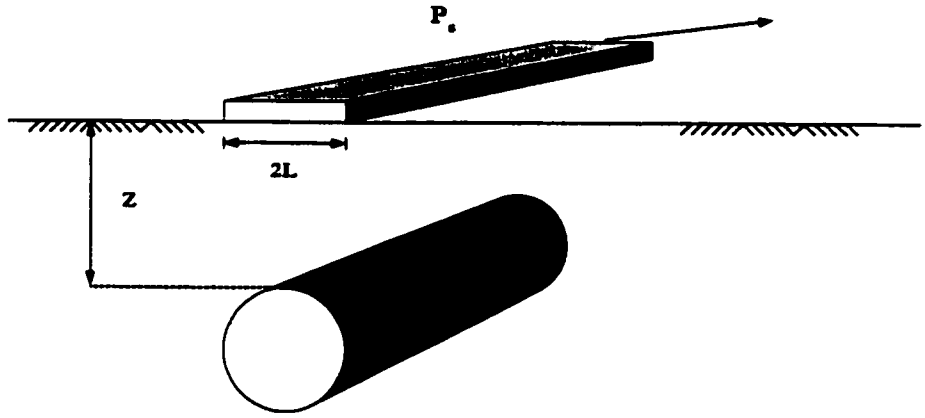

(b) Pressure Strip for Plain Strain Formulations

Fig. 3.8: Actual and plainstrain Pressure distribution

tire. The tire pressure may range from 65 to 100 psi because AASHTO specification does not include maximum values for tire air pressure. Katona [59] used H-truck loading instead of H-S truck loading. He took the upper-bound value of the tire pressure and also assumed the length of the footprint in the direction of travel to be 10 inches and found the values of the width of the footprint for various trucks using the following formula:

$$A = \frac{P}{p} \tag{3.4}$$

where,

A = area of the footprint (approximated as rectangle),

P = load on the tire, and

p = tire pressure

Furthermore, the area is taken as:

$$A = 2b \times 2L \tag{3.5}$$

Where,

$2b$ = width of the footprint, and

$2L$ = length of the footprint in the direction of travel

Table 3.2 summarizes the footprint widths and lengths for various H-trucks.

As can be seen from Fig 3.8, in the two-dimensional plain strain formulations, the footprint length $2L$ can be modeled exactly. However, the plain strain analysis infers that the footprint width is infinitely deep. So, to reasonably simulate a finite footprint width as

TABLE 3.2: Footprint widths and lengths for various H-trucks

Truck type	Gross Wt. (kips)	Rear tire Wt. (kips)	Tire length. (inches)	Tire width. (inches)
H10	20	8	10	8
H15	30	12	10	12
H20	40	16	10	16
H25	50	20	10	20
H30	60	24	10	24

Tire (single or dual) pressure = 100 psi

shown in the figure, the plain strain pressure P_s should be reduced from that of the actual tire footprint pressure P_t; that is

$$P_s = rP_t \tag{3.6}$$

where, r is a reduction factor (less than 1.0). This reduction is required because the soil stress associated with P_t diminishes more rapidly with depth than does the soil stress associated with P_s (i.e. two-dimensional loading versus the one-dimensional load spreading).

To compute the reduction factor, use is made of an exact elasticity solution for a homogenous half space (no pipe) loaded by the pressure P_t acting on a rectangular footing with dimensions $2L$ by $2b$. The solution for the vertical soil stress as a function of depth Z beneath the center of the pressure is given by

$$S_t = \frac{2Pt}{\pi}\left[\tan^{-1}\frac{B}{ZR_3} + BZ\left(\frac{1}{R_1^2R_3} + \frac{1}{R_2^2R_3}\right)\right] \tag{3.7}$$

where

$$\begin{aligned} B &= \frac{b}{L} \\ Z &= \frac{z}{L} \\ R_1 &= \sqrt{1+Z^2} \\ R_2 &= \sqrt{B^2+Z^2} \\ R_3 &= \sqrt{1+B^2+Z^2} \\ \pi &= 3.14 \end{aligned}$$

Similarly, the vertical soil stress for the pressure P_s acting on an infinite strip of dimension

$2L$ (i.e., width $2b$ is infinite) is given by

$$S_s = \frac{\tan^{-1}\left(\frac{B}{ZR_3}\right) + BZ\left(\frac{1}{R_1^2 R_3} + \frac{1}{R_2^2 R_3}\right)}{\tan^{-1}\left(\frac{1}{Z}\right) + \frac{Z}{R_1^2}} \tag{3.8}$$

Values for the reduction factors are given in Table 3.3

3.9 Soil Modeling

The finite element method provides a powerful technique for the analysis of stresses and movements in the earth mass, and it has been applied to a number of practical problems including embankment dams, open excavations, braced excavations and a variety of soil structure interaction problems. However for the results of the soil deformation analysis to be realistic and meaningful, it is very important that the stress-strain characteristic of the soil be represented in a reasonable way. This is extremely difficult because soils are multi-phase materials that consists of variable amount of solid particles, water and gas(air); the soil mass is often found to be inhomogeneous and anisotropic, thereby rendering the mechanical behavior dependent upon a number of factors such as mineralogical composition, dry density(void ratio), stress level, stress path, stress history, temperature, time, degree of saturation, etc.

Therefore it is very difficult to evolve a general constitutive (stress-strain) law, which is valid for all soils under all placement conditions. By necessity, simplified constitutive models based largely on phenomenological considerations have been employed to represent soil behavior in analyzing stresses and displacements of soil masses. It is convenient to classify the various simplified models for defining the behavior of soil into four cate-

TABLE 3.3: Reduction factors for various H-Trucks for various depths

Depth Ratio	H-Truck designation and ratio (b/L)				
$Z = \frac{z}{L}$	H 10 (0.8)	H 15 (1.2)	H 20 (1.6)	H 25 (2.0)	H 30 (2.4)
1.2	.72	.86	.93	.96	.98
1.8	.56	.73	.84	.90	.94
2.4	.45	.62	.74	.82	.88
3.0	.37	.52	.65	.74	.81
3.6	.32	.45	.57	.67	.74
4.2	.28	.40	.51	.60	.68
4.8	.24	.35	.46	.55	.62
5.4	.22	.32	.41	.50	.57
6.0	.20	.29	.38	.46	.53
6.6	.18	.27	.35	.42	.49
7.2	.16	.24	.32	.39	.46
7.8	.15	.23	.30	.36	.43

gories: (1) linear elastic models. (2) nonlinear incrementally elastic models, (3) Higher order elasticity models, and (4) plasticity models. Except for the few plasticity and higher order elasticity models, most of the models employ the generalized Hook's law as a deformation model. Consequently, shear dilatancy is not explicitly accounted for. The effects of dilatancy are accommodated implicitly by attempting to model the field conditions in the laboratory and relating the quasi-elastic response to the stress level. Attempts are also made to select a critical set of soil moduli in lieu of accounting for the effect of time.

3.10 Soil Models

The models discussed in this section are those which are most commonly used to predict the mechanical behavior of soil in finite element analyses involving soil structure interaction. Although there are other models which have been proposed for geologic media. these are the ones that have attracted more attention by the researchers.

3.10.1 Linear Elasticity Models

The assumption of linear elasticity constitutes the oldest and simplest approach to modeling the stress-strain behavior of soil. Subject to the further assumption of material isotropy, only two parameters (elastic modulus and Poisson's ratio) are needed to completely describe the mechanical behavior of a linearly elastic soil. The modulus is generally determined from conventional unconfined or triaxial compression tests; and Poisson's ratio is usually estimated. Both values are normally assumed to be constant throughout the entire loading history. While this model has proven very useful for a number of problems, it is

inherently incapable of describing the complicated nonlinear constitutive behavior of most soils. However, the assumption of linear elasticity has the very significant advantage that it reduces considerably the computational time and effort required to solve a given problem. and it is most applicable under conditions of monotonic loading and small strain level.

3.10.2 Nonlinear Incrementally Elastic Models

In Nonlinear incrementally elastic models an approximation of the actual nonlinear behavior of the soil mass is done by using essentially a series of linear behavior. Normally nonlinear behavior is divided in to pieces of linear elastic behavior, and incremental Hooks's law is assumed to describe the behavior. For each piece the model parameters E and ν are revised by making them functions of the state of stress or strain. Thus such model are only approximating nonlinearity by including the nonlinear effects in essentially two parameters E and ν.

3.10.3 Higher-Order Elasticity Models

Two higher-order elasticity models that have been investigated in geotechnical engineering are hyperelastic and Hypoelastic models.

3.10.3.1 Hyperelastic Models

The hyperelastic models rely on finding constitutive relations by differentiation of a strain energy function, U, with respect to invariants of strain, I_1, I_2, and I_3, as follows:

$$\sigma_{ij} = \frac{\partial U}{\partial I_1}\frac{\partial I_1}{\partial \varepsilon_{ij}} + \frac{\partial U}{\partial I_2}\frac{\partial I_2}{\partial \varepsilon_{ij}} + \frac{\partial U}{\partial I_3}\frac{\partial I_3}{\partial \varepsilon_{ij}} \tag{3.9}$$

$$= A_1\delta_{ij} + A_2\varepsilon_{ij} + A_3\varepsilon_{im}\varepsilon_{mj} \tag{3.10}$$

in which σ_{ij} = stress tensor; ε_{ij} = strain tensor; δ_{ij} = Kronecker delta; and A_i are response functions which satisfy the condition $\frac{\partial A_i}{\partial I_j} = \frac{\partial A_j}{\partial I_i}$.

Different order of hyperelastic models can be obtained by retaining higher-order terms in Eqn.(3.10). Depending on the order, the model can account for various factors. Ko and Masson [60] proposed a third order hyperelastic soil model. The model can accommodate dilatancy and strain hardening of soils. the model was verified by examining its ability to predict the overall response and the strain distribution of a cuboidal sample of Ottawa sand tested under plain strain conditions.

It may be noted that in hyperelastic models, the stresses are functions only of the strains. Consequently, the material behavior is assumed to be independent of the path followed during loading [61]. Unfortunately, for most soils, this assumption is only valid over a small stress range. Accordingly, laboratory tests must use stress paths that follow closely those anticipated in the field problem.

3.10.3.2 Hypoelastic Models

Truesdell [62] introduced a time-independent constitutive law, termed Hypoelastic, that relates an increment of stress to the existing stress and an increment of strain. This relationship has received limited use in describing the nonlinear stress-strain behavior of soils during loading. Coon and Evans [63] applied a first-order hypoelastic law to characterize the recoverable deformation of cohesionless soils. Their approach was entirely phenomenological, and the basic form of the law was chosen to correspond to the behavior observed under conventional triaxial test conditions. Although the incremental nature of this relationship offers many advantages regarding its ability to characterize the mechanical

behavior of soils, its ability to adequately handle stress path dependence would require the use of a higher order hypoelastic law.

A modified version of a hypoelastic law was used by Corotis, et al. [64] to develop nonlinear constitutive formulations for two soils (one cohesionless and one cohesive), and the coefficients in the formulations were evaluated from experimental data. The resulting equations were then incorporated into a finite-element program to determine the stresses that exist at different points in the soil surrounding a buried reinforced concrete pipe, and the predicted results agreed reasonably well with experimental measurements and were somewhat better than those determined by use of a more restrictive stress-strain model. Although this form of constitutive law offers many advantages, its usefulness is somewhat limited by the nature and number of tests that are required to adequately characterize the mechanical behavior of soils, especially if such factors as stress path dependence and density are taken into account

3.10.4 Plasticity Models

Plasticity models usually involve (a) a yield criterion (generally assumed to be a function of the stress invariants) to define the onset of plastic yielding, (b) a hardening or softening rule (generally assumed to be a function of plastic work and stress level) to define the yield criterion after plastic deformation has occurred, and (c) a flow rule to relate increments of plastic strain to increments of stress after the yield condition has been satisfied. From an academic point of view, plasticity models are attractive because they are inherently capable of treating conditions of unloading, stress path dependency, dilatancy, and the ef-

fects of the intermediate principal stress, and they usually satisfy the rigorous theoretical requirements of continuity, uniqueness, and stability. However, it is frequently difficult to correlate plasticity models with test data from conventional triaxial tests. thereby rendering it difficult to determine specific values for the parameters involved.

3.11 Soil Models for Analysis of Buried Pipelines

The models explained with some details in this section are those used by many researches for the simulation of buried pipelines. These models are implemented in many of the general finite element programs and most of the geotechnical finite element programs.

3.11.1 Mohr-Coulomb Elasto-Plastic Model

The Mohr-Coulomb failure criterion states that the shear strength of a soil (τ) increases with increasing normal effective stress on the failure plane (σ) according to:

$$\tau = c + \sigma \tan\phi \tag{3.11}$$

where, C is the cohesion of the soil and ϕ the angle of internal friction. This failure criterion is shown graphically in Fig. 3.9(a). The concept of Mohr circle can be used to express the criterion in terms of principal stresses. This yields:

$$\frac{\sigma_1 - \sigma_3}{2} = \frac{\sigma_1 + \sigma_3}{2} sin\phi + c\ cos\phi \tag{3.12}$$

where, σ_1 and σ_3 are the major and minor principal stresses, respectively.

For unconfined compressive test ($\sigma_3 = 0$), the cohesion (c) is related to angle of internal

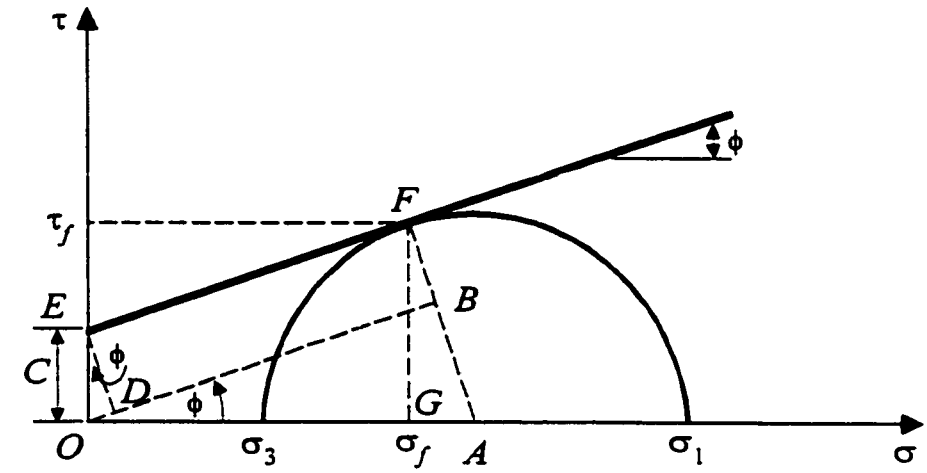

(a)

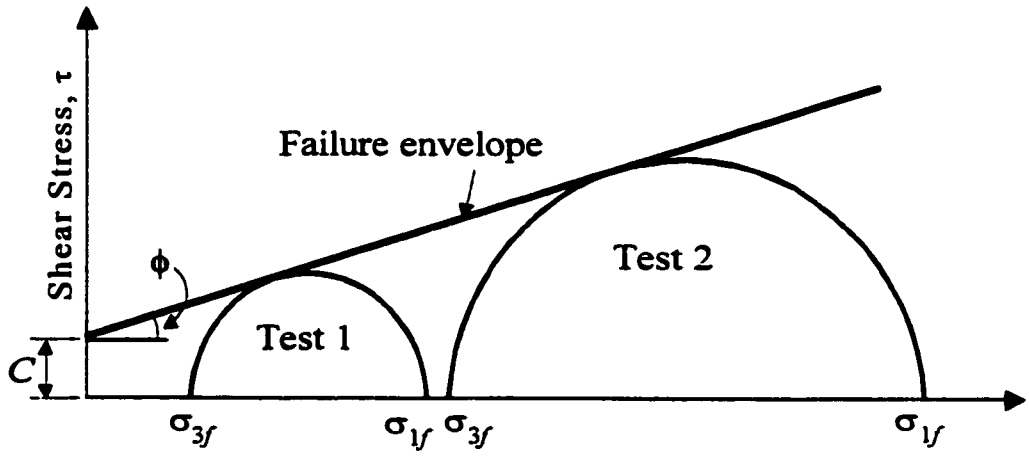

(b)

Fig. 3.9: Mohr circle and failure envelop for Mohr Coloumb Model

friction (ϕ) according to:

$$c = \frac{(1 - sin\phi)}{2cos\phi} * q_u \tag{3.13}$$

where q_u is the unconfined compressive strength (i.e. σ_1 at failure).

The two parameters associated with the Mohr-Coulomb failure criterion, angle of internal friction (ϕ) and cohesion (c), can be determined from laboratory tests on the material conducted up to the ultimate or failure conditions. The Mohr-Coulomb failure line is the envelope of Mohr circles at failure, and the values of ϕ and c may be determined as shown in Fig. 3.9(b). Conventional triaxial compression tests with cylindrical specimens are commonly used in determining the cohesion and angle of internal friction. A minimum of two tests is required to determine c and ϕ.

3.11.2 Overburden-Dependent Model

The overburden-dependent model is the application of the linear model in a series of steps. Each step represents an increment of soil fill or overburden pressure so that the elastic moduli are modified at each step to account for an increased stiffness due to increased overburden.

The overburden-dependent model is only valid insofar as the soil is predominantly in a state of confined compression. Generally, gravity loading of the soil promotes states of confined compression; however, in regions of interaction, such as certain areas in the vicinity of the pipe, the assumption of confined compression is questionable.

Keeping the above limitations in mind, the overburden-dependent model is best illustrated by considering a typical soil specimen undergoing a confined compression test.

Fig. 3.10(a) shows a typical overburden pressure versus axial strain. The relationship between overburden stress, σ_y, and axial strain, ϵ_y, is measured by the "secant" confined modulus, M_s

$$\sigma_y = M_s \varepsilon_y \tag{3.14}$$

From the measurements plotted in Fig. 3.10(a), M_s can be obtained for various values of overburden stress σ_y, $M_s = \sigma_y/\varepsilon_y$, Fig. 3.10(b).

The increments of overburden stress are related to increments of axial strain by the "chord" of the confined modulus, M_c;

$$\Delta\sigma_y = M_c \Delta\epsilon_y \tag{3.15}$$

The "chord" modulus, M_c (or average tangent) can be determined directly from the secant modulus, M_s, for any increment n to $n+1$ by:

$$M_c = \frac{\Delta\sigma_y}{\Delta\varepsilon_y} = \frac{\sigma_{y_{n+1}} - \sigma_{y_n}}{\left(\frac{\sigma_{y_{n+1}}}{M_{s_{n+1}}} - \frac{\sigma_{y_n}}{M_{s_n}}\right)} \tag{3.16}$$

The advantage of an overburden-dependent model over the fully nonlinear model (described later) is that, to advance the solution from step n to $n+1$, the chord modulus, M_c, can be determined directly by estimating $\sigma_{y_{n+1}} = \Delta\sigma_y + \sigma_{y_n}$, where $\Delta\sigma_y$ is estimated as the increment of overburden pressure (fill height equivalent). Since the secant modulus function, $M_s(\sigma_y)$, is known input data, M_c can be directly computed from Eqn. (3.16).

The complete description of the model requires a second elastic parameter, such as the lateral pressure coefficient, K_o, or Poisson's ratio (ν), since $K_o = \nu/(1-\nu)$. Poisson's

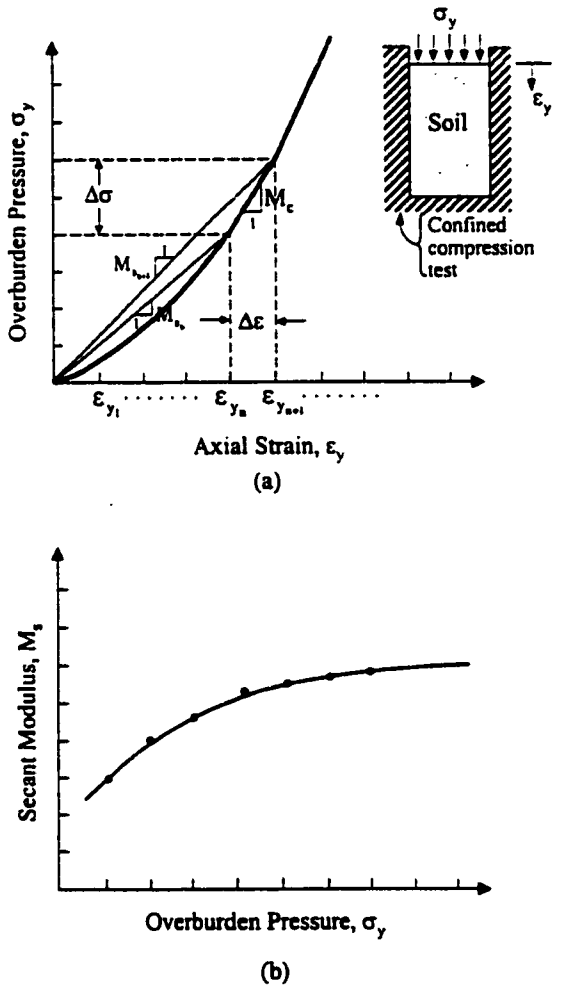

Fig. 3.10: Representation for overburden-dependent model

ratio remains practically constant in the case of confined compression, and therefore a constant value for Poisson's ratio can be used. Furthermore, it is generally more common to describe a model with Young's modulus and Poisson's ratio. Young's modulus is related to the confined modulus by a simple factor of Poisson's ratio as follows

$$E_s = \frac{(1+\upsilon)(1-2\nu)}{1-\nu} M_s \tag{3.17}$$

3.11.3 Duncan and Selig Models

Duncan and Chang's non-linear stress-strain curve is based on a hyperbolic type of relation between the $\sigma_1 - \sigma_3$ and the axial strain space. The Duncan model is defined by a variable Young's modulus and a variable bulk modulus. Young's modulus increases with increasing confining stress and decreases with increasing shear stress. Bulk modulus also increases with confining pressure. This model uses isotropic linear-elastic stress-strain relationships but with the elastic parameters varied according to the stress state. A tangent, rather than secant, formulation is used for Young's modulus so that this model is particularly suited to incremental simulation. Bulk modulus is related to the power of the confining stress.

Selig [65] extended the Duncan model by using the same Young's modulus formulation but with an alternative bulk modulus having a hyperbolic formulation. It is a tangent bulk modulus which is a function of the mean normal stress state. It was found to better represent hydrostatic compression than Duncan's power law form. The hyperbolic form was also found capable of representing uniaxial (confined) and triaxial compression.

3.11.3.1 Young's Modulus

Both the Duncan and Selig parameters were derived using the same Young's modulus obtained from constant confining pressure triaxial tests. The definitions of parameters used are those recommended by Duncan et al. [66]. However, a different method of fitting the triaxial data was used to develop the Selig parameters [67].

A typical stress-strain relationship from a constant confining pressure triaxial compression test is shown by the dashed curve in Fig. 3.11(a). This relationship is assumed to be represented mathematically by a hyperbola of the form

$$\sigma_1 - \sigma_3 = \frac{\varepsilon}{\frac{1}{E_i} + \frac{\varepsilon}{(\sigma_1 - \sigma_3)_u}} \tag{3.18}$$

where E_i = initial tangent modulus, $(\sigma_1 - \sigma_3)_u$= ultimate deviator stress at large strain as shown by the solid curve in Fig. 3.11(b).

The hyperbola is considered valid up to the actual soil failure point A. Thus, the ultimate deviator stress is defined in terms of the actual failure deviator stress by the failure ratio R_f as

$$R_f = \frac{(\sigma_1 - \sigma_3)_f}{(\sigma_1 - \sigma_3)_u} \tag{3.19}$$

To find the parameters E_i and $(\sigma_1 - \sigma_3)_u$, the actual test data are plotted in the linearized hyperbolic form of Fig. 3.11(b). Then the most appropriate straight line is used to represent the transformed Eqn. (3.18). The equation of this line is

$$\frac{\varepsilon}{(\sigma_1 - \sigma_3)} = \frac{1}{E_i} + \frac{\varepsilon}{(\sigma_1 - \sigma_3)_u} \tag{3.20}$$

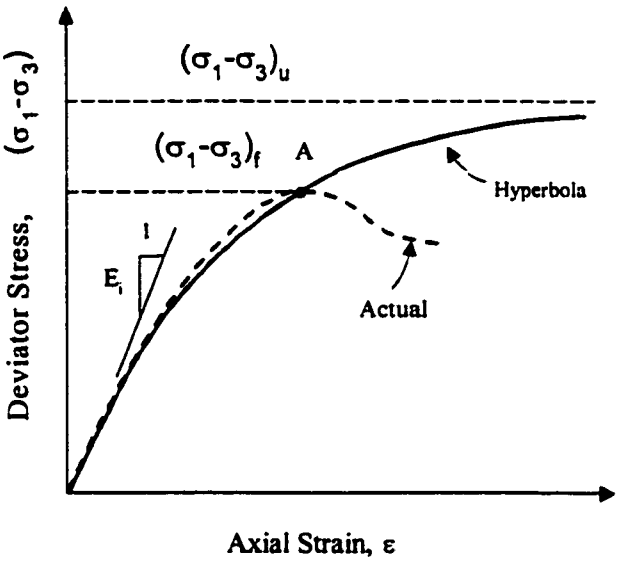

(a)

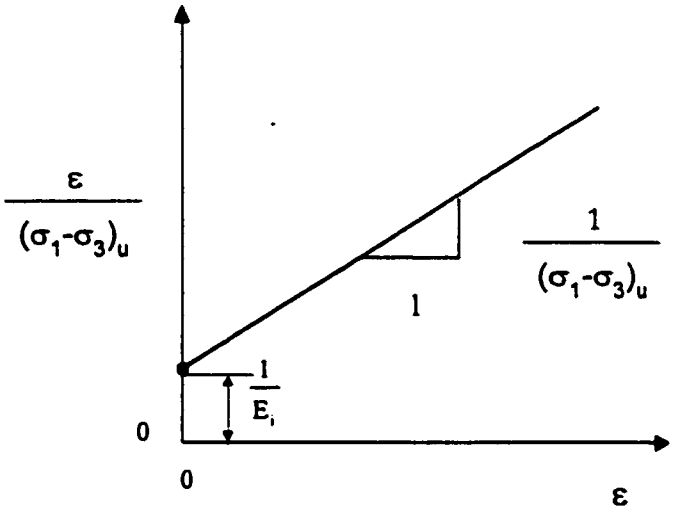

(b)

Fig. 3.11: (a) Hyperbolic representation of stress strain curve (b) Linearization of stress strain curve

The initial tangent modulus is assumed to increase with confining pressure as given by

$$E_i = Kp_a\,(\sigma_3/p_a)^n \tag{3.21}$$

where P_a is the atmospheric pressure which is used only to nondimensionalize the parameters K and n. The method of determining K and n is illustrated in Fig. 3.12 by the logarithmic plot.

The failure deviator stress is a function of the confining stress, σ_3. This is illustrated in Fig. 3.13 by the stress-strain curves and the corresponding failure stress Mohr's circles. The failure envelope is represented for simplicity by a straight line with slope ϕ, angle of internal friction, and intercept C.

The failure envelope is expressed mathematically by

$$(\sigma_1 - \sigma_3)_f = \frac{2c\cos\phi + 2\sigma_3 sin\phi}{1 - sin\phi} \tag{3.22}$$

The actual envelope is often curved. Thus, a best fit straight line is used or ϕ may be varied with σ_3. In the latter case, ϕ is represented by

$$\phi = \phi_o - \Delta\phi \log_{10}(\phi_3/P_a) \tag{3.23}$$

where ϕ = value of ϕ for $\sigma_3 = P_a$, and $\Delta\phi$ = reduction in ϕ for a ten-fold increase in ϕ_3. The method of determining ϕ and $\Delta\phi$ is shown in Fig. 3.14

The tangent Young's modulus for any stress state may be determined by differentiating Eqn. (3.18). The resulting equation is

$$E_t = \left(1 - \frac{R_f\,(1 - sin\phi)\,(\sigma_1 - \sigma_3)}{2Ccos\phi + 2\sigma_3 sin\phi}\right)^2 KP_a\,(\sigma_3/P_a)^n \tag{3.24}$$

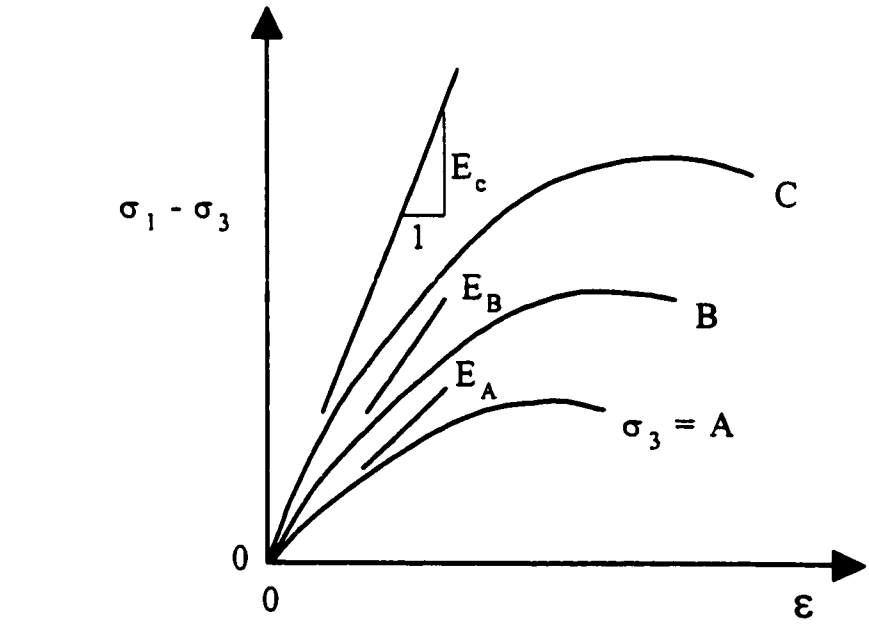

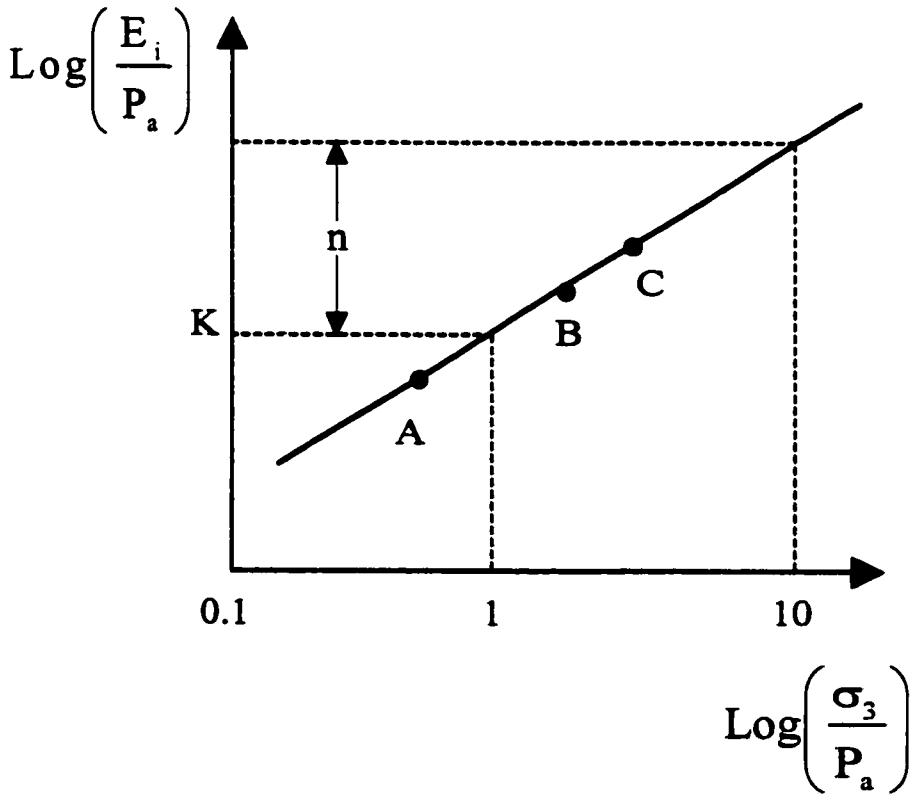

Fig. 3.12: Determination of K and n

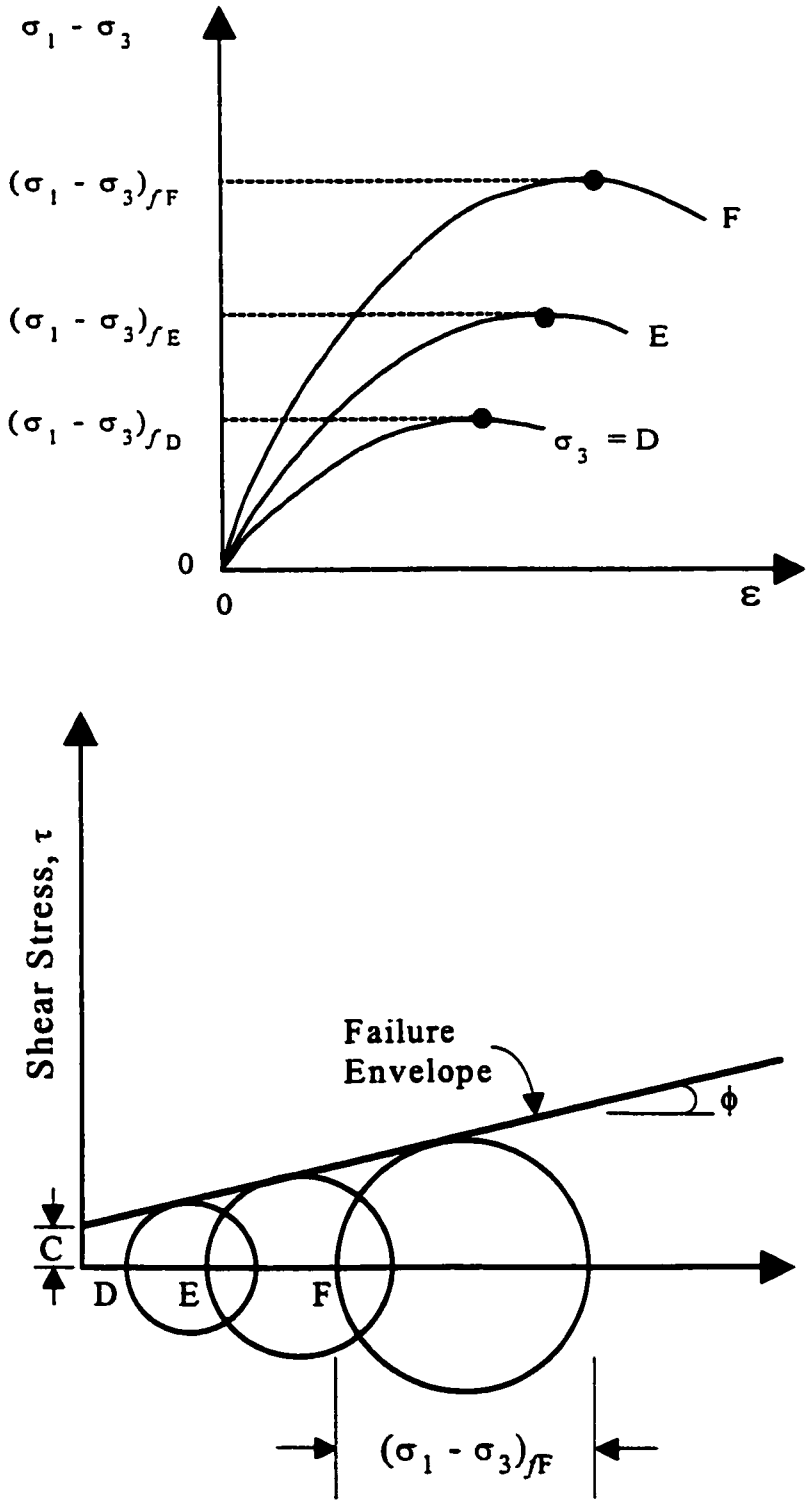

Fig. 3.13: Determination of C and ϕ

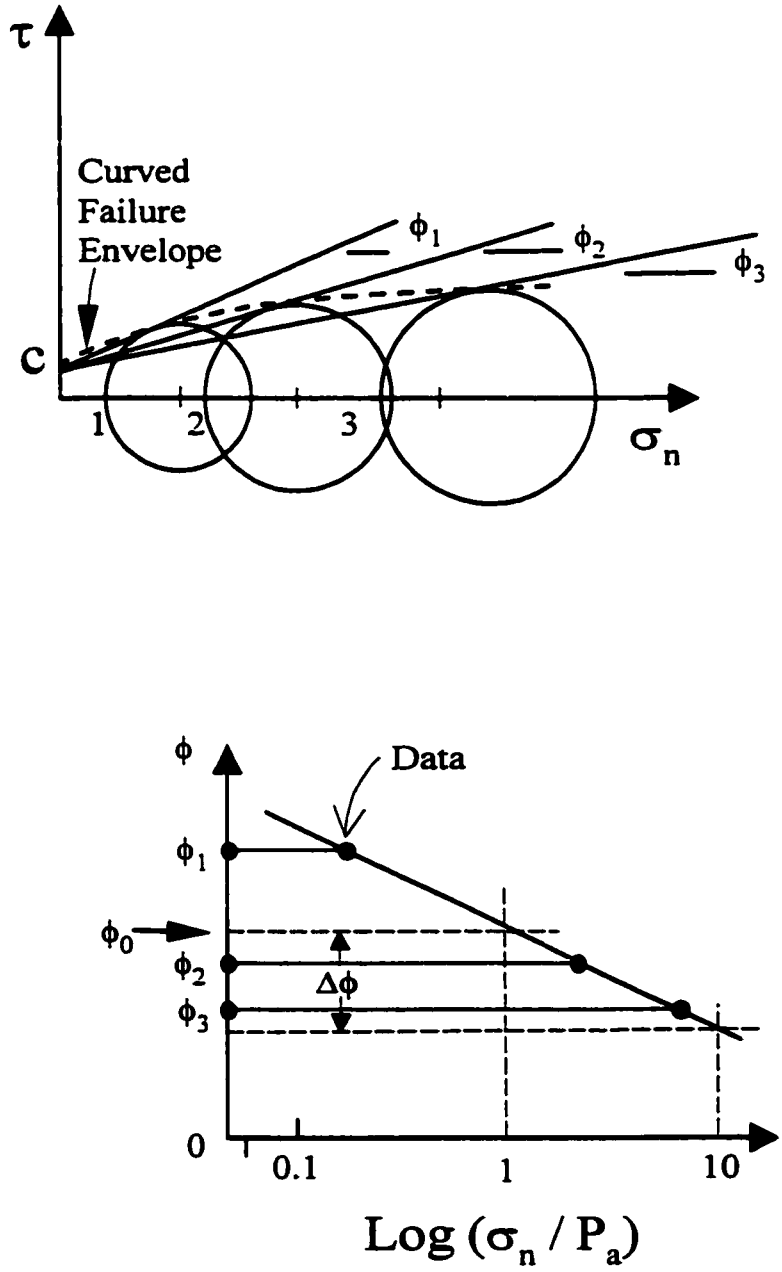

Fig. 3.14: Determination of $\Delta\phi$

3.11.3.2 Bulk Modulus

Bulk modulus, B, is defined as

$$B = \frac{\Delta\sigma_m}{\Delta\varepsilon_{vol}} \tag{3.25}$$

where $\Delta\sigma_m$ = change in mean stress, and $\Delta\varepsilon_{vol}$= change in volumetric strain.

The volumetric strain behavior in the triaxial test is illustrated in Fig. 3.15. The modulus B is determined from triaxial data by

$$B = \frac{\sigma_1 - \sigma_3}{3\varepsilon_{vol}} \tag{3.26}$$

Duncan et al. [66] proposed using the volume change and deviator stress corresponding to the point at which the volume change curve has a horizontal tangent (P in Fig. 3.15) or at which 70 percent of the strength is reached, whichever occurs first. Then the variation of B with σ_3 is assumed to be given by the power formulation

$$B = K_b\,(\sigma_3/P_a)^m \tag{3.27}$$

The parameters K_b and m are determined as shown in Fig. 3.16 . The line in Fig. 3.16 is the logarithmic form of Eqn.(3.27).

An alternative method for obtaining bulk modulus is from a hydrostatic compression test as illustrated in Fig. 3.17. In this test, the soil specimen is compressed under an increasing confining pressure applied equally in all directions. According to Eqn. (3.25), tangent bulk modulus B is the slope of the hydrostatic stress-strain curve.

Selig [65] observed that the curve relating σ_m and ε_{vol} was found to be reasonably

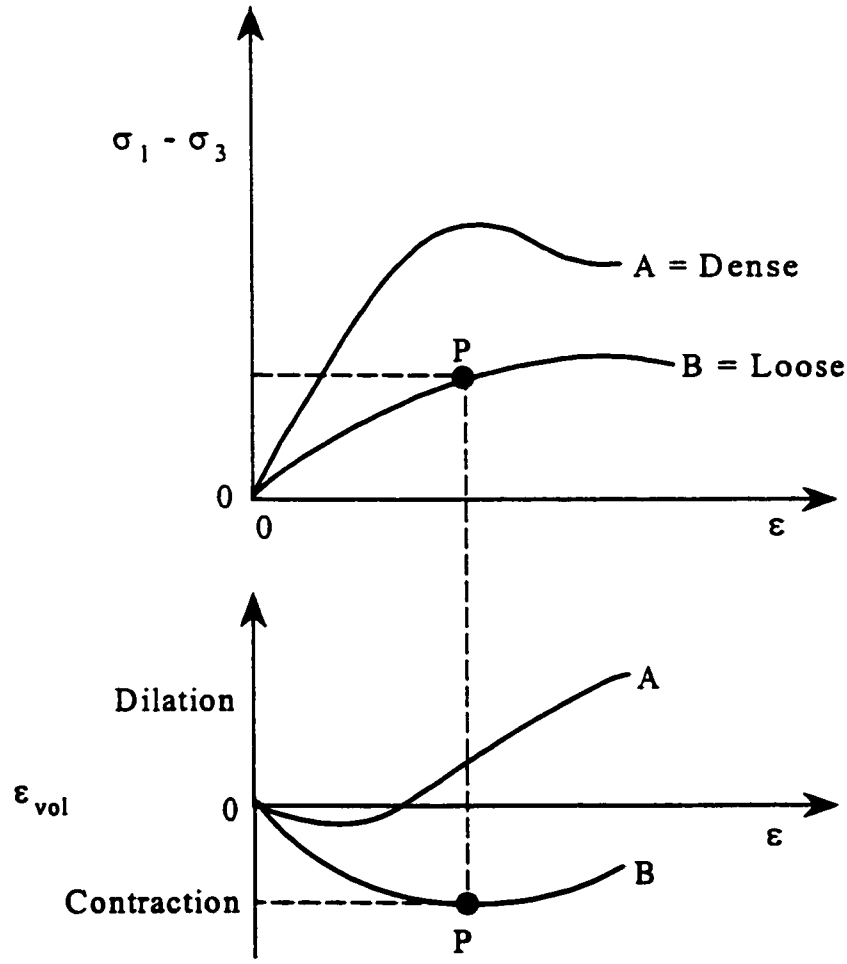

Fig. 3.15: Volumetric strain behavior in the triaxial test

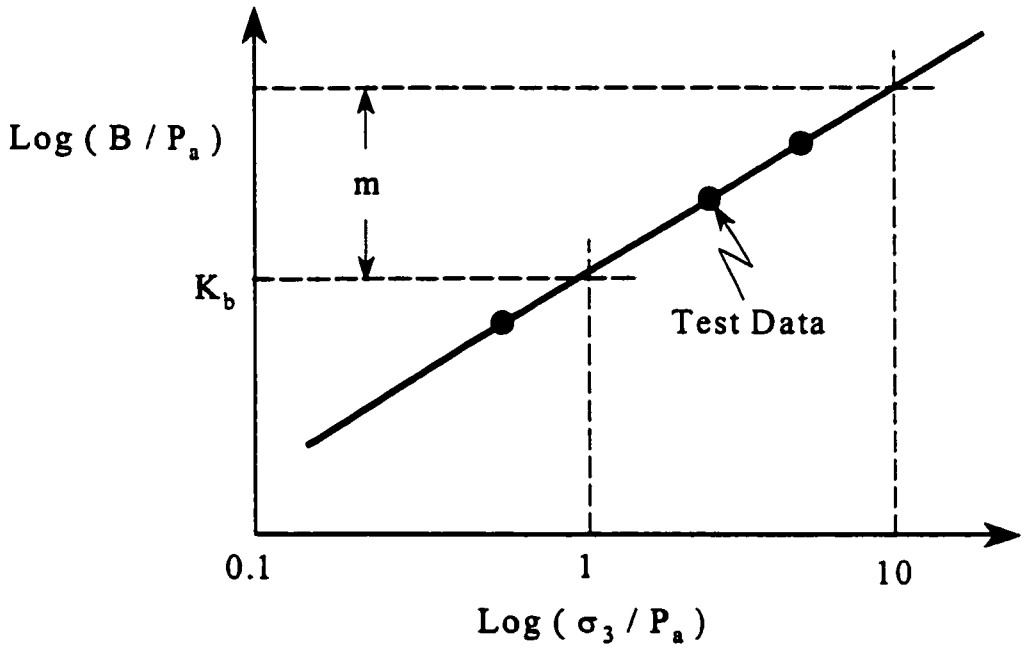

Fig. 3.16: Determination of K_b and m

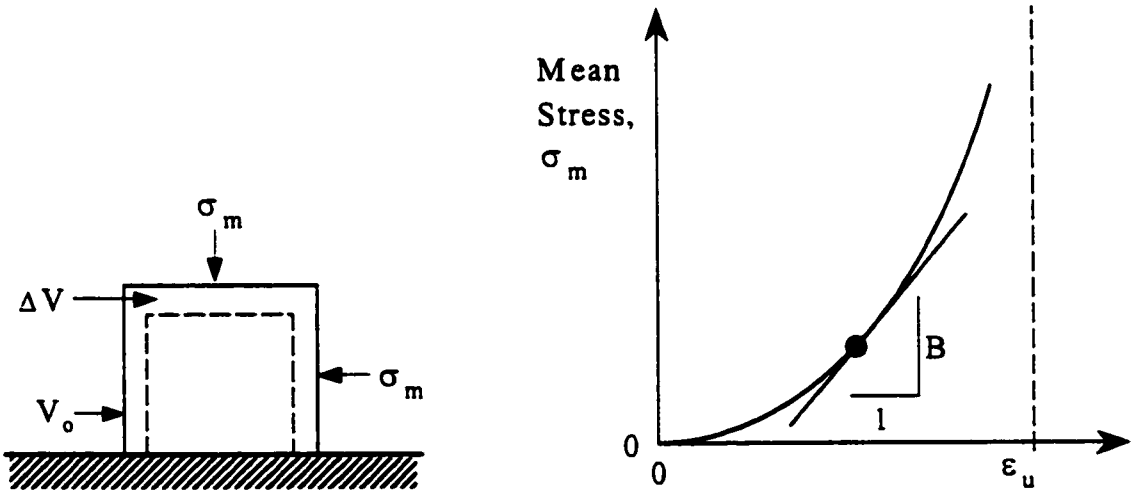

Fig. 3.17: Hydrostatic test

represented by the hyperbolic equation

$$\sigma_m = \frac{B_i \varepsilon_{vol}}{1 - (\varepsilon_{vol}/\varepsilon_u)} \tag{3.28}$$

where B_i = initial tangent bulk modulus, ε_u = ultimate volumetric strain at large stress.

The tangent bulk modulus B is determined by differentiating Eqn. (3.28) and substituting for ε_{vol} from Eqn. (3.28). The result is Selig's bulk modulus expression:

$$B = B_i \left(1 + \sigma_m / \left(B_i \varepsilon_u\right)\right)^2 \tag{3.29}$$

To determine the parameters B_i and ε_u, the test results from the left side of Fig. 3.16 are plotted in the linearized hyperbolic form of Fig. 3.18. Eqn. (3.28) will be a straight line in Fig. 3.18. Once B_i and ε_u are known, the test results can be represented by Eqn. (3.29) which is plotted in the form of Fig. 3.16 (with σ_3 replaced by σ_m) to obtain values of K_b and m.

Several studies have shown that the hyperbolic formulation for bulk modulus, Eqn. (3.29), better represents soil behavior in a hydrostatic compression test than Duncan's power formulation, Eqn. (3.27).

Eqns. (3.24), (3.27), and (3.29) of the former section are tangent moduli expressions for E_t and B_t for a particular principle stress state σ_1 and σ_3. As a load increment is applied, the stress state changes, inferring changes in E_t and B_t. In order to adequately represent the effects of these changes in the above-referenced equations, E_t and B_t should represent "average" values over the load step.

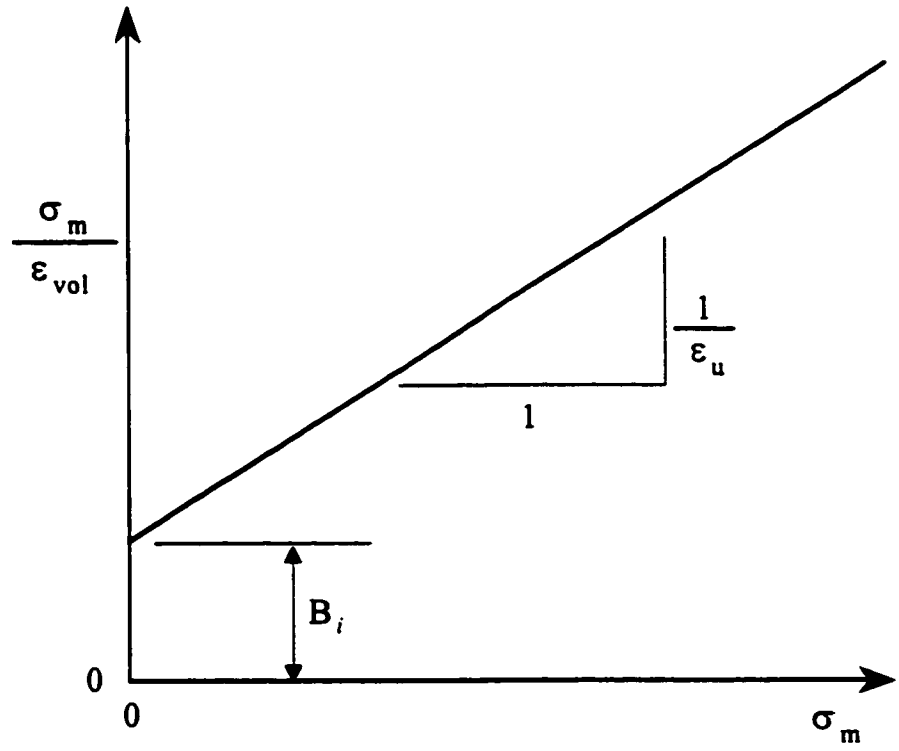

Fig. 3.18: Determination of B_i and ε_u

3.12 Selection of a soil model for analysis of soil pipe interaction problems

The stress strain behavior of the soil plays a very important role in analyzing soil-pipe interaction problems. Poor representation of stress strain characteristics can lead to calculated modes of behavior which is very different from the actual ones. In spite of the considerable work which has been done in this area, a general and versatile way of representing the stress-strain characteristics of soil, has not been established yet. The problem is very complex, and simplifications are essential for "practical" purposes. Accordingly, in selection of soil model, a compromise between accuracy and simplicity is essential. Selection of suitable soil model for soil-pipe interaction problems depend largely on the purpose of analyses. For routine design or preliminary studies, it is desirable to select soil models which don't require soil sampling and laboratory testing. On the other hand, for prediction of soil pipe system responses, development of new design methods, or extensive sensitivity studies, it is desirable to select the most realistic soil model possible within the framework of storage space available, computation time, and prior investigation of validity.

Various researchers have conflicting ideas about the appropriate soil model to be used in the finite element analyses of buried pipelines. Krizek and Atmatzidis [68] reported that reasonably good approximation of a pipe soil system can be obtained by using constant soil moduli with proper order of magnitude and the value of Poisson's ratio can be assumed constant for a given soil. Estimate based on engineering judgement and experience will be satisfactory in virtually all cases. However, they also mentioned that refinement in system behavior especially with increasing flexibility of the pipe can be achieved by using

simplified non-linear stress strain relationship. Leonards, et. al [45] studied the effect on the pipe responses of using different soil model. It was concluded that results obtained with different soil models are very different, especially with respect to deflection and bending moment in the pipe walls. An "equivalent" linear elastic soil model capable of modeling various phases of soil-pipe interaction does not exist. That is different moduli have to be selected when a given factor, say deflection, was considered at different stages in the construction process. Moreover, at any construction stage different moduli are required to predict different response factors, for example, thrust, deflection, or moment. In many instances the error associated with the use of a single set of linear-elastic moduli are very large; accordingly, further use of this model should be abandoned.

Duncan [66] and modified Duncan and Selig model [65] have been used by many researchers [45] [47–49] [69] for realistic finite element simulation of buried pipelines and the results have compared well with the field data. Moreover it has been used by Chua [38] to develop a new design method for design of flexible pipes. Since the Dunacn model has been used extensively and recommended by researchers so it was decided to use the Modified Duncan model which is also known as Selig model [65] for this research.

3.13 Spangler Design Procedure for Design of Buried Pipelines

3.13.1 Introduction

The Spangler approach to the design of pipeline crossings beneath highways and railroads, based on the work presented by Spangler [70–72], is codified in the 5th edition of

the American Petroleum Institute (API) RP 1102 [23]. This section presents the equations used in the Spangler's design procedure.

3.13.2 Calculation of the Total Load on the Pipe

The total load on the crown of the pipe, W_t, is the sum of the dead and the live load:

$$W_t = W_E + W_L \tag{3.30}$$

where W_E and W_L are the soil and live loads per unit length of the pipe, respectively, acting on the pipe due to soil, rail, track load or vehicle load, including impact.

3.13.3 Marston Theory for Estimating Soil Load, W_E

A typical cross-section of a pipe in trench and the prism of the overlying soil which acts upon it is shown in Fig. 3.19. The load on the pipe is the weight of the soil prism above the pipe minus the induced shear along the sides of the soil prism. The resulting load, W_E, acting per unit length of the pipe is given by the expression:

$$W_E = C_d \gamma B^2 \tag{3.31}$$

in which C_d is the load coefficient, γ is the unit weight of the soil, and B is the width of the trench. The parameter C_d can be estimated from either Eqn. (3.32) or the Fig. 3.20. Where H is the distance from the crown of the pipe to the ground surface.

$$C_d = \frac{1 - e^{-2k\mu\left(\frac{H}{B_d}\right)}}{2K\mu} \tag{3.32}$$

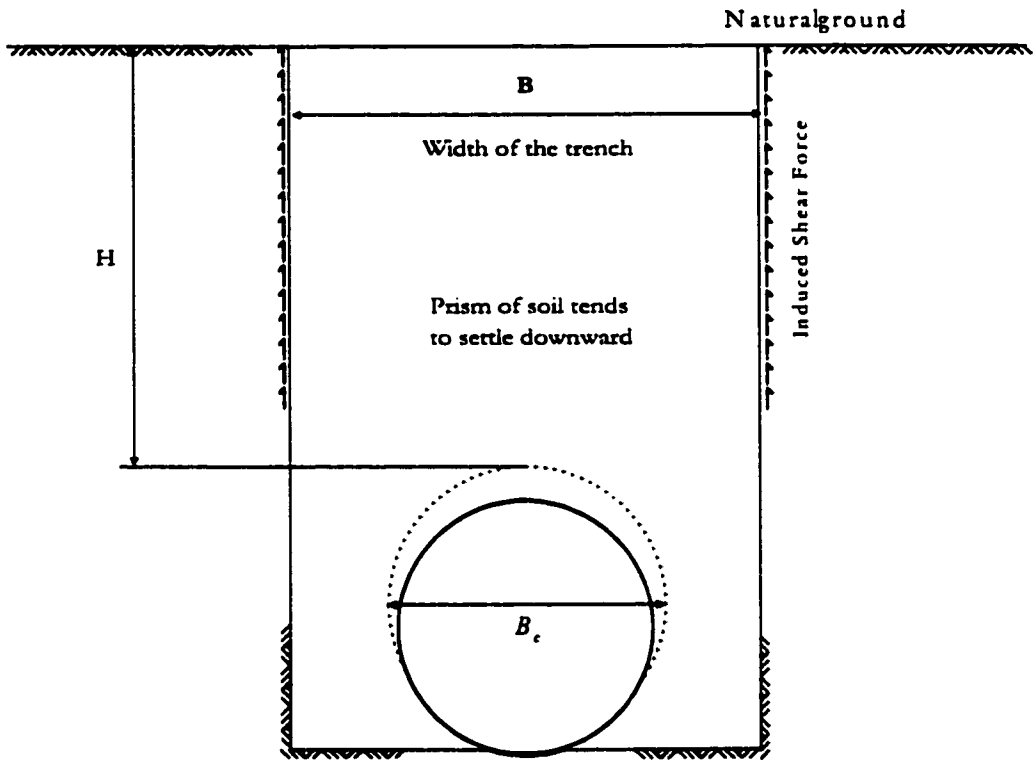

Fig. 3.19: Cross-Section of pipe and soil

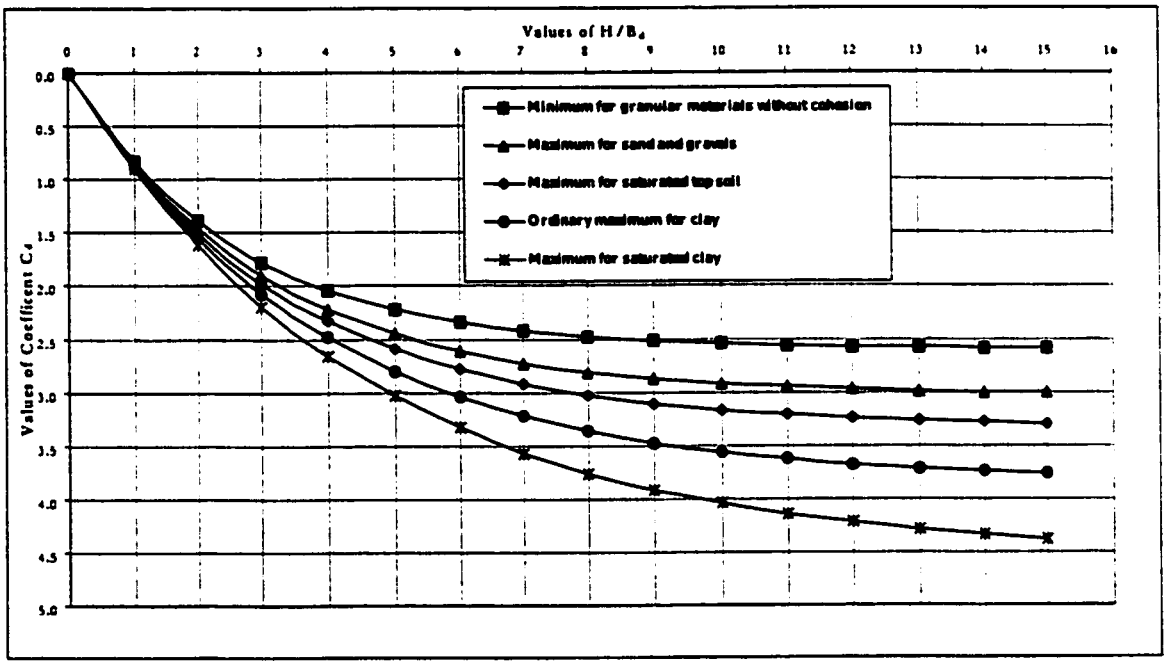

Fig. 3.20: Diagram for Load Coefficent, C_d

Where,

K = Coefficent of lateral earth pressure,

μ = Coefficent of friction between backfill and in situ soil, and

H = Depth of cover.

3.13.4 Newmark Integration of the Boussinesq's Equation for Estimating Live Load, W_L

The simplified vehicular load is shown in Fig. 3.21 as a uniformly distributed rectangular surface pressure. The nominal dimensions depend upon the load coming to the tire and the internal pressure of the tire. The live load acting per linear foot on the crown of the pipe, W_L at a depth, H below the surface is :

$$W_L = 4wF_iI_zD \tag{3.33}$$

Where, W is the idealized vehicular load, I_z is Newmark's influence coefficient as determined from:

$$\begin{aligned} I_z &= \frac{1}{4\pi}\left[\frac{2ABH\sqrt[2]{A^2+B^2+H^2}}{H^2(A^2+B^2+H^2)+A^2B^2}\frac{A^2+B^2+2H^2}{A^2+B^2+H^2}\right] \\ &\quad +\frac{1}{4\pi}\left[\sin^{-1}\left(\frac{2ABH\sqrt[2]{A^2+B^2+H^2}}{H^2(A^2+B^2+H^2)+A^2B^2}\right)\right] \end{aligned} \tag{3.34}$$

Using the geometry of Fig. 3.21, D is the diameter of the pipe, the parameter w is the applied surface pressure usually taken as the tire pressure. The impact factor F_i is given by:

$$F_i = 1.75 - 0.03(H-5) \tag{3.35}$$

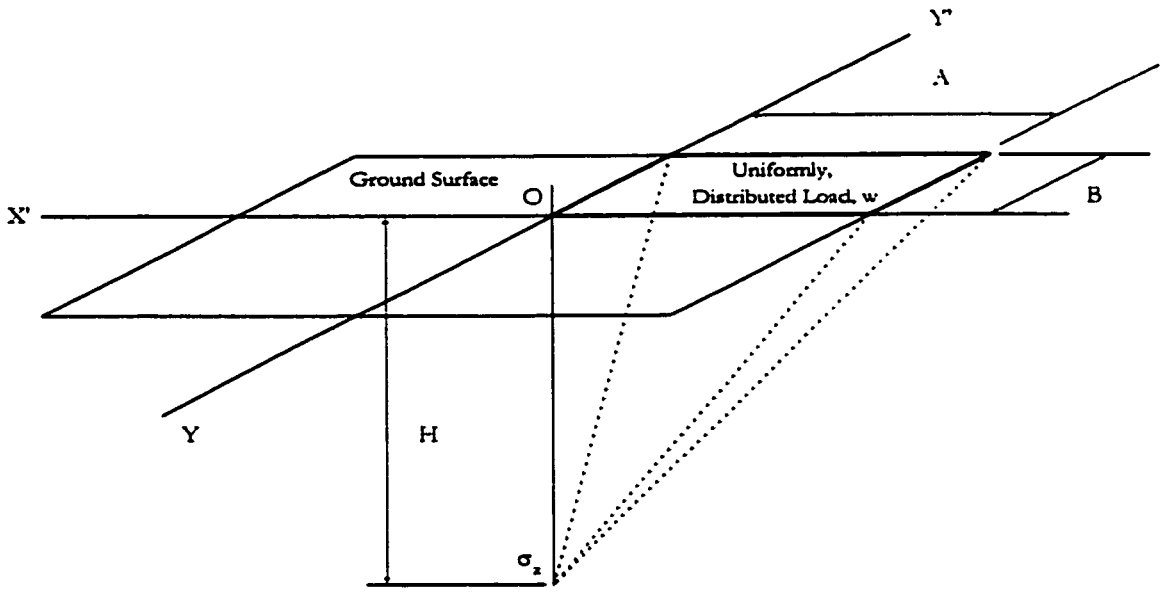

Fig. 3.21: Loading condition for highway live load

in which H is the depth in feet from the ground surface to the crown of the pipe.

3.13.5 The Spangler Formula for Determining Circumferential Stresses Due to External Loads, S_{He}

The Spangler formula, the equation used predicting the circumferential stress, S_{He}, in a pipe due to dead and live loading is given by:

$$S_H = \frac{3K_b W_t E_s D t_w}{E_s t_w^3 + 3K_z p D^3} \tag{3.36}$$

where,

K_b = Bedding angle constant related to pipe moments,

W_E = Total load on the crown of the pipe,

E_s = Young's modulus of the pipe,

D = Diameter of the pipe,

t_w = Pipe wall thickness,

K_z = Bedding angle constant related to pipe displacement, and

p = Internal pressure in the pipe

3.13.6 The Barlow Formula for Calculating Circumferential Stresses Due to Internal Pressure, S_{H_i}

The circumferential stress due to internal pressure, S_{Hi}, is given by the Barlow formula:

$$S_{Hi} = \frac{pD}{2t_w} \tag{3.37}$$

3.13.7 Total Circumferential stress, S_{HT}

the total circumferential stress, S_{HT}, is the sum of the circumferential stress due to the dead and live loading, and the stress due to the pressurization:

$$S_{HT} = S_H + S_{Hi} \tag{3.38}$$

3.14 Summary of the Cornell/GRI Design Procedure for the Design of Buried Pipelines

3.14.1 Introduction

The Cornell/Gas Research Institute (GRI) approach to design pipeline crossings is based on the work presented by Ingraffea, et al [73]. The design procedure for railroad and highways is summarized by Stewart et al. [74] as well as the 6th edition of the American Petroleum Institute RP 1102 [34]. This section presents the design procedure for design of pipelines under highway crossings and dead load. The focus will be on calculation of

stresses and will not include design checks on yield or fatigue.

3.14.2 Calculation of Circumferential Stresses Due to Earth Load, S_{He}

The circumferential stress due to earth load, S_{He} is given by the expression:

$$S_{He} = K_{He} B_e E_e \gamma D \tag{3.39}$$

Where,

K_{He} = Circumferential stiffness factor for earth load

B_e = Burial factor for the earth load

E_e = Excavation factor

γ = Unit weight of the soil

D = Outer diameter of the Pipe

The circumferential stiffness factor, K_{He}, is shown in Fig. 3.22 as a function of the wall thickness to diameter ratios for values of moduli of soil reaction, E'. A value of 500 psi is recommended for E', unless specific soil data indicate otherwise. Fig. 3.23 shows the burial factor, B_e, as a function of the depth to bored diameter ratio for different soil types. The Excavation factor, E_e, is shown in Fig. 3.24. A unit weight of soil $\gamma = 120\ lb/ft^3$ is recommended, unless otherwise warranted by specific soil data.

3.14.3 Calculation of Circumferential stresses Due to Highway Live load, ΔS_{Hh}

The cyclic circumferential stress due to highway load, ΔS_{Hh} may be calculated form:

$$\Delta S_{Hh} = K_{Hh} G_{Hh} R L F_i w \tag{3.40}$$

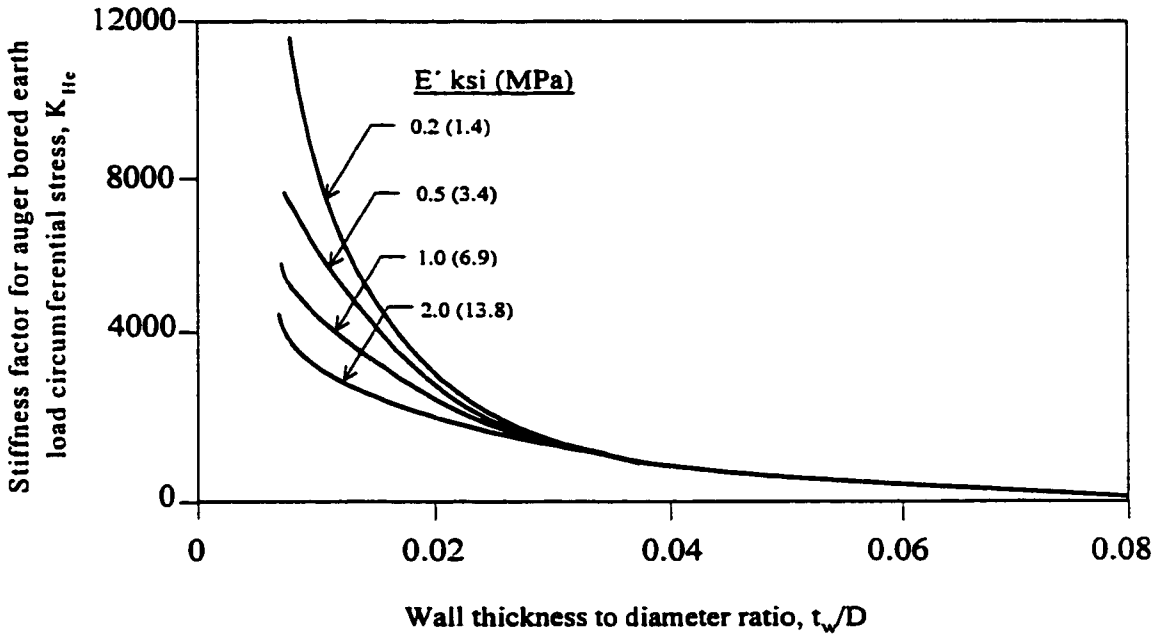

Fig. 3.22: Stiffness factor for earth load circumferential stress, K_{He}

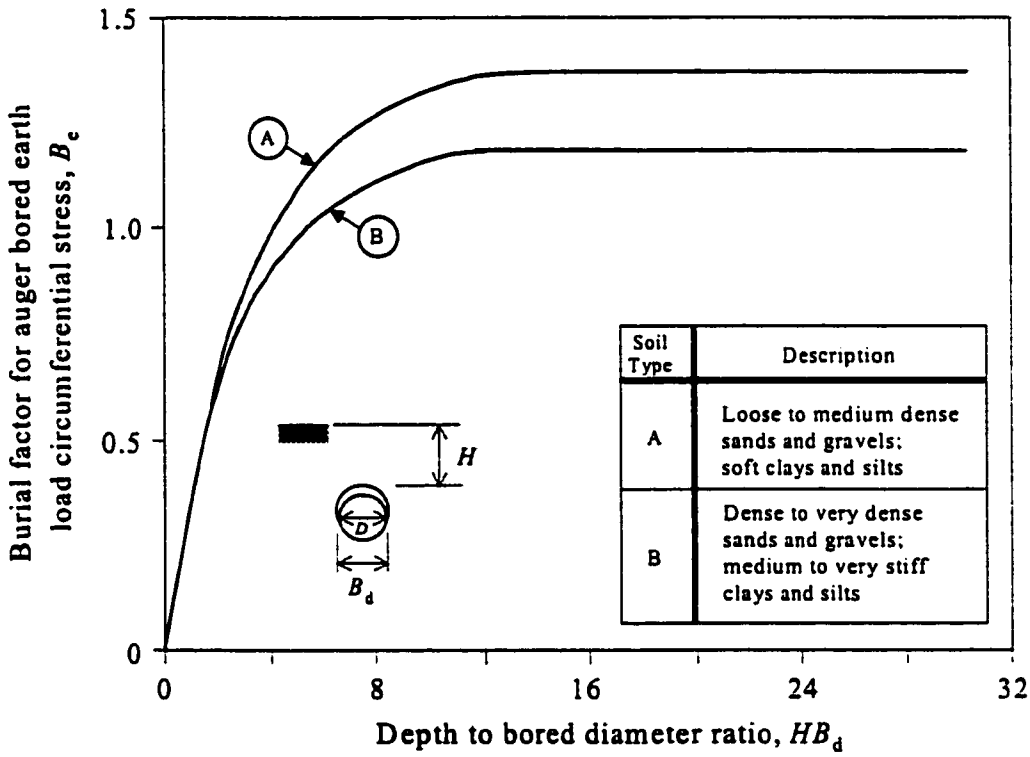

Fig. 3.23: Burial Factor for earth load circumferential stress, Be

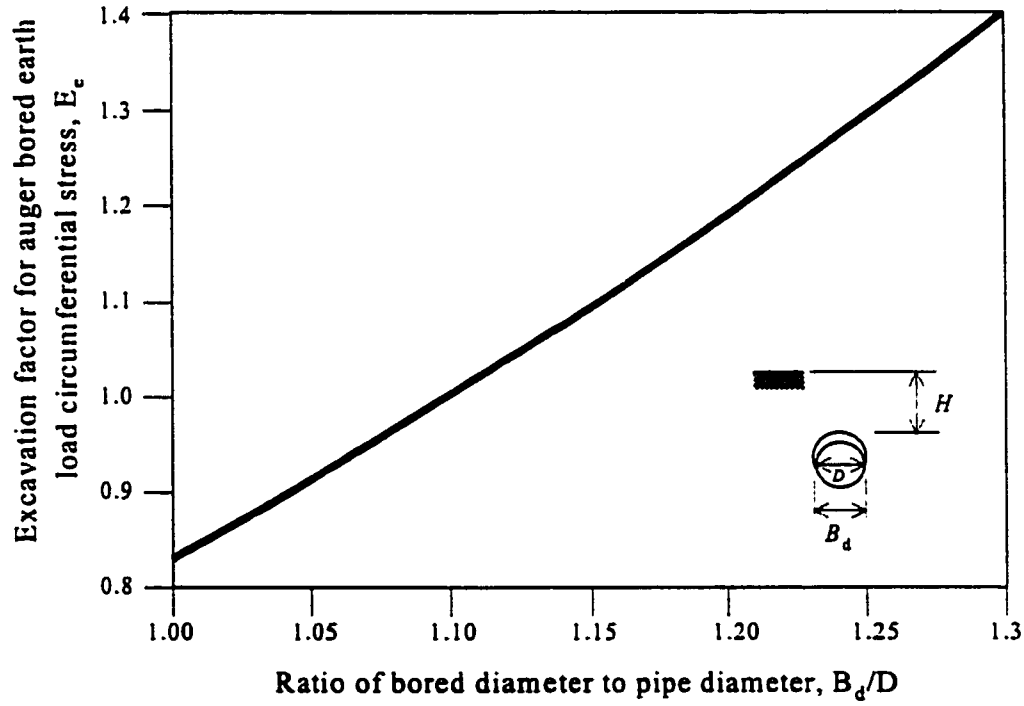

Fig. 3.24: Excavation factor for earth load circumfernetial stress, *Ee*

Where,

K_{Hh} = Highway stiffness factor for cyclic circumferential stress,

G_{Hh} = Highway geometry factor for cyclic circumferntial stress,

R = Highway pavement type factor,

L = Highway axle configuration factor,

F_i = impact factor, and

w = live external highway load, lb.per square inch or kilopascals .

The circumferential highway stiffness factor is presented in Fig. 3.25 as a function of the pipe wall thickness to diameter ratio, t_w/D, and the resilient modulus. E_r. The circumferential highway geometry factor, G_{Hh}, is presented in Fig. 3.26 as a function of pipe diameter and the burial depth. The Highway pavement type factor, R, and Highway Axle configuration factor, L, are given in Table 3.4. The live external highway load. w. is due to the wheel load P, applied at the surface of the roadway. For design only the load from one of the wheel sets is need to be considered. The wheel load from a truck's single axle, P_s, or the maximum wheel load from a truck's tandem axle, P_t. Fig. 3.27 shows the methods by which axle loads are converted in to equivalent single wheel loads P_s and P_t. The impact factor, F_i, is calculated based on the depth of the pipe, H, is given by the equation:

$$F_i = 1.5 \qquad \text{for } H \leq 5\,\text{ft} \tag{3.41}$$

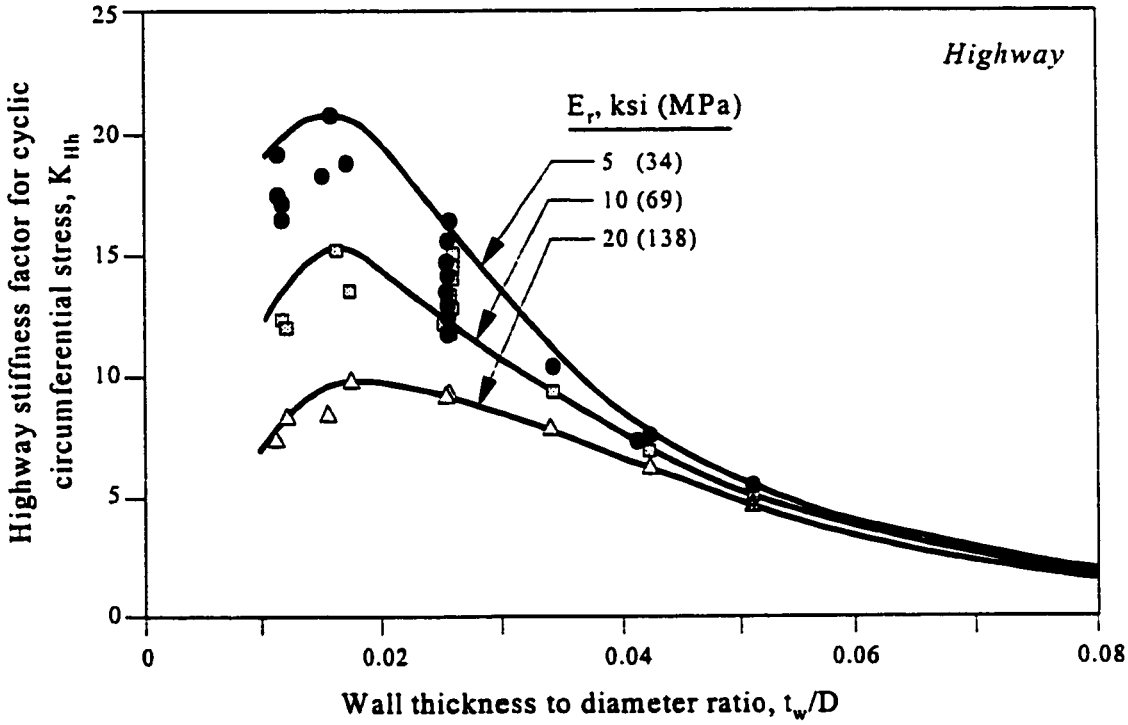

Fig. 3.25: Highway stiffness factor for circumferential stress, KHr

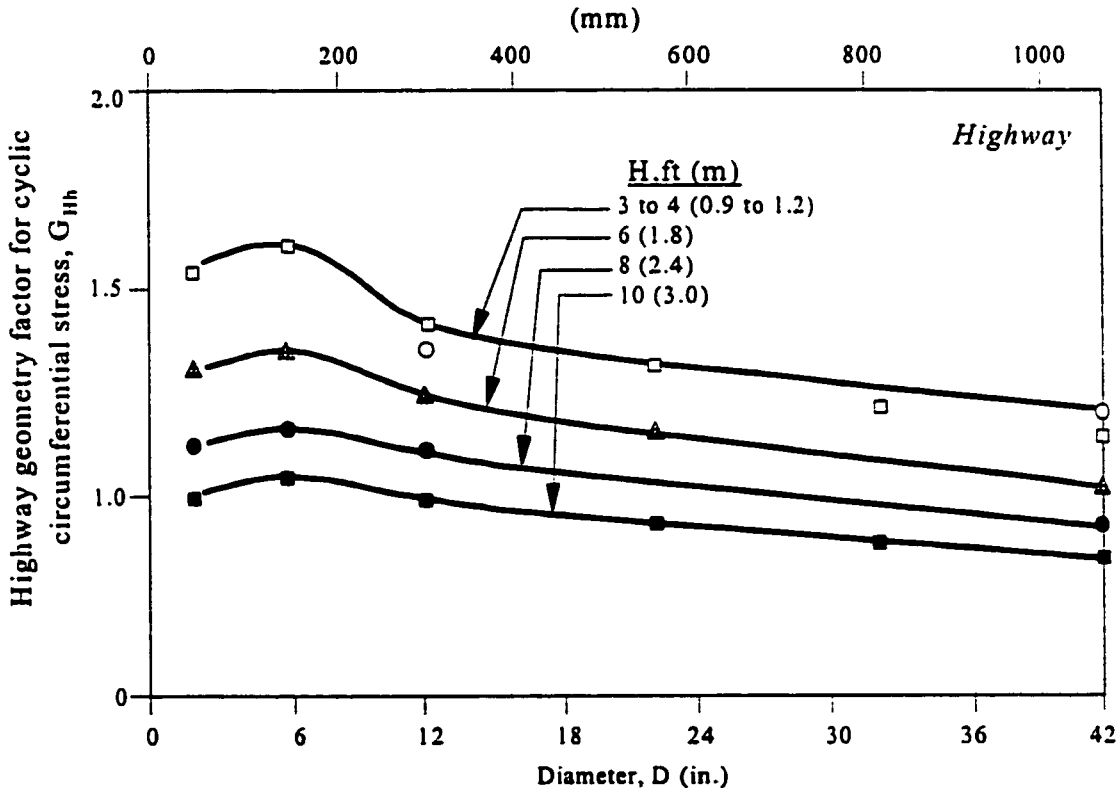

Fig. 3.26: Highway geometry factor for circumferential stress, G_{Hr}

TABLE 3.4: Highway Pavement Type Factors, R, and Axle Configuration Factors, L

Depth, H, < 4 feet and Diameter, D, ≤ 12inches			
Pavement Type	Design Axle Configuration	R	L
Flexible pavement	Tandem axle	1.00	1.00
	Single axle	1.00	0.75
No pavement	Tandem axle	1.10	1.00
	Single axle	1.20	0.80
Rigid Pavement	Tandem axle	0.90	1.00
	Single axle	0.90	0.65
Depth, H, < 4 feet and Diameter, D, > 12 inches			
Depth, H, > 4 feet for all diameters			
Pavement Type	Design Axle Configuration	R	L
Flexible pavement	Tandem axle	1.00	1.00
	Single axle	1.00	0.65
No pavement	Tandem axle	1.10	1.00
	Single axle	1.10	0.65
Rigid Pavement	Tandem axle	0.90	1.00
	Single axle	0.90	0.65

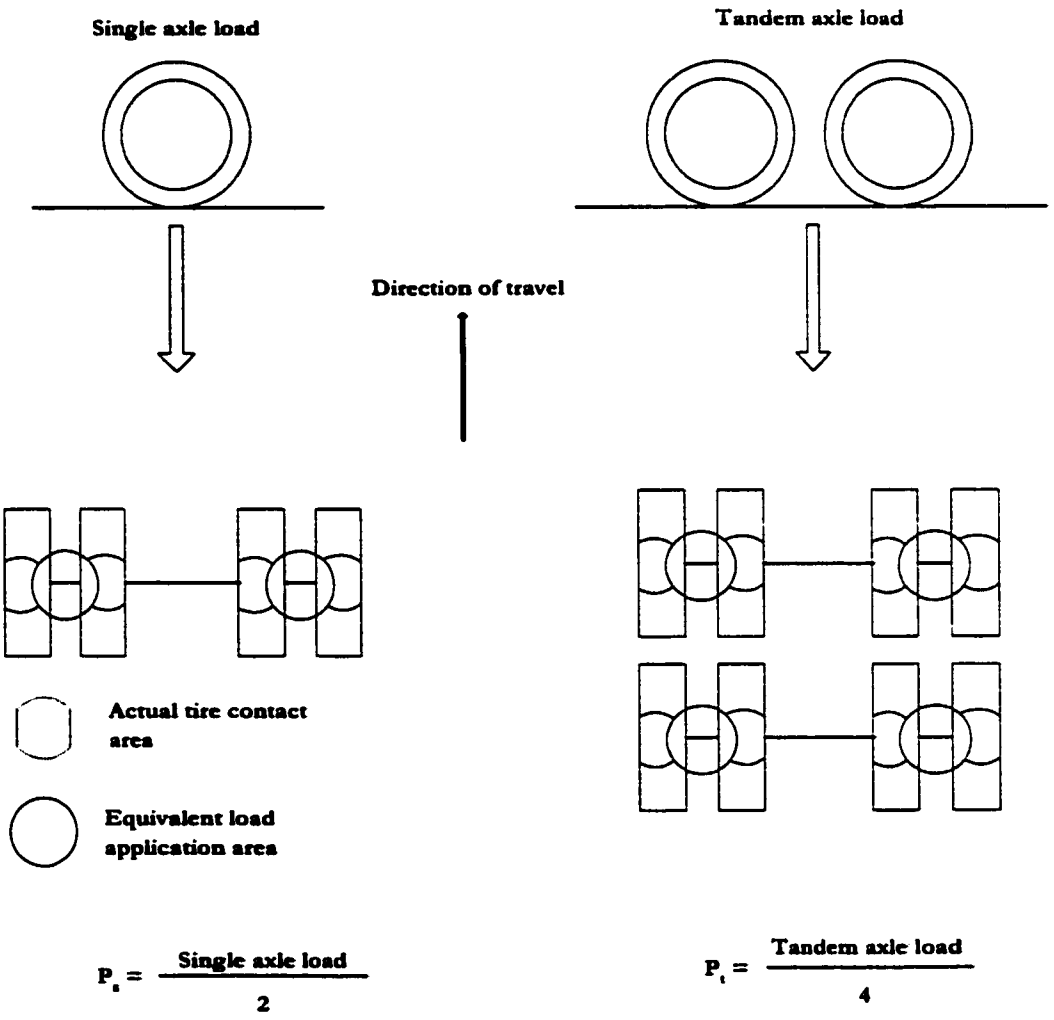

Fig. 3.27: Single and tandem wheel loads, P_s, and P_t

$$F_i = 1.5 - .03\,(H - 5) \qquad \text{for } 5 \text{ ft} \leq H \leq 21 \text{ ft} \tag{3.42}$$

3.14.4 Calculation of Circumferential Stress Due to Internal Pressure S_{Hi}

The circumferential stress due to internal pressure, S_{Hi}, is calculated using the equation:

$$S_{Hi} = \frac{p(D - t_w)}{2t_w} \tag{3.43}$$

Where,

p = Internal pressure,

D = Outer diameter of the pipe, and

t_w = Thickness of the pipe.

This is a slightly modified form of Barlow's formula.

3.14.5 Check for Allowable Stresses

Two checks for allowable stresses are required. The first on the circumferential stress due to internal pressurization. Using the Barlow formula, $SH_i(Barlow)$and is specified by Department of Transportation, US Government printing office 49 code of Federal Regulations part 192 and 195 and is given by,

$$[S_{H_i} = PD/2t_w] \leq F * E * T * SMYS \tag{3.44}$$

For natural gas, and

$$[S_{H_i} = PD/2t_w] \leq F * E * T * SMYS \tag{3.45}$$

For liquids and other products:

P = internal pressure,taken as the maximum allowable operating pressure (MAOP) or maximum allowable pressure (MOP), in psi or kpa,

D = pipe outside diameter,in inches or millimeters,

t_w = wall thickness,in inches or millimeters,

F = design factor chosen in accordance with 49 code of Fedral Regulations part 192 .111 or part 195.106 [75, 76],

E = longitudenal joint factor, and

$SMYS$ = specified minimum yild strength, in psi or kpa.

Strength design is also concerned with determining the stress which most closely approaches the yield or ultimate strength of the material. Therefore, the combined effect of internal pressure and external load must be considered.

Internal pressure causes a large proportion of the stress in the pipe, pressurization induces a circumferential strain which results in a circumferential stress, and due to Poisson effect, a longitudinal stress. Both of these stress components always are tensile.

Blewitt, et al. [77] proposed the use of the von Mises yield criterion for pipeline crossing of railroads and highways. This criterion is used in American society of mechanical engineers (ASME) B31.4 (1989a) [78]. In this formulation the effective stress, S_{eff} is given by:

$$S_{eff} = \sqrt{\frac{1}{2}\left[(S_1 - S_2)^2 + (S_2 - S_3)^2 + (S_3 - S_1)^2\right]} \tag{3.46}$$

in which S_1, S_2 and S_3 are the principal stresses and are calculated from the following:

$$S_1 = S_{He} + \Delta S_H + S_{Hi} \tag{3.47}$$

where,

S_1 = maximum circumferencial stress,

ΔS_{He} = circumferencial stress due to earth load,

ΔS_{Hh} = circumferencial stress due to highway load, and

SHi = circumferencial stress due to internal pressurization.

$$S_2 = \Delta S_L - E_S \alpha_T (T_2 - T_1) + \nu_S (S_{He} + S_{Hi}) \tag{3.48}$$

where,

S_2 = maximum longitudenal stress,

ΔS_L = longitudenal stress in the pipe due to tire load,

E_S = Young's modulus of steel, in pounds per square inch,

α_T = coefficient of thermal expansion of steel, per°F or per°C,

T_1 = temperature at time of installationin°F or°C, and

ν_S = poisson's ratio of steel.

$$S_3 = -P = -MAOP \text{ or } -MOP \tag{3.49}$$

The check against yielding of the pipelines may be accomplished by assuring that the total effective stress is less than the factored specified minimum yield strength (SMYS) using

the following equation:

$$S_{eff} \leq SMYS * F \tag{3.50}$$

The value of the design F factor should be consistent with the standard practice or the code requirements.

CHAPTER 4

Experimental Program and Soil Properties

4.1 Introduction

In order to determine the required soil parameters to be used in the finite element simulations an extensive soil-testing program was carried out at the soil testing facility of King Fahd University of Petroleum and Minerals. The experimental program started with identification of the local soils associated with the pipelines of Eastern province of Saudi Arabia. After the identification of the soils, samples were collected making sure that soil samples are representative of the soils associated with the buried pipelines. After the collection of samples routine soil tests were carried out to characterize the soils followed by specialized tests to determine the required soil parameters to be used in the finite element simulations.

4.2 Site Selection for Soil Materials

Natural soil types that are associated with the local pipeline network were selected for characterization by employing geological maps and pipeline network maps. Emphasis was made on the surface geology of the area. Three different types of soils were considered namely: sand, marl, and, sabkha.

4.3 Experimental Program

An extensive laboratory testing was made to help characterize soil materials. First of all, basic soil properties were determined for the three different soil types. These include the following:

1. Determination of particle size distribution for sand and marl soils using sieve analysis, according to ASTM Standards *D* 421 and *D* 422. Particle size distribution for sabkha soil was found using a combination of sieve analysis and hydrometer method.
2. Determination of specific gravity (G_s) for all soil types, according to ASTM Standard Test Method for Specific Gravity of Soils *D* 854.
3. Determination of maximum and minimum density (relative density) for sand, according to ASTM Standards *D* 4253 and *D* 4254.
4. Determination of moisture-density relationships for marl and sabkha soils, according to ASTM Standard *D*1557 (modified).
5. Determination of natural water content and Atterberg limits (liquid limit and plastic

limit) for sabkha soil, according to ASTM D 2216 and D 4318, respectively.

Sand was tested at two different relative densities (D_r), 30% and 80%. These will be indicated as " loose" and " dense" , respectively. As will be shown in Subsection 4.4.4, these correspond to dry densities of 1.587 and 1.725 g/cm^3, respectively. Marl was tested at two different dry densities of 1.64 and 1.87 g/cm^3, corresponding to relative compactions of 81.4 and 92.8%, respectively. These conditions will be indicated as " low density" and " high density" , respectively. Marl samples were prepared with water content equal to the optimum moisture content. Sabkha soil was tested at two different dry densities of 1.64 and 1.86 g/cm^3, corresponding to relative compactions of 85.2 and 96.8%, respectively. These conditions will be indicated in this thesis as " low density" and " high density" , respectively. Sabkha soil samples were prepared with water content wet of optimum moisture content. The three soil types at the two different conditions stated above were subjected to triaxial and hydrostatic tests.

4.3.1 Triaxial Tests

A set of at least four triaxial tests were conducted for each soil type at loose (low density) and dense (high density) conditions. These tests were done at confining pressures of 100, 200, 300, and 1000 kPa. Measurements included axial strain, deviator stress, and volume change. Tests were performed according to ASTM Standards D 2850 and D 4767. Tests were made at a very slow rate of loading of 0.0466 mm/min. Samples continued to be loaded to a very high strain level up to about 50%. Each test took about one day.

4.3.2 Hydrostatic Compression Tests

One test was conducted for each soil type at loose (low density) and dense (high density) conditions at confining pressures of 25, 50, 100, 200, 400, and 1200 kPa. Volume change and confining pressure were measured. This test is similar to the triaxial test, but without applying any deviator stress, and with the confining pressure being increased in stages for each specimen. Each stage of confining pressure was maintained for about one day for the volume change to reach a final value. The triaxial cell used for these tests was calibrated to find the expansion upon applying the pressure. A steel solid cylinder with a volume equal to that of the soil sample was used in the calibration.

4.4 RESULTS

4.4.1 Particle Size Distribution

Particle size distribution (PSD) curve for sand, marl and sabkha are shown in Fig. 4.1. The coefficient of uniformity (C_u) for the sand is 1.56 and coefficient of curvature (C_c) is 1.0. The sand is classified as 'SP" (poorly-graded sand) according to the Unified Soil Classification System. The grain size distribution curve for the marl is for the portion passing sieve #4. For dry sieving, the values of C_u and C_c are 3.285 and 0.922, respectively. This marl can be classified as "SP" (gravelly sand with fines). The 15% coarser than sieve #200 for sabkha soil was visually inspected and found to contain fine sand and remains of marine organisms. Clay fraction ($< 2mm$) was about 50%.

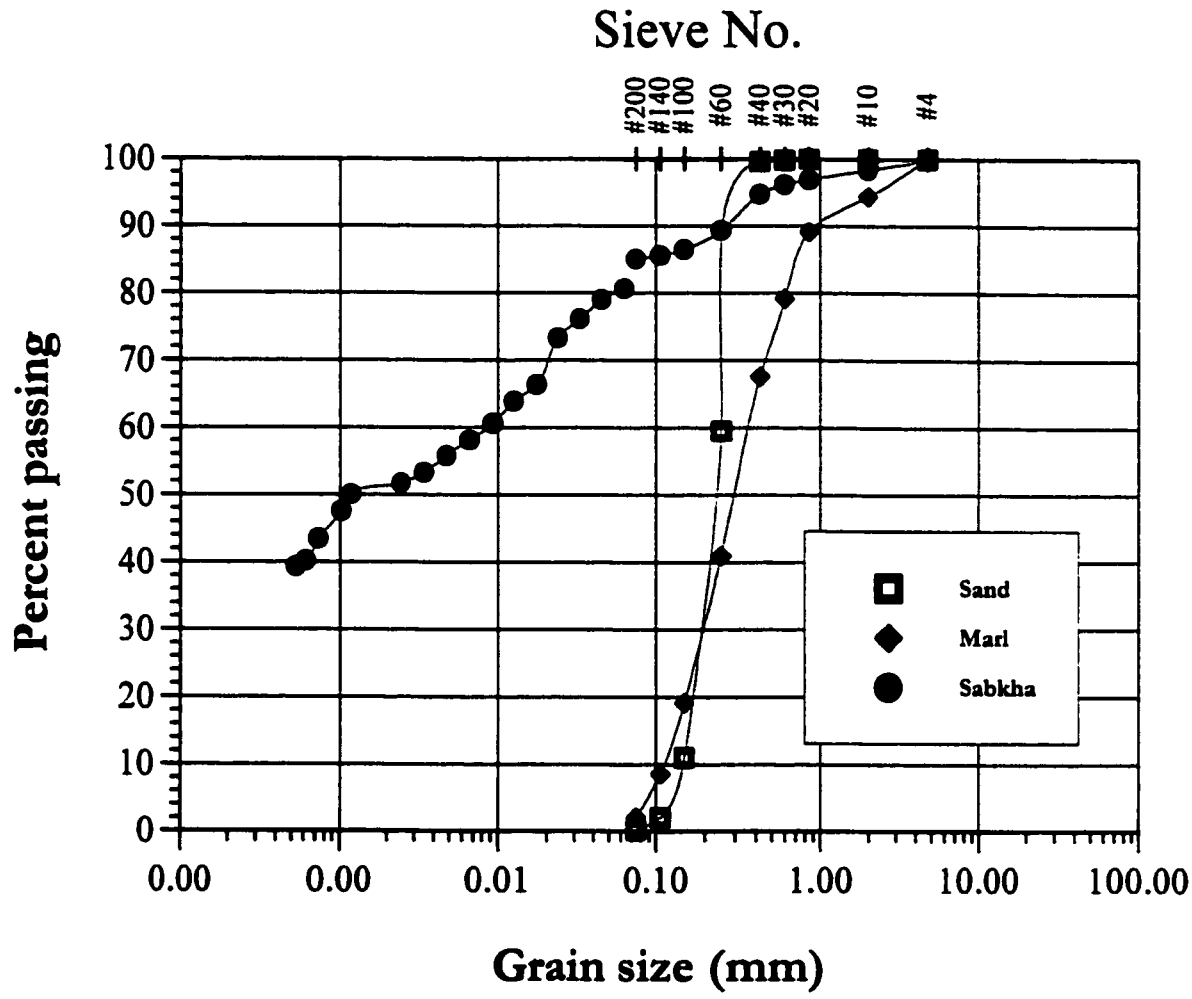

Fig. 4.1: Grain size distribution curve for sand, marl and sabkha

4.4.2 Specific Gravity

The specific gravity (G_s) for various soil types considered in this research was found in the laboratory. The specific gravties are found to 2.659, 2.639, and 2.853 for sand. marl and sabkha respectivly. The high value of specific gravity for sabkha was attributed to the calcareous nature of these deposits, which may contain dolomite and calcium carbonate minerals that are known to have higher values for G_s [79].

4.4.3 Atterberg Limits

The natural water content (w_n) of sabkha soil was found to be 25.6%. The liquid limit (LL) and the plastic limit (PL) for sabkha soil were found to be 28.3 and 22.9. respectively. The plasticity index (PI) is 5.4. This sabkha can be classified as "$CL-ML$" (silty clay).The graph for liquid limit for sabkha soil is shown in Fig. 4.2.

4.4.4 Relative Density

Relative density (D_r) for the sand was calculated using the maximum and minimum densities measured in the laboratory and in-situ density measured by the nuclear gauge in the field according to

$$D_r = \frac{(\rho_{field} - \rho_{\min})}{(\rho_{\max} - \rho_{\min})} * \frac{\rho_{\max}}{\rho_{\min}} \tag{4.1}$$

Where

ρ_{field} = Dry density in the field

$\rho_{\max}$ = Maximum dry density achieved in the lab

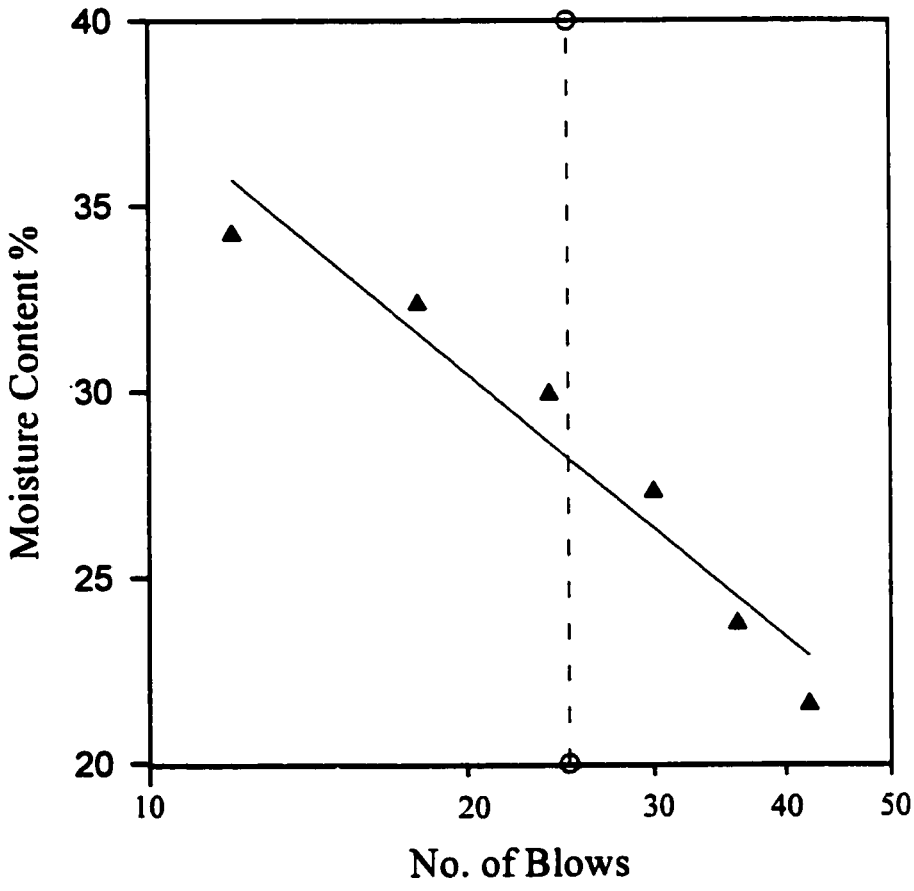

Fig. 4.2: Determination of liquid limit for sabkha soil

ρ_{min} = Minimum dry denity achieved in the lab

The maximum dry density ρ_{max} and minimum dry density ρ_{min} were found to be 1.787 and 1.515 g/cm^3, respectively and For loose and dense conditions used in the experimental program, the values of D_r were chosen to be 30 and 80%.Therefore, sand samples were prepared for loose and dense conditions at dry densities of 1.587 and 1.725, respectively.

4.4.5 Moisture-Density Relationship

The compaction curves for marl and sabkha from modified Proctor tests are shown in Fig. 4.3. The maximum dry density ($\gamma_{d,max}$) for marl is 2.022 g/cm^3 and the optimum moisture content (w_{opt}) is 9.1%. The maximum dry density ($\gamma_{d,max}$) for sabkha is 1.925 g/cm^3 he optimum moisture content (w_{opt}) is 13.55%. The wet of optimum moisture contents at "low" and "high" density of γ_d equal to 1.64 and 1.86 g/cm^3 are 23.25% and 17.8%, respectively.

4.4.6 Analysis Of Triaxial Test Results

This section presents soil parameters obtained from triaxial tests performed on various types of soils (sand, marl, and sabkha), at both loose and dense conditions. The maximum value for deviator stress, $(\sigma_1 - \sigma_3)_f$, is taken as the value of deviator stress at the peak, provided that peak occurs at a strain (ε) less than 15%. In the cases where the peak is not evident or it occurs at $\varepsilon > 15\%$, the $(\sigma_1 - \sigma_3)_f$ is taken to be the value of deviator stress at $\varepsilon = 15\%$, , $(\sigma_1 - \sigma_3)_{\varepsilon=15\%}$ as suggested by [80].

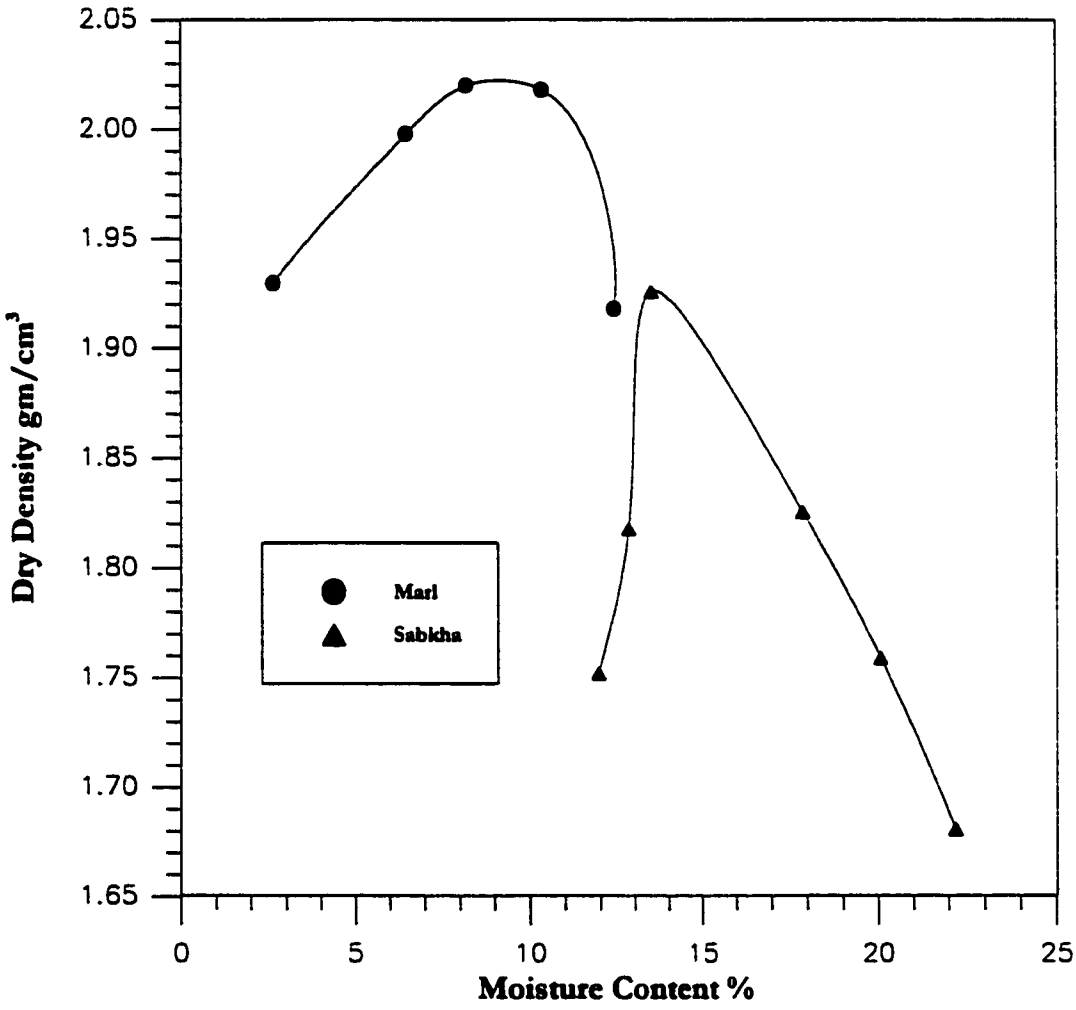

Fig. 4.3: Compaction curves for marl and sabkha

4.4.6.1 Parameters for Sand

Fig. 4.4 presents the triaxial test results for sand at low density (relative density. D_r = 30%), in terms of deviator stress $(\sigma_1 - \sigma_3)$ vs. axial strain (ε). Using the Mohr-Coulomb failure criterion, presented in Subsection 3.11.1, the Mohr circles and the failure envelope were drawn in Fig. 4.5. For this sand, the cohesion (C) is zero, and the angle of internal friction (ϕ_o) is taken as the slope of the tangent of the first three circles $(\phi_o = 38.30°)$. The reduction in angle of internal friction $(\Delta\phi)$ is taken to be the difference between the slope of the tangents of Mohr circles at confining pressure (σ_3) of 100 and 1000 kPa, $(\Delta\phi = 3.16°)$. The same results are presented in $p - q$ diagram in Fig. 4.6. Notice that $P = \frac{\sigma_1 - \sigma_3}{2}$ and $q = \frac{\sigma_1 + \sigma_3}{2}$. The slope of the $p - q$ diagram is ψ, α is the intercept, $\phi = sin^{-1}(tan\psi)$. and $C = \alpha/cos\phi$.

The parameters for hyperbolic model were obtained from the triaxial data, according to the explanation given in Subsection 3.11.3 . Triaxial tests at σ_3 = 100, 200, and 300 kPa were considered for obtaining the parameters. The first step is to find initial tangent modulus (E_i) and the failure ratio (R_f) by plotting $\varepsilon/(\sigma_1 - \sigma_3)$ $vs.\varepsilon$, where ε is the axial strain and $(\sigma_1 - \sigma_3)$ is the deviator stress. Plots of $\varepsilon/(\sigma_1 - \sigma_3)$ vs. ε are presented in Fig. 4.7. The slope of each line gives $1/(\sigma_1 - \sigma_3)_u$ and the intercept gives $1/E_i$. Therefore, E_i is the reciprocal of the intercept, and R_f is the slope times the peak value of deviator stress $(\sigma_1 - \sigma_3)_f$. The value of R_f is found to be 0.90, 0.91, and 0.91 for σ_3 = 100, 200, and 300 kPa, respectively, with an average value of 0.90.

The second step is to find the parameters K and n by plotting the variation of $log\,(E_i/P_a)$ vs. $log(\sigma_3/P_a)$, where p_a is the atmospheric pressure, Fig. 4.8. The slope of the line is n,

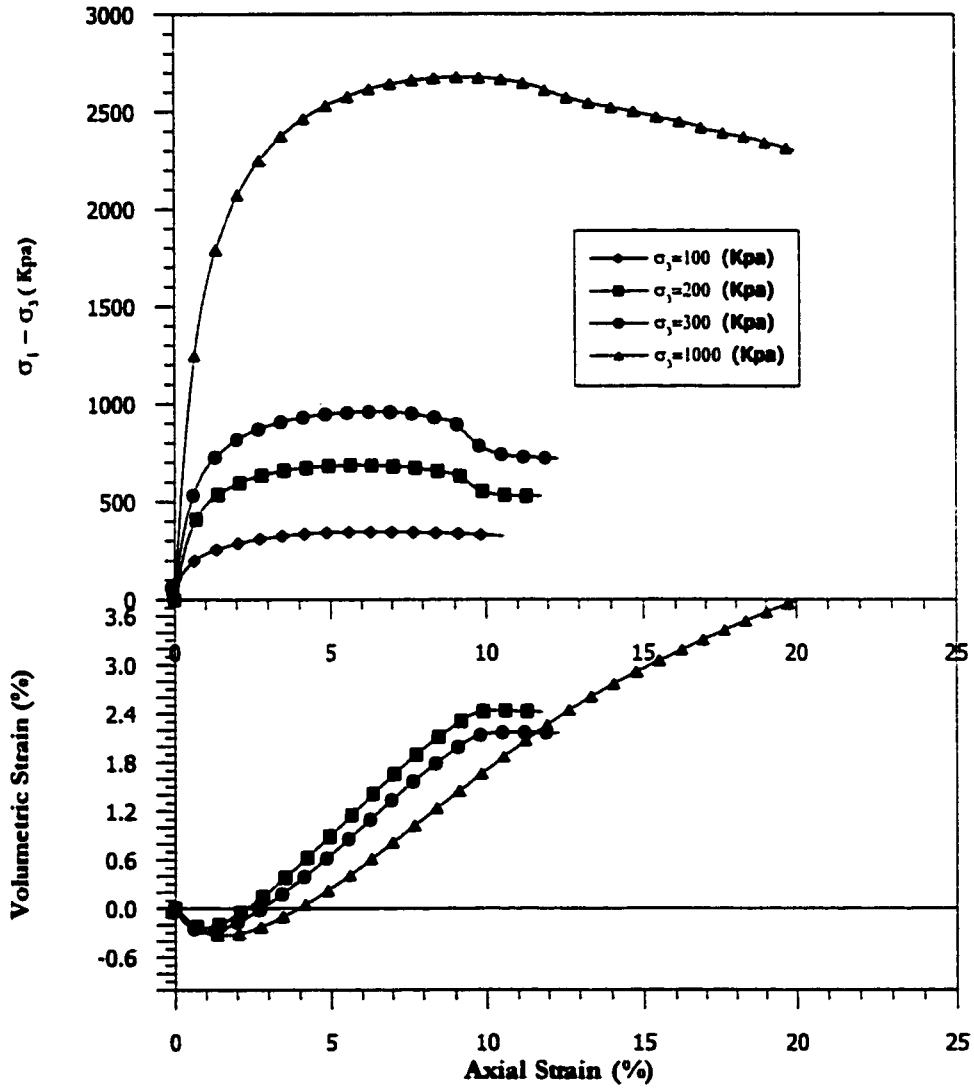

Fig. 4.4: Triaxial test for sand at low density

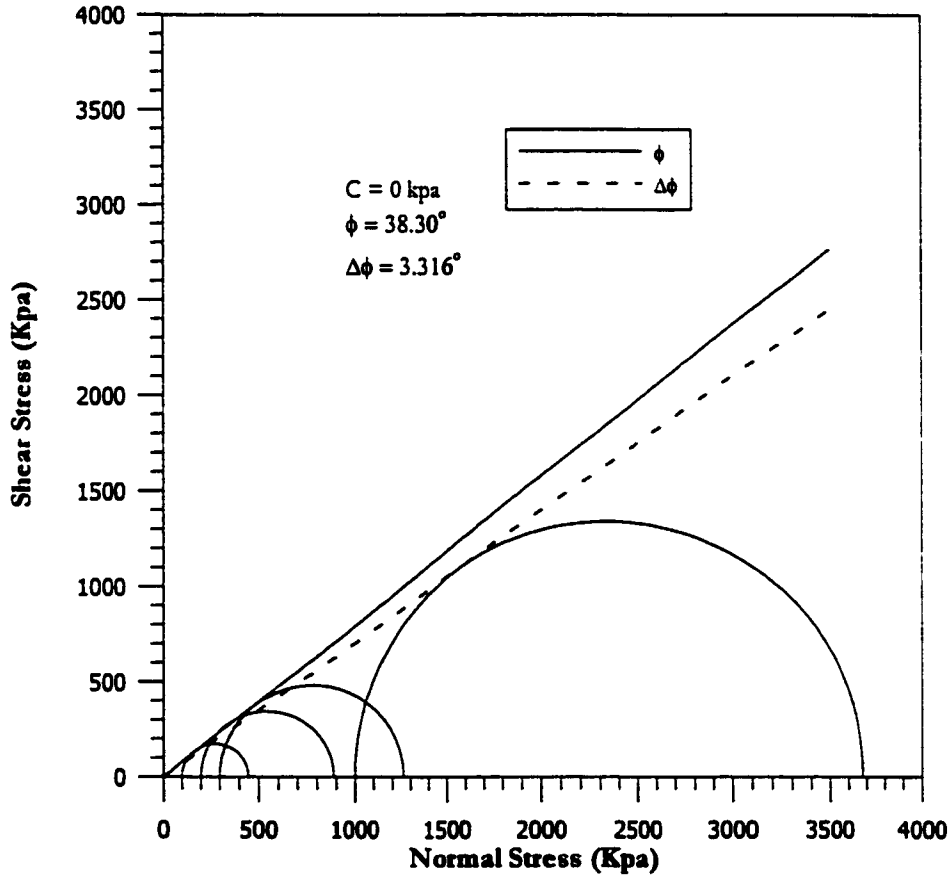

Fig. 4.5: Mohr circle for sand at low density

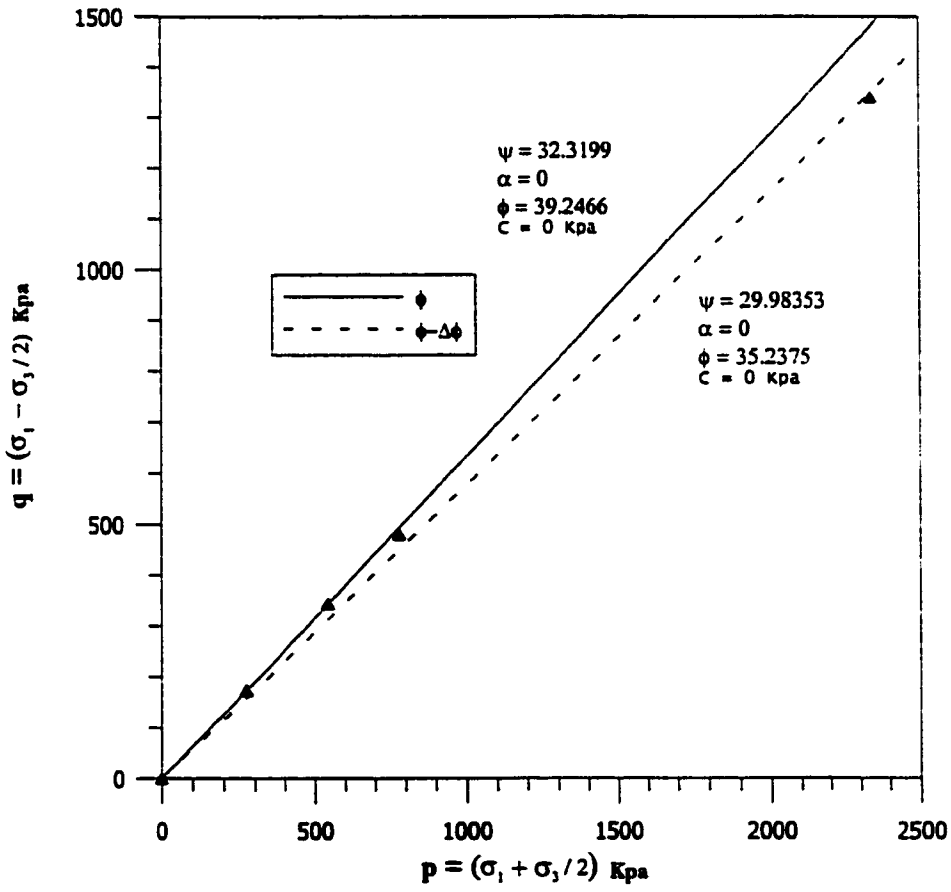

Fig. 4.6: p-q diagram for sand at low density

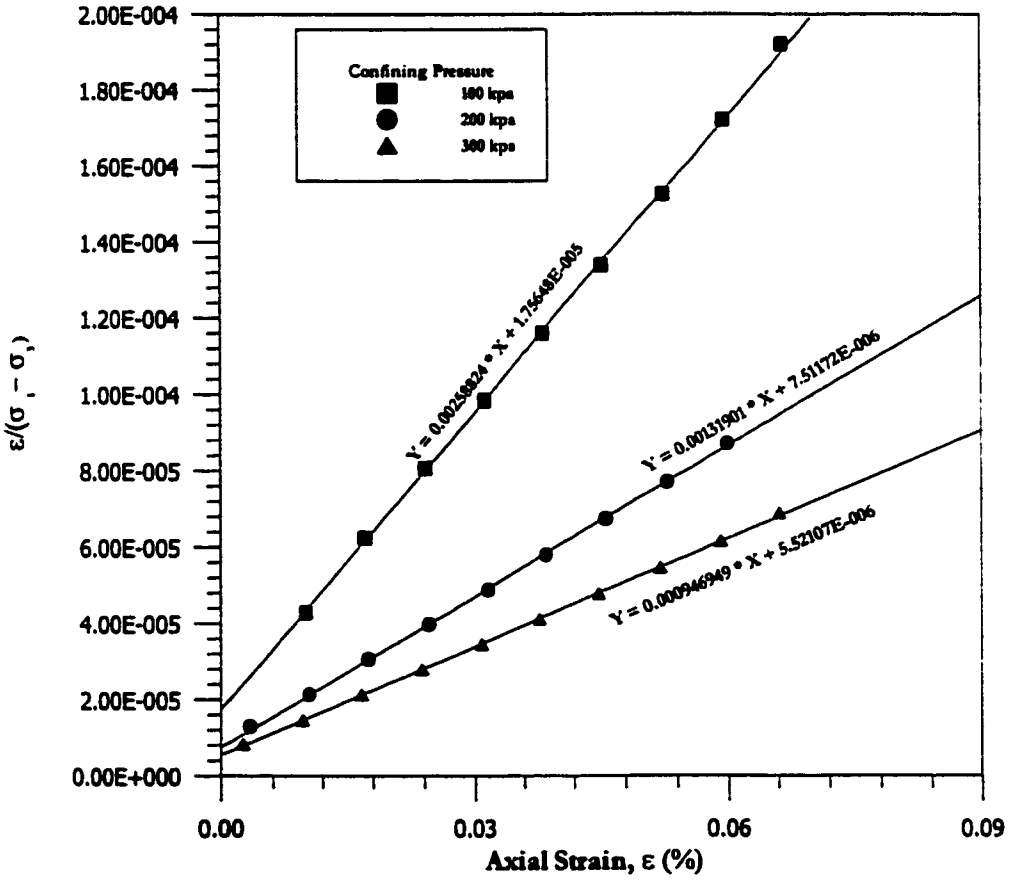

Fig. 4.7: Determination of E_i and R_f for sand low density

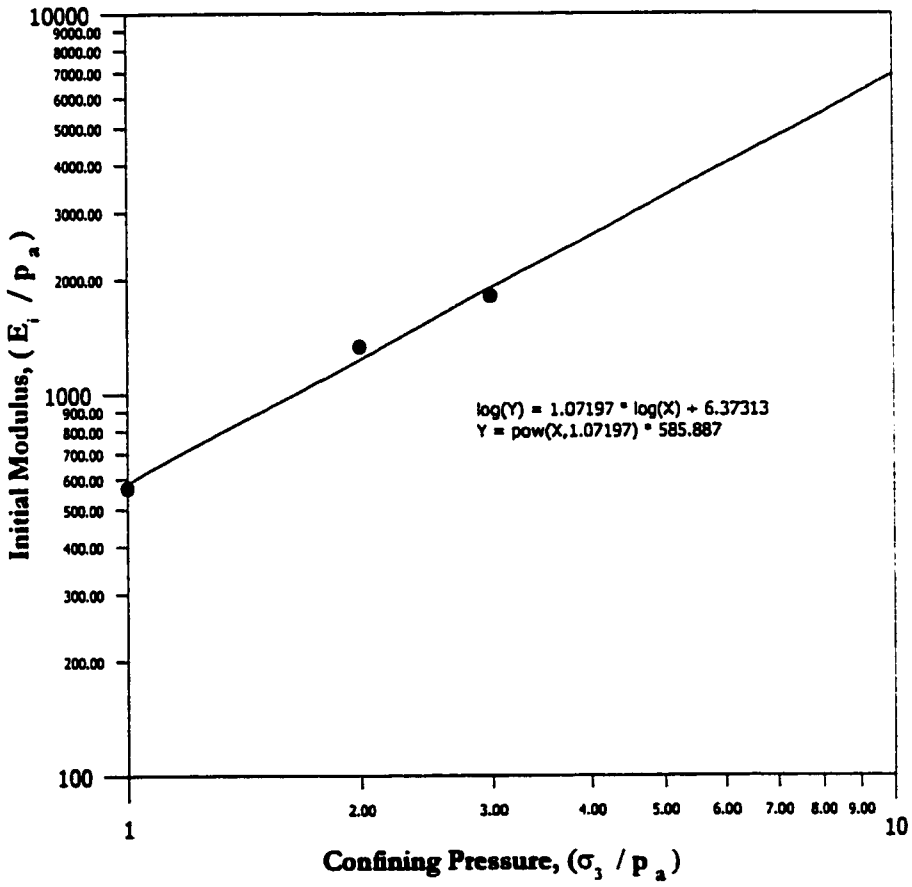

Fig. 4.8: Determination of K and n for sand at low density

and the intercept at is K. The values of K and n are 585.89 and 1.07, respectively.

For sand at high density (D_r = 80%), the triaxial test results are given in Fig. 4.9. Mohr circles and failure envelope are shown in Fig. 4.10, which gives $C = 0$, $\phi_o = 46.39°$, and $\Delta\phi = 3.47°$. The $p - q$ diagram is shown in Fig. 4.11. The plots of $[\varepsilon/(\sigma_1 - \sigma_3)]$ $vs.$ ε are presented in Fig. 4.12. The value of R_f is found to be 0.87, 0.89, and 0.79 for $\sigma 3$ = 100, 200, and 300 kPa, respectively, with an average value of 0.85. The plot of $log(E_i/P_a)$ vs. $log(\sigma_3/P_a)$ is shown in Fig. 4.13, which gives K and n values to be 1.963.22 and 0.62, respectively.

4.4.6.2 Parameters for Marl

Triaxial test results for marl at low density (relative compaction, RC = 81.4%) are given in Fig. 4.14. Mohr circles and failure envelope are presented in Fig. 4.15, in which C = 21.34 kPa, $\phi_o = 30.81°$, and $\Delta\phi = 0.0$. The $p - q$ diagram is shown in Fig. 4.16.The plots of $[\varepsilon/(\sigma_1 - \sigma_3)]$ $vs.$ ε are given in 4.17. The value of R_f is found to be 0.92, 0.89, and 0.84 for σ_3 = 100, 200, and 300 kPa, respectively, with an average value of 0.88. The plot of $log(E_i/P_a)$ $vs.$ $log(\sigma_3/P_a)$ is shown in Fig. 4.18, from which K and n are obtained to have values of 272.46 and 0.10, respectively.

For marl at high density (RC= 92.8%), triaxial test results are given in Fig. 4.19. Mohr circles and failure envelope are presented in Fig. 4.20, in which C = 71.73 kPa, $\phi_o = 33.24°$, and $\Delta\phi = 0.0$. The p-q diagram is shown in Fig. 4.21. The plots of $[\varepsilon/(\sigma_1 - \sigma_3)]$ $vs.$ ε are given in Fig. 4.22. The value of R_f is found to be 0.65, 0.67, and 0.70 for σ_3 = 100, 200, and 300 kPa, respectively, with an average value of 0.67. The plot of $log(E_i/P_a)$ $vs.$ $log(\sigma_3/P_a)$ is shown in Fig. 4.23, from which K and n values are obtained to be 916.98

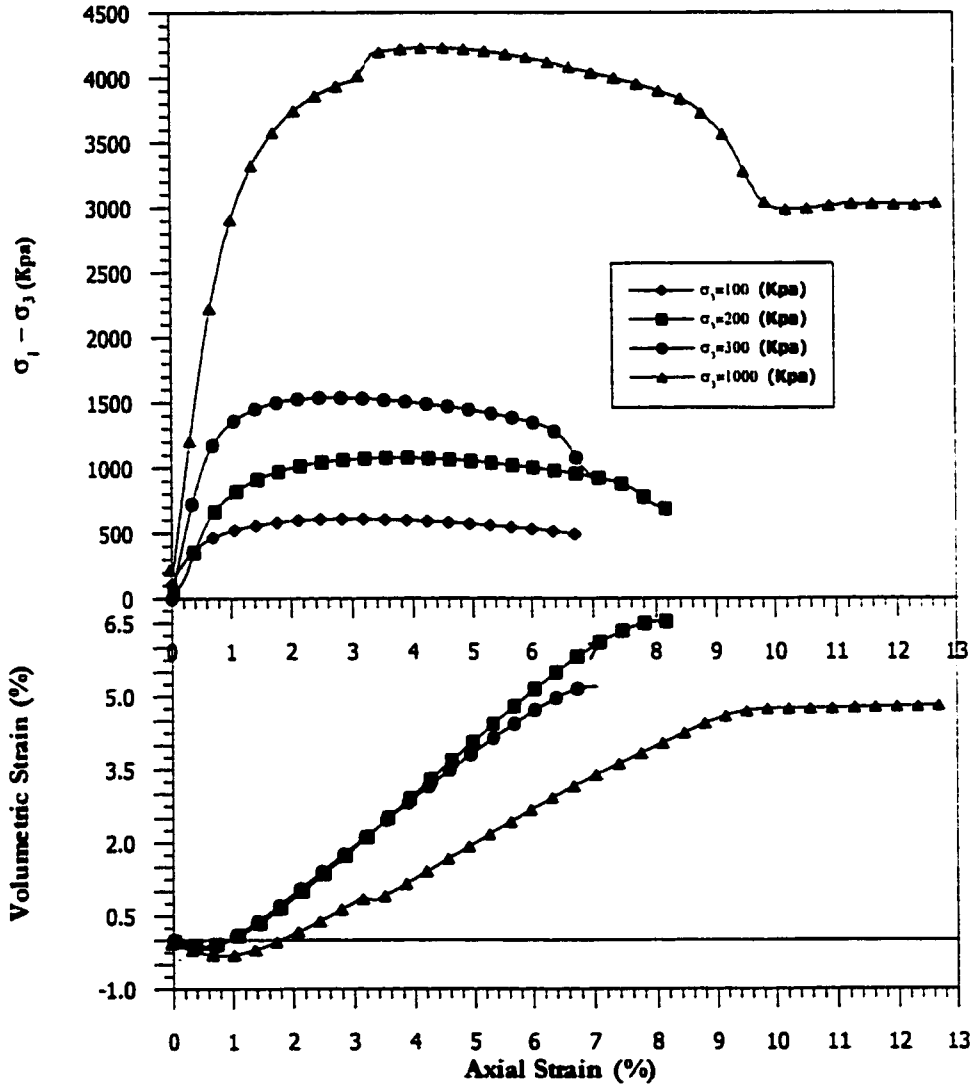

Fig. 4.9: Triaxial test for sand at high density

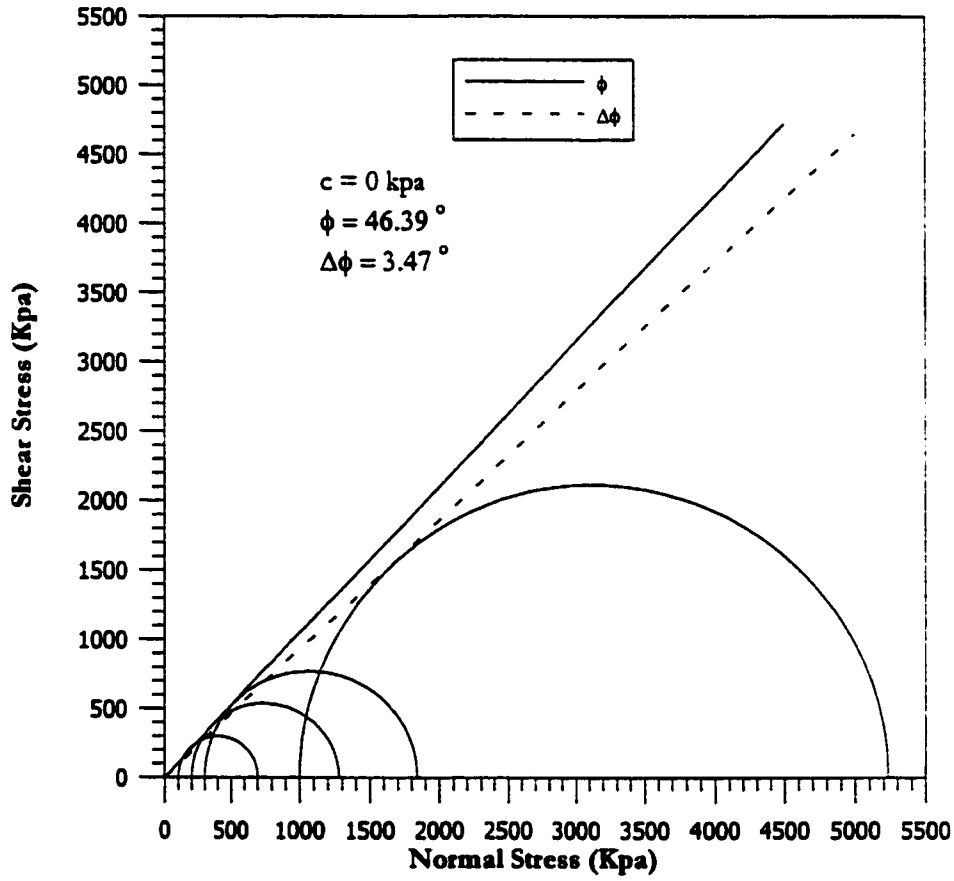

Fig. 4.10: Mohr circle for sand at high density

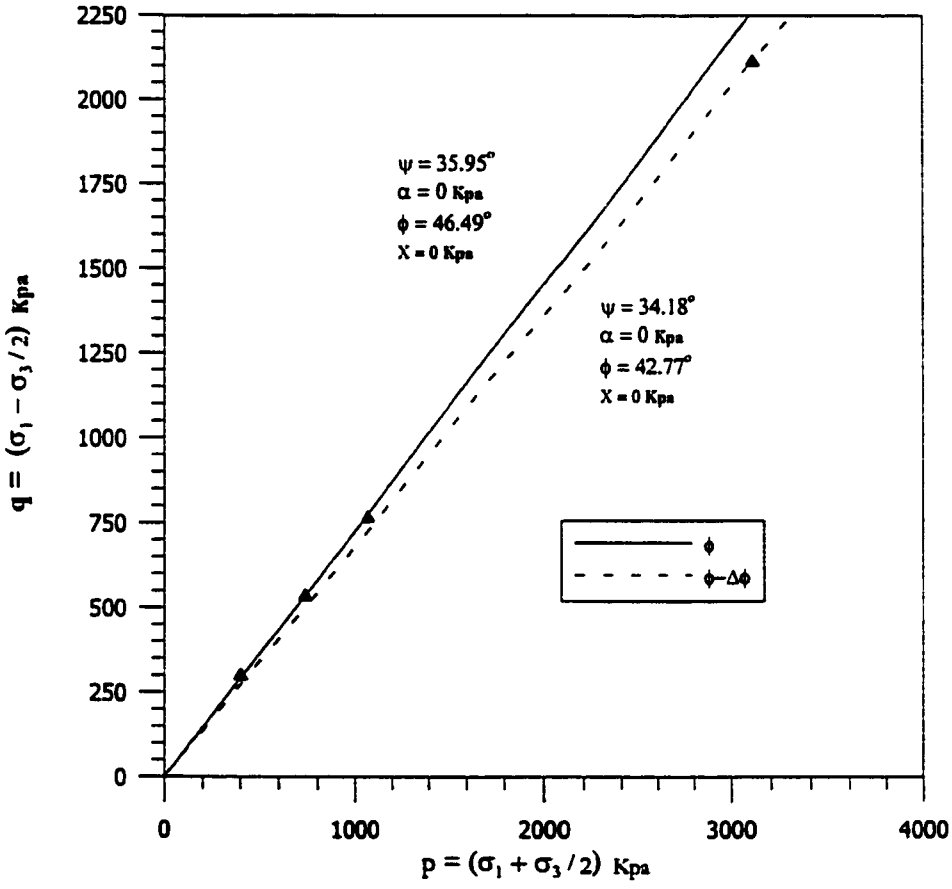

Fig. 4.11: p-q diagram for sand at high density

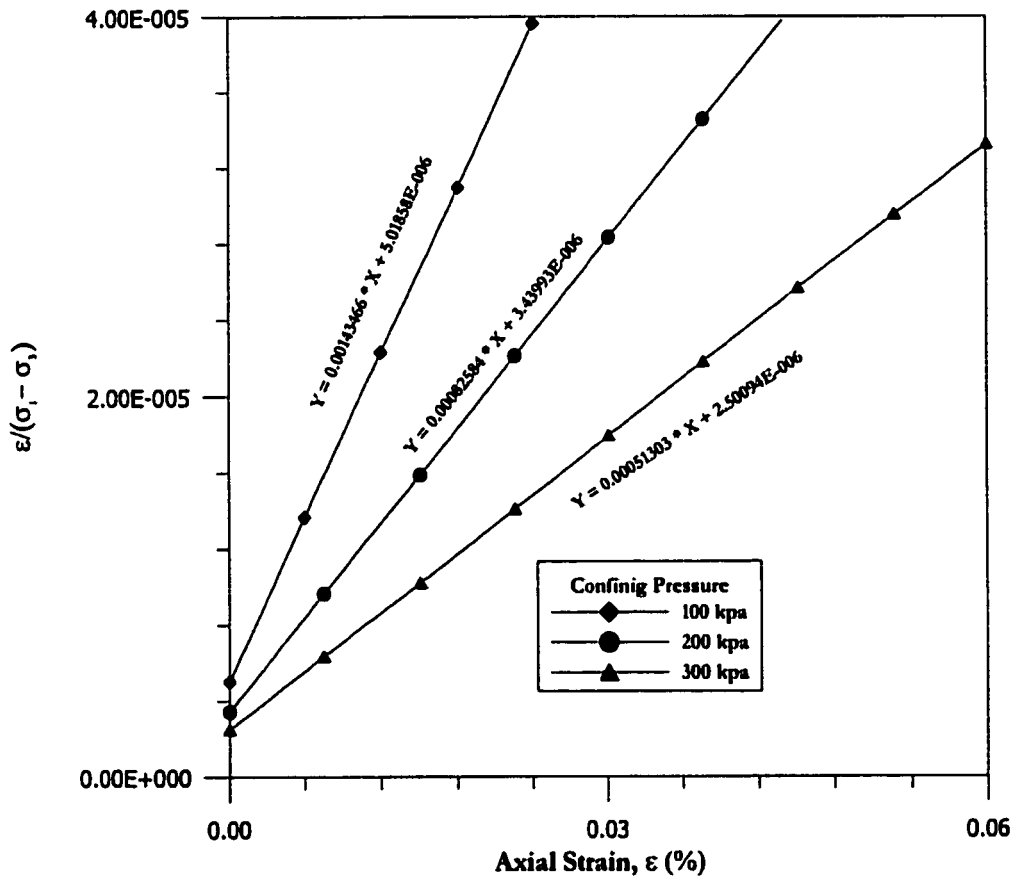

Fig. 4.12: Determination of E_i and R_f for Sand at high density

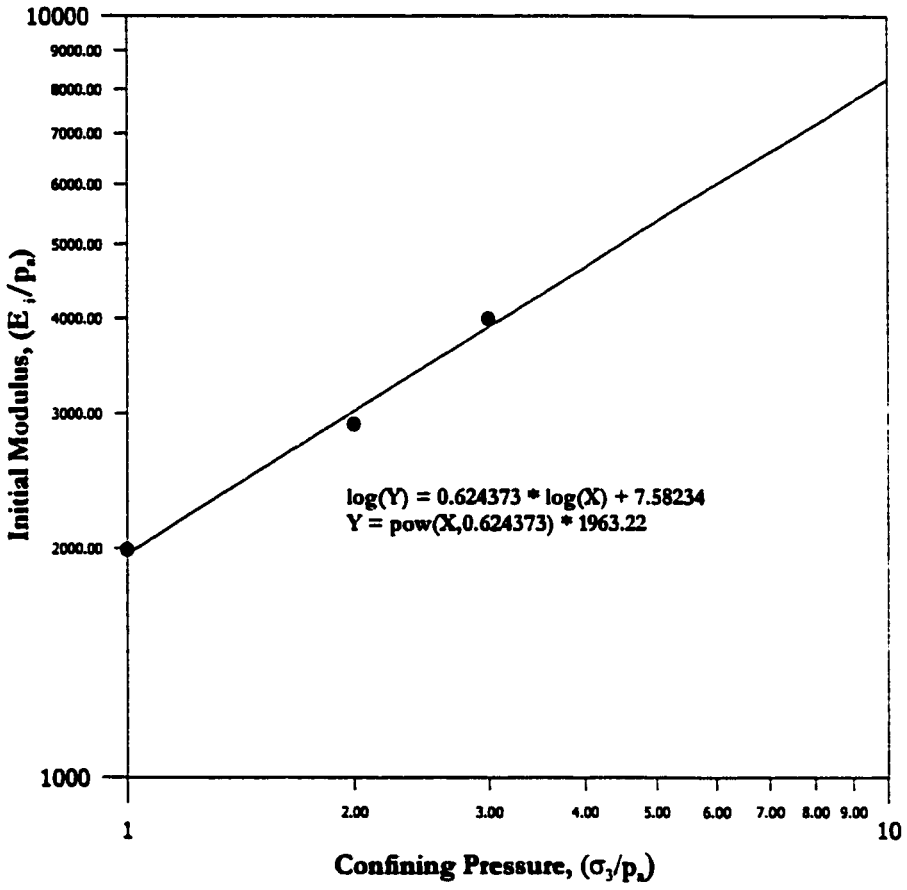

Fig. 4.13: Determination of K and n for sand high density

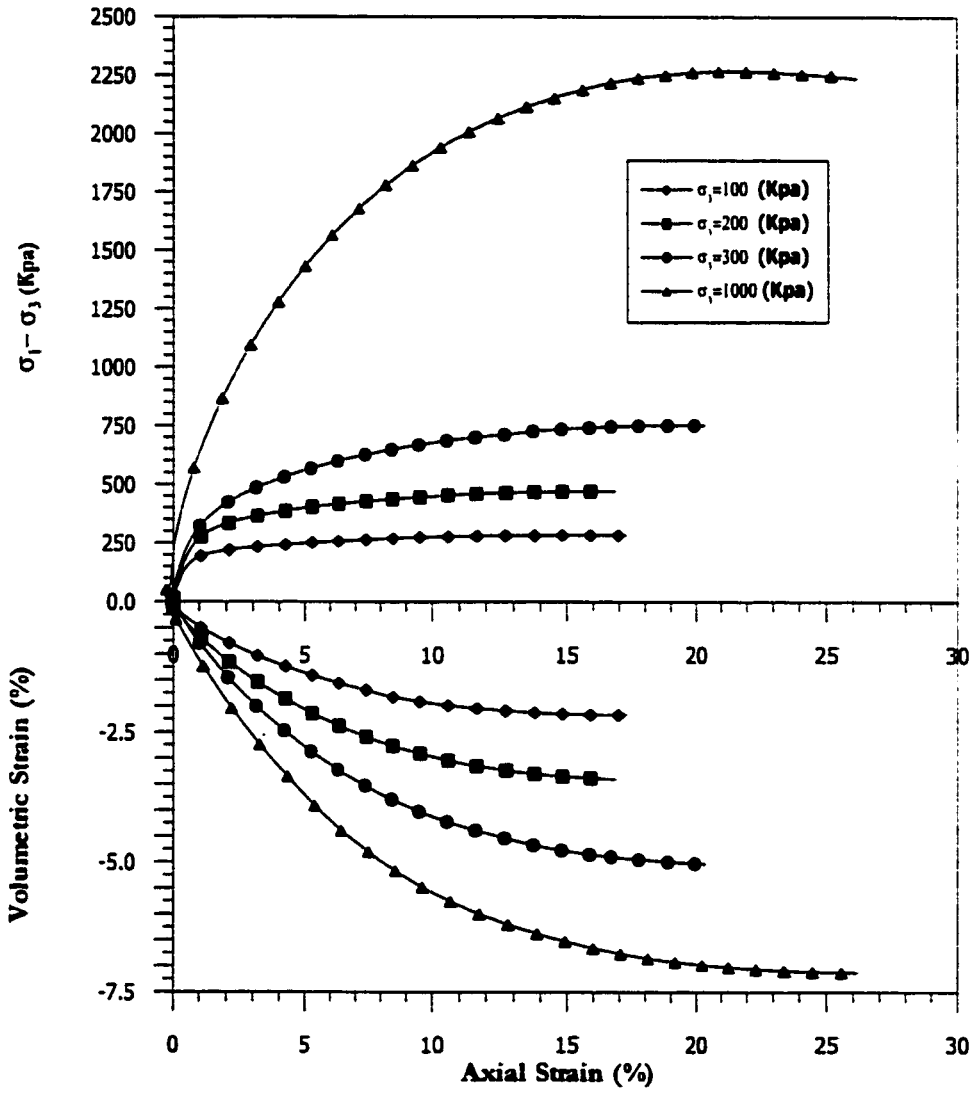

Fig. 4.14: Triaxial test for marl at low density

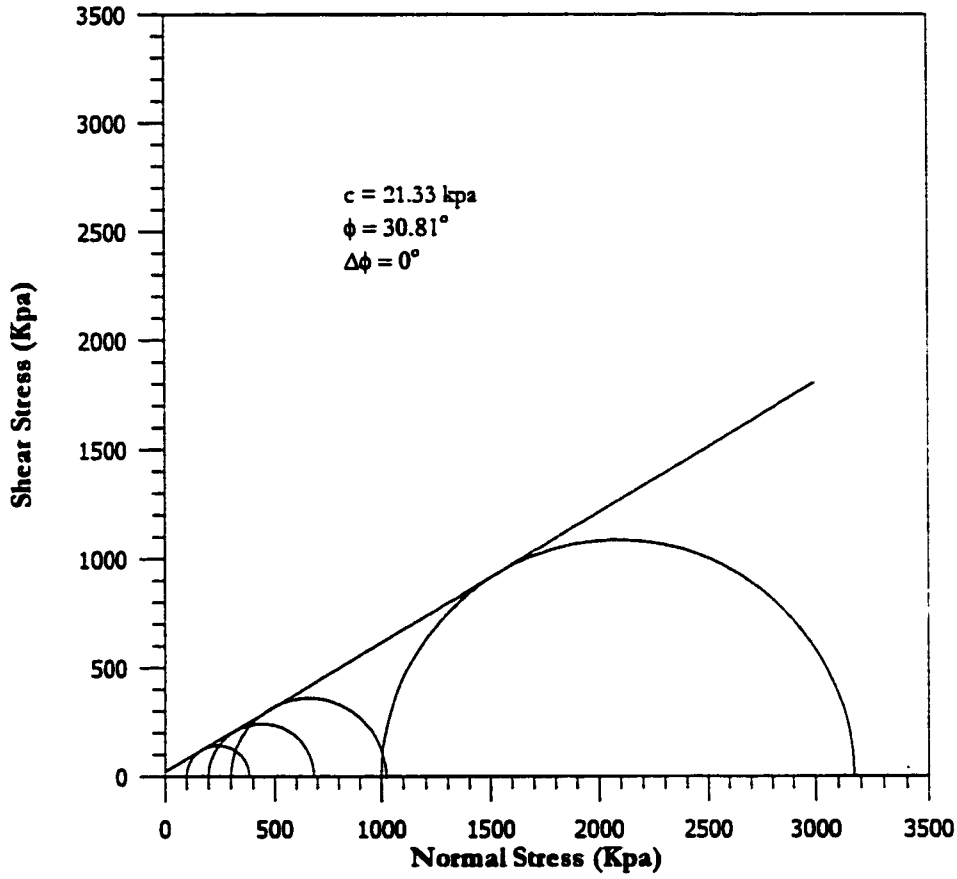

Fig. 4.15: Mohr circle for marl at low density

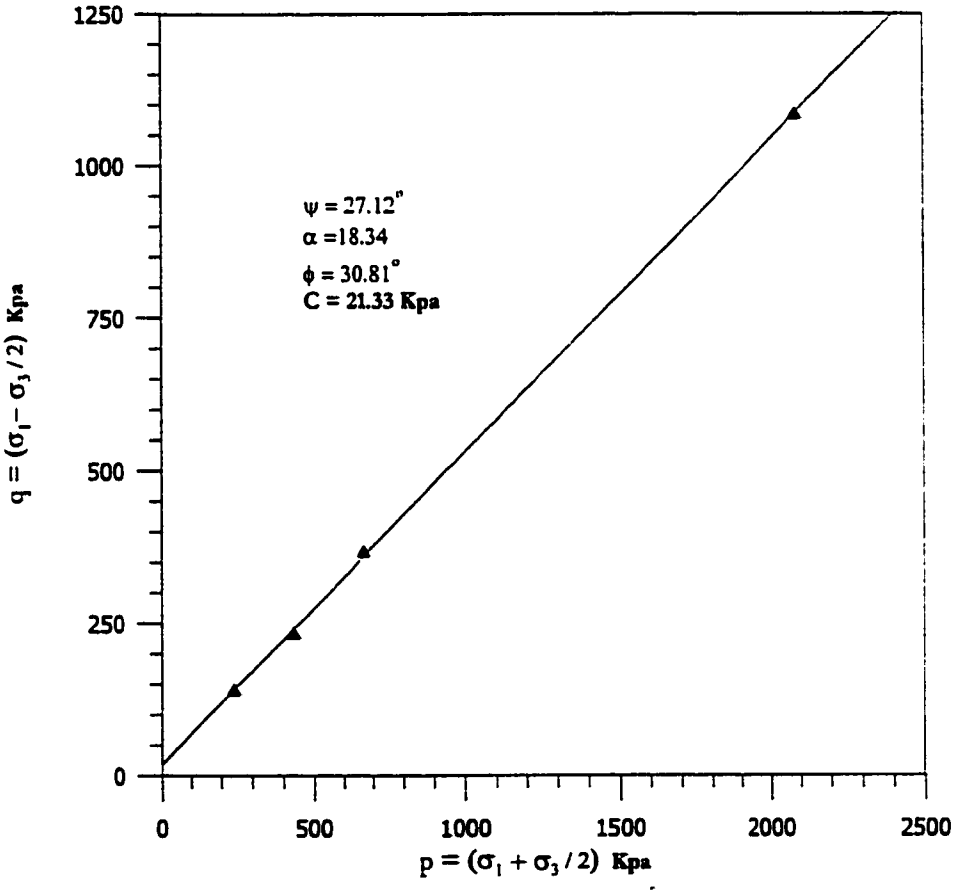

Fig. 4.16: $p - q$ diagram for marl at low density

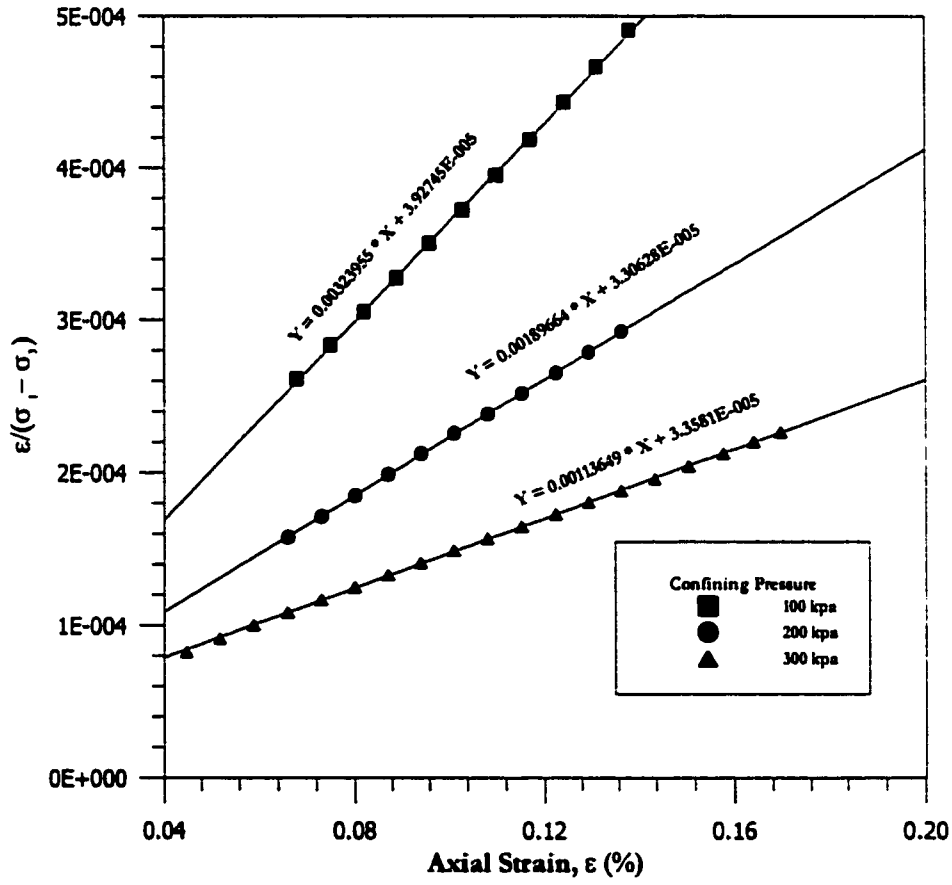

Fig. 4.17: Determination of E_i and R_f for marl at low density

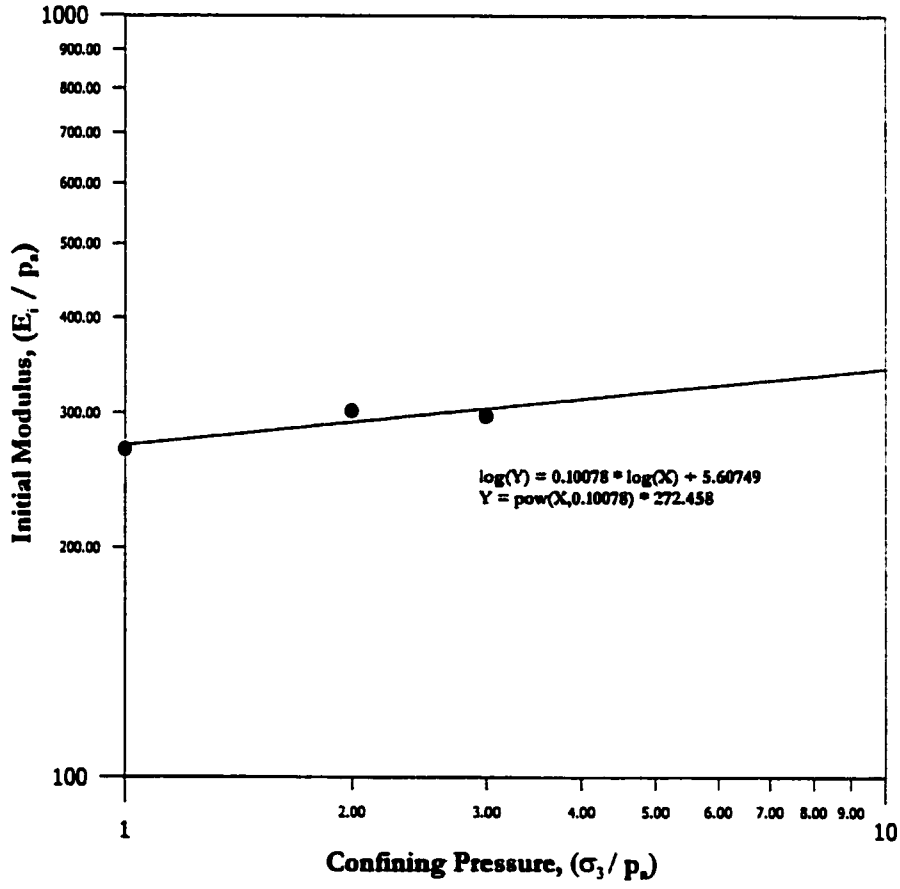

Fig. 4.18: Determination for K and n for marl at low density

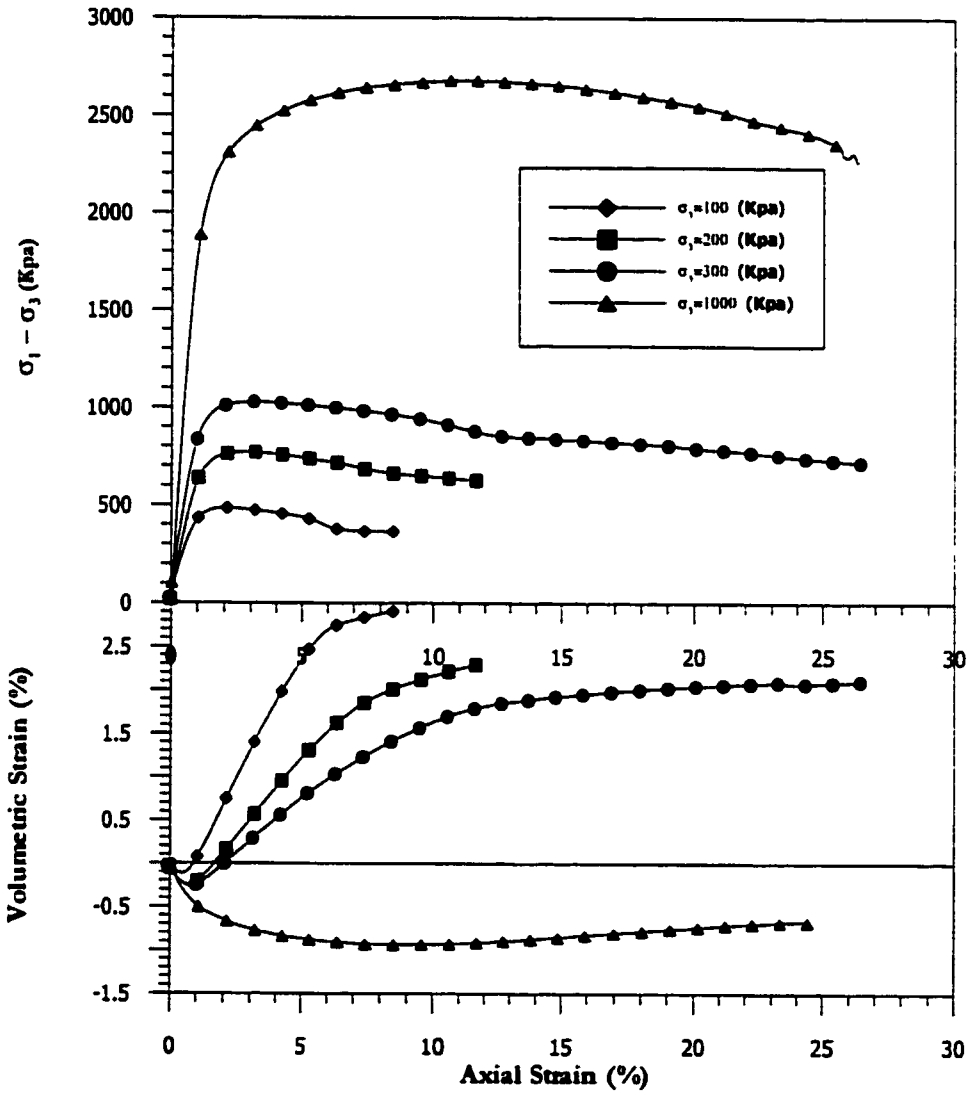

Fig. 4.19: Triaxial test for marl at high density

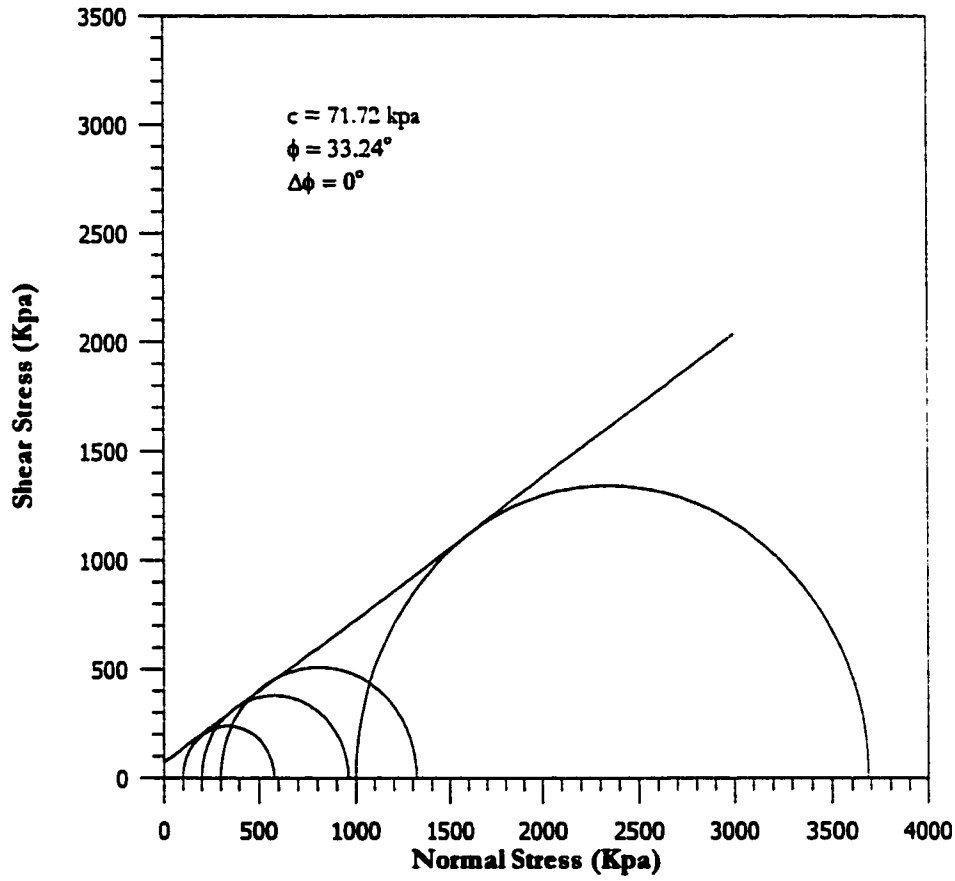

Fig. 4.20: Mohr circle for marl at high density

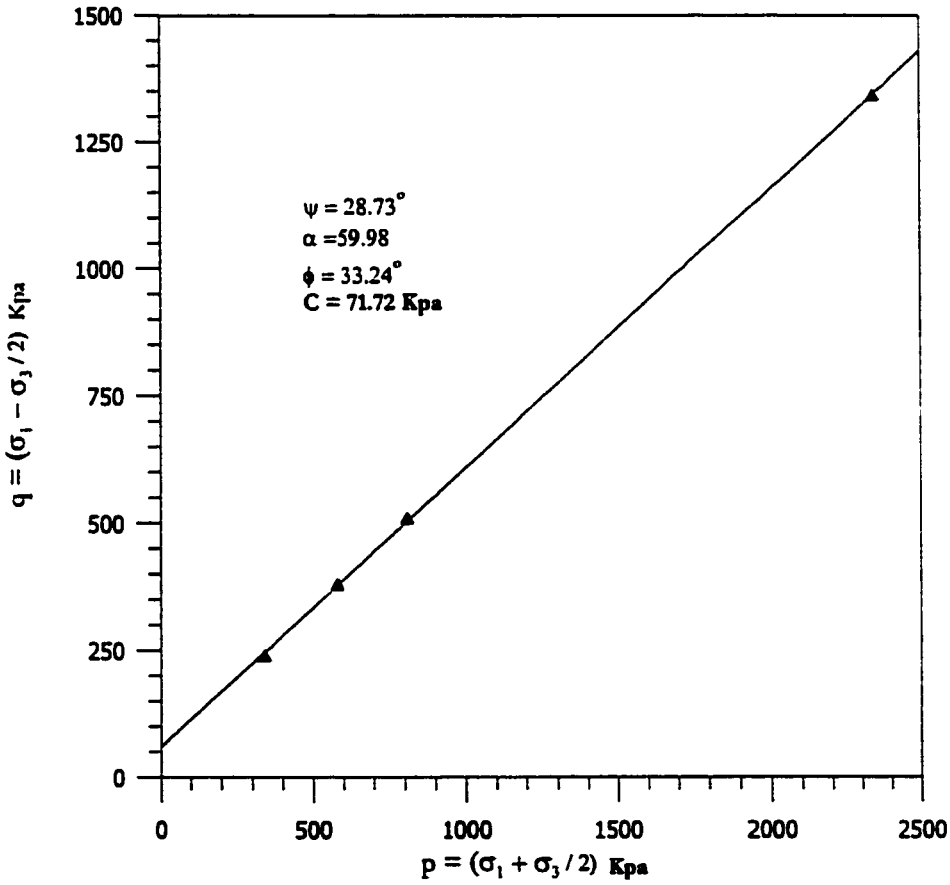

Fig. 4.21: $p - q$ diagram for marl at high density

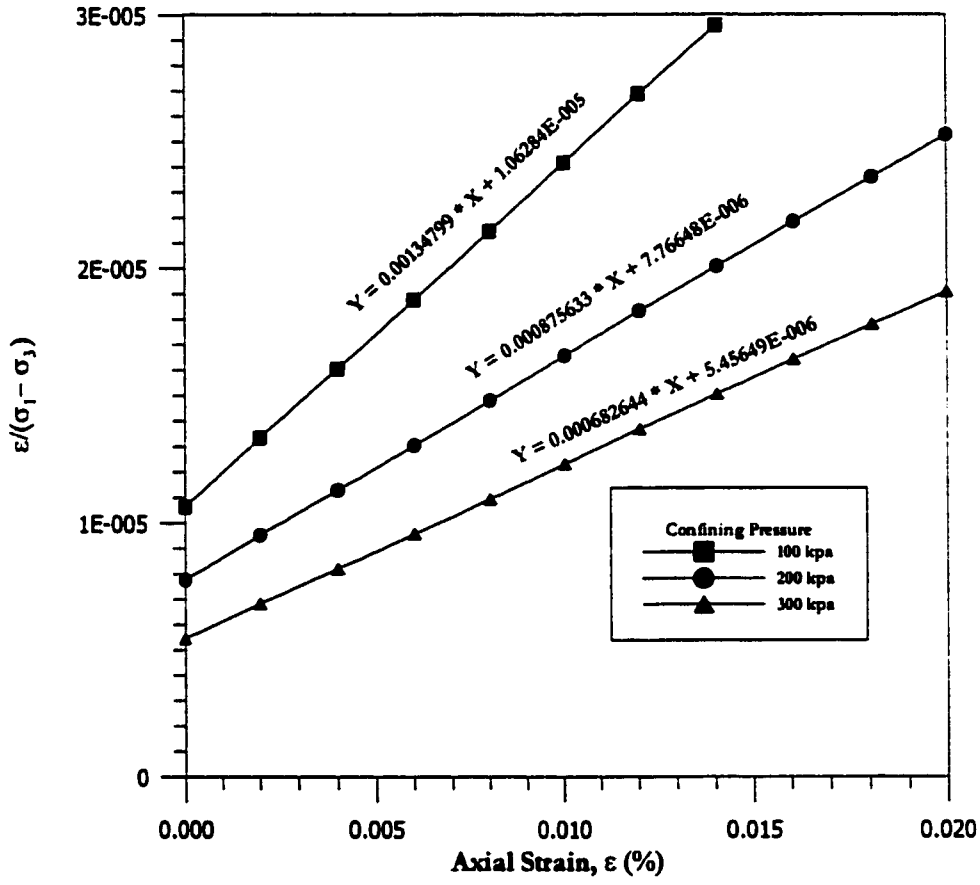

Fig. 4.22: Determination of E_i and R_f for marl at high density

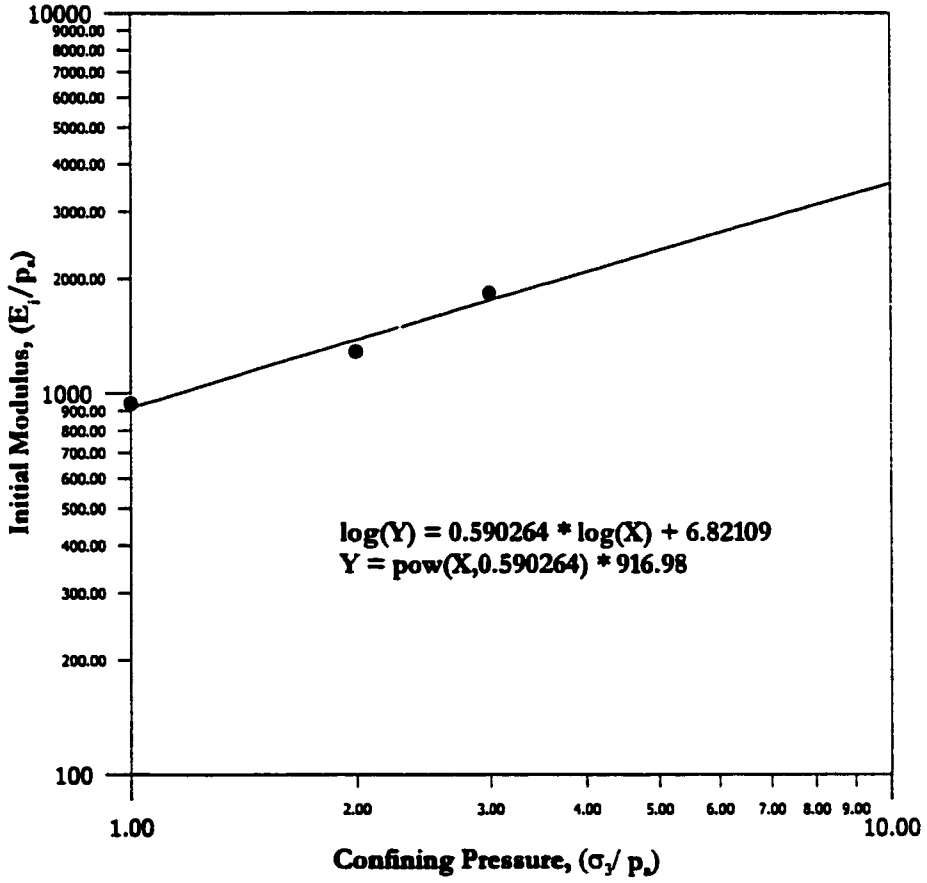

Fig. 4.23: Determination of K and n for marl at high density

and 0.60, respectively.

4.4.6.3 Parameters for Sabkha

Triaxial test results for sabkha at high density (RC = 96.8%) are given in Fig. 4.24. These results are for unconsolidated drained (UD) condition, with wet of optimum water content. Mohr circles and failure envelope are presented in Fig. 4.25, in which C = 84.2 kPa, ϕ_o = 33.3°, and $\Delta\phi$ = 0.0. The $p - q$ diagram is shown in Fig. 4.26. The plots of $[\varepsilon/(\sigma_1 - \sigma_3)]$ $vs.$ ε are given in Fig. 4.27. The value of R_f is found to be 0.72, 0.71, and 0.70 for σ_3 = 100, 200, and 300 kPa, respectively, with an average value of 0.71. The plot of $log(E_i/P_a)$ $vs.$ $log(\sigma_3/P_a)$ is shown in Fig. 4.28, from which K and n values are obtained to be 141.75 and 0.39, respectively.

Sabkha at low density (RC = 85.2%), tested under UD triaxial condition, produced inconsistent soil parameters. This is attributed to the fact that the low density of the clayey sabkha and the high water content produced unusual behavior under drained triaxial tests. Therefore, the results were not reported.

4.4.6.4 Backprediction

Table 4.1 provides a summary of soil parameters obtained from triaxial tests on various types of soils at different conditions. These parameters are used to backpredict the stress-strain behavior of these soils. The predicted stress-strain curve for each soil type is compared with the actual curves obtained from the experimental tests. The hyperbolic stress-strain equation is of the form

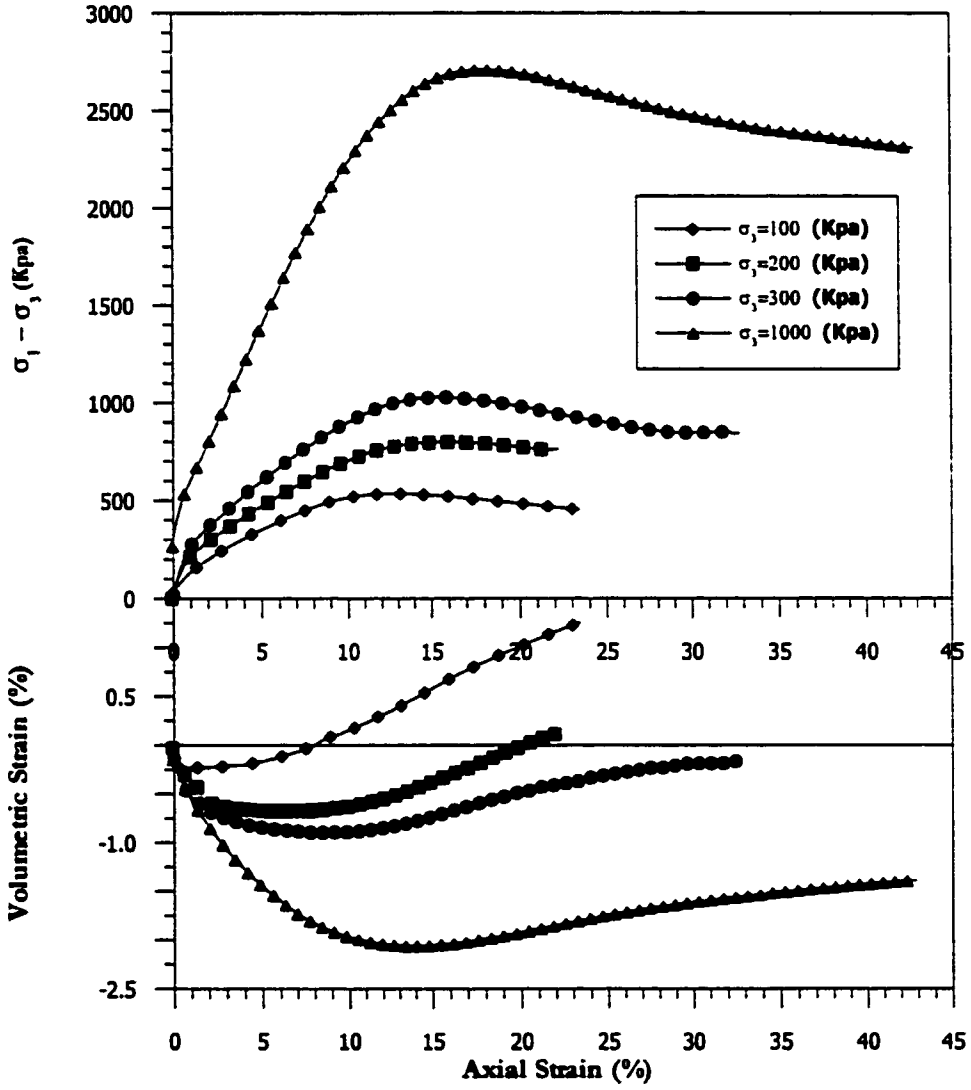

Fig. 4.24: Triaxial test for sabkha at high density

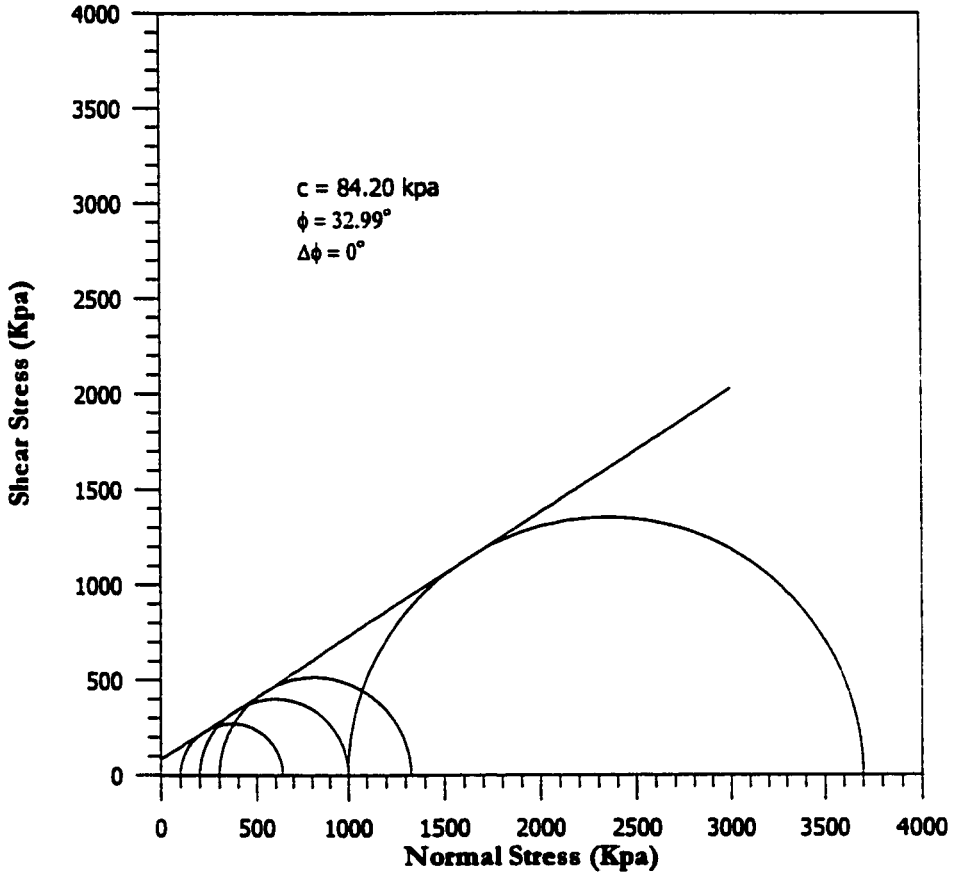

Fig. 4.25: Mohar circle for sabkha at high density

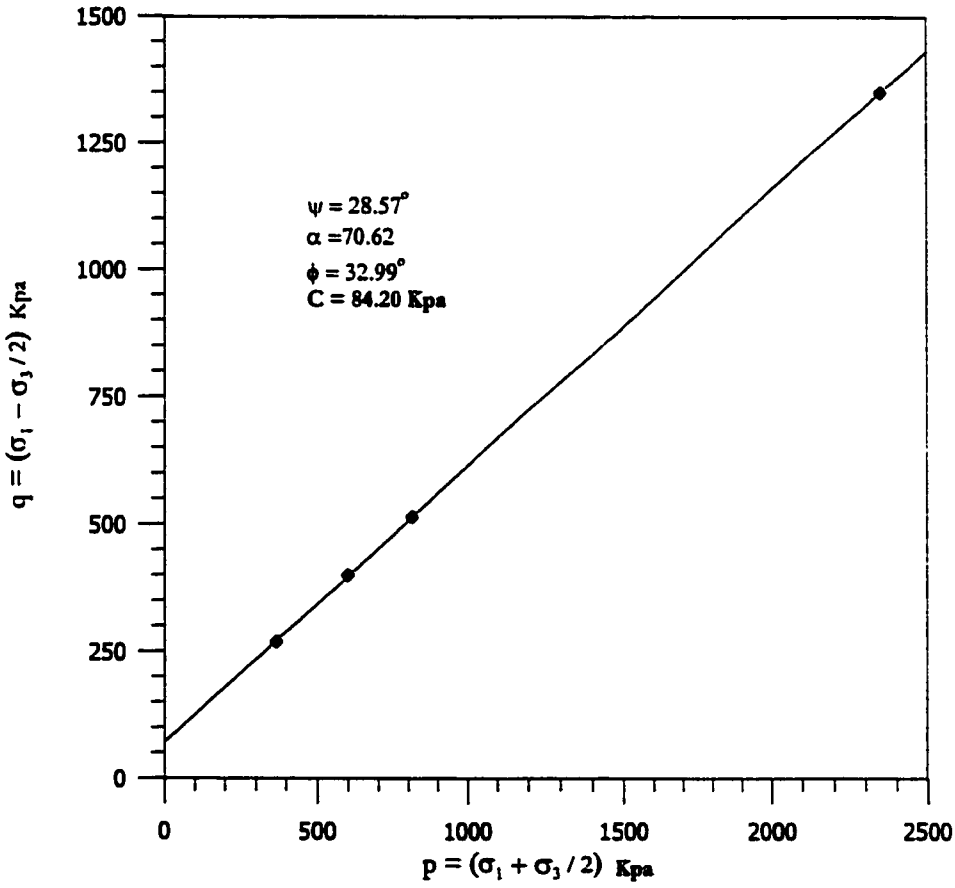

Fig. 4.26: $p - q$ diagram for sabkha at high density

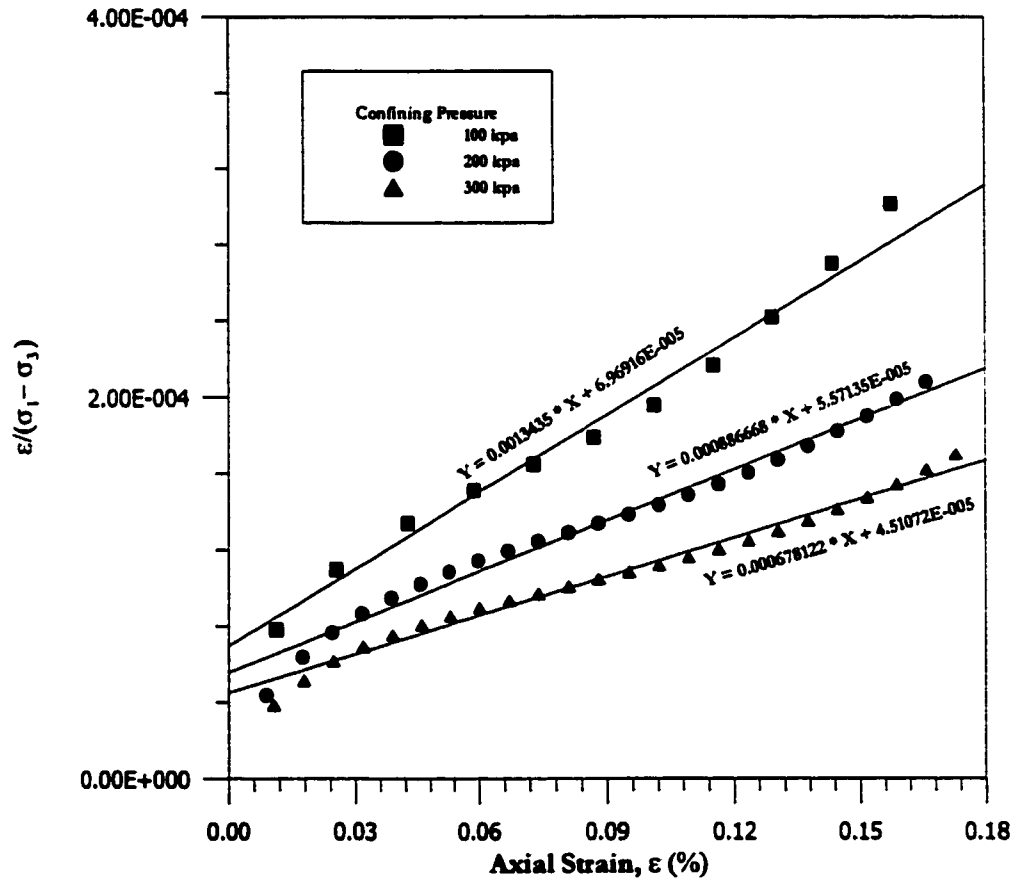

Fig. 4.27: Determination of E_i and R_f for sabkha at high density

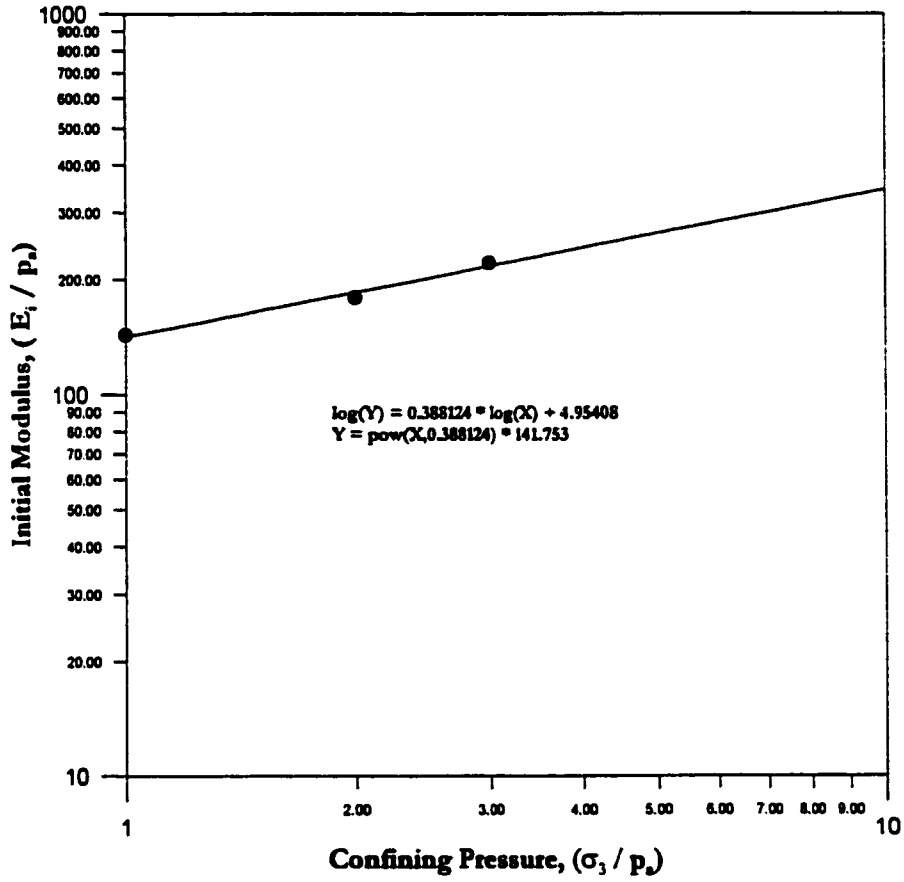

Fig. 4.28: Determination of K and n for sabkha at high density

TABLE 4.1: Triaxial test parameters

Soil	ϕ	ϕ_o	$\Delta\phi$	$C\ Kpa$	$C\ (psi)$	K	n	R_f
Sand at low density	35.46	38.31	3.32	0.00	0.00	585.89	1.07	0.90
Sand at high density	43.36	46.40	3.47	0.00	0.00	1963.22	0.62	0.85
Marl at low density	30.81	30.81	0.00	21.34	3.095	272.46	0.10	0.88
Marl at high density	33.24	33.24	0.00	71.73	10.40	916.98	0.60	0.67
Sabkha at high density	33.00	33.00	0.00	84.20	12.21	141.75	0.39	0.71

$$\sigma_1 - \sigma_3 = \frac{\varepsilon}{\frac{1}{E_i} + \frac{\varepsilon}{(\sigma_1 - \sigma_3)_u}} \tag{4.2}$$

where,

$$E_i = K p_a \left(\sigma_3 / p_a\right)^n \tag{4.3}$$

$$(\sigma_1 - \sigma_3)_u = \frac{(\sigma_1 - \sigma_3)_f}{R_f} \tag{4.4}$$

and

$$(\sigma_1 - \sigma_3)_f = \frac{2C cos\phi + 2\sigma_3 sin\phi}{1 - sin\phi} \tag{4.5}$$

Using Equations (4.3) to (4.5) into Equation (4.2) yields

$$(\sigma_1 - \sigma_3) = \frac{\varepsilon}{\frac{1}{K p_a \left(\sigma_3 / p_a\right)^n} + \frac{\varepsilon * R_f * (1 - sin\phi)}{(2C cos\phi + 2\sigma_3 sin\phi)}} \tag{4.6}$$

where,

$$\phi = \phi_o - \Delta\phi log_{10}\left(\frac{\sigma_3}{p_a}\right) \tag{4.7}$$

Equation (4.6) is used for backprediction of stress-strain relationship.

Fig. 4.29 presents a comparison between experimental and backpredicted stress-strain curves for low density sand, for σ_3 = 100, 200, 300 and 1000 kPa. The experimental and backpredicted curves are in excellent agreement. Similar results were obtained for high density sand, as shown in Fig. 4.30.

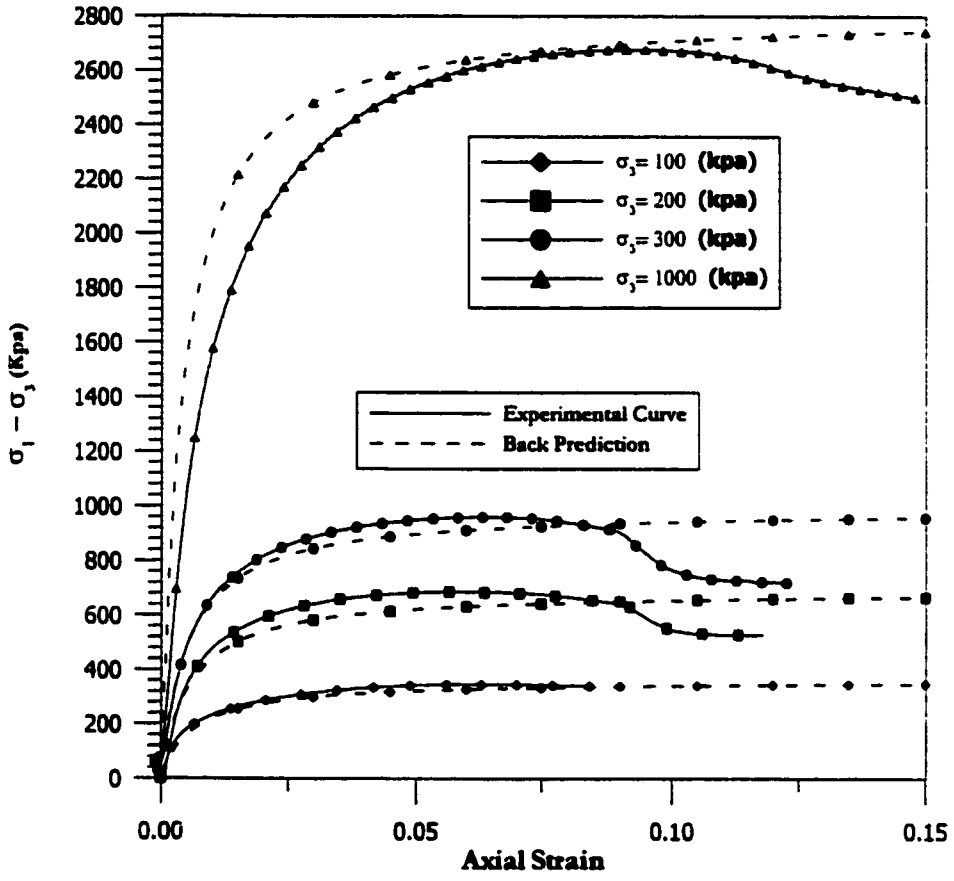

Fig. 4.29: Back prediction for sand at low density

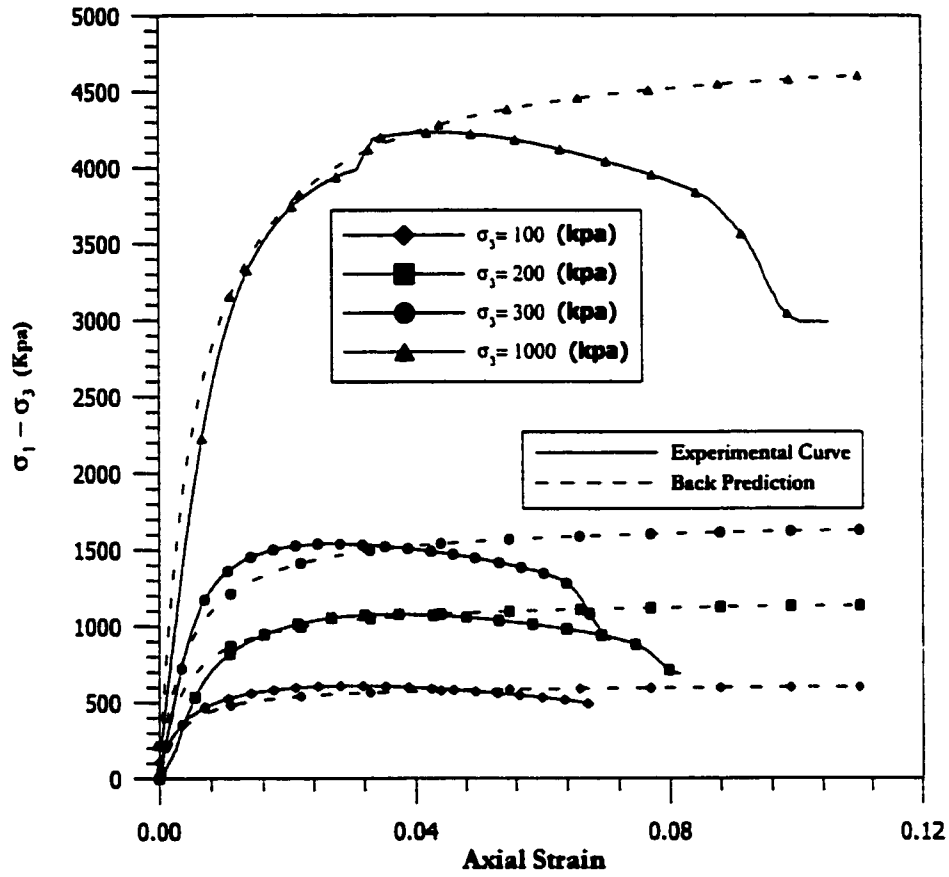

Fig. 4.30: Back prediction for sand high density

Fig. 4.31 and Fig. 4.32 show the experimental and backpredicted curves for marl at low and high density, respectively. The curves are in very good agreement, especially up to the peak. Fig. 4.33 gives similar curves for sabkha soil at high density.

4.4.7 Analysis of Hydrostatic Test Results

Soil parameters were obtained from hydrostatic tests performed on various types of soils (sand, marl, and sabkha) at both loose and dense conditions.

4.4.7.1 Parameters for Sand

Fig. 4.34 presents the results of hydrostatic tests performed on sand at low density, in terms of hydrostatic stress (σ_m) vs. volumetric strain (ε_{vol}). The plot of ($\varepsilon_{vol}/\sigma_m$) vs. σ_m is shown in Fig. 4.35, whose intercept represents the initial bulk modulus (B_i) and its slope represents the reciprocal of the ultimate volumetric strain at large stress ($1/\varepsilon_u$) . The values for B_i and ε_u are 3,836.95 kPa and 0.0251, respectively.

For sand at high density, the results of hydrostatic tests are given in Fig. 4.36. The plot of ($\varepsilon_{vol}/\sigma_m$) vs. σ_m is shown in Fig. 4.37, which gives values for $B_i$and ε_u to be 23,275.9 kPa and 0.0337, respectively.

4.4.7.2 Parameters for Marl

Fig. 4.38 presents the results of hydrostatic tests performed on marl at low density. The plot of ($\varepsilon_{vol}/\sigma_m$) vs. σ_m is shown in Fig. 4.39, which gives values of $6,243.87kPa$ and 0.0915 for B_i and ε_u, respectively.

For marl at high density, the results of hydrostatic tests are given in Fig. 4.40. The plot of ($\varepsilon_{vol}/\sigma_m$) vs. σ_m is shown in Fig. 4.41, which gives values of 5,356.65 kPa and

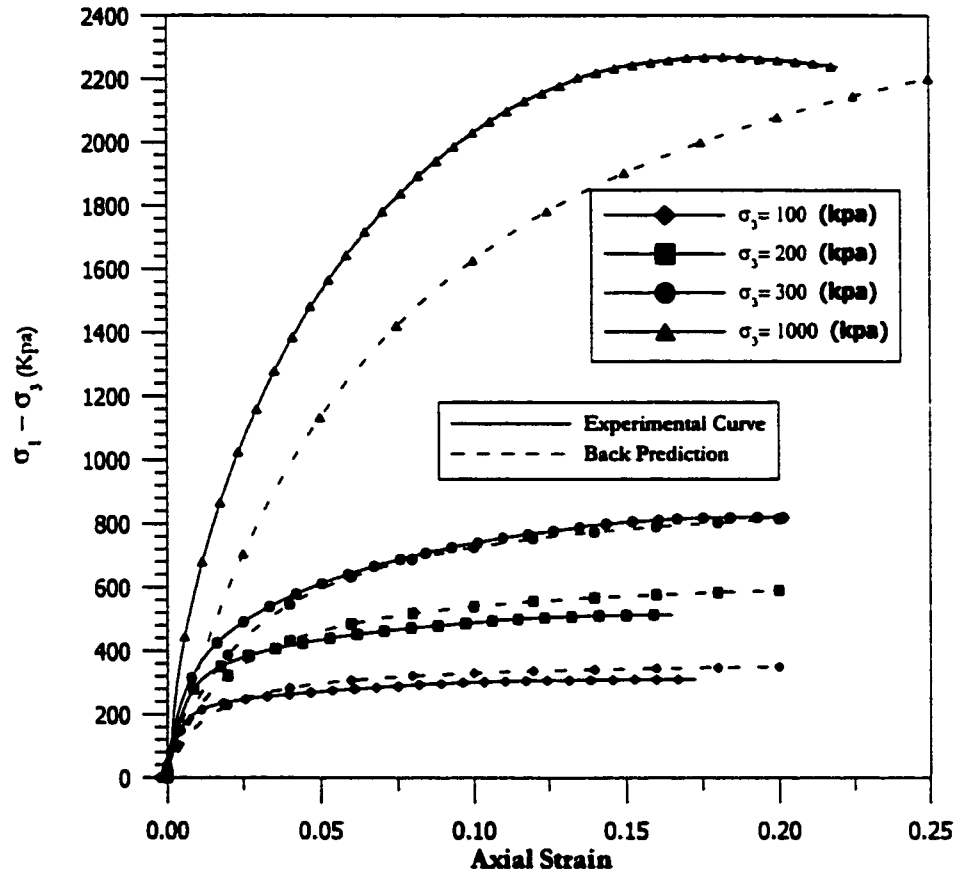

Fig. 4.31: Back prediction for marl at low density

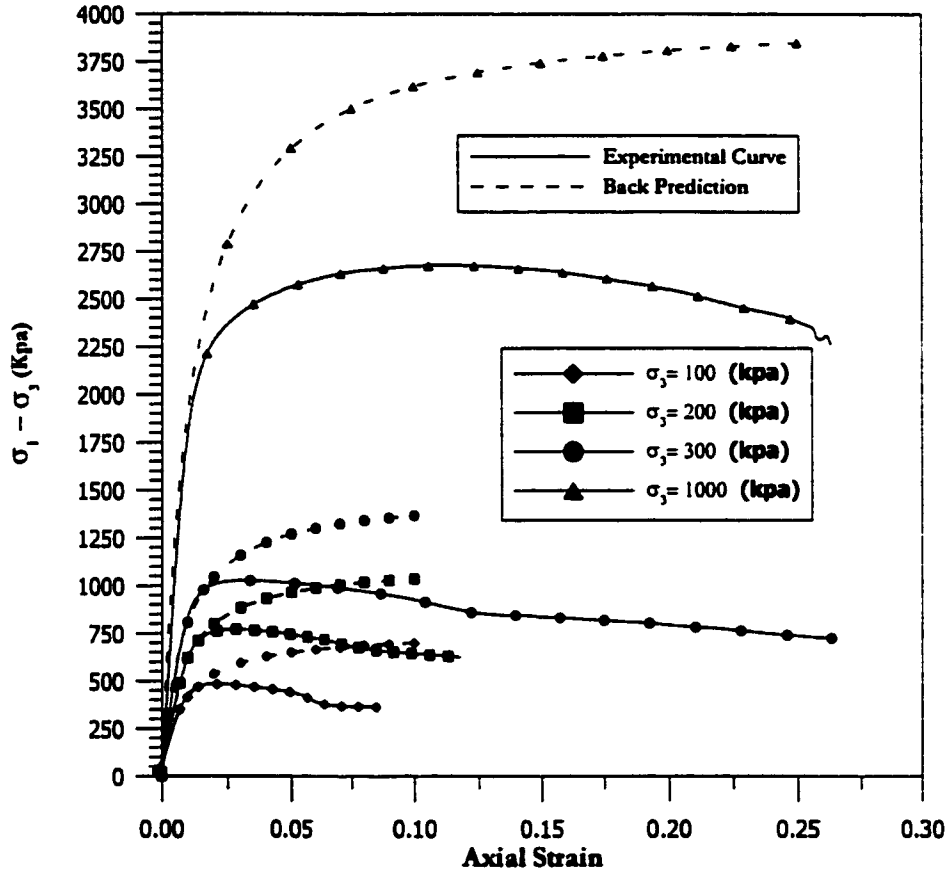

Fig. 4.32: Back prediction for marl at high density

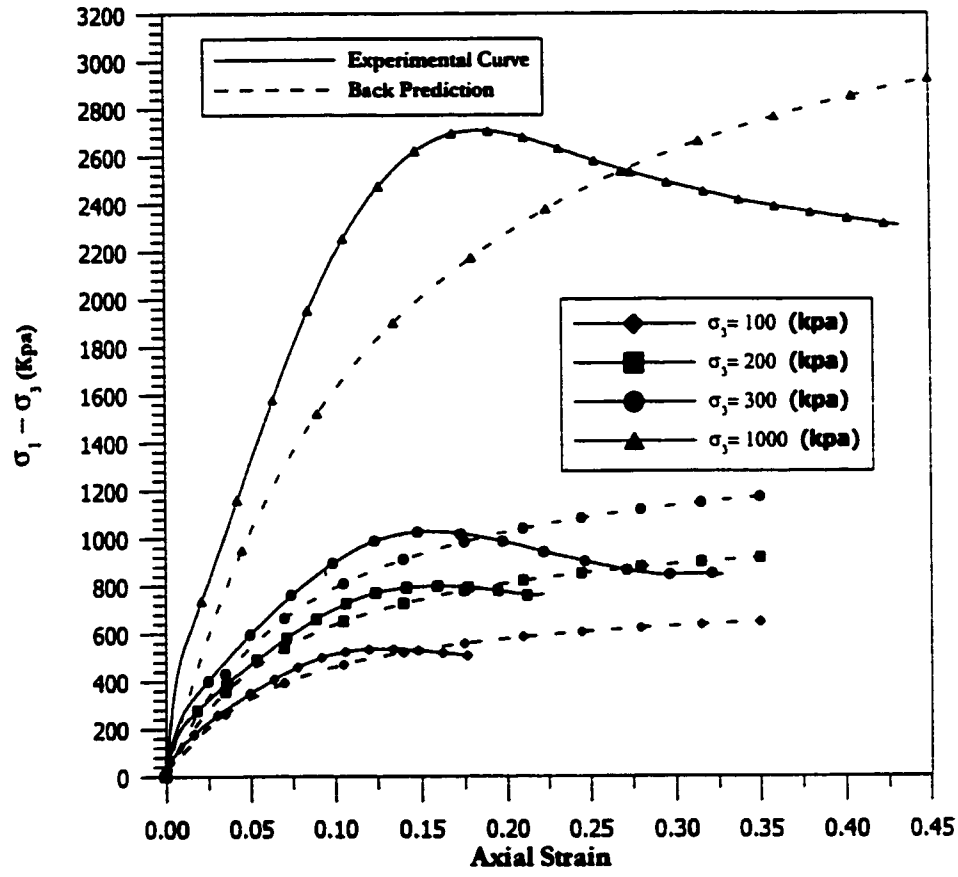

Fig. 4.33: Back prediction for sabkha at high density

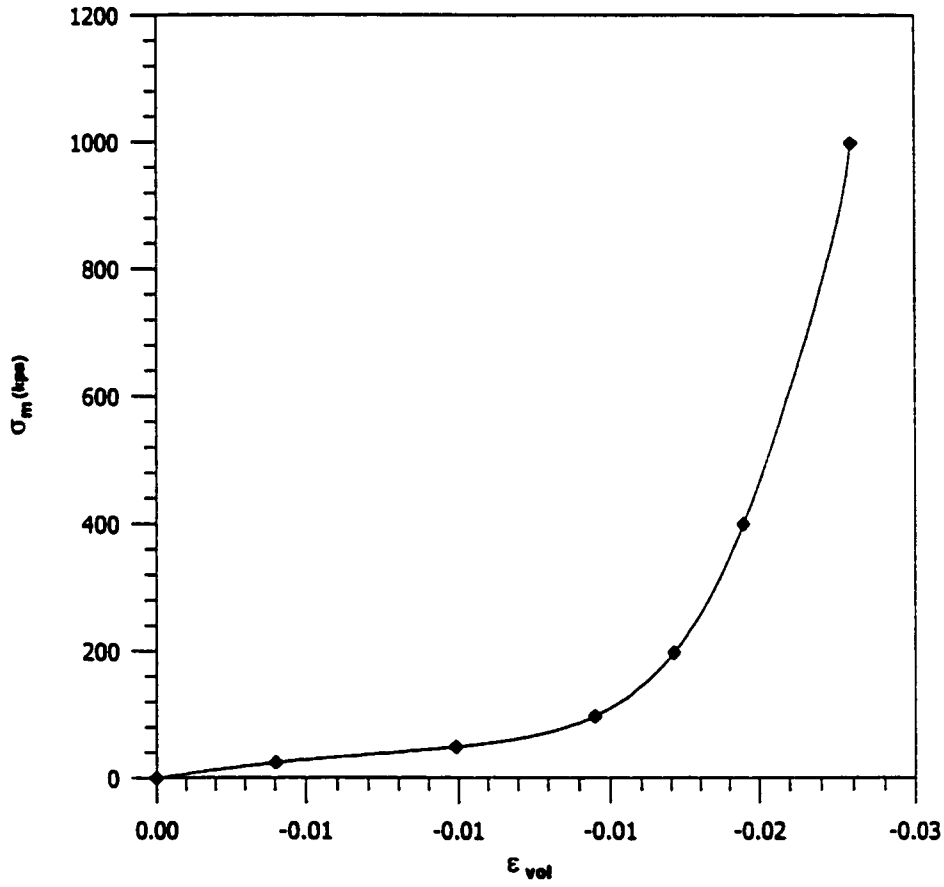

Fig. 4.34: Hydrostatic test for sand at low density

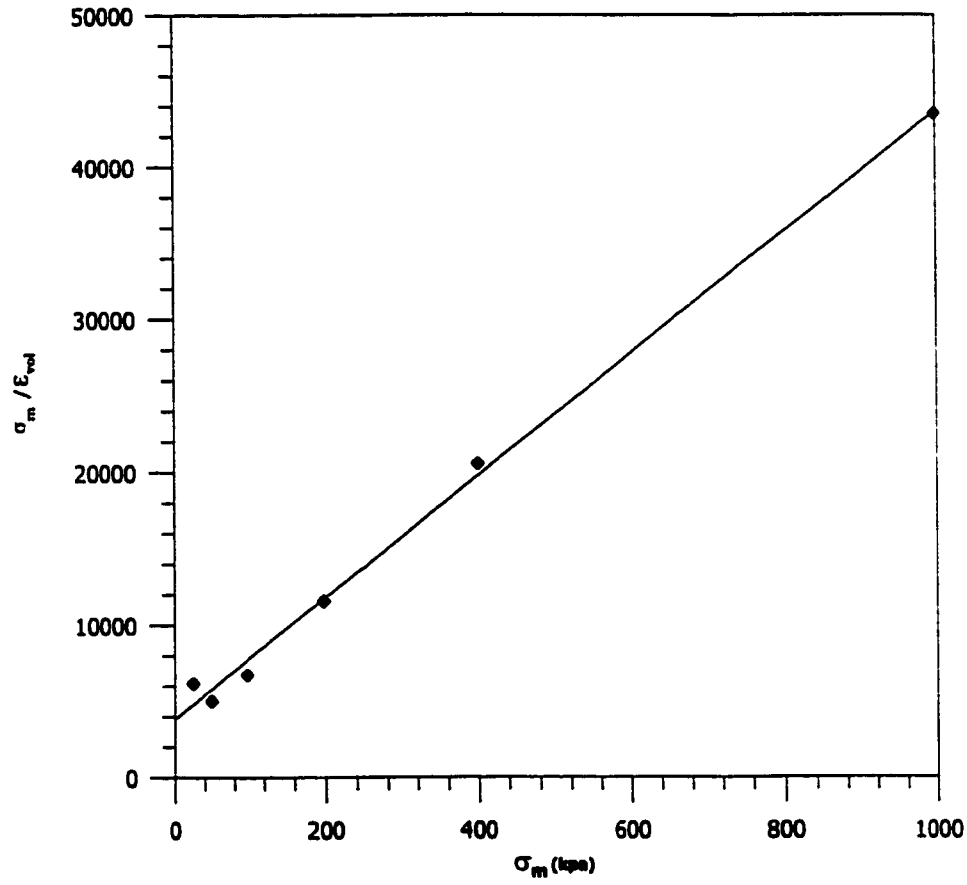

Fig. 4.35: Determination of B_i and ε_u for sand at low density

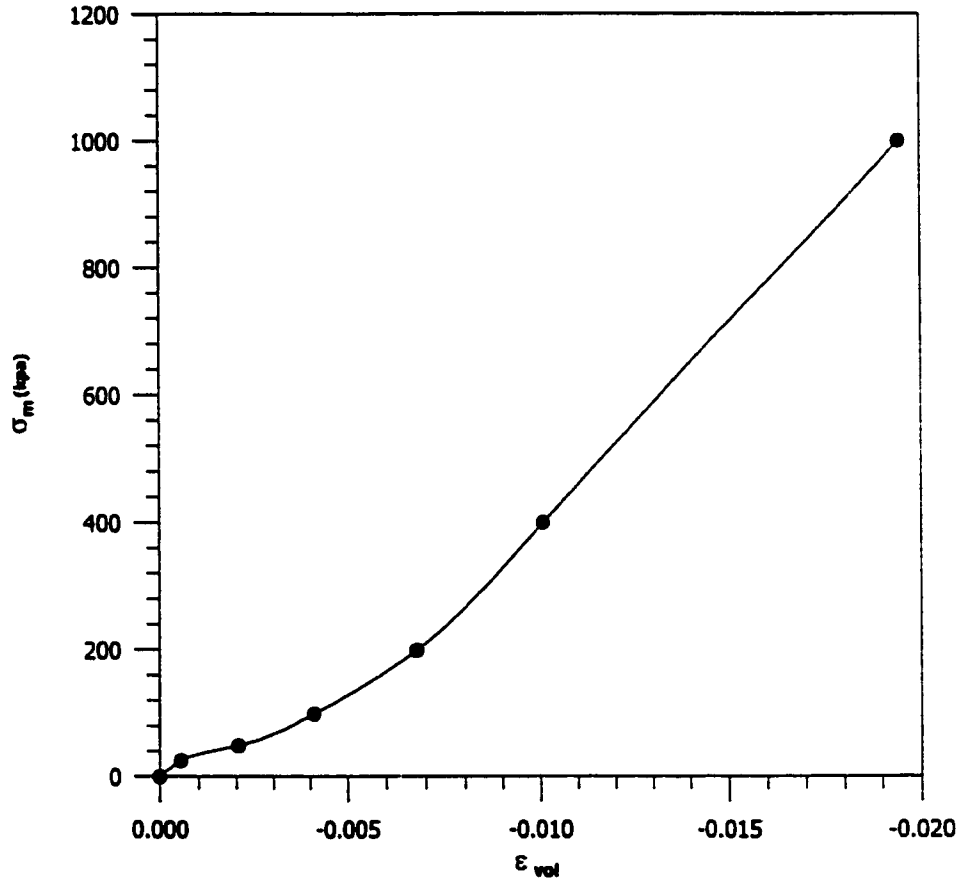

Fig. 4.36: Hydrostatic test for sand at high density

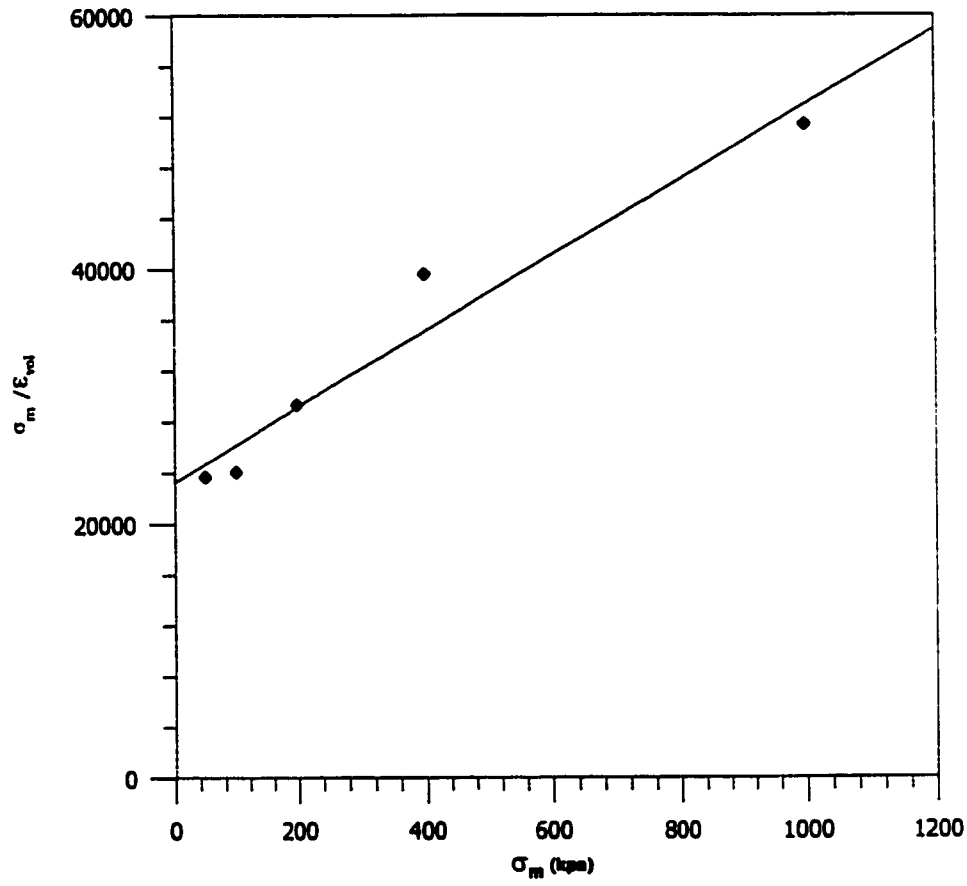

Fig. 4.37: Determination of B_i and ε_u for sand at high density

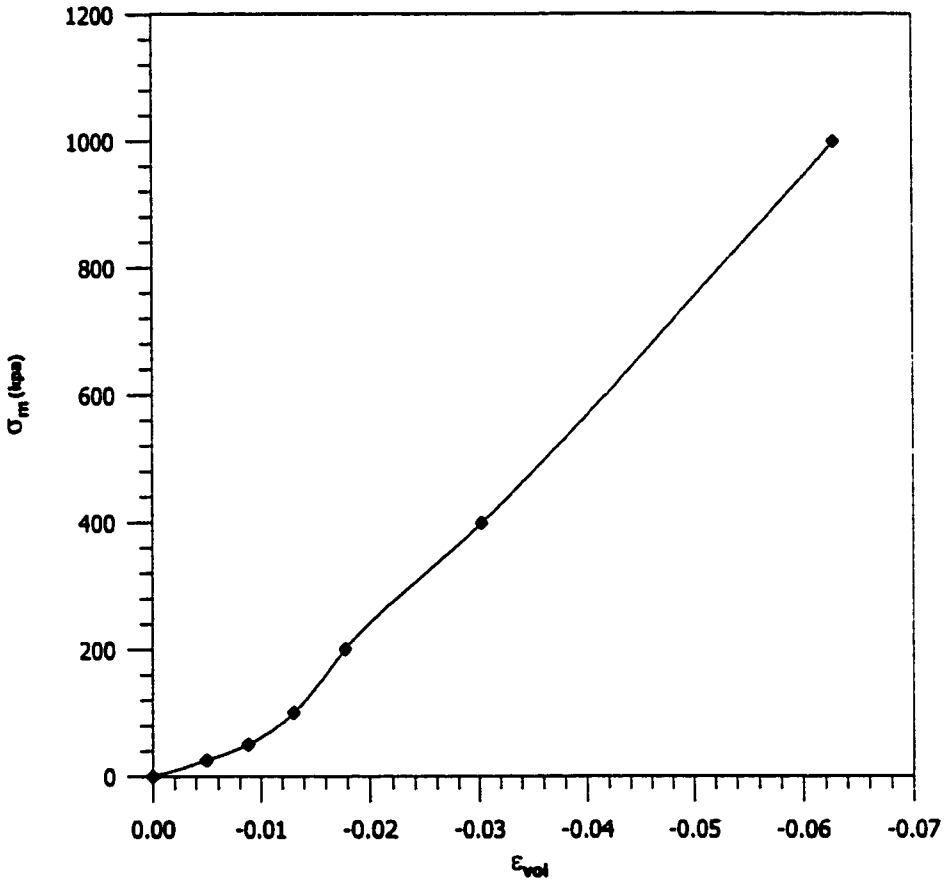

Fig. 4.38: Hydrostatic test for marl at low density

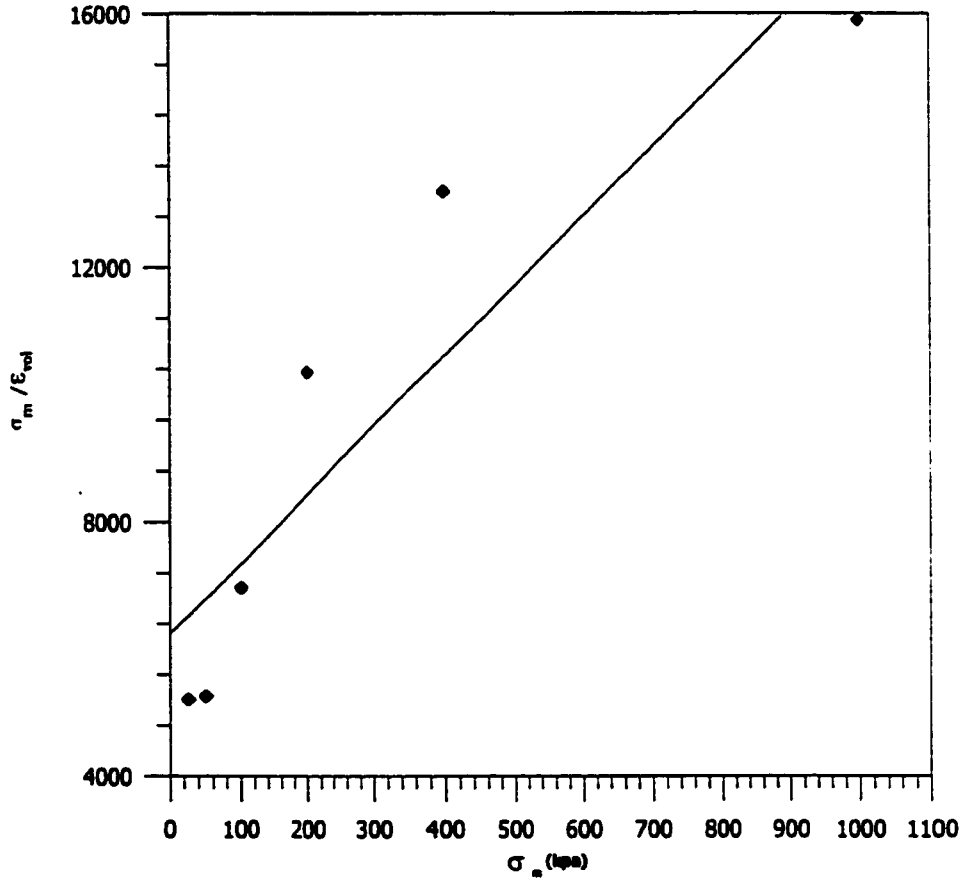

Fig. 4.39: Determination of B_i and ε_u for marl at low density

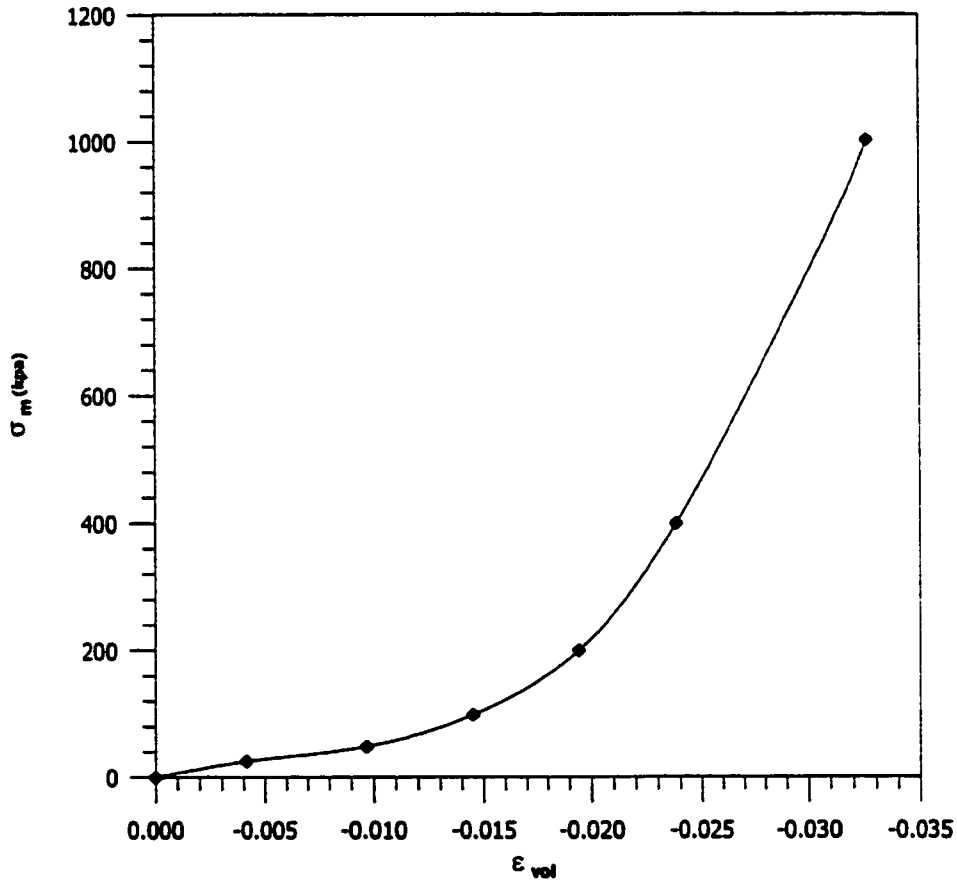

Fig. 4.40: Hydrostatic test for marl at high density

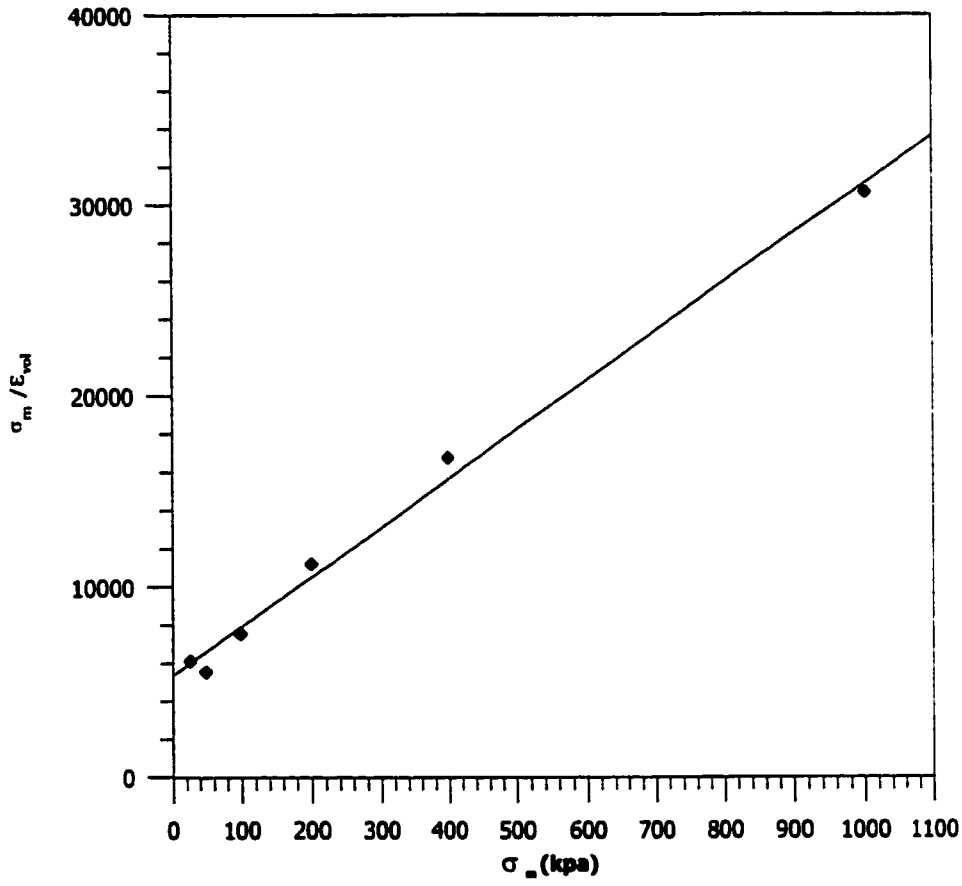

Fig. 4.41: Determination of B_i and ε_u for marl at high density

0.0388 for B_i and ε_u, respectively.

4.4.7.3 Parameters for Sabkha

Fig. 4.42 presents the results of hydrostatic tests performed on sabkha at low density. The plot of $(\varepsilon_{vol}/\sigma_m)$ vs. σ_m is shown in Fig. 4.43, which gives values of 620.84 kPa and 0.1420 for B_i and ε_u, respectively.

For sabkha at high density, the results of hydrostatic tests are given in Fig. 4.44. The plot of $(\varepsilon_{vol}/\sigma_m)$ vs. σ_m is shown in Fig. 4.45, which gives values of 2,608.77 kPa and 0.0618 for B_i and ε_u, respectively.

4.4.7.4 Backprediction

Table 4.2 provides a summary of soil parameters obtained from hydrostatic tests on various types of soils at different conditions. These parameters are used to backpredict the behavior of these soils under hydrostatic stress condition. The predicted behavior for each soil type is compared with the actual curve obtained from the experimental tests. Selig [65] provided the following hyperbolic equation

$$\sigma_m = \frac{B_i \varepsilon_{vol}}{1 - (\varepsilon_{vol}/\varepsilon_u)} \tag{4.8}$$

Equation (4.8) is used to backpredict the behavior of soils under hydrostatic loading.

Figs. 4.46 and 4.47 present comparisons between experimental and backpredicted $\sigma_m - \varepsilon_{vol}$ curves for sand at low and high density, respectively. The experimental and backpredicted curves are in excellent agreement.

Similar results are obtained for marl at low and high densities, as given in Figs. 4.48

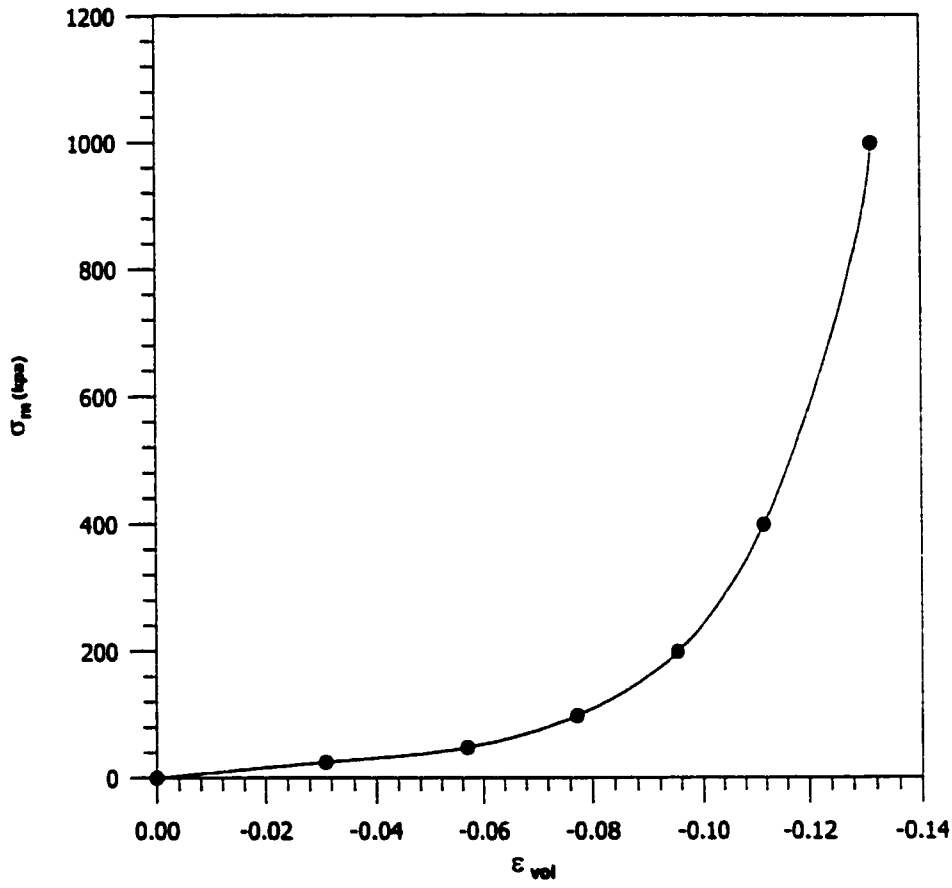

Fig. 4.42: Hydrostatic test for sabkha at low density

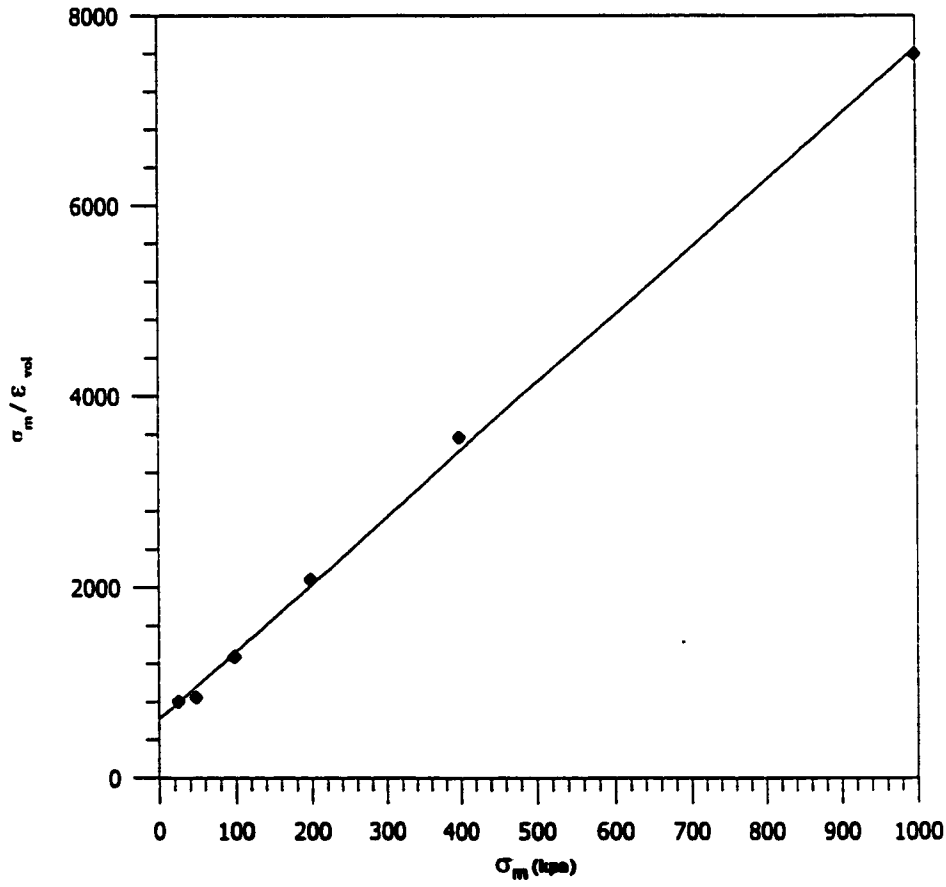

Fig. 4.43: Determination of B_i and ε_u for sabkha at low density

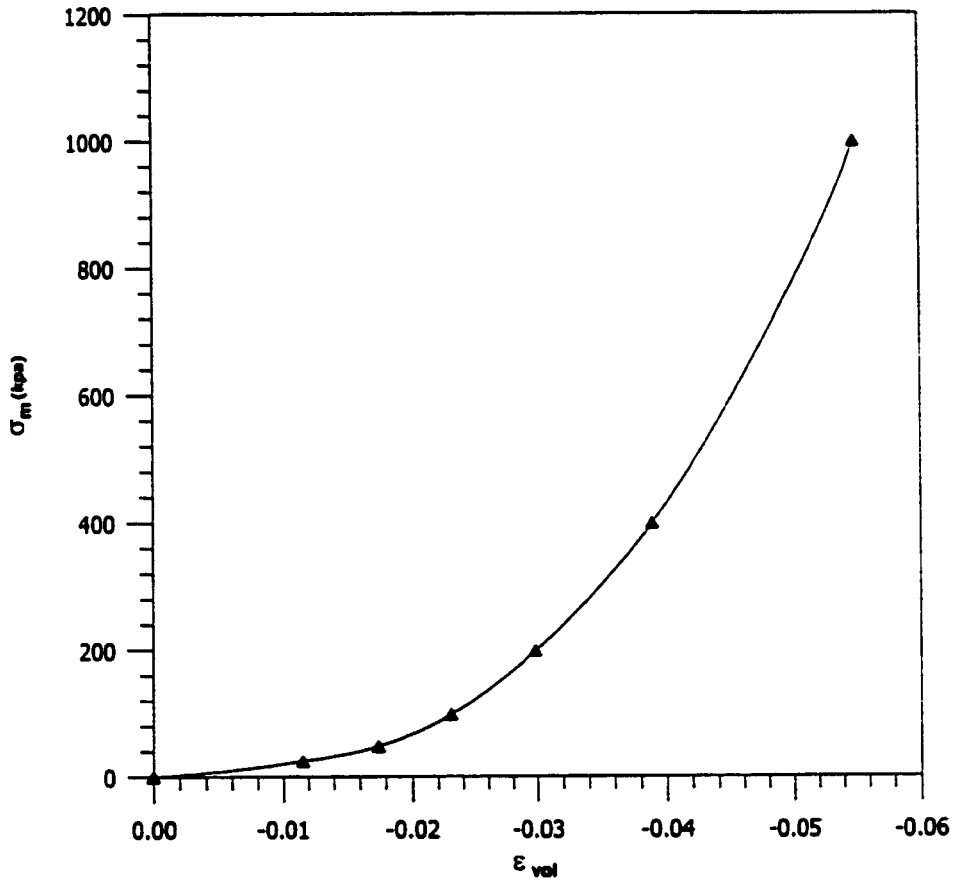

Fig. 4.44: Hydrostatic test for sabkha at high density

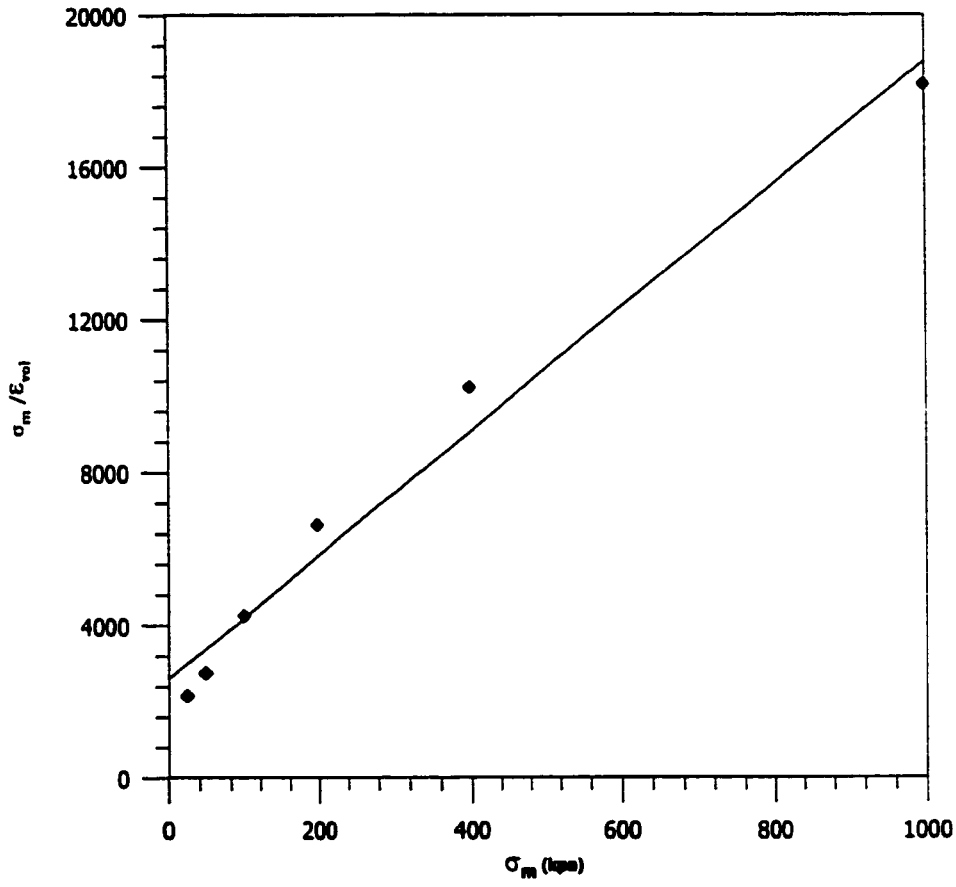

Fig. 4.45: Determination of B_i and ε_u for sabkha at high density

TABLE 4.2: Parameters for hydrostatic test

Soil	B_i (kpa)	B_i (psi)	B_i/P_a	ε_u
Sand at low density	3836.95	556.50	38.37	0.025068625
Sand at high density	23275.90	3375.88	232.76	0.033654736
Marl at low density	6243.87	905.59	62.44	0.0915105656
Marl at high density	5356.65	776.91	53.57	0.038837214
Sabkha at low density	620.84	90.04	6.21	0.141962979
Sabkha at high density	2608.77	378.37	26.09	0.061766141

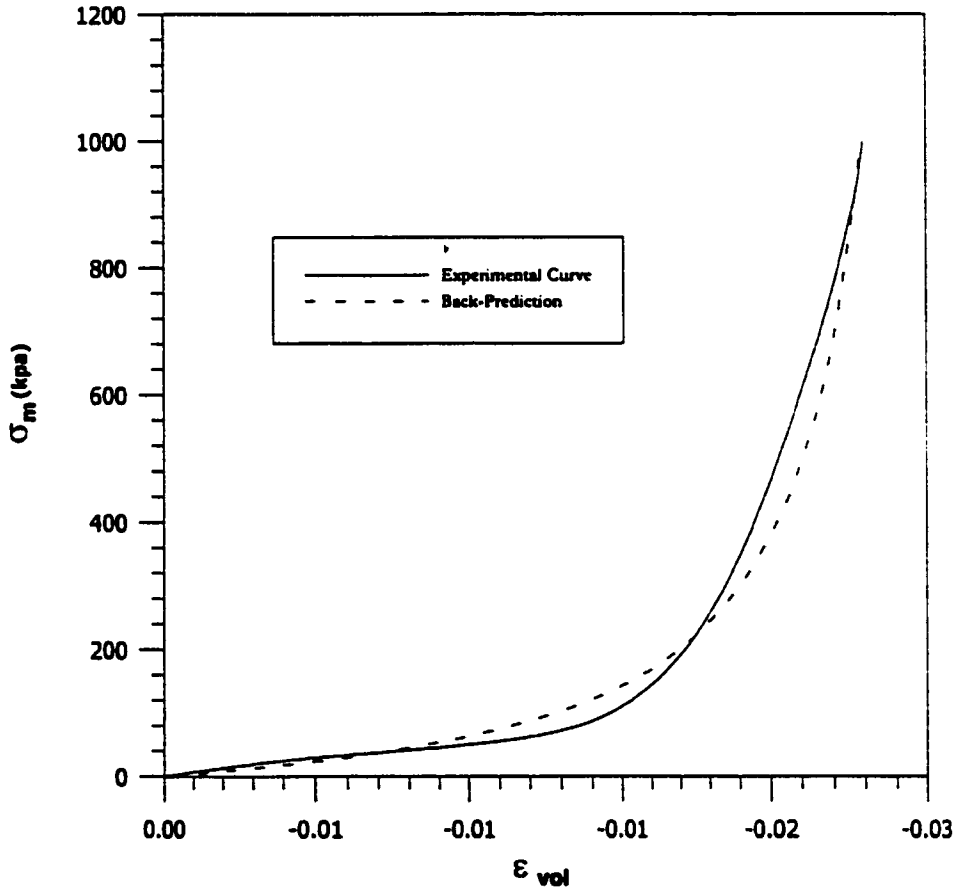

Fig. 4.46: Back prediction for sand at low density

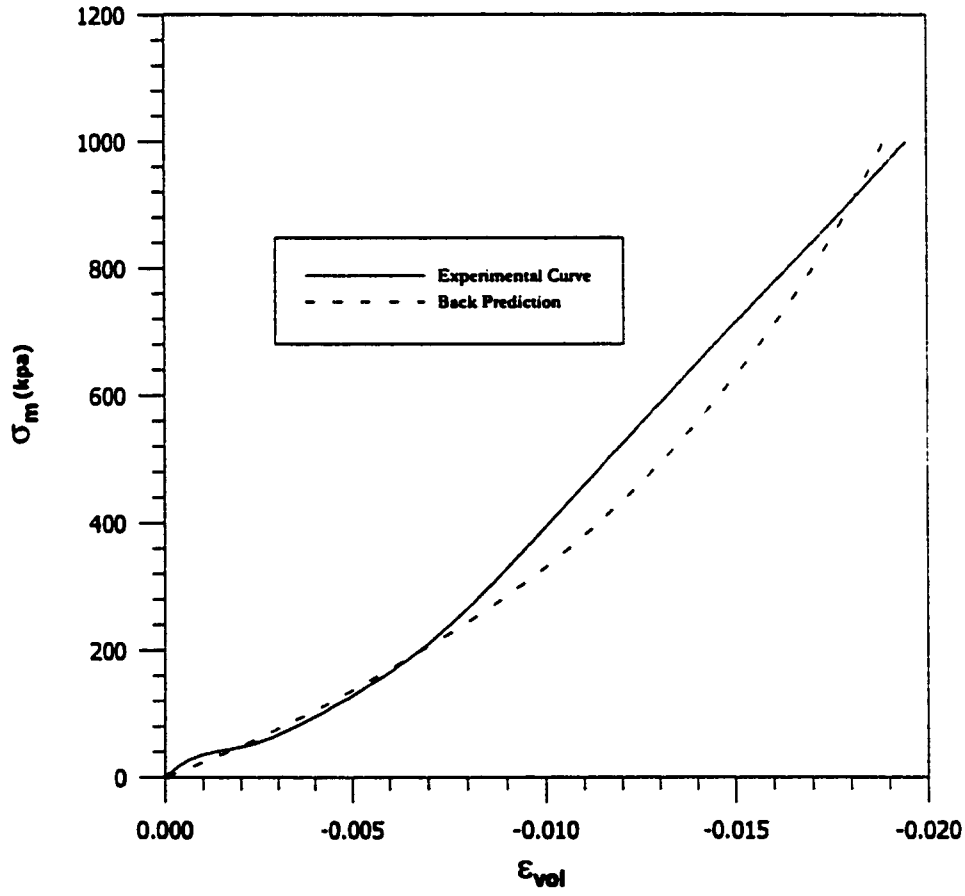

Fig. 4.47: Back prediction for sand at high density

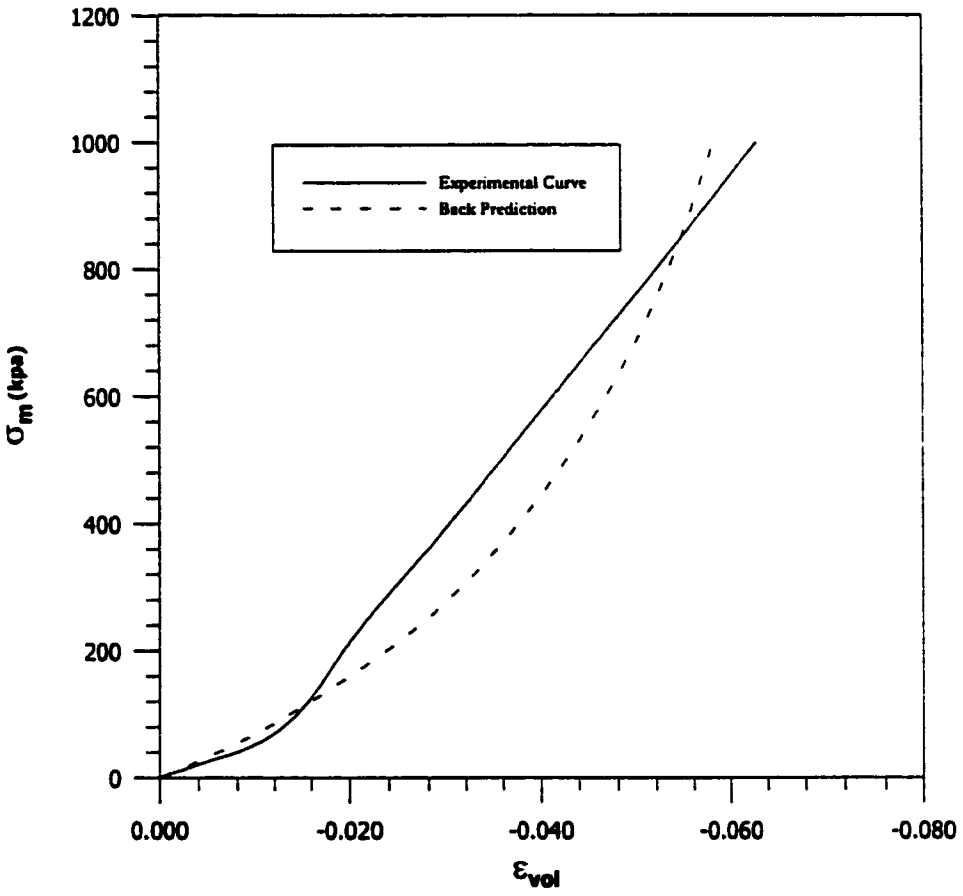

Fig. 4.48: Back prediction for marl at low density

and 4.49, respectively. Also, similar curves for sabkha at low and high densities are given in Figs. 4.50 and 4.51, respectively.

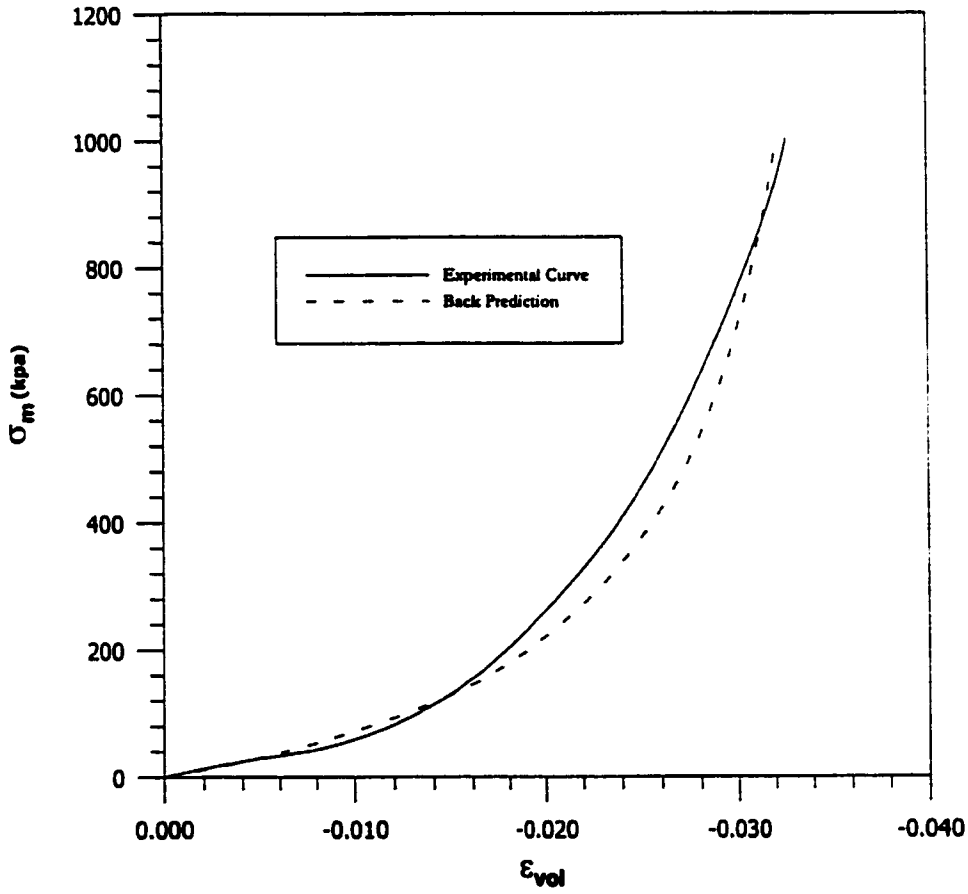

Fig. 4.49: Back prediction for marl at high density

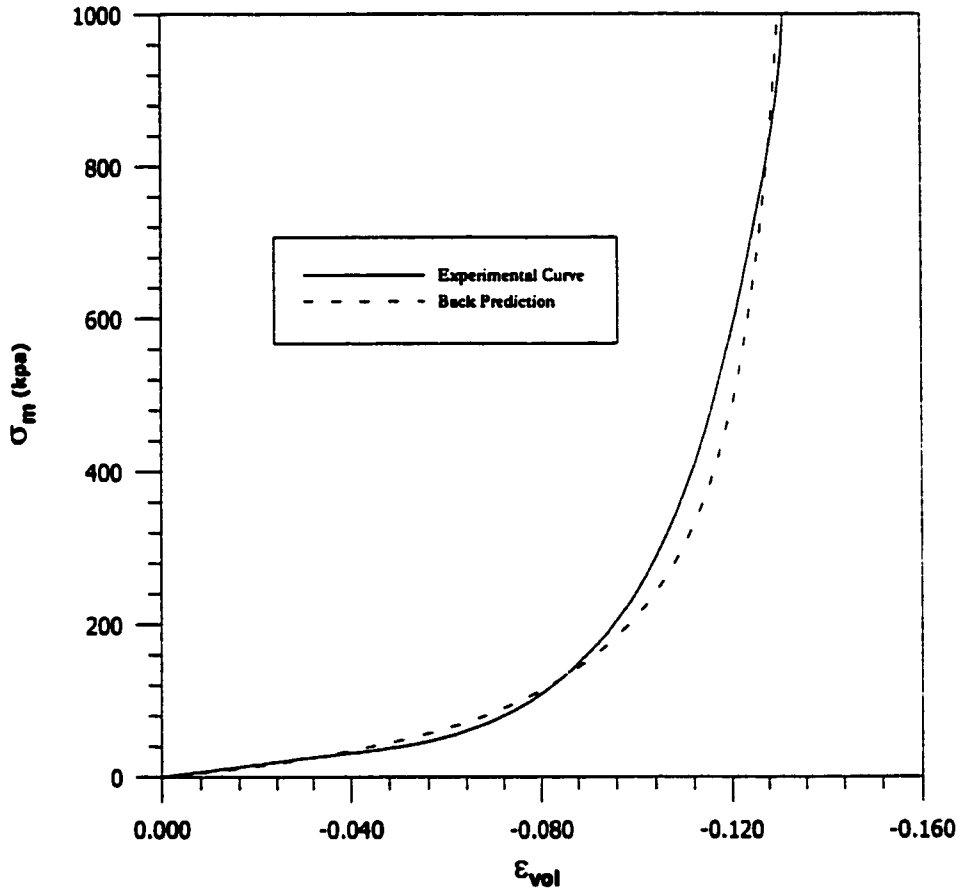

Fig. 4.50: Back prediction for sabkha at low density

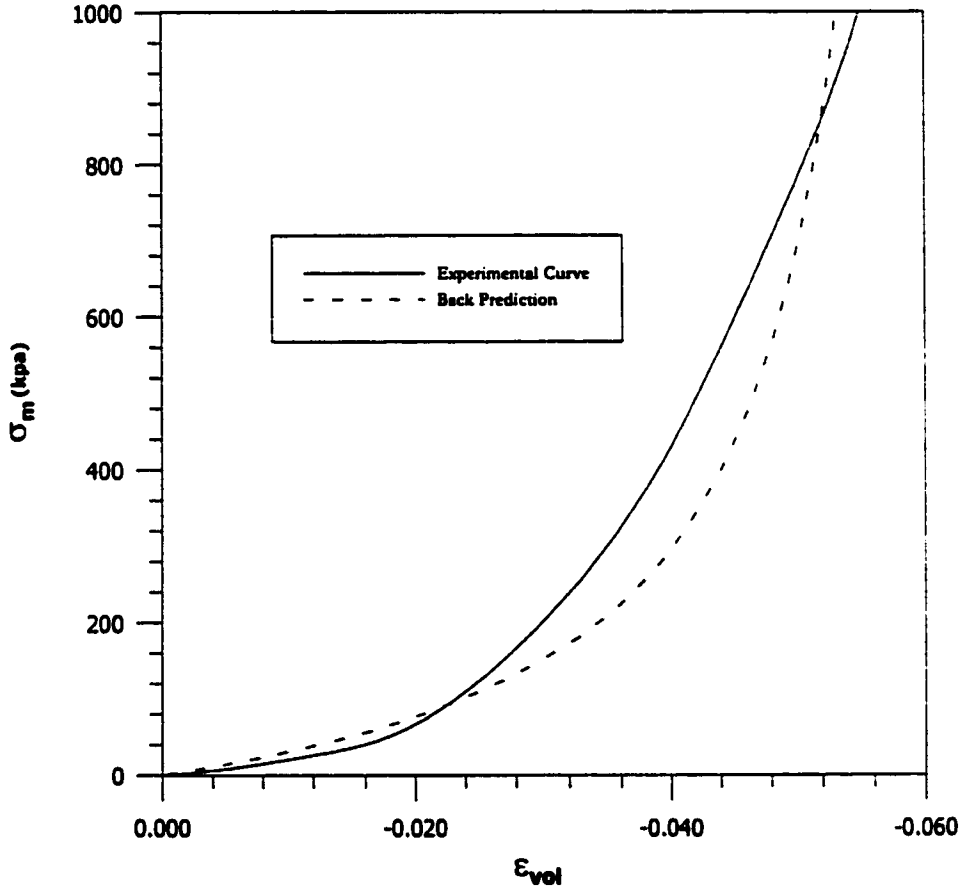

Fig. 4.51: Back prediction for sabkha at high density

CHAPTER 5

NUMERICAL MODELING

5.1 Introduction

A numerical model of the soil-pipe system must be available to analyze or predict the detailed behavior of buried pipelines. Theories of soil-structure interaction such as ring compression provide mathematical models that are currently used to design or analyze buried pipelines. These theories do not account for the actual interaction between the pipe and the surrounding soil during construction, service, and ultimate conditions; due to the nonlinearities, nonhomogeneity and other complexities. Numerical modeling is the best approach to adeqautely model the pipeline-soil system. The finite element method is the most common numerical technique that can be used to analyze and design buried pipelines.

5.2 Existing Finite Element Programs

There are a number of different finite element programs that have been or might be applied to the analysis of pipe-soil systems. A few of these have been specifically designed

for buried conduit problems or for soil-structure interaction studies. Perhaps the most general of these is Culvert ANalysis and DEsign (CANDE), developed by M.G. Katona et al. [57]. Others in a descending order of sophistication, include FINLIN developed by Roy at Purdue university [81], Soil-Structure interaction program (SSTIP) developed by Dunacn et al. at the University of California at Berkeley [82], Nonlinear Soil-Structure Interaction Program (NLSSIP) also developed by Duncan et al. at the University of California at Berkeley [69]. In addition, there exist several general purpose finite element programs that could be applied to the problem. A partial list includes SAP IV, NONSAP, ADINA, MARC, NASTRAN, ASKA, STRUDL II and ANSYS. Most of these general-purpose programs have a structural mechanics orientation, and are lacking sophisticated soil model capable of simulating the actual soil behavior behavior [83]. SMAP is a family of packages (SMAP-S2, SMAP-S3, SMAP-2D, SMAP-3D, SMAP-T2, SMAP-T3, TUNA, TUNA PLUS) for static, dynamic, consolidation, heat conduction, geotechnical, and, structural engineering applications. The oldest version of this program was only two dimensional (2-D) static model, but a later version (1997-98) extended the program to cover three dimensional (3-D) problems. Although the program has the capacity to simulate most of the processes in this research, but for 3-D models it is unfeasible to be used for a large number of simulations which are essential for this research owing to the very complex procedure of data file preparation and high processing time.

A 2-D plain strain finite element simulations with incremental construction and initial stress effects will be used in this research. Moreover a nonlinear material model for soil and interface element and linear elastic material model for pipe was also used. Considering all

of the above software and many others it was decided to use CANDE. A brief introduction of CANDE is given in next section

5.3 CANDE

CANDE an acronym derived from Culvert ANalysis and DEsign, is a computer program for structural analysis, design and evaluation of buried culverts and other soil structures systems. The CANDE methodology incorporates the soil mass along with the structure into an incremental, static, plain-strain boundary value problem. Although CANDE was developed primarily for the design and analysis of buried culverts ranging from the smallest diameter plastic pipe to the largest long span metal arches, the generality offered by the finite element method solution methodology permits other class of soil-structure problems to be analyzed. Some examples are tunnels, retaining walls, ammunition igloos, and underground openings. The only restrictions are 2-D geometry, quasi-static loading conditions and small strain theory.

Since its introduction 1976 [57], the CANDE program has been widely distributed by the Federal Highway Administration (FHWA). It is used by state highway departments, federal agencies (domestic and military), research laboratories, consulting firms, industry, and universities in the United States of America, Canada, and Europe.

In a comprehensive study [69] sponsored by state and federal agencies CANDE was compared with other finite element codes for the analysis and design of buried pipelines, and it was found that CANDE is the only one to possess more versatility than other programs. The interface element of CANDE is capable of modeling not only the pipe soil

interface but also the interface between two different soil types. This element has been tested and found to be numerically very stable and has been compared exceptionally well with analytical solutions [69]. Another reason for the selection of CANDE is that it has an excellent implementation of Dunacn and Selig model [65]. This soil model has been used and recommended by a number of researches for realistic simulations of buried pipelines [45–49], [69]. CANDE has also been used by researchers to model compaction loads during the backfilling [69].

CANDE provides a wide range of user offerings. At one extreme, the program can be efficiently used as a black box without any special knowledge of finite element mesh construction or even the design criteria for a particular class of pipe. Because CANDE has an option that only needs the definition of a few physical input parameters such as type of pipe material (corrugated steel, corrugated aluminum, reinforced concrete, plastic), pipe wall section properties, inside diameter, and depth of burial. CANDE will automatically generate a finite element mesh, provide a solution record of deformations and stress throughout the incremental loading schedule and the summarize results in terms of safety factors against various modes of distress depending upon the type of culvert. However, in this research it was not possible to use the automated finite element mesh options of CANDE because of the different trench inclination angles, and large sized problems which result in very coarse meshes that could affect the accuracy of the results. The level 3 option of the CANDE, which permits the user to develop their own finite element meshes to analyze and design nonstandard pipe shapes has been used in this study.

5.4 Upgrading of CANDE.

The last version of CANDE was released in 1989. Digital computers at that time were not efficient enough to handle large sized problems so the maximum number of elements that CANDE-89 can handle was limited to 300 elements. Moreover there was also a size limitation on number of boundary conditions and maximum bandwidth size that CANDE can handle. Since this study requires the use of large sized finite element meshes. It was essential to increase the number of element, boundary conditions, and the bandwidth size. After making the necessary modification in the subroutines BAKSUB, BEAMST, HEROIC, PRHERO, REDUCI, STIFNS, and STRESS CANDE was capable of handling problems up to 3000 elements. Moreover the double precision option was also invoked to increase the numerical accuracy. After making the necessary modification the program was recompiled and all the 11 problems, which come with the CANDE distribution media, were run on the modified version of CANDE, and results were compared with those reported in the CANDE manual. The results show an excellent comparison.

5.5 Mesh Generation and Finite Element Visualization

As indicated earlier that level 3 of the CANDE which supports the user finite element mesh generation, will be used. The procedure used in CANDE is quite tedious and cumbersome. Therefore it was decided to use a general purpose three dimensional finite element mesh generator and visualization software Finite Element Modeler and Postprocessor (FEMAP) [84]. FEMAP is currently a state of the art finite element conceptualiza-

tion and visualization commercial software available in the market. Various subroutines were programmed in the FEMAP macro language to create versatile meshes for use in this research. After the mesh generation from FEMAP, it was essential to write a translation program which can communicate between CANDE and FEMAP and can translate the meshes generated by FEMAP into CANDE input file format. Once the mesh generation and translation program are working properly another translation program was written to translate the CANDE output back to FEMAP. This was essential because visualization of the results decreases the time for post processing dramatically. The translation program for post processing is powerful enough to plot not only the stresses and deformations for every increment, but also the Duncan moduli and stress level flags for each construction increment. A sample figure from FEMAP showing Duncan moduli for a specific increment is shown in Fig. 5.1.

5.6 Data File Preparation

CANDE doesn't have the post processing capabilities of software of 90's. The program runs in a batch mode, and data file is a text file in the form of formatted FORTRAN fields. This makes the preparation of a single data file very cumbersome, especially in level 3 which contains a large number of input statements as complete mesh and other relevant information has to be defined in the data file. Moreover CANDE also doesn't have the provision that a large number of data files can be specified which CANDE can run one after another. Therefore, it was essential to automate the data file preparation and running a sequence of data files for different problems. VBA (Visual Basic for Applications) was

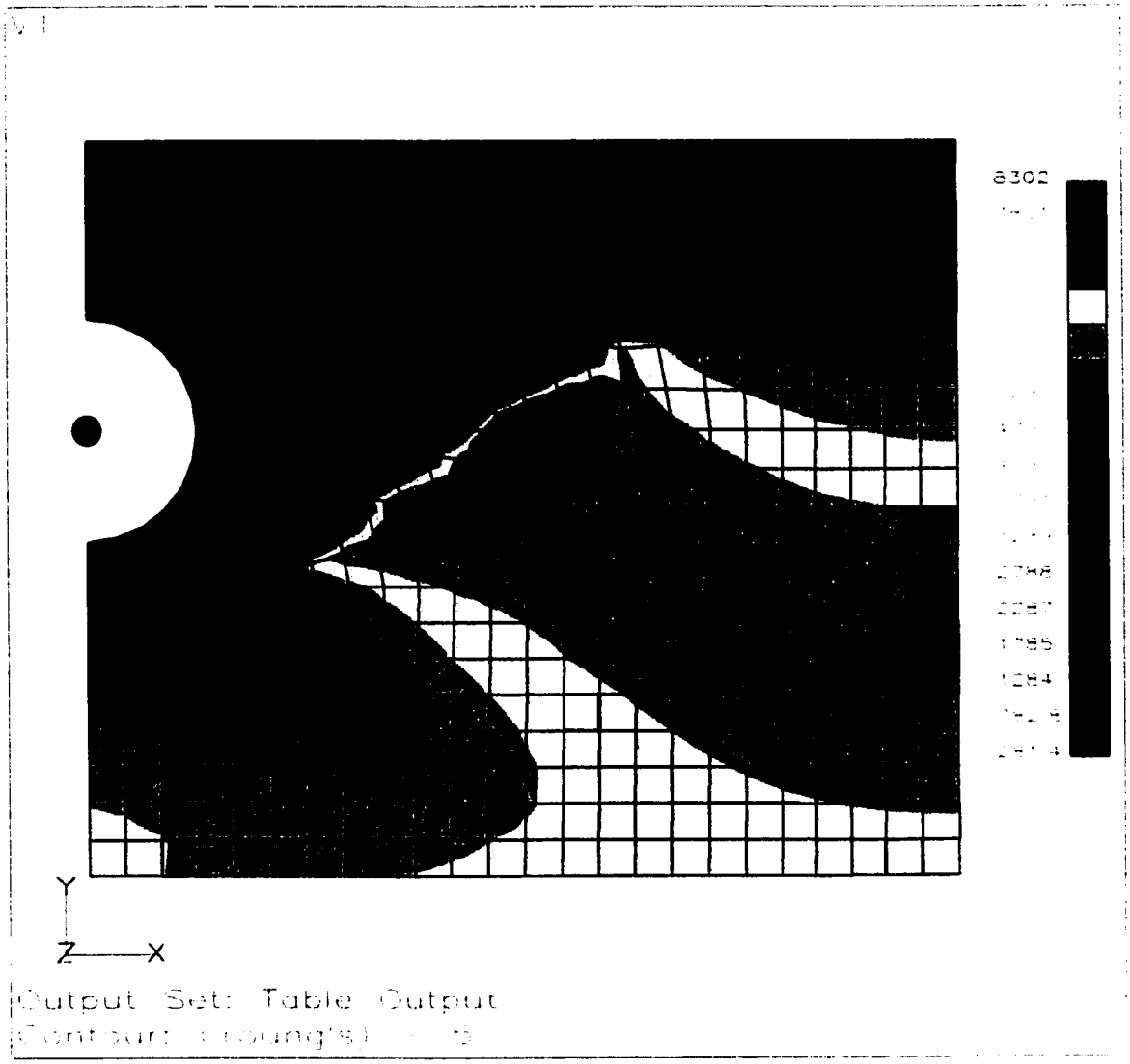

Fig. 5.1: Young's modulus plot from CANDE plotted on FEMAP

used in fulfilling this task. A program was made in VBA with Excel as host application. The programs has two modules. The first module is capable of generating data files while the second module is capable of running many user selected data files one after another and shutting down the computer after completion of the simulations A sample sheet of the program is shown in Fig. 5.2.

The first module of the program is capable of generating data files. The CANDE-FEMAP translation program mentioned in Section 5.5 was incorporated in this module so that mesh geometry and other relevant information can be automatically placed at the appropriate place in the input data file. All the user has to do is to give the name and location of the relevant FEMAP neutral file in column 4 of the sheet shown in Fig. 5.2. A large number of text files were made and placed at certain locations in the computer's hard drive. These text files contain various portions of the input file formatted in the required FORTRAN fields. The program selects the appropriate file based on the user selection and after making necessary modification produces a complete file. The program is capable of handling up to three different material zones in addition to the identification for pavement and interface material. The application of the internal pressure can be handled by the program provided that the user manually identifies the nodes connecting the pipe elements. The live load can be entered as pressure in the last column, with the location where it is applied and the construction increment number at which it should be activated entered in the preceding columns.

The second module of the program is capable of running a sequence of user specified data files one after another. There is no limitation on the number of files that can be run

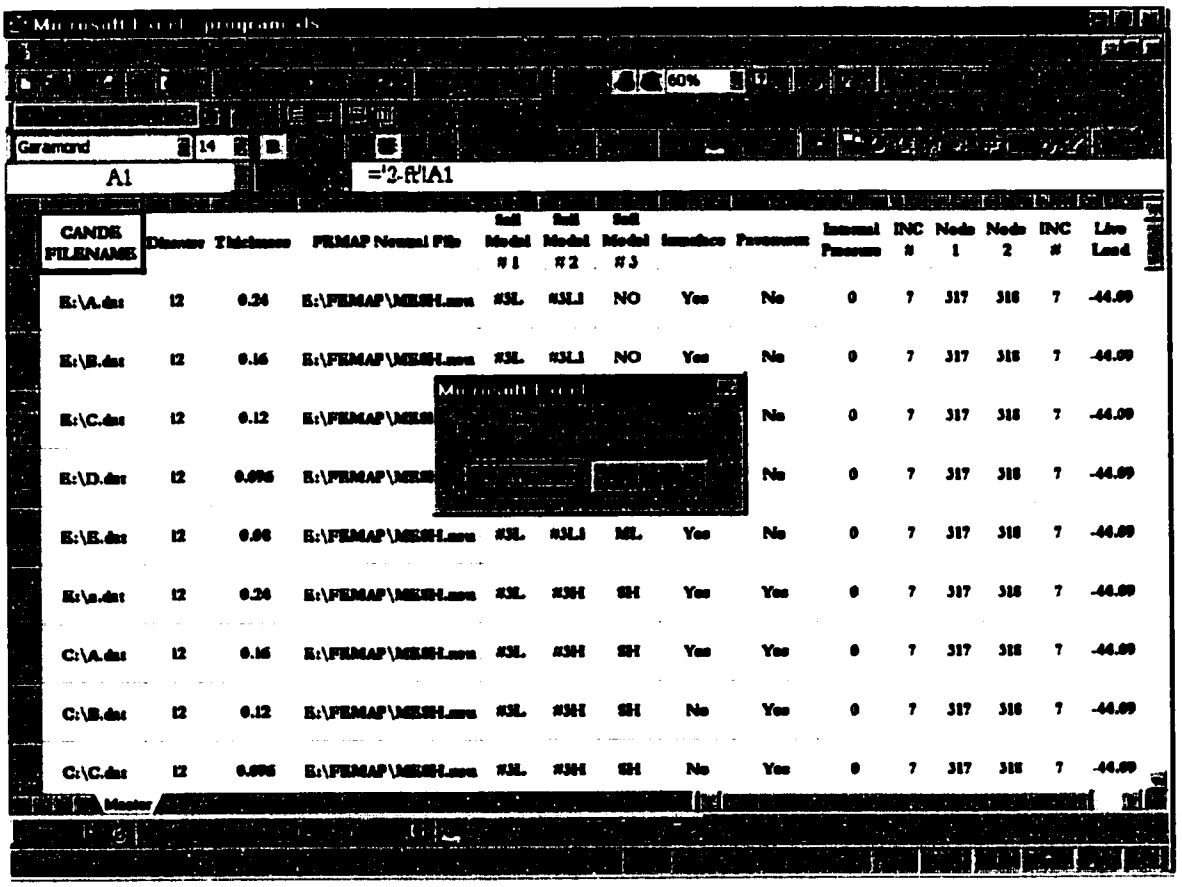

Fig. 5.2: Sample sheet from the input program

with this module. Moreover the module also has the capability of notifying the user after all the files have been run and doesn't want to shut down the computer.

5.7 Post Processing of Results

CANDE creates various output files in ASCII text format. One of the most important output files is the *filename.prn*, which contains the element responses and nodal values of stresses and deformations. The size of this file depends upon the problem size, options selected , and the number of construction increments. In general, the size of the output file is very large especially if there are large number of construction increments. The simulation of the sand overburden problem requires more than 60 construction increments, which usually results in output file containing the element responses which contains more than 6000 pages each containing at least 48 lines with single spacing on the standard A4 paper. Moreover the mesh size is not less than 2000 elements which makes retrieving the required output as looking for a needle in the haystack.

There are two more complications: first that CANDE doesn't report circumferential stresses but the thrust and the bending stresses separately; Also, the location of maximum circumferential stresses along the pipe periphery is also not reported. Therefore results from output file have to be processed to find the maximum circumferential stresses and their locations. Secondly, for the sand overburden problem stresses from all the increments (more than 60) are of interest and have to be retrieved from a single output file. For highway crossing problem, the results from the last two increments representing the complete dead load and live load are of interest and have to be retrieved from multiple files in a single shot.

Two separate programs were developed in VBA with Excel as the host application. A sample sheet for the two programs is shown in Fig. 5.3. The first program is capable of retrieving the results for more than 60 construction increments from a single output file and then analyzing the results for each construction increment and preparing two summary sheets. The summary sheets are shown in Figs. 5.4 and 5.5. In the first summary sheet shown in Fig. 5.4, the maximum tensile and compressive stresses together with their location on the pipe periphery as well as their fiber location is reported together with the maximum deflection and diameter change for the pipe. The second summary sheet reports the thrust, bending moment and associated stresses at the pipe locations of crown, springline and invert as shown in Fig. 5.5. In addition to all of the above, the following factors of safety (FOS) are also calculated in the summary sheets:

$$FOS_{Stress} = \frac{\sigma_{Maximum}}{\sigma_{Allowable}} * 100 \tag{5.1}$$

where,

FOS_{Stress} = factor of safety for maximum stress,

$\sigma_{Maximum}$ = maximum circumferential stress regardless of position and sign, and

$\sigma_{Allowable}$ = 0.72 SMYS = 43,200 lb/in^2(allowable stress according to API 5L).

$$FOS_{Deflection} = \frac{0.2D}{\Delta D} * 100 \tag{5.2}$$

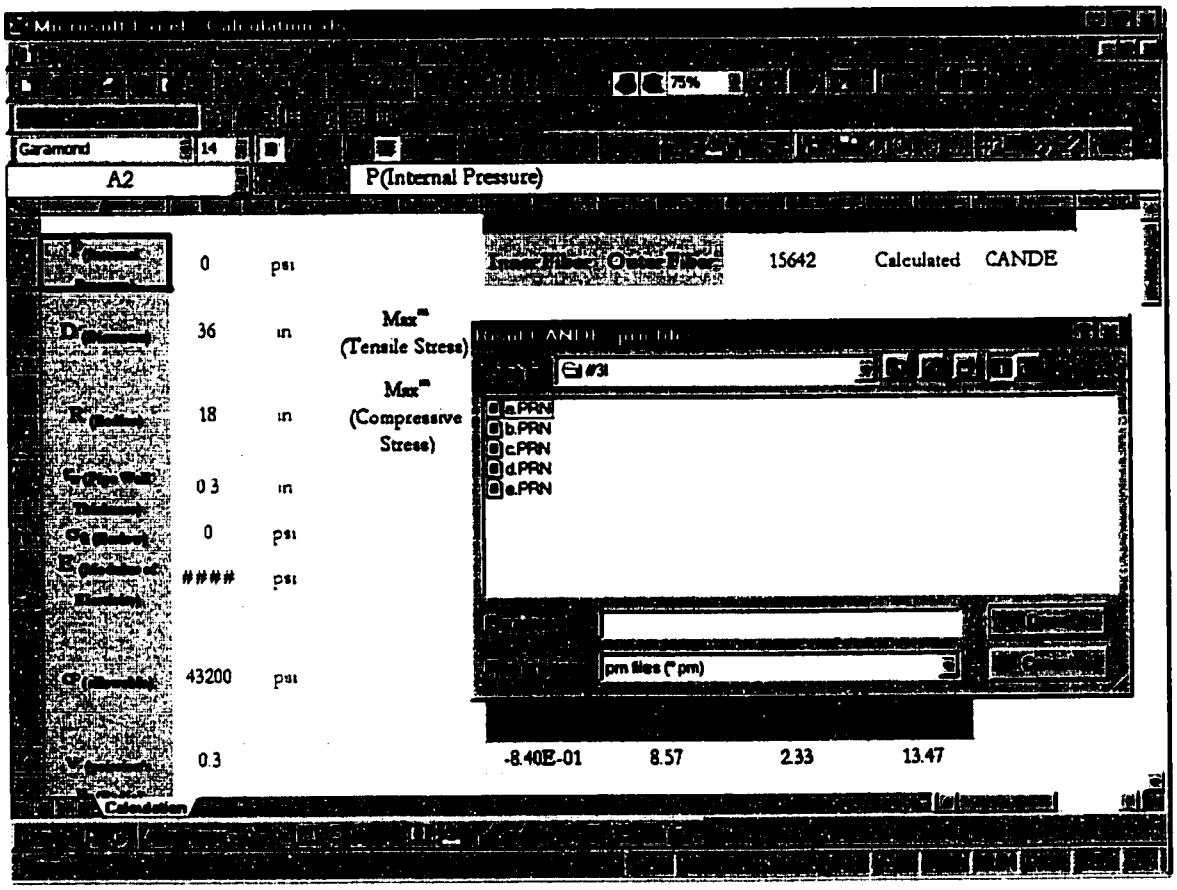

Fig. 5.3: A sample sheet from post processing program

Increment	Max" Inner Fiber Stress (psi)				Max" Outer Fiber Stress (psi)				Abs. Maxm Stress (psi)			FOS	Max" Defln.	Diam. Change	FOS
	Tnsl.	Angle	Comp.	Angle	Tnsl.	Angle	Comp.	Angle	Stress	Angle	Loca	(stress)	(in)	(in)	(Deflu.)
1	143.035	90	-171.64	0	166.36	0	-142.965	90	171.64	0	IN	251.6896	0.0251	-0.0016	1500
2	201.479	90	-248.66	0	243.34	0	-200.521	90	248.66	0	IN	173.7312	0.0279	-0.0026	923.0769
3	263.05	-90	-340.04	-14.9	329.96	-14.9	-276.95	-90	340.04	-14.9	IN	127.0439	0.0303	-0.003	800
4	1054.4	90	-1119.9	0	1020.1	0	-1105.6	90	1119.9	0	IN	38.57487	0.0553	-0.0132	181.8182
5	1628.6	90	-1712.9	0	1527.1	0	-1731.4	90	1731.4	90	OUT	24.95091	0.0761	-0.0203	118.2266
6	2152.6	90	-2255	0	1985	0	-2307.4	90	2307.4	90	OUT	18.72237	0.0959	-0.027	88.88889
7	2666	90	-2746	0	2394	0	-2874	90	2874	90	OUT	15.03132	0.114	-0.0332	72.28916
8	3191	90	-3207	0	2773	0	-3449	90	3449	90	OUT	12.52537	0.131	-0.0395	60.75949
9	3717	90	-3645	0	3135	0	-4023	90	4023	90	OUT	10.73826	0.147	-0.046	52.17391
10	4234	90	-4054	0	3466	0	-4586	90	4586	90	OUT	9.419974	0.161	-0.051	47.05882
11	4730	90	-4442	0	3778	0	-5130	90	5130	90	OUT	8.421053	0.175	-0.057	42.10526
12	5207	90	-4819	0	4081	0	-5653	90	5653	90	OUT	7.64196	0.189	-0.063	38.09524
13	5675	90	-5167	0	4353	0	-6165	90	6165	90	OUT	7.007299	0.201	-0.067	35.8209
14	6122	90	-5494	0	4611	-14.9	-6658	90	6658	90	OUT	6.488435	0.213	-0.072	33.33333
15	6559	90	-5814	-14.9	4886	-14.9	-7141	90	7141	90	OUT	6.049573	0.225	-0.078	30.76923
16	6976	90	-6149	-14.9	5151	-14.9	-7604	90	7604	90	OUT	5.68127	0.236	-0.082	29.26829
17	7383	90	-6474	-14.9	5406	-14.9	-8057	90	8057	90	OUT	5.361797	0.246	-0.086	27.90698
18	7781	90	-6789	15	5651	15	-8499	90	8499	90	OUT	5.082951	0.256	-0.09	26.66667
19	8158	90	-7104	15	5896	15	-8922	90	8922	90	OUT	4.8419e4	0.26e	-0.095	25.26316
20	8525	90	-7408	15	6132	15	-9335	90	9335	90	OUT	4.627745	0.27e	-0.099	24.24242
21	8882	90	-7713	15	6367	15	-9738	90	9738	90	OUT	4.436229	0.285	-0.103	23.30097
22	9230	90	-7997	15	6583	15	-10130	90	10130	90	OUT	4.264561	0.293	-0.106	22.64151
23	9527	90	-8282	15	6798	15	-10473	90	10473	90	OUT	4.124893	0.302	-0.11	21.81818
24	9904	90	-8546	15	6994	15	-10896	90	10896	90	OUT	3.964758	0.31	-0.114	21.05263
25	10182	90	-8810	15	7190	15	-11218	90	11218	90	OUT	3.850954	0.318	-0.117	20.51282
26	10559	90	-9075	15	7385	15	-11641	90	11641	90	OUT	3.711021	0.325	-0.12	20
27	10836	90	-9319	15	7561	15	-11964	90	11964	90	OUT	3.610832	0.333	-0.124	19.35484
28	11113	90	-9563	15	7737	15	-12287	90	12287	90	OUT	3.515911	0.34	-0.127	18.89764
29	11391	90	-9797	15	7903	15	-12609	90	12609	90	OUT	3.426124	0.347	-0.13	18.46154
30	11668	90	-10031	15	8069	15	-12932	90	12932	90	OUT	3.340551	0.353	-0.132	18.18182
31	11945	90	-10260	15	8220	15	-13255	90	13255	90	OUT	3.259147	0.36	-0.135	17.77778
32	12122	90	-10480	15	8380	15	-13478	90	13478	90	OUT	3.205223	0.366	-0.138	17.3913
33	12399	90	-10690	15	8530	15	-13801	90	13801	90	OUT	3.130208	0.372	-0.14	17.14286
34	12676	90	-10900	15	8660	15	-14124	90	14124	90	OUT	3.058624	0.378	-0.143	16.78322
35	12853	90	-11100	15	8800	15	-14347	90	14347	90	OUT	3.011082	0.384	-0.145	16.55172
36	13130	90	-11290	15	8910	15	-14670	90	14670	90	OUT	2.944785	0.39	-0.148	16.21622
37	13307	90	-11520	15	9080	15	-14893	90	14893	90	OUT	2.900692	0.395	-0.15	16
38	13584	90	-11650	15	9150	15	-15216	90	15216	90	OUT	2.839117	0.4	-0.152	15.78947
39	13760	90	-11890	15	9310	15	-15440	90	15440	90	OUT	2.797927	0.406	-0.155	15.48387
40	13937	90	-12020	15	9380	15	-15663	90	15663	90	OUT	2.758092	0.411	-0.157	15.28662
41	14214	90	-12260	15	9540	15	-15986	90	15986	90	OUT	2.702365	0.415	-0.159	15.09434
42	14391	90	-12390	15	9610	15	-16209	90	16209	90	OUT	2.665186	0.42	-0.161	14.90683
43	14567	90	-12630	15	9770	15	-16433	90	16433	90	OUT	2.628857	0.425	-0.163	14.72393
44	14744	90	-12760	15	9840	15	-16656	90	16656	90	OUT	2.59366	0.429	-0.165	14.54545
45	14920	90	-12890	15	9910	15	-16880	90	16880	90	OUT	2.559242	0.434	-0.167	14.37126
46	15100	90	-13130	15	10070	15	-17100	90	17100	90	OUT	2.526316	0.438	-0.169	14.20118
47	15270	90	-13260	15	10140	15	-17330	90	17330	90	OUT	2.492787	0.442	-0.17	14.11765
48	15450	90	-13400	15	10200	15	-17550	90	17550	90	OUT	2.461538	0.446	-0.172	13.95349
49	15630	90	-13530	15	10270	15	-17770	90	17770	90	OUT	2.431064	0.45	-0.174	13.7931
50	15800	90	-13670	15	10330	15	-18000	90	18000	90	OUT	2.4	0.454	-0.175	13.71429
51	15880	90	-13900	15	10500	15	-18120	90	18120	90	OUT	2.384106	0.458	-0.177	13.55932
52	16050	90	-14040	15	10560	15	-18350	90	18350	90	OUT	2.354223	0.461	-0.178	13.48315
53	16230	90	-14170	15	10630	15	-18570	90	18570	90	OUT	2.326333	0.465	-0.18	13.33333
54	16310	90	-14310	15	10690	15	-18690	90	18690	90	OUT	2.311396	0.469	-0.182	13.18681
55	16480	90	-14440	15	10760	15	-18920	90	18920	90	OUT	2.283298	0.472	-0.183	13.11475
56	16660	90	-14580	15	10820	15	-19140	90	19140	90	OUT	2.257053	0.475	-0.184	13.04348
57	16740	90	-14710	15	10890	15	-19260	90	19260	90	OUT	2.242991	0.479	-0.186	12.90323
58	16910	90	-14850	15	10950	15	-19490	90	19490	90	OUT	2.216521	0.482	-0.187	12.83422
59	16990	90	-14980	15	11020	15	-19610	90	19610	90	OUT	2.202958	0.485	-0.188	12.76596
60	17160	90	-15120	15	11080	15	-19840	90	19840	90	OUT	2.177419	0.488	-0.19	12.63158
61	17240	90	-15250	15	11150	15	-19960	90	19960	90	OUT	2.164329	0.491	-0.191	12.56545
62	17320	90	-15390	15	11210	15	-20080	90	20080	90	OUT	2.151394	0.494	-0.192	12.5
63	17490	90	-15520	15	11280	15	-20310	90	20310	90	OUT	2.127031	0.497	-0.194	12.37113

Fig. 5.4: First summary sheet for the sand overburden results

Increment	Crown				Springline				Invert			
	Thrust	Bending Moment	Outer Fibber	Inner Fibber	Thrust	Bending Moment	Outer Fibber	Inner Fibber	Thrust	Bending Moment	Outer Fibber	Inner Fibber
1	0.00415	0.344	-142.965	143.035	-0.317	-0.406	1xx.36	-171.64	-0.595	0.108	-49.86	39.94
2	0.0575	0.483	-200.521	201.479	-0.319	-0.591	243.34	-248.66	-0.628	0.42	-180.23	169.77
3	-0.0502	0.404	-168.418	167.582	-0.52x	-0.72x	298.61	-307.39	-0.834	0.649	-276.95	2x3.05
4	-3.07	2.59	-1105.6	1054.4	-3.99	-2.4x	1020.1	-1119.9	-3.56	2.54	-1089.7	1010.3
5	-6.17	4.02	-1731.4	1628.x	-11.1	-1.88	1527.1	-1712.9	-6.67	3.96	-1705.5	1594.5
6	-9.29	5.36	-2307.4	2152.x	-1x.2	-x.08	1984	-2255	-9.8	5.31	-2291.7	2128.3
7	-12.4	6.65	-2874	2xxx	-21.2	-x.17	2394	-2746	-12.9	6.61	-2857	2643
8	-15.4	7.97	-3449	3191	-2x	-7.17	2773	-3207	-15.9	7.88	-3412	3148
9	-18.3	9.3	-4023	3717	-30.x	-8.13	3135	-3645	-18.7	9.12	-3956	3644
10	-21.2	10.6	-4586	4234	-35.2	-9.03	34xx	-4054	-21.5	10.3	-4479	4121
11	-23.9	11.8	-5130	4730	-39.8	-9.88	3778	-4442	-24.3	11.5	-4982	4578
12	-26.7	13	-5653	5207	-44.3	-10.7	4081	-4819	-27	12.6	-5475	5025
13	-29.4	14.2	-6165	5675	-48.8	-11.4	4353	-5167	-29.7	13.7	-5948	5452
14	-32.1	15.3	-6658	6122	-53.2	-12.1	4600	-5494	-32.5	14.7	-6401	5859
15	-34.9	16.4	-7141	6559	-57.6	-12.8	4850	-5810	-35.2	15.7	-6843	6257
16	-37.6	17.5	-7604	697x	-62	-13.4	5073	-6107	-37.9	16.7	-7276	6644
17	-40.4	18.5	-8057	7383	-66.4	-14	5287	-6393	-40.7	17.6	-7689	7011
18	-43.1	19.5	-8499	7781	-7C.7	-14.6	5481	-6659	-43.4	18.5	-8091	7369
19	-45.9	20.5	-8922	8158	-75	-15.1	5665	-6915	-46.1	19.4	-8474	770x
20	-48.6	21.4	-9335	8525	-79.2	-15.x	583C	-7150	-48.8	20.3	-8856	8044
21	-51.3	22.3	-9738	8882	-83.5	-16.1	5994	-738x	-51.5	21.1	-9219	8361
22	-54	23.2	-10130	9230	-87.7	-16.5	6149	-7611	-54.2	21.9	-9581	8679
23	-56.8	24.1	-10473	9527	-92	-16.9	6284	-7816	-56.9	22.7	-9924	8976
24	-59.5	24.9	-10896	9904	-9x.2	-17.3	6418	-8022	-59.6	23.4	-10256	9264
25	-62.2	25.7	-11218	10182	-100	-17.7	6533	-8207	-62.2	24.2	-10619	9581
26	-64.9	26.5	-11641	10559	-105	-18.1	6648	-8392	-64.9	24.9	-10941	9859
27	-67.7	27.3	-11964	1083x	-109	-18.4	6753	-8567	-67.x	25.6	-111x4	1003x
28	-70.4	28	-12287	11113	-113	-18.7	6848	-8732	-70.3	26.2	-11486	10314
29	-73.1	28.8	-12609	11391	-117	-19	6943	-8897	-73	26.9	-11809	10591
30	-75.9	29.5	-12932	11668	-121	-19.3	7030	-9050	-75.7	27.5	-12131	10869
31	-78.6	30.2	-13255	11945	-12x	-19.x	7100	-9200	-78.4	28.1	-12354	1104x
32	-81.4	30.8	-13478	12122	-130	-19.8	7180	-9340	-81.2	28.7	-1267x	11324
33	-84.1	31.5	-13801	12399	-134	-20.1	7240	-9480	-83.9	29.3	-12899	11501
34	-86.9	32.1	-14124	12676	-138	-20.3	7310	-9610	-86.6	29.9	-13122	11678
35	-89.6	32.7	-14347	12853	-142	-20.5	73x0	-9740	-89.3	30.4	-13444	11956
36	-92.4	33.3	-14x70	13130	-147	-20.7	7410	-9850	-92	30.9	-13xx7	12133
37	-95.2	33.9	-14893	13307	-151	-20.9	7450	-9970	-94.8	31.5	-13890	1231C
38	-98	34.5	-1521x	13584	-155	-21.1	7500	-10080	-97.5	32	-14113	12487
39	-101	35.1	-15440	13760	-159	-21.3	7530	-10190	-100	32.5	-14336	12664
40	-104	35.6	-15663	13937	-163	-21.4	757C	-10290	-103	32.9	-14558	12842
41	-106	36.2	-15986	14214	-168	-21.6	7600	-10400	-106	33.4	-14781	13019
42	-109	36.7	-16209	14391	-172	-21.7	763C	-10490	-109	33.9	-15004	1319x
43	-112	37.2	-16433	14567	-176	-21.9	7650	-10590	-111	34.3	-15227	13373
44	-115	37.7	-16656	14744	-180	-22	7670	-10670	-114	34.7	-15450	13550
45	-118	38.2	-16880	14920	-185	-22.1	7680	-10760	-117	35.2	-15673	13727
46	-120	38.7	-17100	15100	-189	-22.3	7700	-10840	-120	35.6	-15797	13803
47	-123	39.1	-17330	15270	-193	-22.4	7710	-10930	-122	36	-16020	1398C
48	-126	39.6	-17550	15450	-197	-22.5	7720	-11000	-125	36.4	-16240	14160
49	-129	40	-17770	15630	-202	-22.6	7720	-11080	-128	36.8	-16370	14230
50	-132	40.4	-18000	15800	-206	-22.7	7720	-11160	-131	37.1	-16590	14410
51	-135	40.9	-18120	15880	-210	-22.8	773C	-11230	-134	37.5	-16710	14490
52	-137	41.3	-18350	16050	-214	-22.8	7720	-11300	-136	37.8	-16940	14660
53	-140	41.7	-18570	16230	-219	-22.9	7730	-11370	-139	38.2	-17060	14740
54	-143	42.1	-18690	16310	-223	-23	7720	-11440	-142	38.5	-17280	14920
55	-146	42.5	-18920	1x480	-227	-23	7710	-11490	-145	38.9	-17410	14990
56	-149	42.9	-19140	16660	-231	-23.1	7700	-11560	-148	39.2	-17530	15070
57	-152	43.2	-19260	16740	-236	-23.2	7690	-11610	-150	39.5	-17750	15250
58	-155	43.6	-19490	16910	-240	-23.2	768C	-11680	-153	39.8	-17880	1532C
59	-158	44	-19610	16990	-244	-23.3	7x6C	-11740	-156	40.1	-18000	15400
60	-160	44.3	-19840	17160	-249	-23.3	7650	-11790	-159	40.4	-18120	15480
61	-163	44.7	-19960	17240	-253	-23.4	7620	-11840	-162	40.7	-18350	15650
62	-166	45	-20080	17320	-257	-23.4	7610	-11890	-165	41	-18470	15730
63	-169	45.3	-20310	17490	-261	-23.4	759C	-11950	-167	41.3	-18600	15800

Fig. 5.5: Second summary sheet for the sand overburden results

where,

$FOS_{Deflection}$ = factor of safety for deflection,

D = diameter of the pipe, and

ΔD = change in diameter of the pipe.

The maximum circumferential stress in the pipe is always compressive, and it does not occur at the same location. The location of the maximum stress may change when the depth of cover, H, is changed. So, it is decided to consider the maximum circumferential stress regardless of its sign and location along the pipe's periphery. This is named the *Absolute Maximum Stress.*

The change in the diameter is calculated by subtracting the Y-deflections at the pipe crown and invert, and is reported along with its factor of safety mentioned above.

The second program for post processing was made for analyzing the results for the highway crossing problem. The program is capable of retrieving the values form multiple files for the last two construction increments as these two construction increments contain stresses due to dead load and dead plus live load. Like the first program, this one retrieves the values from the output file, and after making the necessary calculations reports the results in the summary sheets. The summary sheets for this program are shown in Figs. 5.6 a & b. The summary sheets are identical to the summary sheets for the output of sand overburden problem, in addition to reporting the file name for which the results have been transferred.

Filename	Increment	Max^m Inner Fiber Stress (psi)				Max^m Outer Fiber Stress (psi)				Abs. Maxm Stress (psi)			FOS	Max^m Defln.	Diam. Change	FOS
		Tnsl.	Angle	Comp.	Angle	Tnsl.	Angle	Comp.	Angle	Stress	Angle	Locn.	(stress)	(in)	(in)	(Defln.)
a	12	5310.2	-90	-5226	0	4854	0	-5469.8	-90	5469.8	-90	OUT	7.897912	1.67	-0.16	75
	13	5809.4	-90	-5777	0	5383	0	-5970.6	-90	5970.6	-90	OUT	7.235454	1.72	-0.18	66.66667
b	12	7652	-90	-7561	0	7039	0	-7908	-90	7908	-90	OUT	5.462822	1.75	-0.34	35.29412
	13	8329	-90	-8336	0	7784	0	-8591	-90	8591	-90	OUT	5.028518	1.81	-0.37	32.43243
c	12	8225	-90	-8093	0	7427	0	-8595	-90	8595	-90	OUT	5.026178	1.84	-0.49	24.4898
	13	9254	90	-8841	0	8139	0	-9626	90	9626	90	OUT	4.487845	1.92	-0.55	21.81818
d	12	8382	90	-7736	0	6924	0	-8858	90	8858	90	OUT	4.876947	1.92	-0.61	19.67213
	13	9508	90	-8378	0	7522	0	-10012	90	10012	90	OUT	4.314822	2	-0.67	17.91045
e	12	8273	90	-7281	0	6319	0	-8867	90	8867	90	OUT	4.871997	1.99	-0.71	16.90141
	13	9403	90	-7826	0	6814	0	-10037	90	10037	90	OUT	4.304075	2.08	-0.78	15.38462

(a) Summary of stresses and deformation

Filename	Increment	Crown				Springline				Invert			
		Thrust	Bending Moment	Outer Fiber	Inner Fiber	Thrust	Bending Moment	Outer Fiber	Inner Fiber	Thrust	Bending Moment	Outer Fiber	Inner Fiber
a	12	-79.9	1140	-4796.5	4663.5	-225	-1210	4854	-5226	-95.8	1290	-5469.8	5310.2
	13	-80.6	1290	-5427.2	5292.8	-236	-1340	5383	-5777	-96.7	1410	-5970.6	5809.4
b	12	-94.1	771	-7348	7112	-209	-779	7039	-7561	-103	830	-7908	7652
	13	-96.8	873	-8301	8059	-221	-860	7784	-8336	-105	902	-8591	8329
c	12	-106	501	-8517	8163	-200	-465	7427	-8093	-111	505	-8595	8225
	13	-112	567	-9626	9254	-211	-509	8139	-8841	-115	544	-9261	8879
d	12	-114	331	-8858	8382	-195	-281	6924	-7736	-116	316	-8472	7988
	13	-121	375	-10012	9508	-205	-305	7522	-8378	-120	339	-9080	8580
e	12	-119	229	-8867	8273	-192	-181	6319	-7281	-119	208	-8107	7513
	13	-127	259	-10037	9403	-203	-195	6814	-7826	-123	222	-8647	8033

(a) Summary for pipe response at crown, springline, and invert

Fig. 5.6: Summary sheets for highway crossing problem

5.8 Validation and Comparison

Although CANDE has been used extensively by so many researches, it was essential to check its capabilities in representing the buried pipeline behavior. Moreover, it was also essential to make comparison of CANDE results with other finite element programs to insure its numerical accuracy.

5.8.1 Modeling of Arching

The capability of CANDE to simulate the arching effect was verified by analyzing the behavior of two pipes having the same diameter but different thickness and stiffness. The flexible pipe has a Young's modulus of 1×10^6 psi and a wall thickness of 0.25 inch while the rigid pipe has a Young's modulus of 29×10^6 psi and a wall thickness of 6 inch. Both pipes have an outer diameter of 48 inches. The trench type of installation was used for both pipes with the same depth of cover and width of trench. Fig. 5.7 shows a sketch of one of the problems solved with CANDE. The distribution of vertical stress in the soil at the crown level for flexible and rigid pipes is shown in Figs. 5.8 and 5.9 respectively. The results from CANDE clearly show that in case of rigid pipe the stresses in the soil just above the pipe crown level decrease as we move away from the center of the pipe. This is a clear indication of the phenomena of negative arching in which the load carried by pipe is more than the sum of the overburden soil pressure. Similarly for the flexible pipe it is clear from Fig. 5.8 that as we move towards the pipe the stress reduces, which is a clear indication of the phenomena of positive arching. This clearly indicate that CANDE is capable of modeling soil arching in soil structure interaction problems.

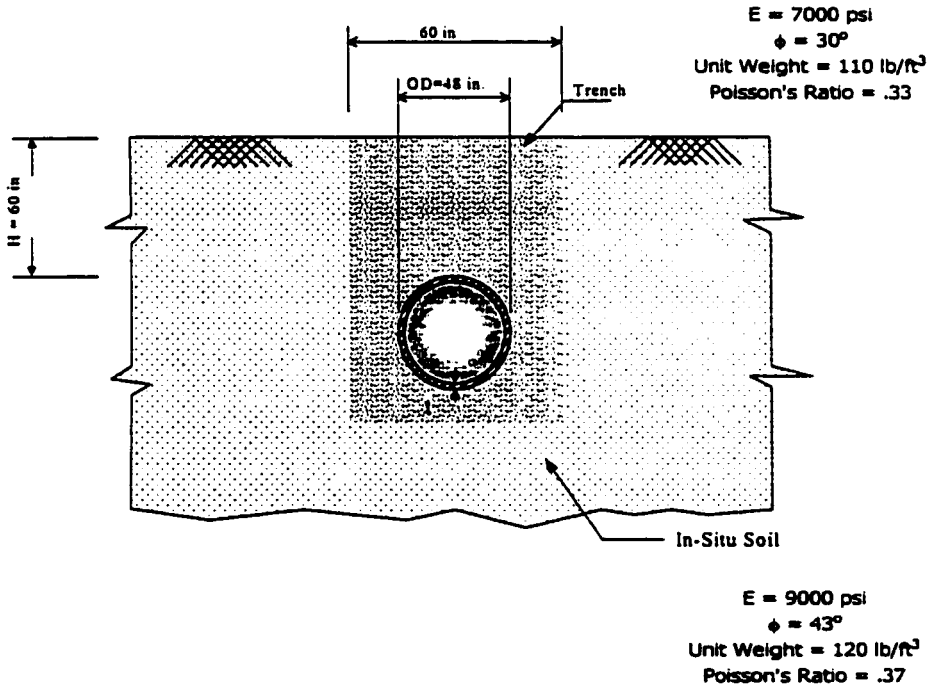

Fig. 5.7: Soil and pipe properties

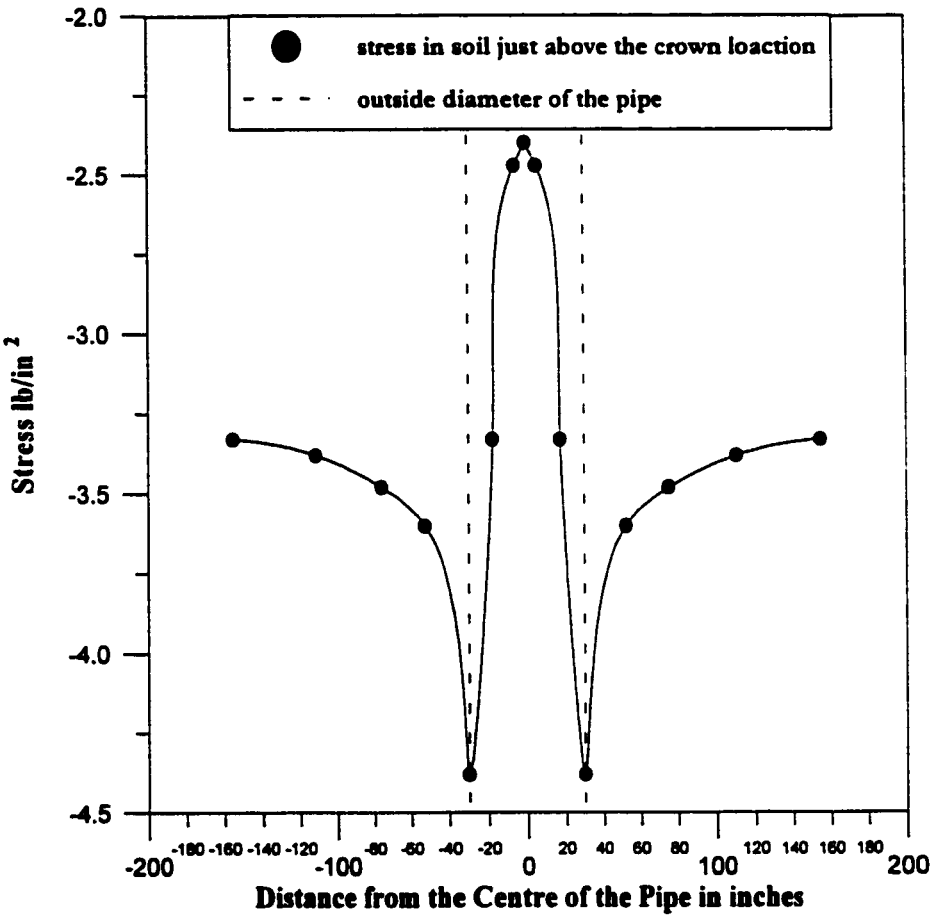

Fig. 5.8: Arching effect for flexible pipe

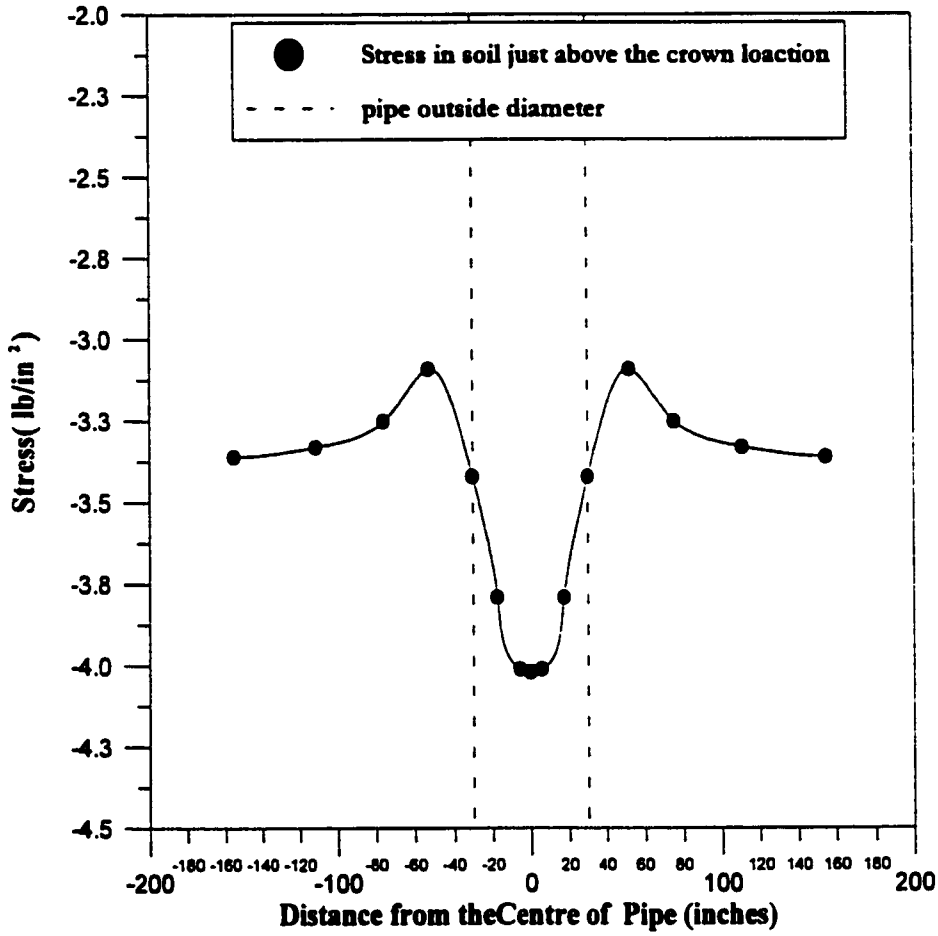

Fig. 5.9: Arching effect for rigid pipe

5.8.2 Comparison of CANDE and SMAP-3D

To check the results of CANDE software, which is a plain strain 2-D program.. a comparison between the performance of CANDE and SMAP 3-D has been conducted. The diameter of the selected pipe is 36 inches, and the D/t ratios of 50, 75, 100, 125, and 150 have been considered. A mesh of 492 elements is created in FEMAP and is later translated to CANDE input by means of the translation program. The pipe is modeled by 24 beam elements and the soil by 468 quadrilateral elements. The mesh is developed in such a way that the top six inches of the soil is assigned a different material number than the other soil. This enables the use of the upper six inches as a pavement layer. The depth of the soil cover is fixed to 24 inches. The finite element mesh used in the CANDE analysis is shown in Fig. 5.10.

A total of seventy runs were executed. Out of the 70 runs, thirty-five runs were carried out using CANDE and the rest using SMAP-3D. In the thirty-five runs by CANDE, for the first twenty runs the soil modulus was kept constant at 500 psi and the soil modulus for the top six inches was varied from 500 to 500, 000 psi to simulate the no-pavement and various pavement conditions. For the last 15 runs, the soil modulus of the soil was changed to 5000 psi, and the modulus of the top six inches was varied from 5000 to 500, 000 psi. Details of the runs are shown in Table 5.1.

The same mesh was then modified for SMAP-3D. The mesh was extruded in the third dimension with a unit thickness. The beam elements were replaced by an equal number of shell elements and the quadrilateral soil elements were replaced by 3-D continuum elements. The resulting 3-D SMAP-3D model is shown in Fig. 5.11.

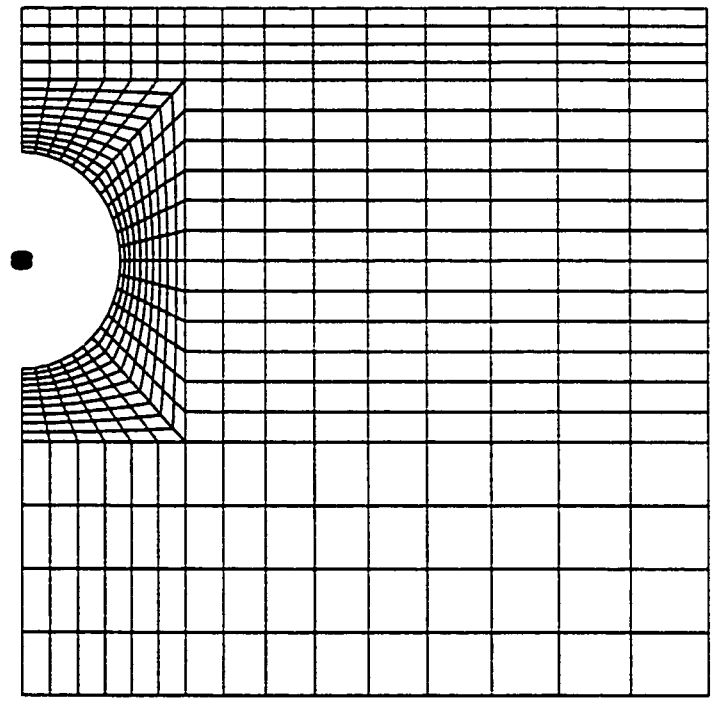

Fig. 5.10: Finite element mesh used in the CANDE analysis

TABLE 5.1: Details of finite element runs

Run no	D/t	t	SoilModulus(psi)	PavementModulus (psi)
1	50	.72	500	500
2	50	.72	500	5000
3	50	.72	500	50000
4	50	.72	500	500000
5	50	.72	5000	5000
6	50	.72	5000	50000
7	50	.72	5000	500000
8	75	.48	500	500
9	75	.48	500	5000
10	75	.48	500	50000
11	75	.48	500	500000
12	75	.48	5000	5000
13	75	.48	5000	50000
14	75	.48	5000	500000
15	100	.36	500	500
16	100	.36	500	5000
17	100	.36	500	50000
18	100	.36	500	500000
19	100	.36	5000	5000
20	100	.36	5000	50000
21	100	.36	5000	500000
22	125	.288	500	500
23	125	.288	500	5000
24	125	.288	500	50000
25	125	.288	500	500000
26	125	.288	5000	5000
27	125	.288	5000	50000
28	125	.288	5000	500000
29	150	.24	500	500
30	150	.24	500	5000
31	150	.24	500	50000
32	150	.24	500	500000
33	150	.24	5000	5000
34	150	.24	5000	50000
35	150	.24	5000	500000

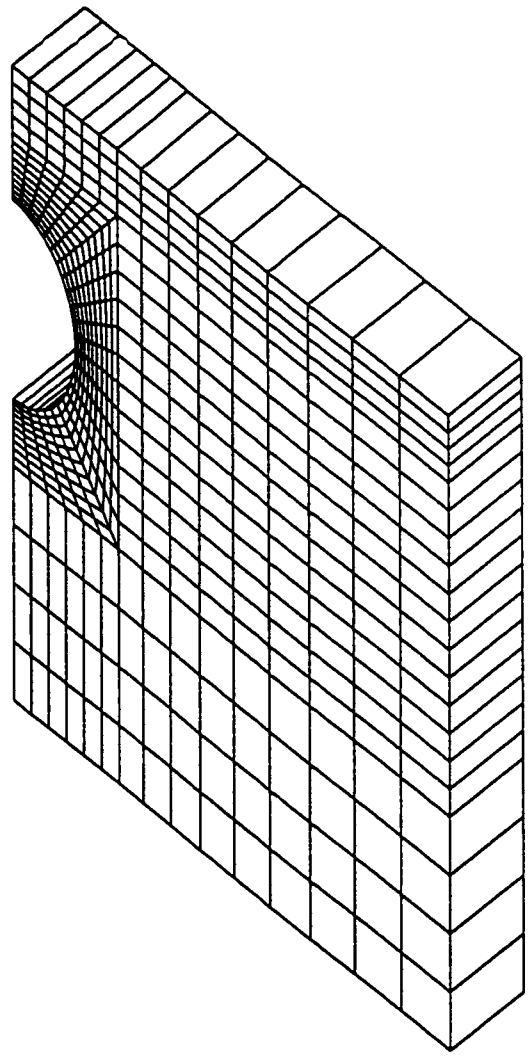

Fig. 5.11: Finite element mesh used in SMAP-3D analysis

This mesh is locked in the third dimension to simulate the plane-strain conditions to be consistent with the CANDE model. Another thirty-five simulations were run using the SMAP-3D program. The same parameters, already stated in Table 5.1, were used.

The vertical pipe deflection predicted by the two programs was comapred. The Y-deflection was selected because it is the primary output from the finite element analyses. The results are shown in Figs. 5.12 to 5.18. These figures show the percent difference in the Y-deflection at all positions along the pipe's periphery. The percent difference in the Y-deflection is defined as:

$$\Delta\% = \frac{(\Delta SMAP-3D) - (\Delta CANDE)}{\{\Delta SMAP-3D)} * 100 \qquad (5.3)$$

where

$\Delta\%$ = percent difference inY-deflection predicted by the two software programs,

$\Delta SMAP-3D$ = Y-deflection predicted by SMAP-3D, and

$\Delta CANDE$ = Y-deflection predicted by CANDE.

The figures indicate an excellent agreement between the predictions of the two programs. The percent difference the Y-deflections is within $\pm$ 1.5 % for most cases; however, a difference up to $\pm$5.0% was observed for certain cases, which is still with in the tolerable range.

The Figs. 5.19 and 5.20 show the percent difference, (δ) between the absolute maxi-

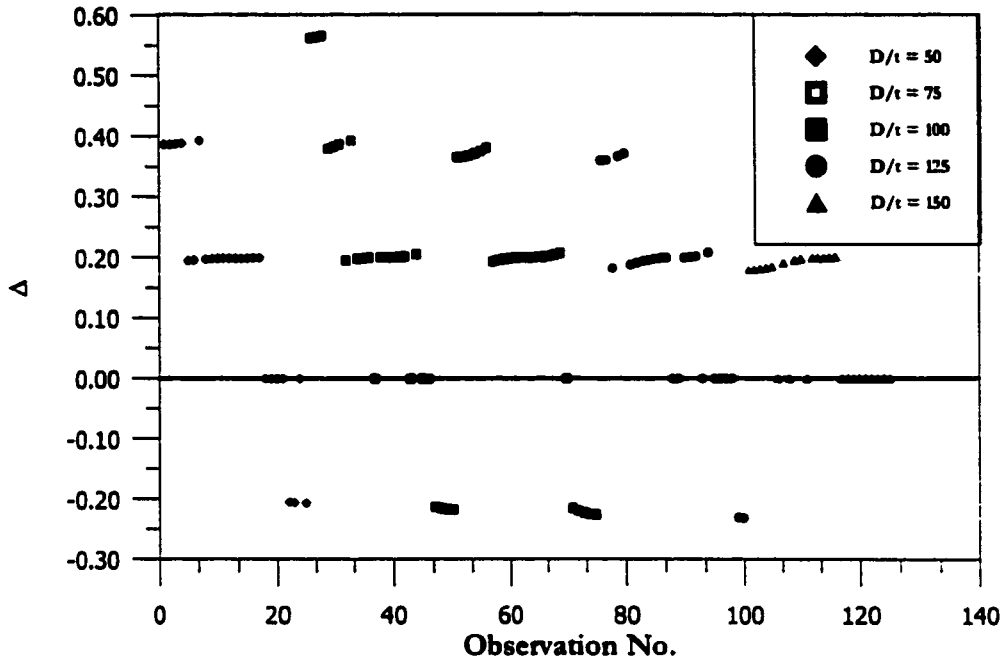

(a) Dead Load only

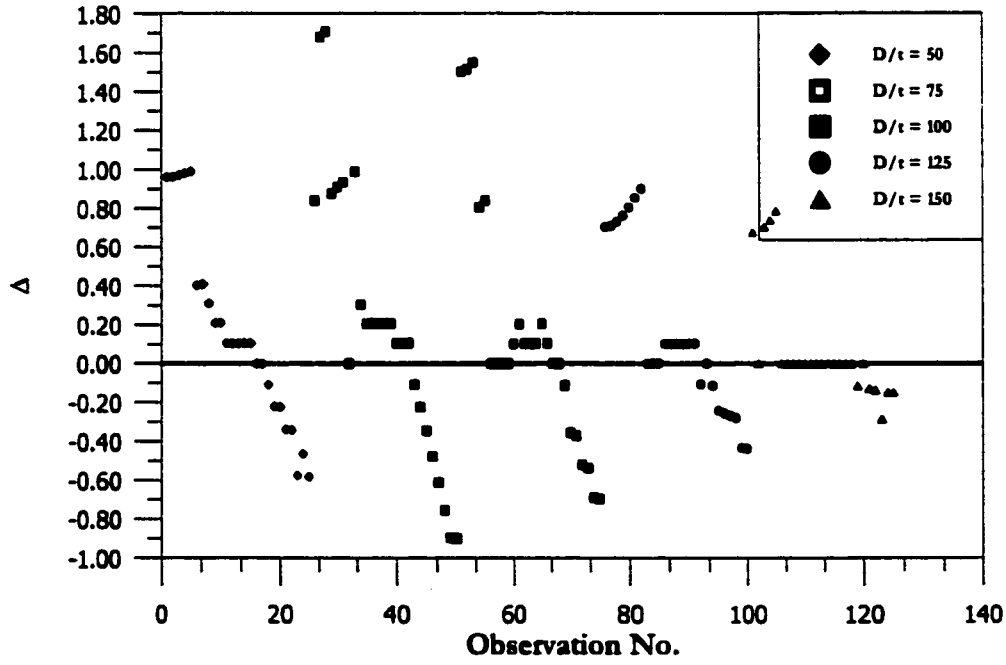

(b) Dead plus live load

Fig. 5.12: Comparison for soil modulus 500 psi and pavement stiffness 500 psi

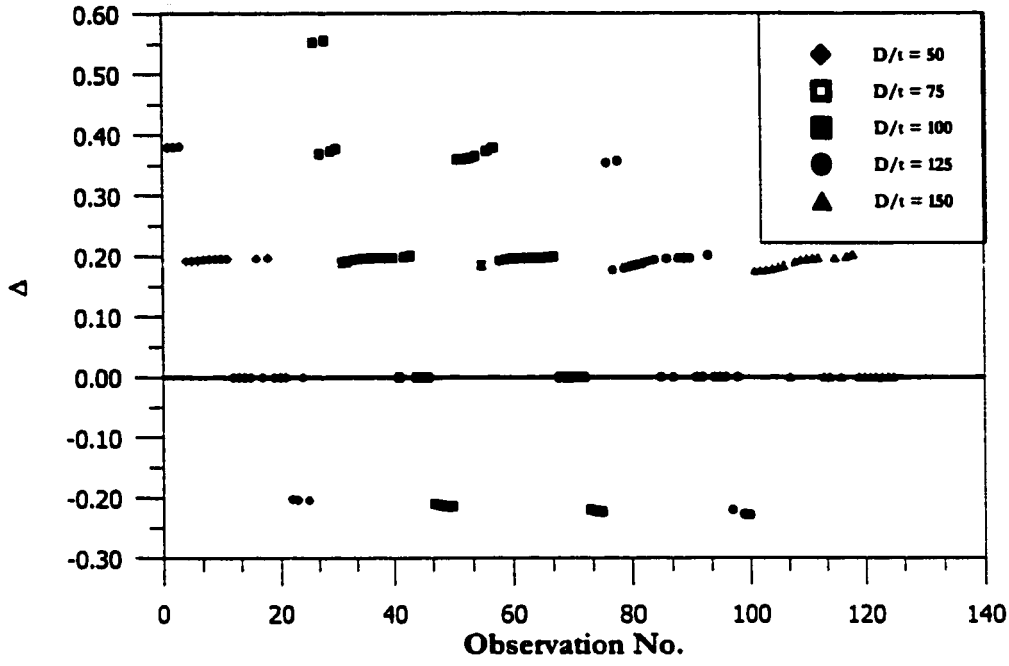

(a) Dead load only

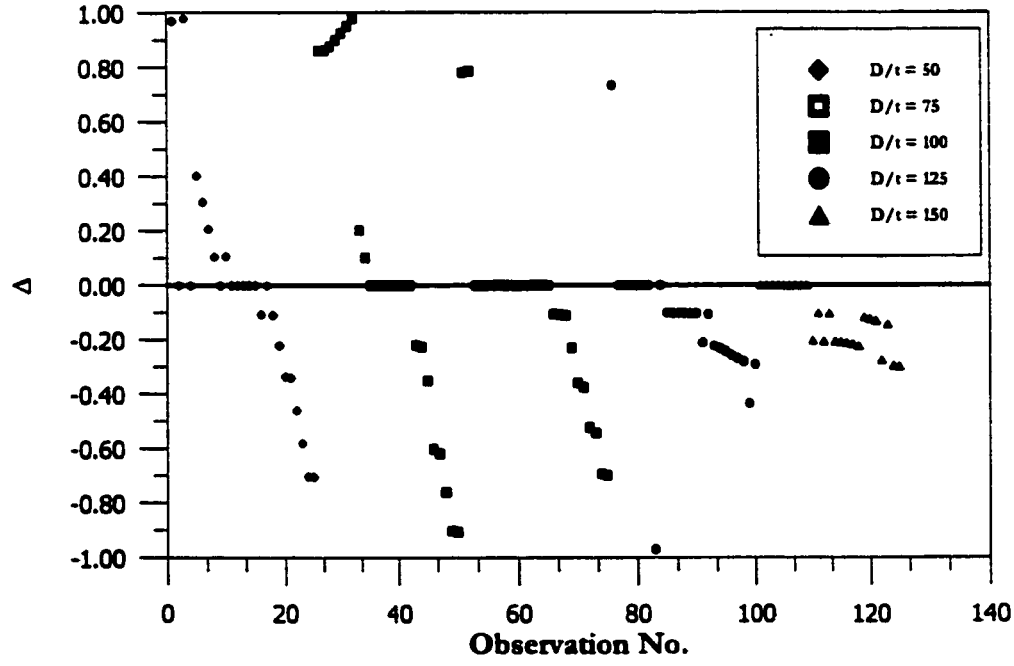

(b) Dead plus live load

Fig. 5.13: Comparison for soil modulus 500 psi and pavement stiffness 5000 psi

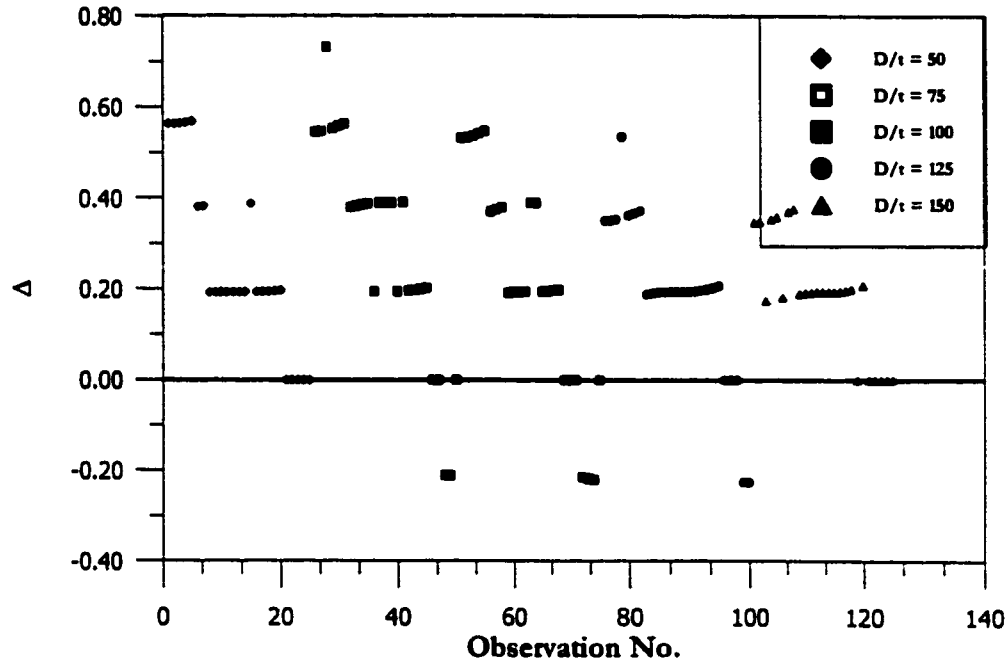

(a) Dead load only

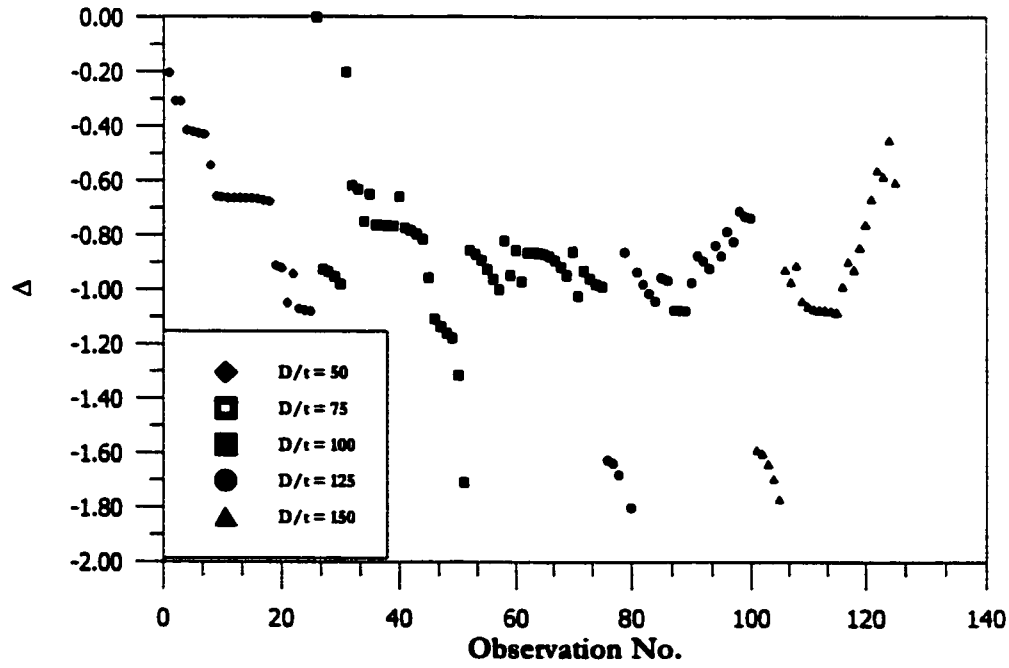

(b) Dead plus live load

Fig. 5.14: Comparison for soil modulus 500 psi and pavement stiffness 50000 psi

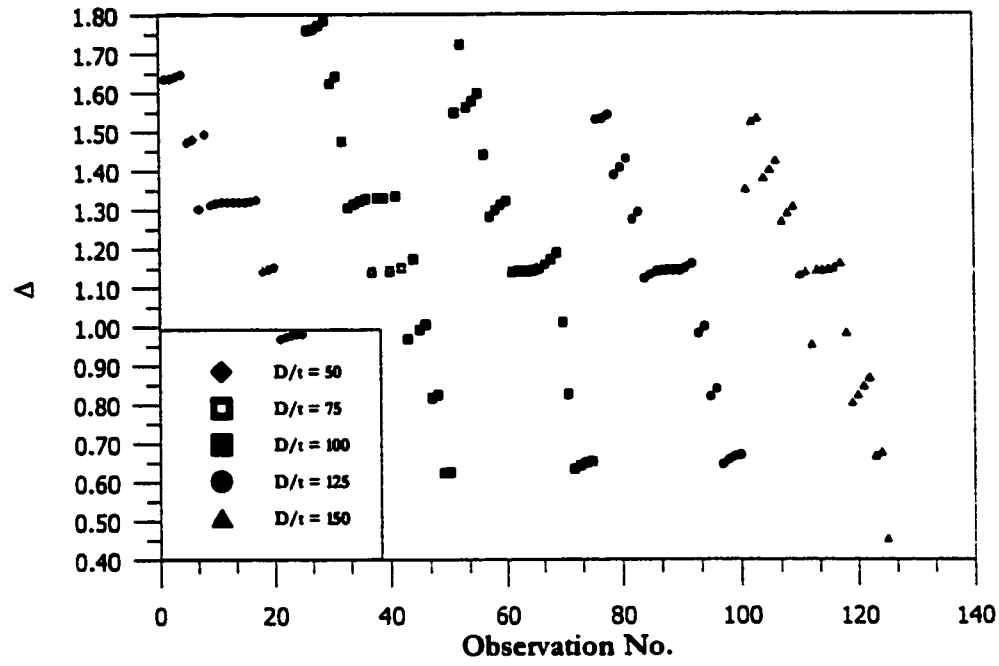

(a) Dead load only

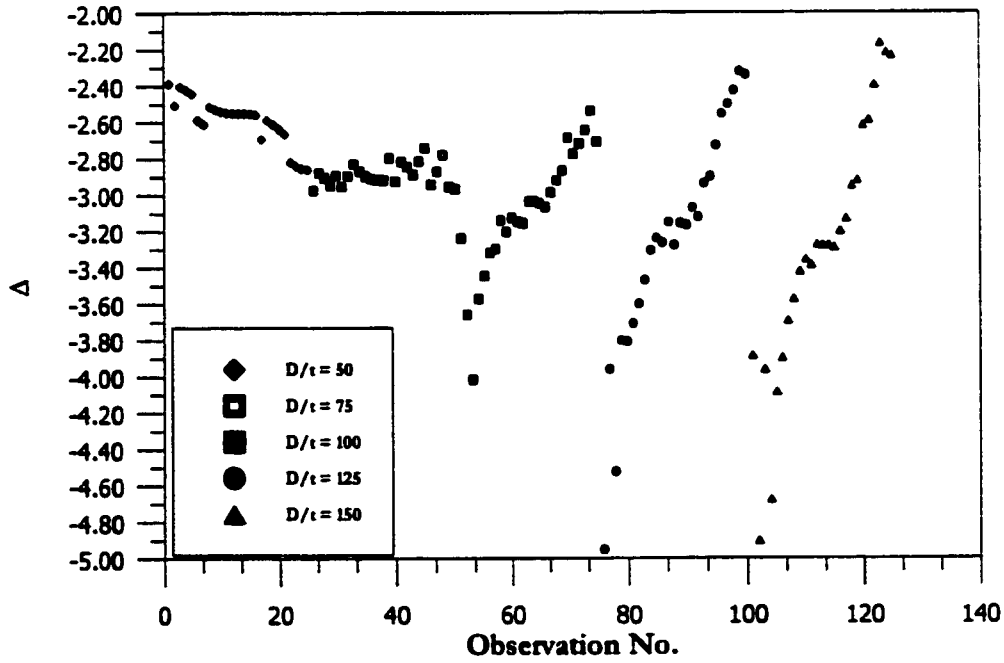

(b) Dead plus live load

Fig. 5.15: Comparison for soil modulus 500 psi and pavement stiffness 500000 psi

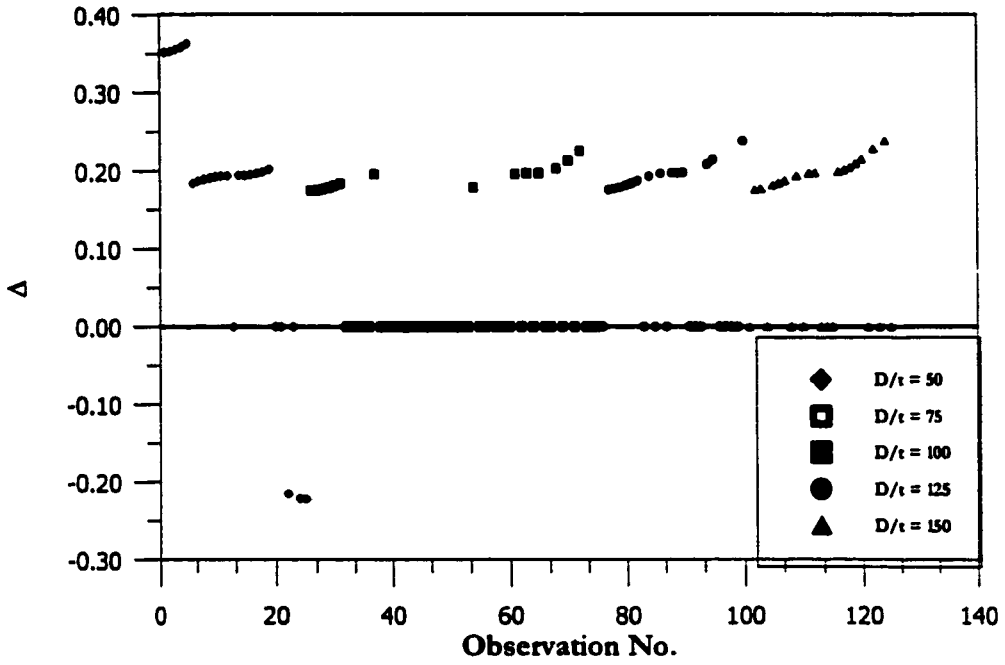

(a) Dead load only

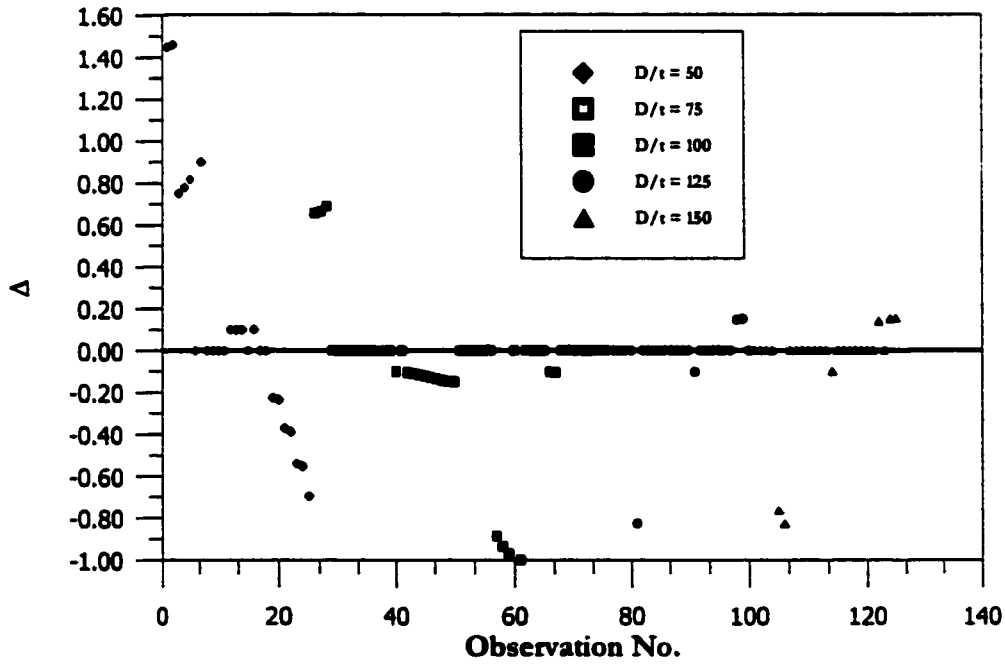

(b) Dead plus live load

Fig. 5.16: Comparison for soil modulus 5000 psi and pavement stiffness 5000 psi

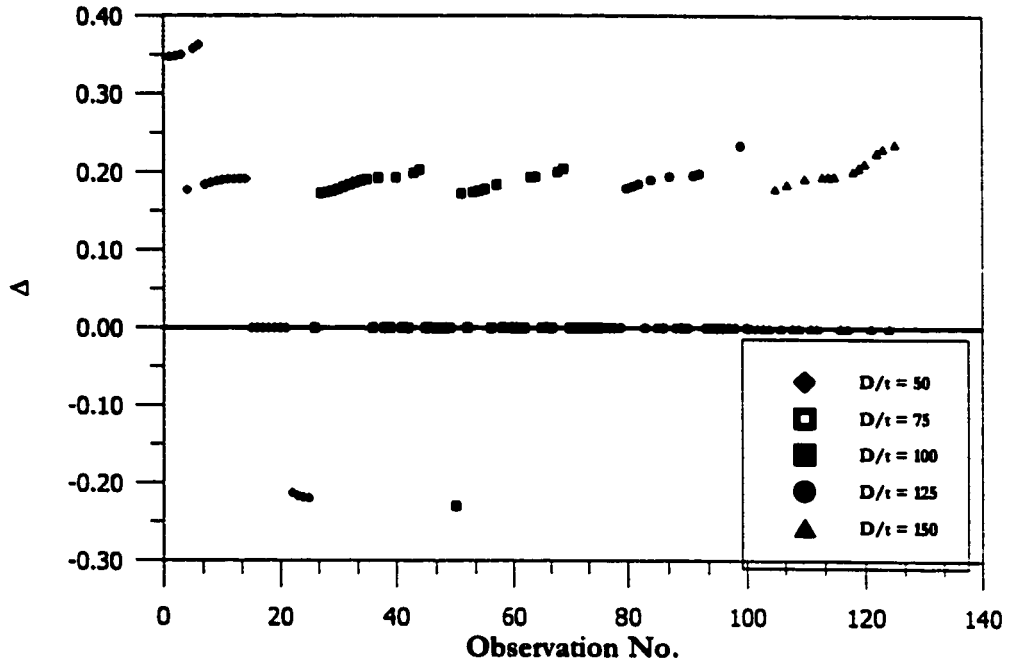

(a) Dead load only

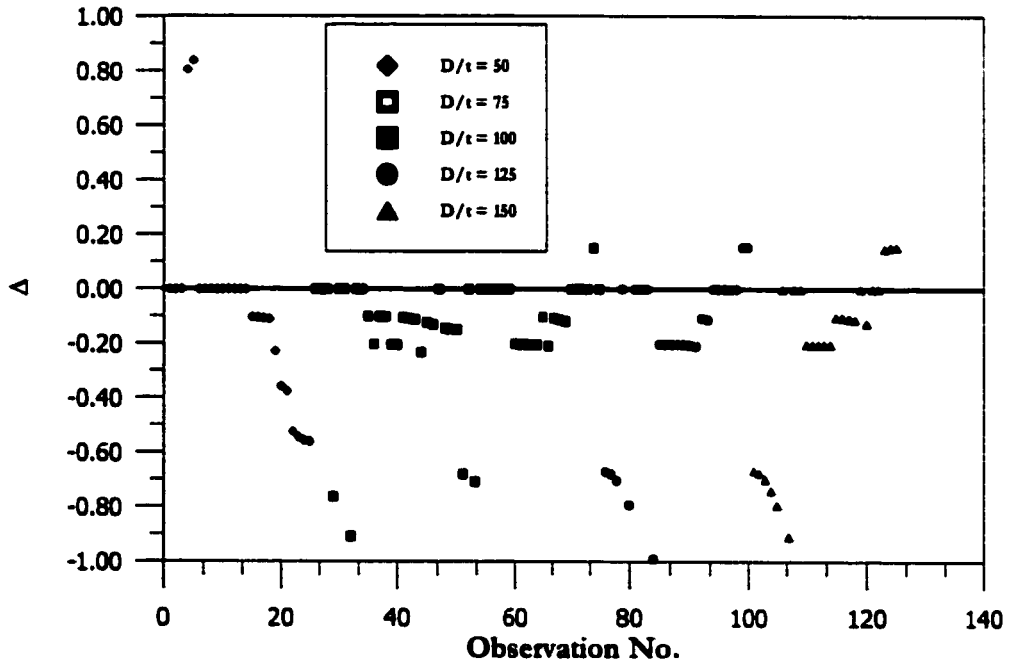

(b) Dead plus live load

Fig. 5.17: Comparison for soil modulus 5000 psi and pavement stiffness 50000 psi

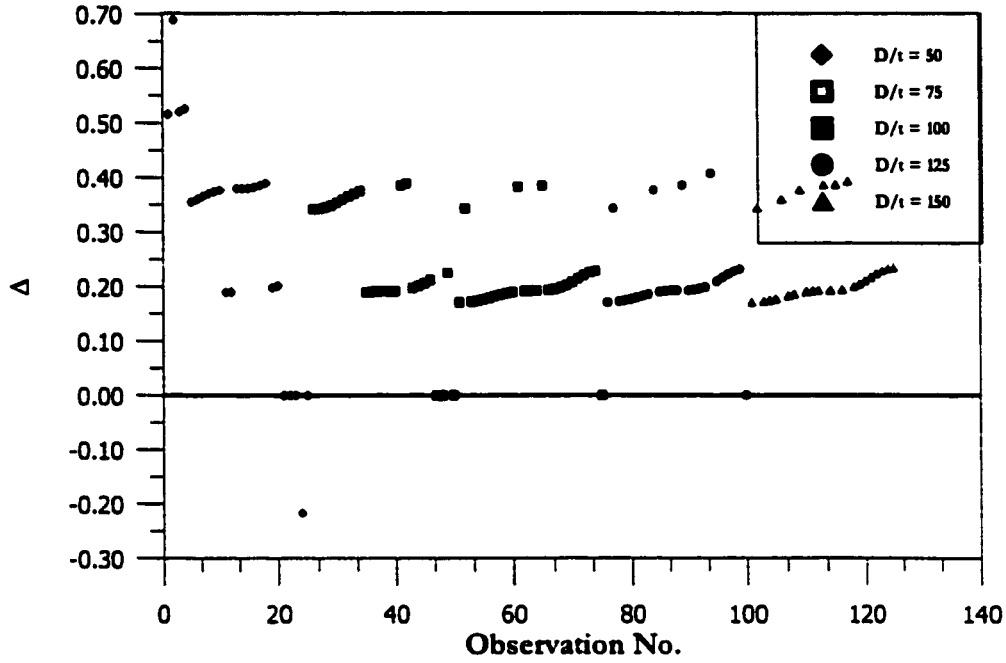

(a) Dead load only

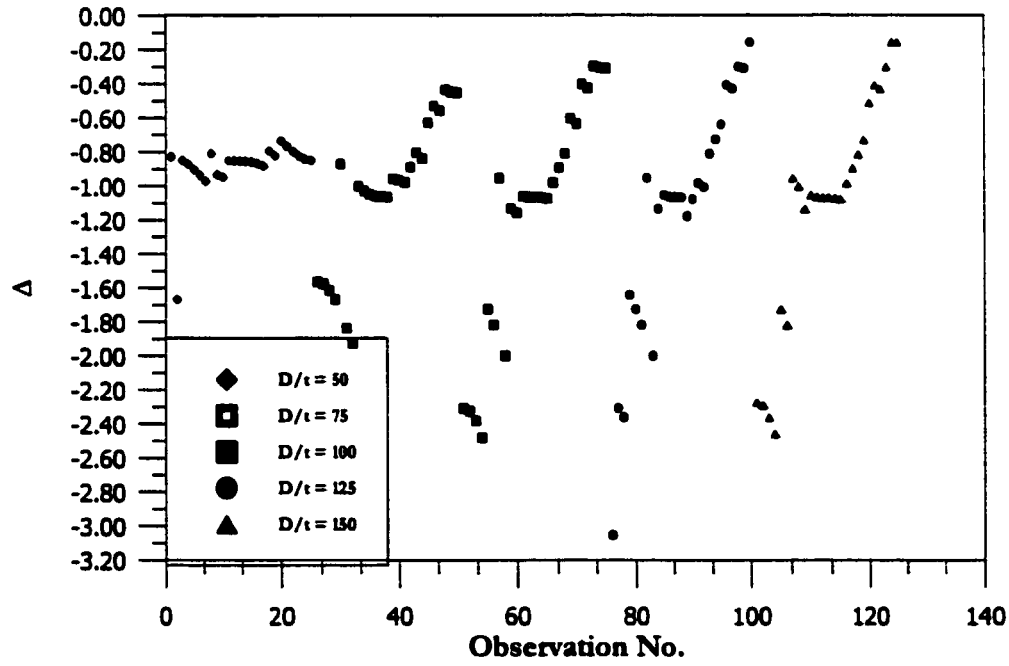

(b) Dead plus live load

Fig. 5.18: Comparison for soil modulus 5000 psi and pavement stiffness 500000 psi

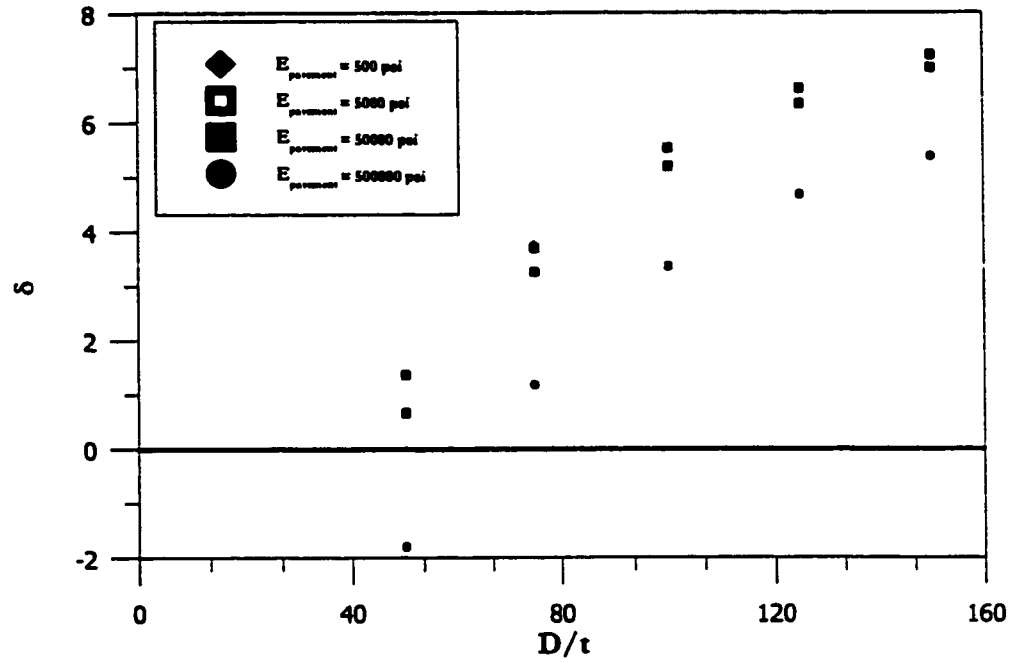

(a) Dead Load only

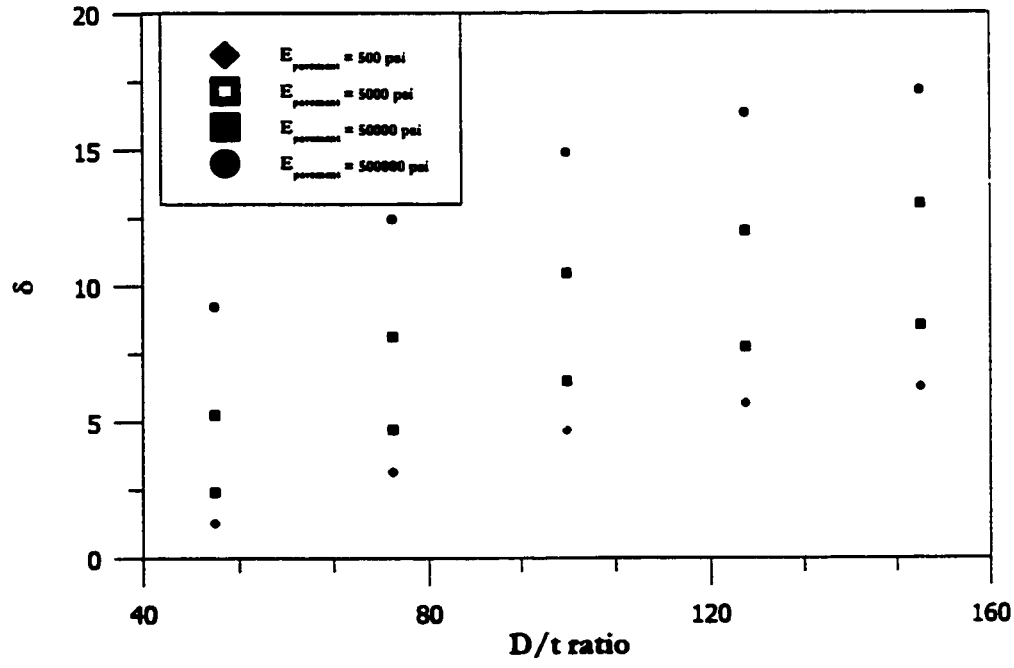

(b) Dead plus live load

Fig. 5.19: Comparison of stress for soil modulus 500 psi and various pavement stiffness

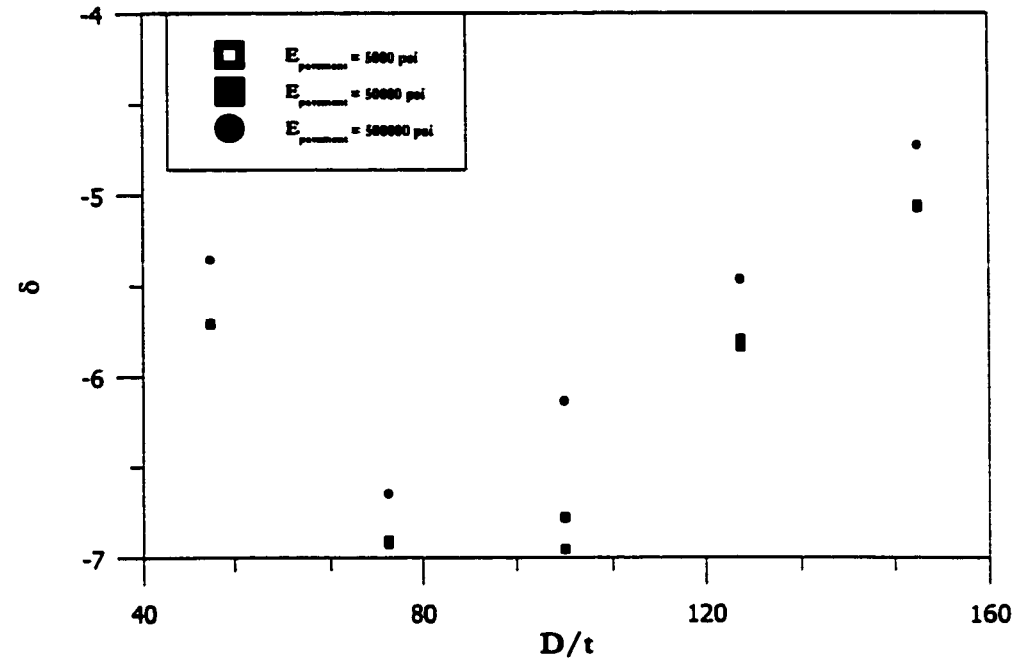

(a) Dead Load only

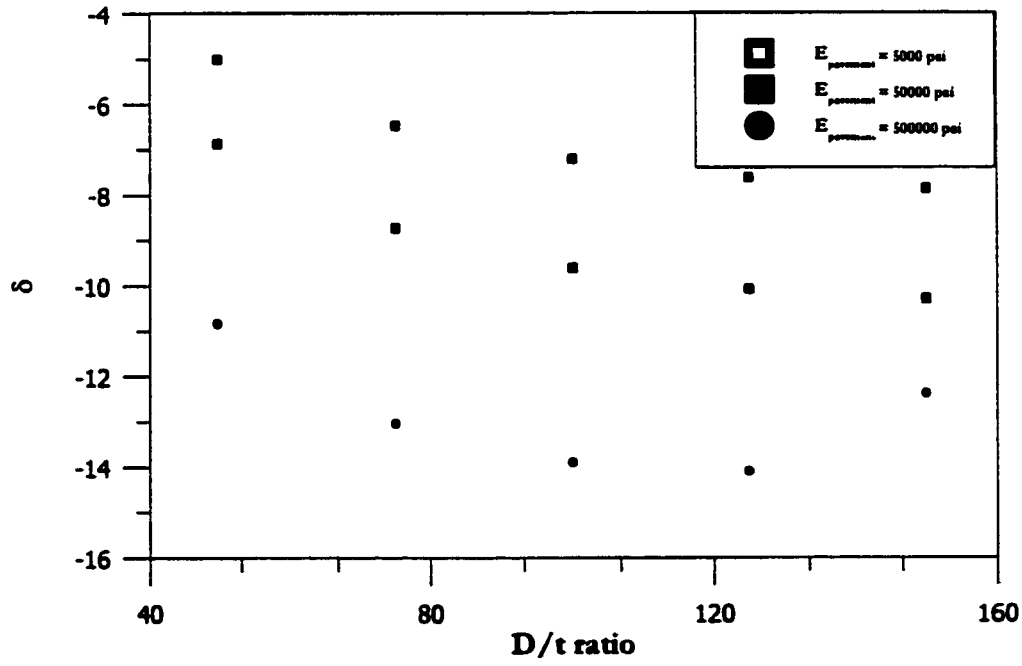

(b) Dead plus live load

Fig. 5.20: Comparison of stress for soil modulus 5000 psi and various pavement stiffness

mum stresses predicted by the two software.

$$\delta\% = \frac{\sigma_{Smap-3D} - \sigma_{CANDE}}{\sigma_{Smap-3D}} * 100\% \tag{5.4}$$

where

$\delta\%$ = percent difference in the absolute maximum stress predicted by the two software programs,

$\sigma_{Smap-3D}$ = absolute maximum stress predicted by SMAP-3D, and

σ_{CANDE} = absolute maximum stress predicted by CANDE.

The results again show a good agreement between the prediction of the two software. The difference for most cases was within ±10 %. However, for a few cases, a difference of 17 % was noted. This is an acceptable result because the stresses are a secondary results, and the two elements used to model the pipe are quite different (beam vs. shell). This does not fully justify the shortcoming of CANDE to predict accurate results for large D/t ratios. Nevertheless, it can be concluded that CANDE can handle D/t ratios within the range of 50 to 150 with a good accuracy.

CHAPTER 6

INITIAL PARAMETRIC STUDY

6.1 Introduction

Since the present scope of this research involves a large number of finite element simulations, it is necessary to carry out an initial parametric study to identify the influence of various parameters. Important factors regarding the mesh geometries and material zone identifications are identified and their influence on the results is established, as reported in this chapter.

6.2 Trench Inclination Angle

To install a buried pipeline, the soil is usually excavated, thus forming a trench. The finite element simulations to model the sand overburden are based on a trench-type installation configuration. The trench-type installation has an inherent assumption that the trench is relatively narrow and dug in passive or undisturbed soil with the sides of the trench inclined at 90°. However, in the field, the trench sides are not always inclined at 90°, espe-

cially when the pipe is to be laid in the cohesionless soil. In the case of sand, the sides of the trench are normally inclined at an angle that is equal to the angle of repose. Moreover, the trench-fill material is usually loose sand without much compaction, so the interaction of the trench-fill sand with the native soil may also be a major factor influencing the results. The various material zones in a typical ninety-degree trench-type installation are shown in Fig. 6.1. The trench model shown in that figure clearly identifies the four material zones within the trench, assuming the trench side to be at 90°.

The angle of inclination of the trench can influence the pipe-soil system in a number of ways, e.g., an angle smaller than 90° means that the trench soil is extended into the zone considered as native soil in the 90° model. Also, the soil elements in the native soil region just next to the trench fill are in different states of stress in the two cases, because the native soil elements are activated in the first construction increment, as shown in Fig. 6.2. Thus, to study the effect of the trench inclination angle, it becomes necessary to run some simulations with varying angles of inclination for different types of soil material. The task becomes easier because of the subroutines programmed in FEMAP mentioned in Section 5.5.

In order to understand the physics of the problem and use an angle of inclination that simulates the field conditions accurately, it is decided to look into the dead load and live load separately. As mentioned earlier, the aim is to simulate a trench, so a construction increment sequence representing the field installation procedure is made in the runs, as illustrated in Fig. 6.2. First, the problem of dead load is considered. Three types of meshes are developed with 90°, 60°, and 35° angles for the trench inclination. These meshes along

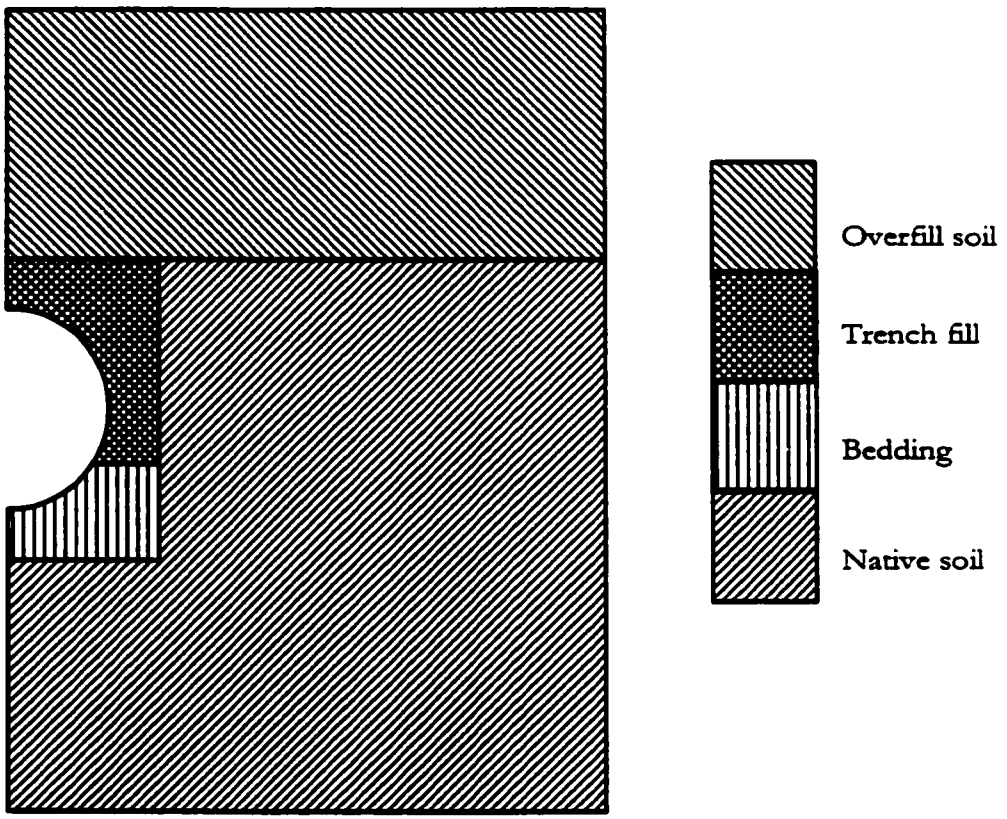

Fig. 6.1: Typical trench type installation

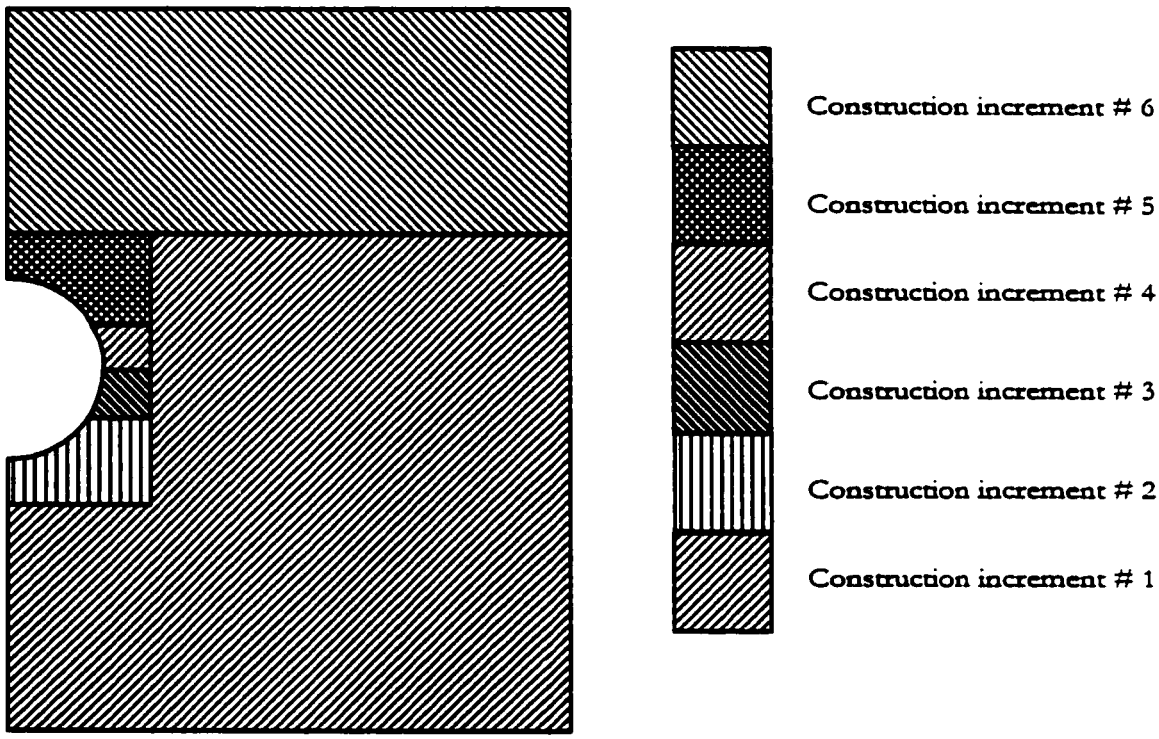

Fig. 6.2: Construction increments for trench type installation

with the material zone identification are shown in Figs. 6.3 to 6.5. A typical pipe diameter of 36 in. is selected for these analyses, with D/t ratios equal to 50 and 150. These D/t ratios represent the maximum and minimum values. The dead load is increased by placing the cover depth in increments. Ten increments are used for a cover depth of 10 ft., one foot each. The trench fill and the overfill are always sand at low density to be consistent with the field condition, but the native soil is different for each of the runs. The four soil types used in the analysis as native soils are: sand at low density, sand at high density, marl at low density, and sabkha at high density, for reasons discussed in another section.

The results of the dead load analyses are shown in Figs. 6.6 to 6.7. The results for sand at low density as the native soil, trench fill, and overfill is shown in Fig. 6.6. These results show an increase in the stress with an increasing angle of inclination for the trench. Since this is the case of homogenous soil conditions, the difference cannot be attributed to the extension of the trench fill soil into the native soil but rather due to the fact that the native soil, that is activated in the first construction increment, may not be stable with a higher angle of inclination because of the unsupported length. This is confirmed by the fact that when an embankment type of construction increment is used, all three trench inclination angles predict exactly the same value of stress. The results for the high density sand show a much more complex phenomenon than that of the low density; the result are shown in Fig. 6.7. These results show that the unsupported side of the trench does not play an important role. This is due to the stiffness of the soil, compared with the low density sand and the pipe stiffness. The D/t ratio also has a significant effect since it changes the relative stiffness of the pipe and soil. For D/t ratio of 50 , the 60° angle of inclination for the trench predicts

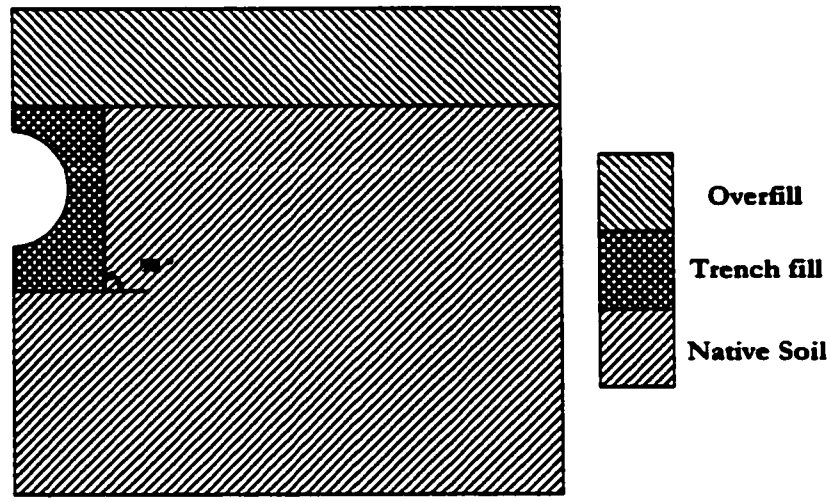

(a) Material zone identification

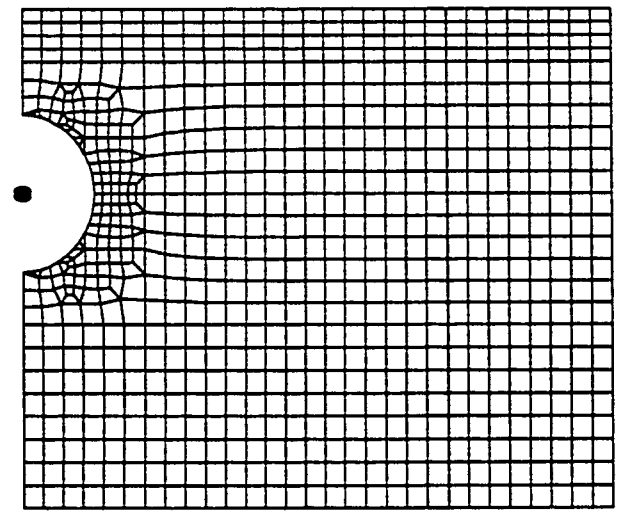

(b) Typical mesh

Fig. 6.3: Material zone identification and typical mesh for 90 degree, trench inclination

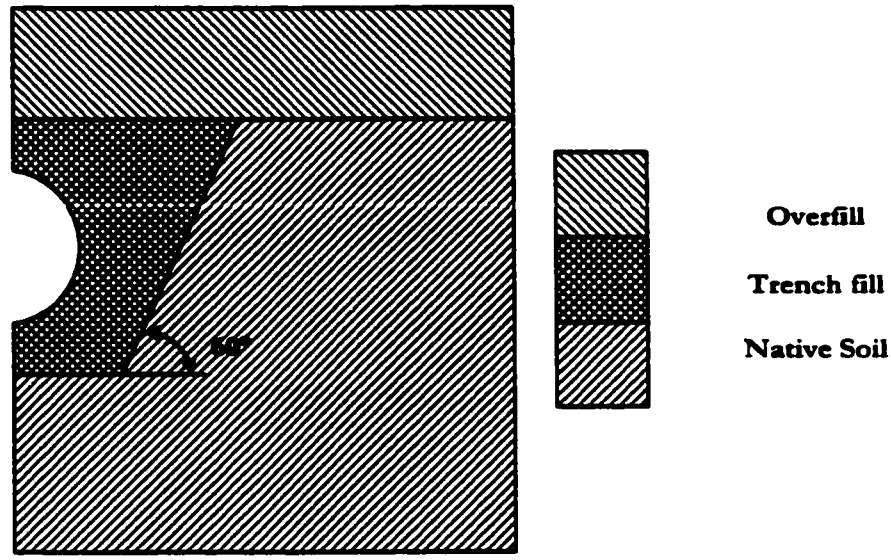

(a) Material zone identification

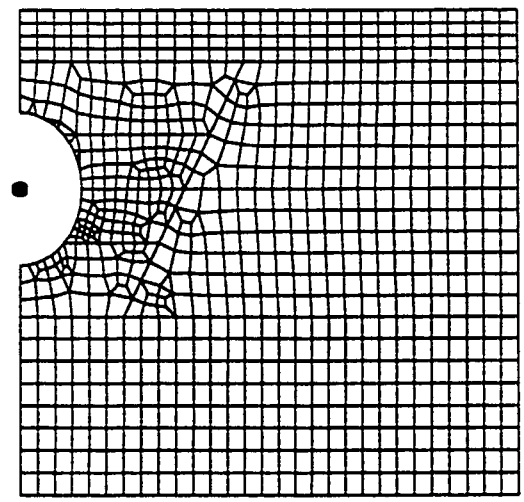

(b) Typical mesh

Fig. 6.4: Material zone identification and typical mesh for 60 degree, trench inclination

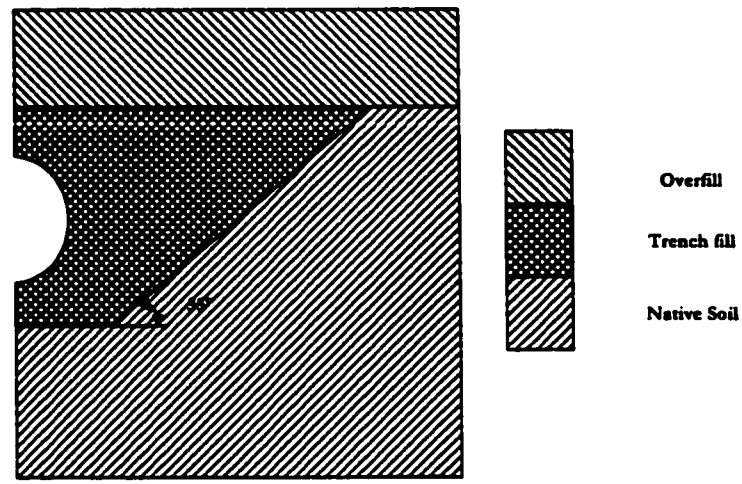

(a) Material zone identification

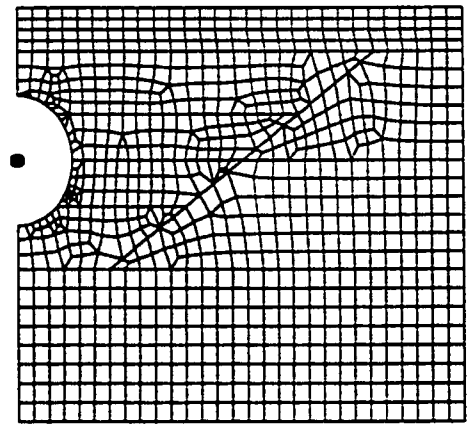

(b) Typical mesh

Fig. 6.5: Material zone identification and typical mesh for 35 degree, trench inclination

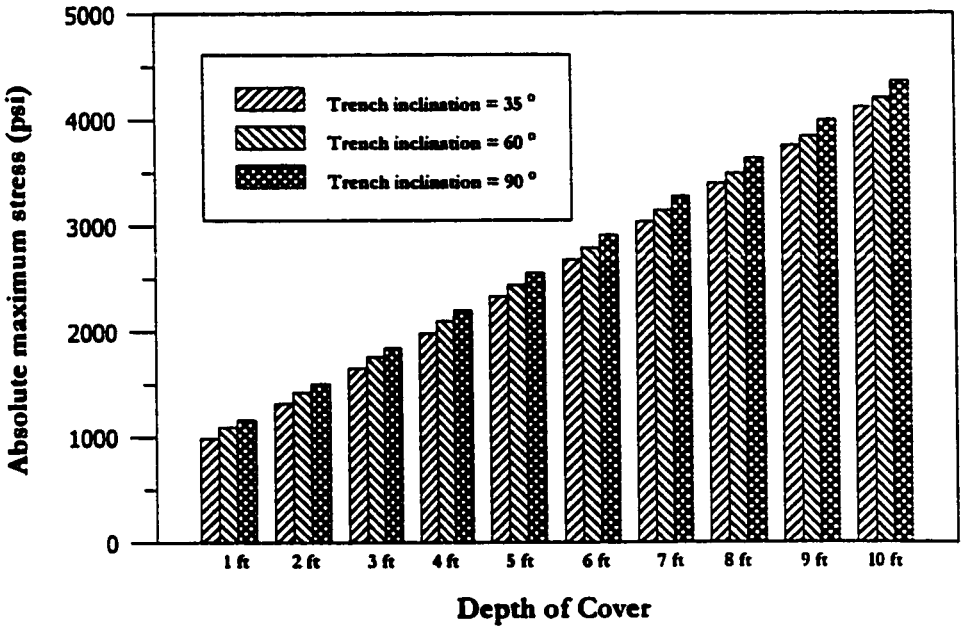

(a) D/t = 50 for dead load condition

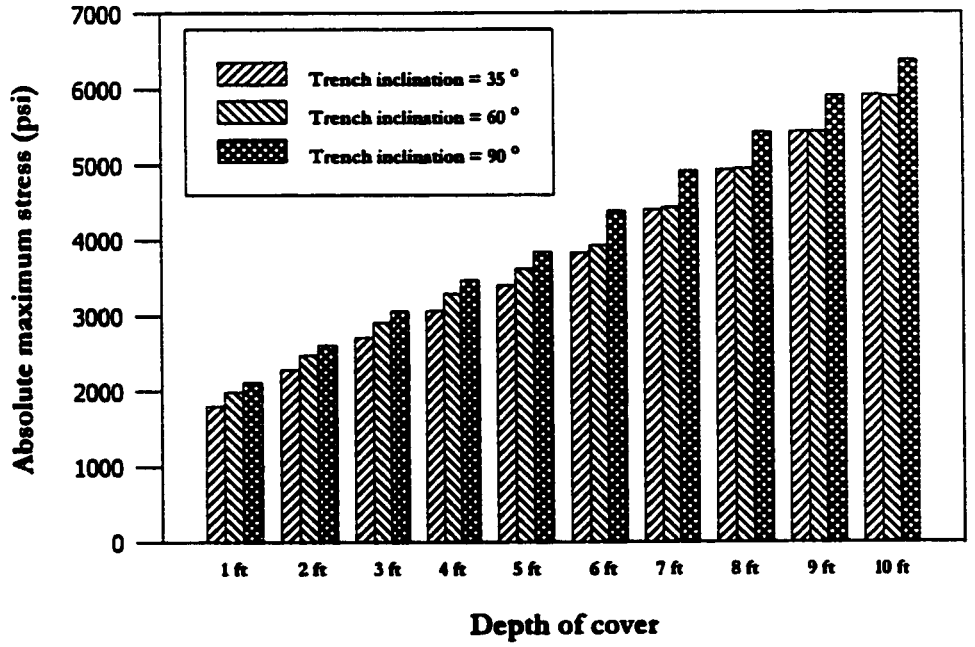

(b) D/t = 150 for dead load condition

Fig. 6.6: Absolute maximum stress for sand at low density for different trench inclination angles

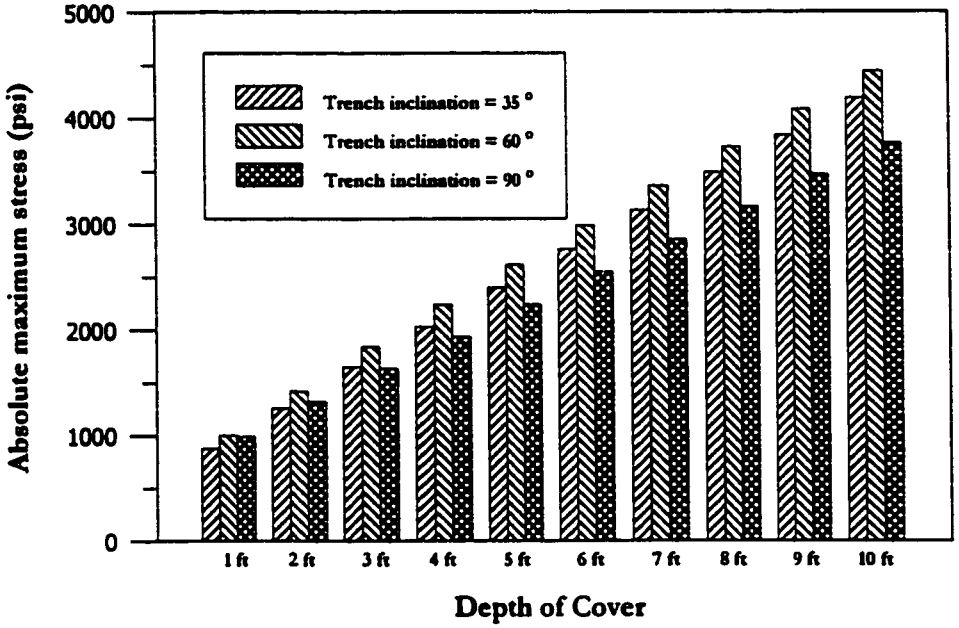

(a) D/t = 50 for dead load condition

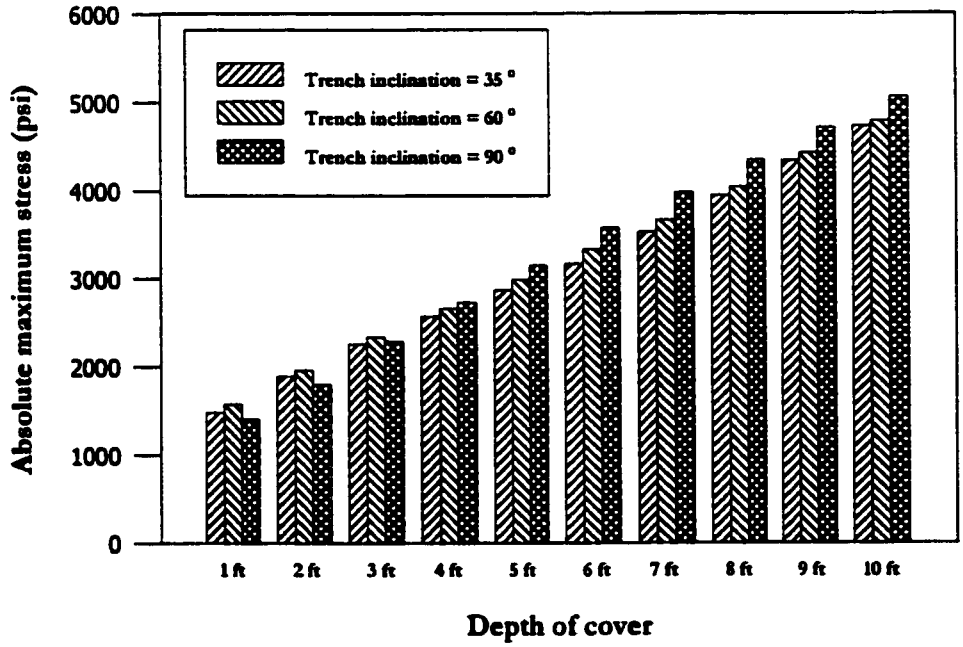

(b) D/t = 150 for dead load condition

Fig. 6.7: Absolute maximum stress for sand at high density for different trench inclination angles

more stresses; however, for a D/t of 150, which represents the most flexible pipes, the stresses increase again with an increasing trench inclination angle.

For marl at low density and sabkha at high density, the larger trench angle gives higher stresses, a behavior similar to that of low density sand as shown in Figs. 6.8 and 6.9. In summary, it can be stated that the absolute maximum pipe stress increases with an increase in the trench inclination angle, except for the high density sand.

The live load problem is studied next. Instead of examining all cover depths, it is decided to study only the case of 2 feet depth of cover, which is the most critical case for the live load. The live load stresses are found to be independent of the dead load stresses, a highly anticipated result. The homogenous case of low density sand did not show any variations in the stresses over the trench inclination angle, as shown in Fig. 6.10(a), while in all other cases the 35° trench inclination angle predicts much higher stresses, as shown in Figs. 6.10 (b) and 6.11. On the other hand, there is a negligible difference between the stress values of the 60° and the 90° trench inclination angles.

6.3 Construction Increment Sequence

In a soil-pipe system, soil backfilling is usually carried out in a series of lifts. For a realistic analysis of stresses and deformations in the soil-pipe system, it is necessary to account for the effects introduced by the sequential loading. Leonards et al. [69] reported that the larger the pipe diameter and the shallower the soil cover, the more the effects of the sequential construction. A procedure for simulating the sequential construction of soil mass commonly used in the finite element analysis is derived from an idea proposed by

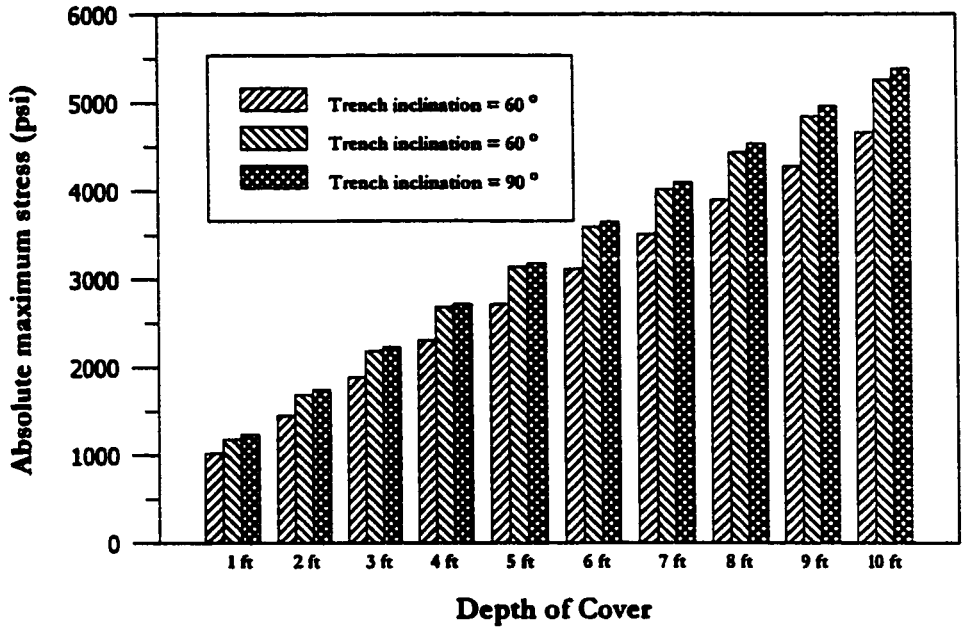

(a) D/t = 50 for dead load condition

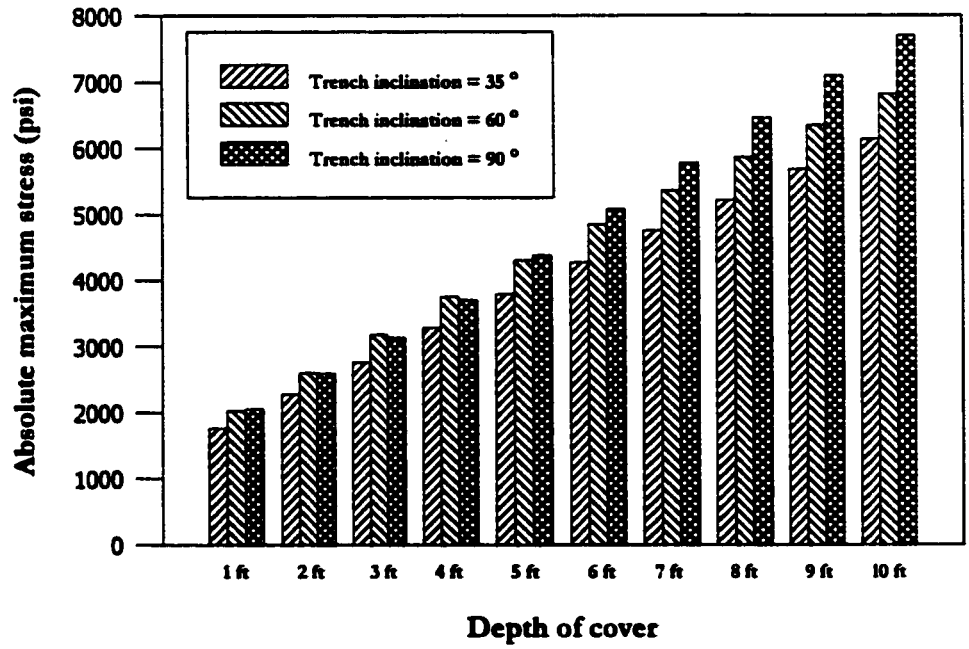

(b) D/t = 150 for dead load condition

Fig. 6.8: Absolute maximum stress for marl at low density for different trench inclination angles

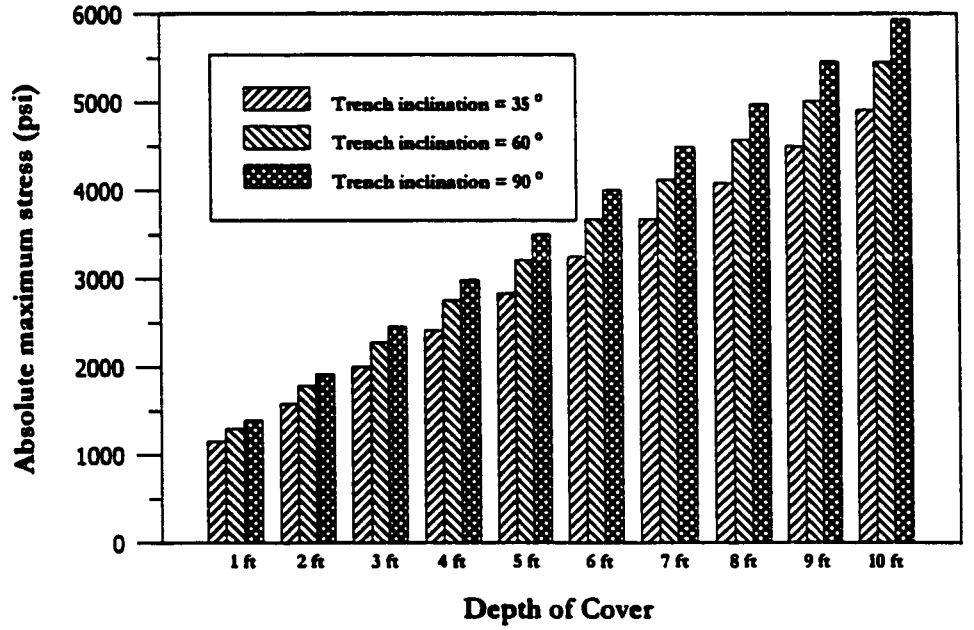

(a) D/t = 50 for dead load condition

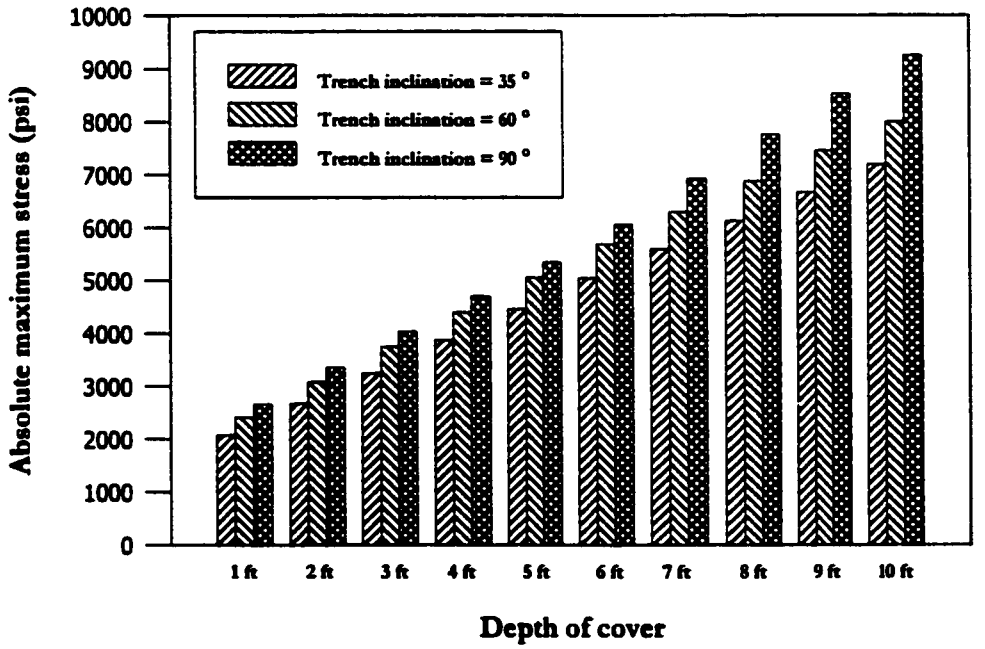

(b) D/t = 150 for dead load condition

Fig. 6.9: Absolute maximum stress for sabkha at high density for different trench inclination angles

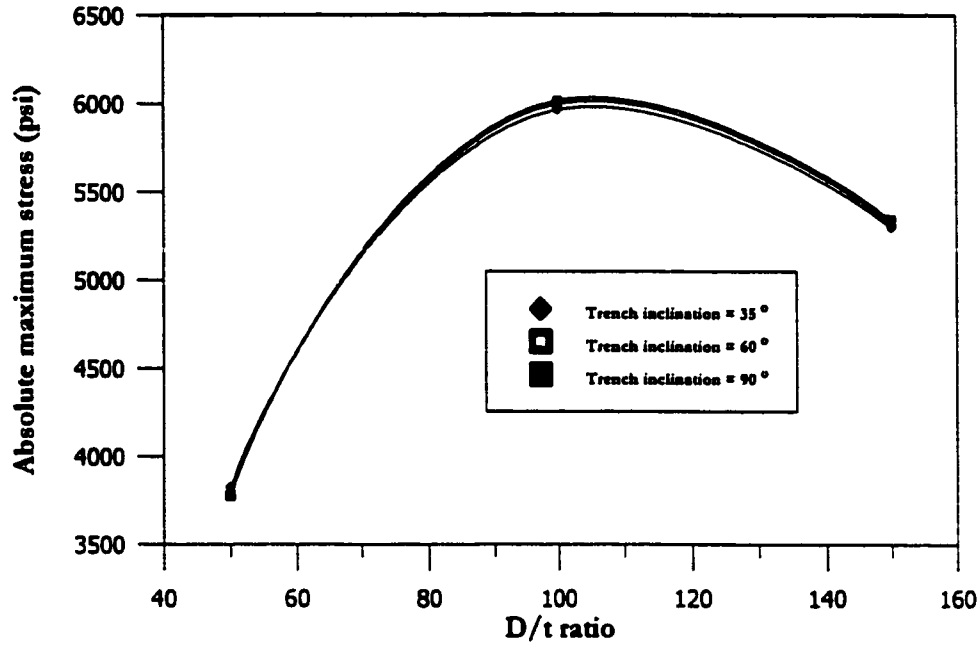

(a) Live load condition with sand at low density as native soil

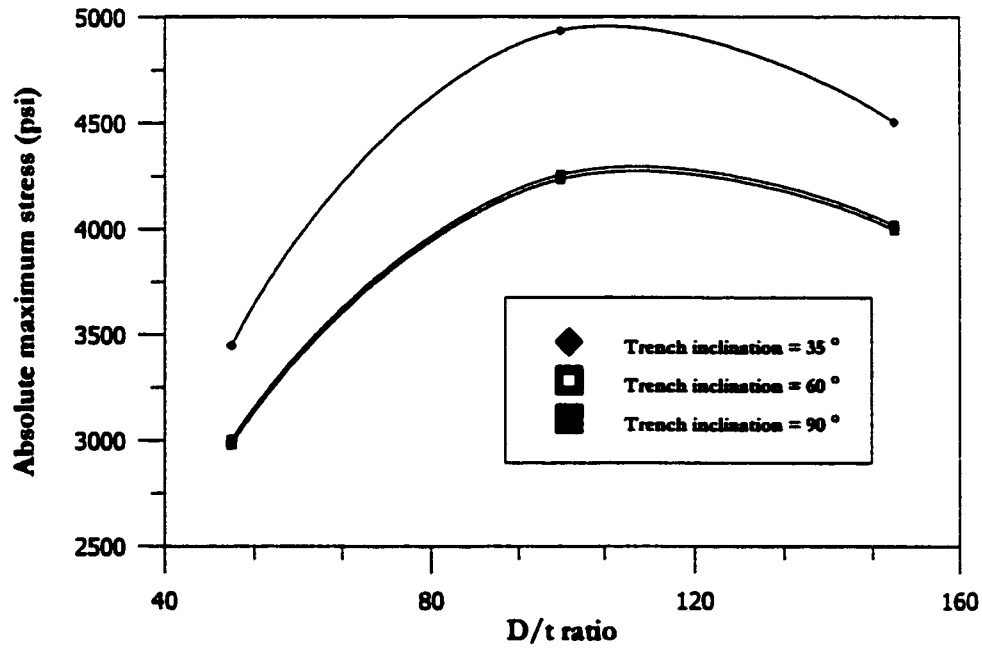

(b) Live load condition with sand at high density as native soil

Fig. 6.10: Absolute maximum stress for sand at low and high density for diffrent trench inclination angles subjected to live load only

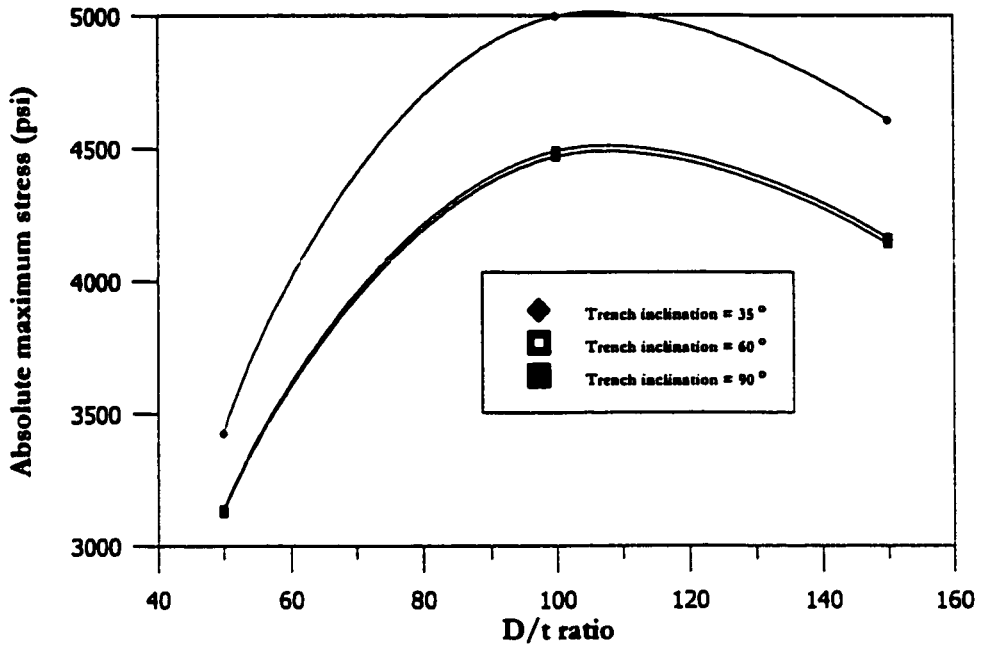

(a) Live load condition with marl as native soil

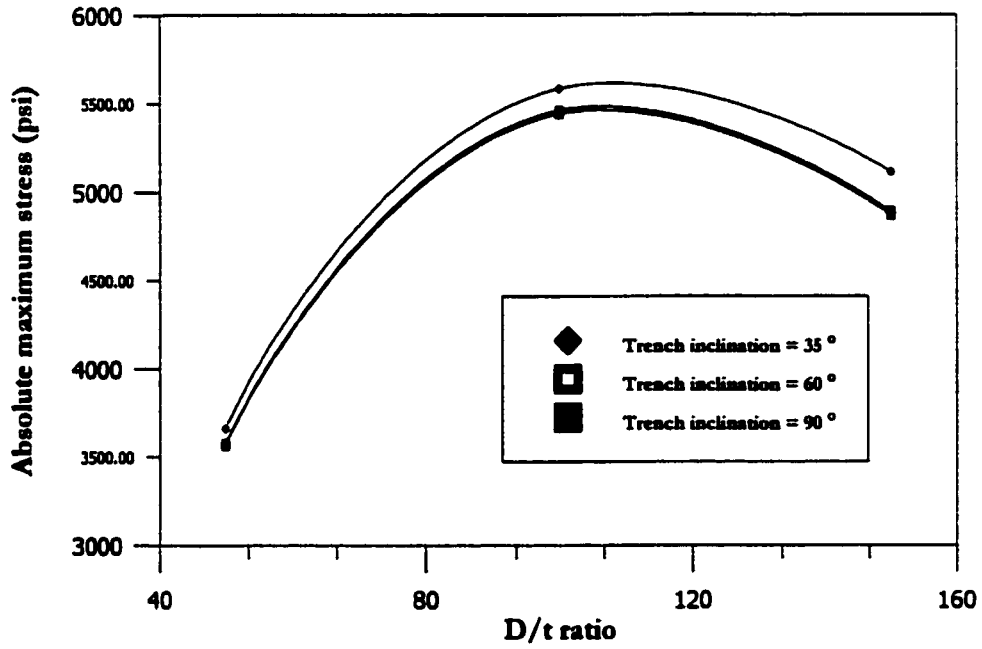

(b) Live load condition with sabkha as native soil

Fig. 6.11: Absolute maximum stress for marl and sabkha for diffrent trench inclination angles subjected to live load only

[85]. The following four steps describe the procedure:

1. Introduce the initial stresses in the foundation soil before the construction starts (Fig. 6.12(a)). The initial stresses can be obtained by performing one cycle of the finite element analysis or simply by estimation.
2. Evaluate the stiffness matrix and the load vector associated with the configuration after the first soil lift is laid down (Fig. 6.12(b)). Solve for the system responses, and add the stresses to the initial stresses; store the results.
3. Compute the combined stiffness matrix corresponding to the configuration after the second soil lift is laid down. Solve for the system responses due to the loads from the second soil lift, add them to the results from step 2, and store the results.
4. Continue the same process for each soil lift as in step 3 (Fig. 6.12(c)). The final state is the sum of all responses.

Unfortunately, regardless of the accuracy of the techniques for simulating the basic construction process, there are many details in construction, such as construction equipment loads and non-uniform backfilling, which can strongly influence the system response but are very difficult to simulate rationally. Knowing the effects of these details is essential to keep a reasonable perspective about possible perturbations due to the factors not included in the analysis.

The CANDE program manual shows the construction increment sequence for the embankment and trench-type installation; they are reproduced here in Figs. 6.13 and 6.14. The embankment-type construction increment sequence tries to simulate the actual embankment-

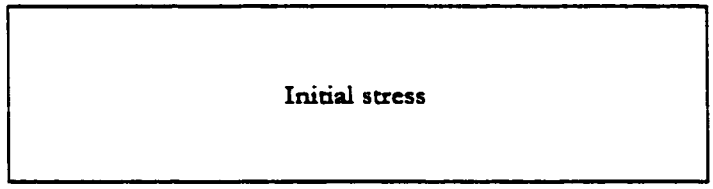

(a) Initial state

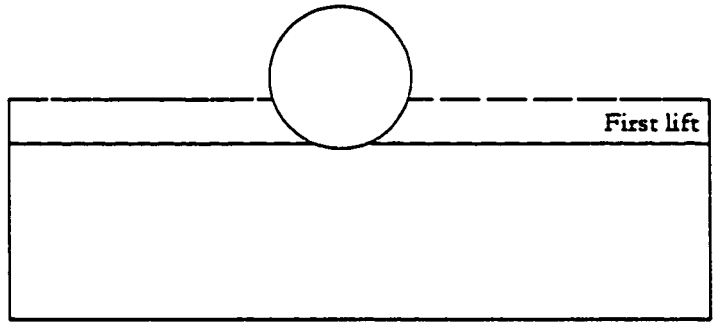

(b) First lift

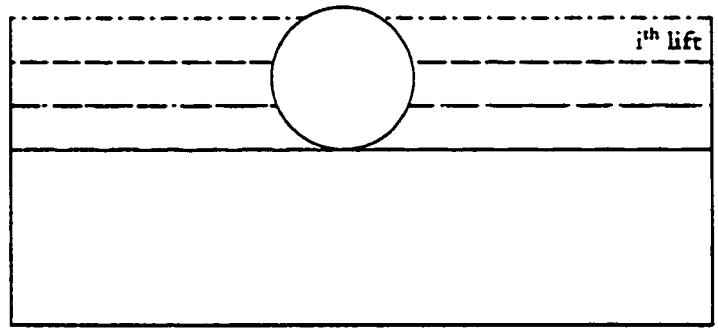

(c) Lift i

Fig. 6.12: Analytical simulation of sequential construction

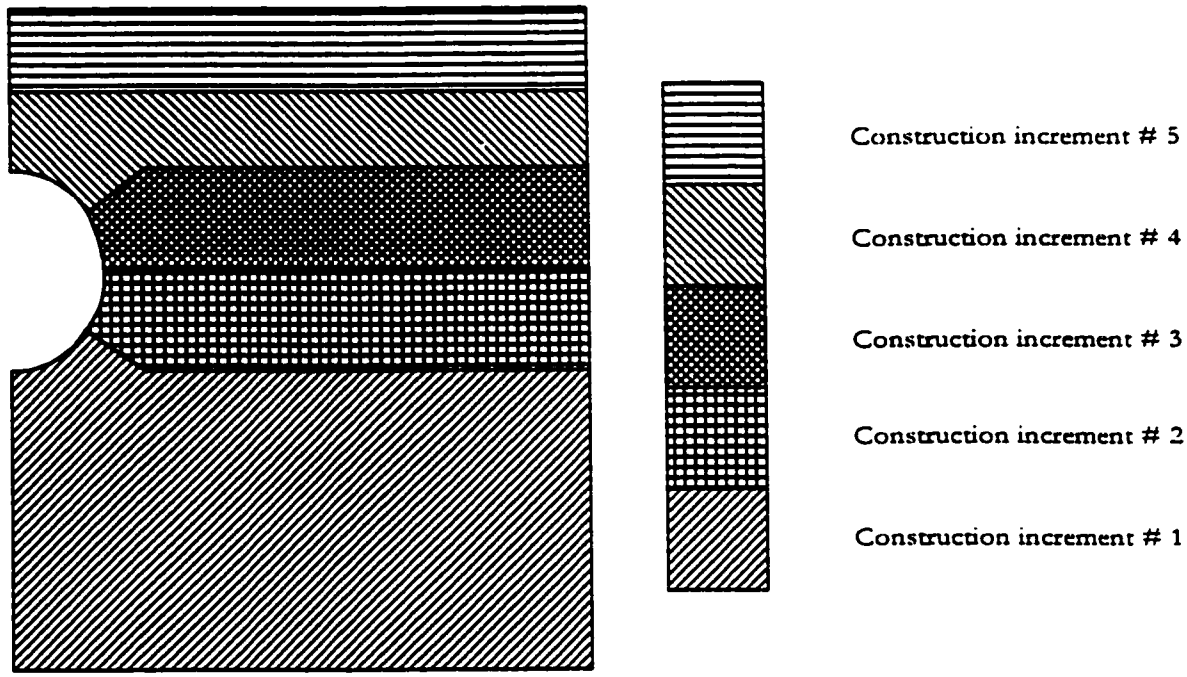

Fig. 6.13: Construction increment sequence for embankment type of installation (CANDE)

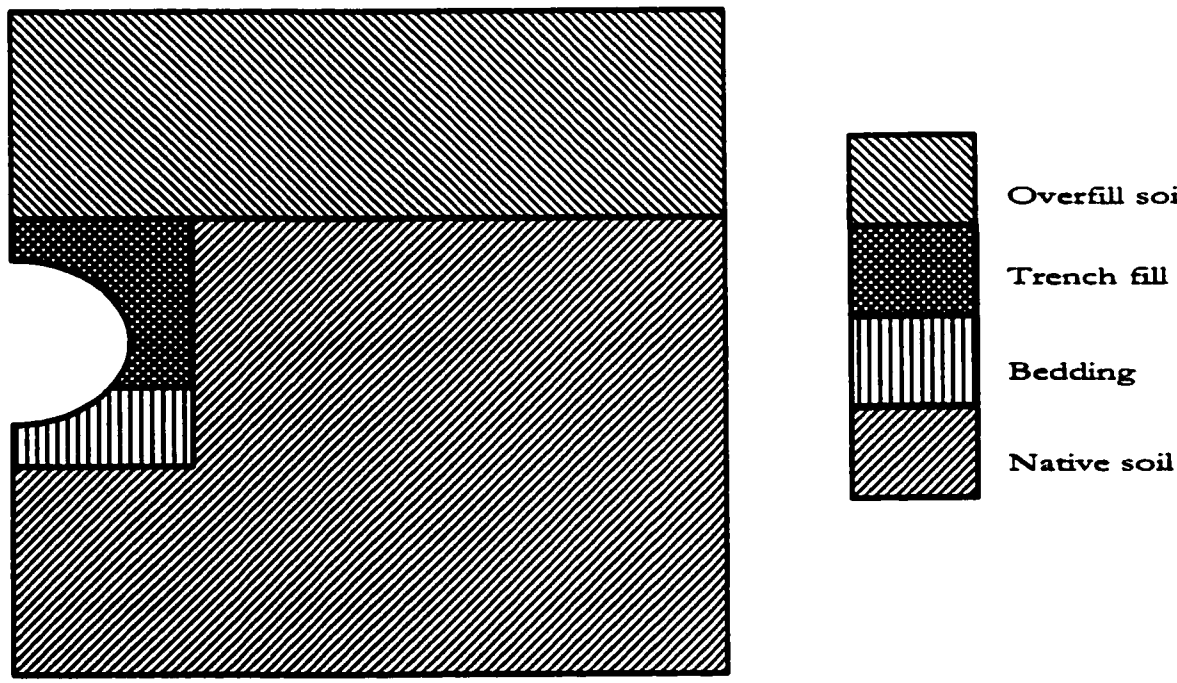

Fig. 6.14: Construction increment sequence for trench type of installation (CANDE)

type installation in the field, while the trench-type installation increment sequence simulates the trench-type installation in the field. Leonards et al. [45] defined a favorable and unfavorable construction increment sequence. His unfavorable construction increment sequence resembles the trench-type construction increment sequence, while the favorable construction increment sequence is almost similar to the embankment-type construction increment sequence of CANDE. He noted that the unfavorable construction increment sequence results in unusually high bending moments, which ultimately results in higher stresses; however, the pipe diameter used in his analysis was unusually large, being 12.5 feet.

As is evident from the above-mentioned discussion, the construction increment sequence plays an important role in the simulation of the pipe-soil system, and it becomes necessary to run several test simulations in order to understand the physics of the problem and come up with a construction increment sequence which simulates the field conditions accurately, and at the same time gives reliable results. Two types of mesh routines are programmed in FEMAP, one with the construction increment sequence similar to the embankment type, and the other with the construction increment sequence similar to the trench type. These construction increment sequences are shown in Figs. 6.15 and 6.16. Note that the meshes which have inclined sides are only used for sand at low and high densities as the native material; for marl and sabkha, meshes with similar construction increment sequences but inclined at 90^{o} are used. As mentioned in the literature, the construction increment sequence is more sensitive to shallow depths of cover; therefore, shallow depths of 3 and 4 feet are selected for the initial runs. It is also decided to first investigate the

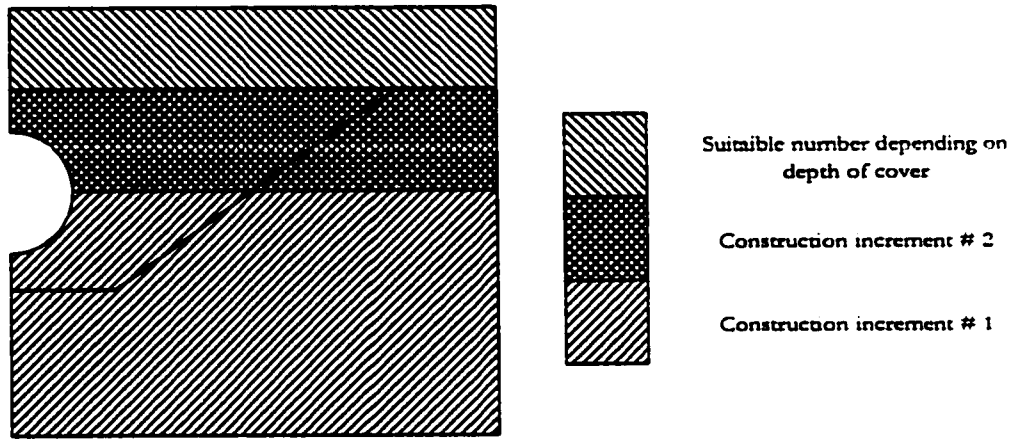

Fig. 6.15: Construction increment sequence for embankment type of installation used in test runs

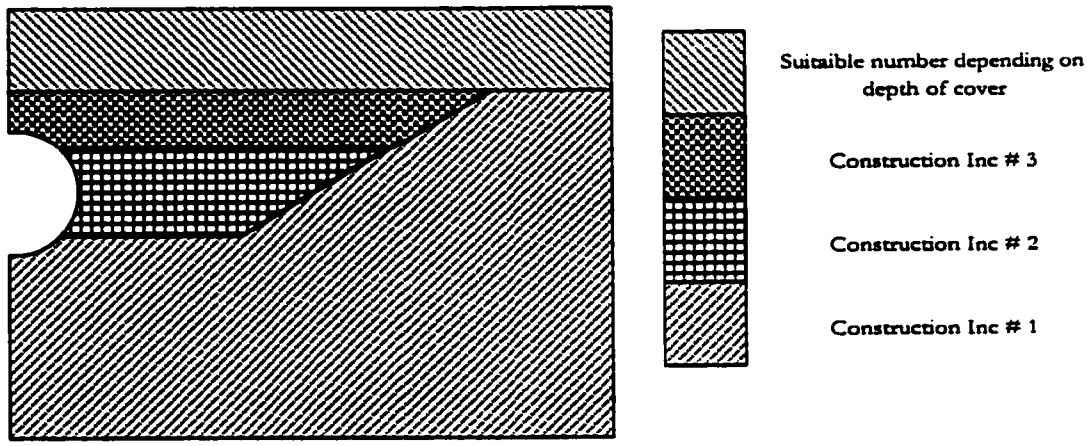

Fig. 6.16: Construction increment sequence for trench type of installation used in test runs

problem for dead load and then for live load. The pipe diameter of 36 inches is used and D/t ratios of 50, 75, 100, 125, and 150 are investigated. The four soil types used are sand at low density, sand at high density, marl at low density, and sabkha at high density as the native soils. The trench fill and overfill are always sand at low density. The material zone identification for the simulations is shown in Fig. 6.17. Note that the asphalt layer is only used for live load runs.

For the dead load problem, two depths of cover are investigated first. These depths of cover are 3 and 4 feet. The results are shown in Figs. 6.18 to 6.19. The results show that for a depth of cover of 3 feet, sand at low and high densities show less variation in the stresses than the marl at low density and sabkha at high density (Fig. 6.18); moreover. the difference in the diameter changes is less than the difference in the absolute maximum stresses. Fig. 6.19, for the depth of cover of 4 feet shows less variations in stresses and diameter changes than the depth of cover of 3 feet; therefore, it was decided to run several problems for the sand overburden problem up to 60 feet. The two extreme D/t ratios of 50 and 150 were selected and the results are shown in Figs. 6.20 to 6.23. The results support the Leonards' observation that the difference in the stresses and diameter changes become less as the depth of cover is increased. Moreover, the difference in diameter change for the two construction increments is minimal.

Next, the problem of live load was taken into account; the two depths of cover used in the analysis were 3 feet and 4 feet. The results are shown in Figs. 6.24 to 6.25. These results are very much expected. At small cover depths, the live load stresses overshadow the dead load stresses. Since the live load stresses and deformations are not at all sensitive

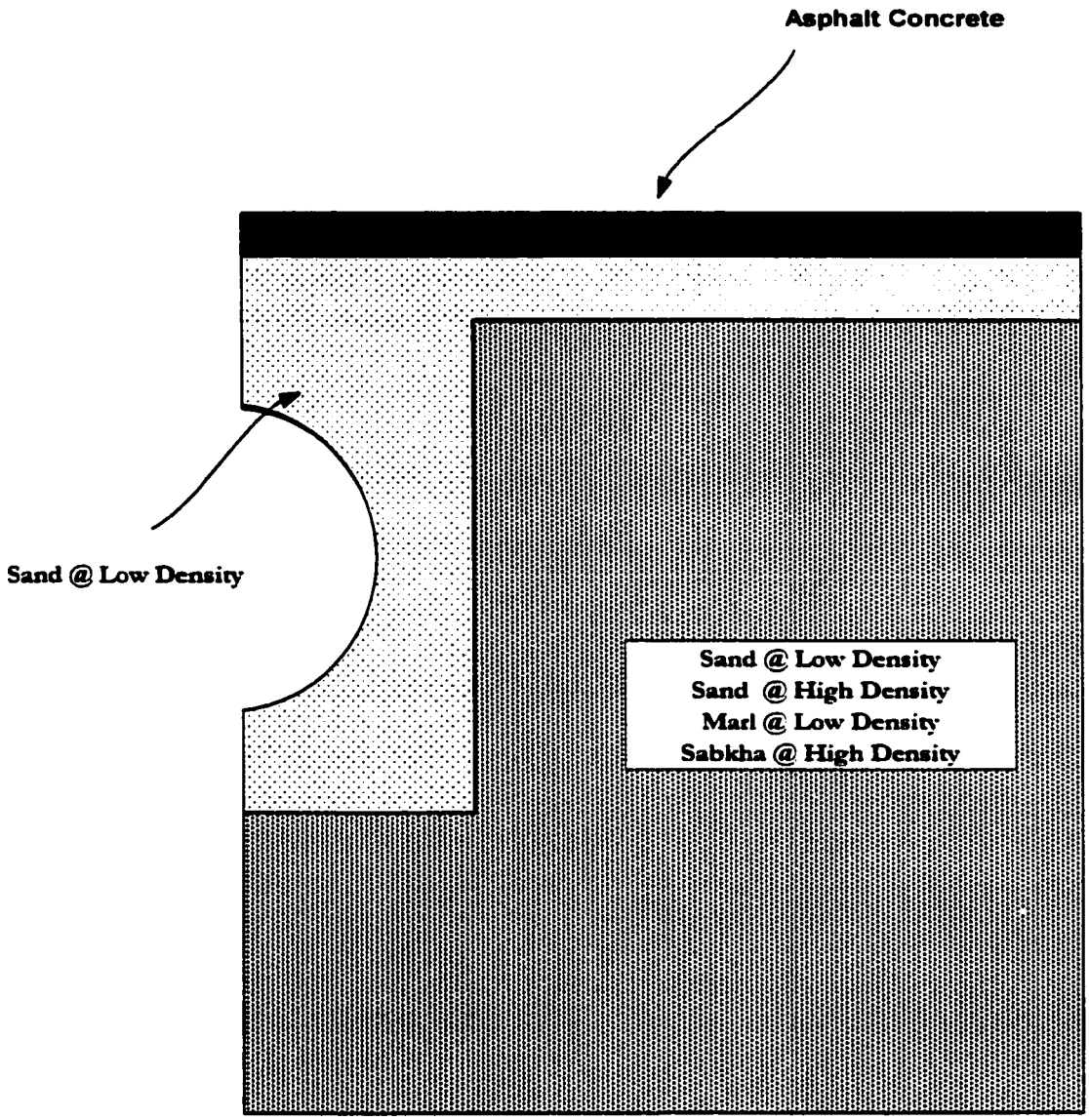

Fig. 6.17: Material zone identification for test runs

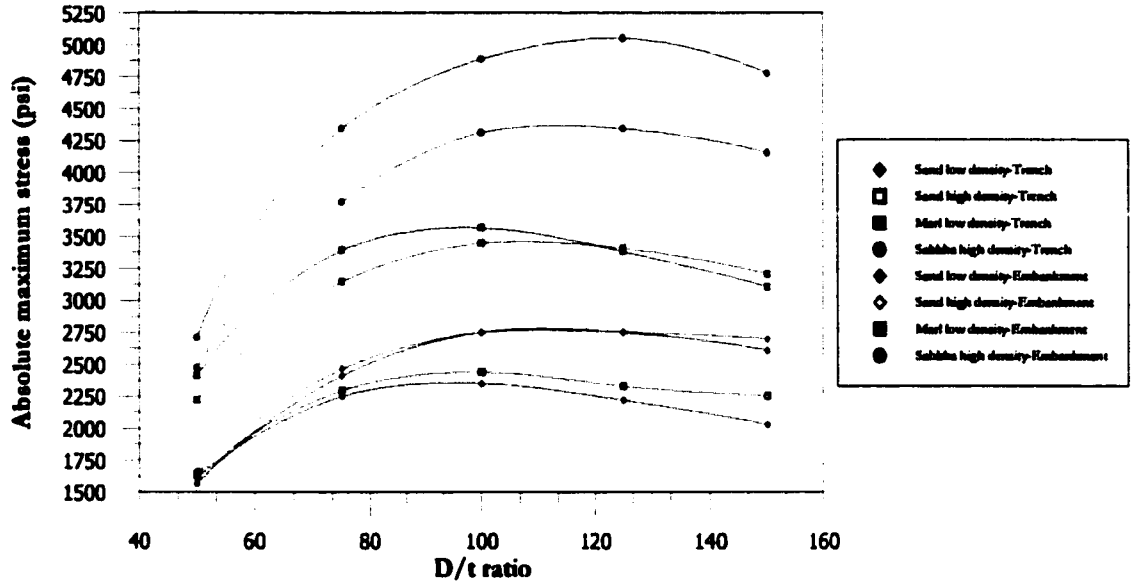

(a) Variation of absolute maximum stress for deal load only

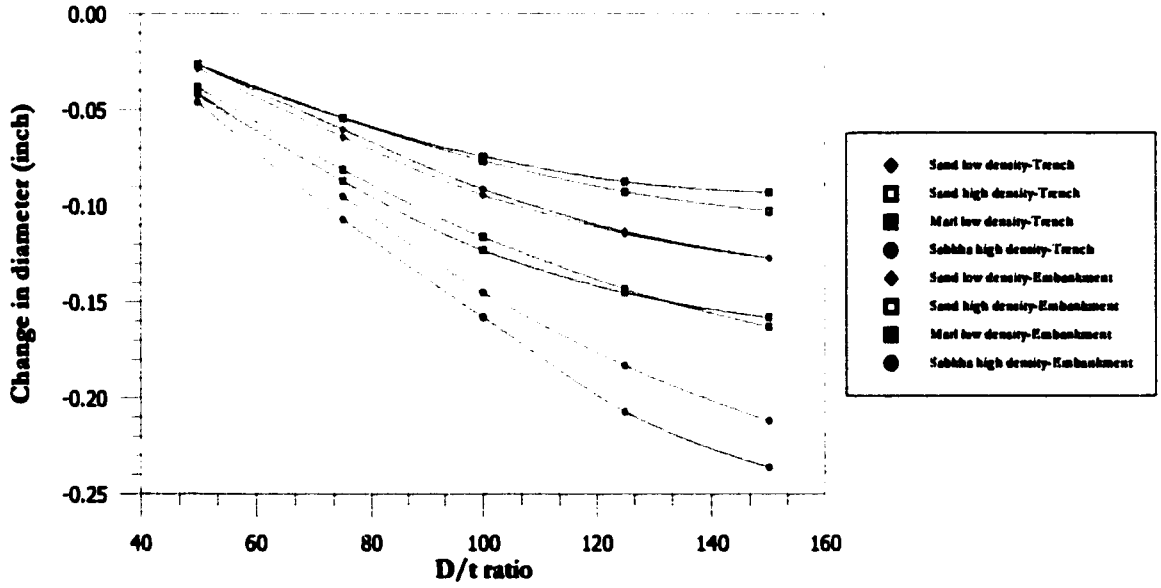

(b) Variation of change in diameter for dead load only

Fig. 6.18: Variation in absolute maximum stress and diameter change for 3 feet depth of cover for trench and embankment type construction increment sequence

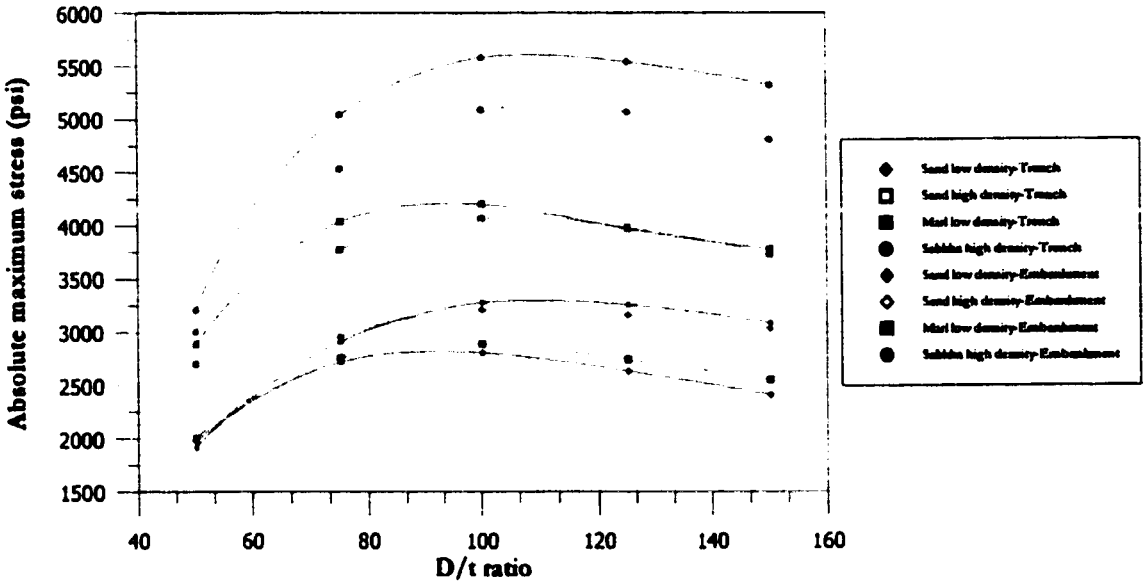

(a) Variation of absolute maximum stress for dead load only

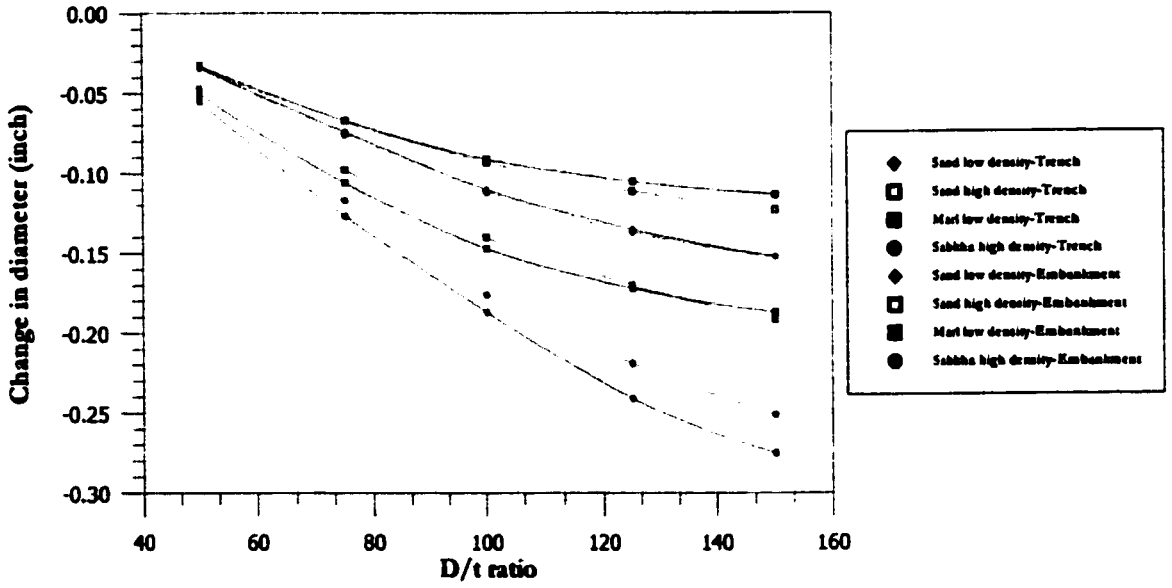

(b) Variation of change in daimeter for dead load only

Fig. 6.19: Variation in absolute maximum stress and diameter change for 4 feet depth of cover for trench and embankemnt type construction increment sequence

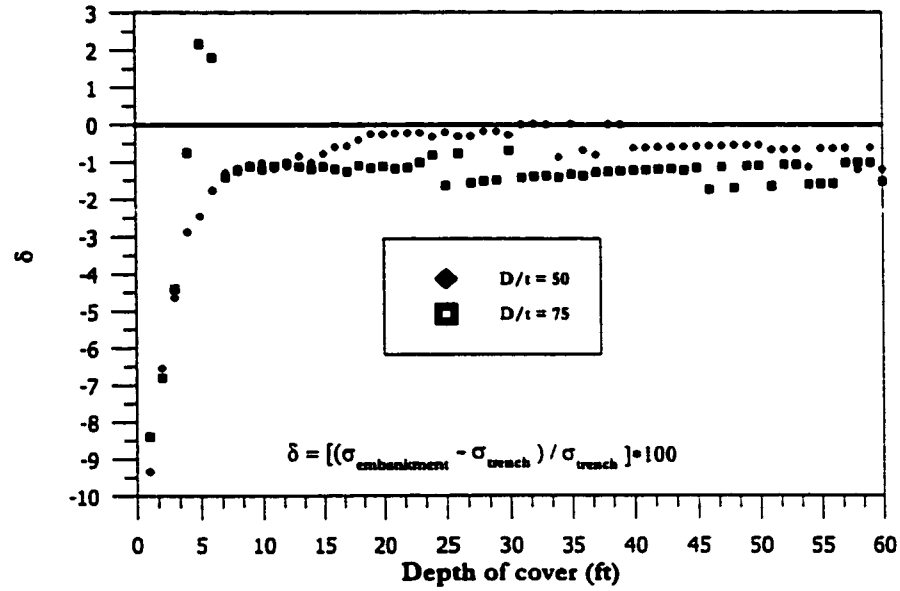

(a) Variation of absolute maximum stress for dead load only

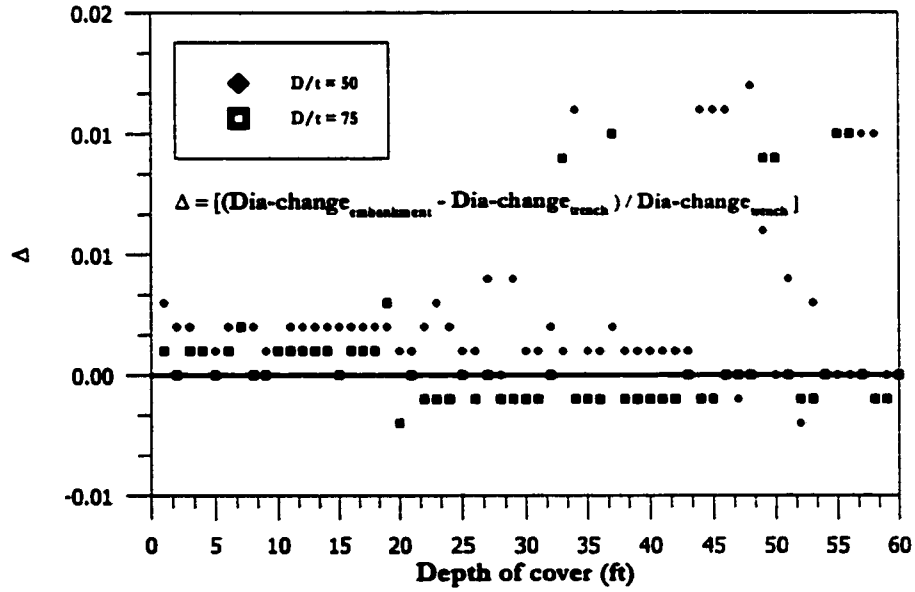

(b) Variation of change in diamter for dead load only

Fig. 6.20: Percent difference in absolute maximum stress and diameter change for sand at low density for trench and emabankment type construction increment sequence

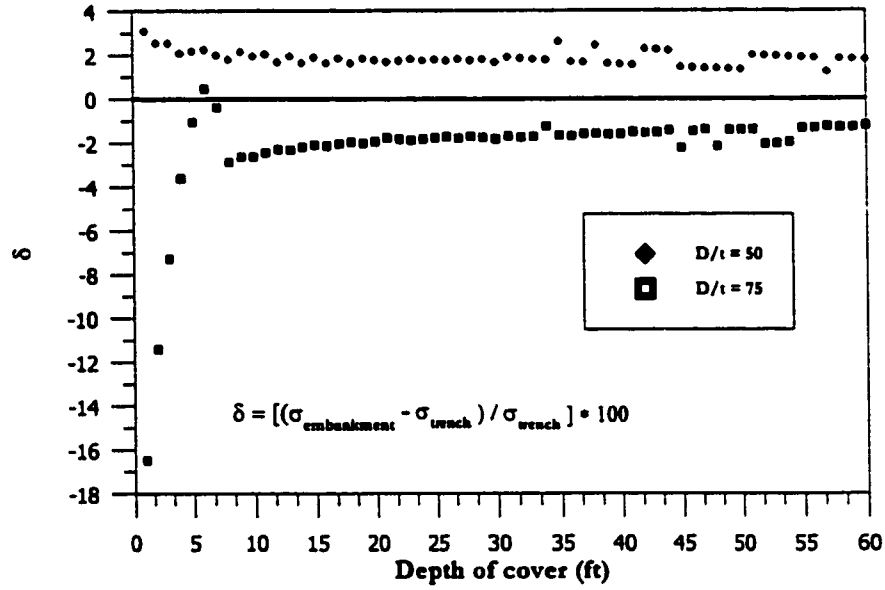

(a) Variation of absolute maximum stress for dead load only

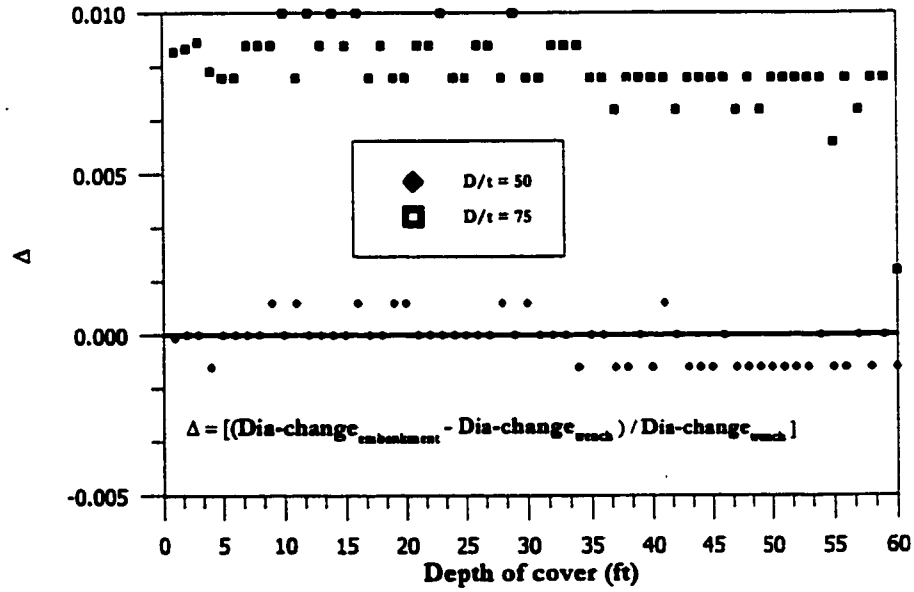

(b) Variation of change in diameter for dead load only

Fig. 6.21: Percent difference in absolute maximum stress and diameter change for sand at high density for trench and embankemnt type construction increment sequence

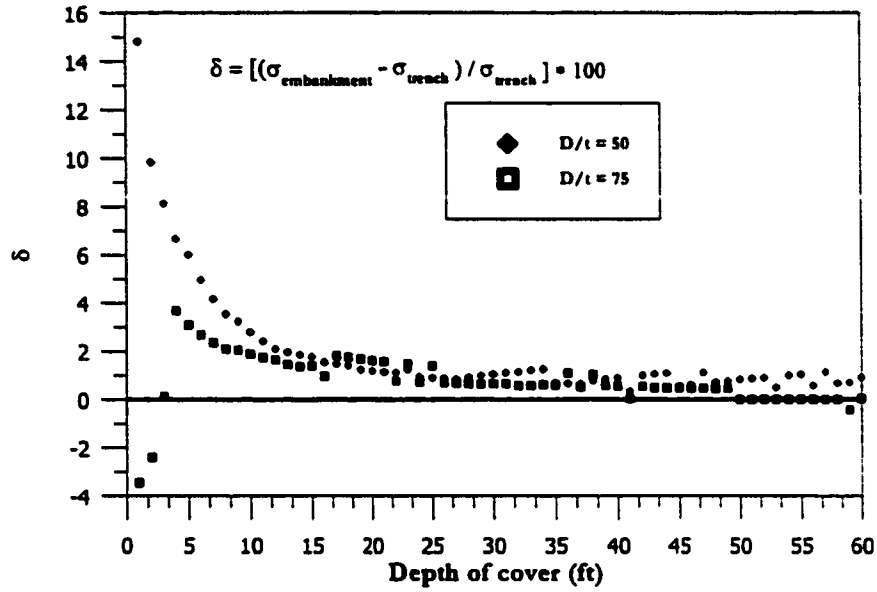

(a) Variation of absolute maximum stress for dead load only

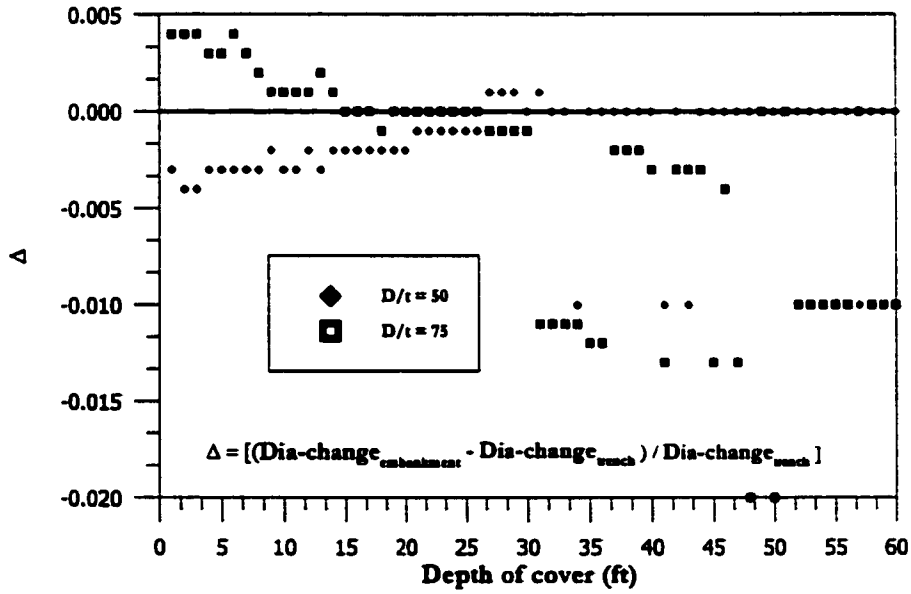

(b) Variation of change in diameter for dead load only

Fig. 6.22: Percent difference in absolute maximum stress and diameter change for marl at low density for trench and embankemnt type construction increment sequence

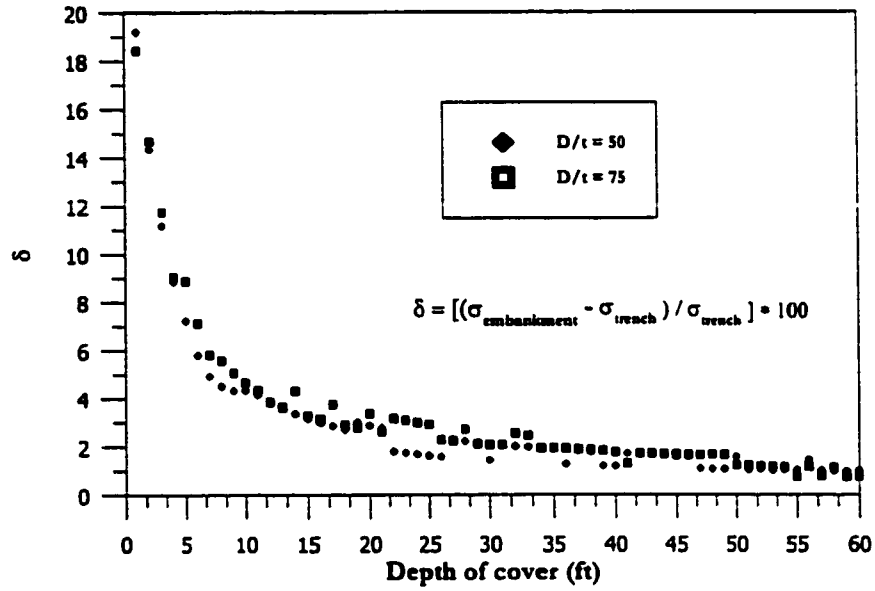

(a) Variation of absolute maximum stress for dead load only

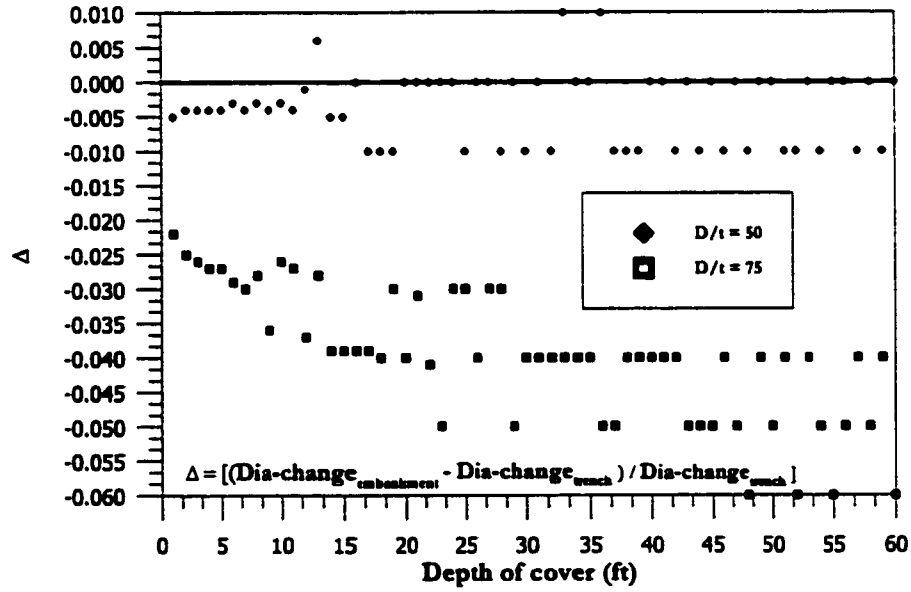

(b) Variation of change in diameter for dead load only

Fig. 6.23: Percent difference in absolute maximum stress and diameter change for sabkha at high density for trench and embankemnt type construction increment sequence

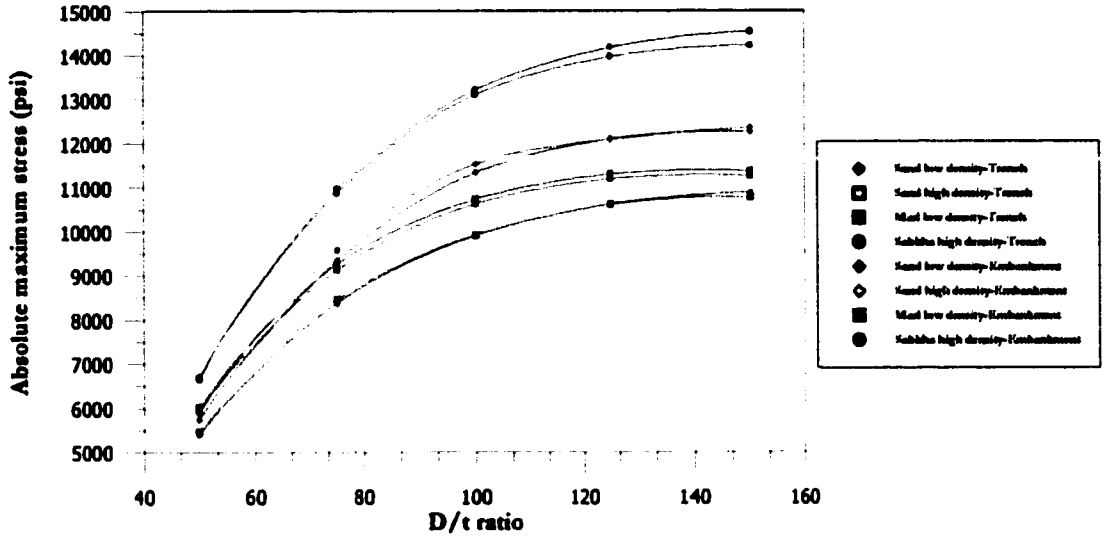

(a) Variation of absolute maximum stress for dead plus live load

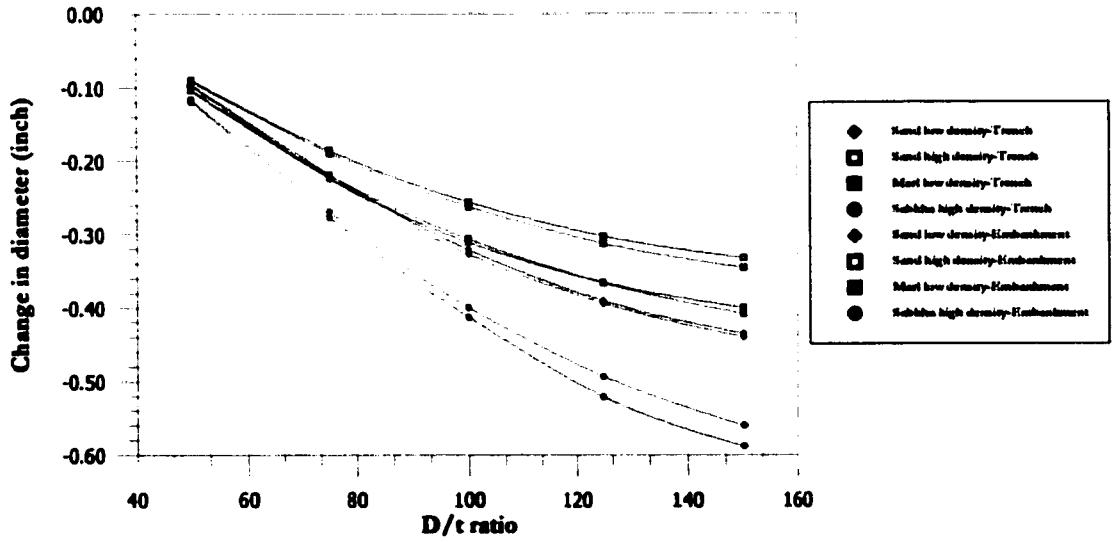

(b) Variation of change in diameter for dead plus live load

Fig. 6.24: Absolute maximum stress and diameter change for 3 feet depth of cover for trench and embankemnt type construction increment sequence under live load condition

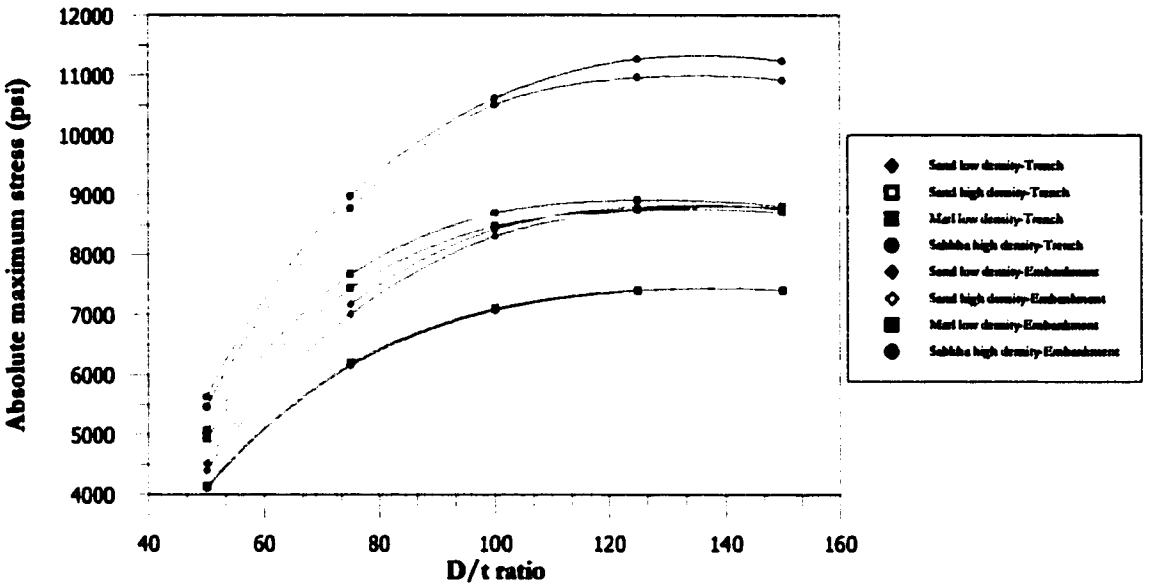

(a) Variation of absolute maximum stress for dead plus live load

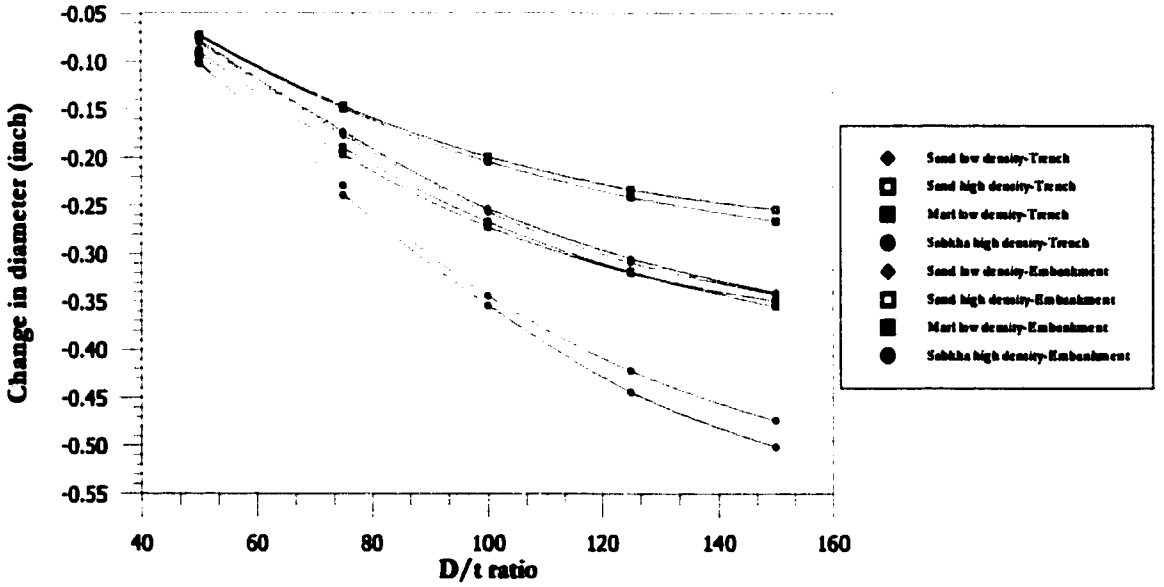

(b) Variation of change in diamter for dead plus live load

Fig. 6.25: Absolute maximum stress and diameter change for 4 feet depth of cover for trench and embankemnt type construction increment sequence under live load conditions

to the construction increment sequence, a very small difference in stresses and diameter changes is observed for the two construction increment sequences.

6.4 Low versus High Density Sand

To simulate different field conditions, and to make compactive studies, sand was assumed to be compacted at two different densities, i.e. relative densities of 35% and 85% were chosen to represent the sand at low and high densities respectively. The Duncan and Selig model parameters were determined for these two densities. The next step was to decide which density of the sand is to be used as the overfill material in the finite element simulations of sand overburden and highway crossing. A set of finite element simulations was made using sand at low and high densities as the overfill material. In all of these finite element simulations, the trench fill is always low density sand. This is because in the field the trench is always filled with sand without any compaction. The native soil materials used in these simulations are sand at low density, sand at high density, marl at low density, and sabkha at high density. First, the problem of sand overburden is considered; a total of 20 simulations are made. Five simulations are carried out for each type of the native soil with D/t ratios of 50, 75, 100, 125, and 150. The construction increments are adjusted in such a way that a depth of cover from 1 to 60 feet can be modeled in a single simulation.

The results of the first 20 simulations for the sand overburden problem are shown in Figs. 6.26 to 6.27. In these figures, the ordinate is the percent difference in the absolute

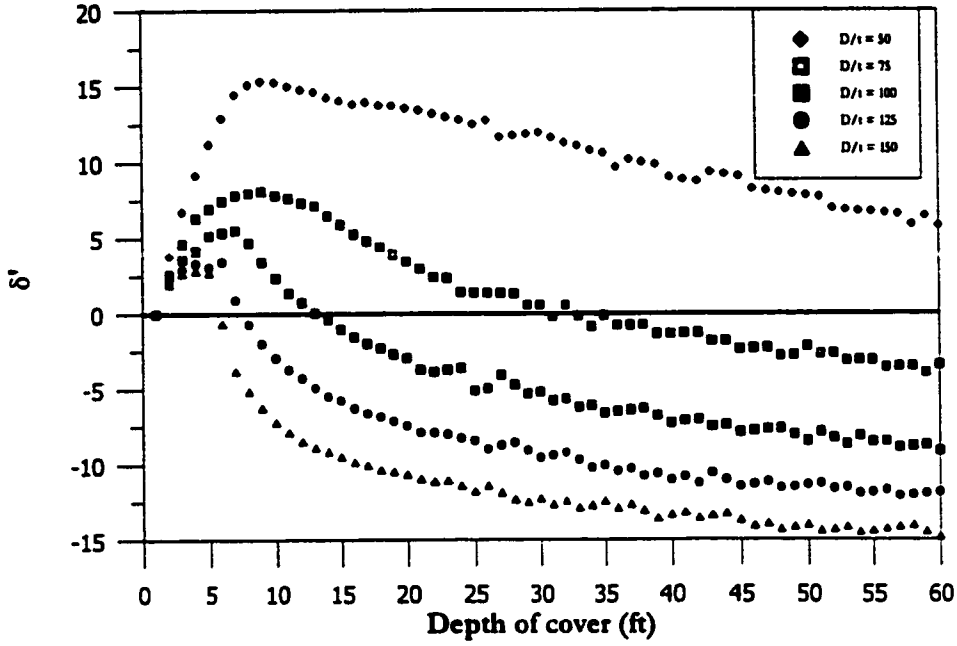

(a) Sand at low density as native material

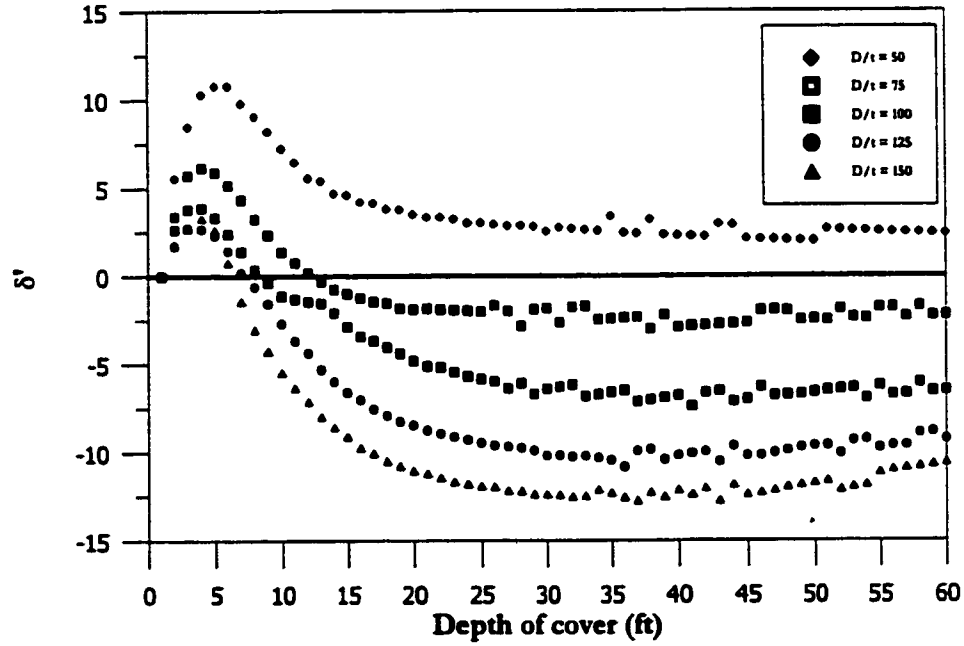

(b) Sand at high density as native material

Fig. 6.26: Percent difference in absolute maximum stress for sand at low and high density

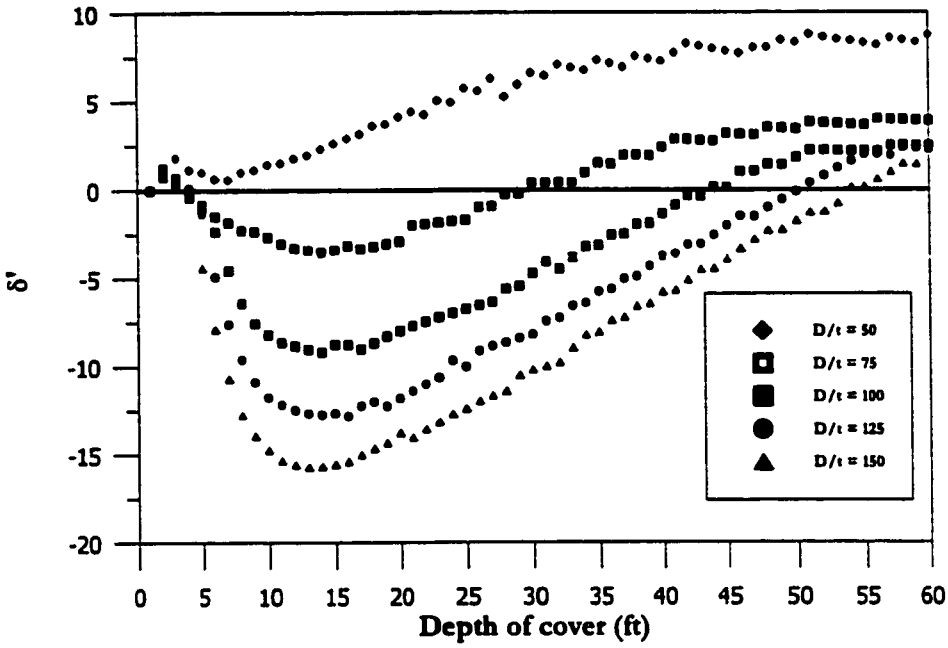

(a) marl at low density as native material

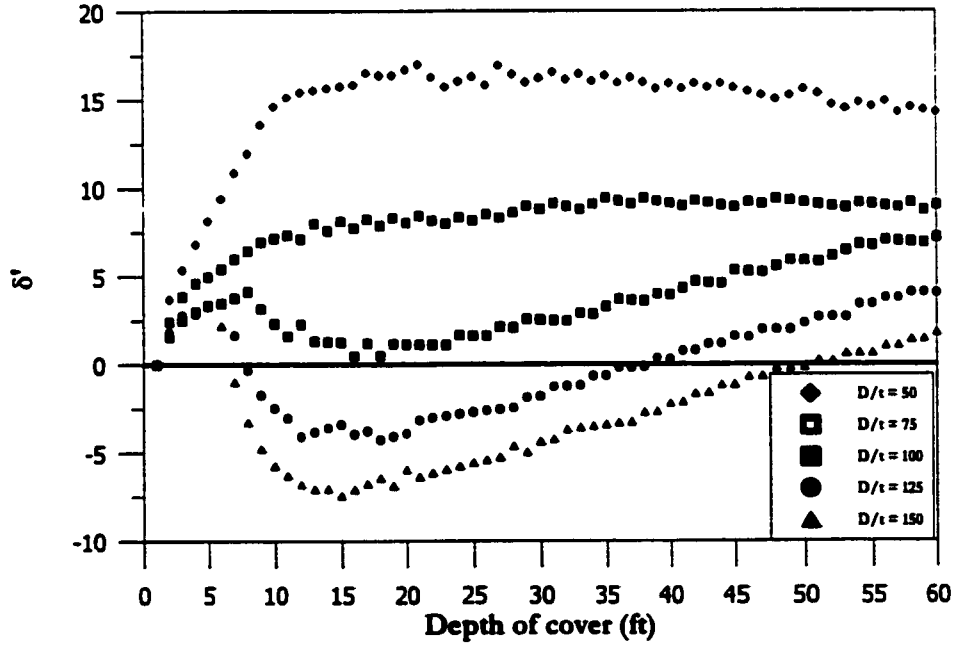

(b) Sabkha at high density as native material

Fig. 6.27: Percent difference in absolute maximum stress for marl low and sabkha high

maximum stress represented by the symbol δ'. Which is defined as follows:

$$\delta' = \frac{\sigma_H - \sigma_L}{\sigma_H} * 100 \tag{6.1}$$

where

σ_H = absolute maximum stress in the pipe with high density soil

σ_L = absolute maximum stress in the pipe with low density soil

The results for the sand overburden problems indicate that there is a very small difference in the absolute maximum stress at small depths of cover. This is expected because small cover depths mean less overfill and thus smaller stress. Furthermore, the results also indicate that for small D/t ratios, the absolute maximum stress for sand at high density as the overfill material is more than that for sand at low density as the overfill material. This is contrary to the large D/t ratios where the absolute maximum stresses for sand at low density as the overfill material are more than that for the high density sand as the overfill material. This can be explained in terms of positive arching. For small D/t ratios, in which the pipe is very rigid, the sand at high density as the overfill material produces more stresses because of a higher unit weight than the sand at low density. However, for large D/t ratios, the pipe is relatively flexible, and the sand at high density, being stiffer than the sand at low density, decreases the stresses as a result of positive arching. So, to be on the safe side, it was decided to use sand at low density as the overfill material in sand overburden problems.

Another set of 40 simulations were executed to study the effect of sand density on overfill material for highway crossing problems. The two depths of cover investigated

were 2 feet and 3 feet. The results for the live load problems is shown in Fig. 6.28. The results clearly indicate that, owing to its greater stiffness, high density sand as the overfill material is more successful in dissipating the live load than the sand at low density. Also, the difference is more pronounced for larger D/t ratios due to the reasons mentioned above. Another important observation is that at a cover depth of 3 feet, the percentage difference in the absolute maximum stresses is more than that of the cover depth of 2 feet. This is also expected because for a cover depth of 2 feet the overfill is only one foot, while for a cover depth of 3 feet the overfill is 2 feet, which results in a better dispersion of the live load. Hence, it was decided to use sand at low density as the overfill material since it represents the more critical case.

6.5 Low versus High Density Marl

In the preliminary study of this investigation, it was noted that the marl compacted at low and high densities of 111 lb/ft^3 and 127.54 lb/ft^3, respectively, show a marginal difference in the pipe stresses and deflection. Therefore, a study was made to compare the pipeline stresses and deflection for high and low-density marl. The diameter chosen in this study is 36 inches, which is the middle of the diameter range. First, the dead load is considered; ten simulations are made for marl of low and high density. The D/t ratio is varied from 50 to 150 in increments of 25. The construction increments of the mesh are taken in such a way that in each increment one foot of soil is placed. This enabled getting the pipeline stresses and deflection for each foot of the cover. The depths of covers simulated are from 1 foot to 60 feet. The percent difference in the absolute maximum stress

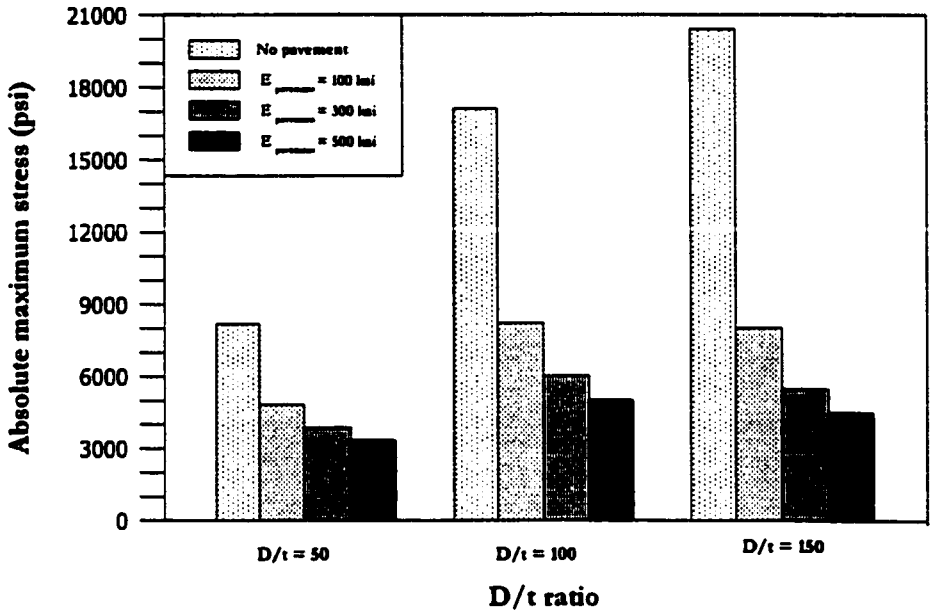

(a) Absolute maximum stress for various values of pavement stiffness

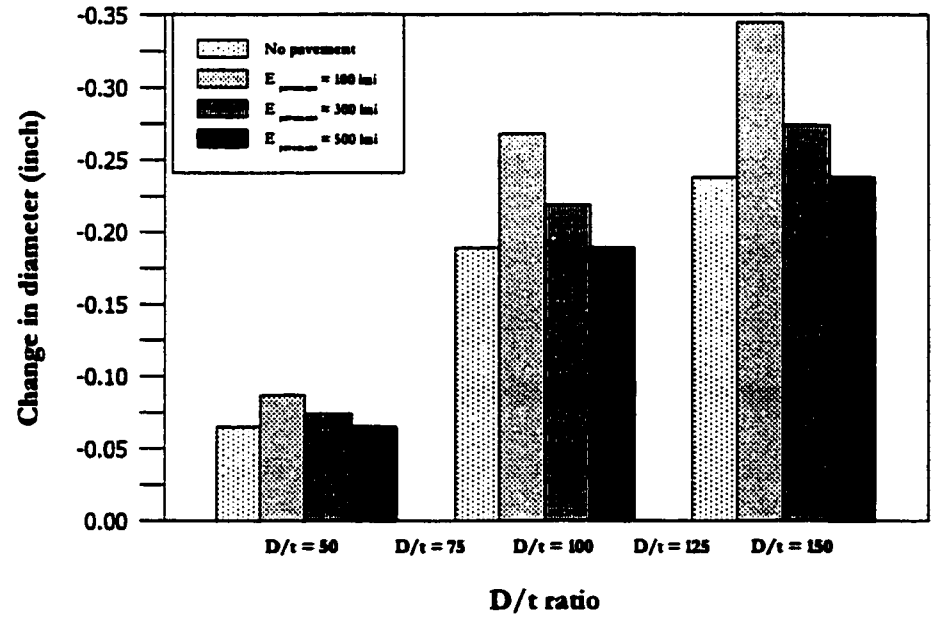

(b) Diamter change for various values of pavement stiffness

Fig. 6.28: Percent difference in absolute maximum stress for 2 and 3 feet depth of cover under live load conditions

(δ) for the two soils is shown in Fig. 6.29(a). From the figure, it is obvious that for all D/t ratios except 50, the percent difference is within $\pm$ 5%. However, for the D/t ratio of 50, the percent difference is 10 % for certain depths of cover. This difference is not very large either, owing to the fact that a D/t ratio of 50 represents a very rigid pipe which develops much less stresses and deflection than higher D/t ratios. The percent difference in the diameter change (Δ) is shown in Fig. 6.29(b). The percent difference in the diameter change also shows the same trend as that of the absolute maximum stress. The maximum difference between the two soils is for the D/t ratio of 50, which is 14% at certain depths of cover. However, this is also not significant because the factor of safety against the change in diameter is very high for the D/t ratio of 50 as the pipe is quite rigid and the absolute value for the deflection is very small.

The next step was a comparison between the low and high-density marl for the live load case. A pipe diameter of 36 inches was chosen. The most critical depth of cover, which is 2 feet, was selected. This depth of cover gives the upper bound for the stresses and deformation for the live loads. As before, the D/t ratios were varied from 50 to 150. The results for the percent difference in the absolute maximum stress and diameter change for the two soils are shown in Fig. 6.30. The percent difference in the absolute maximum stress is within the range of 4 %; however, the percent difference in the diameter change is 12 % for certain cases, which is not large, owing to the large factor of safety in the diameter change for stiff pipes.

Based on the above discussion, it was decided to use only low-density marl in the analysis as it is the upper bound for the stresses and deflections.

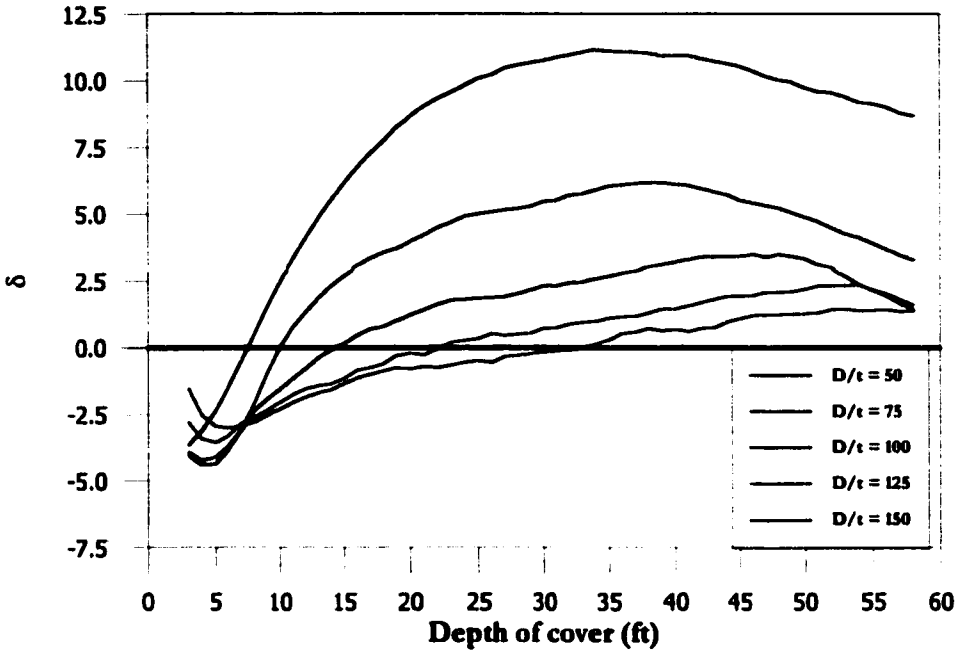

(a) Percent difference in absolute maximum stress

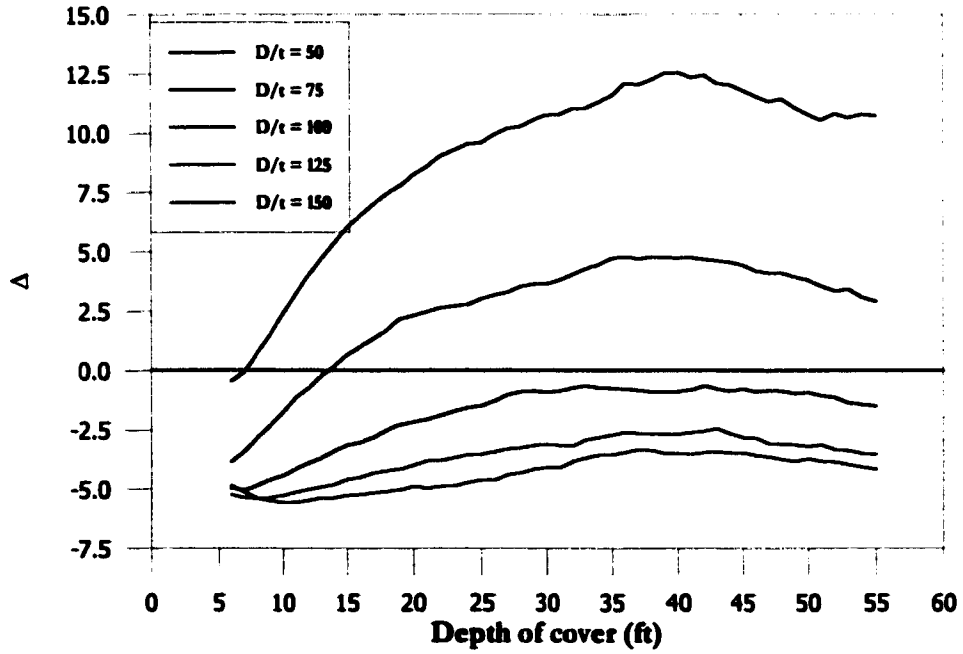

(b) Percent difference in diameter change

Fig. 6.29: Percent difference in marl low density and high density for dead load only

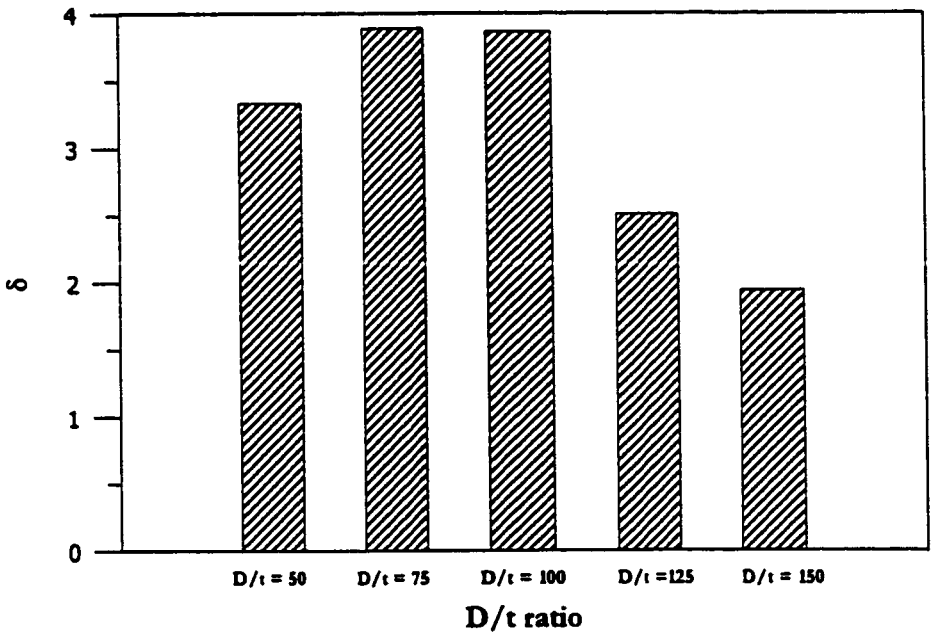

(a) Percent difference in absolute maximum stress

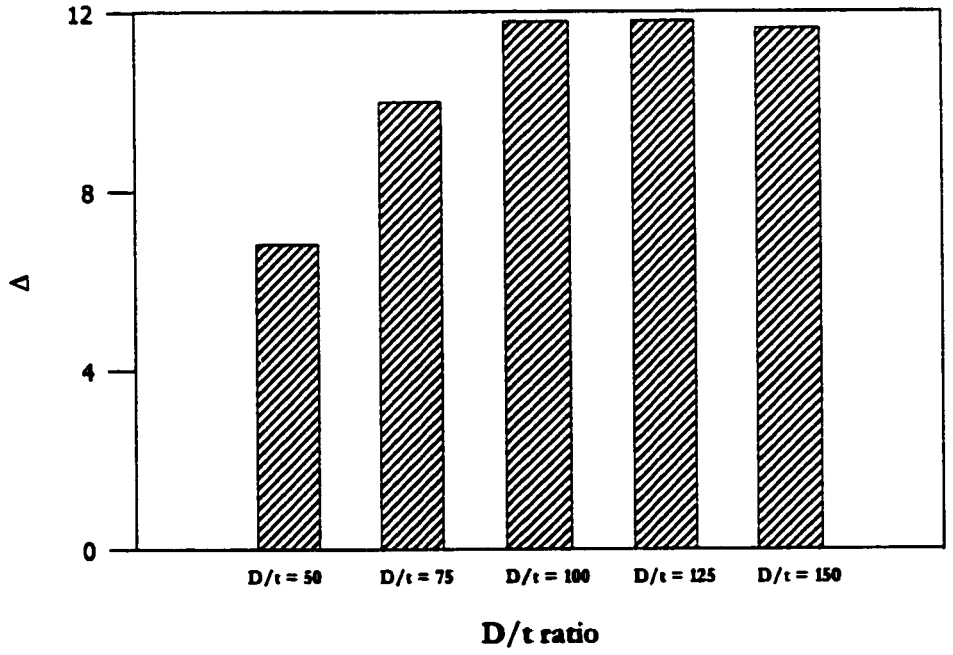

(b) Percent difference in Diameter change

Fig. 6.30: Percent difference in marl low density and high density for dead plus live load

6.6 Effect of Pavement

In the field, it is very common to have a layer of pavement on the top of the soil mass covering the buried pipelines. The stresses and deformation of such pipelines depend not only on the traffic loading, but also on the material properties of the pavement system and foundation soils. Highway pavements are generally grouped in two categories: rigid pavements with a top course of cement concrete and flexible pavements with a top layer of asphalt concrete. A typical highway cross-section consists of a rigid or flexible pavement, a compacted granular base course, and a subgrade of pre-existing natural material or compacted fill.

Katona [59] reported that pavements, both asphalt and concrete, are extremely effective in reducing the live load distress on a shallow buried pipe. Nevertheless, the pavement thickness is not customarily included as part of the minimum soil cover requirement because a minimum soil cover to withstand the construction loads prior to the placement of the pavement must protect the pipe. However, if the engineer is confident that construction loads prior to the placement of the pavement will be minimal, the inclusion of the pavement thickness into the soil cover is justifiable.

Since the stiffness of the overlying layers, especially the pavement, is the most influencing factor in the stress analysis of pipeline crossing, it is essential to use a realistic value for pavement modulus in the finite element analysis of pipeline crossing. The stiffness of the cement concrete may be determined on the basis of the uniaxial compressive strength, f'_c [86]. Average concrete compressive strengths of 3 to 6 ksi result in an elastic moduli of

3,100 to 4,400 ksi. Unfortunately, the stiffness of the asphalt concrete pavements varies over a much broader range, owing to the temperature-dependent viscosity of asphalt and its viscoelastic behavior. Data reported by Witczak [87] and Bissada et al. [88] indicate that in temperate climate, pavement temperatures may range from approximately $30°F$ to over $100°F$, and the modulus of elasticity of asphalt pavements over this temperature range may vary from 70 ksi to 2,000 ksi. This wide range for the modulus of elasticity makes the selection of a single value for it a difficult task. Fatani et al. [89] proposed an average value of 300 ksi for the modulus of elasticity of asphalt pavements, taking into account the local conditions of Saudi Arabia.

In order to study the effect of pavement stiffness variation on pipe stresses at crossing, a number of finite element simulations are carried out with various pavement stuffiness. The pipe diameter used in these simulations is 36 in. and the D/t ratios used are 50, 100, and 150. These D/t ratios represent the upper, lower, and middle values for the D/t ratio range. The finite element simulations are made for no-pavement condition and a 6-inch pavement with moduli of elasticity of 10, 300, and 500 ksi. In all of these simulations, the pavement, if present, is considered as a linear elastic material with a Poisson's ratio value of 0.35. A total of 48 simulations are run. The trench fill and overfill are always sand at low density, while the native soils simulated are sand at low density, sand at high density, marl at low density, and sabkha at high density. The reason behind choosing these types of soil only is discussed earlier in this chapter.

The results for absolute maximum stresses in the pipe and diameter changes are shown in Figs. 6.31 to 6.34. These findings clearly indicate that increasing the pavement stiffness

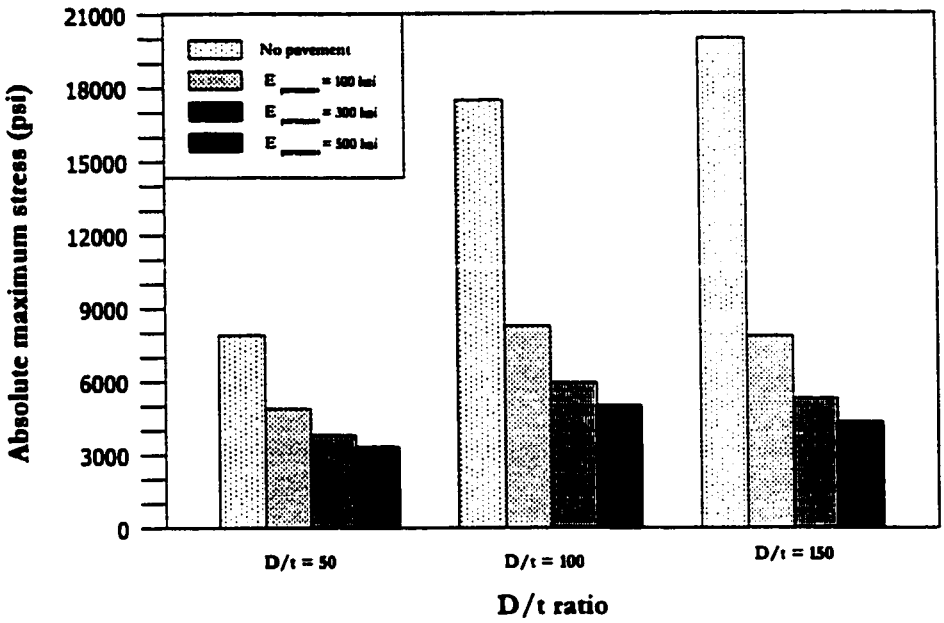

(a) Absolute maximum stress for various values of pavement stiffness

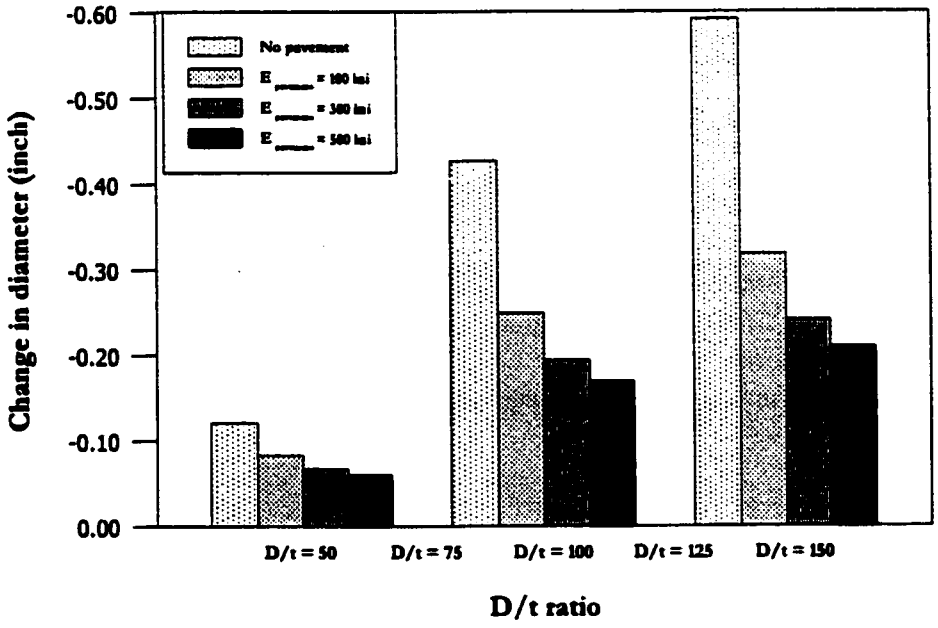

(b) Diamter change for various values of pavement stiffness

Fig. 6.31: Absolute maximum stress and diameter change in the pipe for sand at low density as native soil

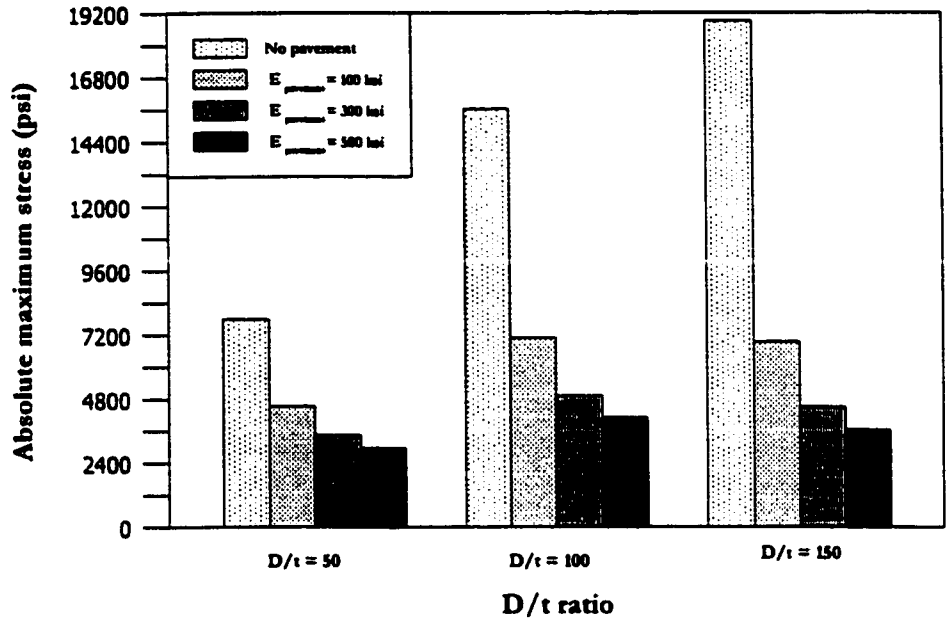

(a) Absolute maximum stress for various values of pavement stiffness

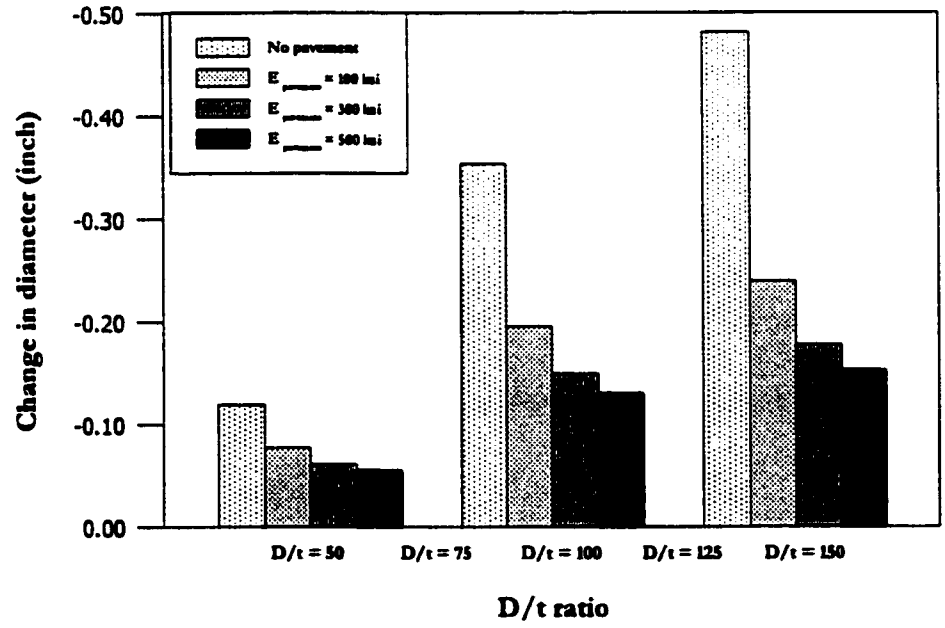

(b) Diamter change for various values of pavement stiffness

Fig. 6.32: Absolute maximum stress and diameter change in the pipe for sand at high density as native soil

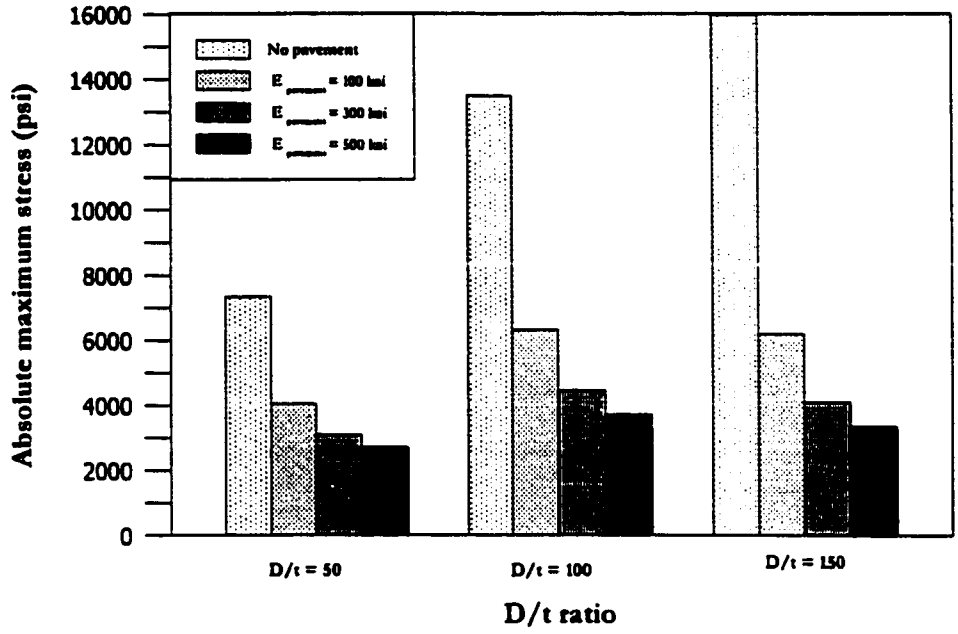

(a) Absolute maximum stress for various values of pavement stiffness

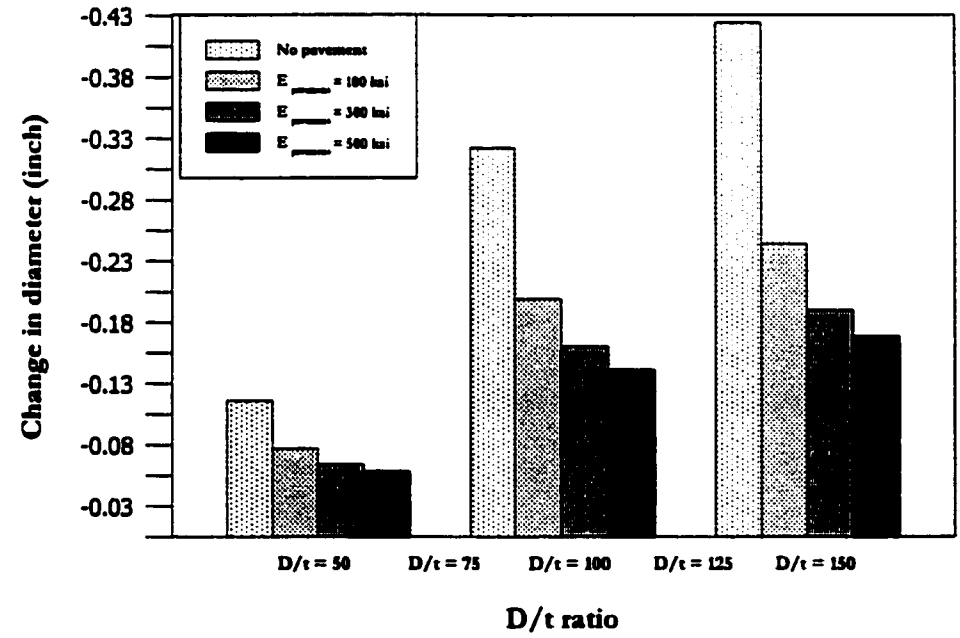

(b) Diamter change for various values of pavement stiffness

Fig. 6.33: Absolute maximum stress and diameter change for in the pipe marl at low density as native soil

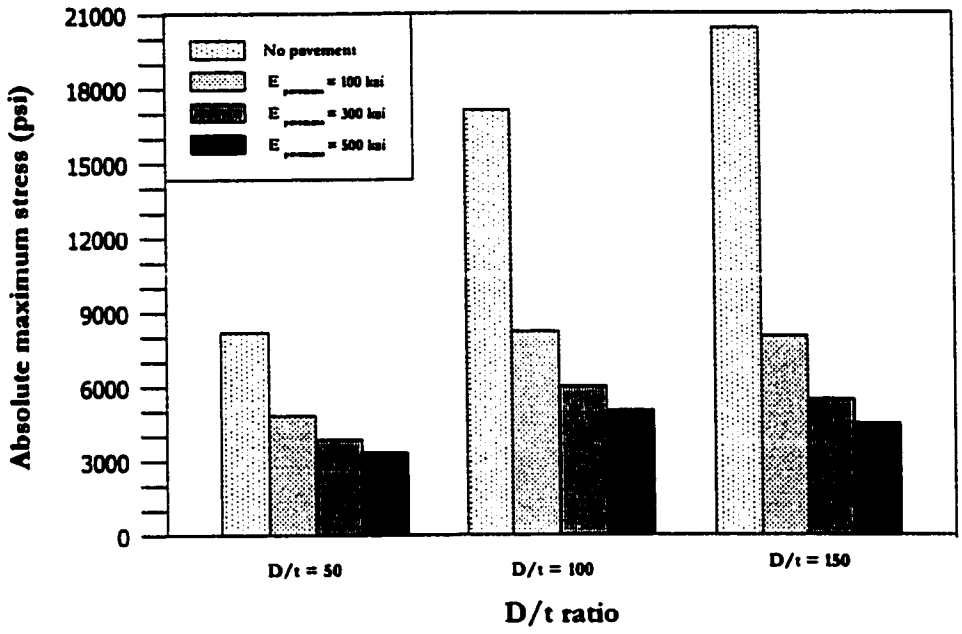

(a) Absolute maximum stress for various values of pavement stiffness

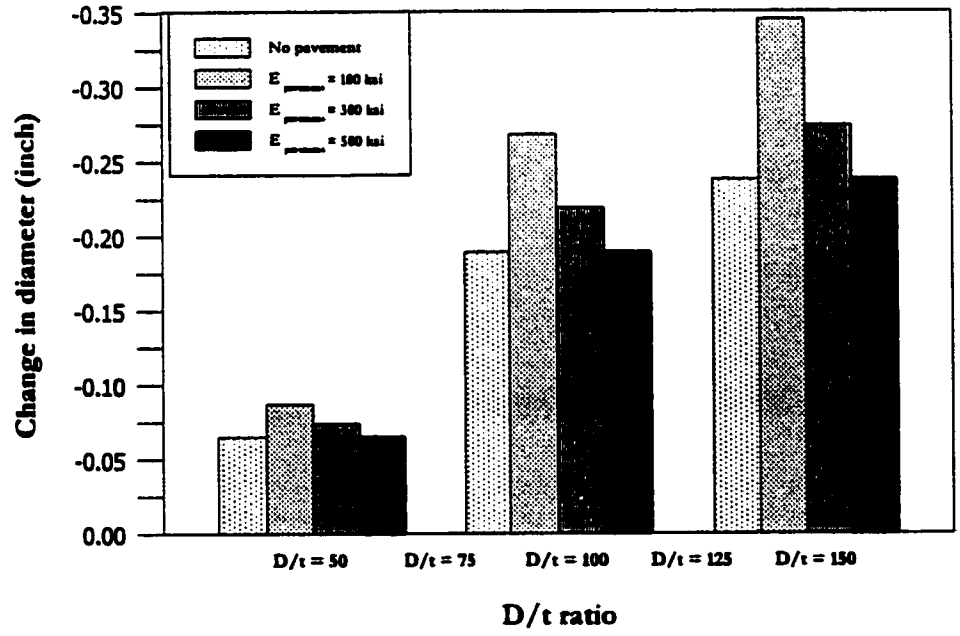

(b) Diamter change for various values of pavement stiffness

Fig. 6.34: Absolute maximum stress and diameter change in the pipe for sabkha at high density as native soil

results in a reduction in the absolute maximum stress and the diameter change. The most drastic difference is between "no-pavement" and "pavement" with very high stiffness. It can also be seen that the larger the D/t ratio the bigger is the difference in stresses and diameter changes. Since it is confirmed that pavement plays an important role in the pipeline stresses, it is decided to use a 6-inch pavement thickness with a modulus of elasticity of 300 ksi and a Poisson's ratio value of 0.35 in the pipeline crossing problem.

CHAPTER 7

RESULTS AND DISCUSSION

7.1 Introduction

In this chapter, results of the finite element analysis will be presented. First, the results of buried pipelines subjected to sand overburden will be discussed followed by results of pipelines subjected to live load due to highway crossings. The results are preceded by the identification of the parameters that have been varied in the finite element analyses followed by the comparison with the existing methods of design.

7.2 Pipelines Subjected to Sand Overburden

Cross-country Pipelines are subjected to dead loads coming from the soil cover provided in accordance with the code requirements. In general, the dead load due to soil cover for cross-country pipelines is quite minimal. However if the pipelines are passing through an active sand area there is a probability of formation of sand dune over the pipeline. In such cases, the pipelines are subjected to the sand overburden load which could have ma-

jor effect on the behavior of the buried pipelines [56]. Thus these pipelines either have to be designed to withstand the anticipated maximum load due to the sand overburden, or a continuous monitoring and removal of sand above a certain height have to be made.

A detailed study on such pipelines in active sand area [56] indicated from a full scale field test that steel pipelines subjected to sand overburden from dune formation can sustain much larger loads than those determined from existing design procedures. Moreover, there is a great need for conducting numerical analyses to simulate the pipes of various diameters and thicknesses under variety of different conditions. The aim is to come up with a design procedure suitable for design of pipelines subjected to sand overburden.

7.3 Parametric Study for Pipelines Under Sand Overburden

Taking advantage of the results and conclusions obtained in the previous chapters, a parametric study was carried out. Thus, only the important factors were considered in this section; the other factors which have little effect, if any, were eliminated. The following explains the various steps for the analysis of the sand overburden problem. It begins with the description of the various variables, which are critical and are varied in the finite element simulations. The variables, which are either marginal in importance or are not changed in the standard trench type pipe installation procedure are also identified. The results of the finite element simulations are then presented. The parameters are discussed under the following headings: boundary conditions, trench configuration, construction increment sequence, soil properties, and pipe properties.

7.3.1 Boundary conditions

The boundary conditions for the finite element simulations are shown in Figs. 7.1 and 7.2. The boundary conditions conform with the specifications in the CANDE manual [39] and the recommendations made by Leonards et al. [69]. Fig. 7.1 shows a typical mesh together with boundary conditions used to simulate the trench-type installation with a 90° angle of trench inclination. This type of mesh is used in the analysis of problems with marl and sabkha as native soils, according to the recommendation given in a Section 6.2. Fig. 7.2 shows a typical mesh for a trench angle of inclination of 35° together with the boundary conditions used for the analysis of problems in which sand at low or high density is encountered as the native soil.

7.3.2 Trench configuration

Five zones are identified in the soil-pipe interaction system corresponding to five different material types. They are shown in Fig. 7.3, except the interface element, which has a zero thickness and is present between the nodes connecting the pipe elements to the soil elements. These zones are:

1. Pipe : steel pipe (appropriate reference).
2. In-situ soil : also termed as native soil meaning which will be effected due to excavation.
3. Trench fill : the soil material used to fill the trench after the pipe has been installed.
4. Overfill : the soil above the trench which is placed after the trench has been filled with sand.
5. Interface : The pipe-soil interface is modeled by the interface elements, which are

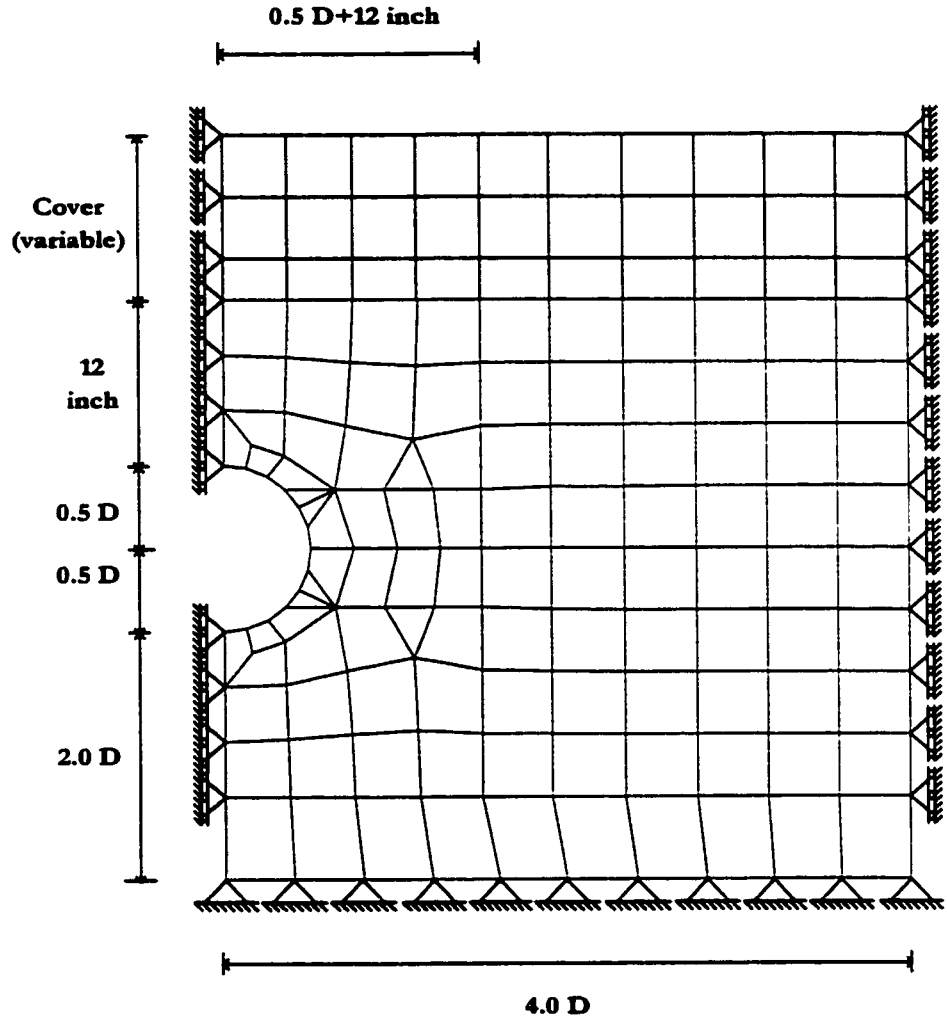

Fig. 7.1: Boundry conditions for a mesh with 90° trench inclination

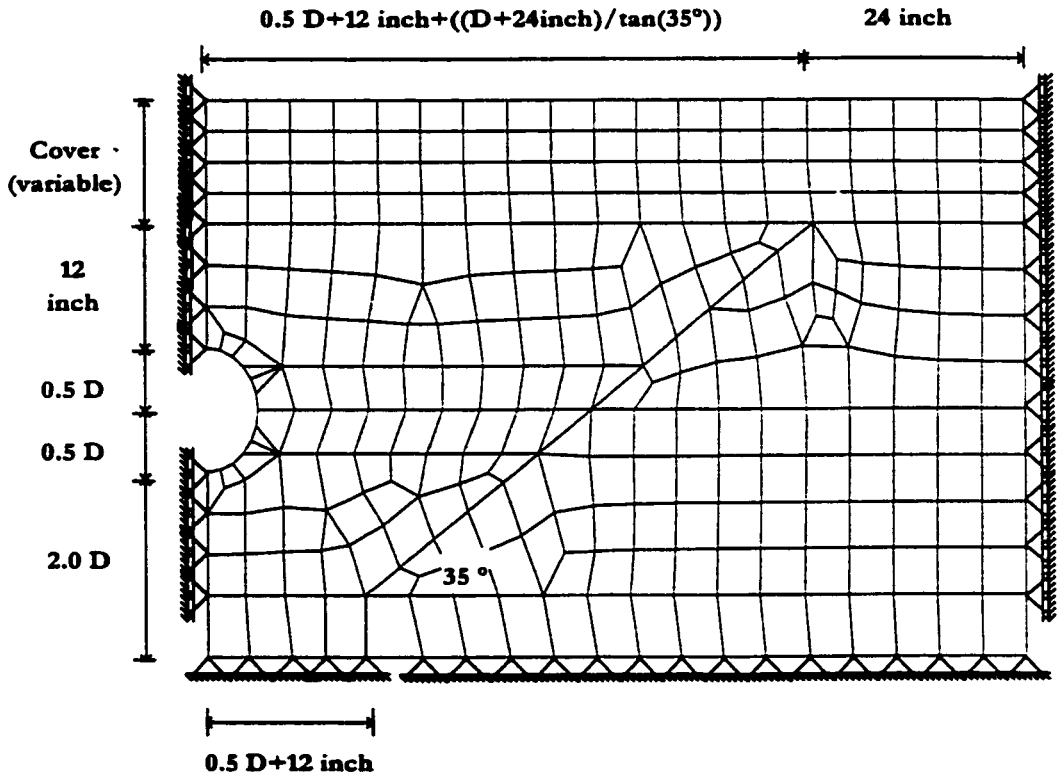

Fig. 7.2: Boundry conditions for a mesh with 35° trench inclination

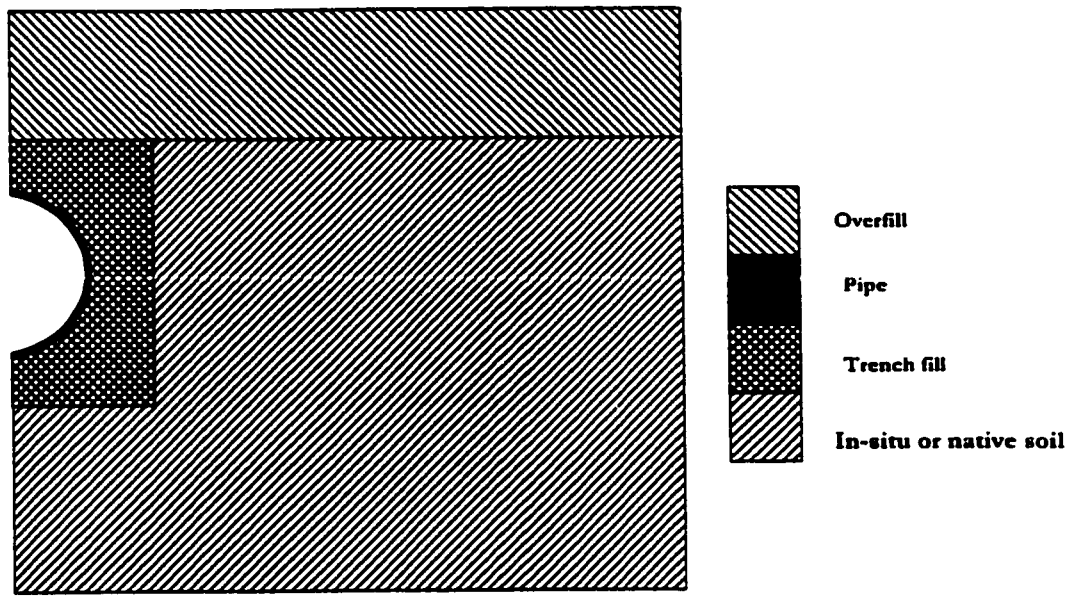

(a) Trench type model with 90 degree, angle of trench inclination

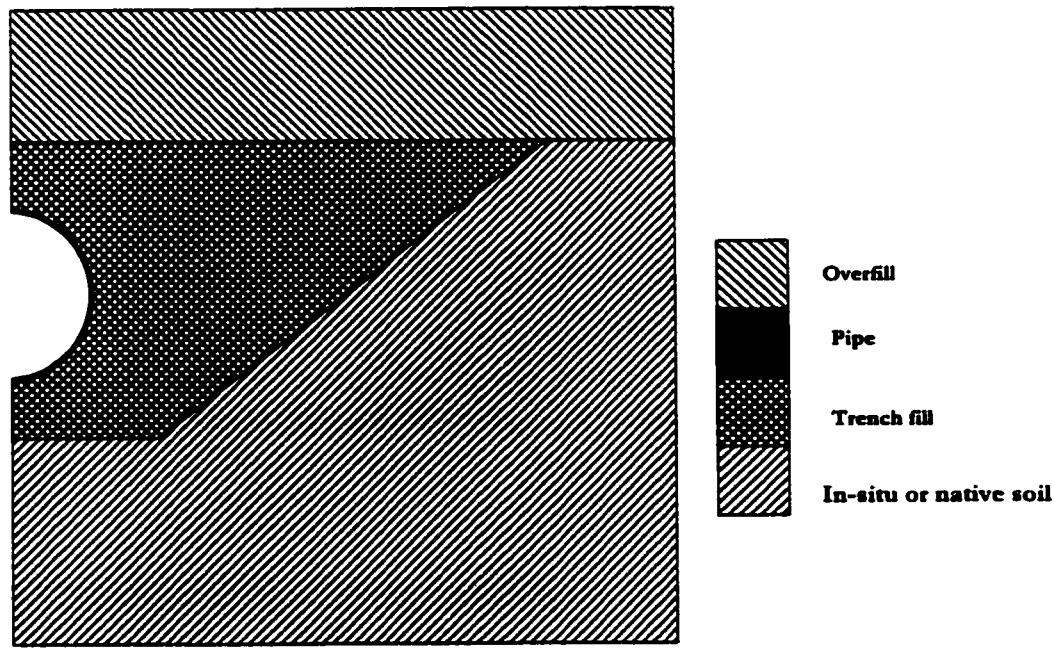

(b) Trench type model with 35 degree, angle of trench inclination

Fig. 7.3: Material zone identification for trench type model

essential to model the conditions of slip and de-bonding at the pipe-soil interface.

7.3.3 Construction increment sequence

The construction increment sequences shown in Fig. 7.4 a & b are used in all of the simulations for the sand overburden problems. This construction increment resembles the standard method of installation used locally. Moreover, the construction increments are arranged in such a way that each foot of depth of cover is simulated in a single construction increment; this makes it possible to get the stresses for depths of cover from 1 to 60 feet in a single simulation. A mesh showing a depth of cover of 60 feet is shown in Fig. 7.5.

7.3.4 Pipe properties

The properties of the pipe material used in the analysis are given in Table 7.1; they conform to the API $5L$ grade $X60$ steel; other grades may be used. The material property of the pipe is kept constant while the section properties are varied for each of the pipe diameters to simulate various D/t ratios. The section properties used in the analysis are given in Table 7.2.

7.3.5 Soil properties

Four types of soil materials are identified: sand at low density, sand at high density, marl at low density, and sabkha at high density. Marl at low density and sabkha at high density will be referred from now on as marl and sabkha. It is also decided to use sand at low density as the trench fill and overfill material, although the native soil is changed. The full description of the material properties was presented in Chapter 4.

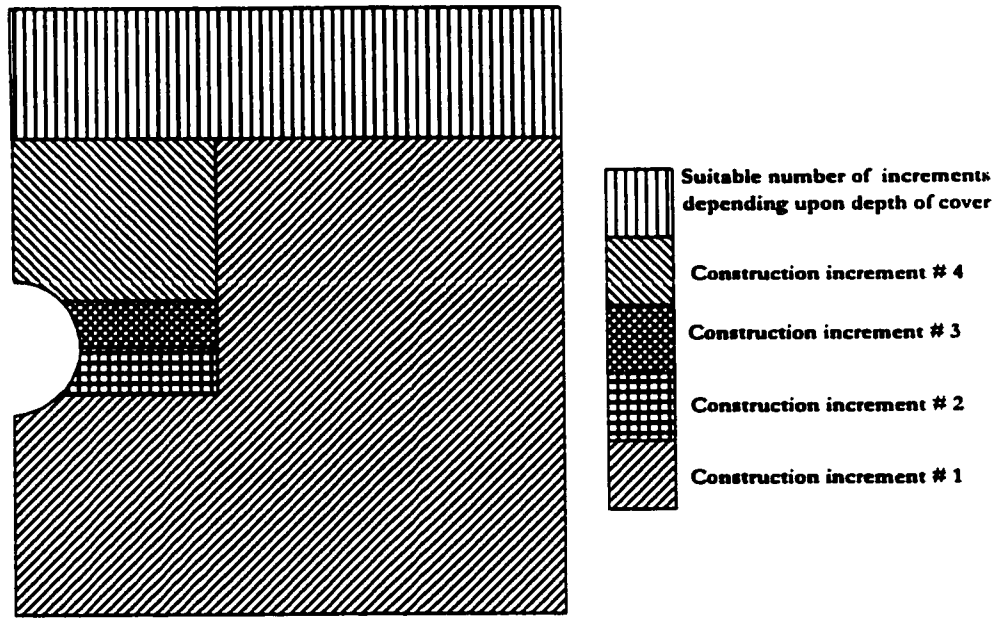

(a) Construction increments for Trench type model with 90 degree, angle of trench inclination

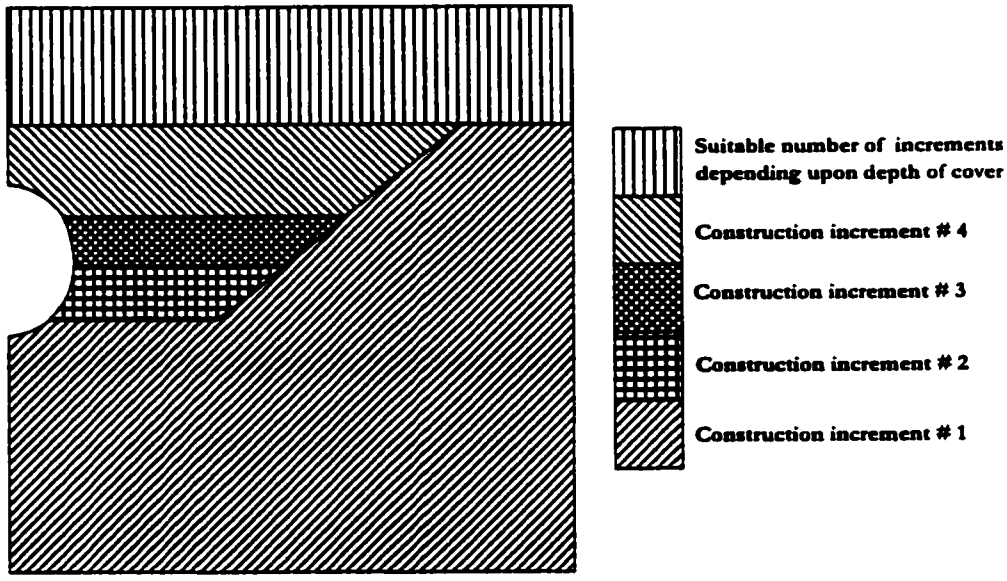

(b) Construction increments for Trench type model with 35 degree, angle of trench inclination

Fig. 7.4: Construction increment sequence for parametric study

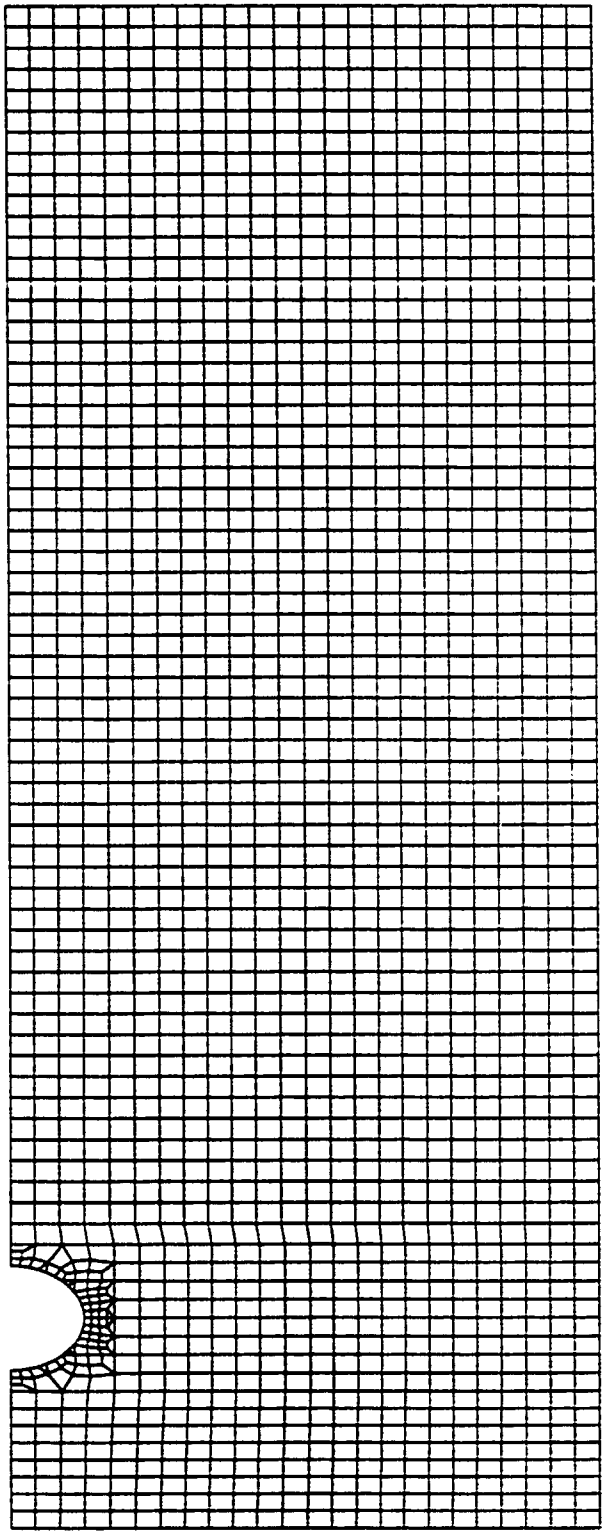

Fig. 7.5: A typical mesh with 60 feet depth of cover

TABLE 7.1: Material properties of the pipe used in the finite element analysis

Specification	API 5L
Grade	X60
Specified minimum yield strength	6,000,000 psi
Weld joint factor, E	1.00
Allowable stress, $\sigma_{allowable}$	43,200 psi
Modulus of Elasticity	290,000,000 psi
Poisson's ratio, μ	0.3
Density, γ_{pipe}	0.28 lb/in^3

TABLE 7.2: Section properties of the pipe used in the finite element analysis

Pipe Diameter (inches)	Thickness (inches)				
	D/t = 50	D/t = 75	D/t = 100	D/t = 125	D/t = 150
12	.24	.16	0.12	0.096	0.08
24	.48	.32	0.24	0.192	0.16
36	.72	.48	0.36	0.288	0.24
48	.96	.64	0.48	0.384	0.32
60	1.2	.8	0.6	0.48	0.4

Based on the above discussions, the parametric study was carried out. A total of 100 finite element simulations were executed for the sand overburden problem. The complete details of the runs data are given in Tables 7.3 & 7.4. As mentioned earlier, the construction increments were programmed in such a way that each finite element simulation gives the results for each foot of depth of cover from 1 to 60 feet. In the first construction increment, the native soil, pipe, and a small amount of trench fill underneath the pipe were activated, followed by the second construction increment in which the trench fill up to springline is activated. In the third increment, the trench is filled up to $\frac{1}{4}$ of diameter above the springline. The first foot of cover is activated in the fourth increment. The rest of the 59 increments follow.

7.4 Results for Sand Overburden Problem

The absolute maximum calculated stress and diameter change for pipes with diameters equal to 12, 24, 36, 48, and 60 inches are shown in Figs. 7.6 to 7.10 for low density sand, in Figs. 7.11 to 7.15 for high density sand, in Figs. 7.16 to 7.20 for marl, and in Figs. 7.21 to 7.25 for sabkha. Each diameter is plotted for depths of cover 1 to 60 feet, and for D/t ratios of 50 to 150 in increments of 25. The general trend which is common to all of the results presented here is that the variation of both stresses and diameter change with increasing depth of cover seem to be approaching an asymptotic value. The trend is very similar to results achieved from the design methods presented in Chapter 3. Another important observation is that stresses for large D/t ratio of 125 and 150 are either very similar to those for D/t ratios of 75 and 100 or sometimes even less. In other words the large increase

TABLE 7.3: Details of first 50 runs for sand overburden problem

Run #	Diameter (inches)	D/t	t (inches)	Soil type	H
1 2 3 4	12	50	.24	Sand at low density Sand at high density Marl Sabkha	1 to 60 feet
5 6 7 8	12	75	0.16	Sand at low density Sand at high density Marl Sabkha	1 to 60 feet
9 10 11 12	12	100	.12	Sand at low density Sand at high density Marl Sabkha	1 to 60 feet
13 14 15 16	12	125	.096	Sand at low density Sand at high density Marl Sabkha	1 to 60 feet
17 18 19 20	12	150	.08	Sand at low density Sand at high density Marl Sabkha	1 to 60 feet
21 22 23 24	24	50	.48	Sand at low density Sand at high density Marl Sabkha	1 to 60 feet
25 26 27 28	24	75	0.32	Sand at low density Sand at high density Marl Sabkha	1 to 60 feet
29 30 31 32	24	100	0.24	Sand at low density Sand at high density Marl Sabkha	1 to 60 feet
33 34 35 36	24	125	0.192	Sand at low density Sand at high density Marl Sabkha	1 to 60 feet
37 38 39 40	24	150	0.16	Sand at low density Sand at high density Marl Sabkha	1 to 60 feet
41 42 43 44	36	50	0.72	Sand at low density Sand at high density Marl Sabkha	1 to 60 feet
45 46 47 48	36	75	0.48	Sand at low density Sand at high density Marl Sabkha	1 to 60 feet
49 50	36	100	0.36	Sand at low density Sand at high density	1 to 60 feet

TABLE 7.4: Details of last 50 runs for sand overburden problem

Run #	Diameter (inches)	D/t	t (inches)	Soil type	H
51 52	36	100	0.36	Marl Sabkha	1 to 60 feet
53 54 55 56	36	125	0.28	Sand at low density Sand at high density Marl Sabkha	1 to 60 feet
57 58 59 60	36	150	0.24	Sand at low density Sand at high density Marl Sabkha	1 to 60 feet
61 62 63 64	48	50	0.96	Sand at low density Sand at high density Marl Sabkha	1 to 60 feet
65 66 67 68	48	75	0.64	Sand at low density Sand at high density Marl Sabkha	1 to 60 feet
69 70 71 72	48	100	.48	Sand at low density Sand at high density Marl Sabkha	1 to 60 feet
73 74 75 76	48	125	.384	Sand at low density Sand at high density Marl Sabkha	1 to 60 feet
77 78 79 80	48	150	0.32	Sand at low density Sand at high density Marl Sabkha	1 to 60 feet
81 82 83 84	60	50	1.2	Sand at low density Sand at high density Marl Sabkha	1 to 60 feet
85 86 87 88	60	75	0.8	Sand at low density Sand at high density Marl Sabkha	1 to 60 feet
89 90 91 92	60	100	0.6	Sand at low density Sand at high density Marl Sabkha	1 to 60 feet
93 94 95 96	60	125	0.48	Sand at low density Sand at high density Marl Sabkha	1 to 60 feet
97 98 99 100	60	'150	0.4	Sand at low density Sand at high density Marl Sabkha	1 to 60 feet

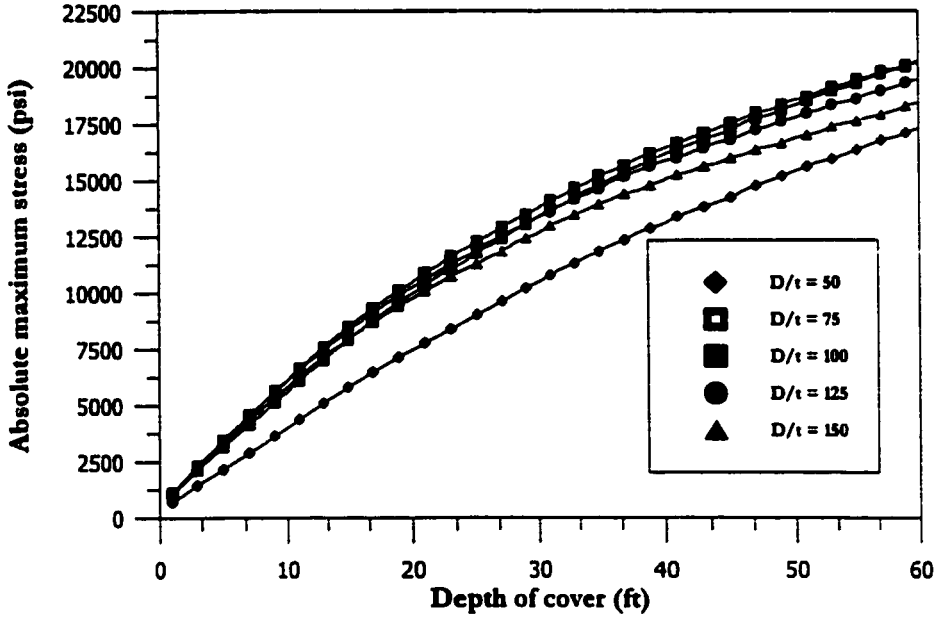

(a) Variation of absolute maximum stress

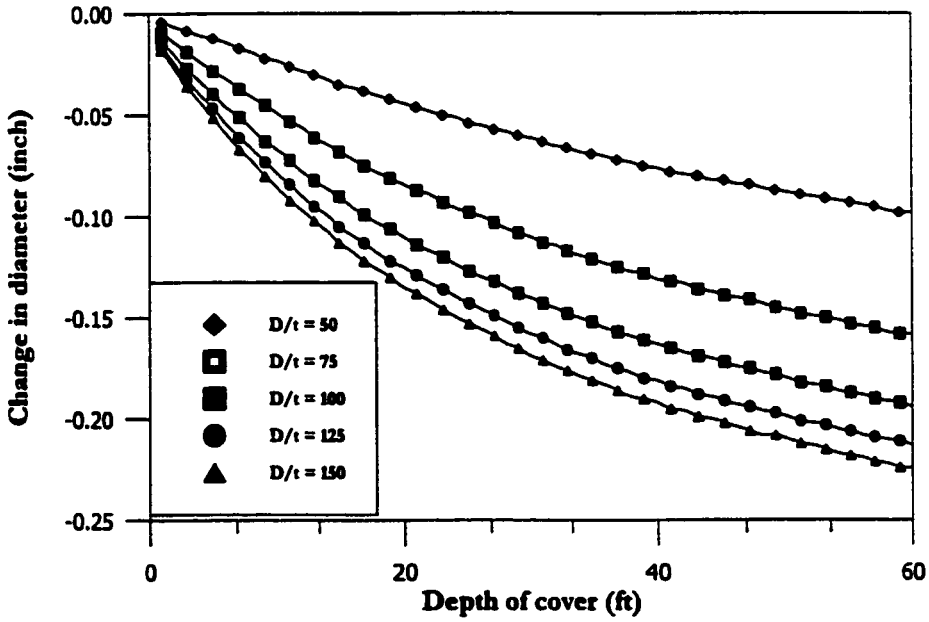

(b) Variation of change in diameter

Fig. 7.6: Absolute maximum stress and diameter change for 12 inches pipe diameter and low density sand as native soil

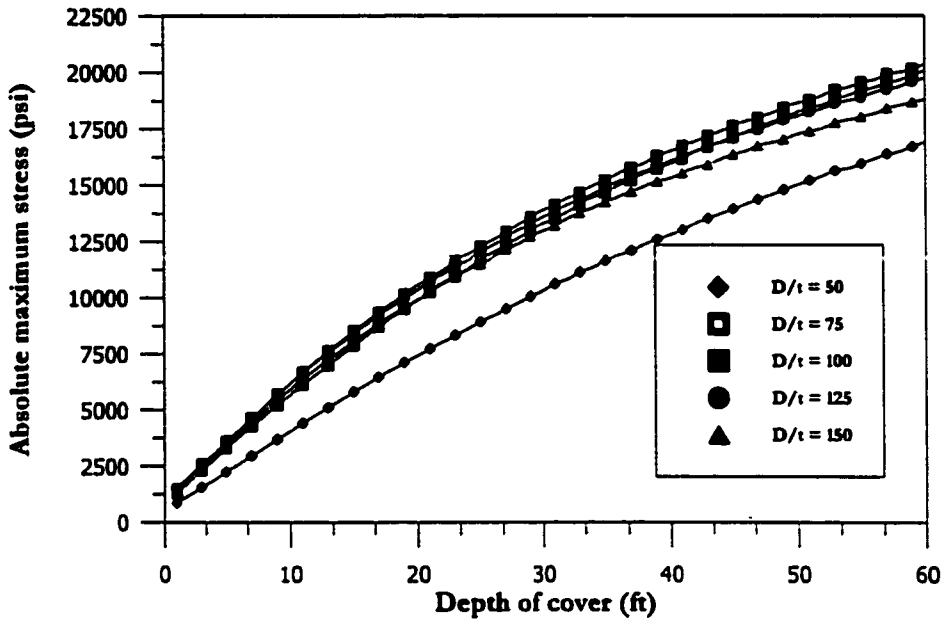

(a) Variation of absolute maximum stress

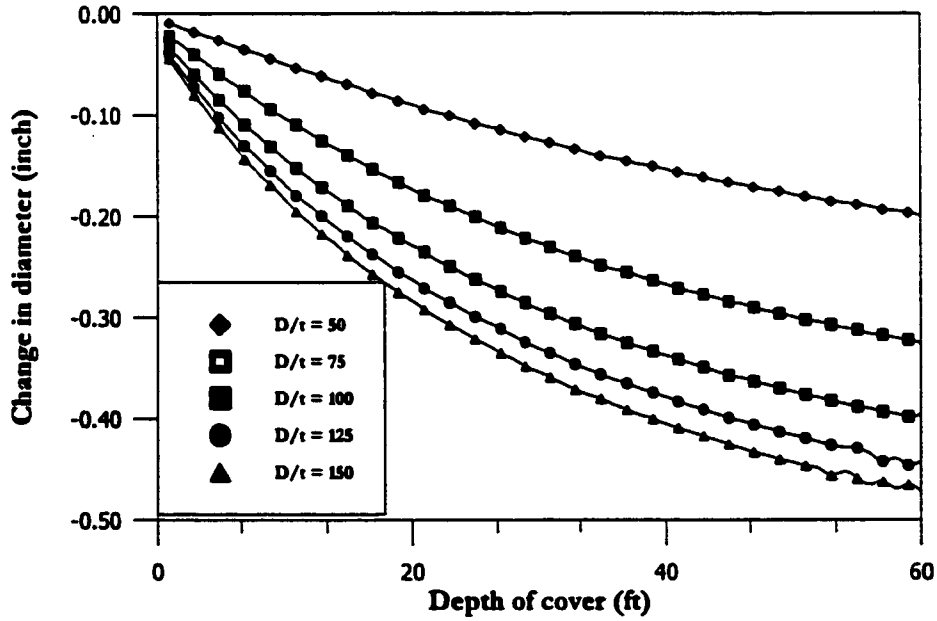

(b) Variation of change in diameter

Fig. 7.7: Absolute maximum stress and diameter change for 24 inches pipe diameter and low density sand as native soil

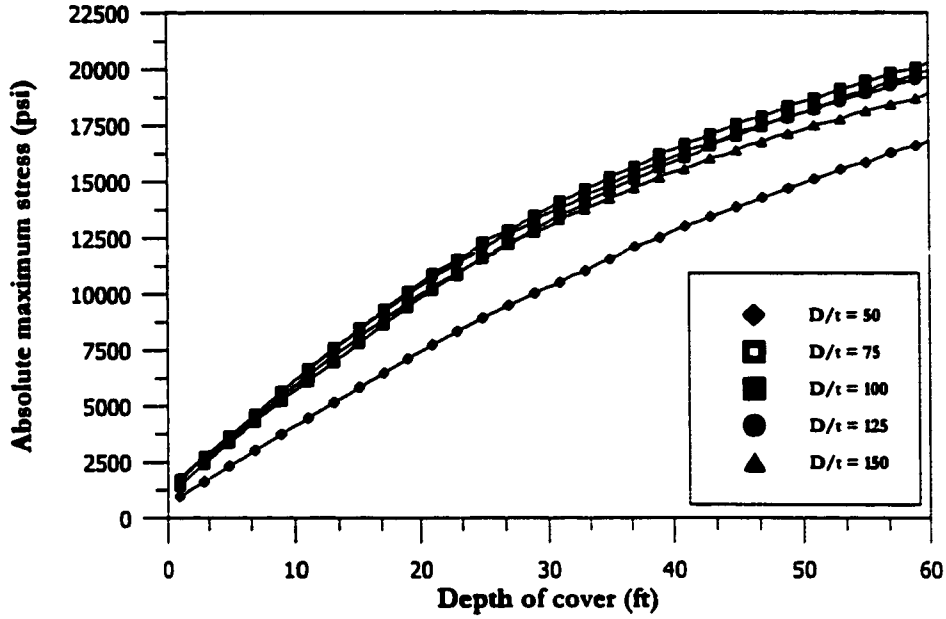

(a) Variation of absolute maximum stress

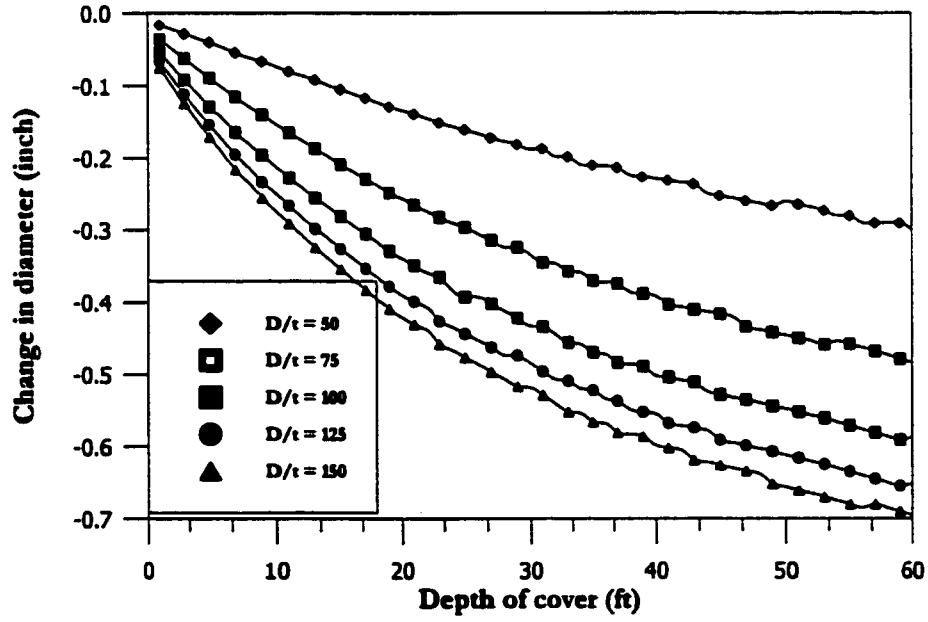

(b) Variation of change in diameter

Fig. 7.8: Absolute maximum stress and diameter change for 36 inches pipe diameter and low density sand as native soil

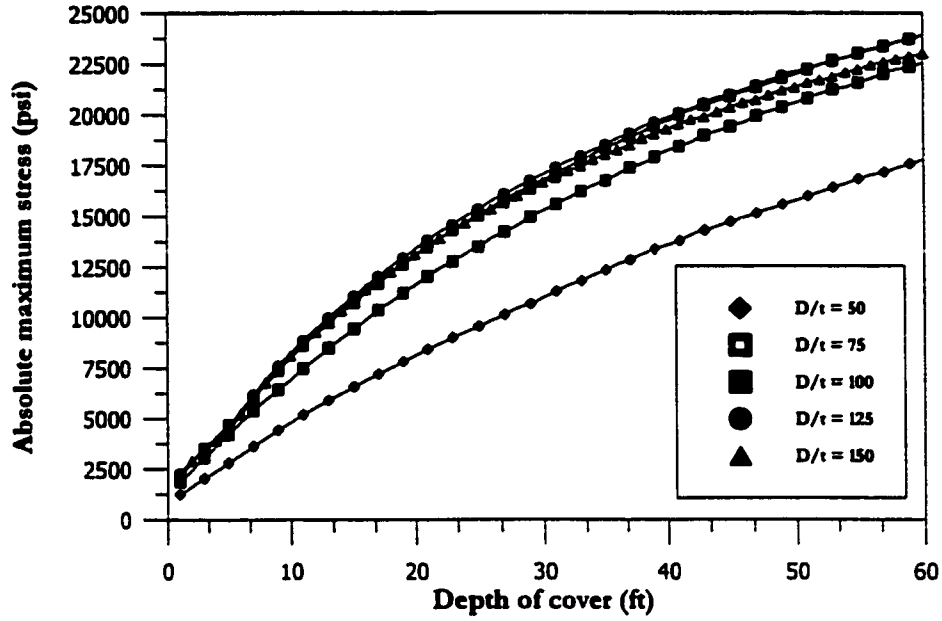

(a) Variation of absolute maximum stress

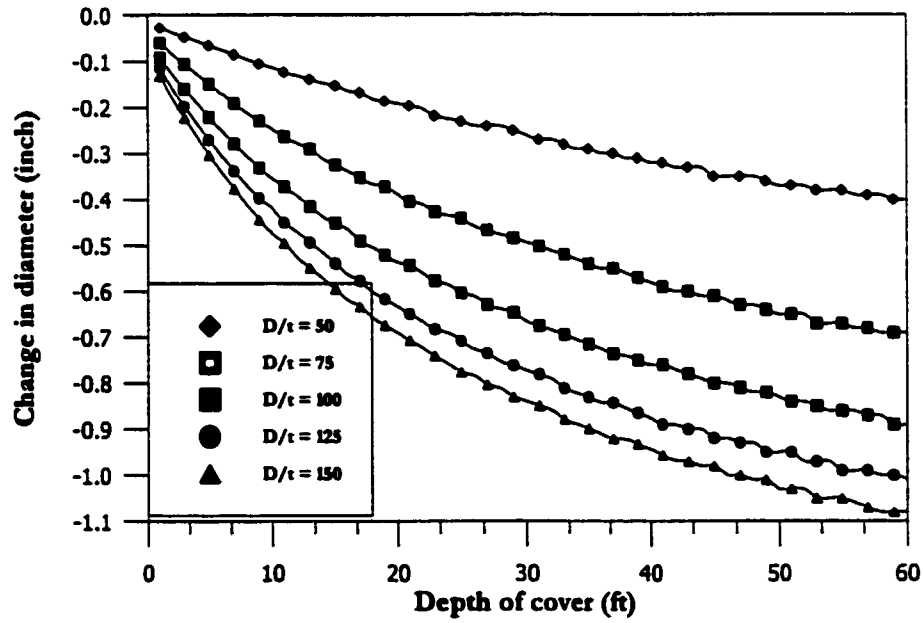

(b) Variation of change in diameter

Fig. 7.9: Absolute maximum stress and diameter change for 48 inches pipe diameter and low density sand as native soil

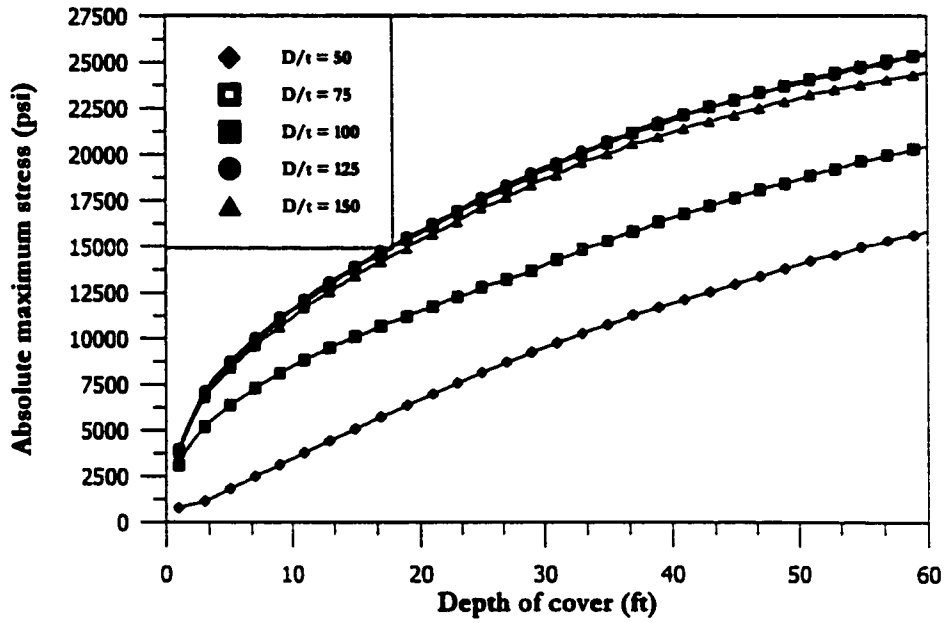

(a) Variation of absolute maximum stress

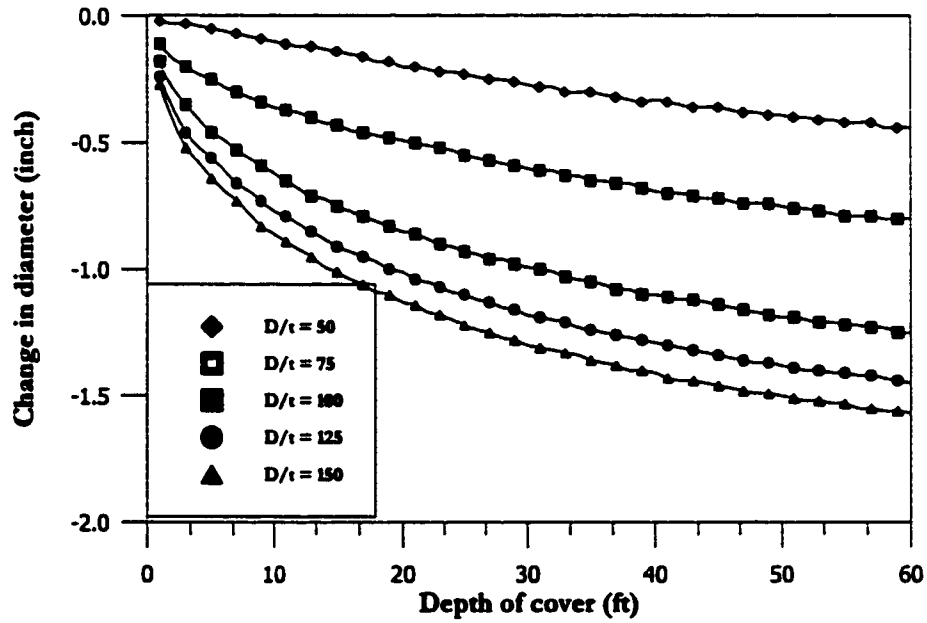

(b) Variation of change in diameter

Fig. 7.10: Absolute maximum stress and diameter change for 60 inches pipe diameter and low density sand as native soil

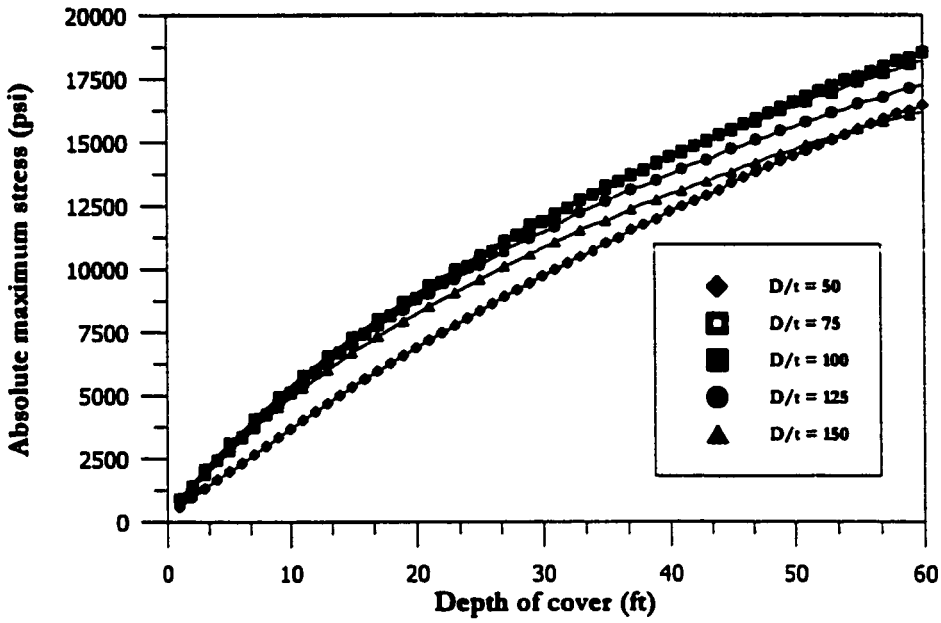

(a) Variation of absolute maximum stress

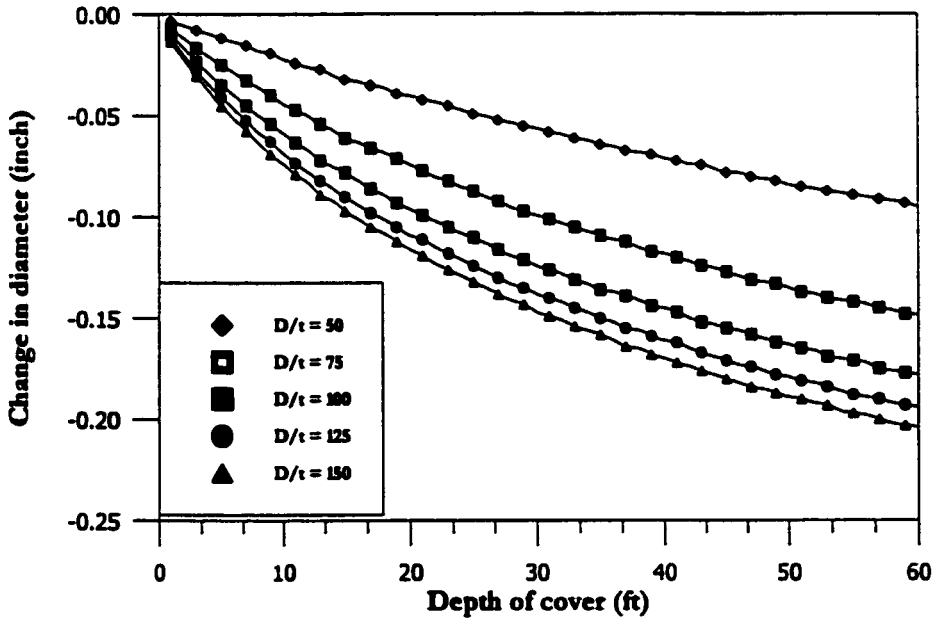

(b) Variation of change in diameter

Fig. 7.11: Absolute maximum stress and diameter change for 12 inches pipe diameter and high density sand as native soil

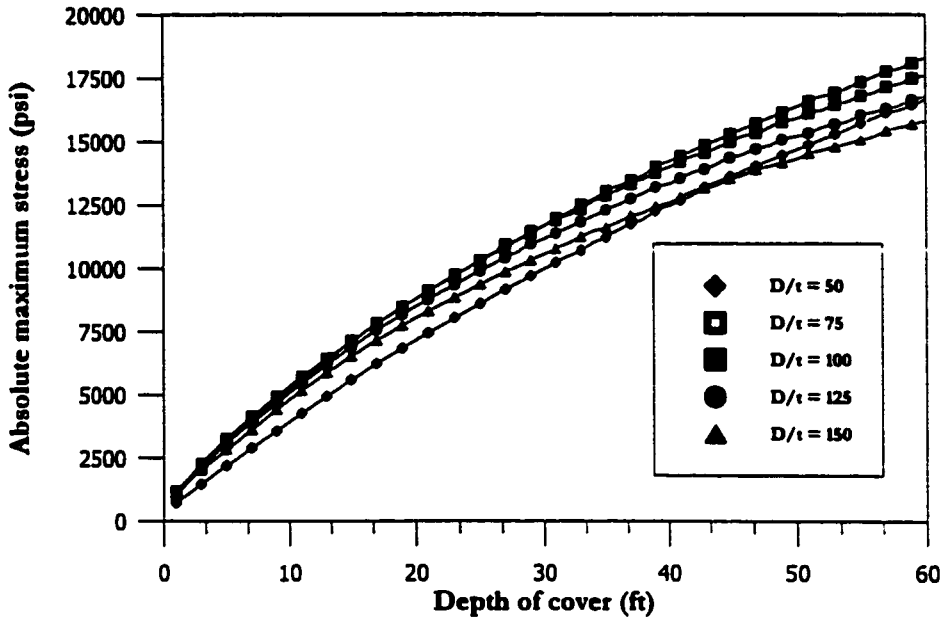

(a) Variation of absolute maximum stress

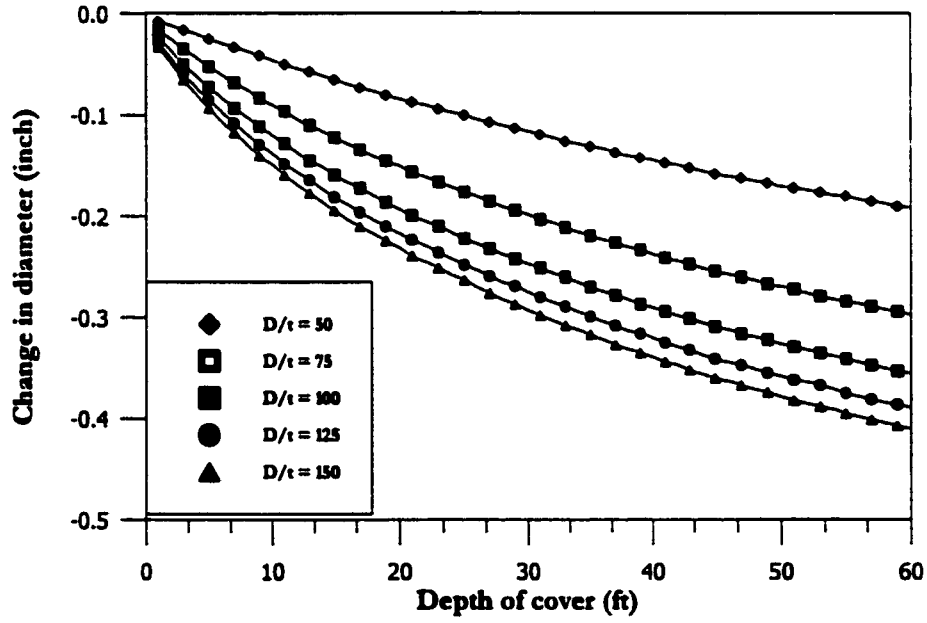

(b) Variation of change in diameter

Fig. 7.12: Absolute maximum stress and diameter change for 24 inches pipe diameter and high density sand as native soil

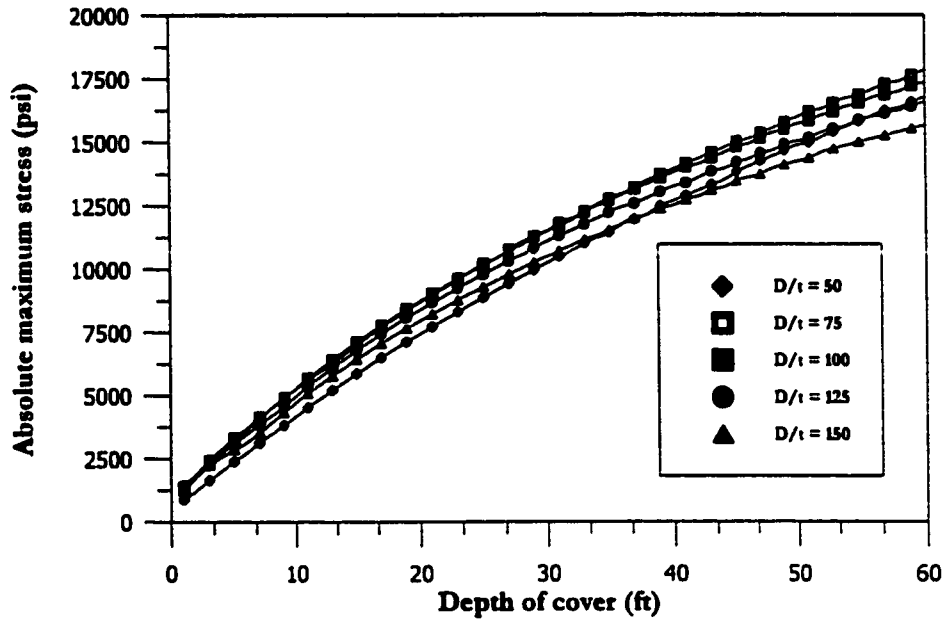

(a) Variation of absolute maximum stress

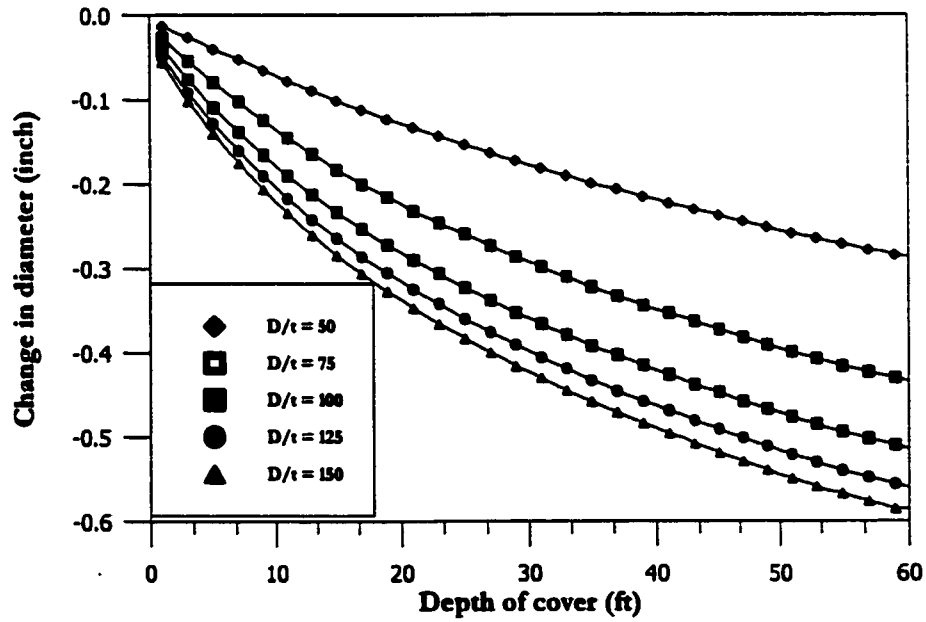

(b) Variation of change in diameter

Fig. 7.13: Absolute maximum stress and diameter change for 36 inches pipe diameter and high density sand as native soil

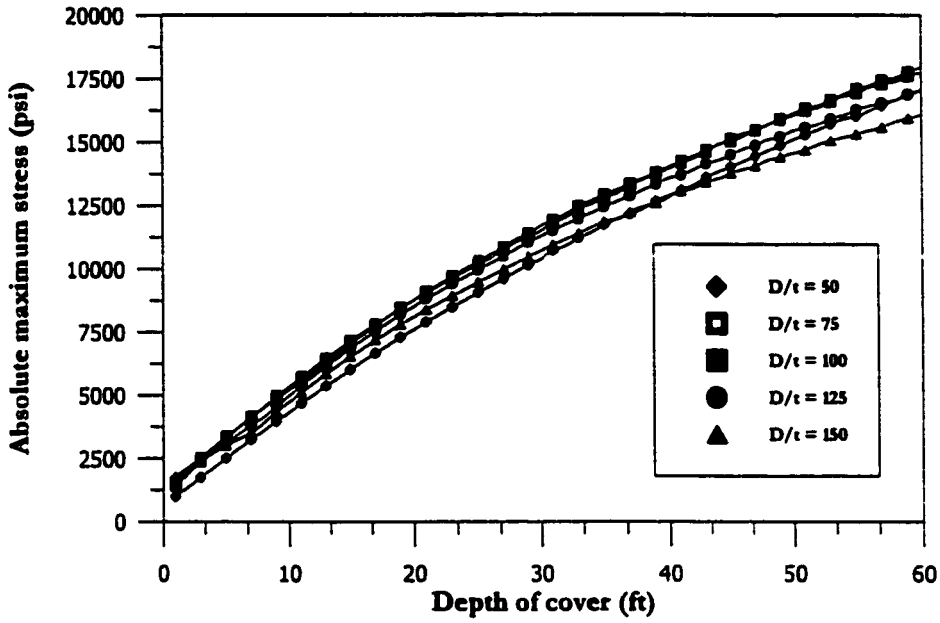

(a) Variation of absolute maximum stress

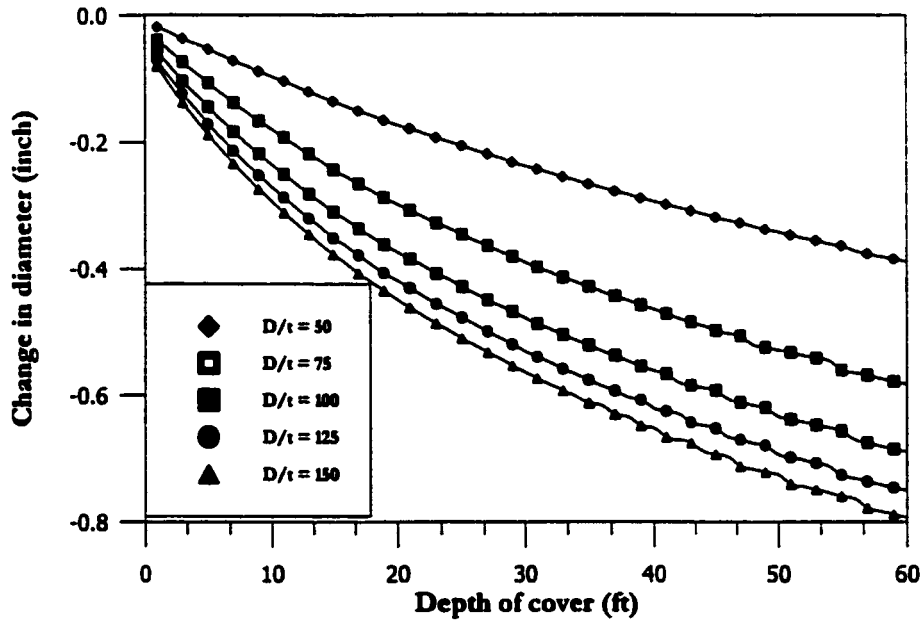

(b) Variation of change in diameter

Fig. 7.14: Absolute maximum stress and diameter change for 48 inches pipe diameter and high density sand as native soil

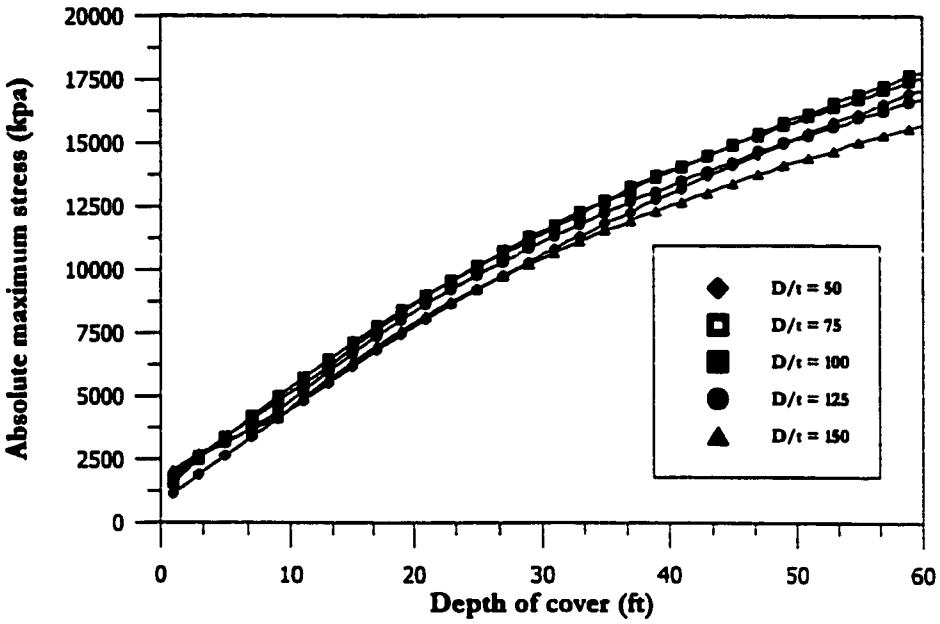

(a) Variation of absolute maximum stress

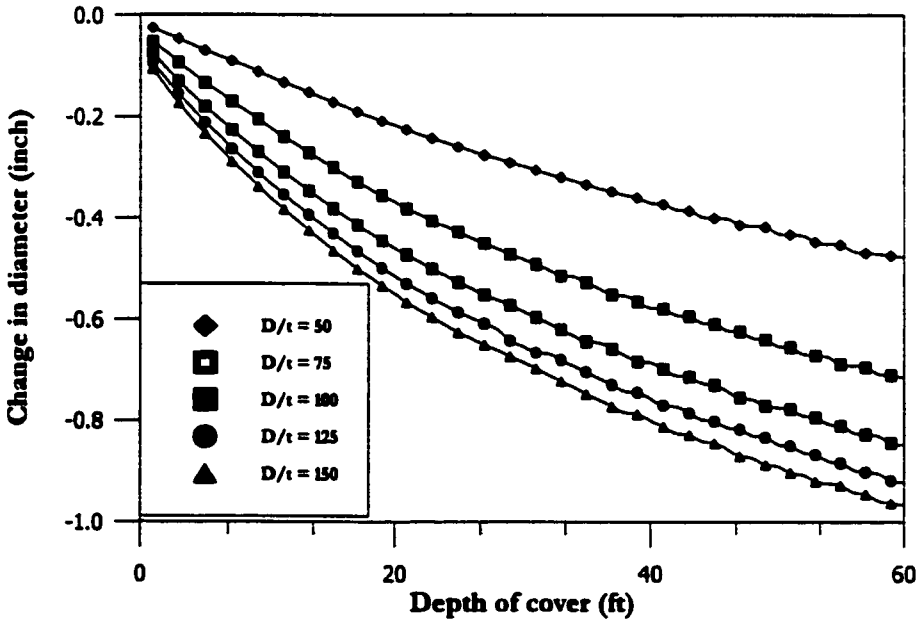

(b) Variation of change in diameter

Fig. 7.15: Absolute maximum stress and diameter change for 60 inches pipe diameter and high density sand as native soil

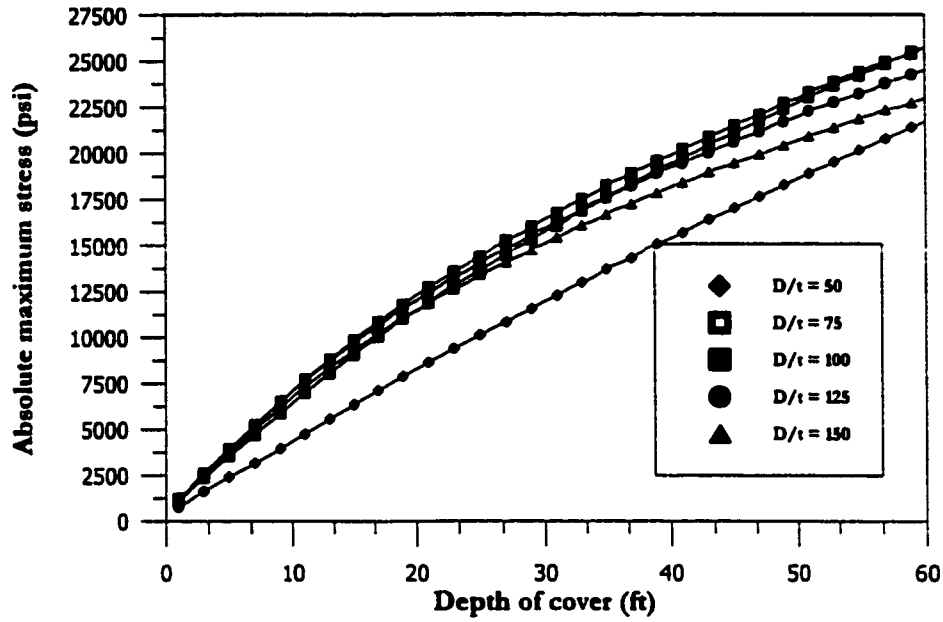

(a) Variation of absolute maximum stress

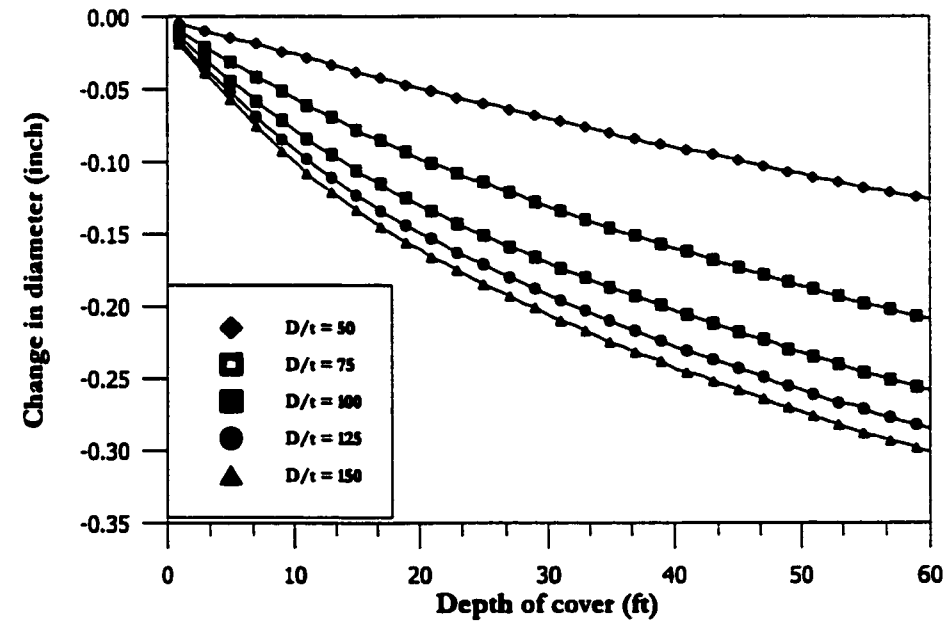

(b) Variation of change in diameter

Fig. 7.16: Absolute maximum stress and diameter change for 12 inches pipe diameter and marl as native soil

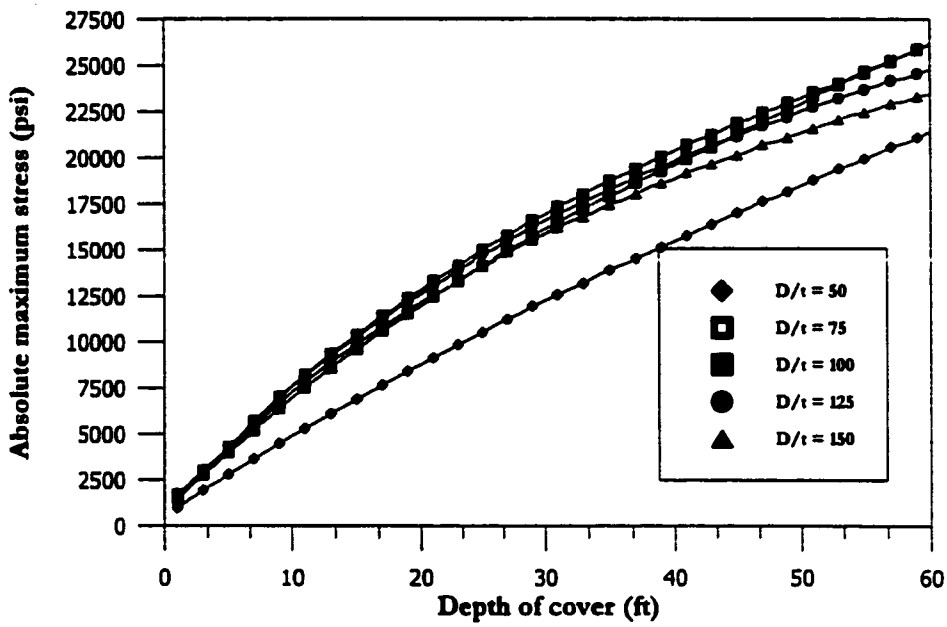

(a) Variation of absolute maximum stress

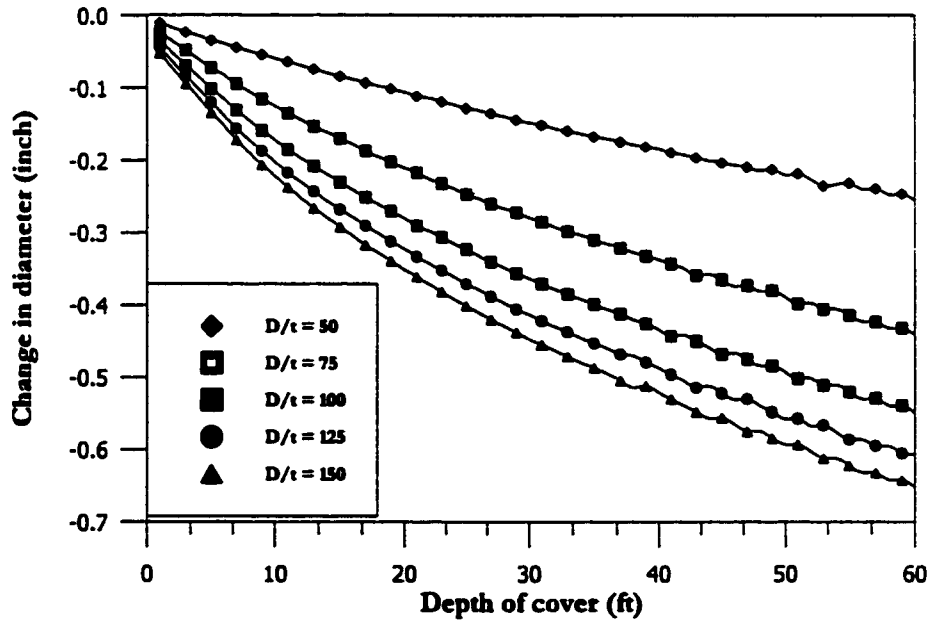

(b) Variation of change in diameter

Fig. 7.17: Absolute maximum stress and diameter change for 24 inches pipe diameter and marl as native soil

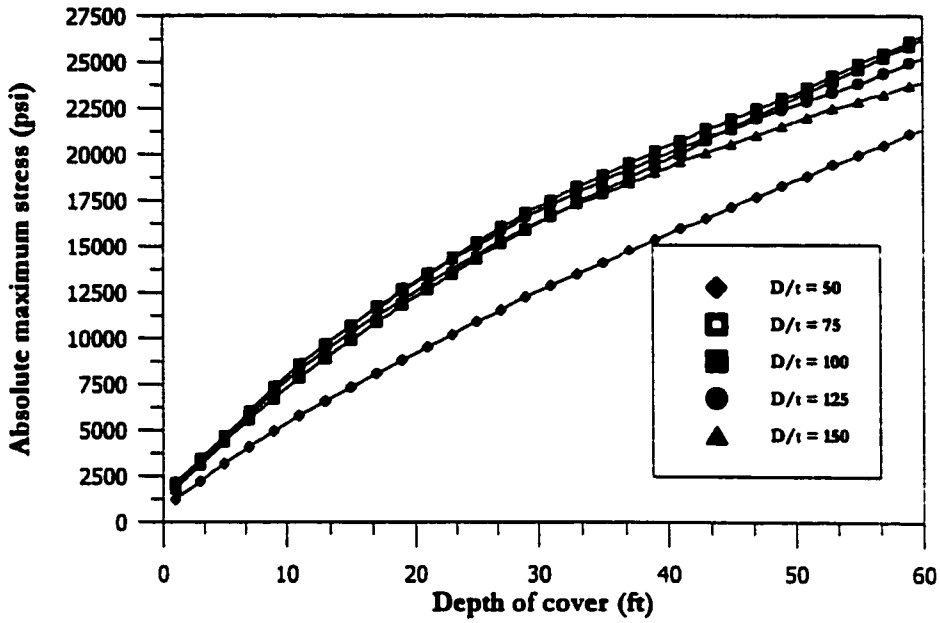

(a) Variation of absolute maximum stress

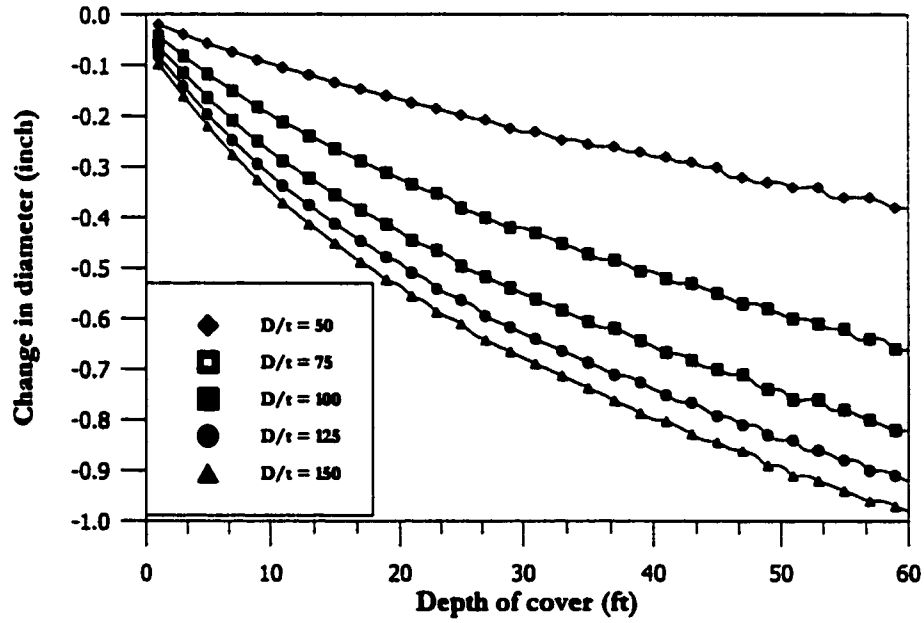

(b) Variation of change in diameter

Fig. 7.18: Absolute maximum stress and diameter change for 36 inches pipe diameter and marl as native soil

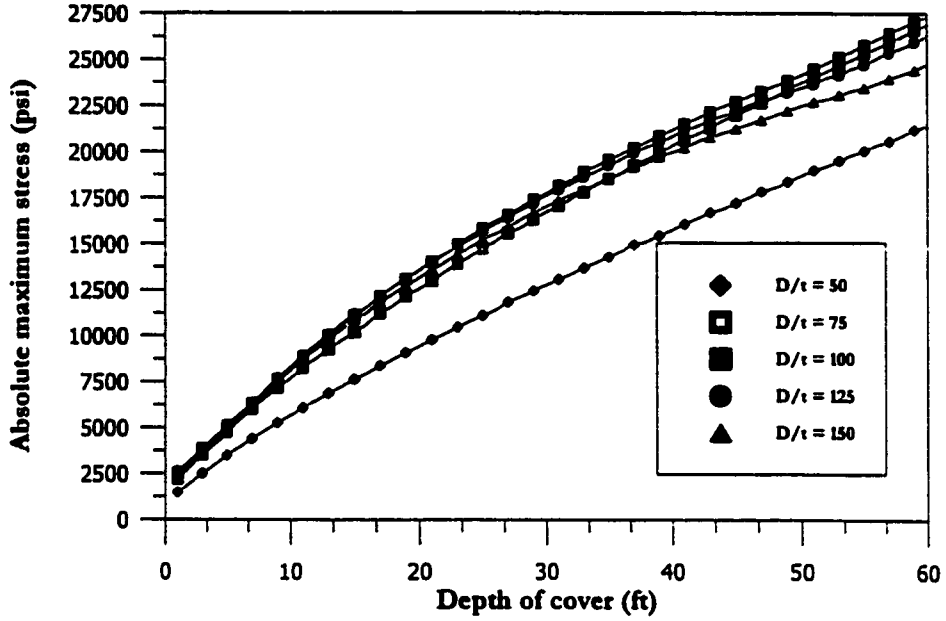

(a) Variation of absolute maximum stress

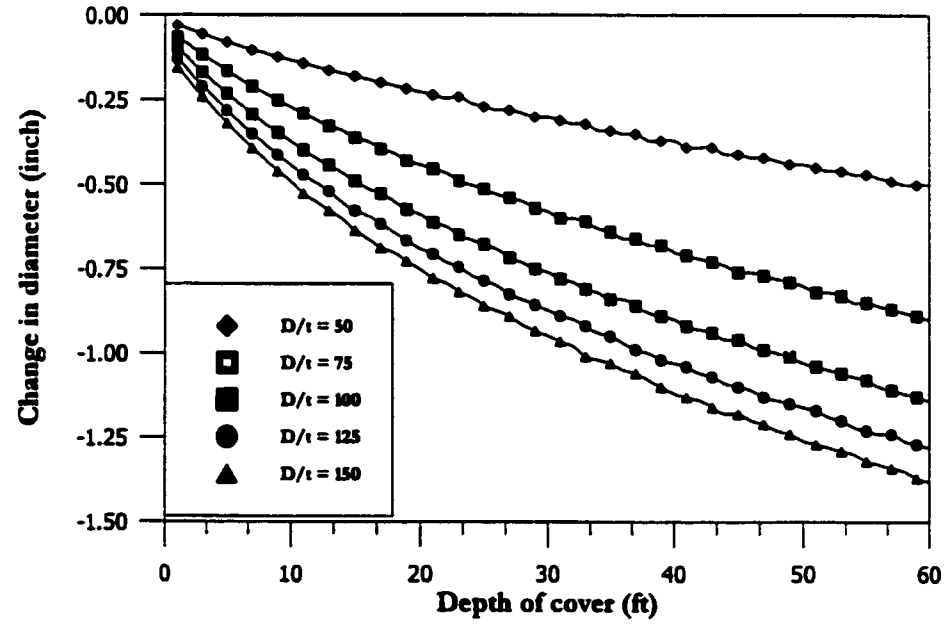

(b) Variation of change in diameter

Fig. 7.19: Absolute maximum stress and diameter change for 48 inches pipe diameter and marl as native soil

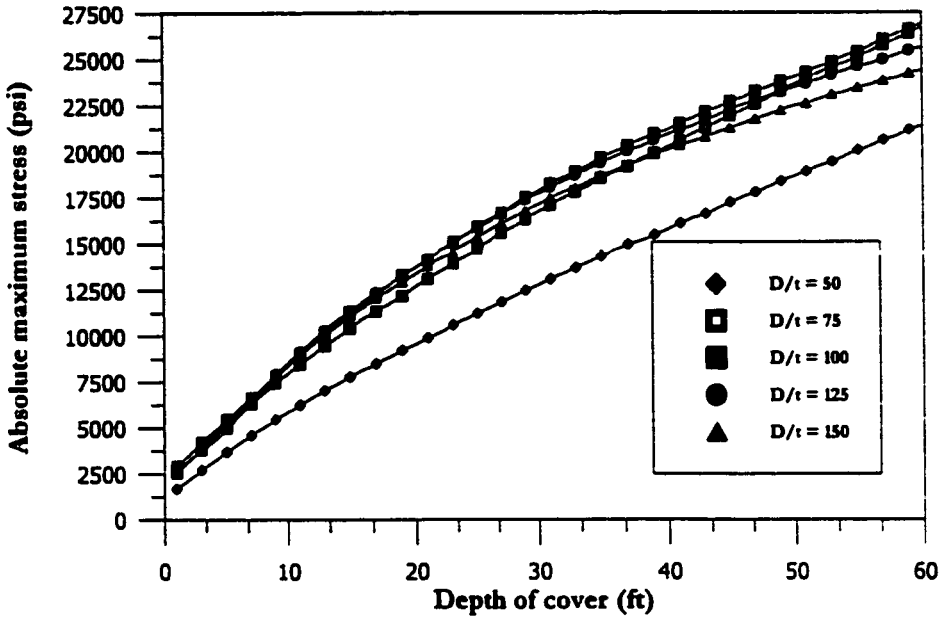

(a) Variation of absolute maximum stress

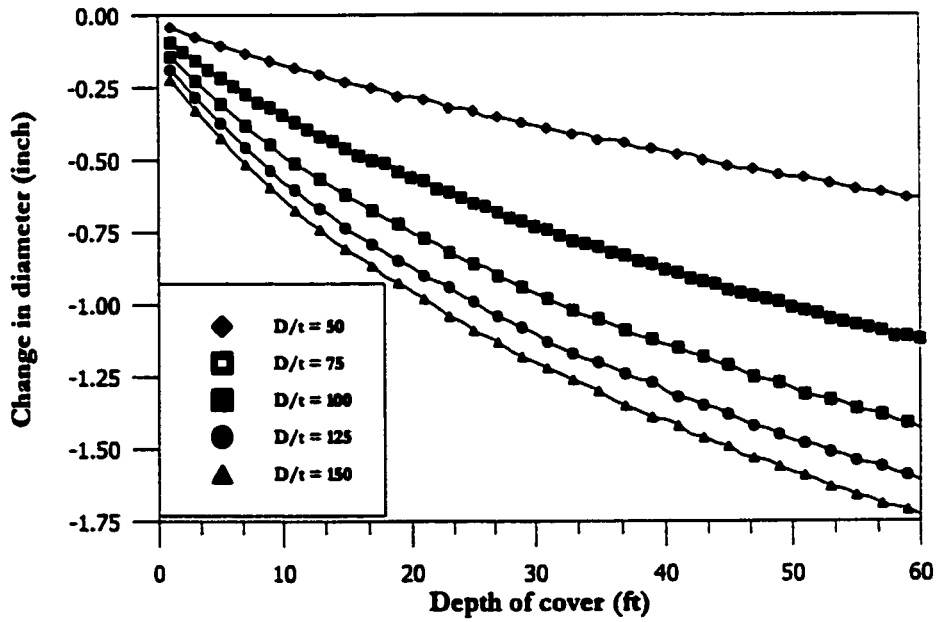

(b) Variation of change in diameter

Fig. 7.20: Absolute maximum stress and diameter change for 60 inches pipe diameter and marl as native soil

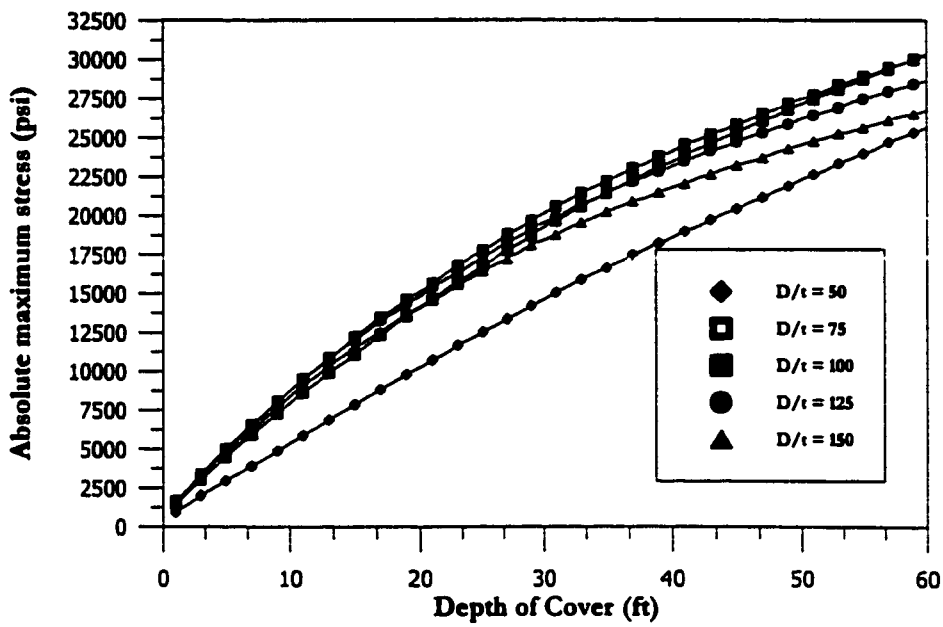

(a) Variation of absolute maximum stress

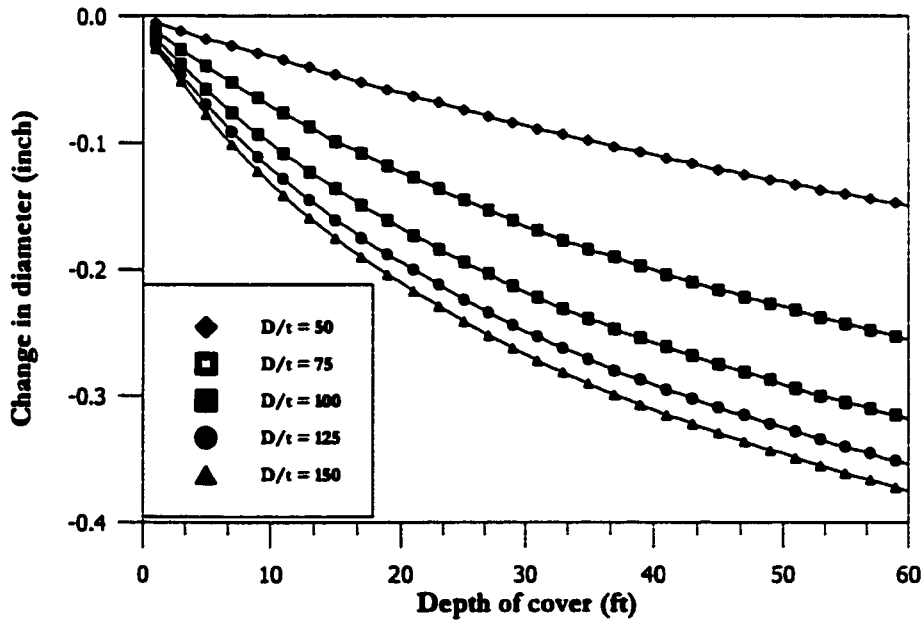

(b) Variation of change in diameter

Fig. 7.21: Absolute maximum stress and diameter change for 12 inches pipe diameter and sabkha as native soil

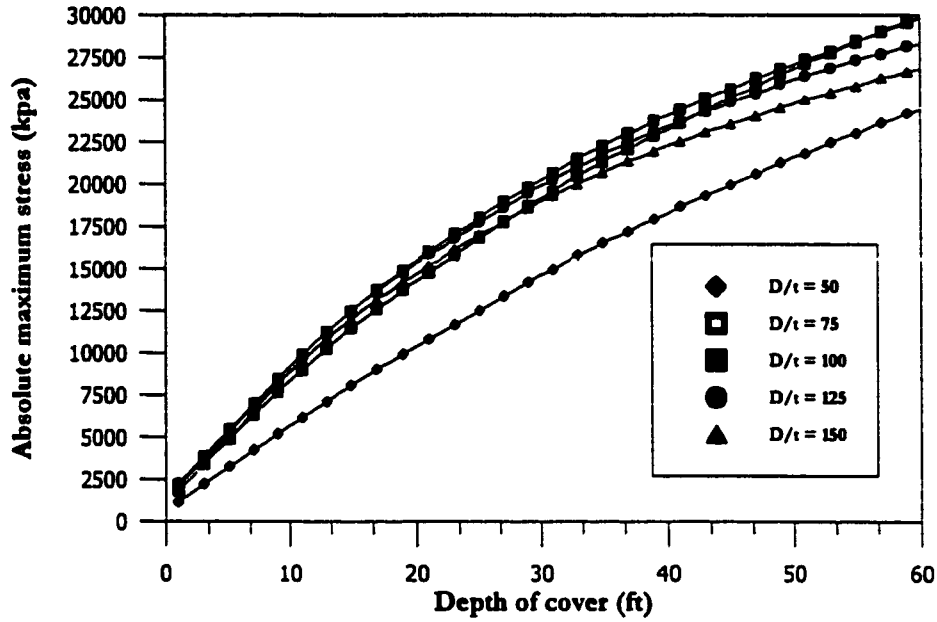

(a) Variation of absolute maximum stress

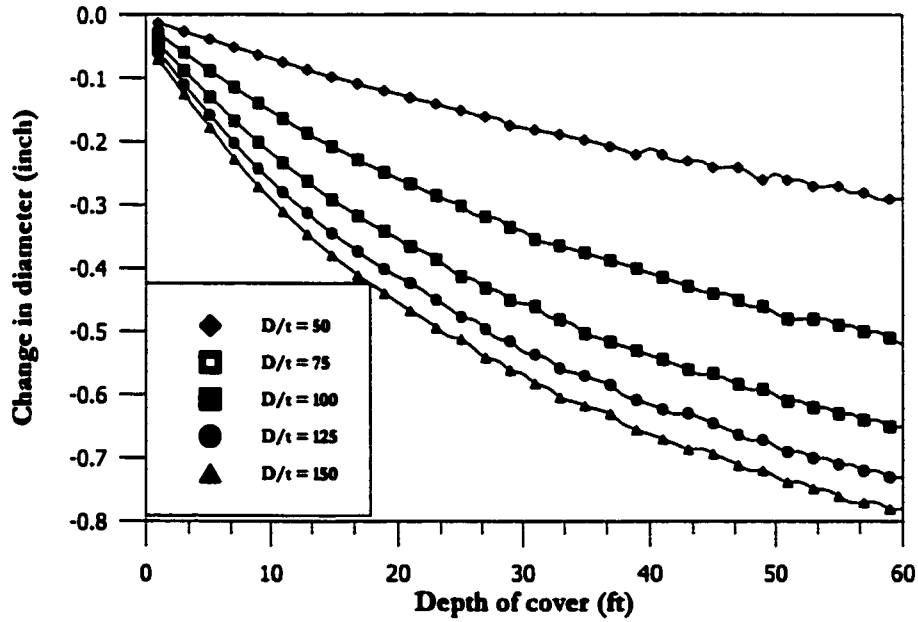

(b) Variation of change in diameter

Fig. 7.22: Absolute maximum stress and diameter change for 24 inches pipe diameter and sabkha as native soil

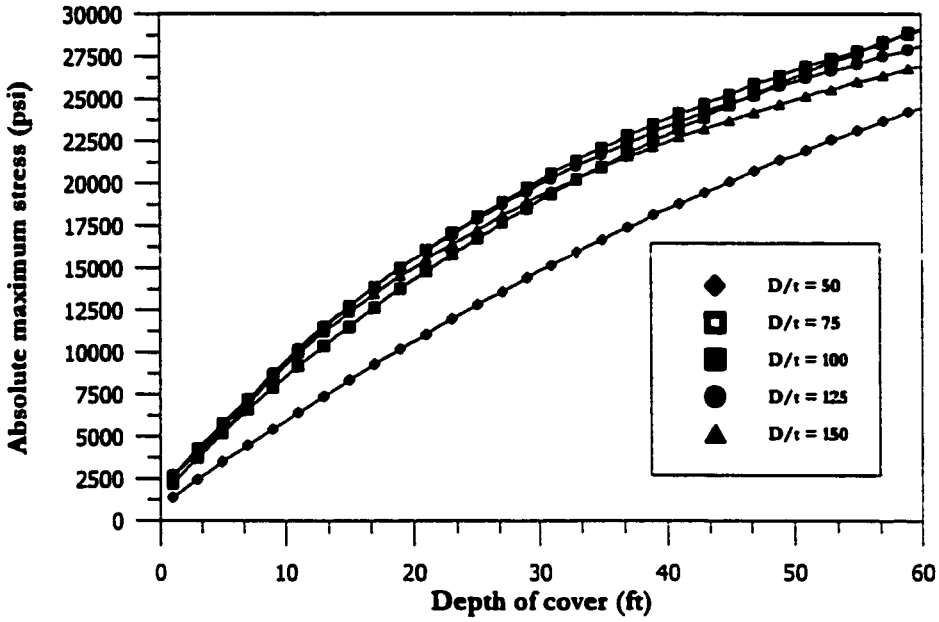

(a) Variation of absolute maximum stress

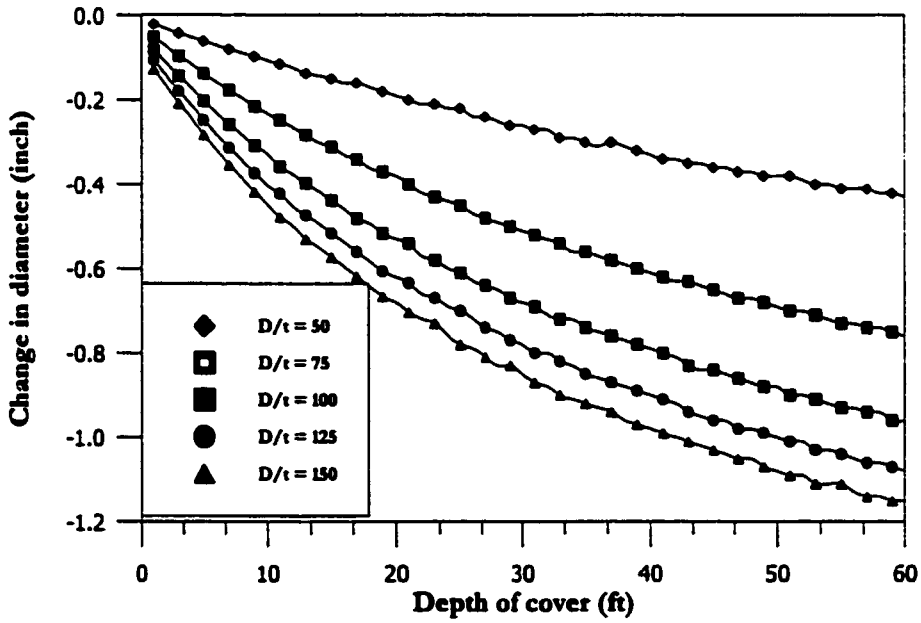

(b) Variation of change in diameter

Fig. 7.23: Absolute maximum stress and diameter change for 36 inches pipe diameter and sabkha as native soil

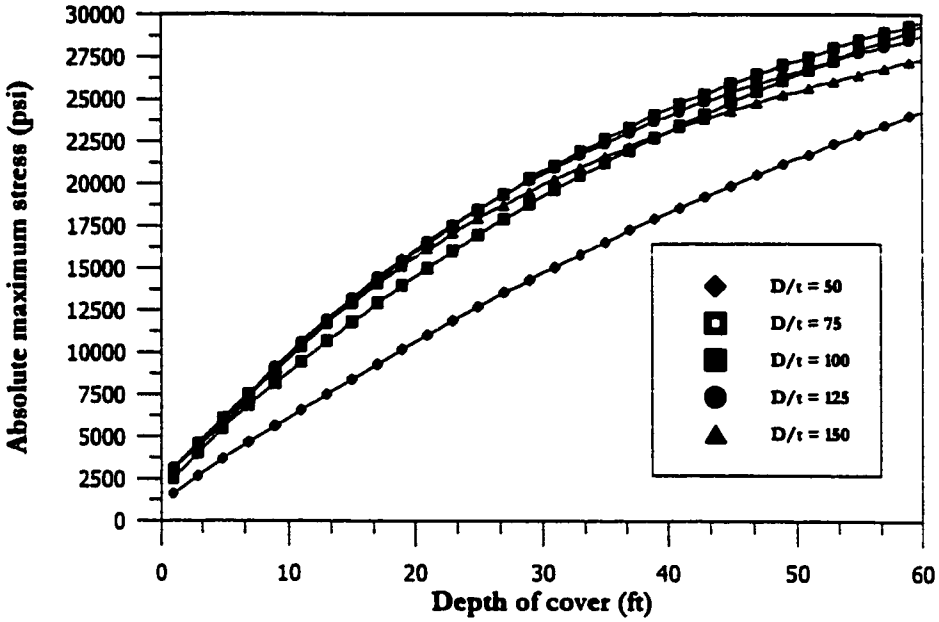

(a) Variation of absolute maximum stress

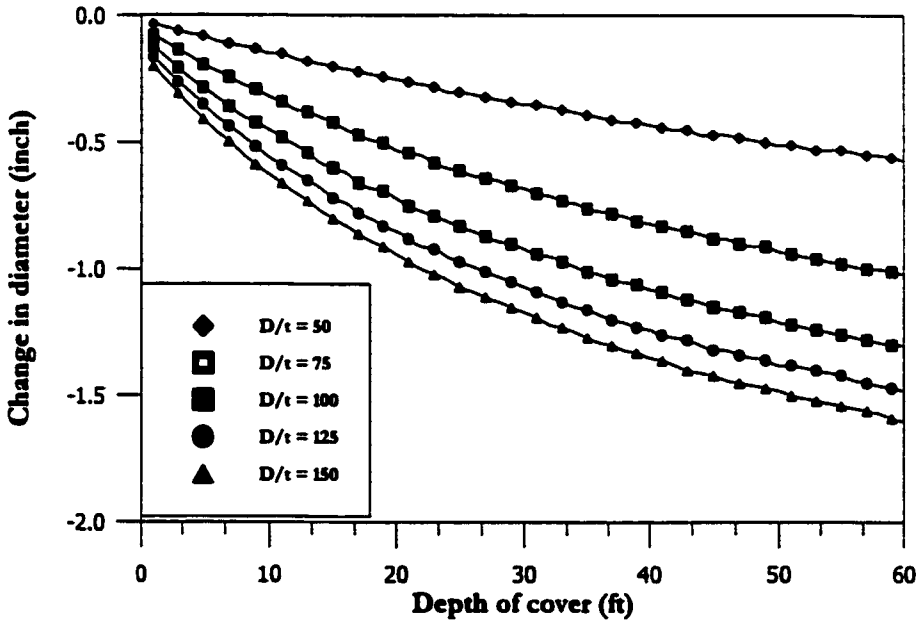

(b) Variation of change in diameter

Fig. 7.24: Absolute maximum stress and diameter change for 48 inches pipe diameter and sabkha as native soil

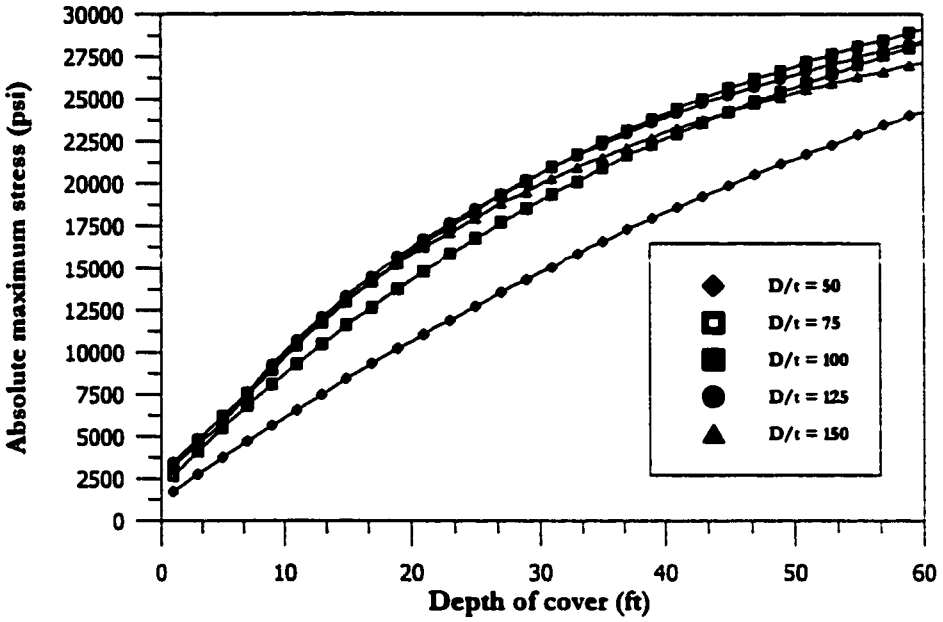

(a) Variation of absolute maximum stress

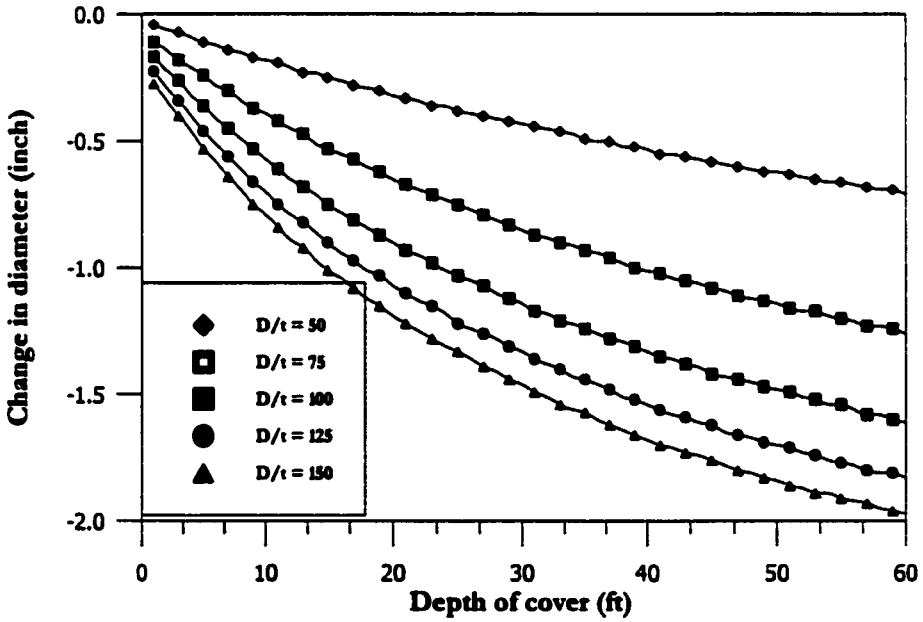

(b) Variation of change in diameter

Fig. 7.25: Absolute maximum stress and diameter change for 60 inches pipe diameter and sabkha as native soil

in stresses from D/t ratio of 50 to 75 is not that evident for D/t ratios of 100, 125, and 150. This trend is more pronounced for certain type of soils types, especially for sand at high density as native soil. Since the bending stiffness ($\frac{EI}{R^2}$) and hoop stiffness ($\frac{EA}{R}$) are both functions of thickness so investigating this matter was essential to look for the phenomenal abstraction which is responsible for this behavior. The diameter of 36 inch under a depth of cover 10 feet was analyzed in more detail to draw some more useful conclusions. All four types of native materials were considered. The normal pressure at two different locations namely: crown and springline was noted for the four different types of native soils and D/t ratios of 50, 75, 100, 125, and 150. The normal pressures at crown and springline are plotted against the respective D/t ratios for each native material. The results are shown in Figs. 7.26 and 7.27.

It can be seen very clearly that normal pressure at the crown for small D/t ratios is always greater than the free field stress indicating a rigid pipe behavior, while for large D/t ratios its is less than the free field stress indicating that the load carried by the pipe is less than the load carried by the surrounding soil. The smooth transition of normal pressure at crown from values above the free field stress at small D/t ratios to values below the free field stress for large D/t ratios, clearly indicate the change in behavior of pipe from rigid at small D/t ratios to flexible at large D/t ratios. The argument can be further strengthened by observing normal pressure at springline, where again it can be noted that the value of normal pressure at springline with increasing D/t ratio is increasing indicating the mobilization of passive resistance at springline for pipes of low stiffness. Since the two arguments are complementing each other, it can be deduced that there is a

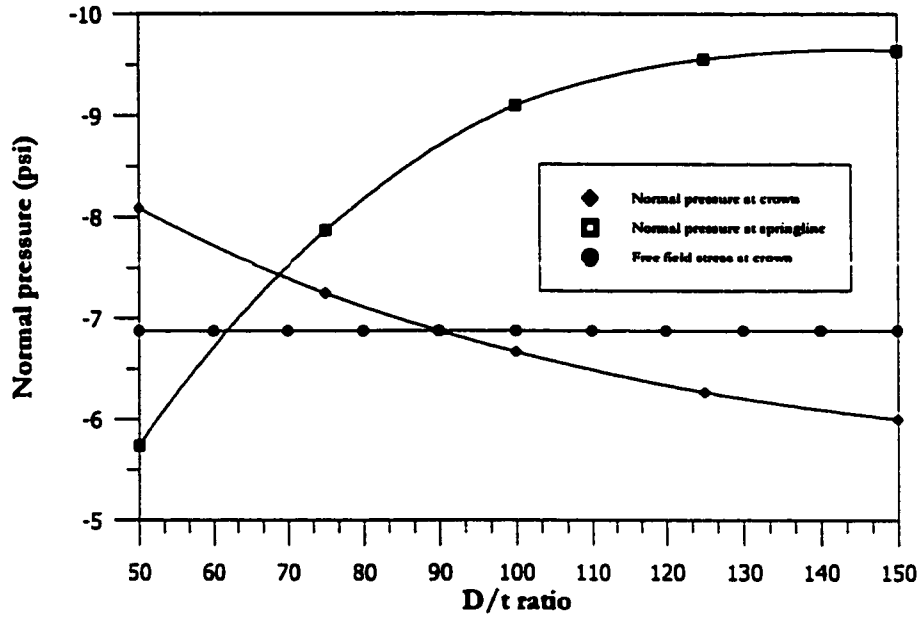

(a) Sand at low density as native soil

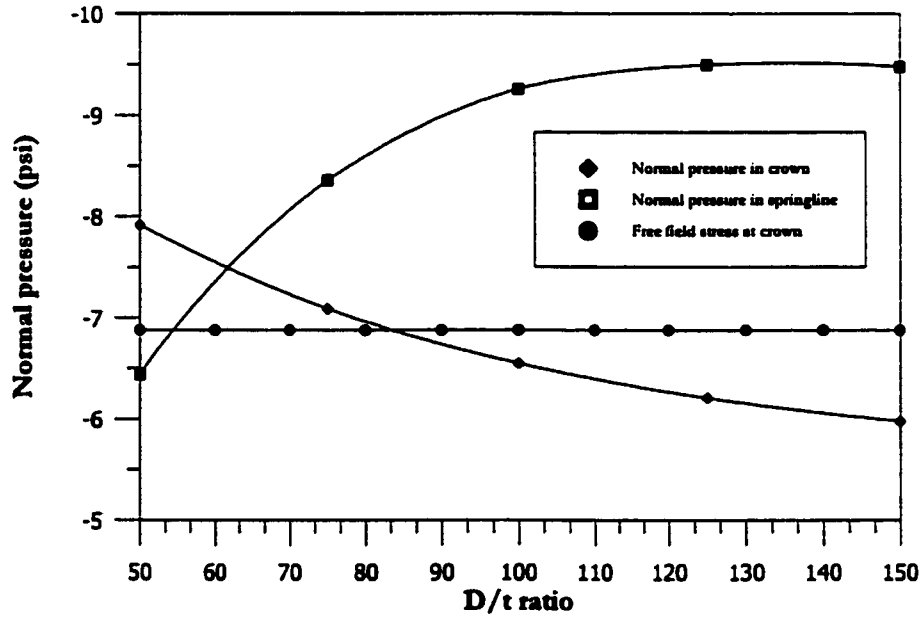

(b) Sand at high density as native soil

Fig. 7.26: Normal pressure at crown and springline for 36 inch pipe diameter and low and high density sand as native soils

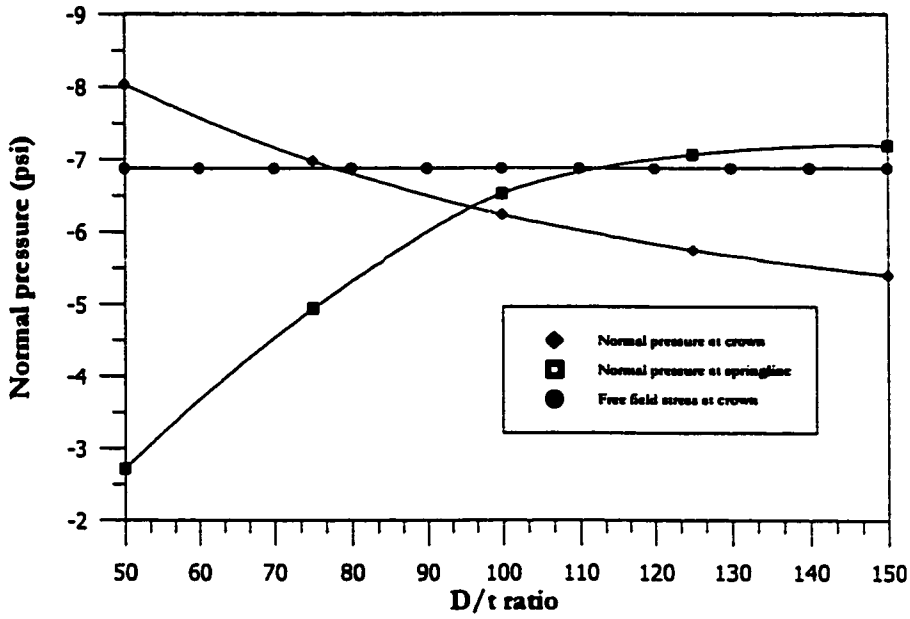

(a) marl as native soil

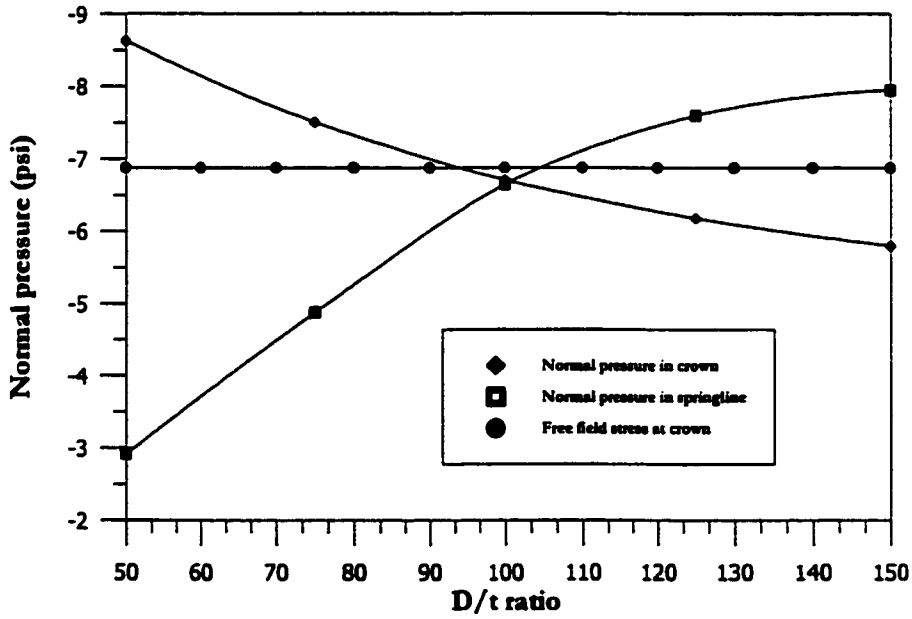

(b) sabkha as native soil

Fig. 7.27: Normal pressure at crown and springline for 36 inch pipe diameter with marl and sabkha as native soils

major change in the pipe behavior due to the variation in D/t ratio. Moreover by comparing the results of sand as native soil to other types it can be noted that the above phenomenon is more pronounced in sand as compared to the other soil types. This is because sand at high density is the more stiff than the other soils considered in this research.

As a next step towards the analysis of results, the effect of internal pressure was added to the dead load stresses. The calculation of the circumferential stresses due to internal pressure has been done by using the modified Barlow's formula, presented in Subsection 3.14.4. The results are plotted only for 36 inch diameter pipe and are shown in Figs. 7.28 to 7.31. The results clearly indicated that the stresses due to internal pressure are dominating as the clear distinction can be made between the results for different D/t ratios. There will be no much difference between the procedure of original and modified Barlow's formula. The maximum difference will be:

$$S_{Hi(Modified)} = \frac{p(D-t_w)}{2t_w} \tag{7.1}$$

$$S_{Hi(Barlow)} = \frac{pD}{2t_w} \tag{7.2}$$

$$S_{Hi(Barlow)} - S_{Hi(Modified)} = \frac{pD}{2t_w} - \frac{p(D-t_w)}{2t_w} \tag{7.3}$$

$$S_{Hi(Barlow)} - S_{Hi(Modified)} = \frac{p}{2} \tag{7.4}$$

7.5 Comparison Study For Sand Overburden Problem

A comparison of CANDE finite element predictions for the sand overburden problem is made with API recommended practice 1102 (API RP 1102) [34] and Spangler's method

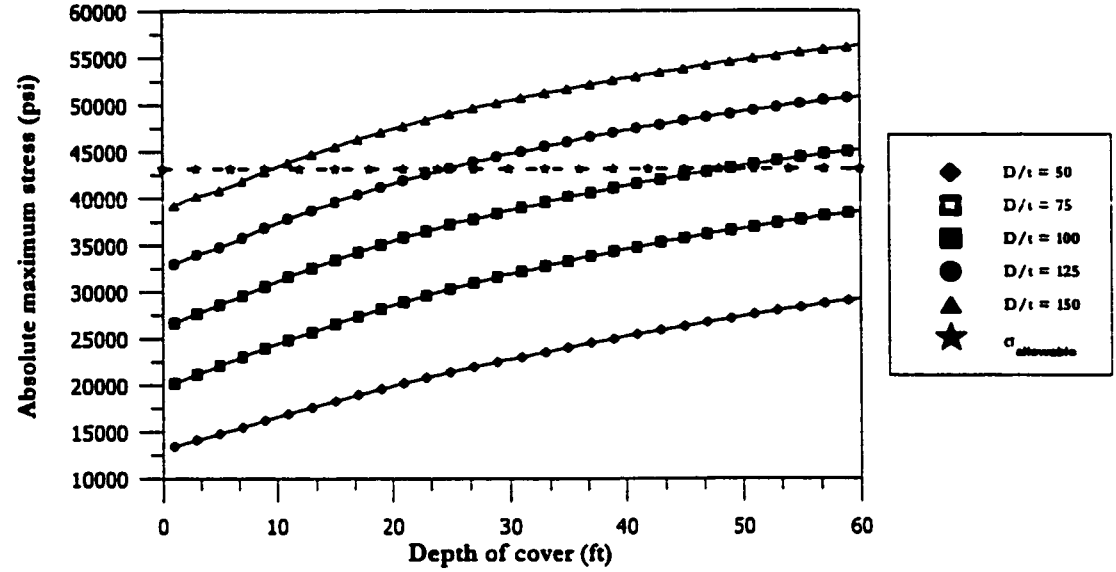

(a) Pipe subjected to internal pressure of 500 psi

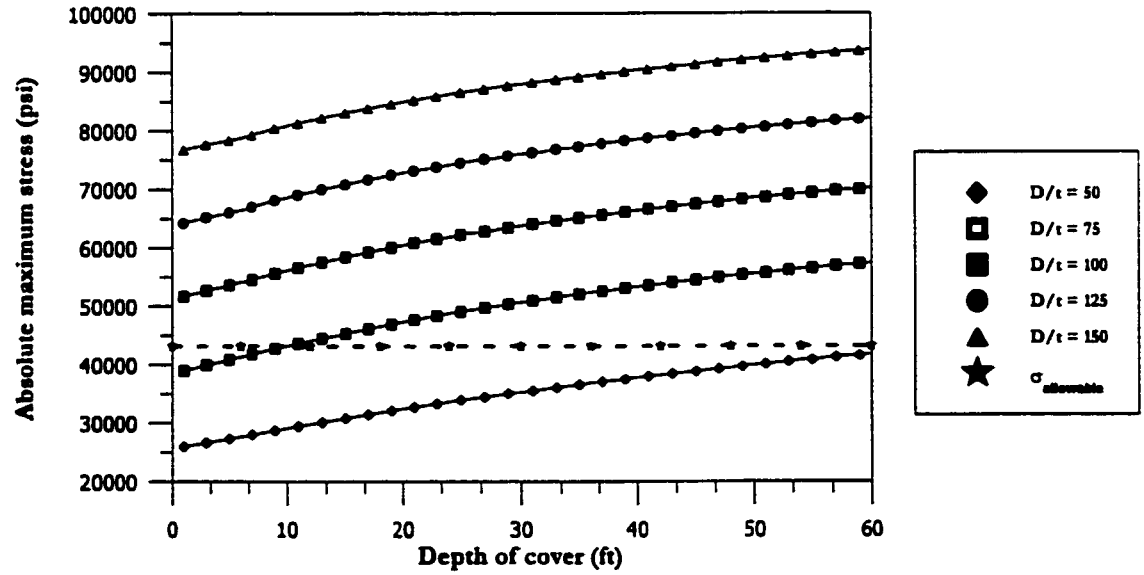

(b) Pipe subjected to internal pressure of 1000 psi

Fig. 7.28: Absolute maxium stress for 36 inches pipe diameter and low density sand subjected to dead load and internal pressure

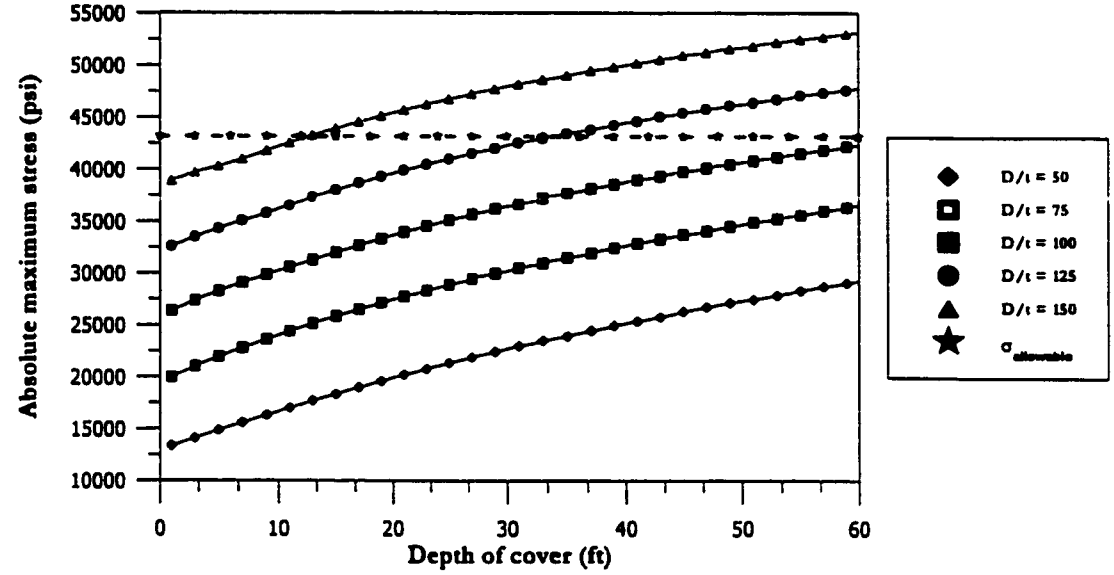

(a) Pipe subjected to internal pressure of 500 psi

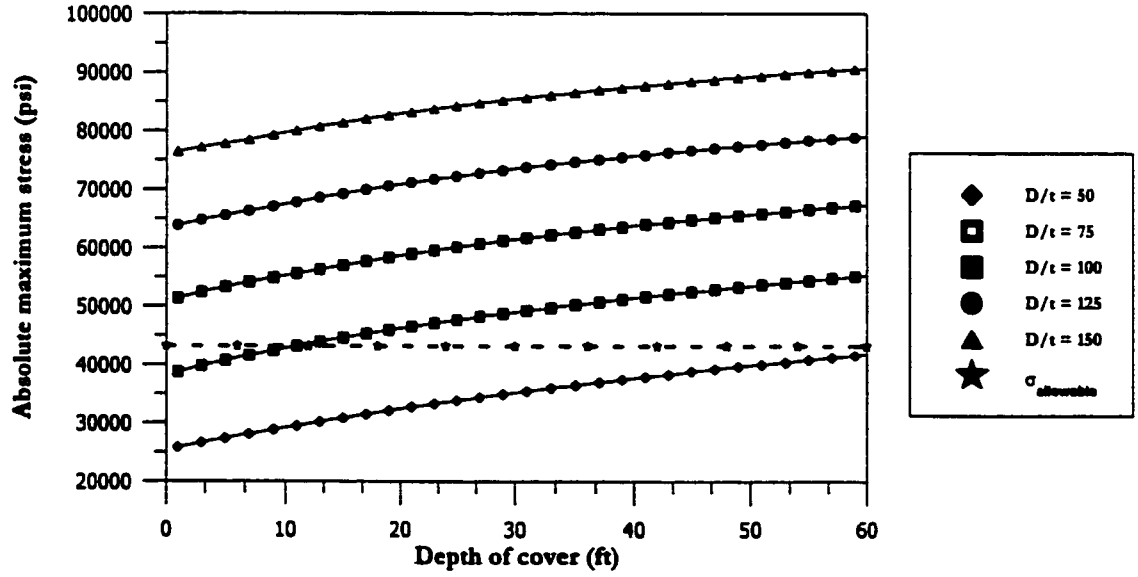

(b) Pipe subjected to internal pressure of 1000 psi

Fig. 7.29: Absolute maxium stress for 36 inches pipe diameter and high density sand subjected to dead load and internal pressure

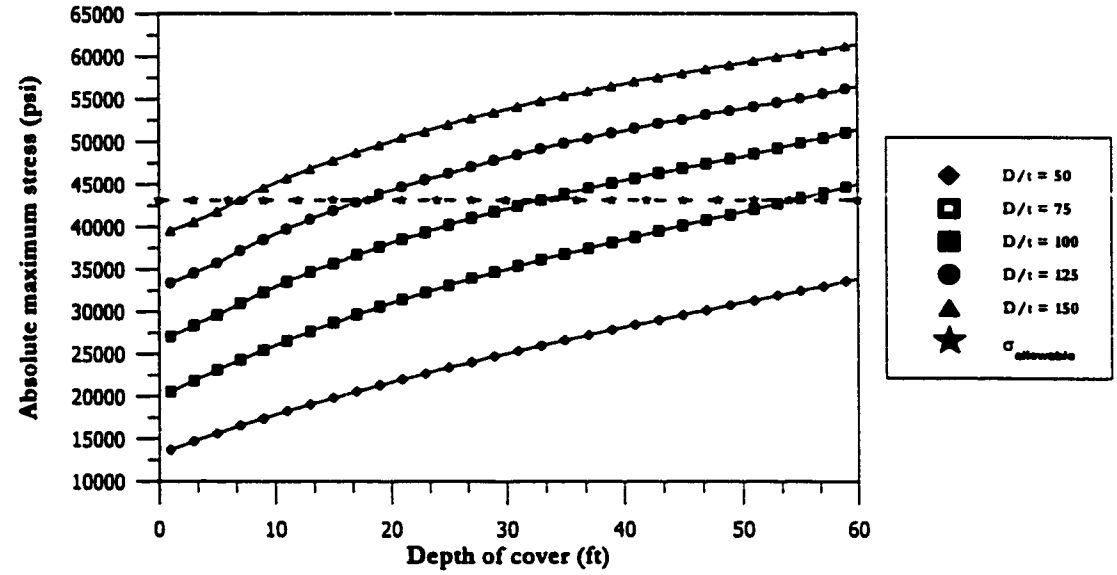

(a) Pipe subjected to internal pressure of 500 psi

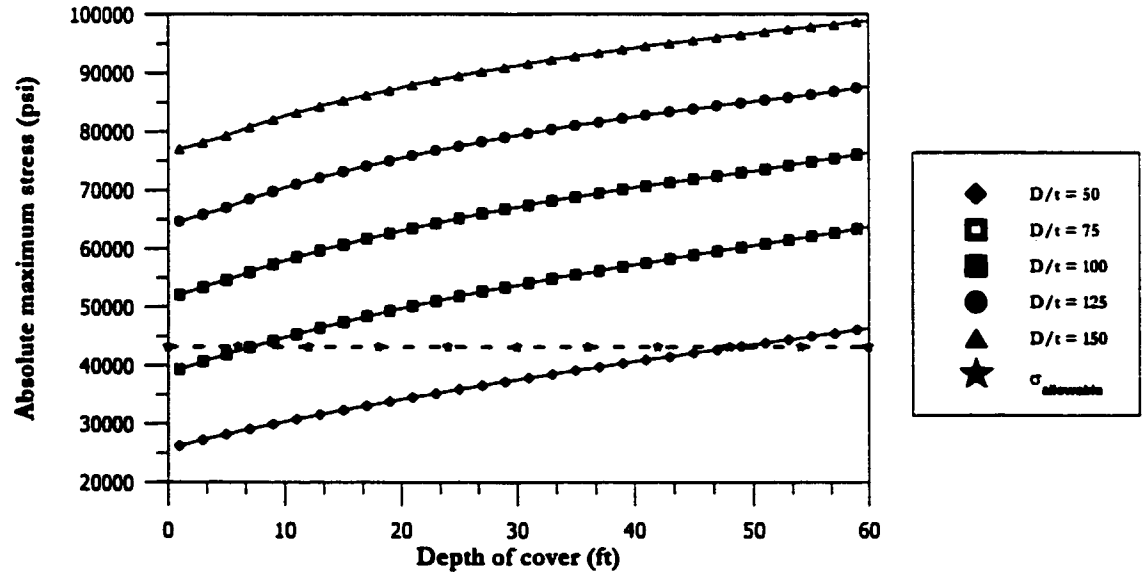

(b) Pipe subjected to internal pressure of 1000 psi

Fig. 7.30: Absolute maxium stress for 36 inches pipe diameter and marl as native soil subjected to dead load and internal pressure

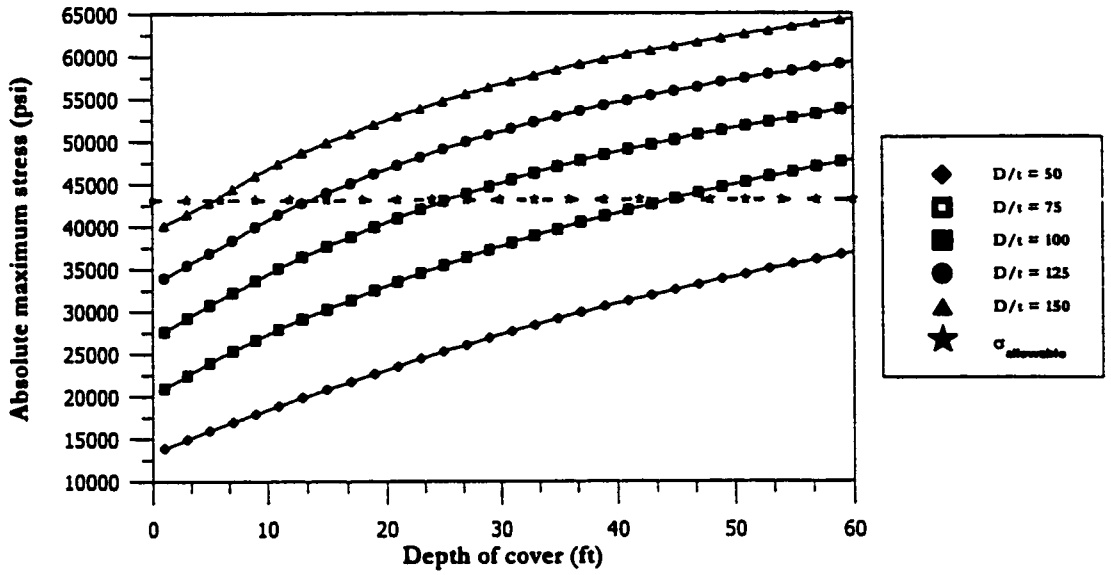

(a) Pipe subjected to internal pressure of 500 psi

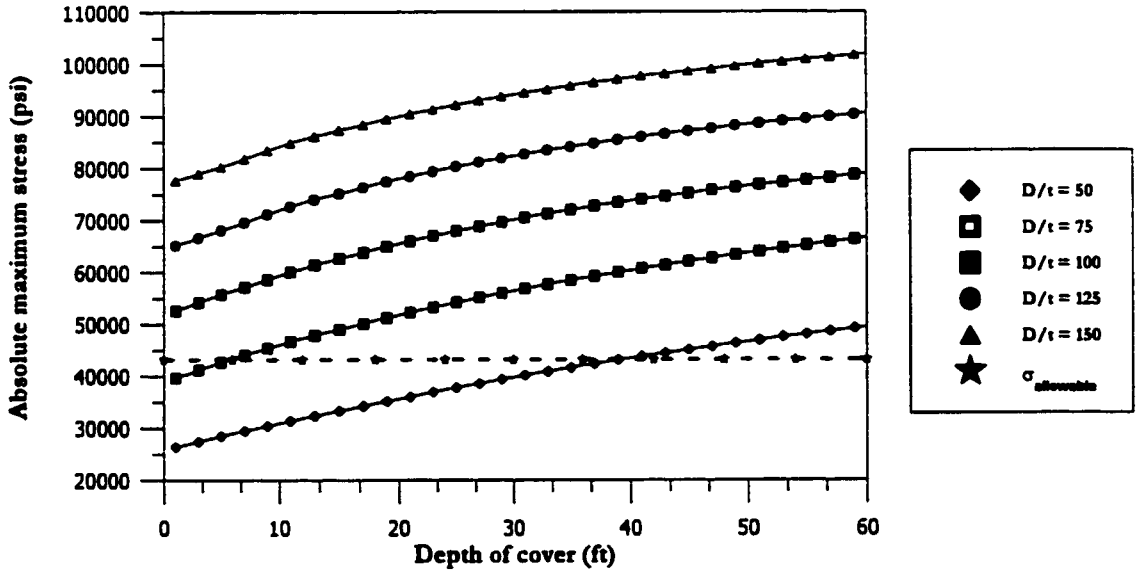

(b) Pipe subjected to internal pressure of 1000 psi

Fig. 7.31: Absolute maxium stress for 36 inchs pipe diameter and sabkha as native soil subjected to dead load and internal pressure

[21]. Two problems are selected from the report by GRI (Gas Research Institute) [73]. These problems are used in the report for the comparison between the API RP 1102 and the Spangler's equation. The complete details of the pipe and soil properties for the two methods are given in Table 7.5.

However it should be emphasized that in all of the finite element simulations by CANDE, a trench-type of installation was used, while the API RP 1102 is based on auger bored pipelines. Moreover, it is noted that API RP 1102 recommends a value of B_d equal to D and E_e equal to 1.0 for trenched construction; however, the PC-PISCESL program (computer implementation of API RP 1102), by default, takes a value for E_e equal to 0.83 if the selected value of B_d is taken as the diameter of the pipe. This clearly indicates a shortcoming in PC-PISCESL to calculate dead load stresses for trenched construction.

The results from the three analyses are given in Tables 7.6 to 7.8. The results from the three methods are quite different. The Spangler's equation is found to be the most conservative at an internal pressure of 0 psi. However, the stresses reduce with the application of internal pressure as a result of the pressure re-rounding effect.

The results for the 12.75-inch diameter pipe show that CANDE is somewhat more conservative than API RP 1102. This is mainly because of the difference in the pipe installation method and the use of a value of E' equal to 1.8 ksi, which is very close to the upper bound of 2.0 used for dense to very dense sand and gravel. While in the local installation procedure and CANDE simulation, both trench installations and loose sand around the pipe are used. Thus, reworking the problem with E' = 0.5 ksi, as recommended in Appendix A of API RP 1102 for loose sand, CANDE results compare well for a diameter of 12.75

TABLE 7.5: Pipe and soil properties for comparison study

Parameter.	a) First pipe	b) Second pipe
D	12.75 inch	36 inch
t_w	0.25 inch	0.606 inch
H	5.7 ft	5.8 ft
B_d	14.75 inch	38 inch
H/B_d	4.64	1.83
γ	0.069 lb/in^3	0.069 lb/in^3
F_i	1	1
E_s	30000000 psi	30000000 psi
K_μ	0.192	0.192
K_b	0.169	0.169
K_z	0.108	0.108
C_d	2.17	1.31
W_E	33 lb/in	131 lb/in
Soil type	B	B
B_d/D	1.16	1.16
E'	1.8 ksi	1.8 ksi
E_r	20 ksi	20 ksi
t_w/D	0.02	0.017
K_{He}	2244	2568
B_e	0.99	0.61
E_e	1.5	0.92

TABLE 7.6: Circumferntial stresses from Spangler's equation for various pipe internal pressures

Diamter	12.75 inch		36 inch	
	ΔS_{He} (psi)	Pressure (psi)	ΔS_{He} (psi)	Pressure (psi)
Spangler Equation	3413.12	0	6510.83	0
	2513.05	250	4157.49	250
	1988.63	500	3053.72	500
	1645.30	500	2413.08	500
	1403.06	1000	1994.62	1000

TABLE 7.7: Circumferential stresses from API RP1102

Diameter, D	12.75 inch		36 inch	
API 1102	ΔS_{He} (psi)	E/ (ksi)	ΔS_{He} (psi)	E/ (ksi)
	2149.86	1.8	3579.85	1.8
	2808.04	0.5	5362.80	0.5

TABLE 7.8: Circumferential stresses from CANDE finite element simulations for different native soils

Diameter, D	12.75 inch	36 inch
thickness, t	0.25 inch	0.606 inch
D/t	51 in/in	54.91 in/in
ΔS_{He} (psi) sand at low density	2614.8 lb/in^2	3252.0 lb/in^2
ΔS_{He} (psi) sand at high density	2441.2 lb/in^2	3238.3 lb/in^2
ΔS_{He} (psi) marl	2913 lb/in^2	4305.2 lb/in^2
ΔS_{He} (psi) sabkha	3580.7 lb/in^2	4916.3 lb/in^2

inch and prove to be less conservative for 36-inch pipe diameter, as shown in Table 7.8. This clearly indicates that the API RP 1102 is more conservative for larger diameters and smaller D/t ratios. In order to investigate this relation and also to come up with a complete picture, it is decided to make a comprehensive comparison between the database generated by the CANDE finite element simulations and the API RP 1102.

Since the PC-PISCESL program is not suitable for predicting the dead load stresses for the trenched construction, so the dead load equation from API RP 1102 is programmed in the EXCEL program, taking the values of the parameters from the relevant graphs of the API RP 1102. The parameters and their respective values used in the analysis by the API RP 1102 are given in Tables 7.9 and 7.10 Diameters of 12, 24, 36, 48, and 60 inches are analyzed for D/t ratios of 50, 75, and, 100 for H/D ratio ranging from 1 to 12 and with E' values of 0.2, 0.5, 1.0, and 2.0 ksi. The results from the API RP 1102 are compared with CANDE finite element simulations having the same pipe properties and four different soil materials as native soils.

The comparison results between CANDE and API RP 1102 for the pipe diameters, 12, 24, 36, 48, and 60 inches and for D/t ratios of 50, 75, and 100 are shown in Figs. 7.32 to 7.34. For these results the soil property used in the API RP 1102 is modulus of soil reaction E'which is taken as 0.2 ksi, while for CANDE analysis, sand at low density is considered as the native soil. These results clearly indicate that API RP 1102 overestimates the circumferential stresses for large D/t ratios. Similarly, the API RP 1102 becomes more conservative with the increase in the pipe's diameter.

A similar comparison was performed to investigate the effect of soil properties on both

TABLE 7.9: Values of K_{He} used in comparison study

D/t_w	t_w/D	E' (ksi)	K_{He}
50	0.2	0.2	3196
		0.5	2931
		1.0	2587
		2.0	2123
75	.013	0.2	6298
		0.5	5051
		1.0	3909
		2.0	2858
100	.01	0.2	9130
		0.5	6460
		1.0	4691
		2.0	3433

TABLE 7.10: Values of B_e used in the comparison study

H/B_d	B_e (A)	B_e (B)
2	0.66	0.63
4	1	0.92
6	1.18	1.06
7	1.23	1.09
8	1.27	1.12
9	1.29	1.14
10	1.31	1.15
11	1.33	1.16
12	1.35	1.165

$B_{\bar{d}} = D$ as recommended by API 1102 for trenched construction

$E_e = 1.0$ as recommended by API 1102 for trenched construction

A, loose to medium dense sands and gravels; of clays and silts

B, dense to very dense sands and gravels; medium to very stiff clays

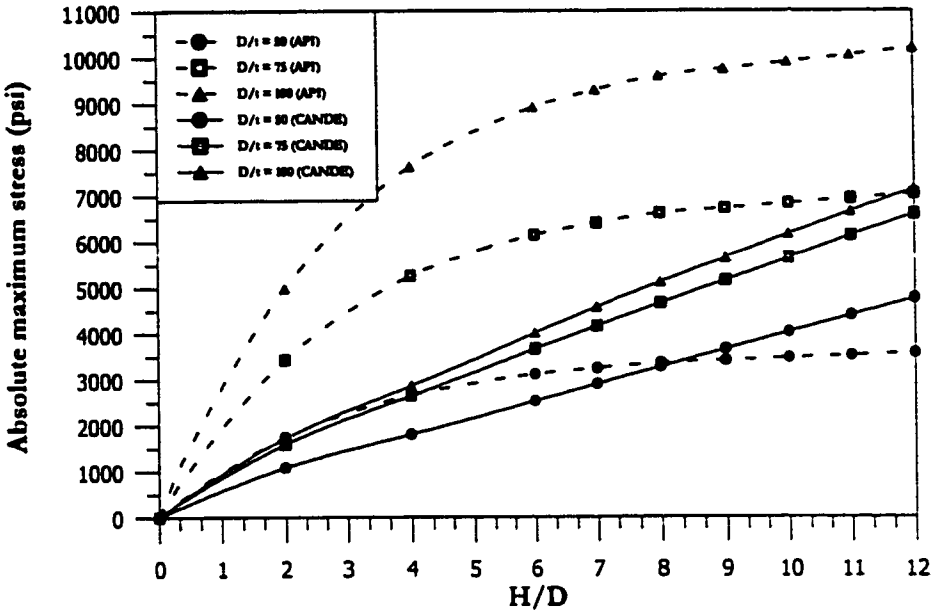

(a) Pipe diameter = 12 inch

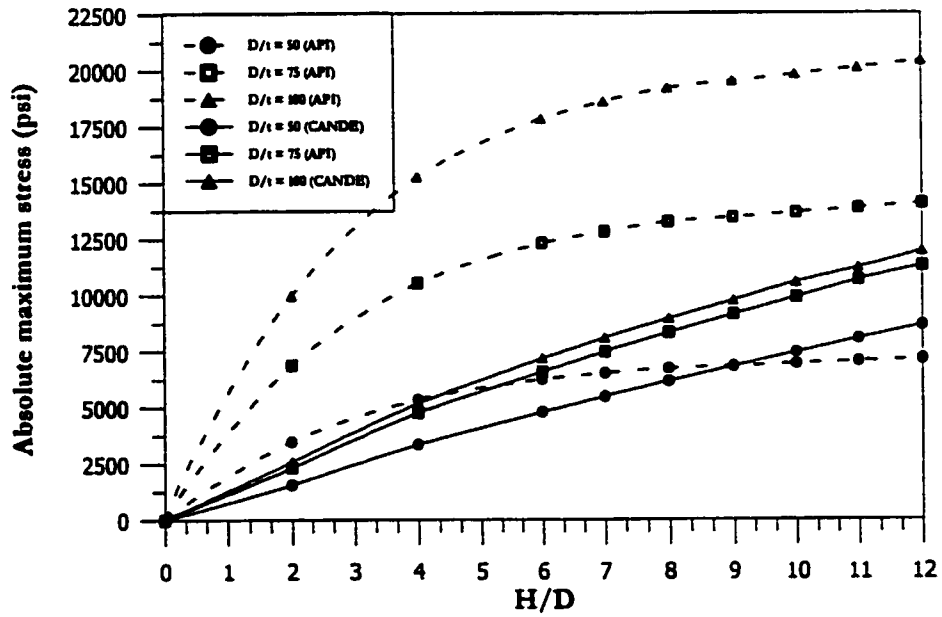

(b) Pipe diameter = 24 inch

Fig. 7.32: Comparison for 12 and 24 inches pipe diameters with low density sand as native soil and E′ = 0.2 ksi for API RP 1102

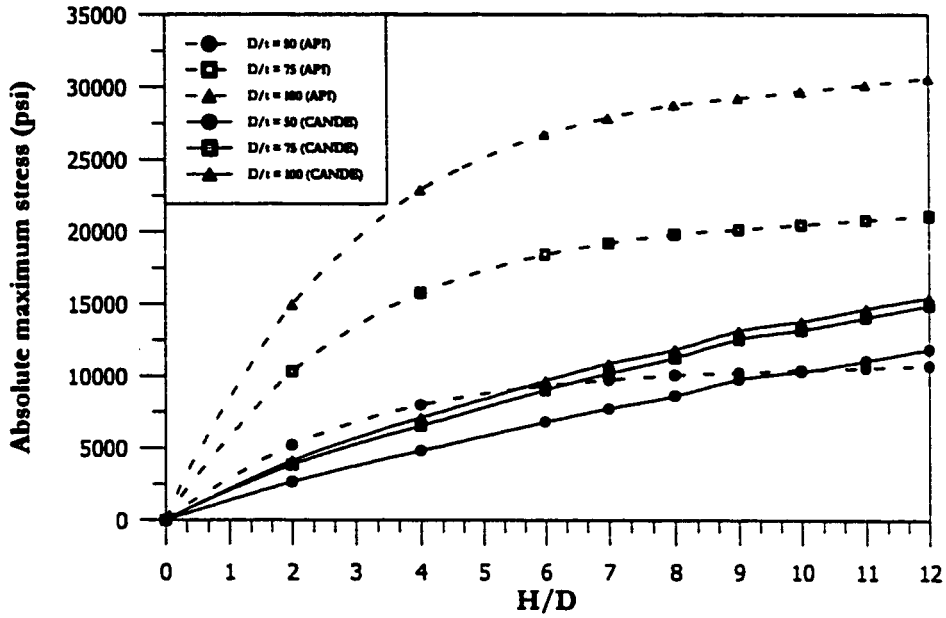

(a) Pipe diameter = 36 inch

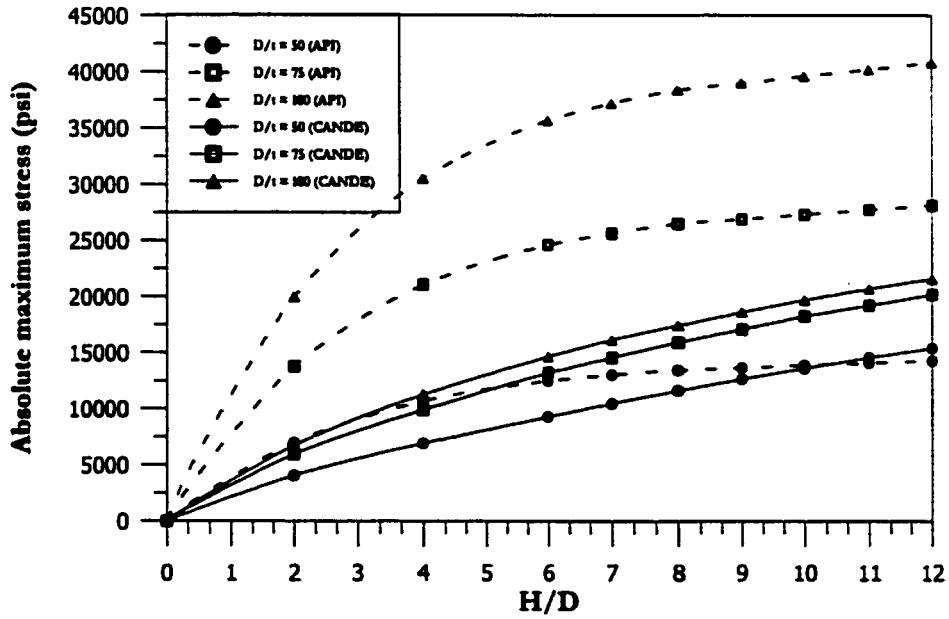

(b) Pipe diameter = 48 inch

Fig. 7.33: Comparison for 36 and 48 inches pipe diameters with low density sand as native soil and E′ = 0.2 ksi for API RP 1102

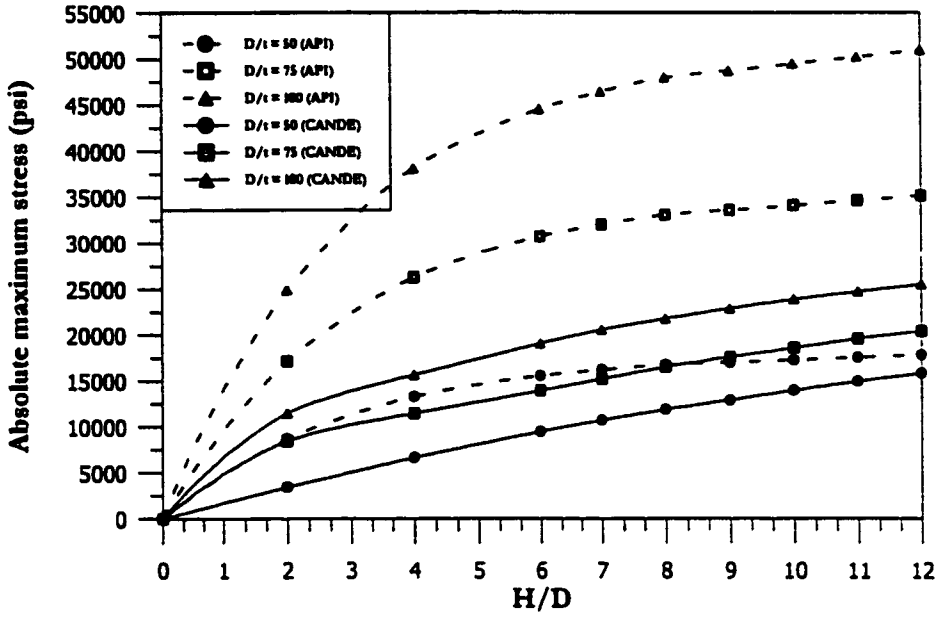

(a) E' = 0.2 ksi

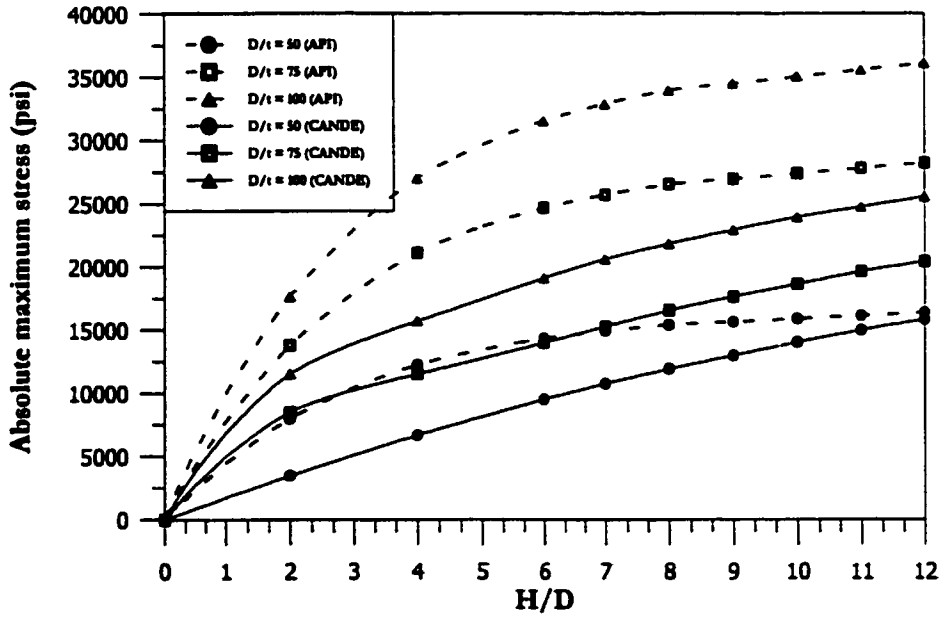

(b) E' = 0.5 ksi

Fig. 7.34: Comparison for 60 inches pipe diameter with low density sand as native soil and E' = 0.2 and 0.5 ksi

API RP 1102 and CANDE results. In the API method, the soil conditions can be varied by taking K_{He} values corresponding to values of soil reaction (E') equal to 0.2, 0.5, 1.0, 2.0., while in CANDE different soil materials. The pipe diameter of 60 inches was selected for the comparison. Figs. 7.34 and 7.35 compare the results of the two methods. It is clear that the API RP 1102 is very sensitive to E' values. For small values of E' such as 0.2, the results of API RP 1102 are more conservative than the CANDE predictions. However, the results from the two procedures converge as the E' value increases. Although the results for the two procedures converge with an increasing value of E', a value of E' equal to 1.0 or 2.0 ksi is not recommended for sands at low density. In addition, API RP 1102 does not recommend the use of an E' value greater than 0.5 [73]. Figs. 7.36 to 7.37 compare the results of the API RP 1102 for E' of 0.2, 0.5, 1.0, and 2.0 with CANDE results in which sand at high density is used as the native soil. It can be depicted that CANDE analysis shows a very small variation over the D/t ratio as compared to the API RP 1102. This is totally expected, owing to the fact that in the CANDE analysis, the effect of arching is dominant for sand at high density being a very stiff soil. Moreover, as compared to the sand at low density, the CANDE results for sand at high density remain less conservative than the API RP 1102. The comparisons for sabkha and marl are shown in Figs. 7.38 to 7.41. The results follow almost the same trend as that for the sand at low density.

7.6 Pipelines Subjected to Highway Live Load

Almost every pipeline crosses public or private roads. These crossings vary in width and complexity, from multilane highways to country roads, city streets, and private or farm

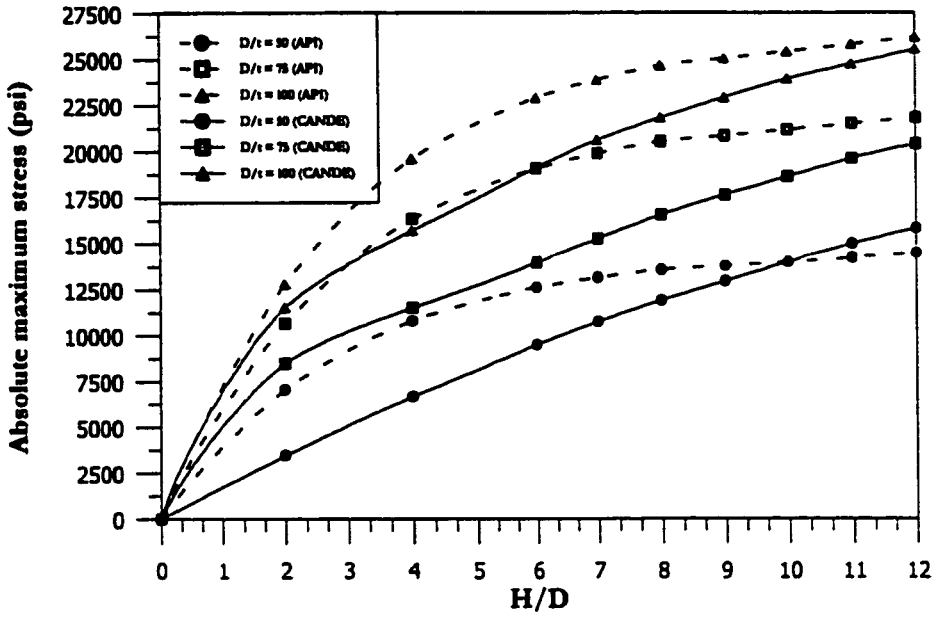

(a) E' = 1.0 ksi

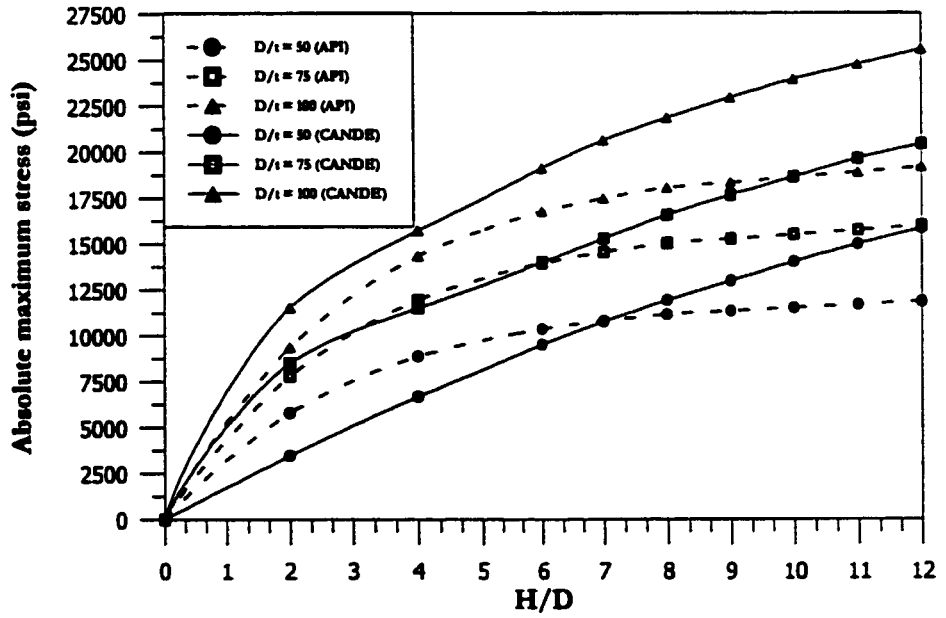

(b) E' = 2.0 ksi

Fig. 7.35: Comparison for 60 inches pipe diameter and low density sand as native soil and E' = 1.0 and 2.0 ksi

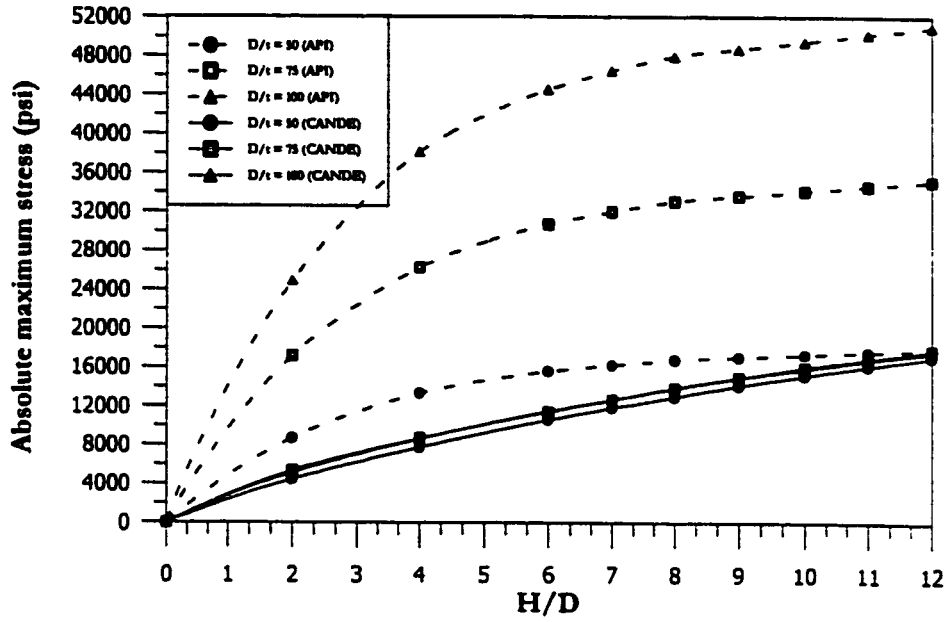

(a) E' = 0.2 ksi

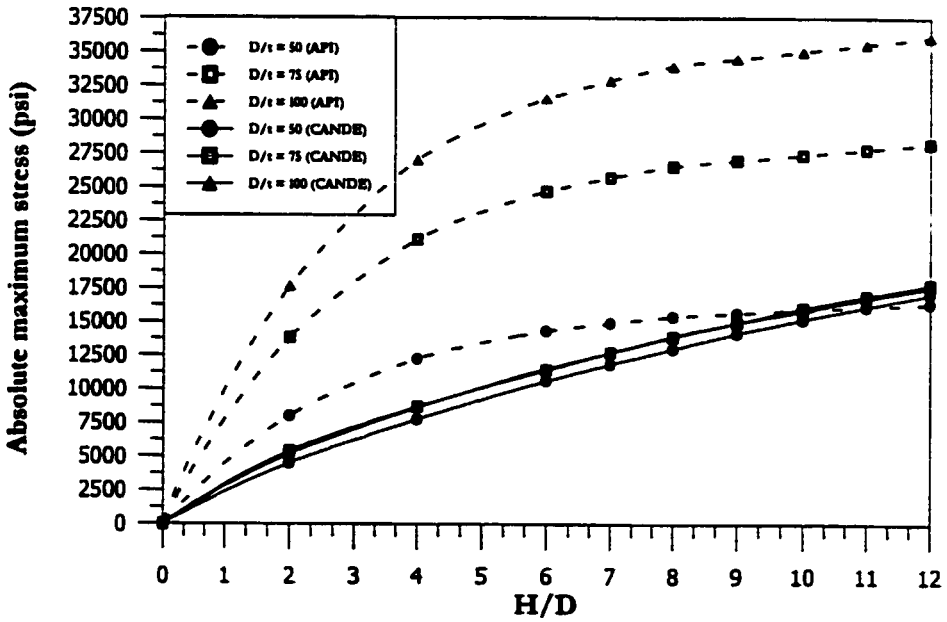

(b) E' = 0.5 ksi

Fig. 7.36: Comparison for 60 inches pipe diameter with high density sand as native soil and E' = 0.2 and 0.5 ksi

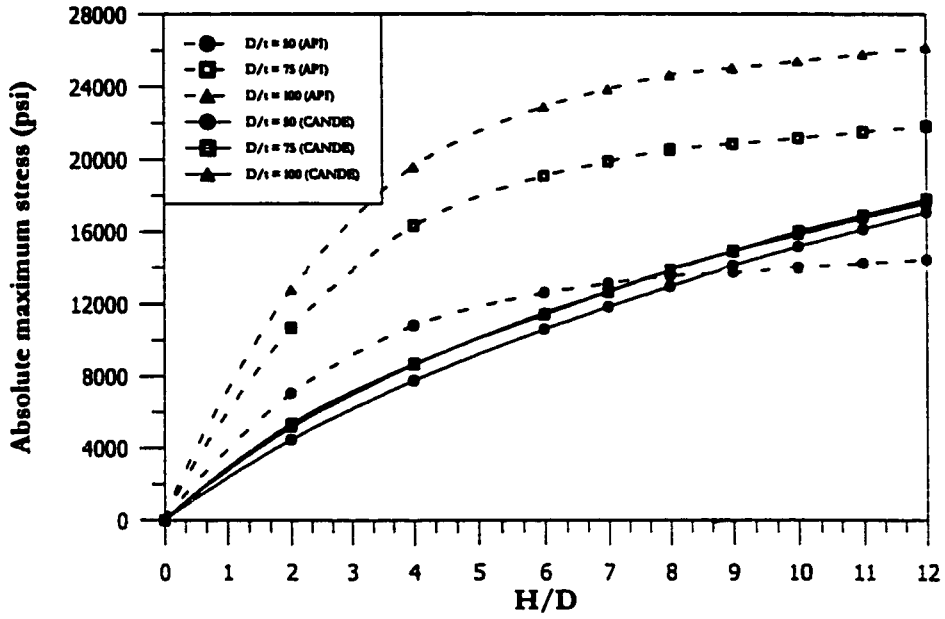

(a) E' = 1.0 ksi

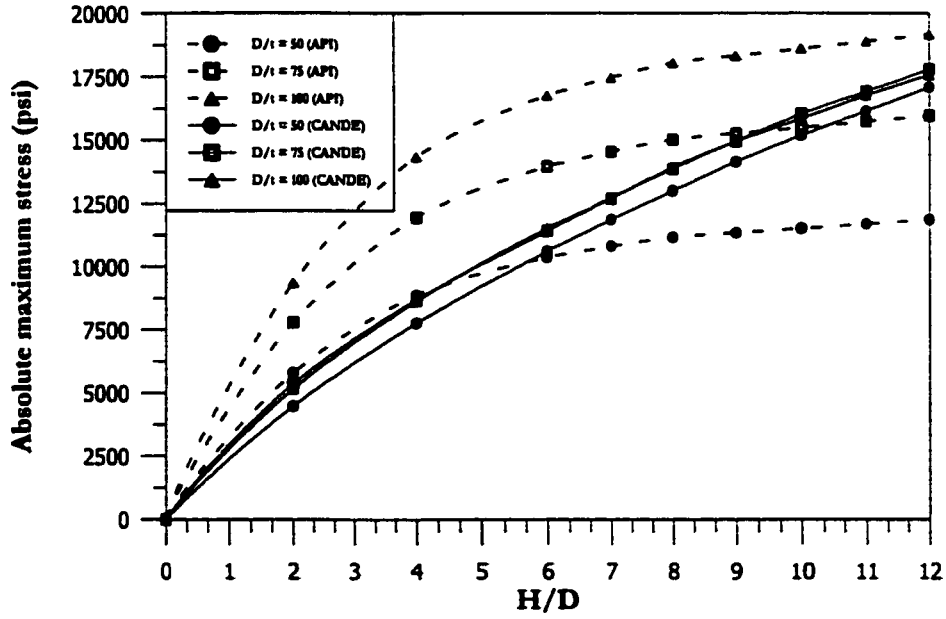

(b) E' = 2.0 ksi

Fig. 7.37: Comparison for 60 inches pipe diameter with high density sand as native soil and E' = 1.0 and 2.0 ksi

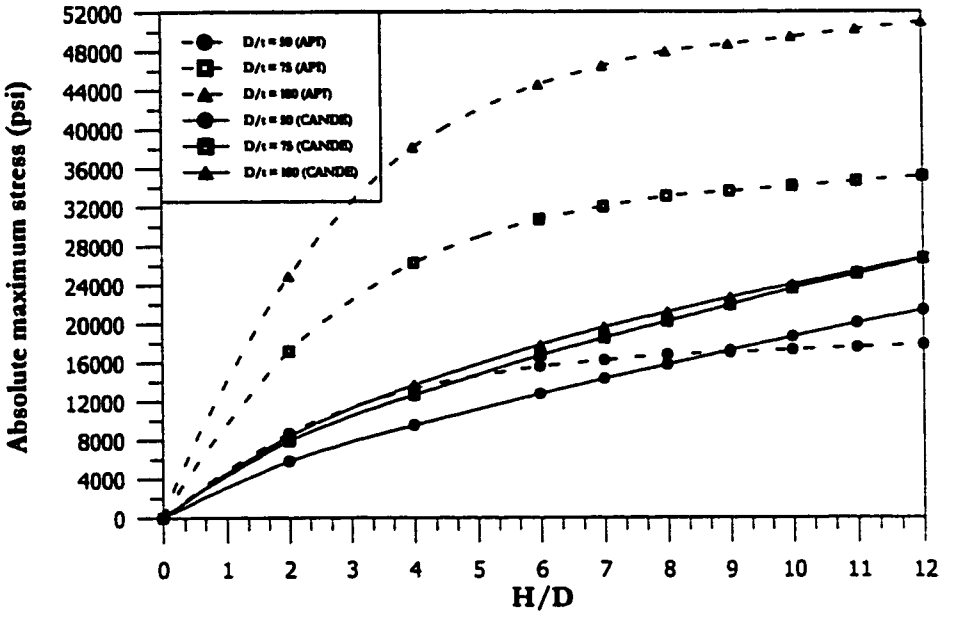

(a) E' = 0.2 ksi

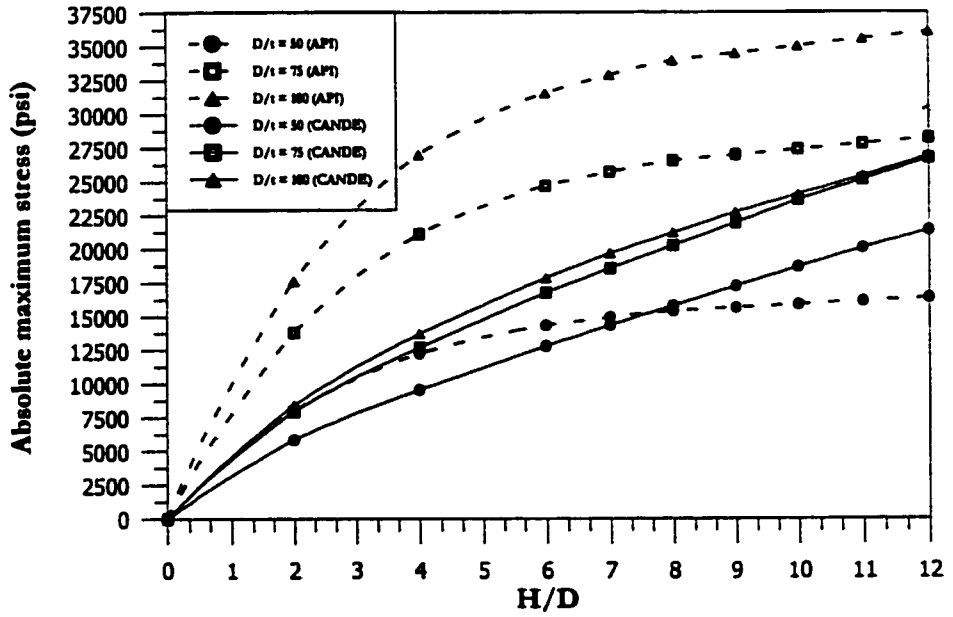

(b) E' = 0.5 ksi

Fig. 7.38: Comparison for 60 inches pipe diameter with marl as native soil and E' = 0.2 and 0.5 ksi

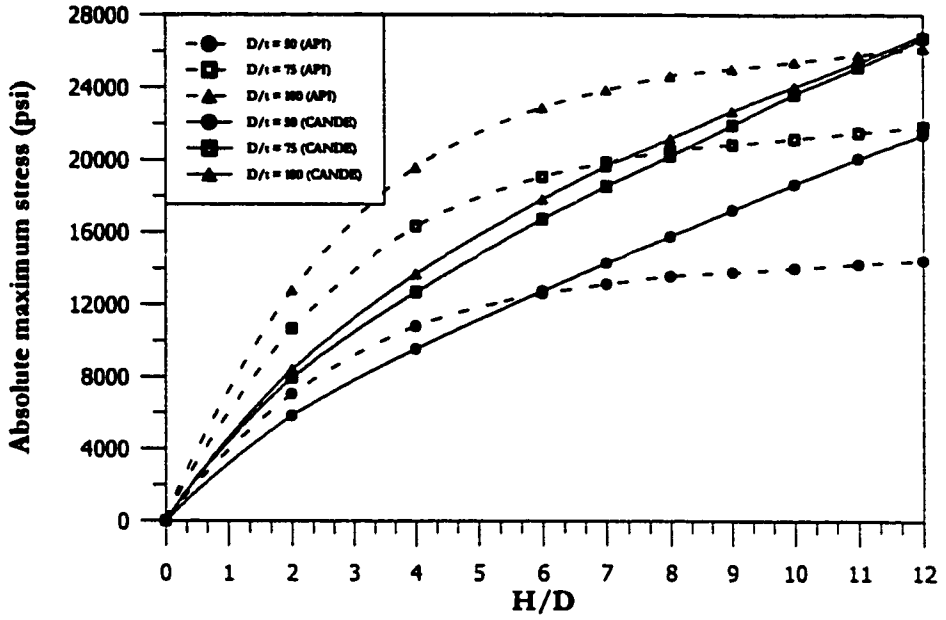

(a) E' = 1.0 ksi

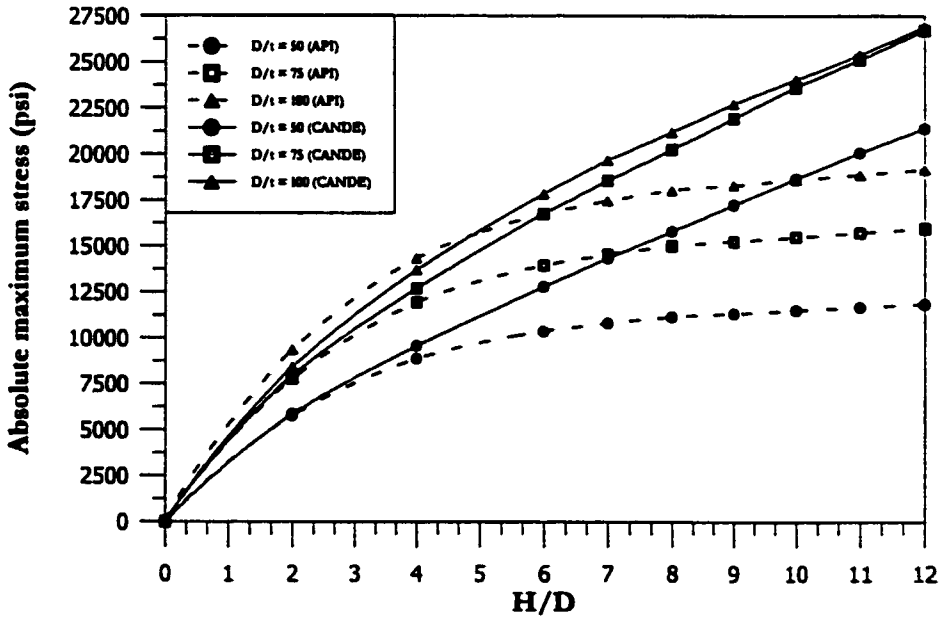

(b) E' = 2.0 ksi

Fig. 7.39: Comparison for 60 inches pipe diameter with marl as native soil and E' = 1.0 and 2.0 ksi

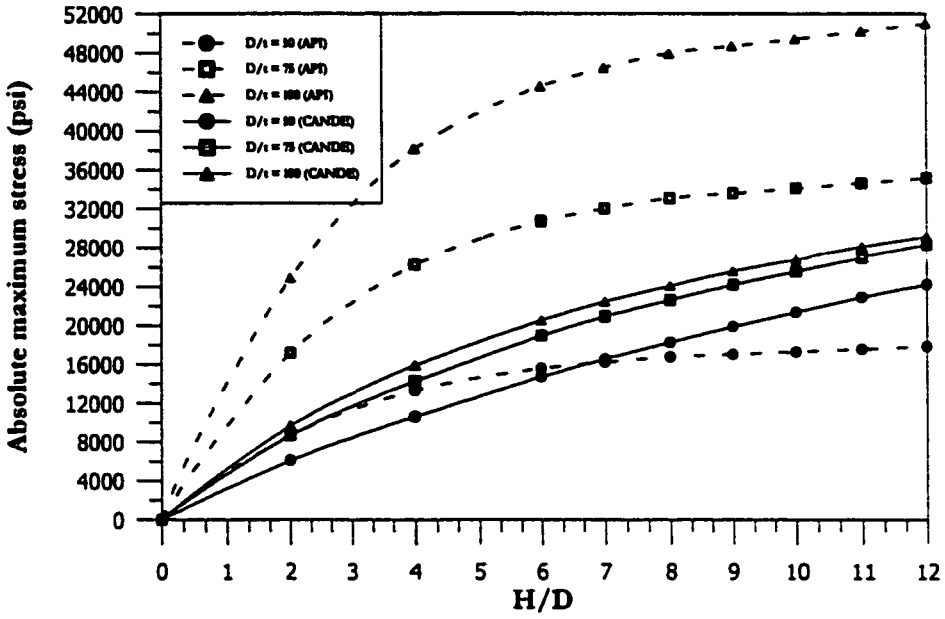

(a) E' = 0.2 ksi

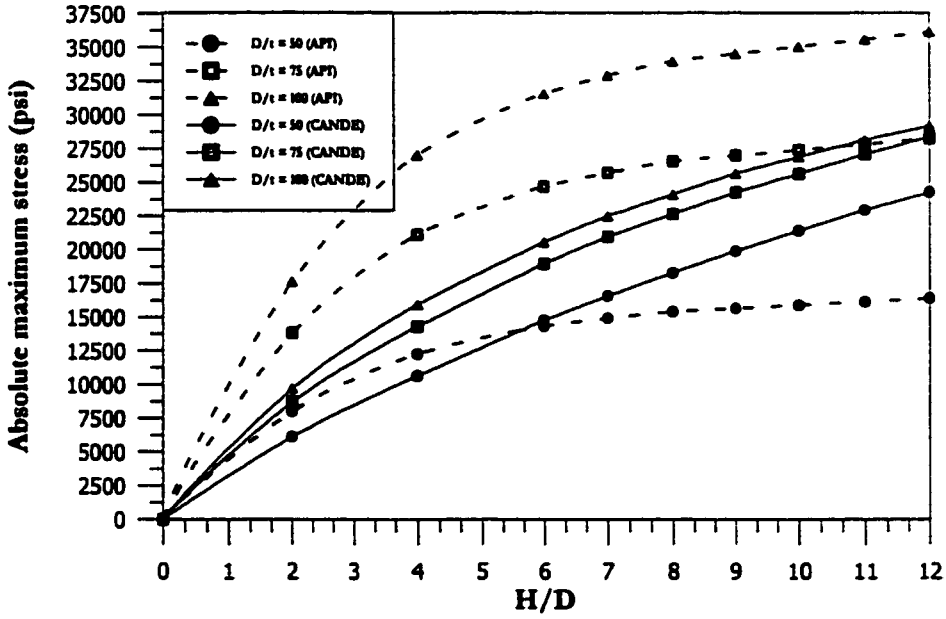

(b) E' = 0.5 ksi

Fig. 7.40: Comparison for 60 inches pipe diameter with sabkha as native soil and E' = 0.2 and 0.5 ksi

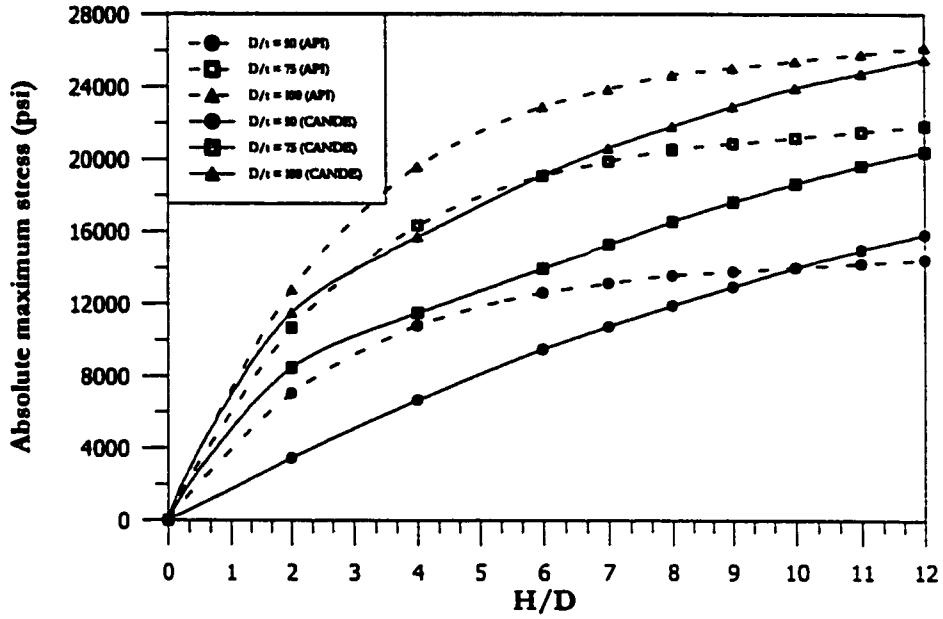

(a) E' = 1.0 ksi

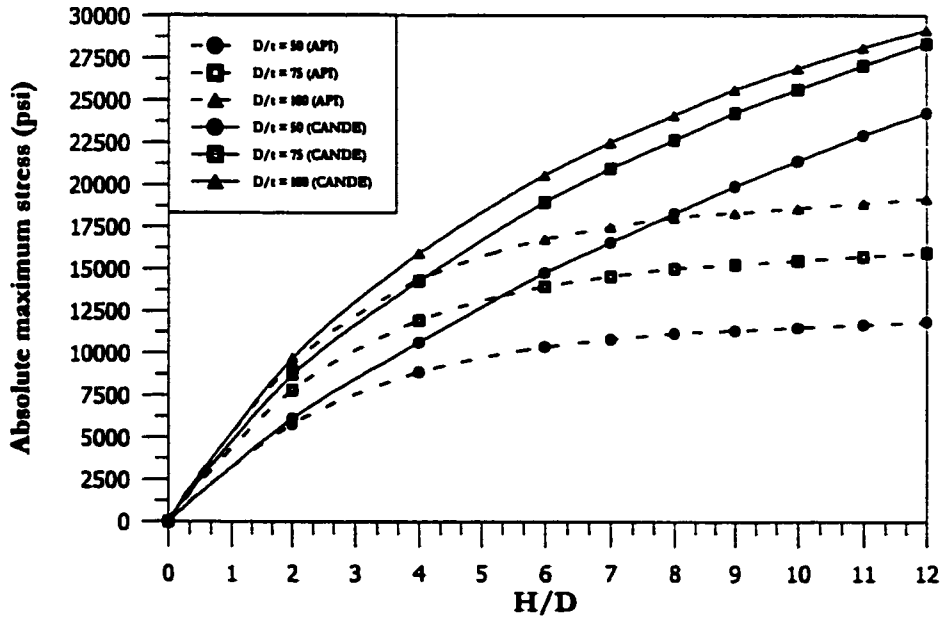

(b) E' = 2.0 ksi

Fig. 7.41: Comparison for 60 inches pipe diameter with sabkha as native soil and E' = 1.0 and 2.0 ksi

roads. The pipelines crossing under highways are subjected to live load in addition to the dead load coming form soil and pavement. Accurate modelling of the phenomenon is much more difficult than the sand overburden problem because of the three dimensional nature of the vehicular load to which the pipeline is subjected. However a reasonable estimate of stresses and deformation in the pipe can be made by considering the live load as an equivalent line load or infinite pressure strip, then carrying out a plain-strain analysis.

7.7 Parametric Study for Pipelines Crossings Highways

A Parametric study was carried out for pipelines crossing highways to generate a database which can be used to develop a regression model to predict the stresses and deformations in the pipelines. The parameters considered in this research are as follows:

1. **Boundary conditions**: The boundary conditions for the finite element simulation of pipeline crossings under highways are exactly the same as those considered for the sand overburden problem.
2. **Trench configuration**: The trench configuration for the pipelines crossing under highways is very similar to the trench configuration for the sand overburden problem. An additional material zone is identified for the overlying pavement. The trench configuration is shown in Fig. 7.42. The pipe, native soil, overfill, and, interface are the same as those of the trench configuration used for sand overburden problem, except a 6 inch thick layer of asphalt pavement is added at the top of the overfill layer.
3. **Construction Increment sequence**: The construction increment sequence is similar to

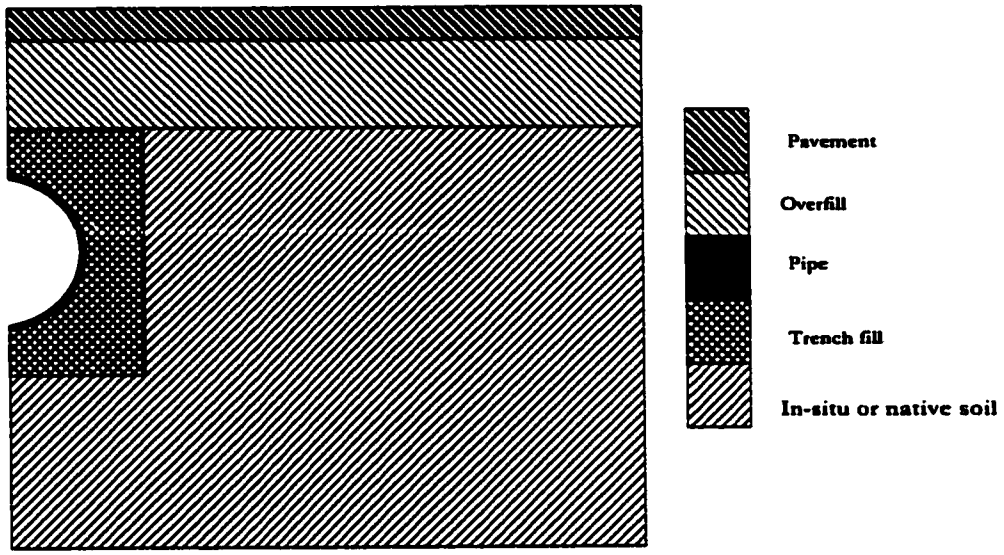

(a) Trench type model with 90 degree, angle of trench inclination

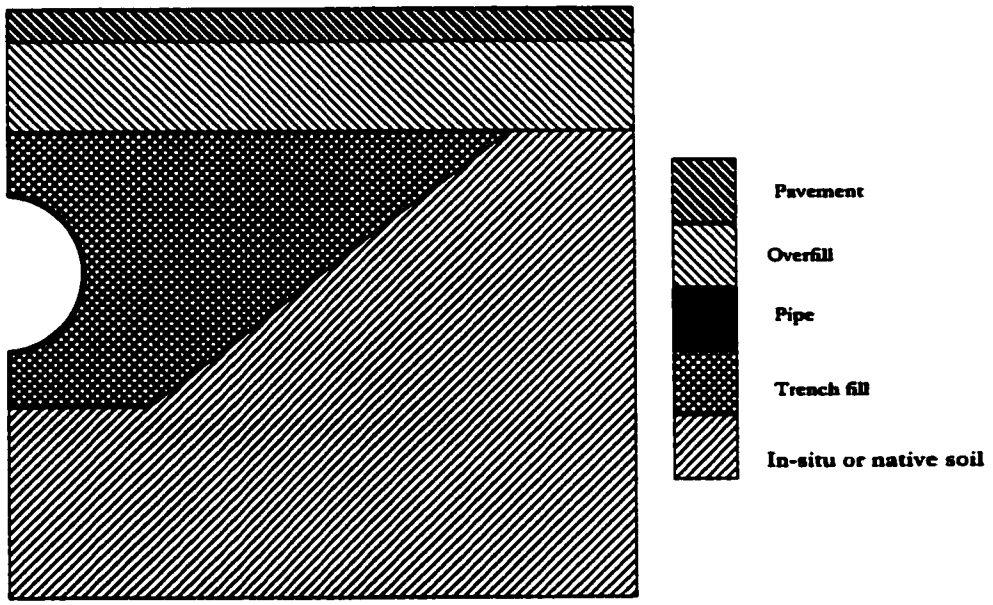

(b) Trench type model with 35 degree, angle of trench inclination

Fig. 7.42: Material zone identification for finite element simulations for pipeline crossing under highways

the one used in the cross-country pipelines under sand overburden with the following two additions. The 6 inch thick pavement layer is activated in a construction after all the over fill is placed and then the live load is applied in the form of pressure in the last increment

4. **Pipe Properties**: The pipe material and section properties are exactly the same as used for the sand overburden problem, Section 7.3.
5. **Soil Properties**: The four type of soil materials identified earlier were used as the native soils, while sand at low density is used for the backfill and over fill layer.
6. **Pavement Properties**: The unit weight, Poisson's ratio, and modulus of elasticity of the pavement used are 145 lb/ft^3, 0.35, 300, 000 psi, respectively.
7. **Live Load**: The live load from a 39 ton Ministry of communication truck (Fig. 7.43) is selected. A single tire load is converted to an equivalent plain strain pressure strip by the procedure outlined in Section 3.8.

A parametric study is carried out for pipelines crossing highways. A total of 500 runs are made. The complete details of the runs are given Tables 7.11 and 7.12. A total of 100 finite element runs were carried out for each of the diameters 12, 24, 36, 48, and 60 inches. The depths of cover considered are 2, 3, 4, 8, and 12 feet.

7.8 Results for Pipelines Crossing Under Highways

As a first step towards the analysis of results from the pipelines crossing problem, it was essential to know the depth of cover at which the effect of live load on the pipe will be

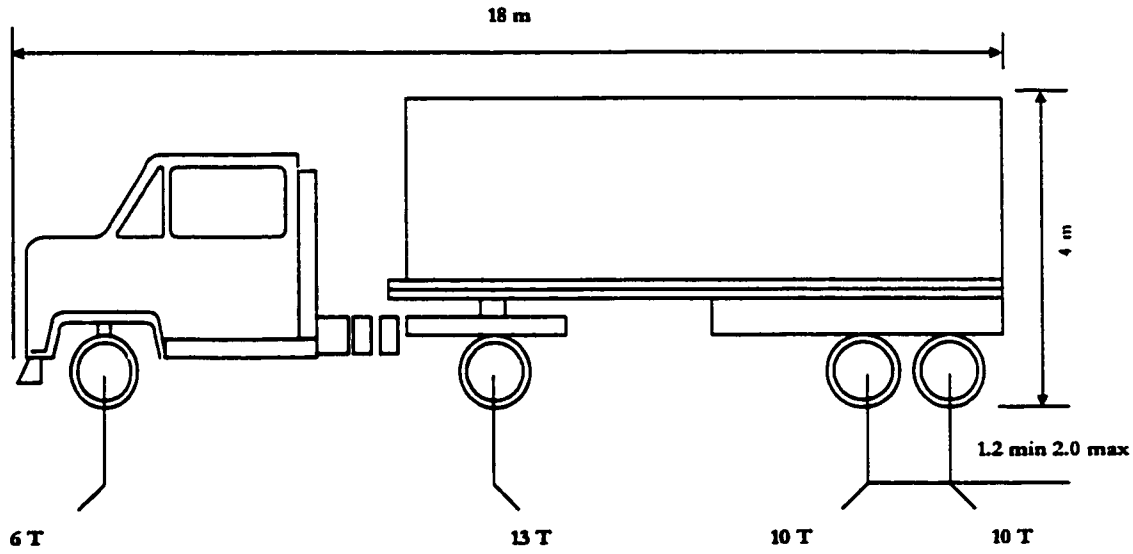

Fig. 7.43: Ministry of communication 39 Ton truck

TABLE 7.11: Details of first 250 runs for pipeline crossing highways

Run #					Diameter	t	Native soil	H				
1	2	3	4	5	12	0.24	Sand at low density	2	3	4	8	12
6	7	8	9	10			Sand at high density	2	3	4	8	12
11	12	13	14	15			Marl	2	3	4	8	12
16	17	18	19	20			Sabkha	2	3	4	8	12
21	22	23	24	25	12	0.16	Sand at low density	2	3	4	8	12
26	27	28	29	30			Sand at high density	2	3	4	8	12
31	32	33	34	35			Marl	2	3	4	8	12
36	37	38	39	40			Sabkha	2	3	4	8	12
41	42	43	44	45	12	0.12	Sand at low density	2	3	4	8	12
46	47	48	49	50			Sand at high density	2	3	4	8	12
51	52	53	54	55			Marl	2	3	4	8	12
56	57	58	59	60			Sabkha	2	3	4	8	12
61	62	63	64	65	12	.096	Sand at low density	2	3	4	8	12
66	67	68	69	70			Sand at high density	2	3	4	8	12
71	72	73	74	75			Marl	2	3	4	8	12
76	77	78	79	80			Sabkha	2	3	4	8	12
81	82	83	84	85	12	.08	Sand at low density	2	3	4	8	12
86	87	88	89	90			Sand at high density	2	3	4	8	12
91	92	93	94	95			Marl	2	3	4	8	12
96	97	98	99	100			Sabkha	2	3	4	8	12
101	102	103	104	105	24	0.48	Sand at low density	2	3	4	8	12
106	107	108	109	110			Sand at high density	2	3	4	8	12
111	112	113	114	115			Marl	2	3	4	8	12
116	117	118	119	120			Sabkha	2	3	4	8	12
121	122	123	124	125	24	0.32	Sand at low density	2	3	4	8	12
126	127	128	129	130			Sand at high density	2	3	4	8	12
131	132	133	134	135			Marl	2	3	4	8	12
136	137	138	139	140			Sabkha	2	3	4	8	12
141	142	143	144	145	24	0.24	Sand at low density	2	3	4	8	12
146	147	148	149	150			Sand at high density	2	3	4	8	12
151	152	153	154	155			Marl	2	3	4	8	12
156	157	158	159	160			Sabkha	2	3	4	8	12
161	162	163	164	165	24	0.192	Sand at low density	2	3	4	8	12
166	167	168	169	170			Sand at high density	2	3	4	8	12
171	172	173	174	175			Marl	2	3	4	8	12
176	177	178	179	180			Sabkha	2	3	4	8	12
181	182	183	184	185	24	0.16	Sand at low density	2	3	4	8	12
186	187	188	189	190			Sand at high density	2	3	4	8	12
191	192	193	194	195			Marl	2	3	4	8	12
196	197	198	199	200			Sabkha	2	3	4	8	12
201	202	203	204	205	36	0.72	Sand at low density	2	3	4	8	12
206	207	208	209	210			Sand at high density	2	3	4	8	12
211	212	213	214	215			Marl	2	3	4	8	12
216	217	218	219	220			Sabkha	2	3	4	8	12
221	222	223	224	225	36	0.48	Sand at low density	2	3	4	8	12
226	227	228	229	230			Sand at high density	2	3	4	8	12
231	232	233	234	235			Marl	2	3	4	8	12
236	237	238	239	240			Sabkha	2	3	4	8	12
241	242	243	244	245	36	0.36	Sand at low density	2	3	4	8	12
246	247	248	249	250			Sand at high density	2	3	4	8	12

TABLE 7.12: Details of next 250 runs for pipeline crossing highways

Run #					Diameter	t	Native soil	H				
251	252	253	254	255	36	0.36	Marl	2	3	4	8	12
256	257	258	259	260			Sabkha	2	3	4	8	12
261	262	263	264	265	36	0.288	Sand at low density	2	3	4	8	12
266	267	268	269	270			Sand at high density	2	3	4	8	12
271	272	273	274	275			Marl	2	3	4	8	12
276	277	278	279	280			Sabkha	2	3	4	8	12
281	282	283	284	285	36	0.24	Sand at low density	2	3	4	8	12
286	287	288	289	290			Sand at high density	2	3	4	8	12
291	292	293	294	295			Marl	2	3	4	8	12
296	297	298	298	300			Sabkha	2	3	4	8	12
301	302	303	304	305	48	0.96	Sand at low density	2	3	4	8	12
306	307	308	309	310			Sand at high density	2	3	4	8	12
311	312	313	314	315			Marl	2	3	4	8	12
316	317	318	319	320			Sabkha	2	3	4	8	12
321	322	323	324	325	48	0.64	Sand at low density	2	3	4	8	12
326	327	328	329	330			Sand at high density	2	3	4	8	12
331	332	333	334	335			Marl	2	3	4	8	12
336	337	338	339	340			Sabkha	2	3	4	8	12
341	342	343	344	345	48	0.48	Sand at low density	2	3	4	8	12
346	347	348	349	350			Sand at high density	2	3	4	8	12
351	352	353	354	355			Marl	2	3	4	8	12
356	357	358	359	360			Sabkha	2	3	4	8	12
361	362	363	364	365	48	0.384	Sand at low density	2	3	4	8	12
366	367	368	369	370			Sand at high density	2	3	4	8	12
371	372	373	374	375			Marl	2	3	4	8	12
376	377	378	379	380			Sabkha	2	3	4	8	12
381	382	383	384	385	48	0.32	Sand at low density	2	3	4	8	12
386	387	388	389	390			Sand at high density	2	3	4	8	12
391	392	393	394	395			Marl	2	3	4	8	12
396	397	398	399	400			Sabkha	2	3	4	8	12
401	402	403	404	405	60	1.2	Sand at low density	2	3	4	8	12
406	407	408	409	410			Sand at high density	2	3	4	8	12
411	412	413	414	415			Marl	2	3	4	8	12
416	417	418	419	420			Sabkha	2	3	4	8	12
421	422	423	424	425	60	0.8	Sand at low density	2	3	4	8	12
426	427	428	429	430			Sand at high density	2	3	4	8	12
431	432	433	434	435			Marl	2	3	4	8	12
436	437	438	439	440			Sabkha	2	3	4	8	12
441	442	443	444	445	60	0.6	Sand at low density	2	3	4	8	12
446	447	448	449	450			Sand at high density	2	3	4	8	12
451	452	453	454	455			Marl	2	3	4	8	12
456	457	458	459	460			Sabkha	2	3	4	8	12
461	462	463	464	465	60	0.48	Sand at low density	2	3	4	8	12
466	467	468	469	470			Sand at high density	2	3	4	8	12
471	472	473	474	475			Marl	2	3	4	8	12
476	477	478	479	480			Sabkha	2	3	4	8	12
481	482	483	484	485	60	0.4	Sand at low density					
486	487	488	489	490			Sand at high density	2	3	4	8	12
491	492	493	494	495			Marl	2	3	4	8	12
496	497	498	499	500			Sabkha					

diminished. In the finite element analyses, the live load is applied in the last increment after the overfill layer has been applied. Stresses and deformations obtained in the last increment were subtracted from the stresses and deformations of the preceding construction increment to get only the live load component. Figs. 7.44 to 7.48 show the results of selected runs for sand at low density as native soils. The results for other soils show a similar trend. It can be seen that after 8 feet depth of cover, regardless of the pipe diameter, the change in stresses and diameter is not significant. Therefore, a depth of cover in this study was limited to 12 feet.

Katona [59] reported that larger diameter pipes require less depth of cover for protection against live load contrary to common belief that large diameter pipes require more depth of cover under live load. An attempt was made to check the Katona's observation. The results for high density sand as native soil are shown in Figs. 7.49 to 7.53. The similar results were obtained for all the other native soil types. The results clearly show that pipes of larger diameter have less stresses as compared to the smaller diameter pipes. The percent change in diameter shows a similar trend indicating the pipes of larger diameter require less cover against live load.

Figs. 7.54 to 7.73 show results of combined dead and live load for D/t ratios of 50, 75, 100, 125, 150 for all soil types. No major variation in stresses for the D/t ratios of 100, 125, and 150. Following the same steps as in sand overburden problem the variation of normal pressure at crown and springline for pipe diameter of 36 inch was investigated for D/t ratios of 50, 75, 100, 125, and 150 and different soil types. Figs. 7.74 and 7.75 clearly indicate that the load carried by the pipe at the crown decreases with the increase in

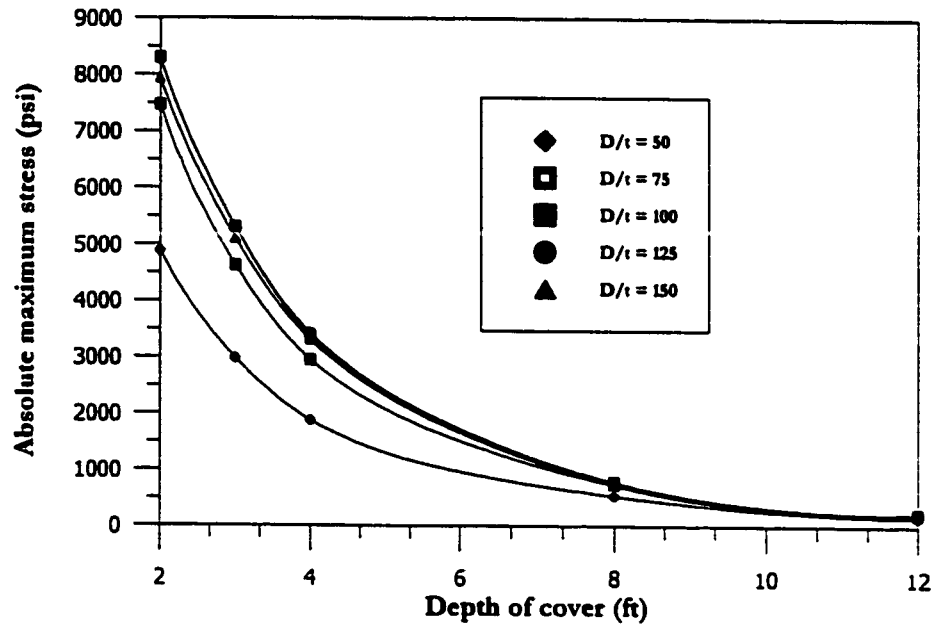

(a) Variation of absolute maximum stress

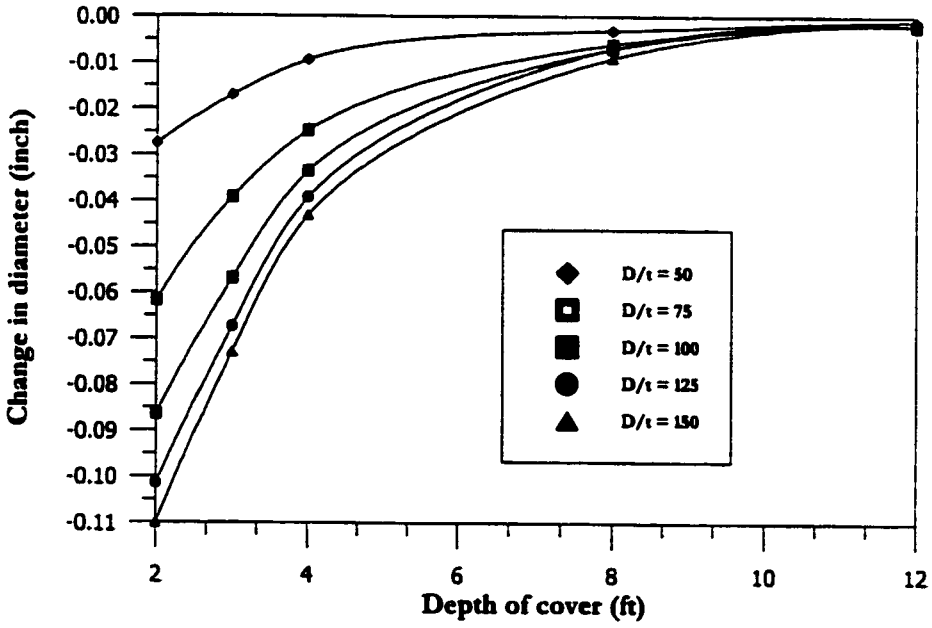

(b) Variation of change in diameter

Fig. 7.44: Effect of live load on 12 inches pipe diameter and low density sand as native soil

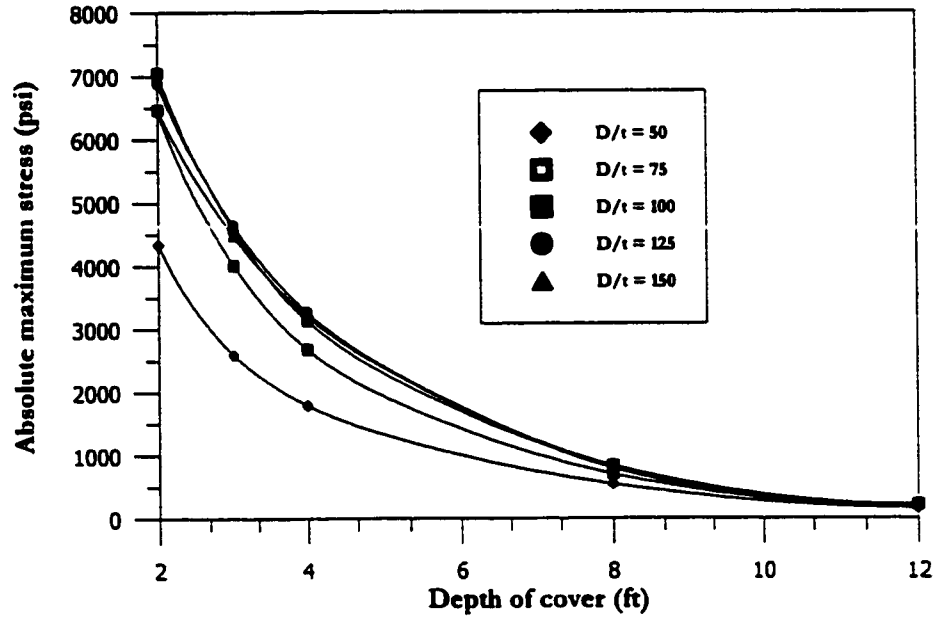

(a) Variation of absolute maximum stress

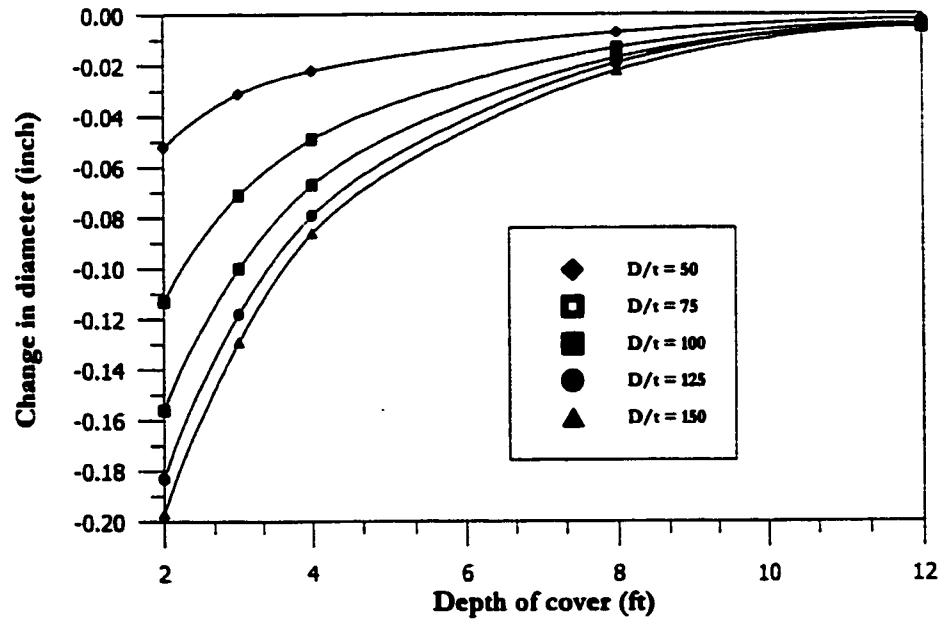

(b) Variation of change in diameter

Fig. 7.45: Effect of live load on 24 inches pipe diameter and low density sand as native soil

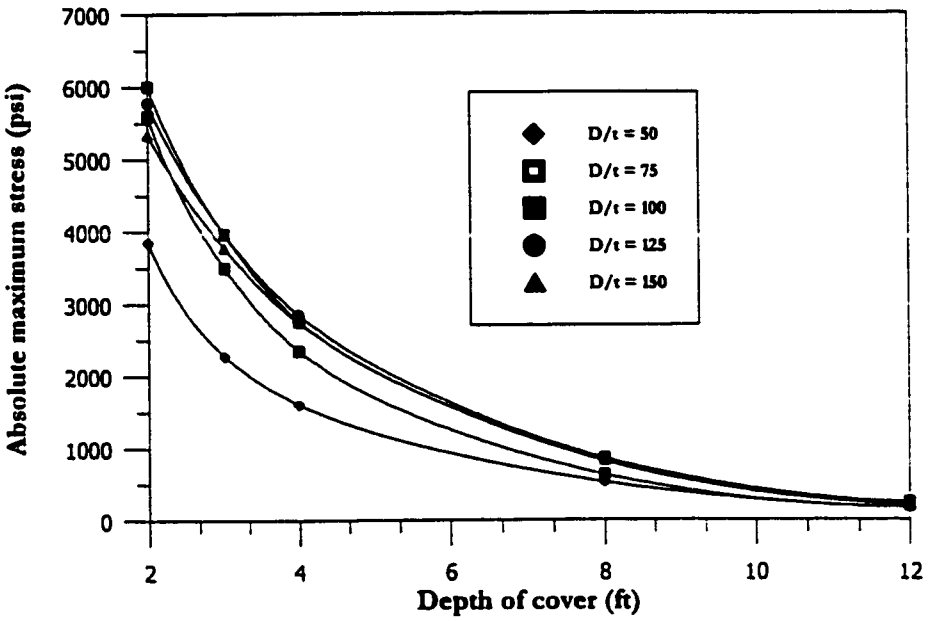

(a) Variation of absolute maximum stress

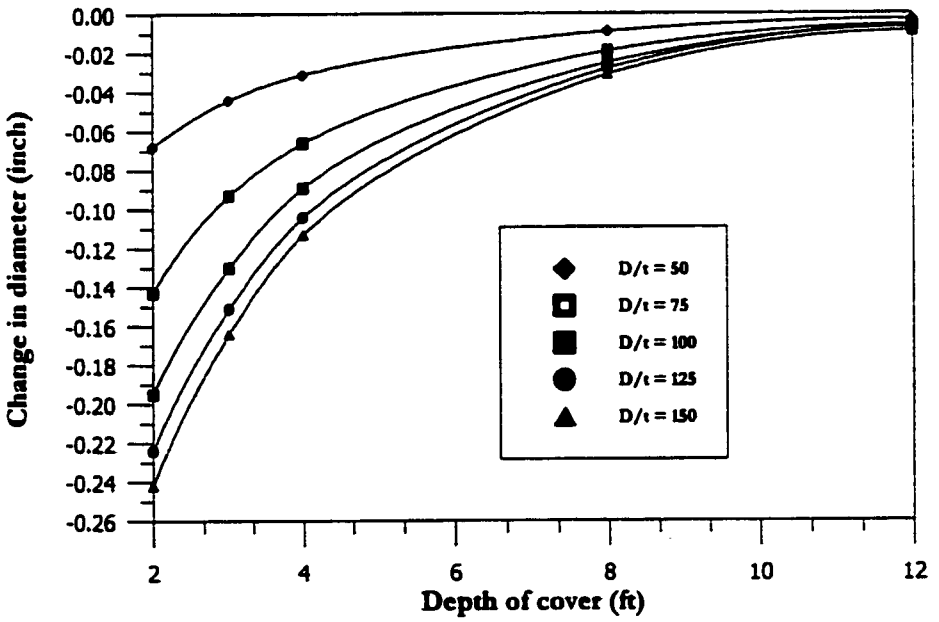

(b) Variation of change in diameter

Fig. 7.46: Effect of live load on 36 inches pipe diameter and low density sand as native soil

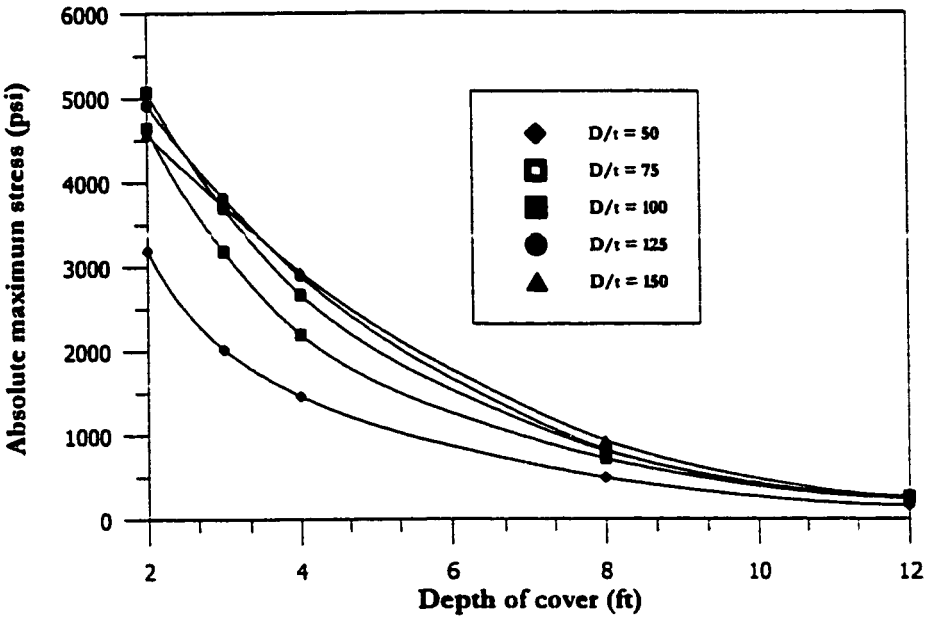

(a) Variation of absolute maximum stress

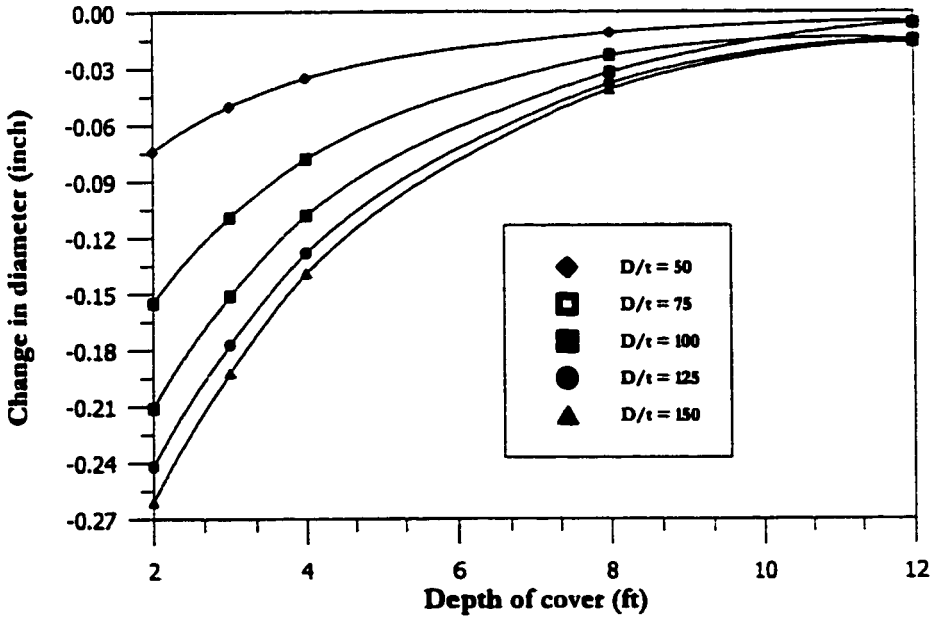

(b) Variation of change in diameter

Fig. 7.47: Effect of live load on 48 inches pipe diameter and low density sand as native soil

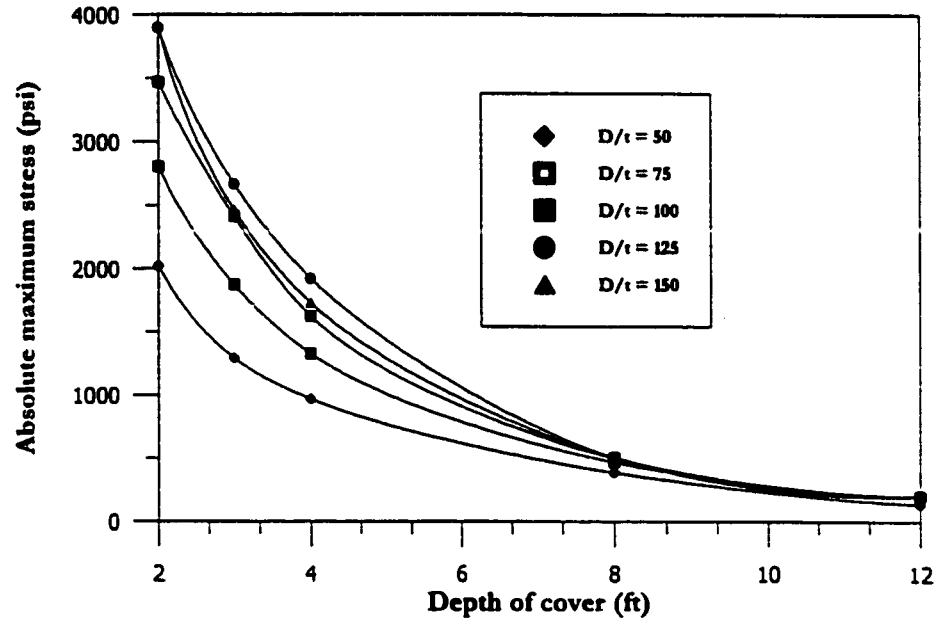

(a) Variation of absolute maximum stress

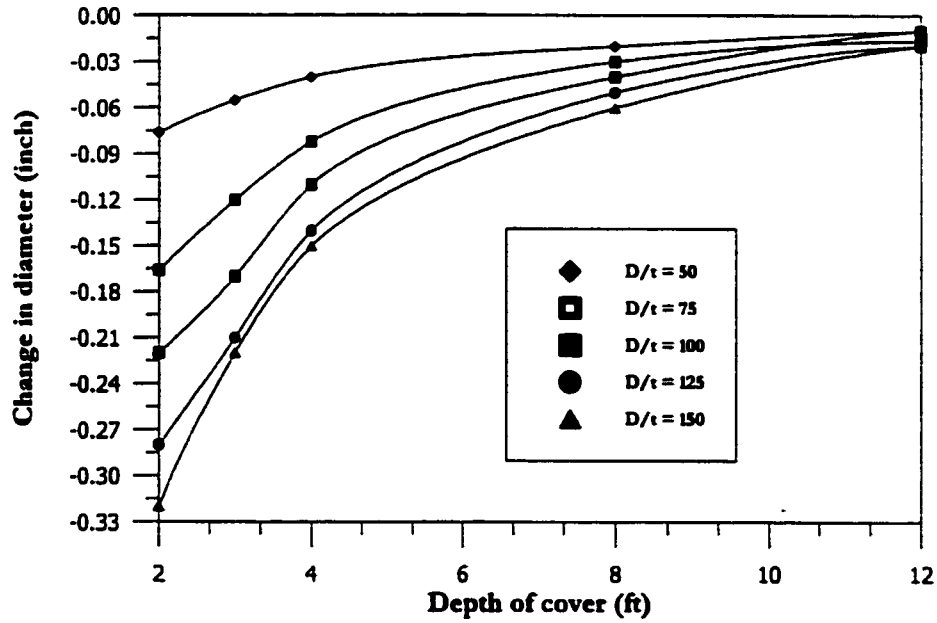

(b) Variation of change in diameter

Fig. 7.48: Effect of live load on 60 inches pipe diameter and low density sand as native soil

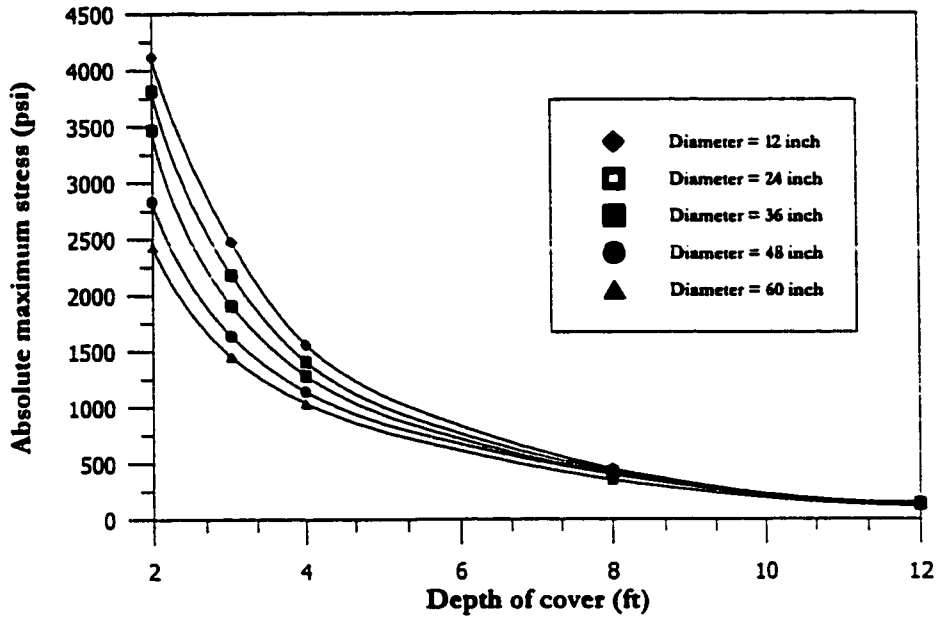

(a) Variation of absolute maximum stress

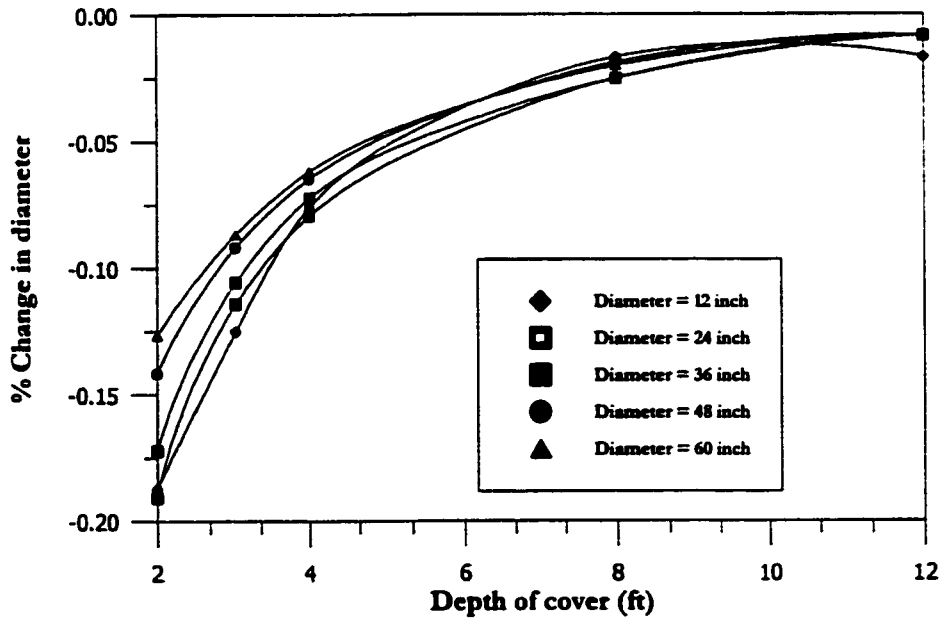

(b) Variation of change in diameter

Fig. 7.49: Variation in absolute maximum stress and percent change in diameter for D/t = 50 and High density sand for live load only

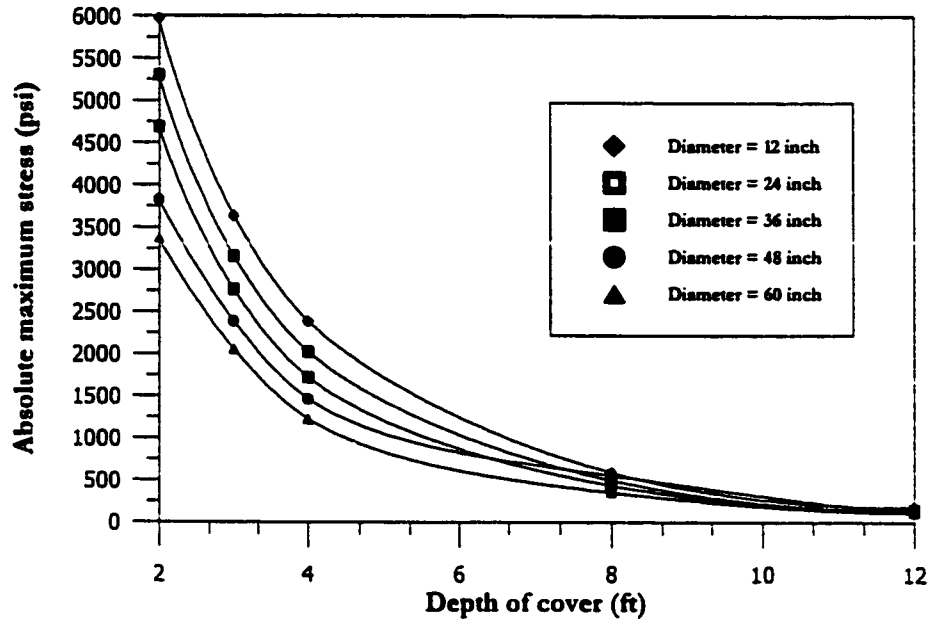

(a) Variation of absolute maximum stress

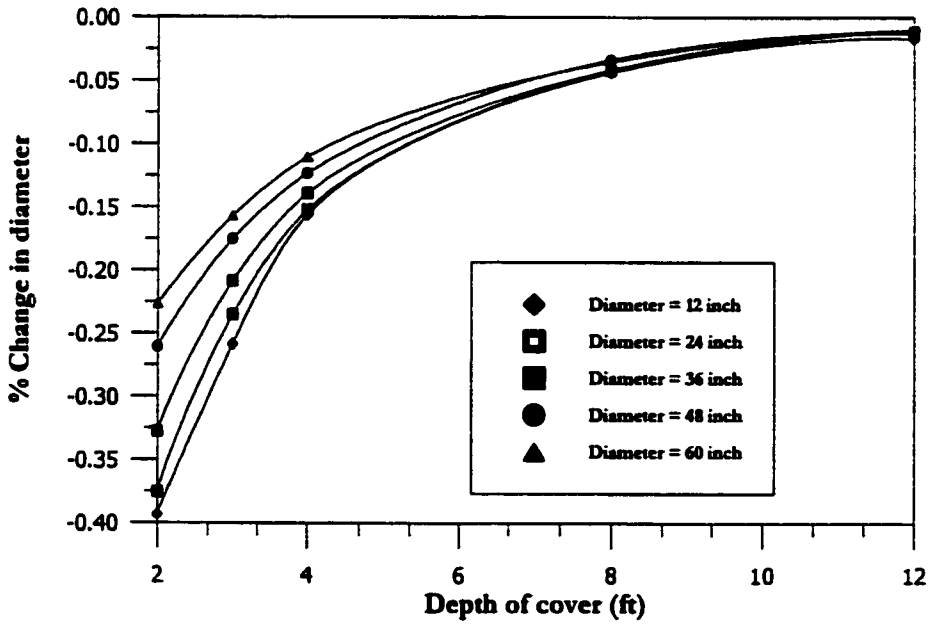

(b) Variation of change in diameter

Fig. 7.50: Variation in absolute maximum stress and percent change in diameter for D/t = 75 and High density sand for live load only

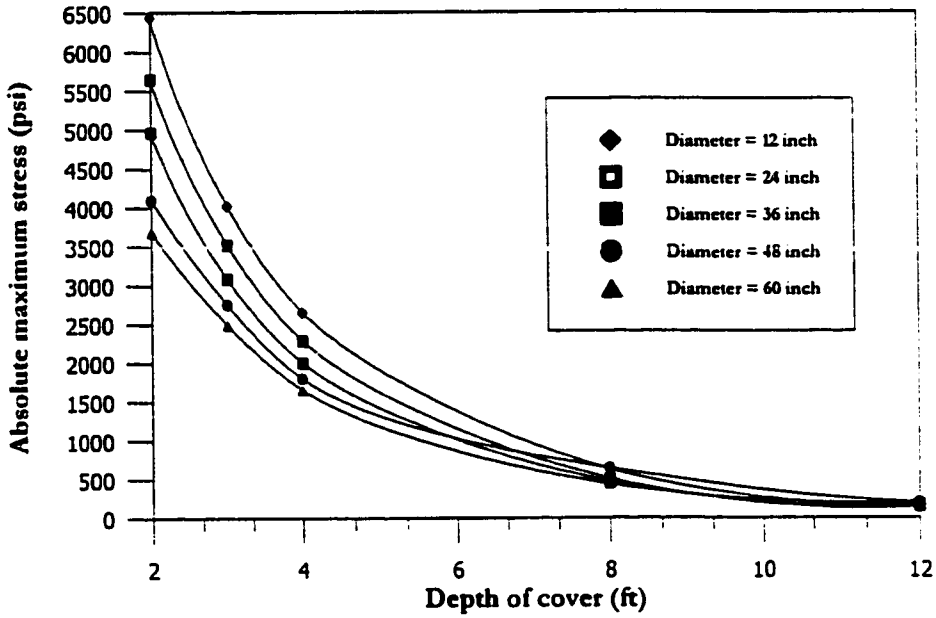

(a) Variation of absolute maximum stress

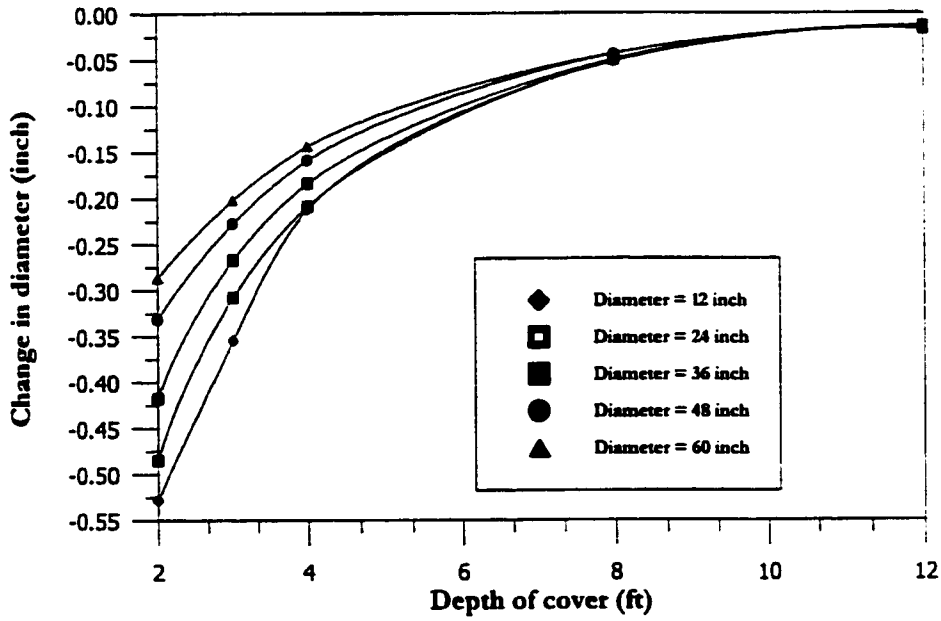

(b) Variation of change in diameter

Fig. 7.51: Variation in absolute maximum stress and percent change in diameter for D/t = 100 and High density sand for live load only

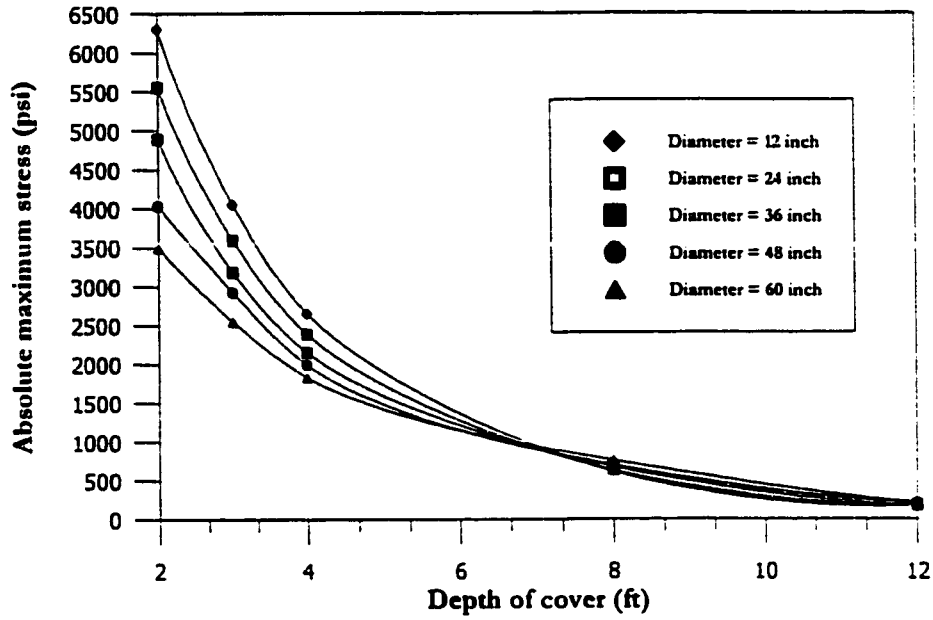

(a) Variation of absolute maximum stress

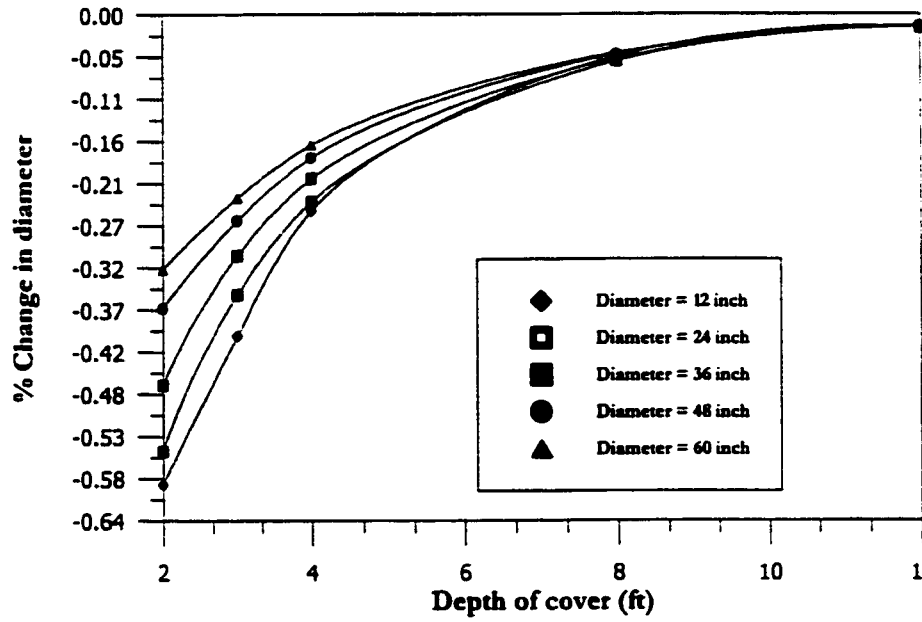

(b) Variation of change in diameter

Fig. 7.52: Variation in absolute maximum stress and percent change in diameter for D/t = 125 and High density sand for live load only

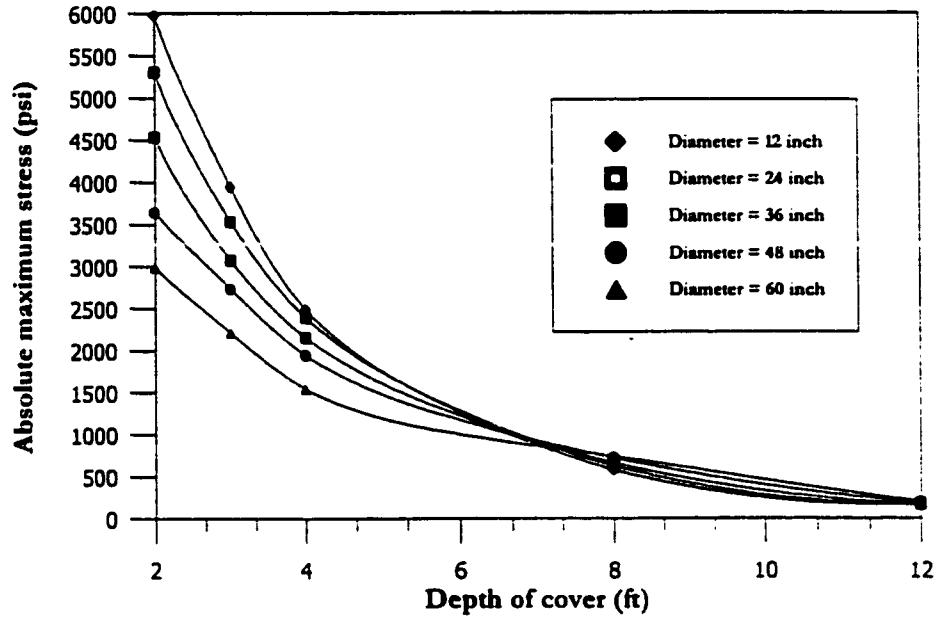

(a) Variation of absolute maximum stress

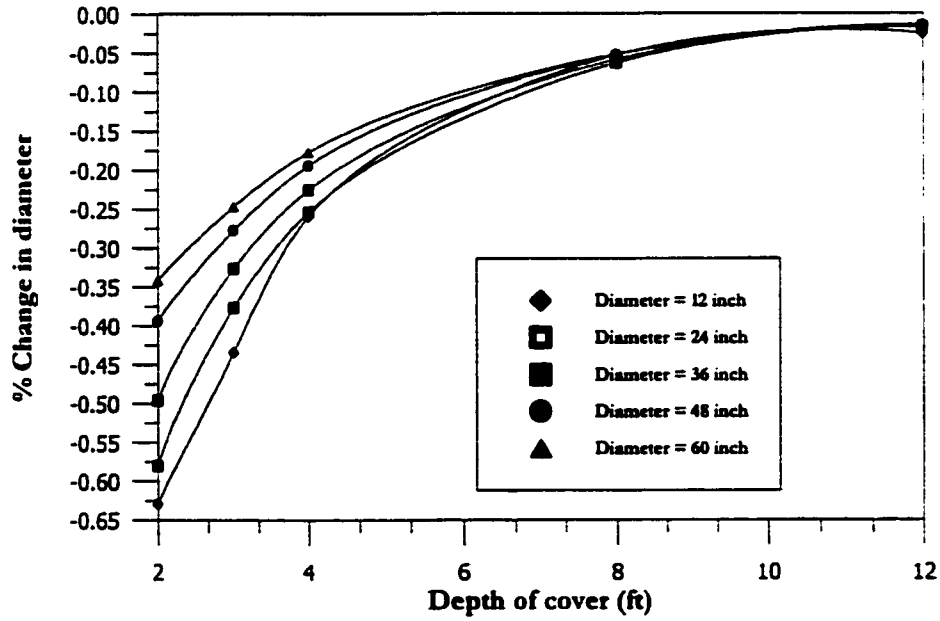

(b) Variation of change in diameter

Fig. 7.53: Variation in absolute maximum stress and percent change in diameter for D/t = 150 and High density sand for live load only

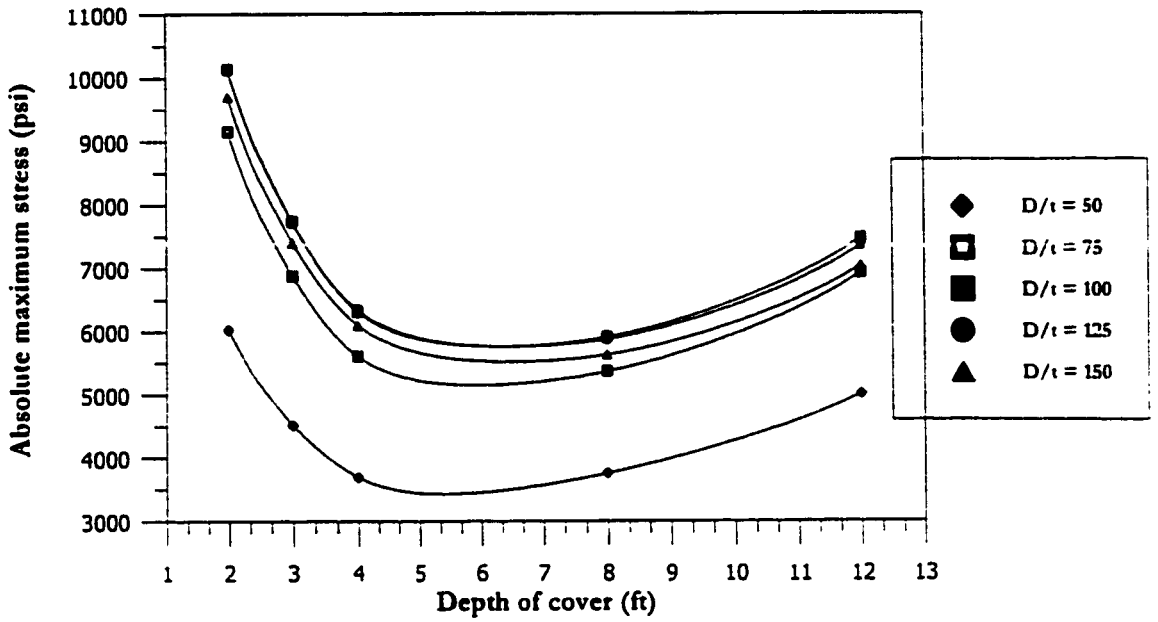

(a) Variation of absolute maximum stress

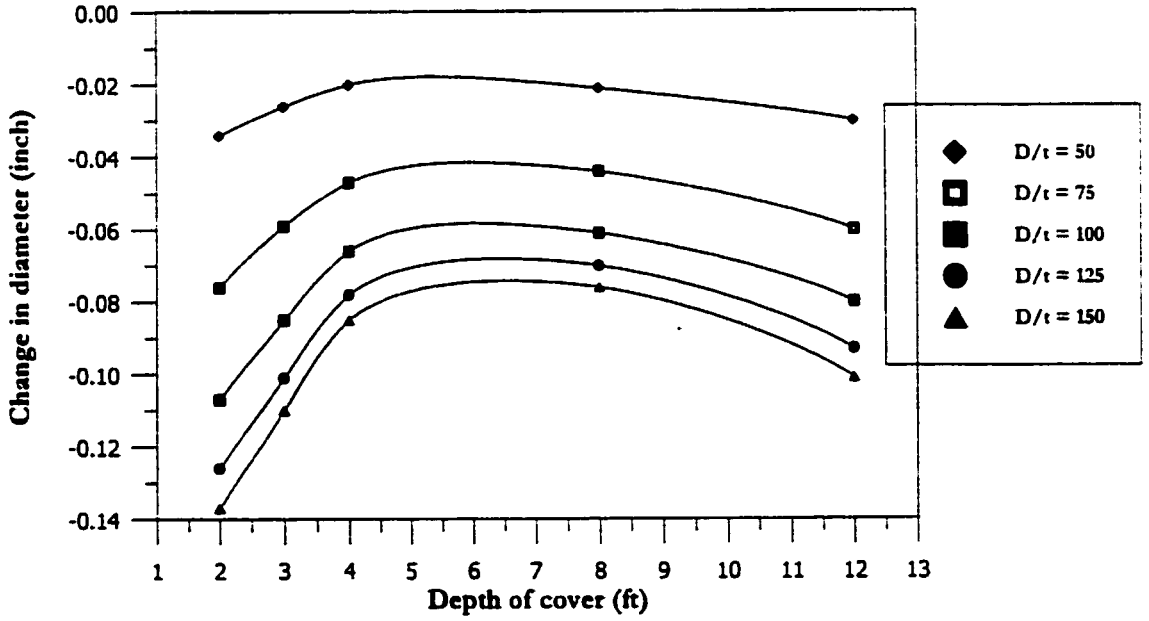

(b) Variation of change in diameter

Fig. 7.54: Variation in absolute maximum stress and diameter change for 12 inches pipe diamter with low density sand subjected to dead plus live load

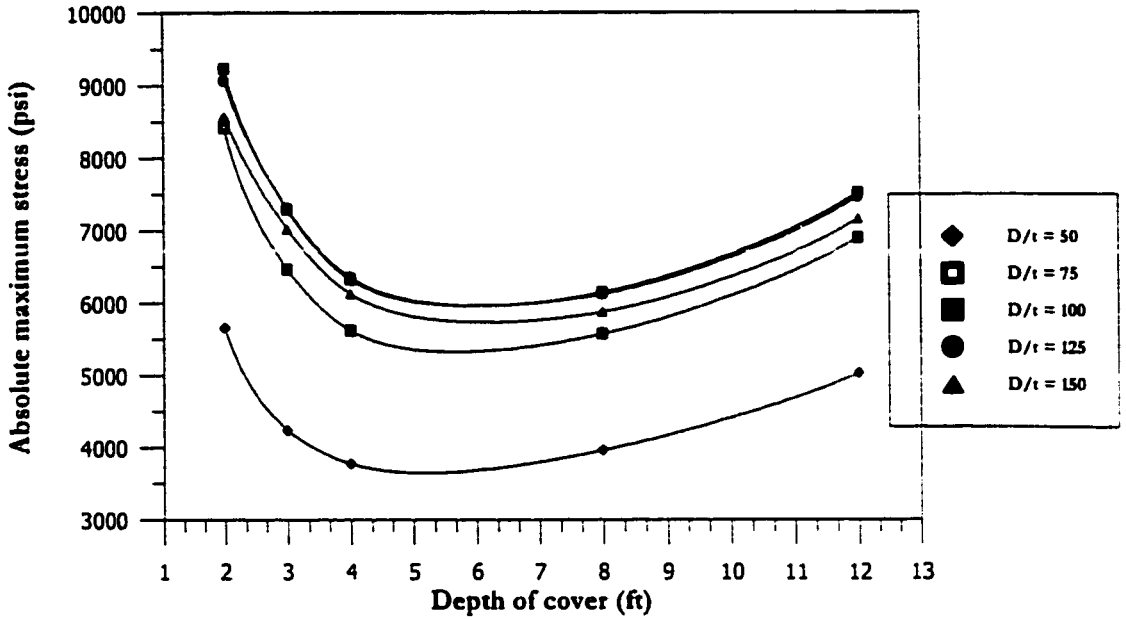

(a) Variation of absolute maximum stress

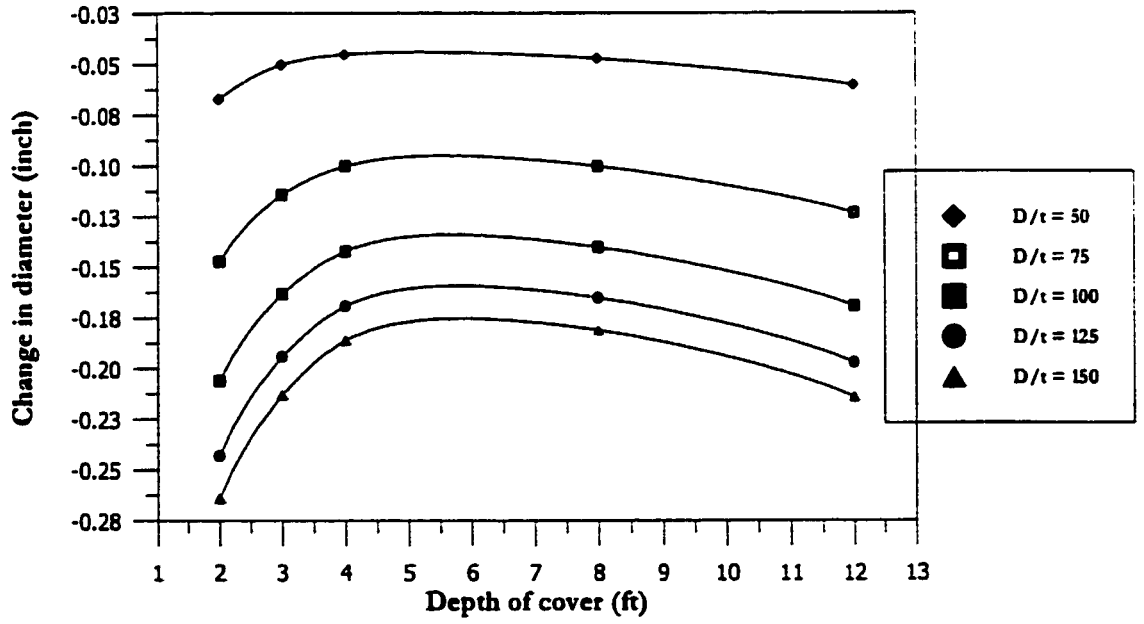

(b) Variation of change in diameter

Fig. 7.55: Variation in absolute maximum stress and diameter change for 24 inches pipe diamter with low density sand subjected to dead plus live load

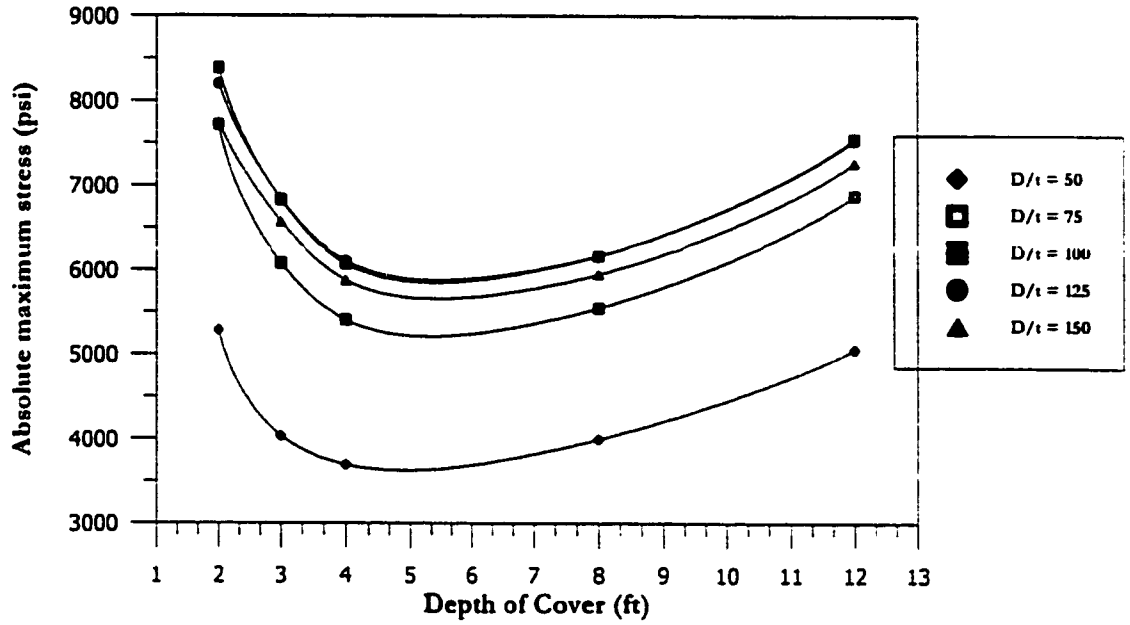

(a) Variation of absolute maximum stress

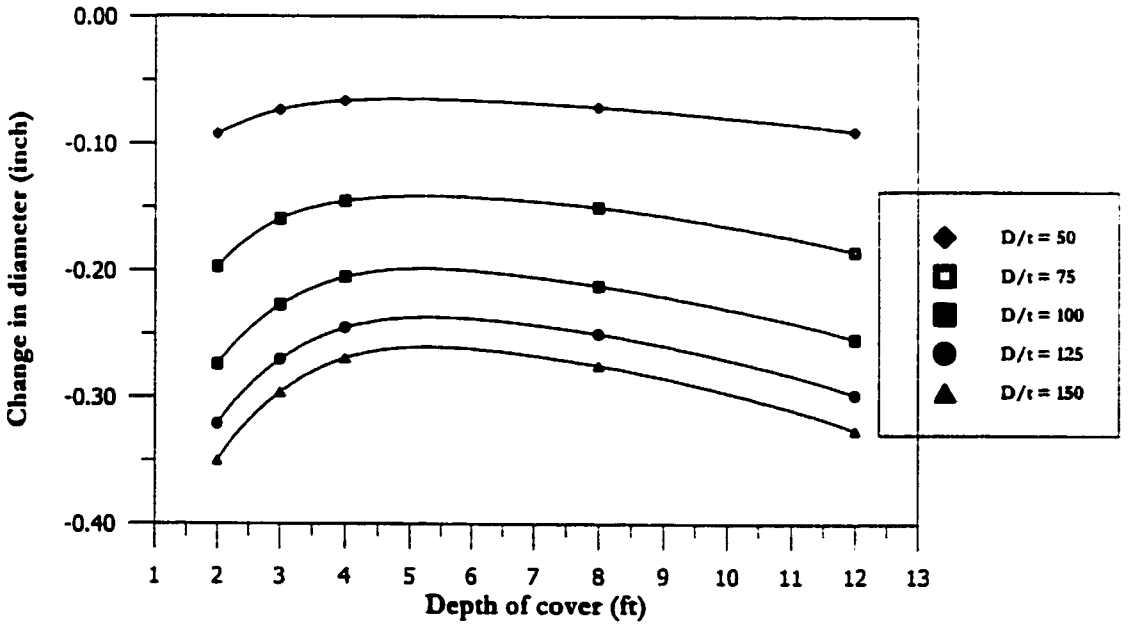

(b) Variation of change in diameter

Fig. 7.56: Variation in absolute maximum stress and diameter change for 36 inches pipe diamter with low density sand subjected to dead plus live load

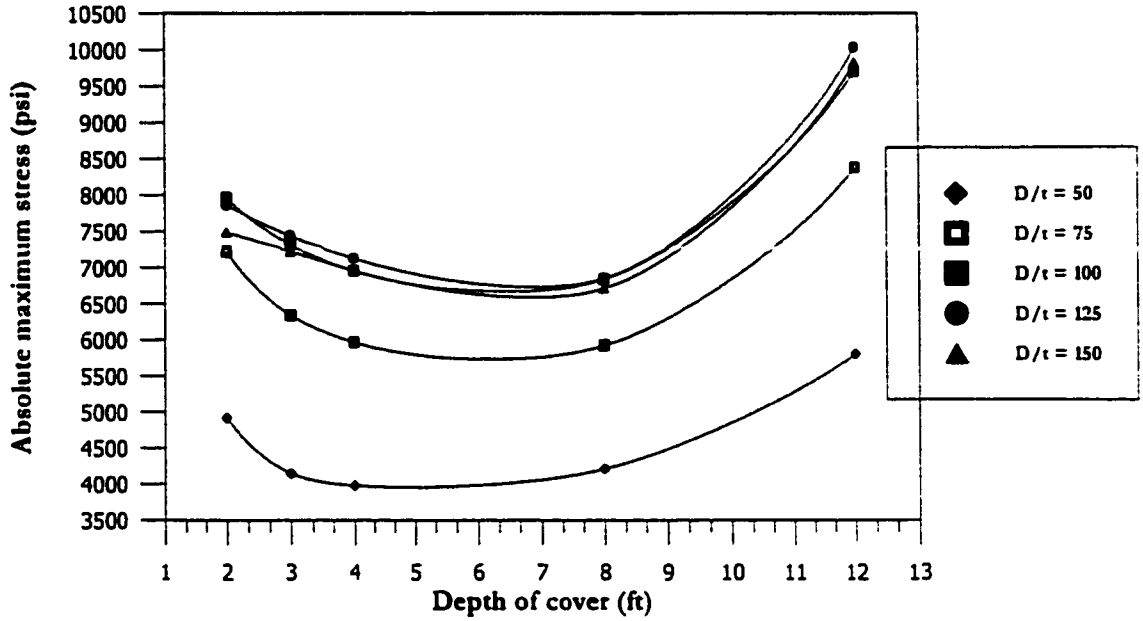

(a) Variation of absolute maximum stress

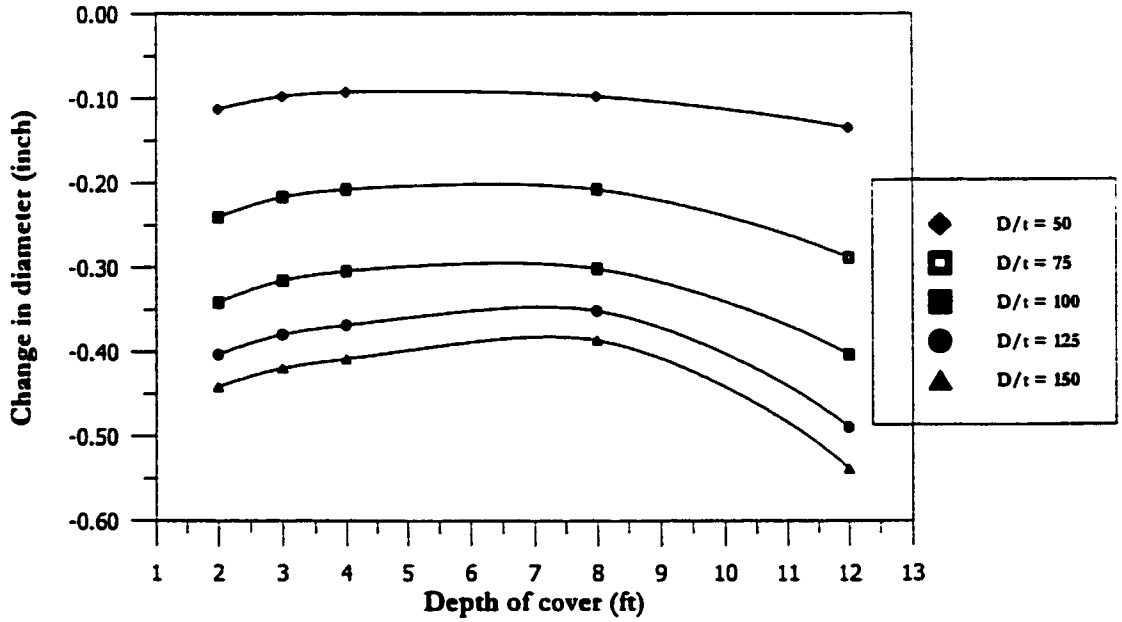

(b) Variation of change in diameter

Fig. 7.57: Variation in absolute maximum stress and diameter change for 48 inches pipe diamter with low density sand subjected to dead plus live load

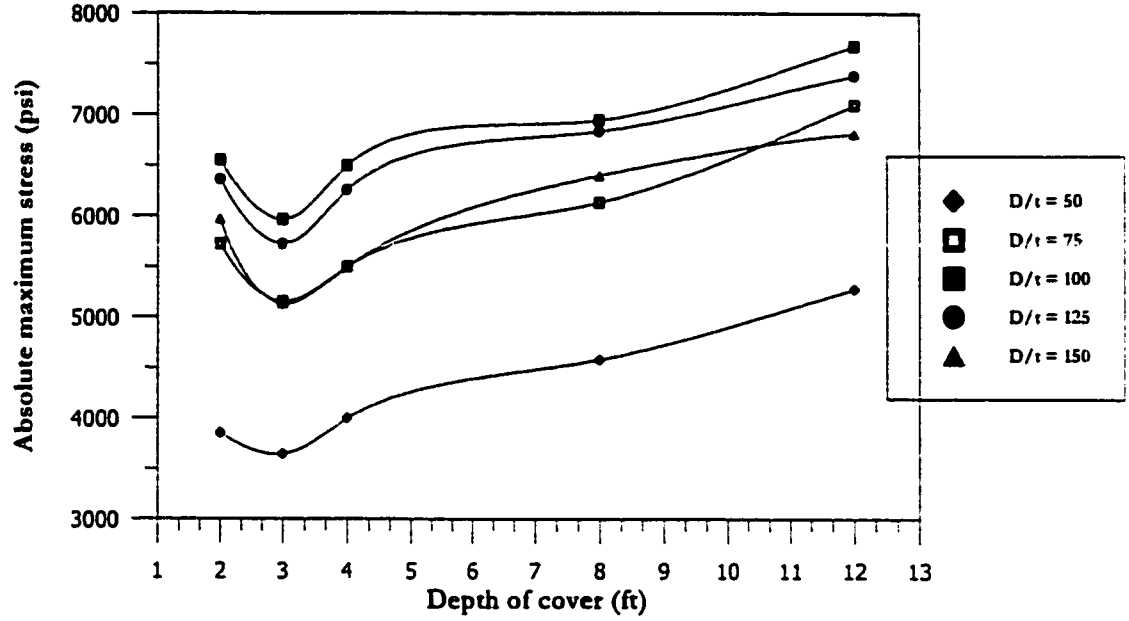

(a) Variation of absolute maximum stress

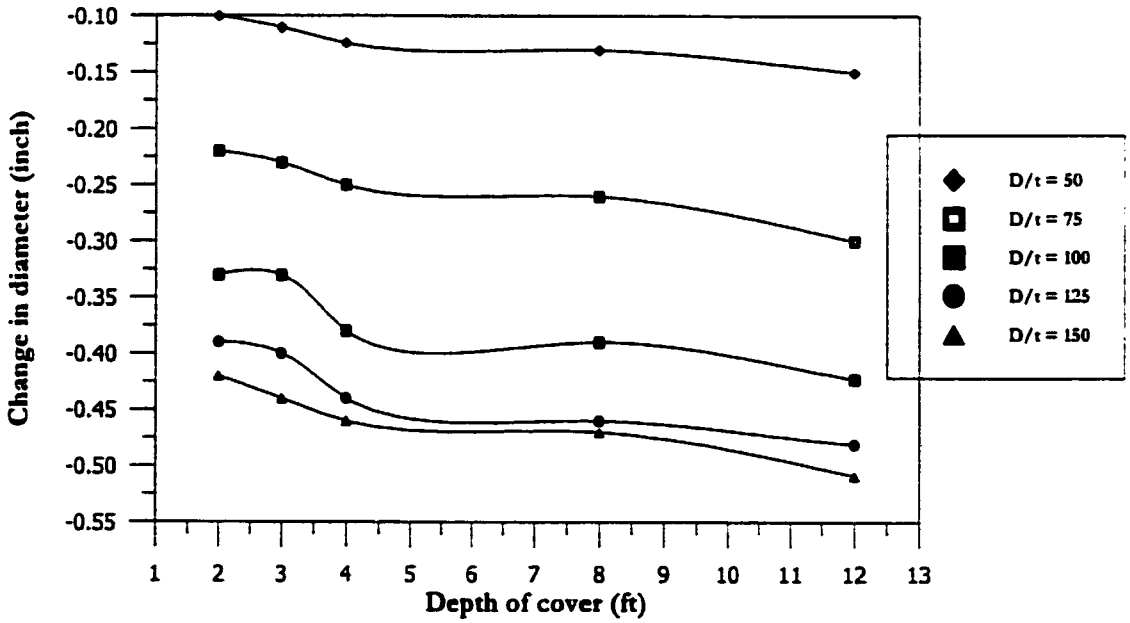

(b) Variation of change in diameter

Fig. 7.58: Variation in absolute maximum stress and diameter change for 60 inches pipe diamter with low density sand subjected to dead plus live load

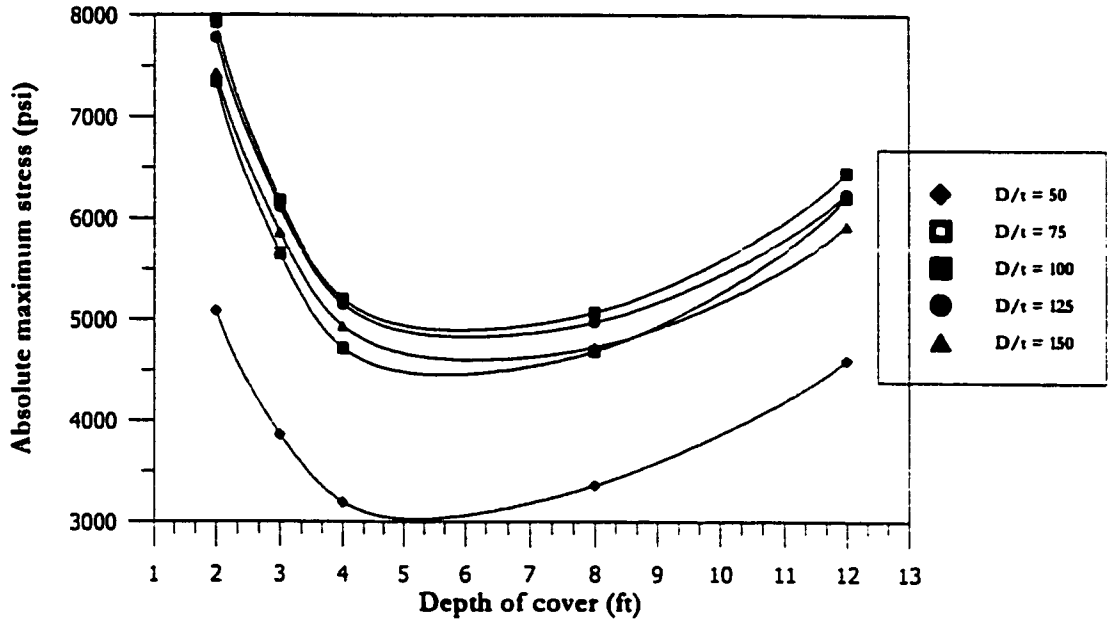

(a) Variation of absolute maximum stress

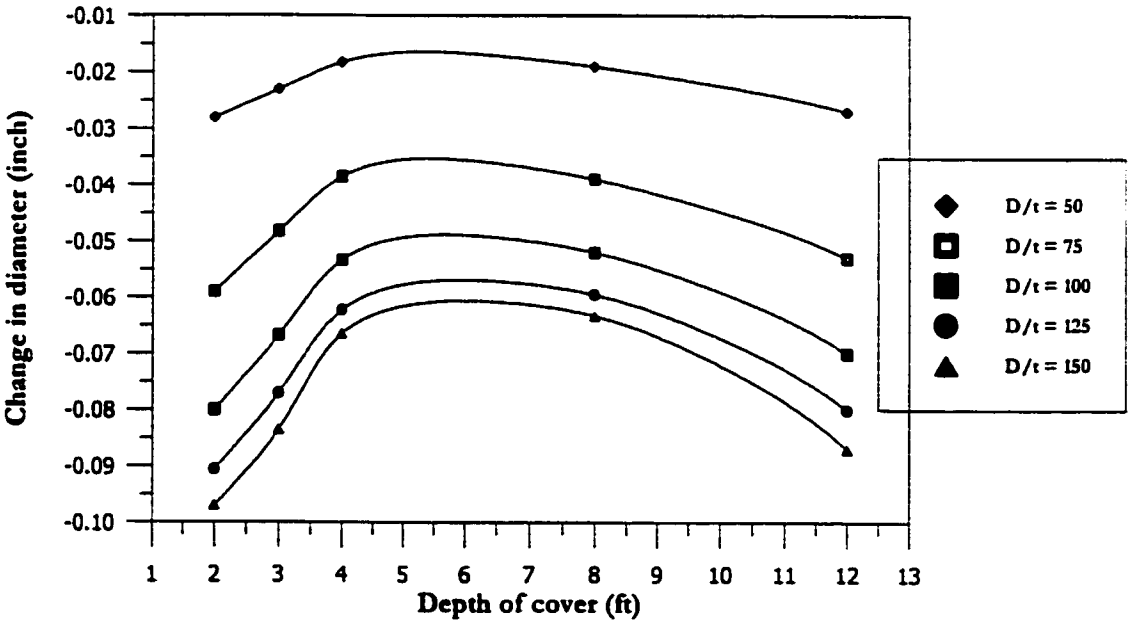

(b) Variation of change in diameter

Fig. 7.59: Variation in absolute maximum stress and diameter change for 12 inches pipe diamter with high density sand subjected to dead plus live load

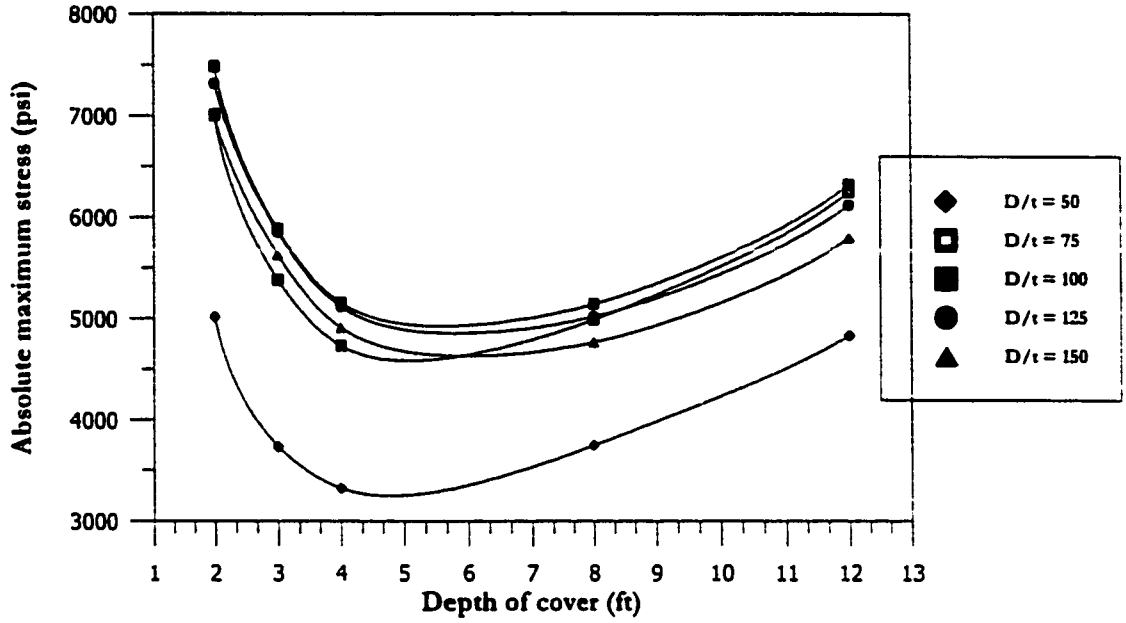

(a) Variation of absolute maximum stress

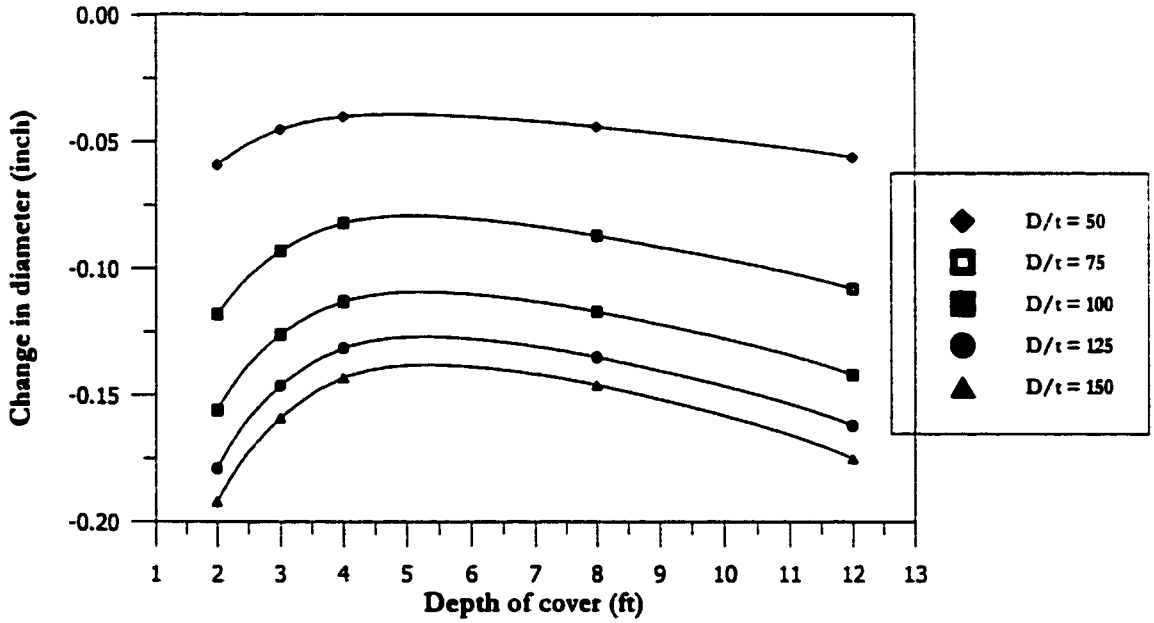

(b) Variation of change in diameter

Fig. 7.60: Variation in absolute maximum stress and diameter change for 24 inches pipe diamter with high density sand subjected to dead plus live load

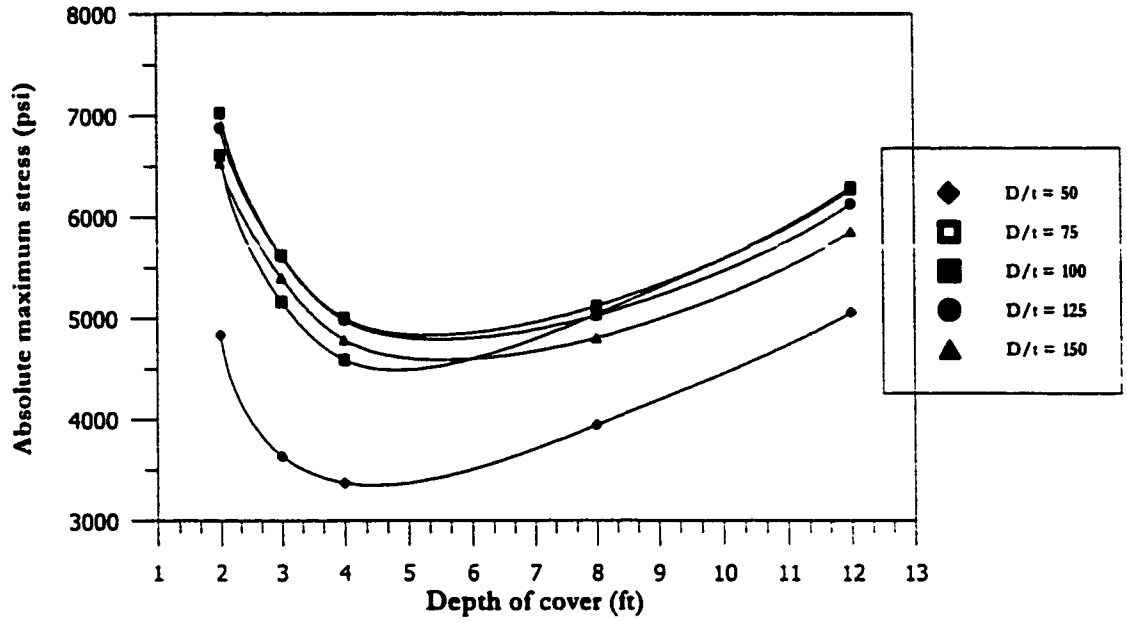

(a) Variation of absolute maximum stress

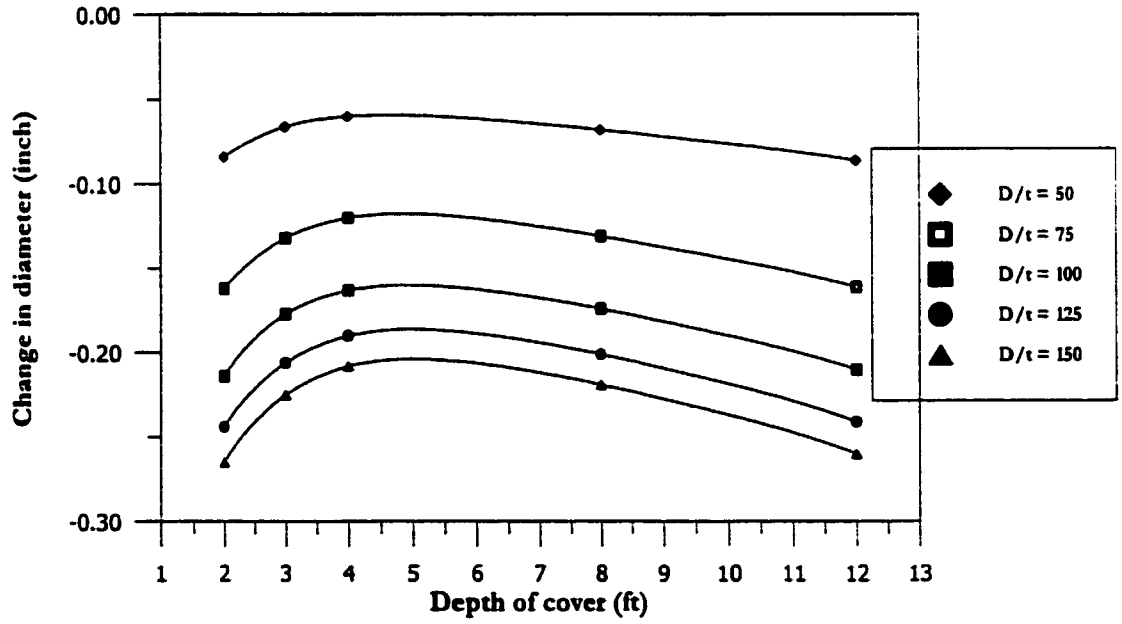

(b) Variation of change in diameter

Fig. 7.61: Variation in absolute maximum stress and diameter change for 36 inches pipe diamter with high density sand subjected to dead plus live load

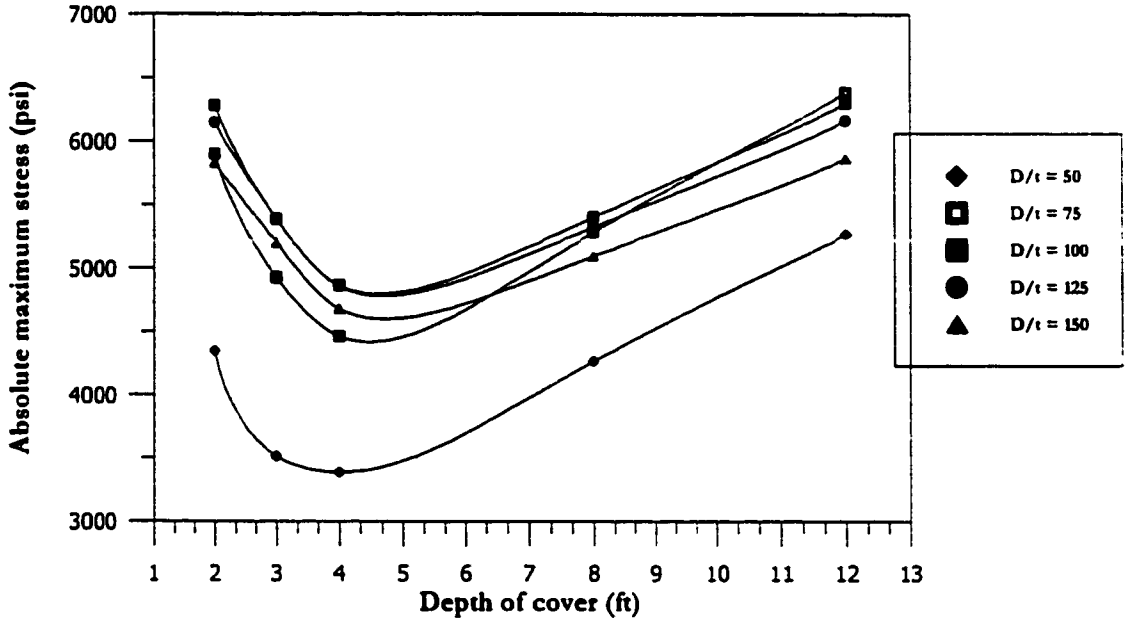

(a) Variation of absolute maximum stress

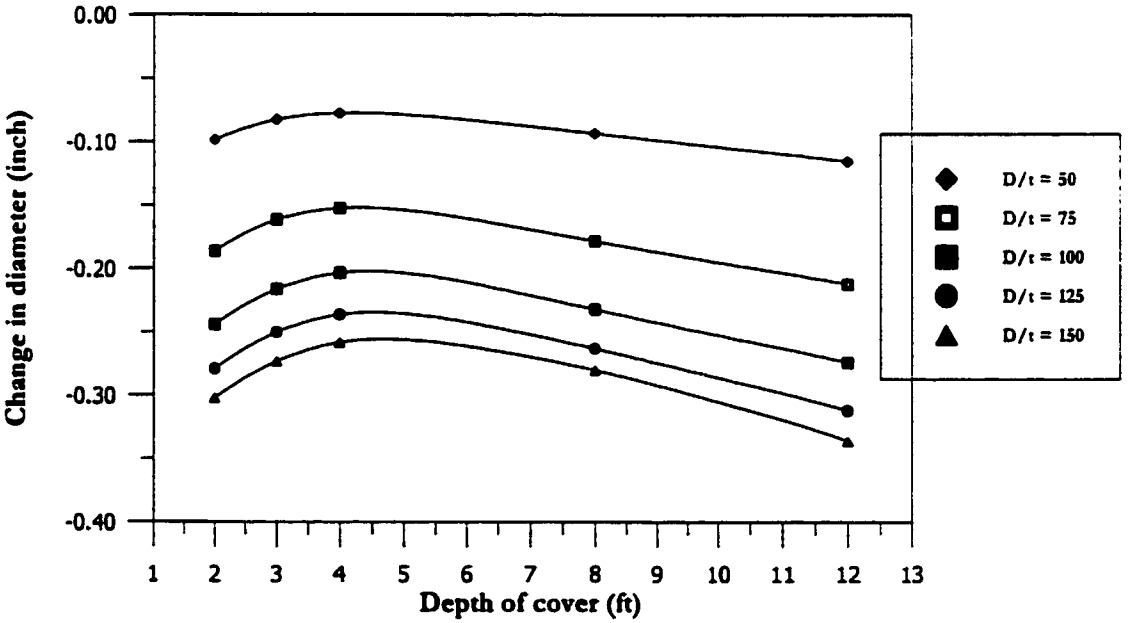

(b) Variation of change in diameter

Fig. 7.62: Variation in absolute maximum stress and diameter change for 48 inches pipe diamter with high density sand subjected to dead plus live load

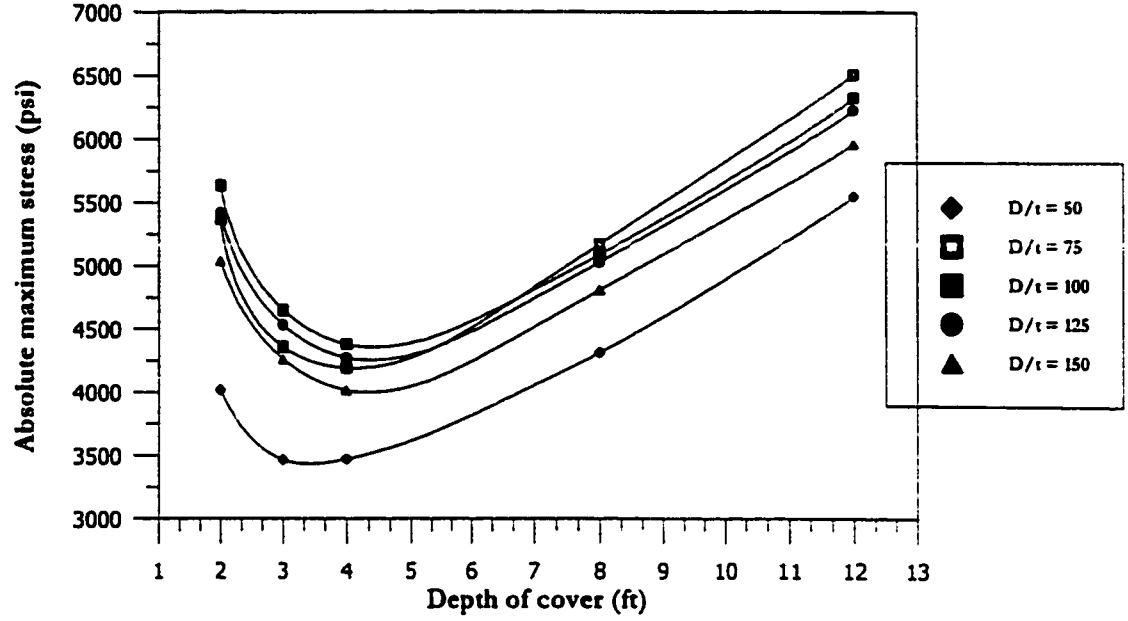

(a) Variation of absolute maximum stress

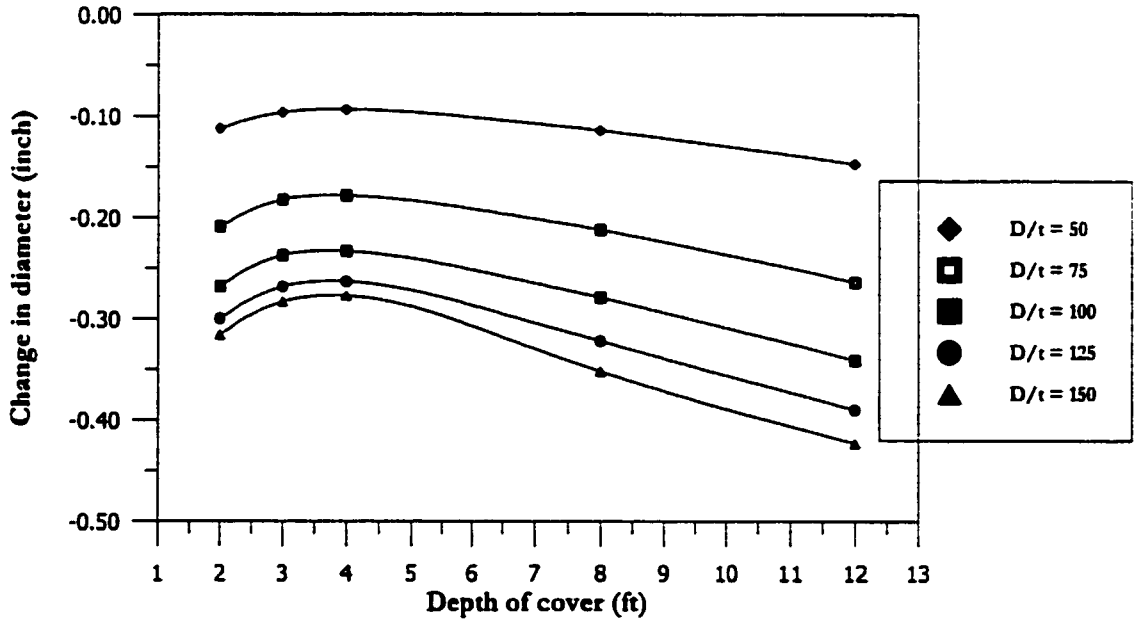

(b) Variation of change in diameter

Fig. 7.63: Variation in absolute maximum stress and diameter change for 60 inches pipe diamter with high density sand subjected to dead plus live load

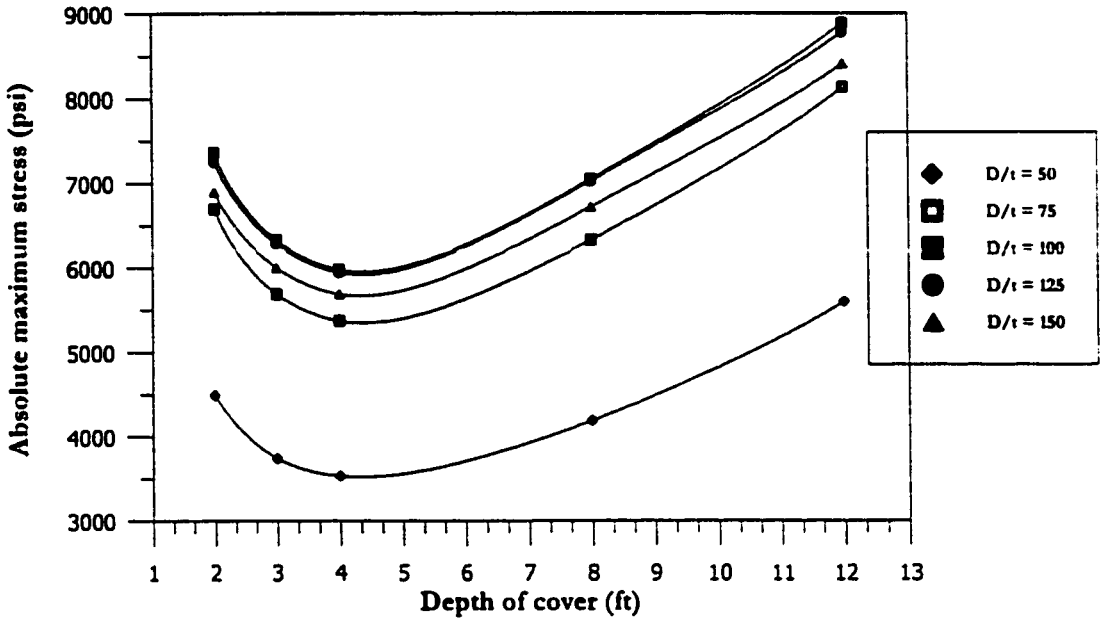

(a) Variation of absolute maximum stress

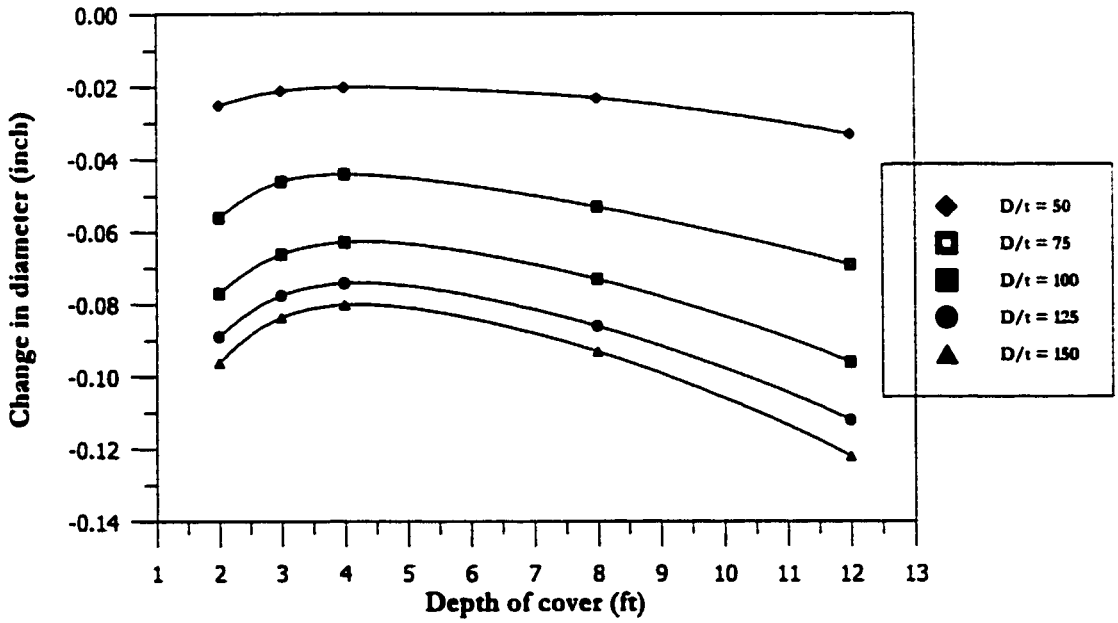

(b) Variation of change in diameter

Fig. 7.64: Variation in absolute maximum stress and diameter change for 12 inches pipe diamter with marl subjected to dead plus live load

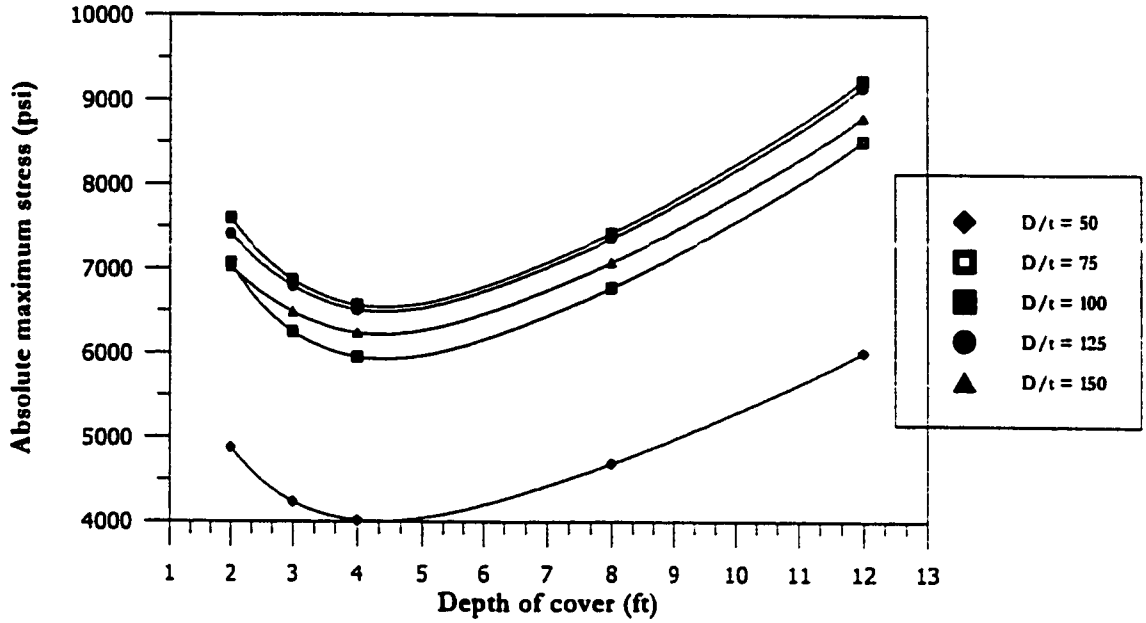

(a) Variation of absolute maximum stress

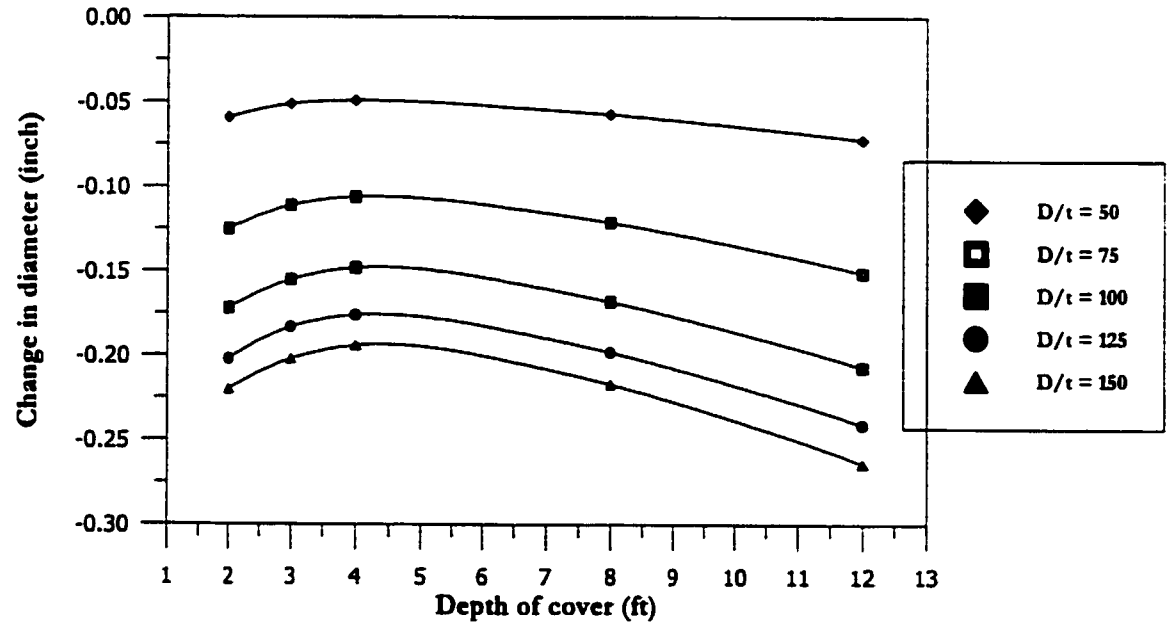

(b) Variation of change in diameter

Fig. 7.65: Variation in absolute maximum stress and diameter change for 24 inches pipe diamter with marl subjected to dead plus live load

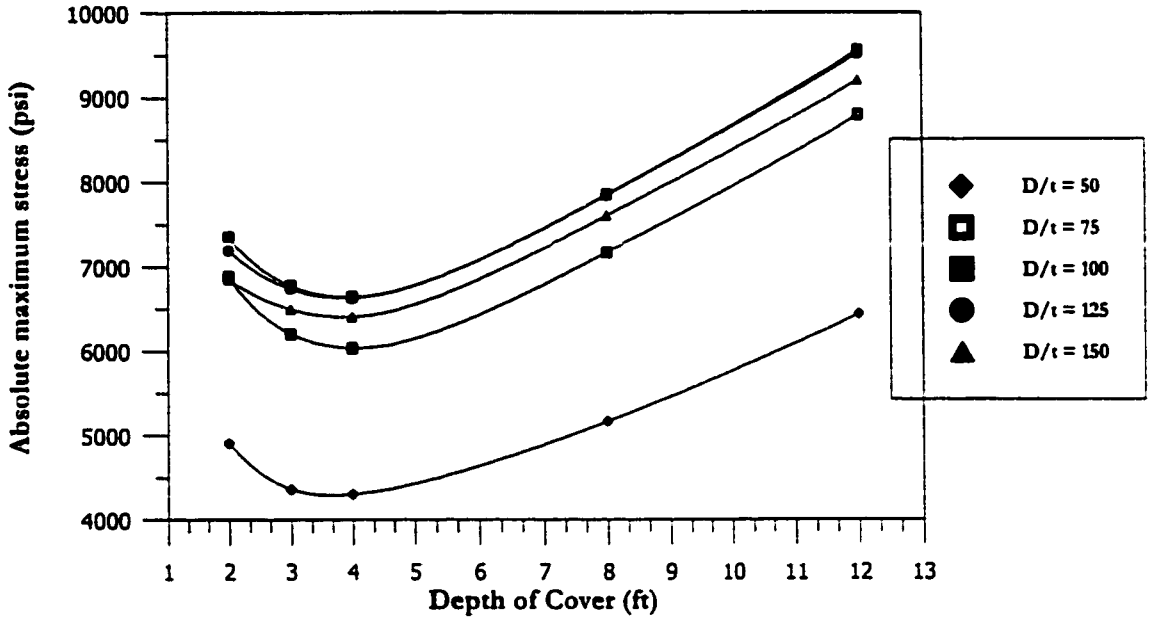

(a) Variation of absolute maximum stress

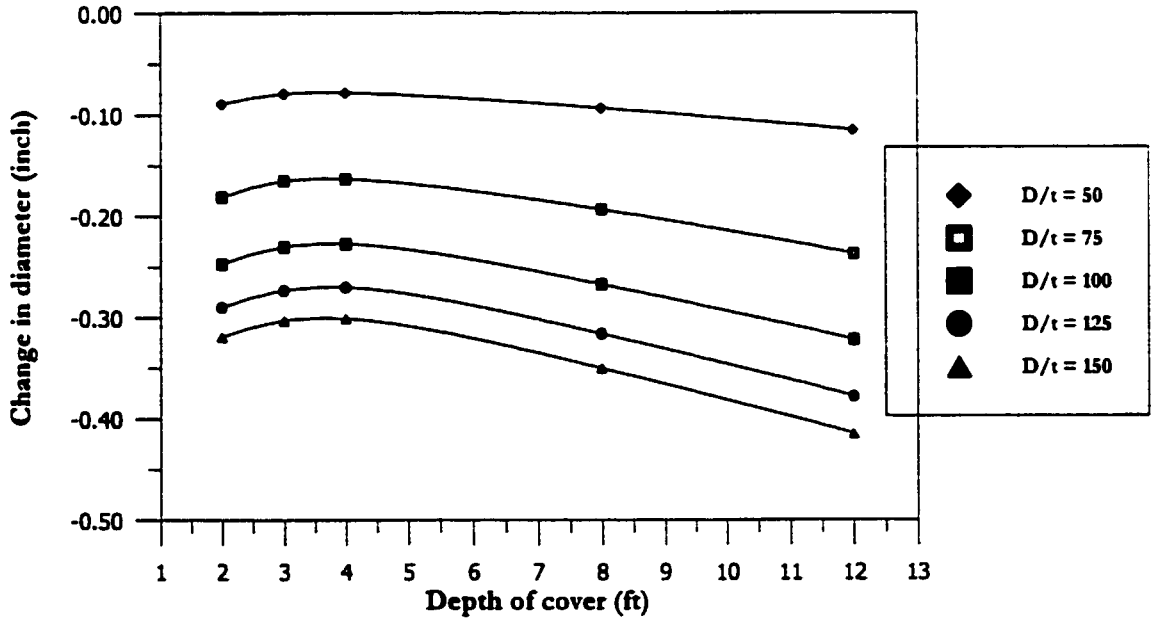

(b) Variation of change in diameter

Fig. 7.66: Variation in absolute maximum stress and diameter change for 36 inches pipe diamter with marl subjected to dead plus live load

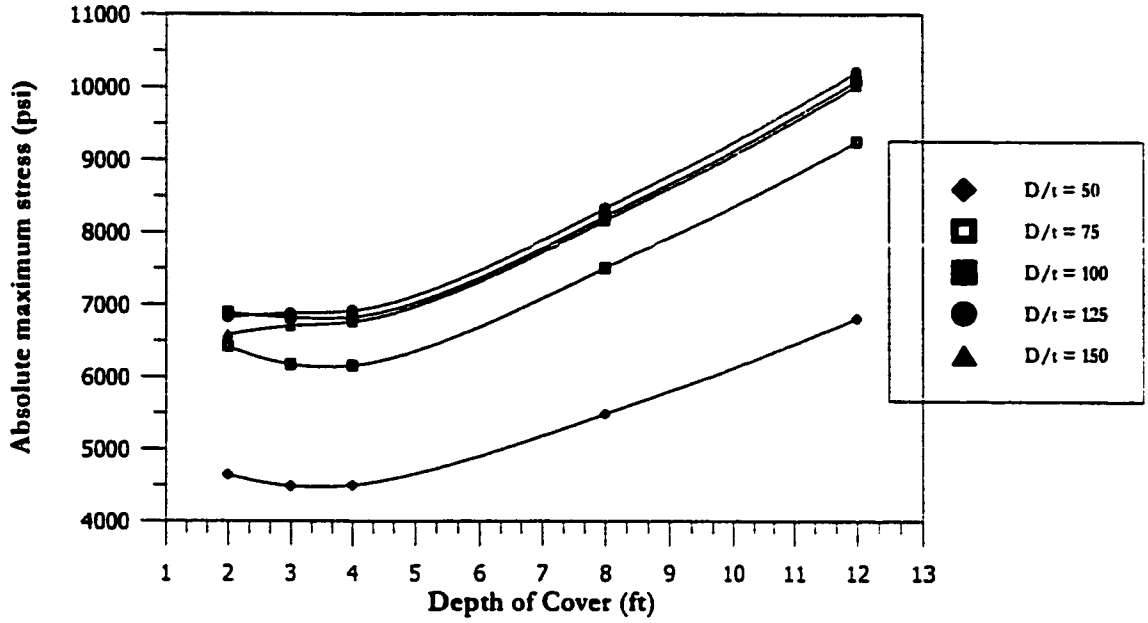

(a) Variation of absolute maximum stress

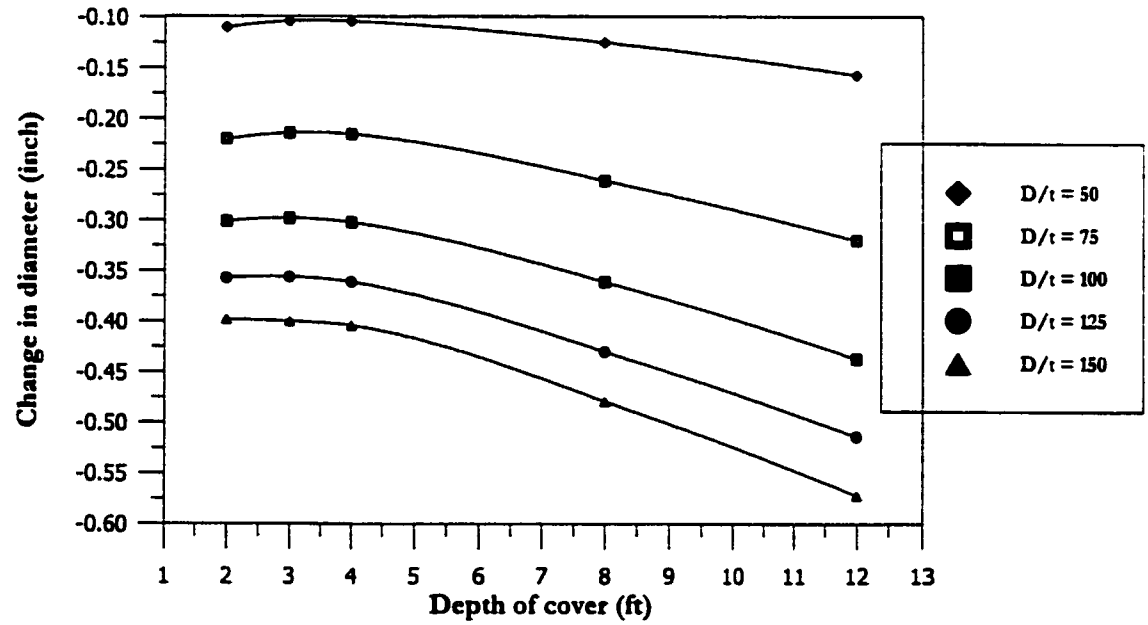

(b) Variation of change in diameter

Fig. 7.67: Variation in absolute maximum stress and diameter change for 48 inches pipe diamter with marl subjected to dead plus live load

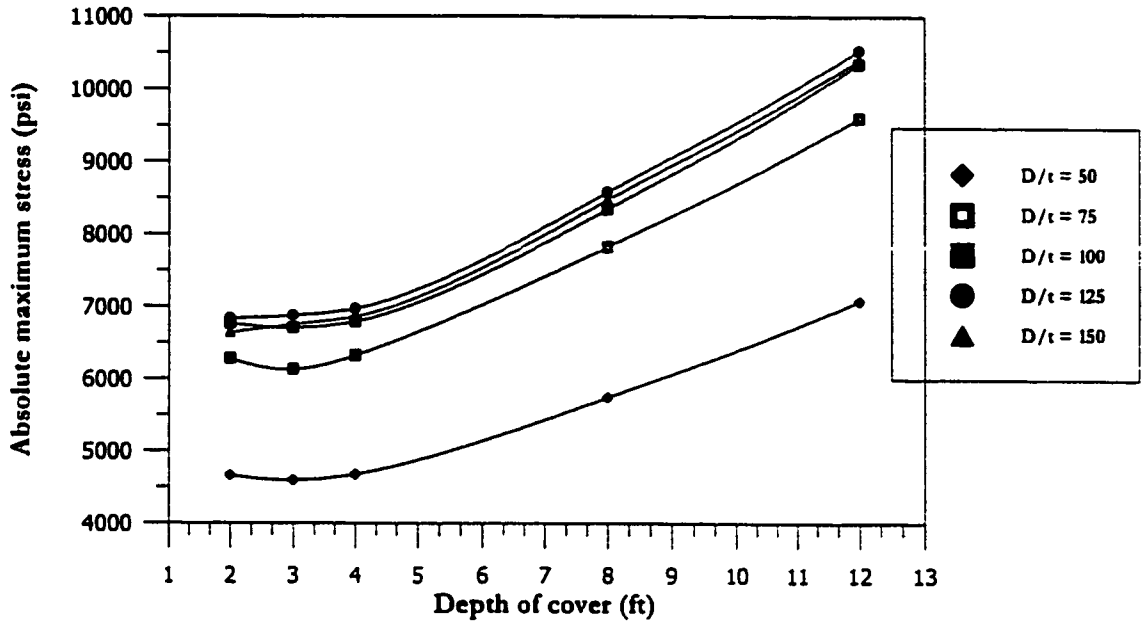

(a) Variation of absolute maximum stress

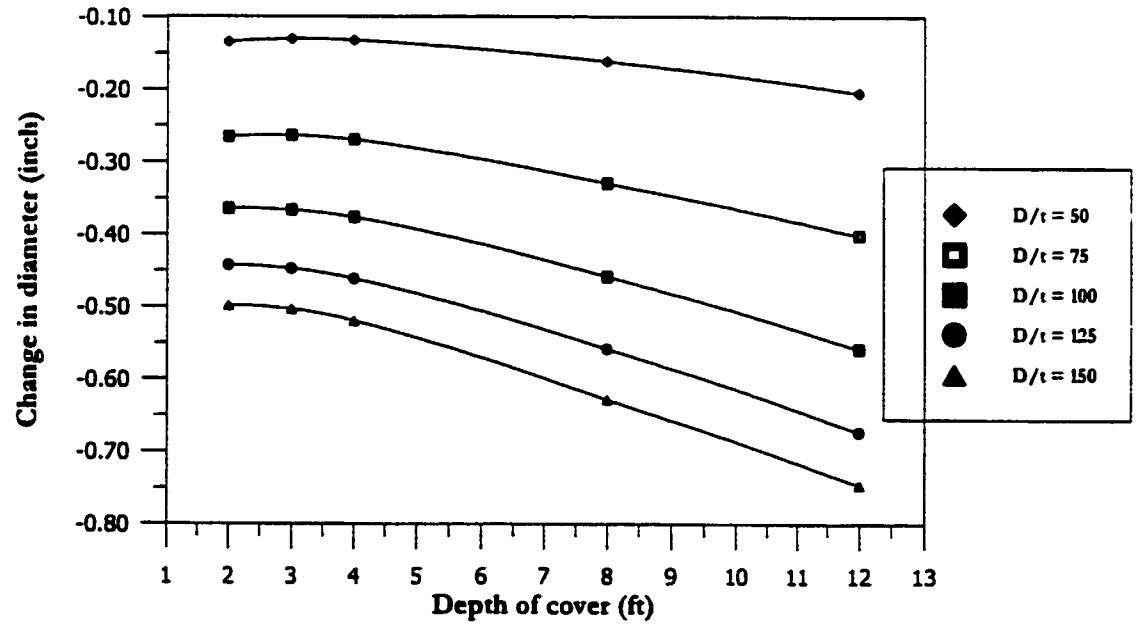

(b) Variation of change in diameter

Fig. 7.68: Variation in absolute maximum stress and diameter change for 60 inches pipe diamter with marl subjected to dead plus live load

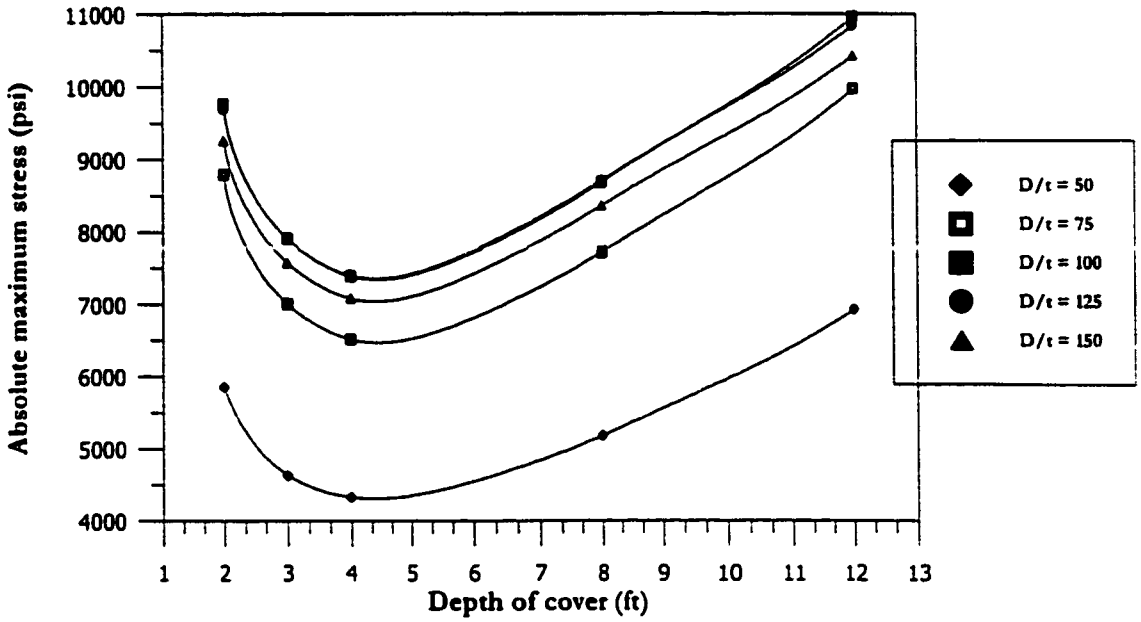

(a) Variation of absolute maximum stress

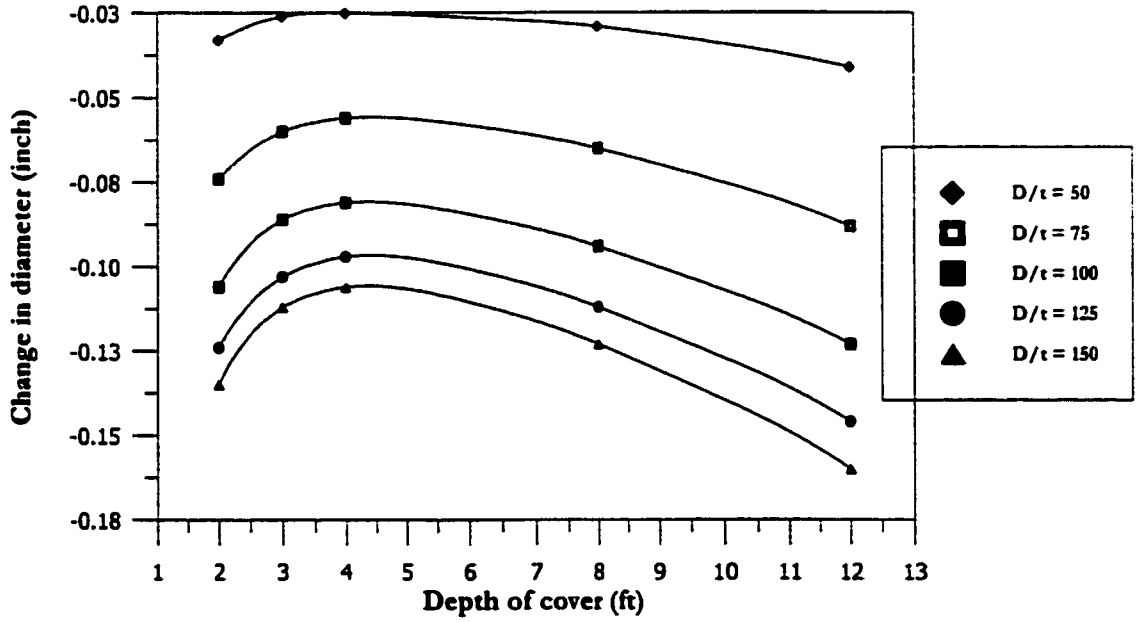

(b) Variation of change in diameter

Fig. 7.69: Variation in absolute maximum stress and diameter change for 12 inches pipe diamter with sabkha subjected to dead plus live load

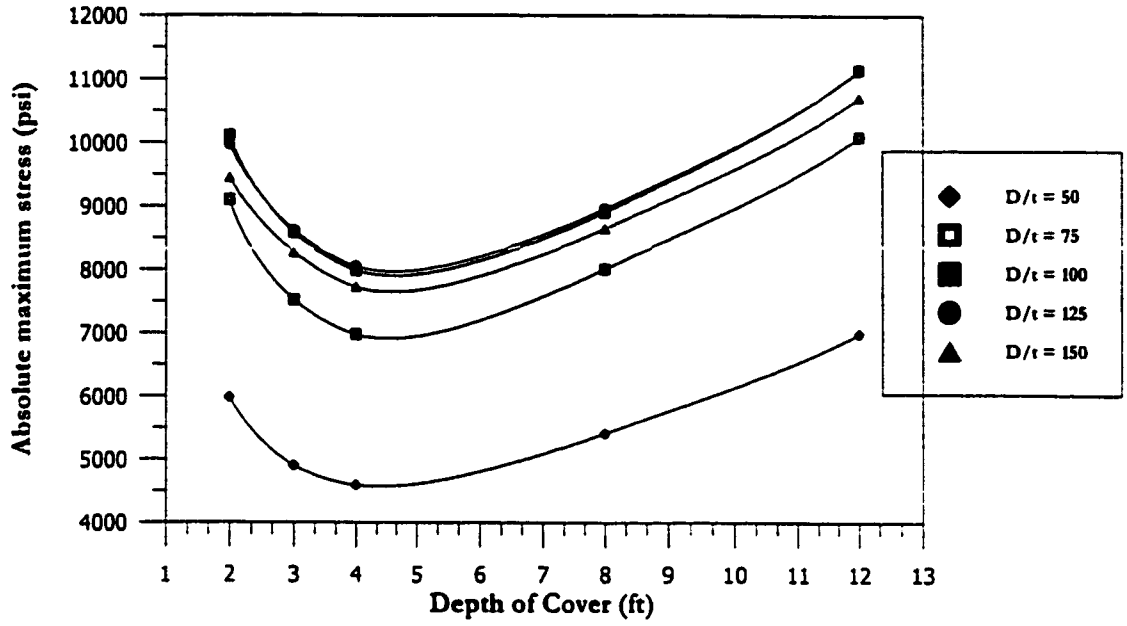

(a) Variation of absolute maximum stress

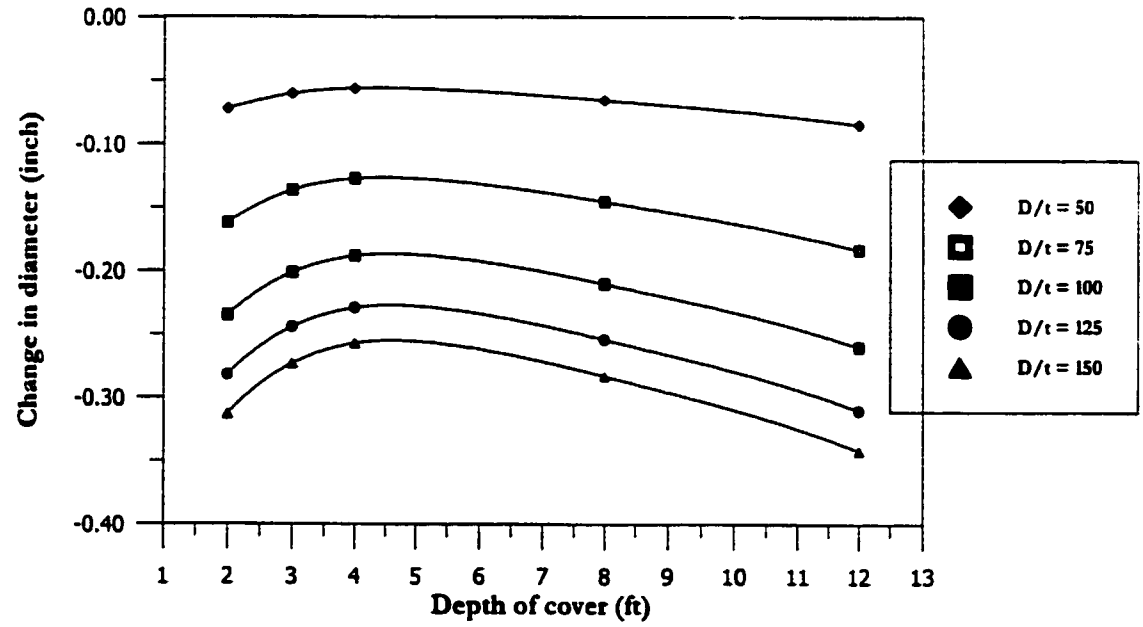

(b) Variation of change in diameter

Fig. 7.70: Variation in absolute maximum stress and diameter change for pipe diamter 24 inches with sabkha subjected to dead plus live load

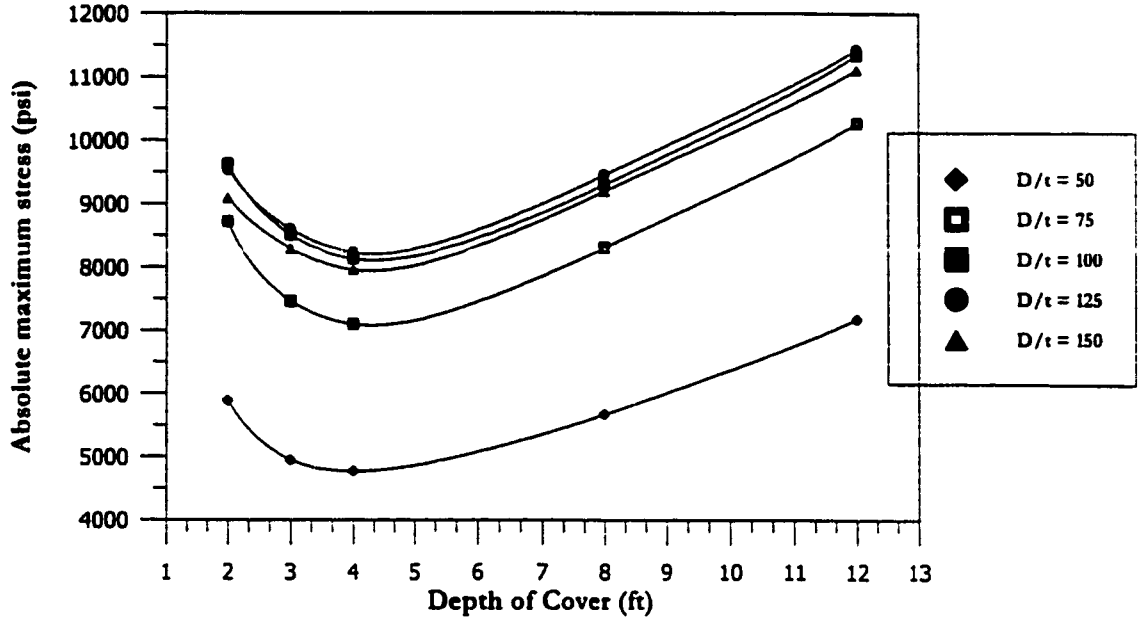

(a) Variation of absolute maximum stress

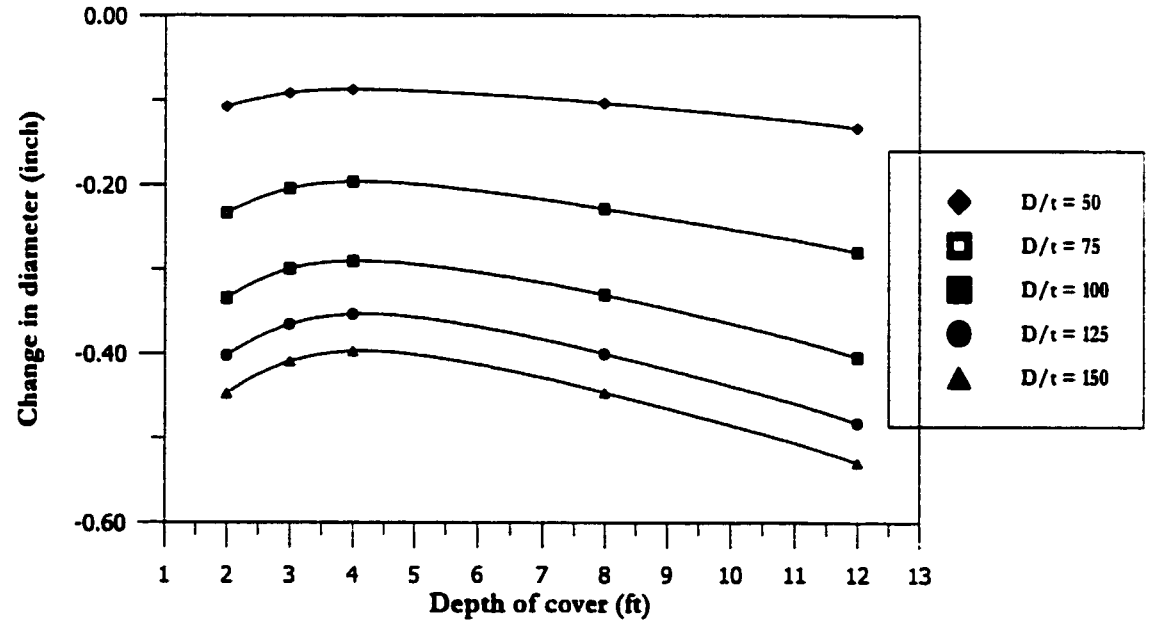

(b) Variation of change in diameter

Fig. 7.71: Variation in absolute maximum stress and diameter change for 36 inches pipe diamter with sabkha subjected to dead plus live load

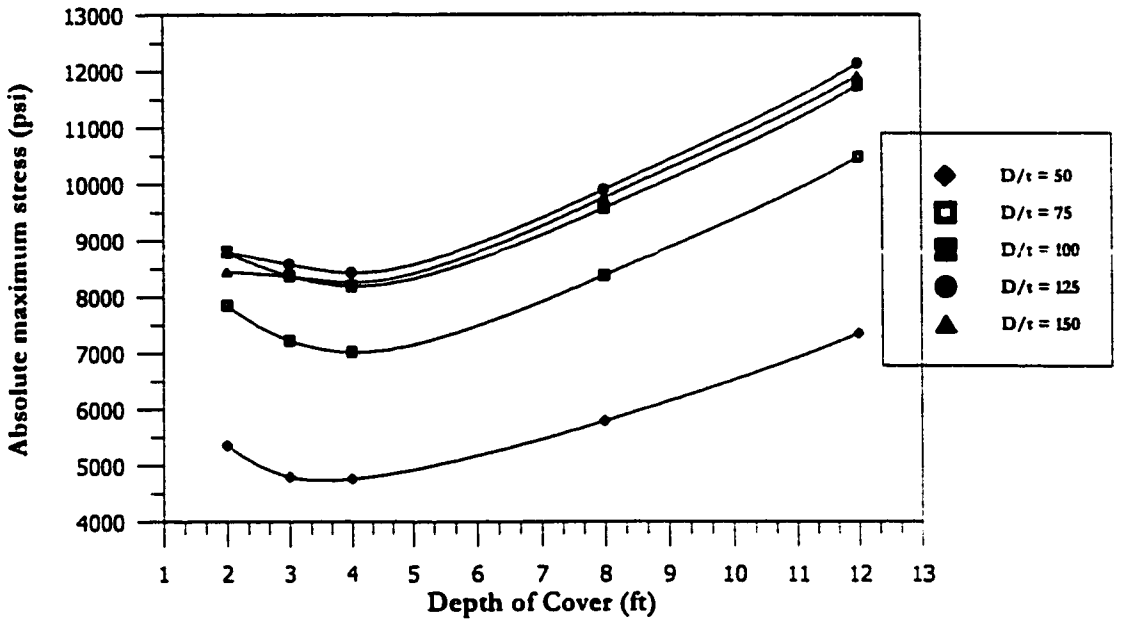

(a) Variation of absolute maximum stress

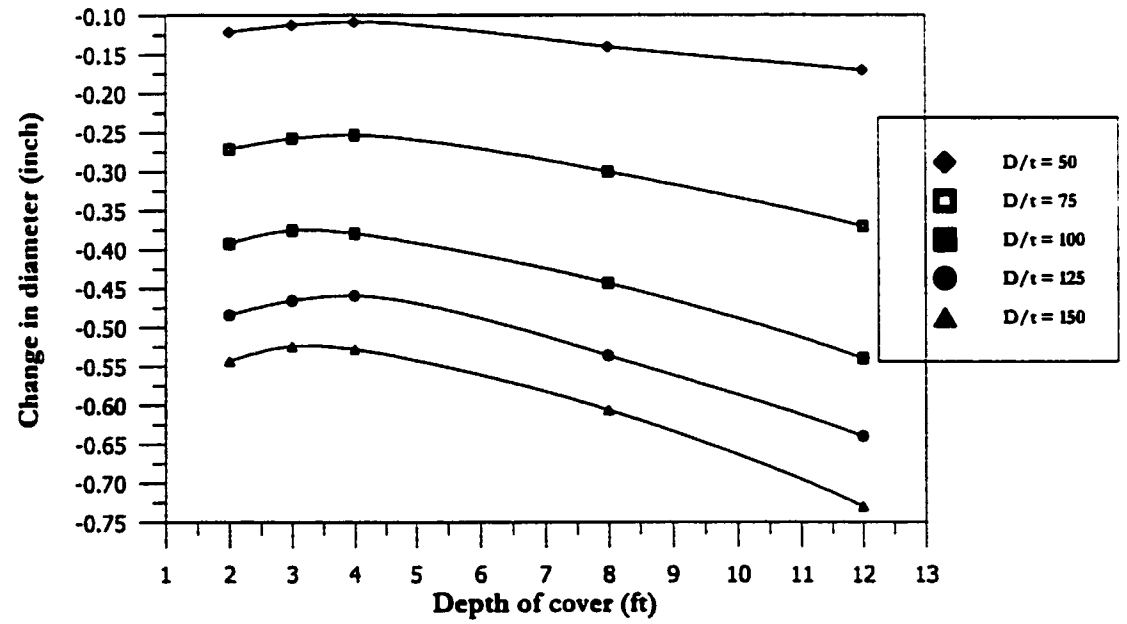

(b) Variation of change in diameter

Fig. 7.72: Variation in absolute maximum stress and diameter change for 48 inches pipe diamter with sabkha subjected to dead plus live load

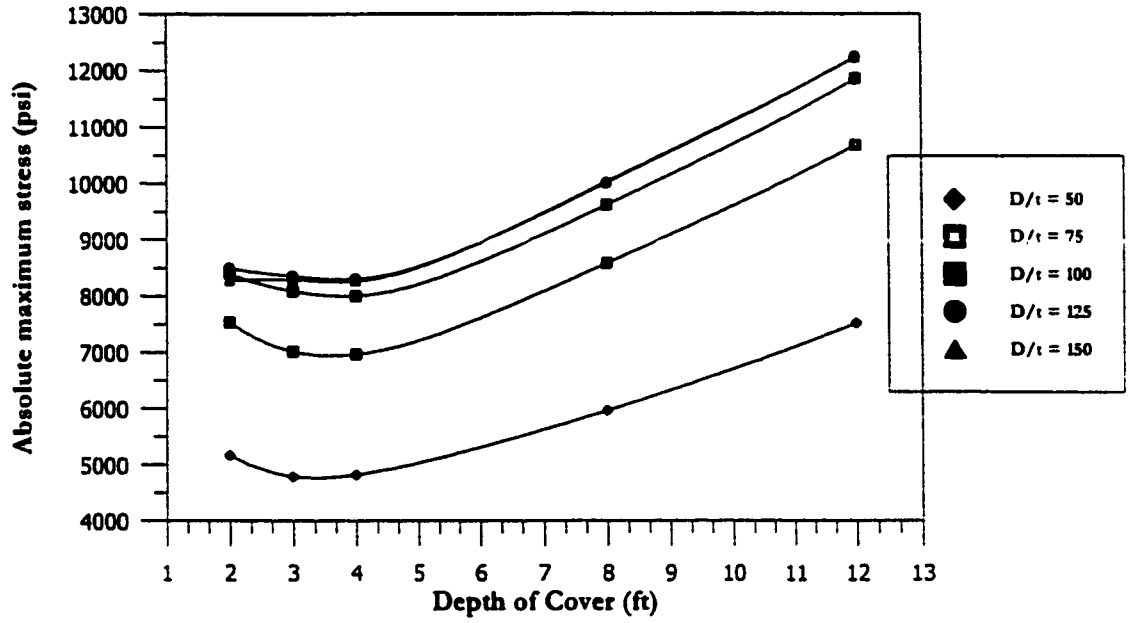

(a) Variation of absolute maximum stress

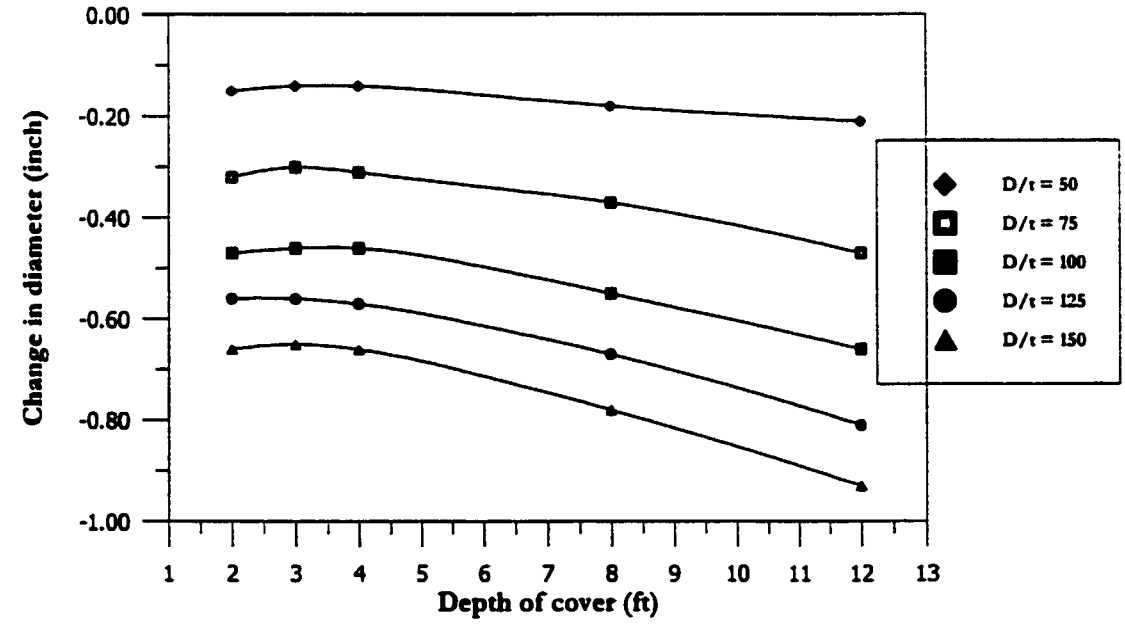

(b) Variation of change in diameter

Fig. 7.73: Variation in absolute maximum stress and diameter change for 60 inches pipe diamter with sabkha subjected to dead plus live load

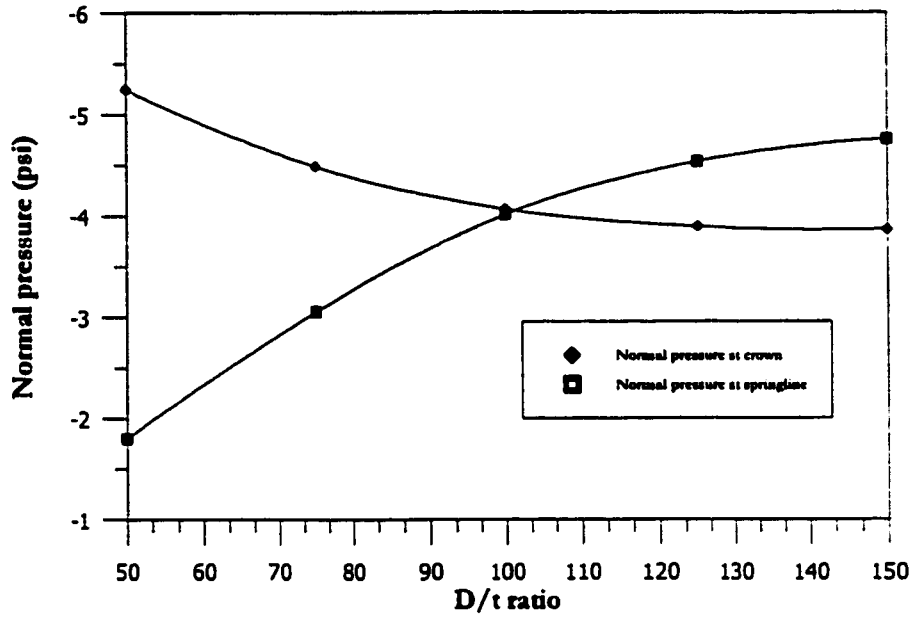

(a) Sand at low density as native soil

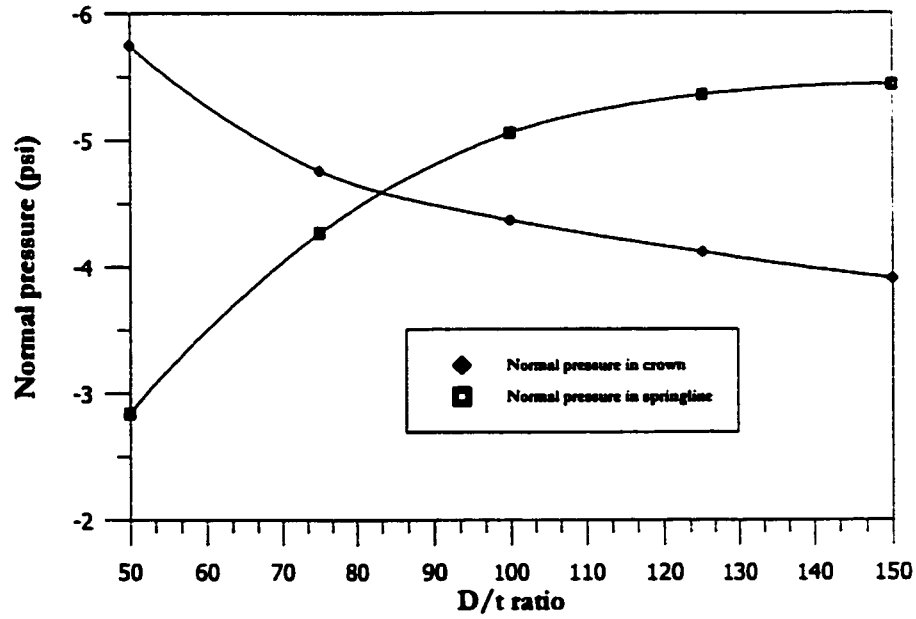

(b) Sand at high density as native soil

Fig. 7.74: Variation of normal pressure at crown and springline for 36 inch pipe diameter with low and high density sand subjected to dead plus live load

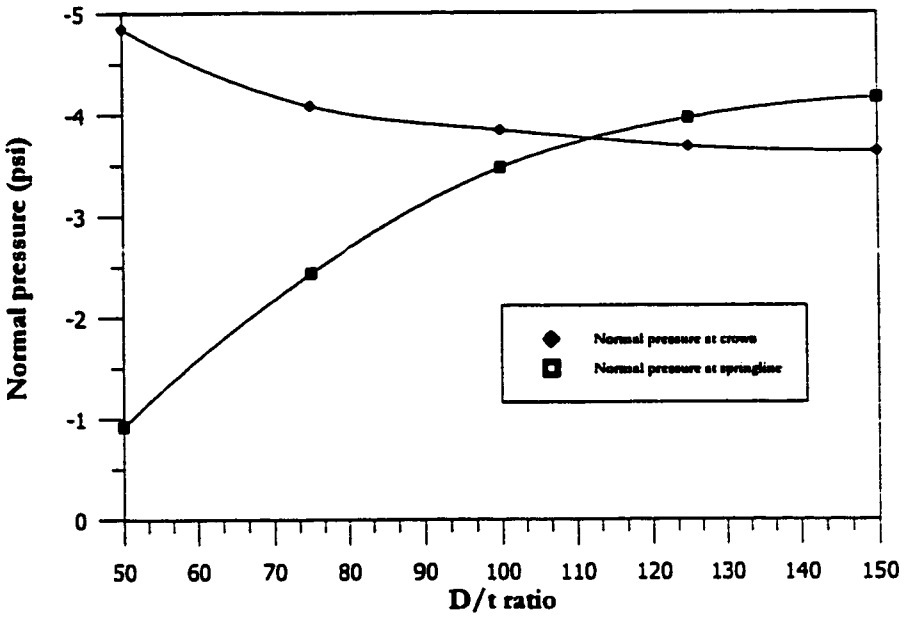

(a) marl as native soil

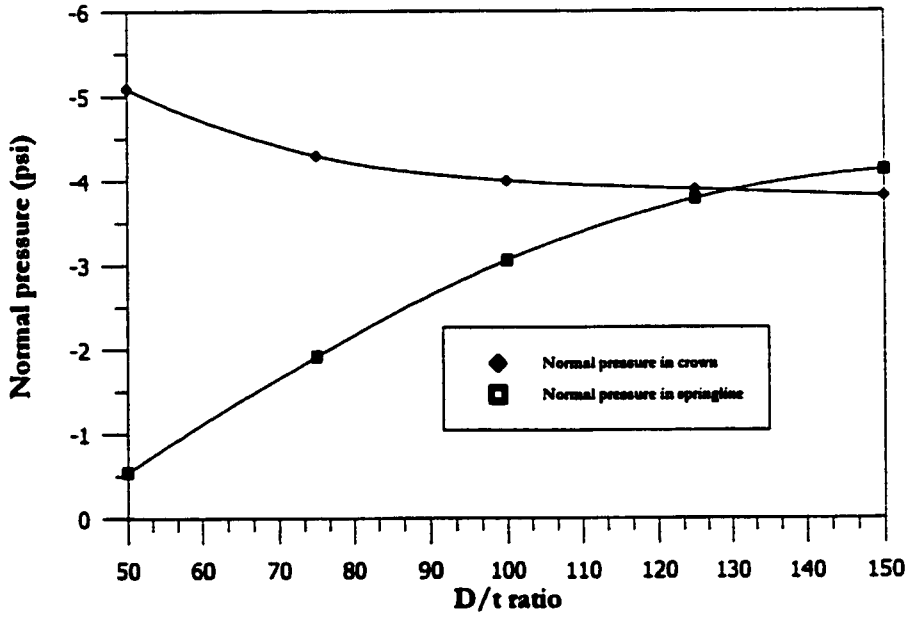

(b) sabkha as native soil

Fig. 7.75: Variation of normal pressure at crown and springline for 36 inch pipe diameter with marl and sabkha subjected to dead plus live load

D/t ratio. Moreover the increase in normal pressure at springline with the increase in the D/t ratio signifies the fact that for pipes of low stiffness the passive resistance is mobilized at the springline and pipe is in the range of flexible behavior.

To get a further insight of the results presented in Figs. 7.54 to 7.73, it was decided to plot stresses due to the live load with the stresses due to the total load. Dead load stresses from the sand overburden problem for the same depths of cover were superimposed. A few of the results are presented in Figs. 7.76 to 7.81. It can be observed that after a certain depth of cover the live load stresses start to dissipate, while the dead load stresses start to dominate. Moreover the dead load stresses form the highway crossing problem and sand overburden problem are quite similar since in highway crossing only 6 inches of soil is replaced by the asphalt concrete layer.

7.9 Calculation of Effective Stresses and Comparison With Existing Design Procedures

In this section the effective stress will be calculated using the methodology recommended by [73] and [34] and presented in Subsection 3.14.5. A comparison of circumferential, longitudinal, and effective stresses calculated using CANDE will be compared with API RP 1102.

7.9.1 Comparison of Circumferential Stresses Due to Live Load

The circumferential stresses due to highway loading predicted by CANDE runs will be compared with circumferential stress calculated by API RP 1102. For the purpose of

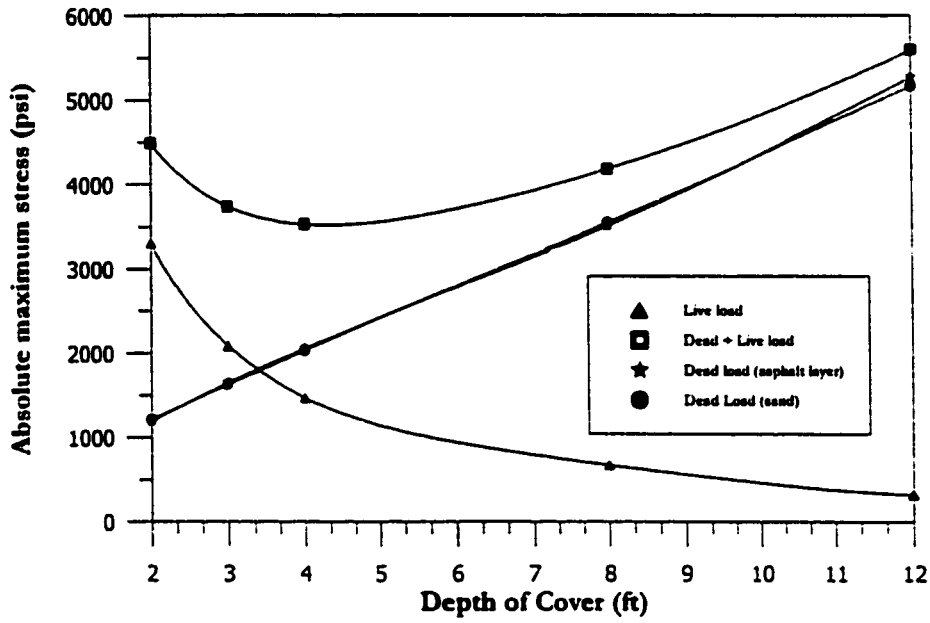

(a) D/t = 50

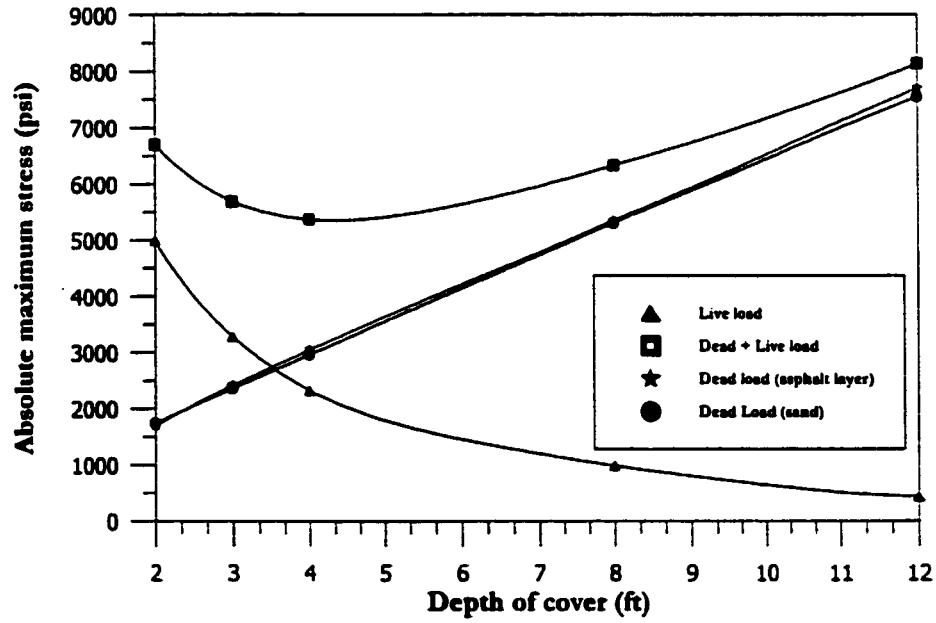

(b) D/t = 75

Fig. 7.76: Combination of stresses for 12 inches pipe diameter and D/t ratios of 50 and 75 with marl as native soil

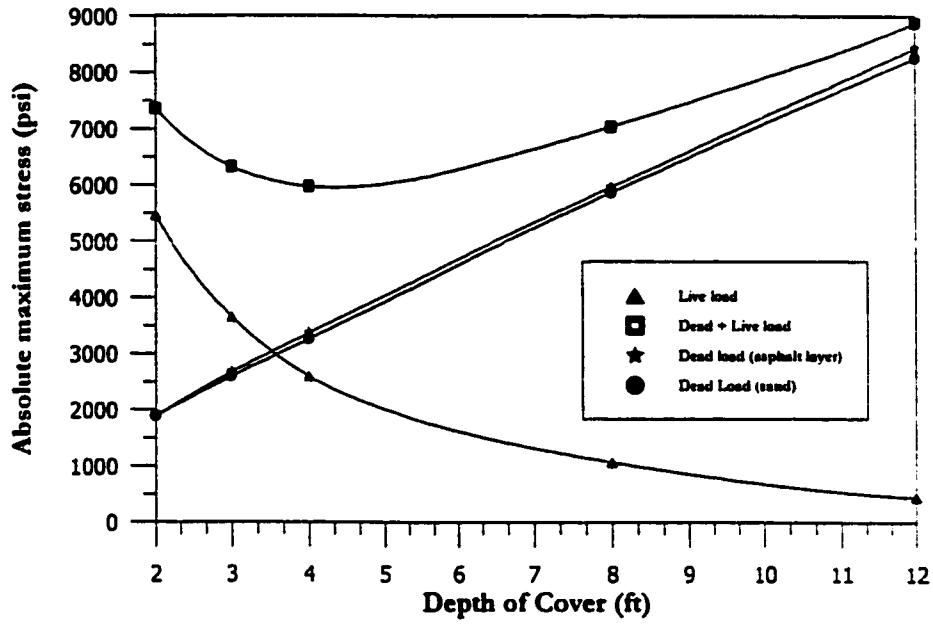

(a) D/t = 100

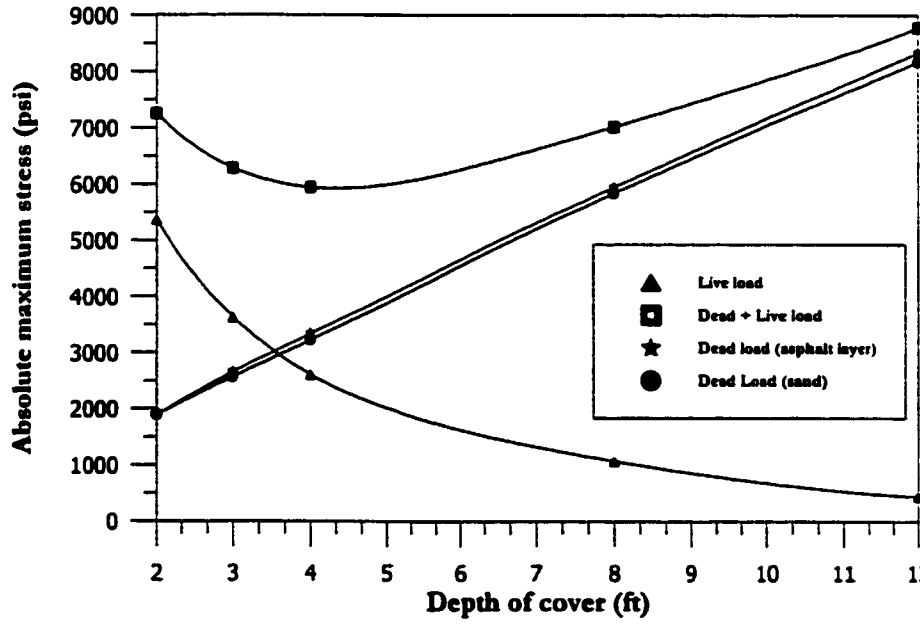

(b) D/t = 125

Fig. 7.77: Combination of stresses for 12 inches pipe diameter and D/t ratios of 100 and 125 with marl as native soil

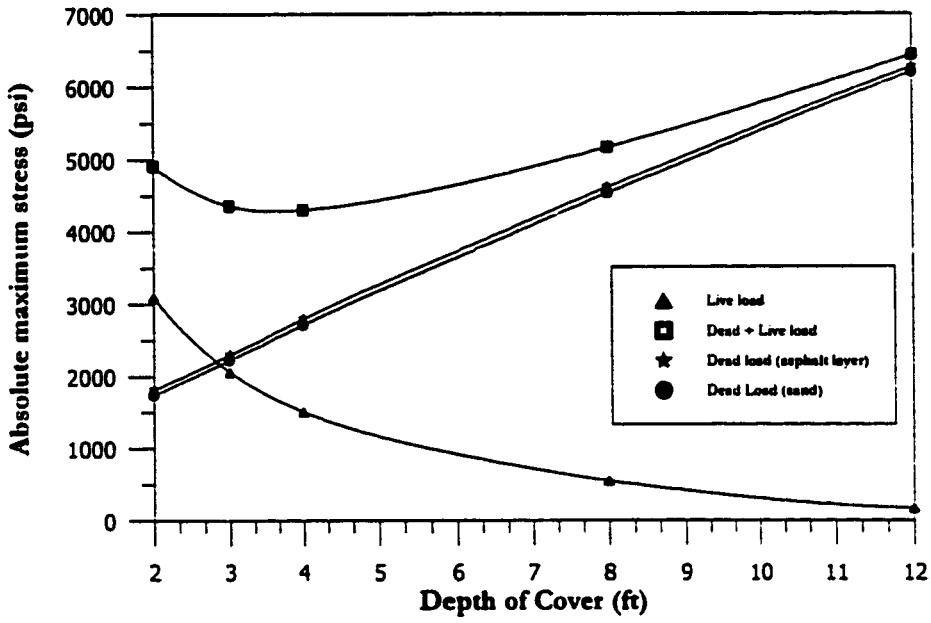

(a) D/t = 50

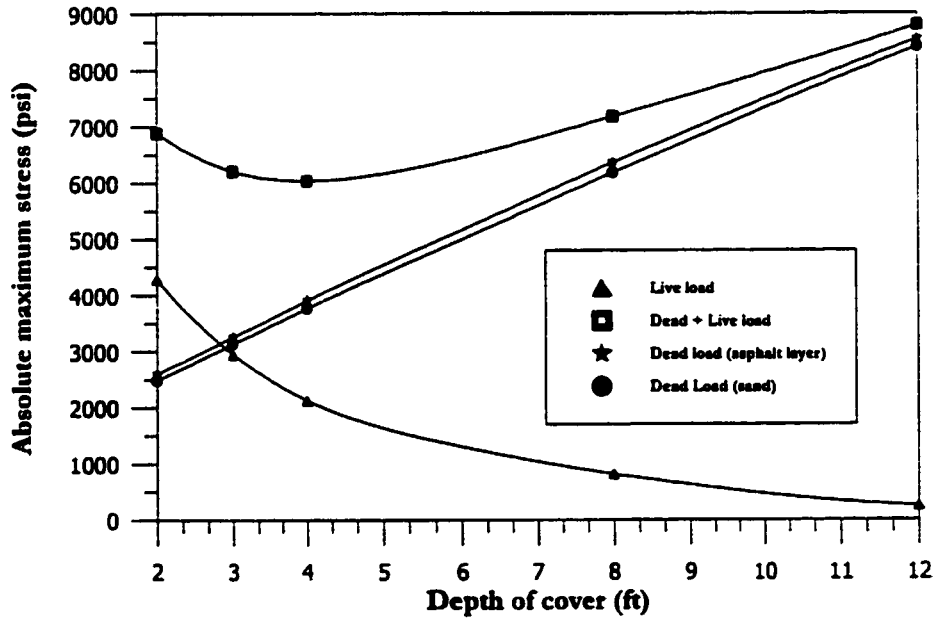

(b) D/t = 75

Fig. 7.78: Combination of stresses for 36 inches pipe diameter and D/t ratios of 50 and 75 with marl as native soil

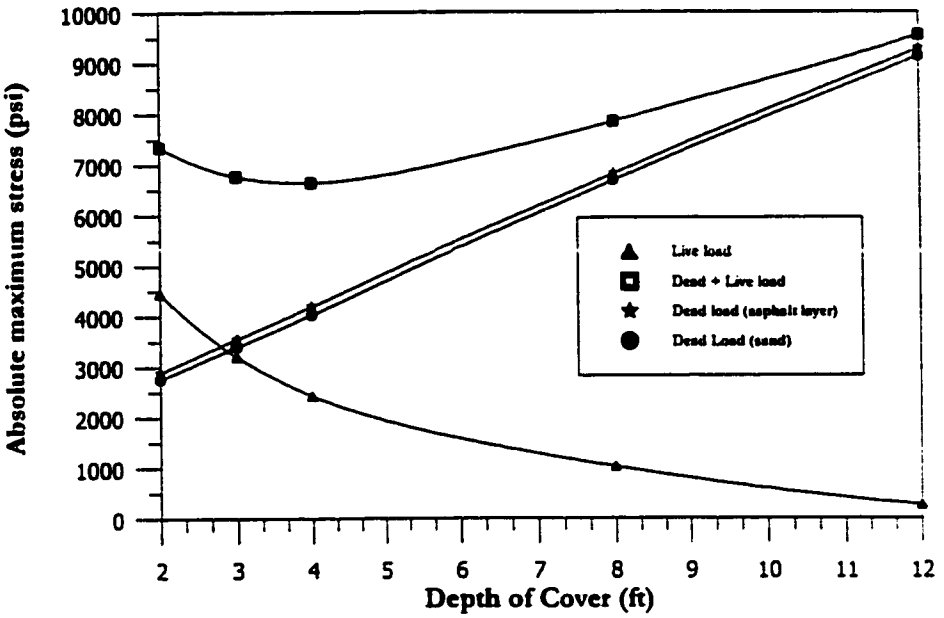

(a) D/t = 100

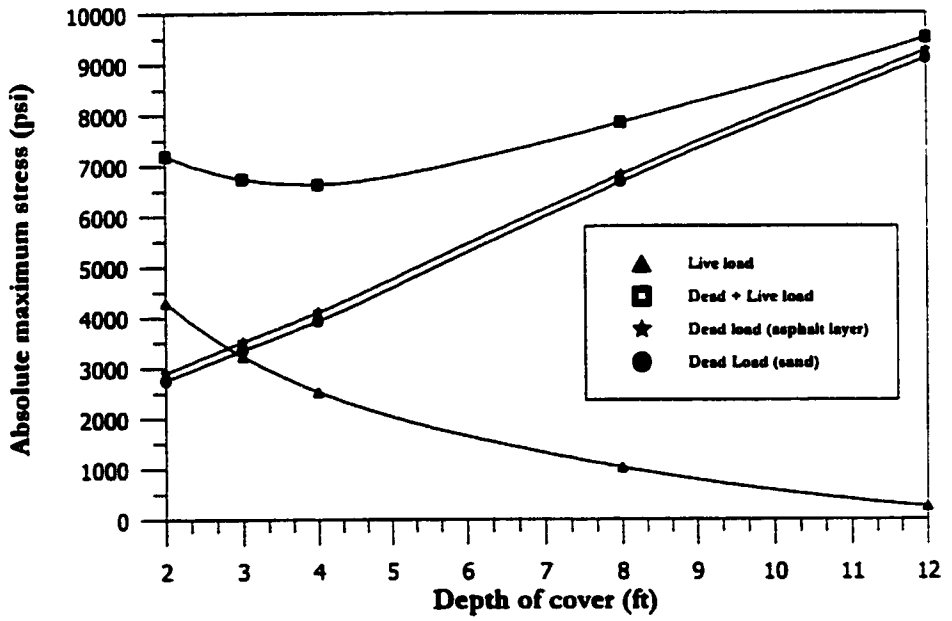

(b) D/t = 125

Fig. 7.79: Combination of stresses for 36 inches pipe diameter and D/t ratios of 100 and 125 with marl as native soil

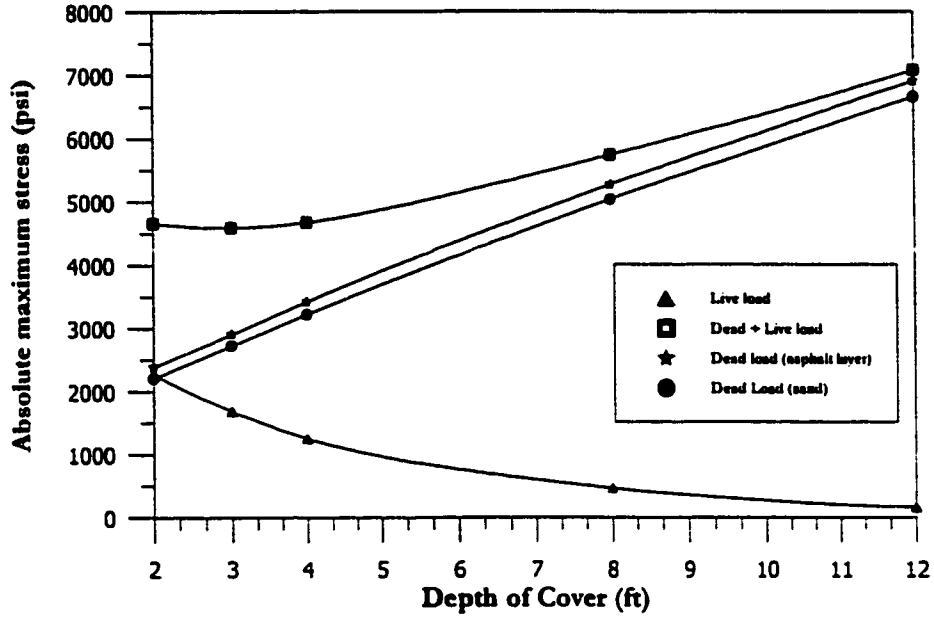

(a) D/t = 50

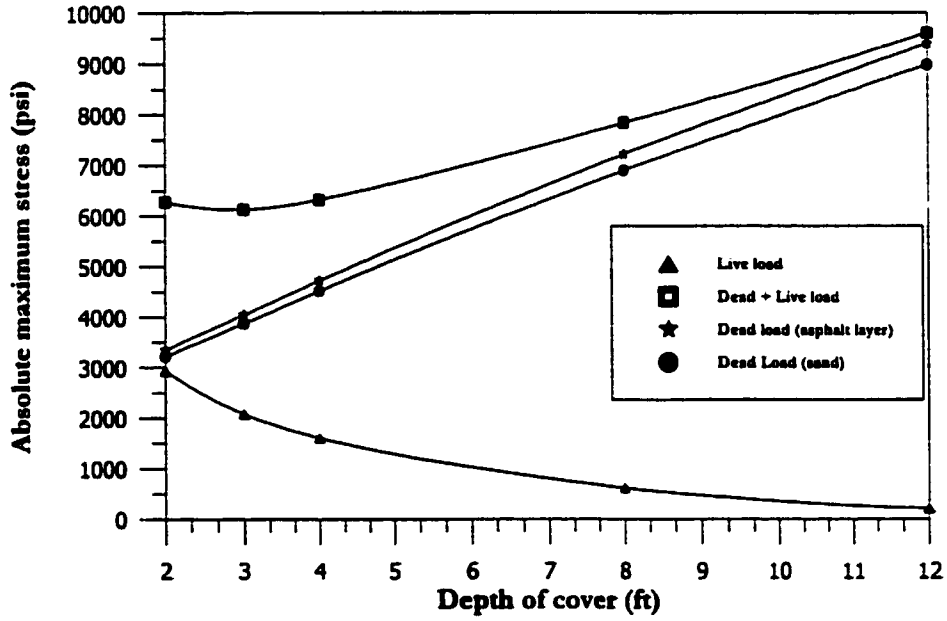

(b) D/t = 75

Fig. 7.80: Combination of stresses for 60 inches pipe diameter and D/t ratios of 50 and 75 with marl as native soil

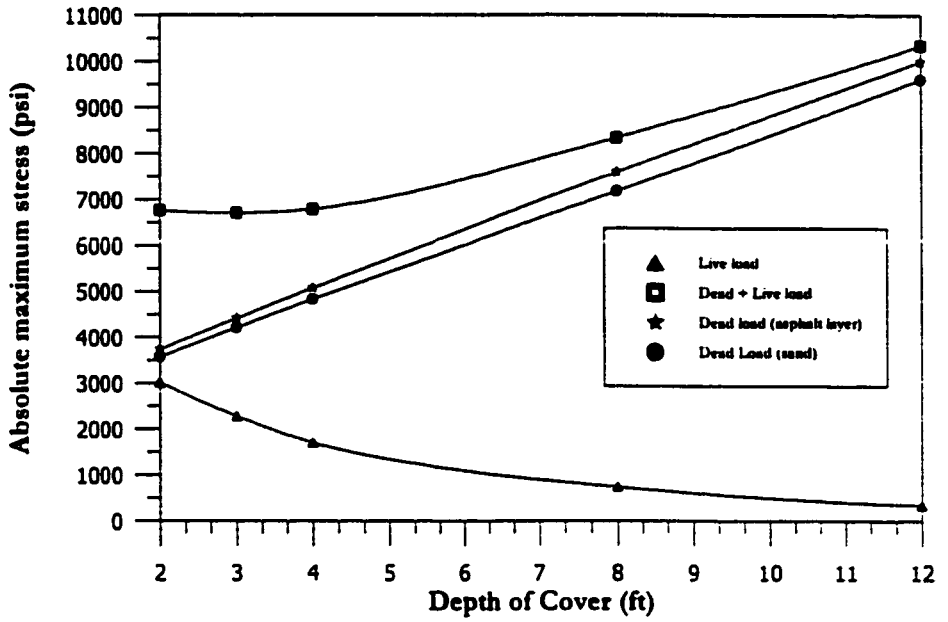

(a) D/t = 100

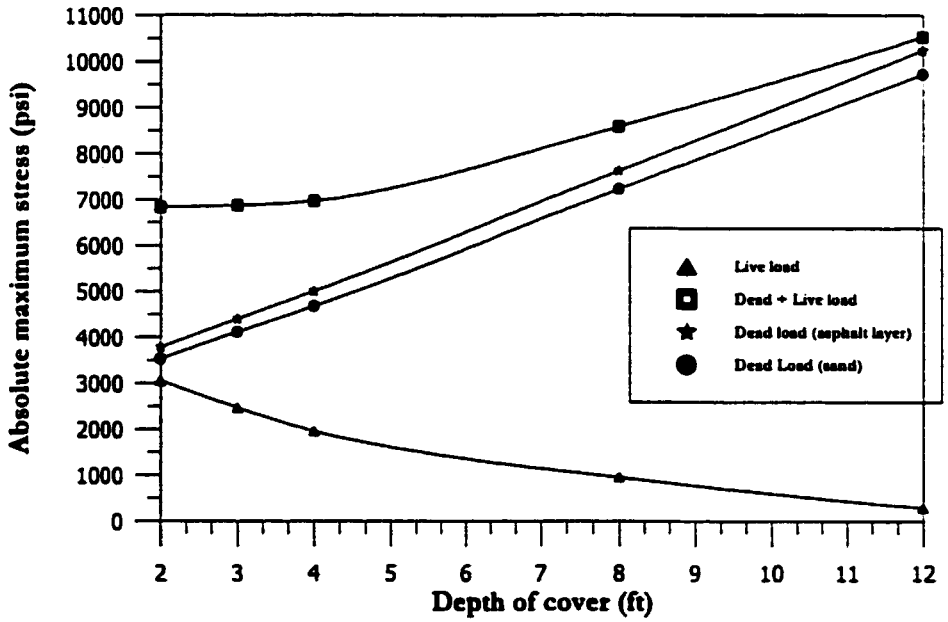

(b) D/t = 125

Fig. 7.81: Combination of stresses for 60 inches pipe diameter and D/t ratios of 100 and 125 with marl as native soil

comparison the diameters of 12, 24, and 36 inches were selected. Larger diameters of 48, and 60 inches can not be compared because in the API RP 1102 the pipe diameter is limited to maximum value of 42 inch. Also, for similar reasons D/t ratios are limited to 50, 75 and 100. The four depths of cover for highway crossing used in the comparison are 3, 4, 6, and 8 feet. However it was noted that API RP 1102 makes no distinction between the live load circumferential stresses for depths of cover of 3 and 4 feet.

Since the CANDE simulations are made with a pavement layer and a single axle loading so the pavement type factor (R), and axle type factor (L) is taken as 1.0 . The loading pressure w for the API RP 1102 is taken as 100 psi, which is the same value used in CANDE. The values of highway stiffness factor for cyclic circumferential stress (F_{Hh}) and highway geometry factor.(G_{Hh}) for cyclic circumferential stress are given in Tables 7.13 and 7.14. The values reported in Tables 7.13 and 7.14 were generated from the computer software PC-PISCESL.

A comparison is made between API RP 1102 and CANDE by changing the values of soil resilient modulus for API RP 1102 and comparing it with same values used in CANDE. Although the results for different soil resilient modulus for API RP 1102 were compared with four native soils identified earlier however the comparison for high density sand is only presented here. The results are shown in Figs. 7.82 to 7.87.

The comparison of results from CANDE simulations and API RP 1102 show a consistent pattern. The following important observations can be made.

1. The API RP 1102 predicts the same live load stress for depths of cover 3 and 4 feet as the value of G_{Hh} is same for depths of cover 3 and 4 feet as shown in Table 7.14.

TABLE 7.13: Highway stiffness factor (K_{Hh}) for cyclic circumferential stress

K_{Hh}			
H ft	D 12 inch	D 24 inch	D 36 inch
3	1.25	1.1	1.02
4	1.25	1.1	1.02
6	1.0	0.86	0.75
8	0.82	0.71	0.62

TABLE 7.14: Highway geometric factor (G_{Hh}) for cyclic circumferential stress

G_{Hh}			
D/t	E_r 5 ksi	E_r 10 ksi	E_r 20 ksi
50	19.1	14.2	9.7
75	20.5	14.5	8.7
100	18.8	12.4	6.8

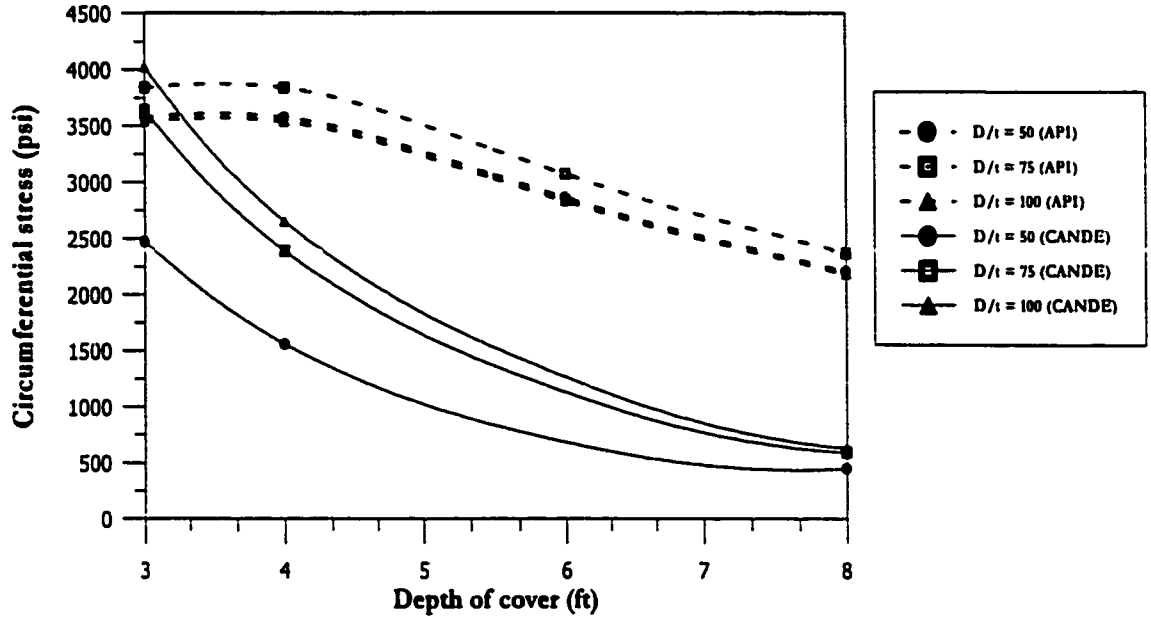

(a) Resilient modulus 5 ksi

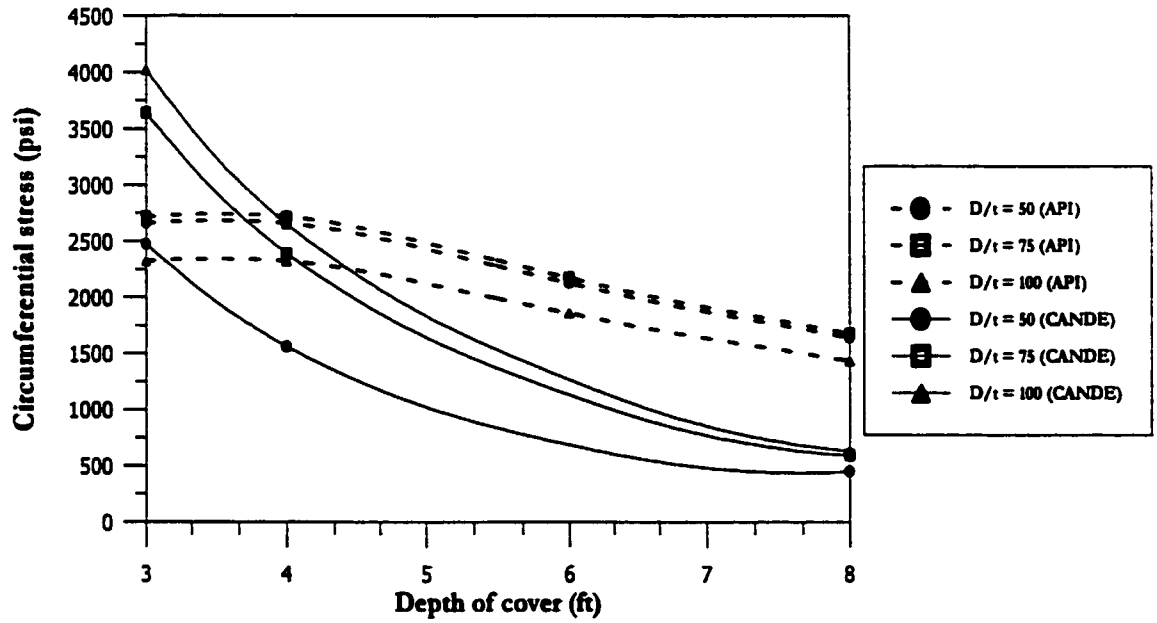

(b) Resilient modulus 10 ksi

Fig. 7.82: Comparison of circumferential stress due to live load for 12-inch diameter pipe with resilient modulus values of 5 and 10 ksi

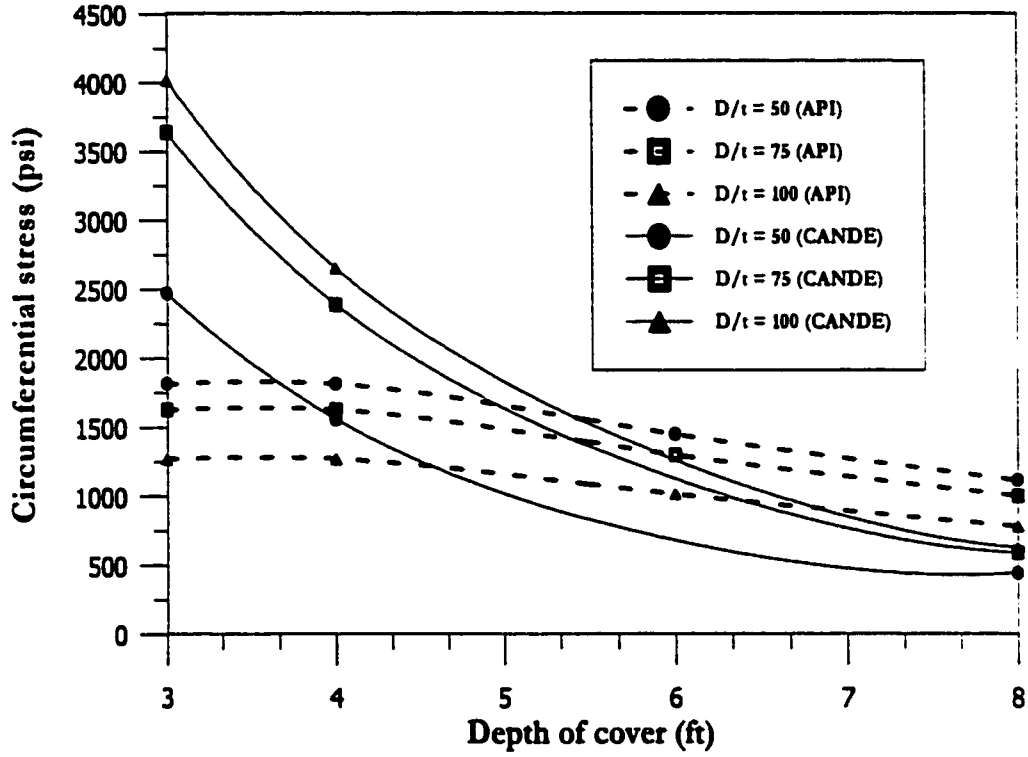

Fig. 7.83: Comparison of circumferential stress due to live load for 12-inch diameter pipe with resilient modulus value of 20 ksi

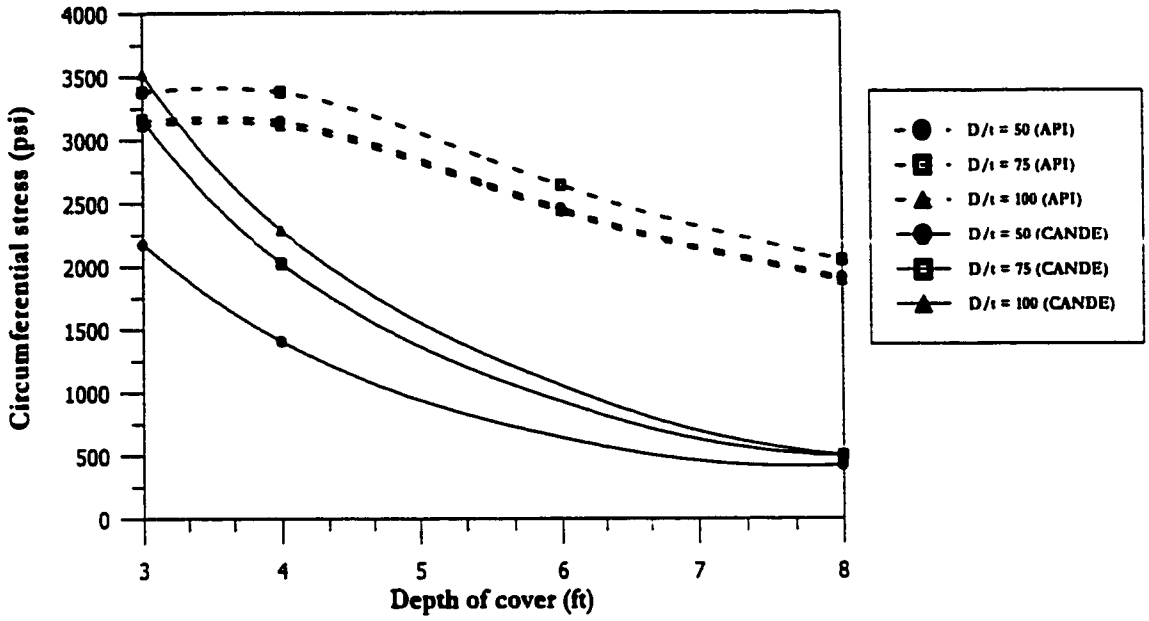

(a) Resilient modulus 5 ksi

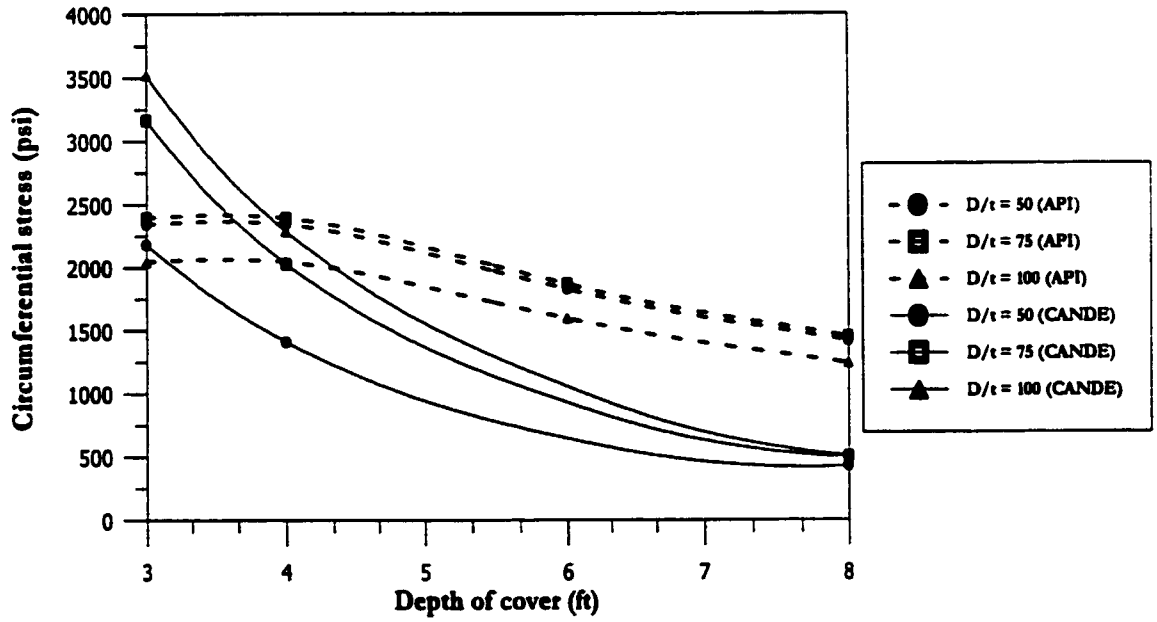

(b) Resilient modulus 10 ksi

Fig. 7.84: Comparison of circumferential stress due to live load for 24-inch diameter pipe with resilient modulus values of 5 and 10 ksi

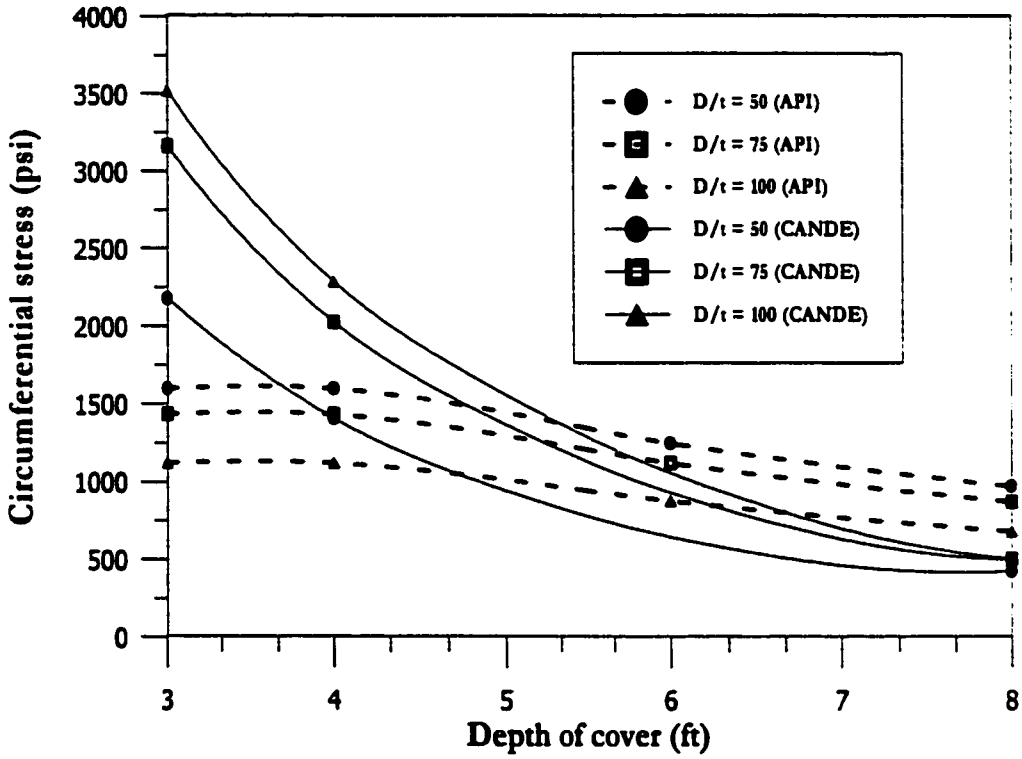

Fig. 7.85: Comparison of circumferential stress due to live load for 24-inch diameter pipe with resilient modulus value of 20 ksi

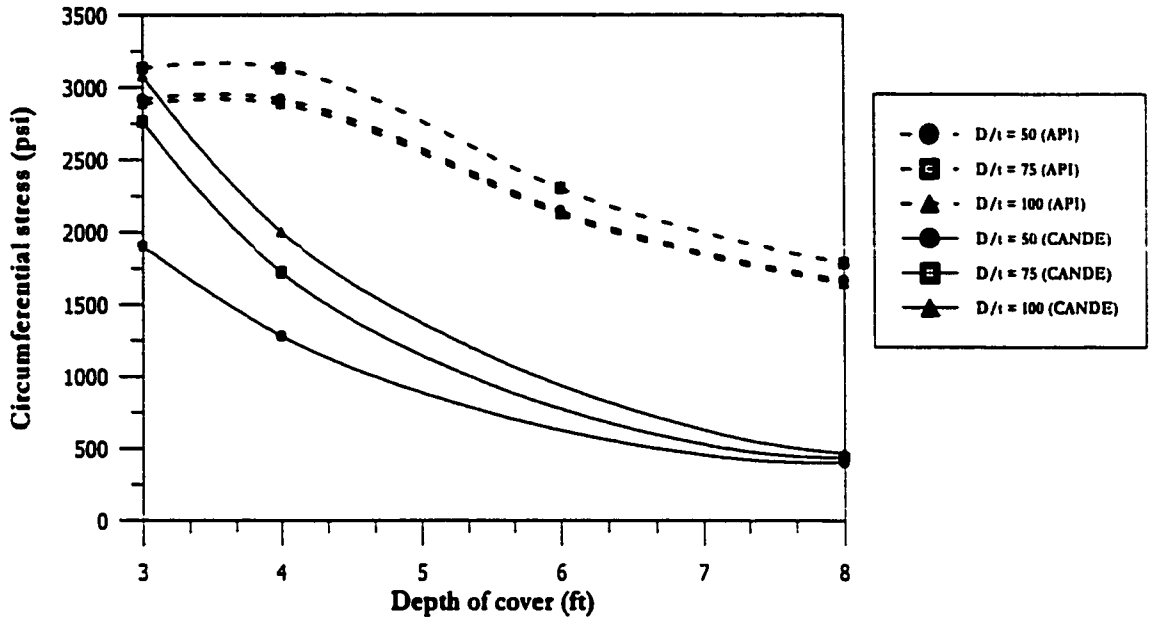

(a) Resilient modulus 5 ksi

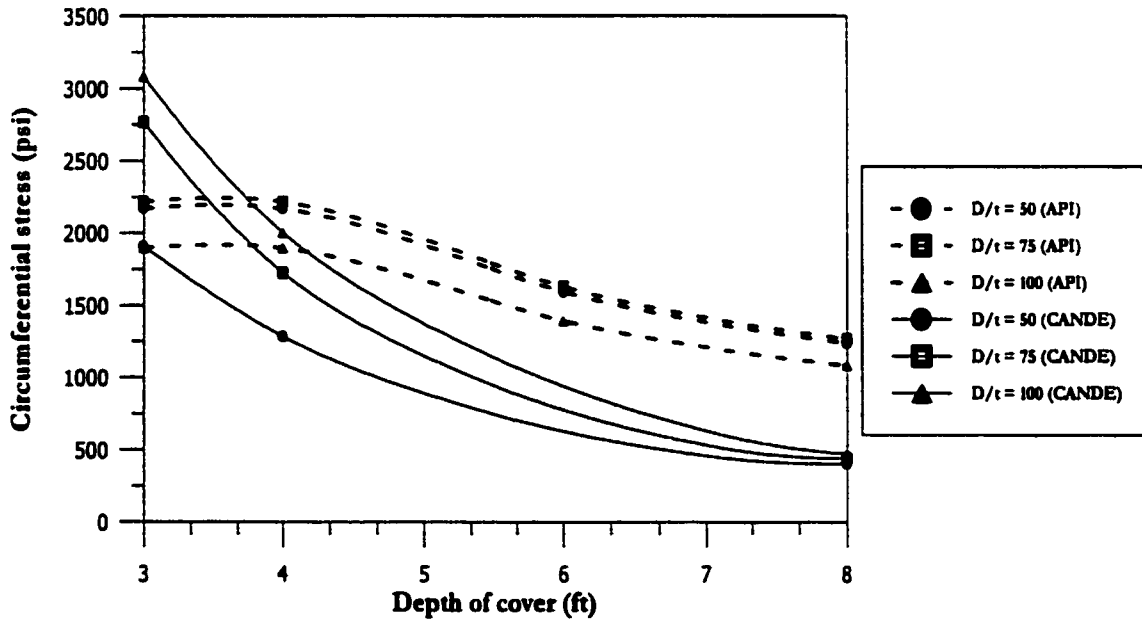

(b) Resilient modulus 10 ksi

Fig. 7.86: Comparison of circumferential stress due to live load for 36-inch diameter pipe with resilient modulus values of 5 and 10 ksi

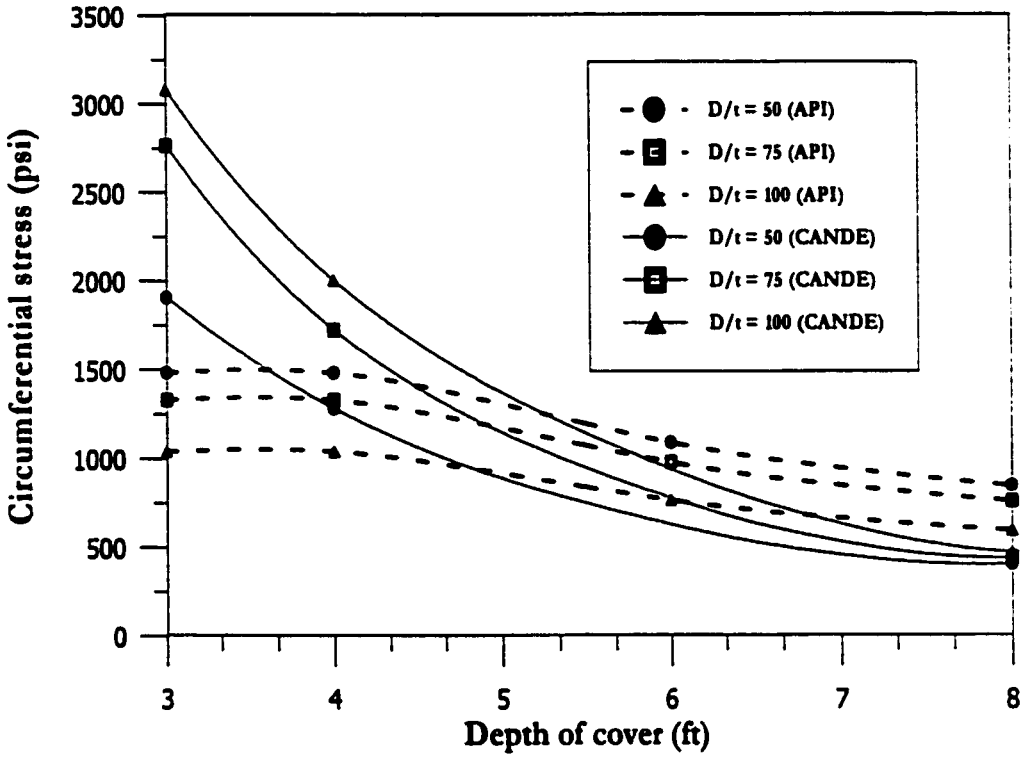

Fig. 7.87: Comparison of circumferential stress due to live load for 36-inch diameter pipe with resilient modulus values of 20 ksi

2. The results from CANDE simulations are less conservative for 4 feet depth of cover and resilient modulus of 5 ksi for all D/t ratios. However if the resilient modulus in API RP 1102 is taken as 10 ksi the CANDE results are less conservative for D/t ratios of 50 and 75 and are almost equal or slightly more conservative than API RP 1102. The use of resilient modulus 20 ksi in API RP 1102 procedure always result in results which are less conservative than CANDE. The reasons for this is that the API recommended practice is developed from finite element simulations in which soil resilient modulus was the only soil material property used [73]. The use of high values of 10 and 20 ksi modulus of resilience in API RP 1102 is based on auger bored pipelines in which the soil has become stiff due to repeated traffic loads. On the other hand in CANDE simulations a trench type of installation is used with a loose soil in the trench. A few representative modulus plots of these simulations in Figs. 7.88 and 7.89 indicate that soil modulus for CANDE simulations is far less than the resilient modulus of 5, 10, and 20 ksi.
3. Another important observation from the above comparison is that API recommended practice predicts less stresses for small D/t ratios as opposed to CANDE simulations. This is because in CANDE simulations a loose soil is used inside the trench so the arching effect and mobilization of passive resistance at springline comes into the picture for D/t ratios of 125 and 150, which are not compared here because API recommended practice is not capable of modeling D/t ratios of 125 and 150. A plot of live load stress vs D/t ratio for 24 inch diameter pipe is shown in Fig. 7.90 It can be observed that for low density sand the arching is effective at D/t ratios of 125 and 150 while for high density sand the arching is also significant at D/t ratios of 75 and 100.

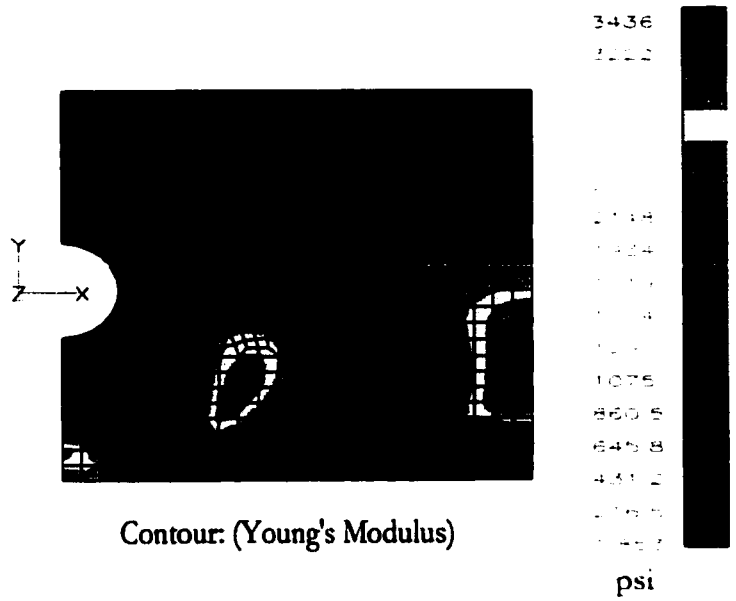

(a) Low density sand as native material

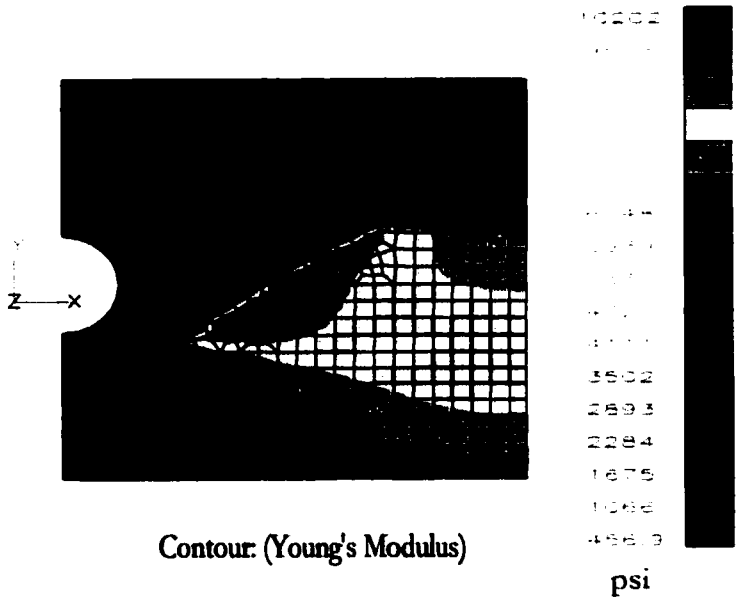

(b) High density sand as native material

Fig. 7.88: Contours of modulus of elasticity for low and high density sand as native soil

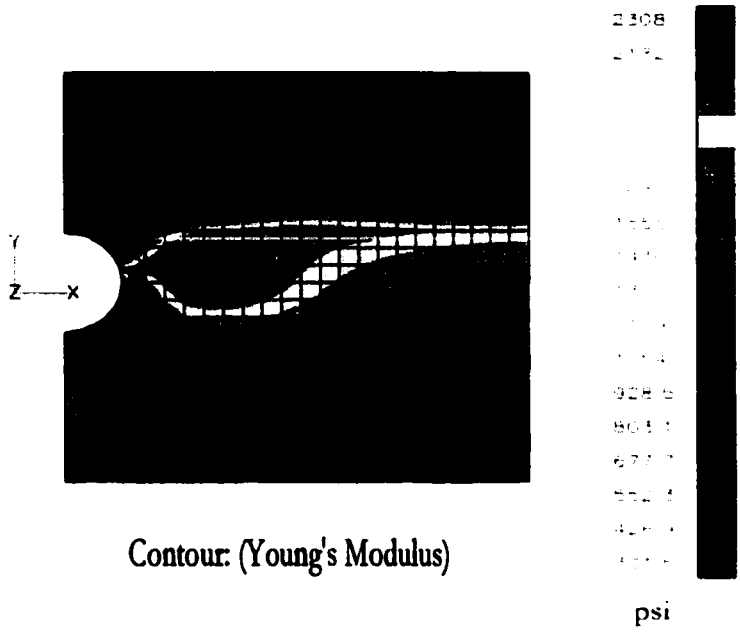

(a) Marl as native material

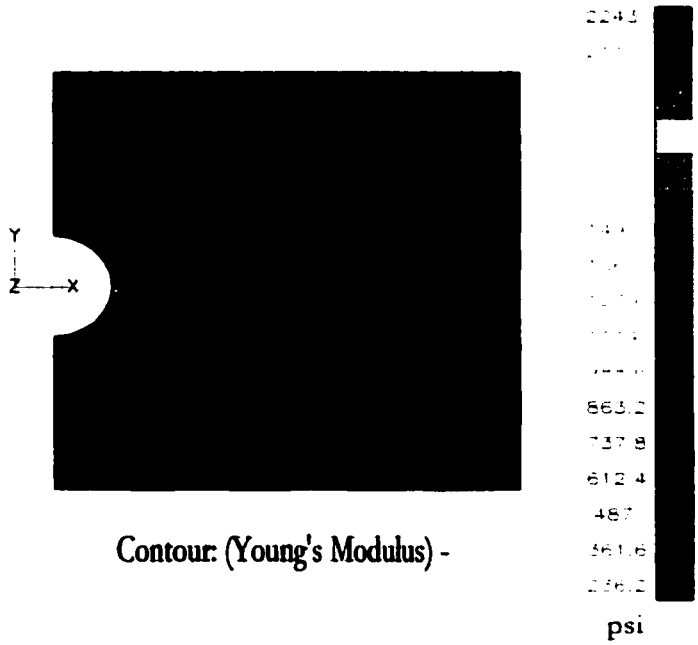

(a) Sabkha as native material

Fig. 7.89: Contours of modulus of elasticity for marl and sabkha as native soil

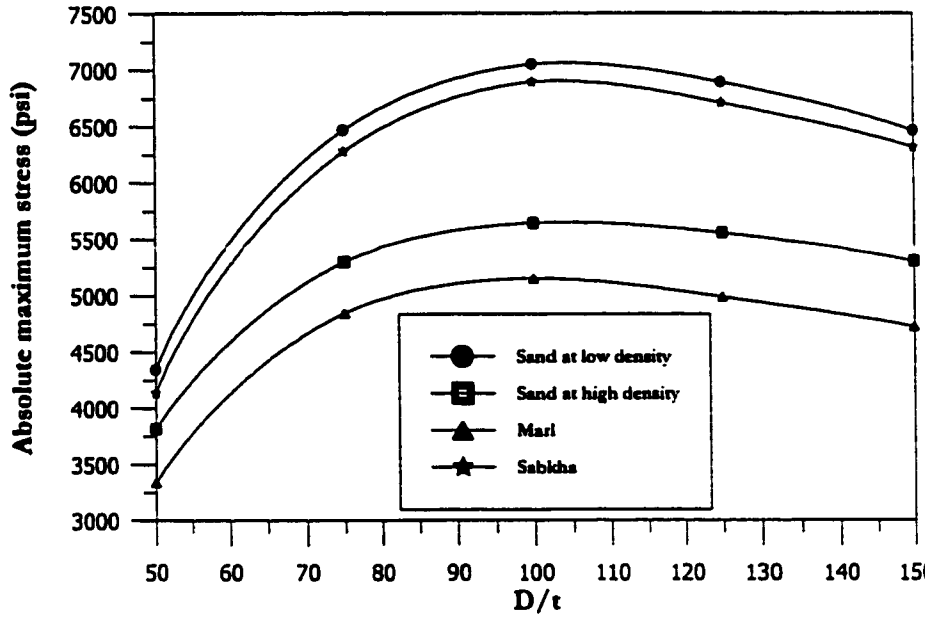

(a) Sand at low density as trench fill and overfill material

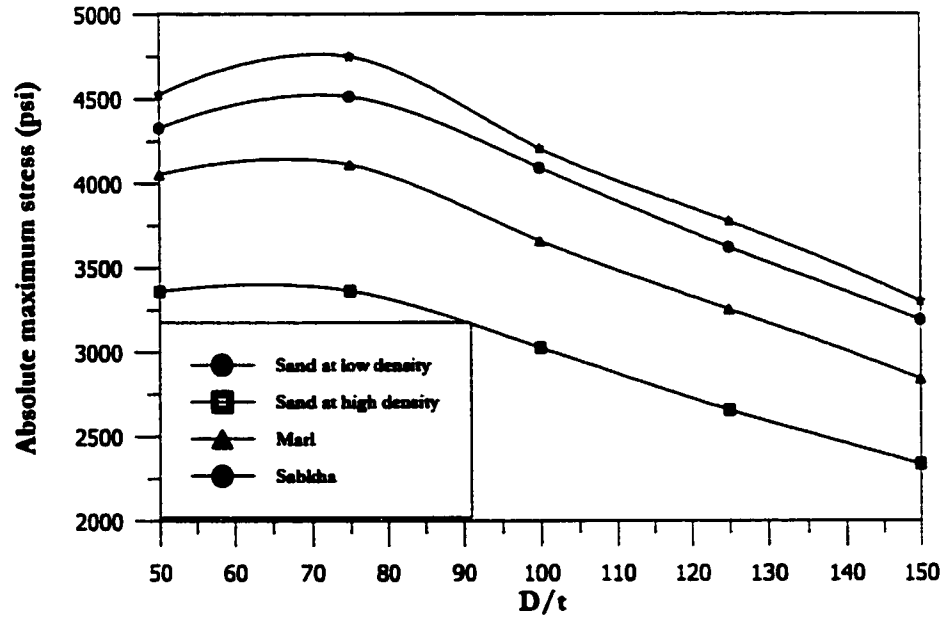

(b) Sand at high density as trench fill and overfill material

Fig. 7.90: Live load circumferential stresses for 24 inch diameter pipe and 2 feet depth of cover using low and high density sand as trench and overfill materials

7.9.2 Comparison of Total Circumferential Stresses

In this section a comparison is made between total circumferential stresses predicted by CANDE and those predicted by API RP 1102. The total circumferential stresses are represented by S_1 in API RP 1102 as defined in Subsection 3.14.5. For calculation of dead load circumferential stresses by API RP 1102 the modulus of soil reaction was taken as 0.5 ksi because it is recommended by API for most of the soils. The live load circumferential stresses for API RP 1102 are calculated for soil resilient modulus values of 5, 10 and 20 ksi. As before, pipe diameters of 12, 24, and 36 with D/t ratios of 50, 75, and. 100 were compared. The values of required parameters to predict dead plus live stresses from API RP 1102 are given in Tables 7.15 to 7.18. Stresses due to an internal pressure of 500 psi are calculated using modified Barlow formula mentioned in Subsection 3.14.4. The results from CANDE and API RP 1102 are compared in Figs. 7.91 to 7.96. The following observations can be made from the results presented.

1. CANDE results are always less conservative than the API RP 1102 except for pipe diameter 12 inches and soil resilient modulus of 20 ksi.
2. At larger depths of cover the difference between CANDE results and API results is more than at small depths of cover.
3. The variation in CANDE and API results is always more at large D/t ratios.
4. The variation in CANDE and API results is always more for larger pipe diameters than the smaller diameters.

TABLE 7.15: Values of Burial factor used in calculation of dead load stresses from API RP 1102

H/D	B_c
1.0	0.38
1.5	0.57
2.0	0.66
2.5	0.77
3.0	0.86
3.5	0.93
4.0	1
4.5	1.06
5.0	1.10
5.5	1.14
6.0	1.18
6.5	1.20
7.0	1.23
7.5	1.25
8.0	1.27
8.5	1.28
9.0	1.29
9.5	1.31
10.0	1.31
10.5	1.33
11.0	1.33
11.5	1.35
12.0	1.35

TABLE 7.16: Values of stiffness factors used in calculation of dead load stresses from API RP 1102

D/t	E'	K_{He}
50	0.5 ksi	2931
75	0.5 ksi	5051
100	0.5 ksi	6460

TABLE 7.17: Values of highway stiffness factor for cyclic circumferential and longitudinal factors used in calculation of live load stresses from API RP 1102

D/t	$E_r = 5ksi$		$E_r = 10ksi$		$E_r = 20ksi$	
	K_{Hh}	K_{Lh}	K_{Hh}	K_{Lh}	K_{Hh}	K_{Lh}
50	19.1	14.3	14.2	9.8	9.7	6.5
75	20.5	15.0	14.5	10.1	8.7	6.4
100	18.9	14.5	12.4	9.7	6.8	6.0

TABLE 7.18: Values of highway geometry factor for cyclic circumferential and longitudinal factors used in calculation of live load stresses from API RP 1102

H (ft)	D = 12 inch		D = 12 inch		D = 12 inch	
	G_{Hh}	G_{Lh}	G_{Hh}	G_{Lh}	G_{Hh}	G_{Lh}
3	1.25	1.17	1.10	1.07	1.02	0.91
4	1.25	1.17	1.10	1.07	1.02	0.91
6	1	1.03	0.86	0.90	0.75	0.76
8	0.82	0.92	0.71	0.77	0.62	0.65

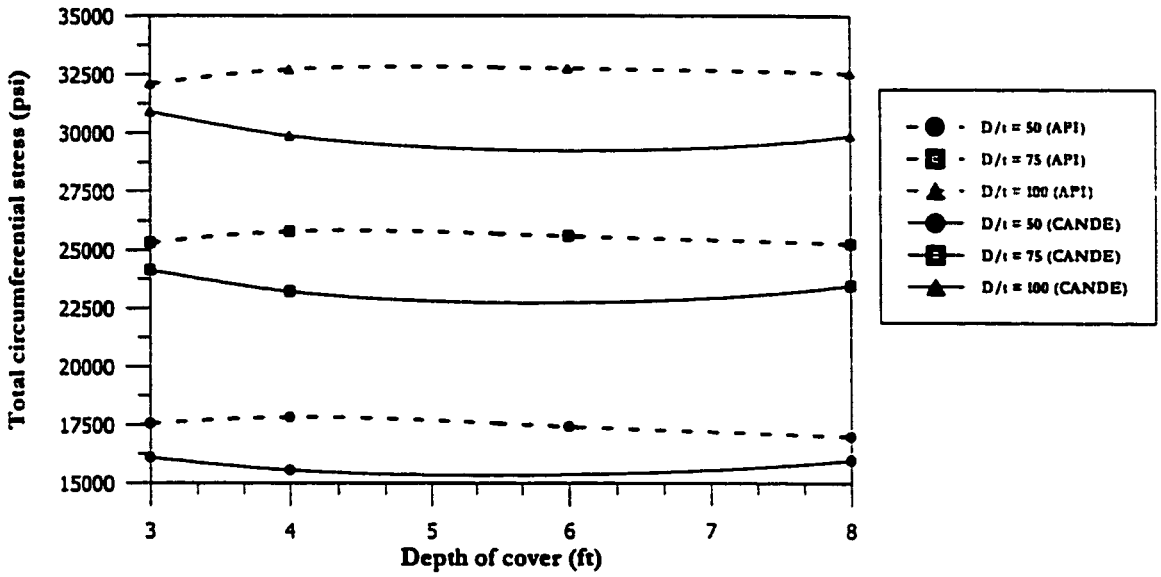

(a) Resilient modulus 5 ksi

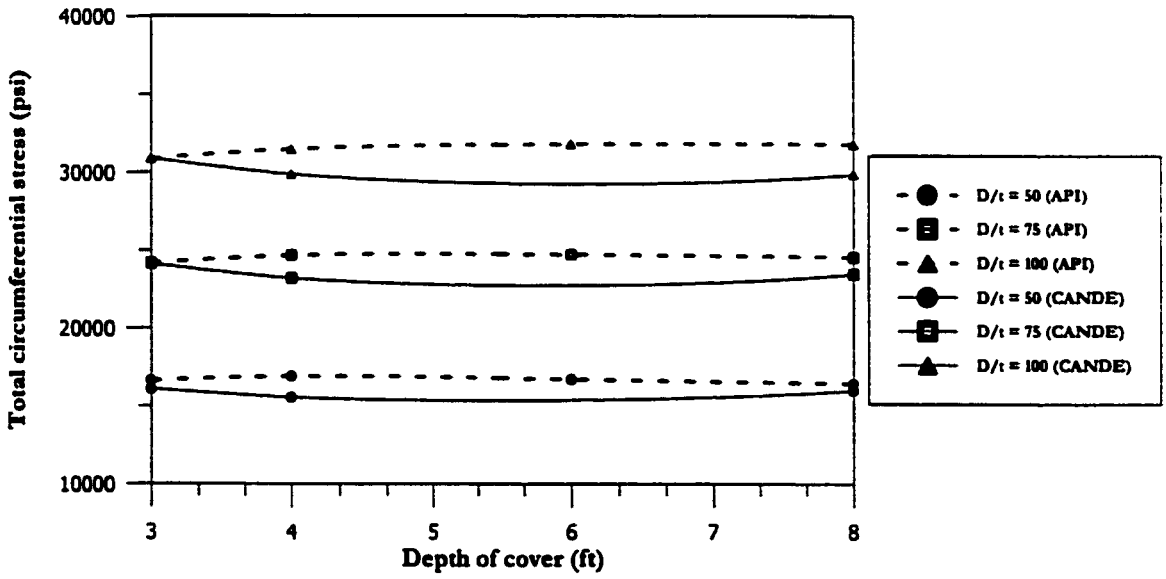

(b) Resilient modulus 10 ksi

Fig. 7.91: Total circumferential stresses for 12 inches pipe diameter and soil resilient modulus values of 5 and 10 ksi

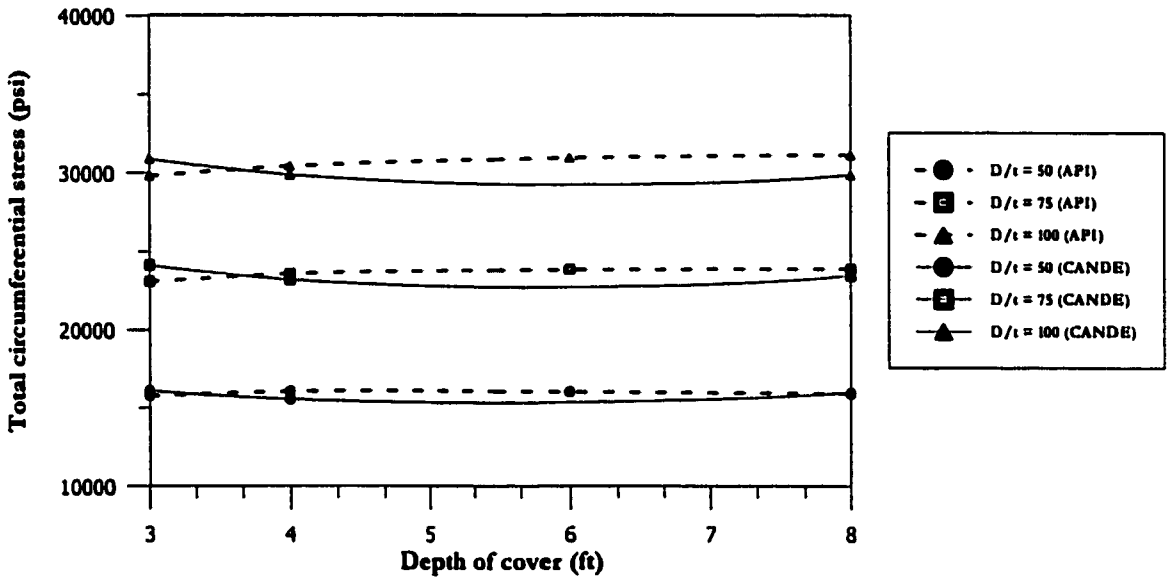

Fig. 7.92: Total circumferential stresses for 12 inches pipe diameter and soil resilient modulus value of 20 ksi

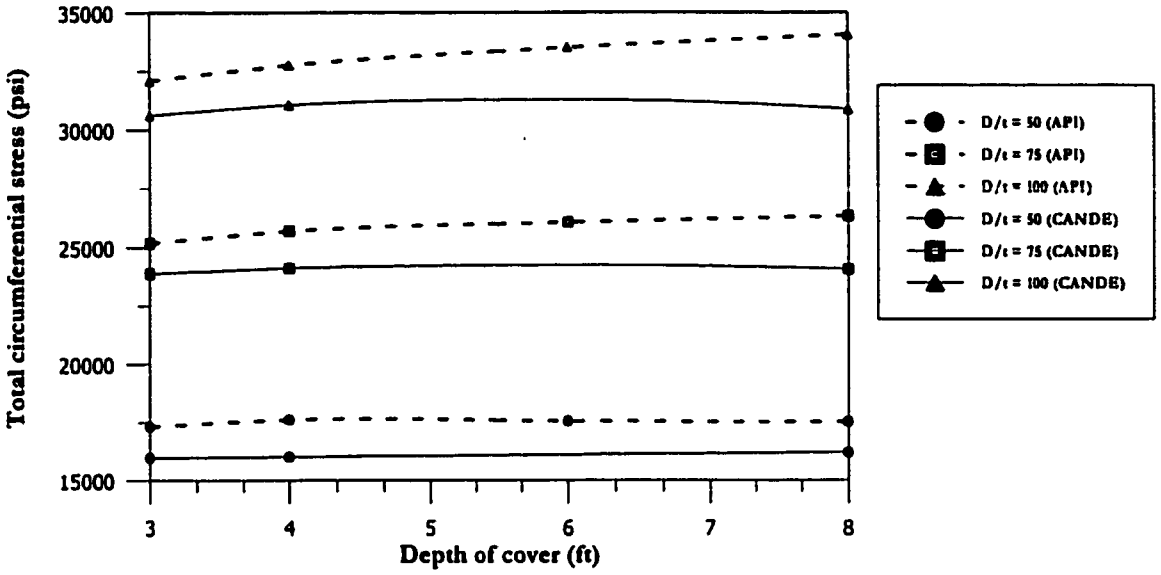

(a) Resilient modulus 5 ksi

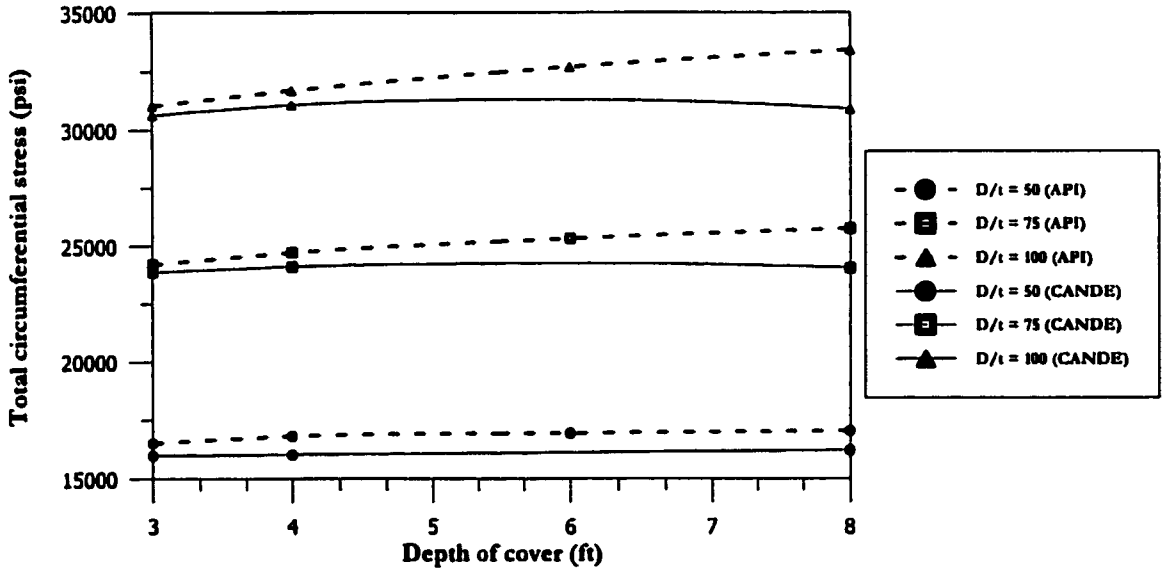

(b) Resilient modulus 10 ksi

Fig. 7.93: Total circumferential stresses for 24 inches pipe diameter and soil resilient modulus values of 5 and 10 ksi

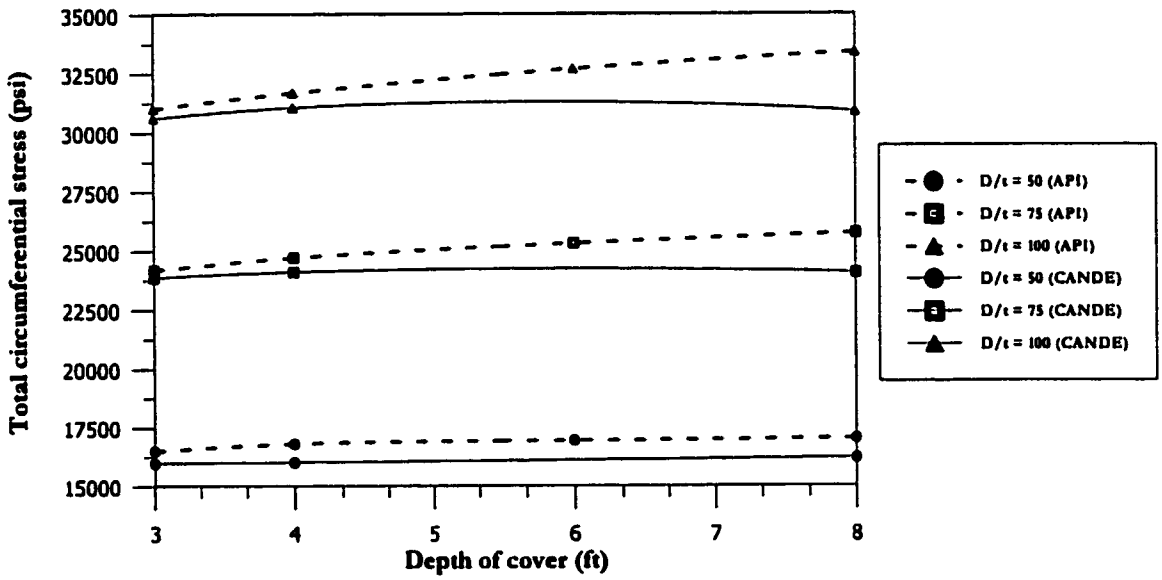

Fig. 7.94: Total circumferential stresses for 24 inches pipe diameter and soil resilient modulus value of 20 ksi

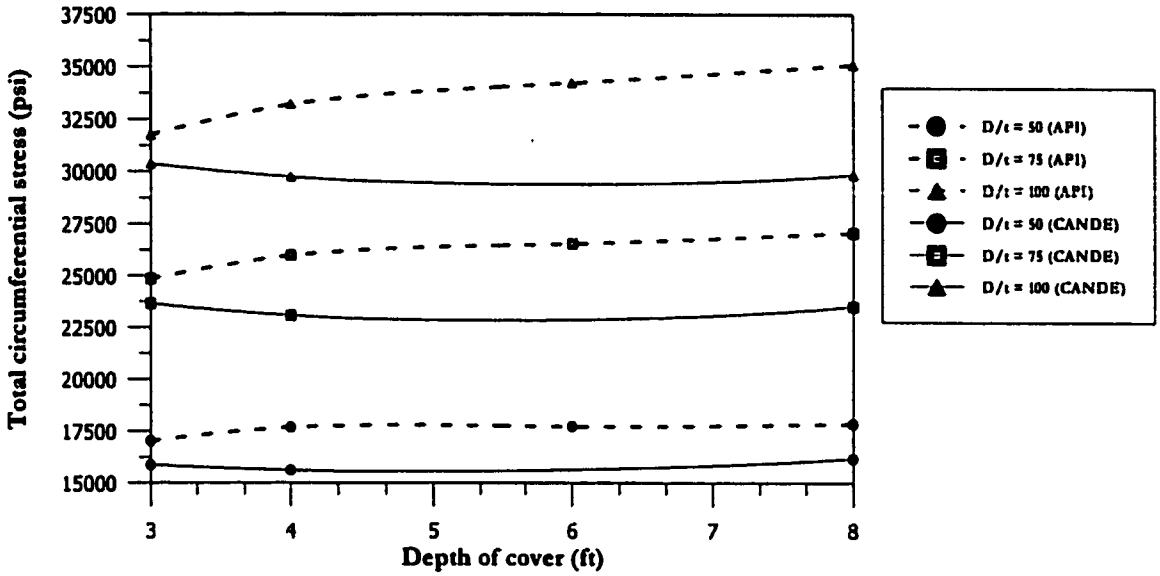

(a) Resilient modulus 5 ksi

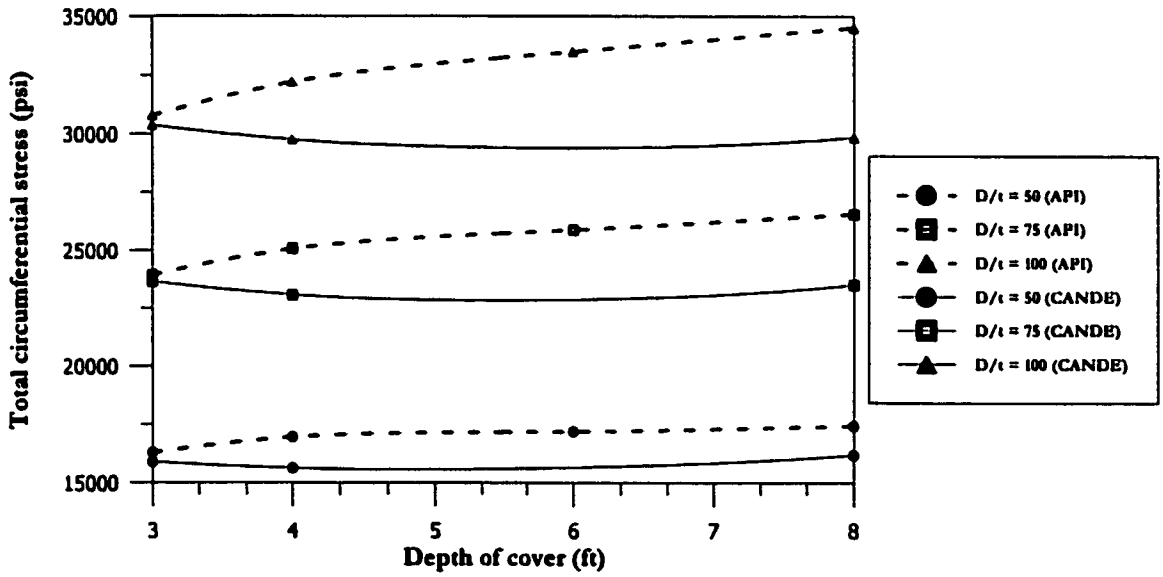

(b) Resilient modulus 10 ksi

Fig. 7.95: Total circumferential stresses for 36 inches pipe diameter and soil resilient modulus values of 5 and 10 ksi

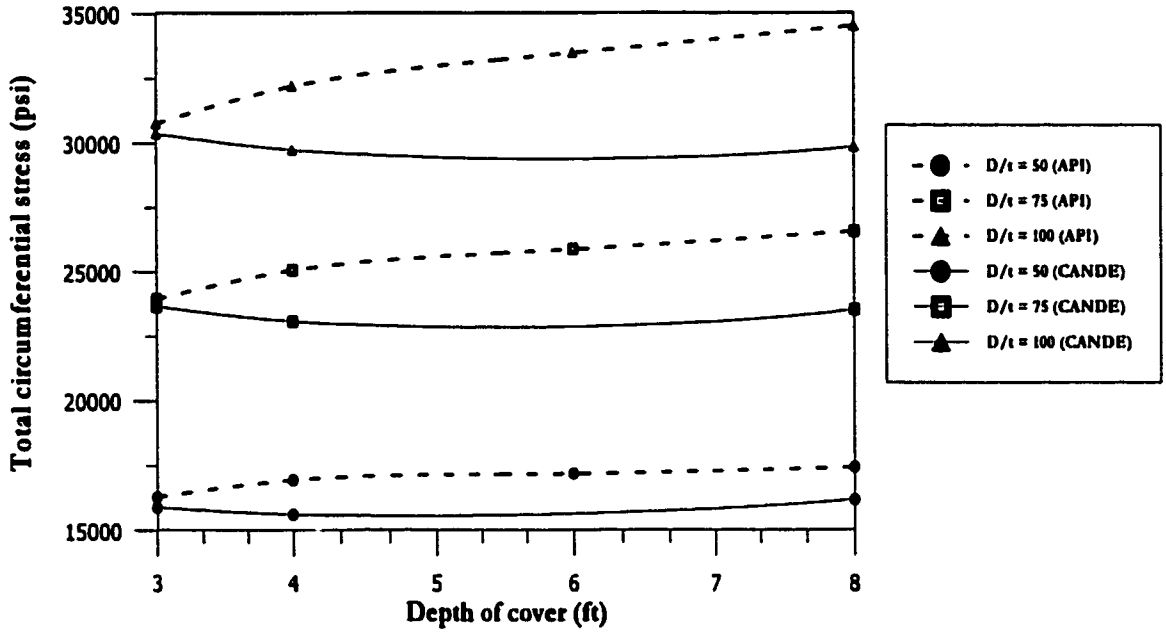

Fig. 7.96: Total circumferential stresses for 36 inches pipe diameter and soil resilient modulus value of 20 ksi

7.9.3 Comparison for Longitudinal Stresses

A comparison of total longitudinal stresses (defined in Subsection 3.14.5) between API RP 1102 and CANDE is presented here. The diameters and D/t ratios compared here are the same as those in Subsection 7.9.1 and Subsection 7.9.2. The parameters for calculating the longitudinal stresses by API 1102 are same as presented in Subsection 7.9.2. The values of longitudinal stresses by API 1102 are calculated with constant modulus of soil reaction of 0.5 ksi and varying soil resilient modulus. The loadings considered are dead load, live load and an internal pressure of 500 psi.

The longitudinal stresses for both CANDE and API 1102 are calculated with and without temperature stresses. A temperature gradient of $120°F$ is used with the assumption that temperature encountered in the field is always greater than the installation temperature. Since CANDE is a plain-strain formulation, therefore longitudinal stresses due to live load for CANDE are calculated using the plain-strain approximation.

The results for longitudinal stresses without the temperature stresses are shown in Figs. 7.97 to 7.102, and the results for longitudinal stresses with temperature stresses are shown in Figs. 7.103 to 7.108. The results for longitudinal stresses without temperature show a consistent pattern that CANDE results are always less conservative than API RP 1102 results and the difference between them is greater for large diameters and D/t ratios, and small soil resilient modulus.

The results for longitudinal stresses including the temperature effect show an appropriate behavior. of longitudinal stresses without the temperature effect. The temperature gradient will cause stresses to act in the direction opposite to the longitudinal stresses due

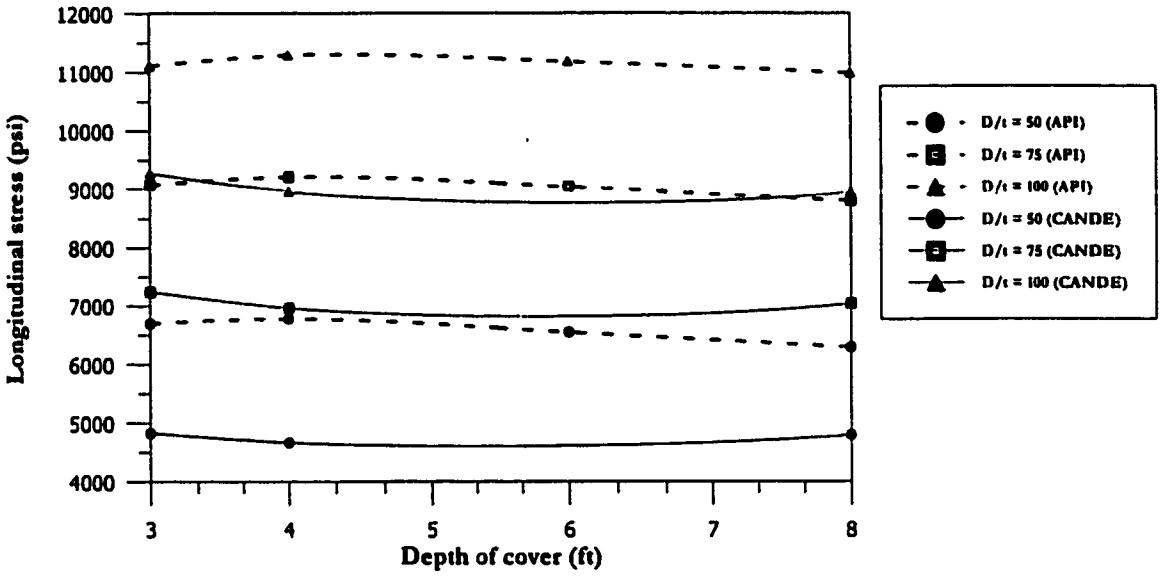

(a) Resilient modulus 5 ksi

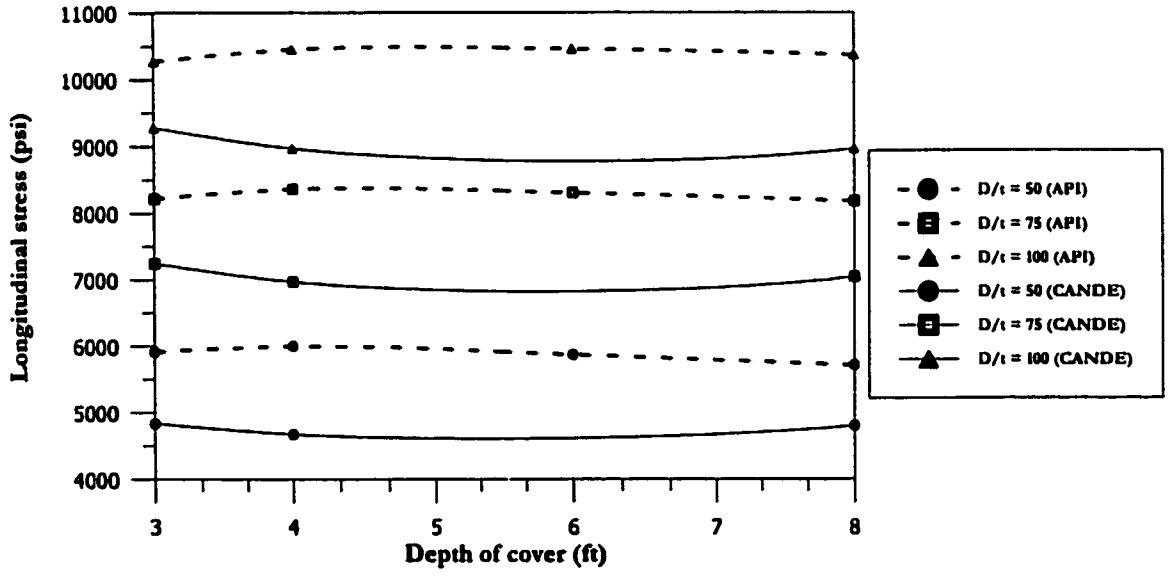

(b) Resilient modulus 10 ksi

Fig. 7.97: Longitudinal stresses for 12 inches pipe diameter and soil resilient modulus values of 5 and 10 ksi without temperature stresses

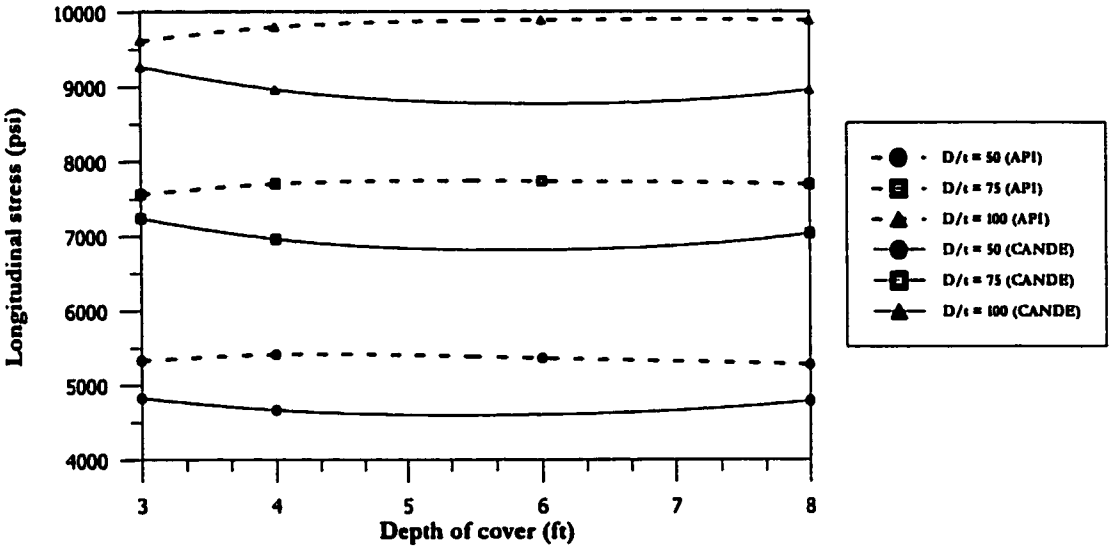

Fig. 7.98: Longitudinal stresses for 12 inches pipe diameter and soil resilient modulus value of 20 ksi without temperature stresses

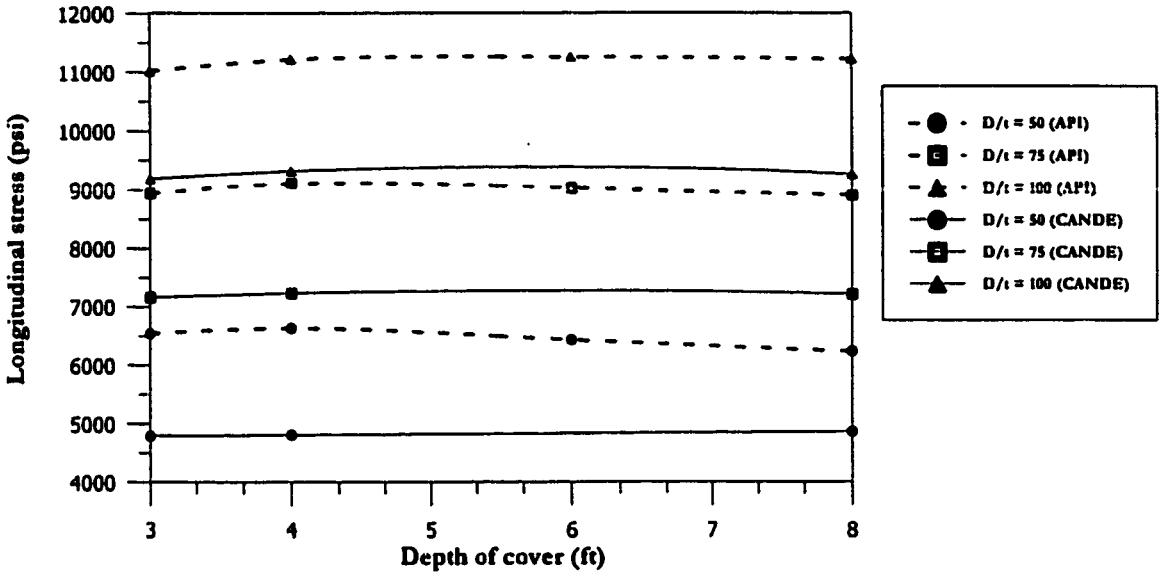

(a) Resilient modulus 5 ksi

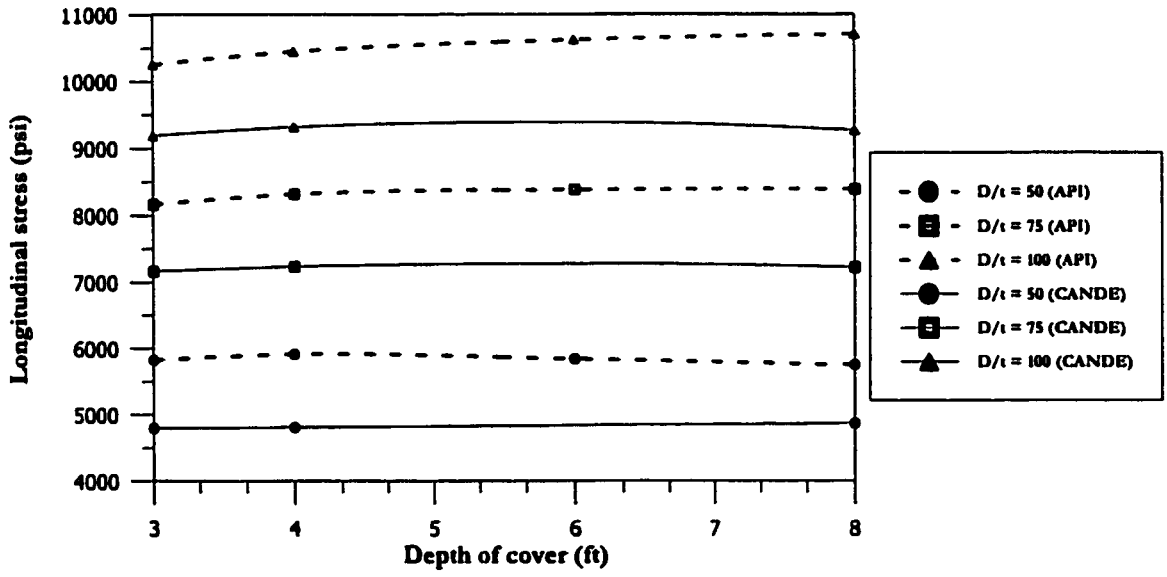

(b) Resilient modulus 10 ksi

Fig. 7.99: Longitudinal stresses for 24 inches pipe diameter and soil resilient modulus values of 5 and 10 ksi without temperature stresses

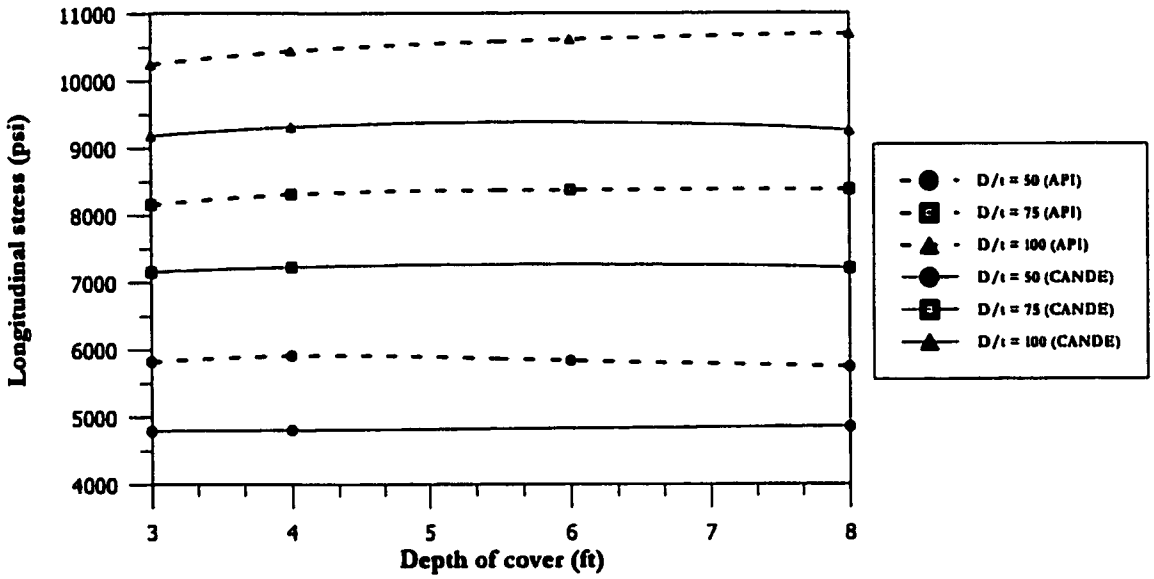

Fig. 7.100: Longitudinal stresses for 24 inches pipe diameter and soil resilient modulus values of 20 ksi without temperature stresses

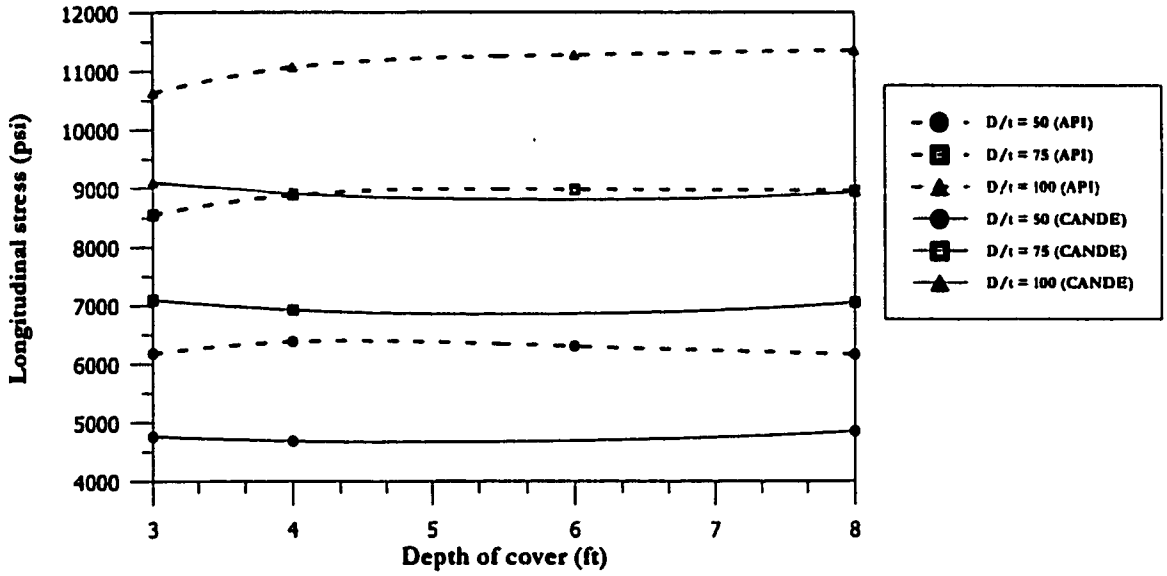

(a) Resilient modulus 5 ksi

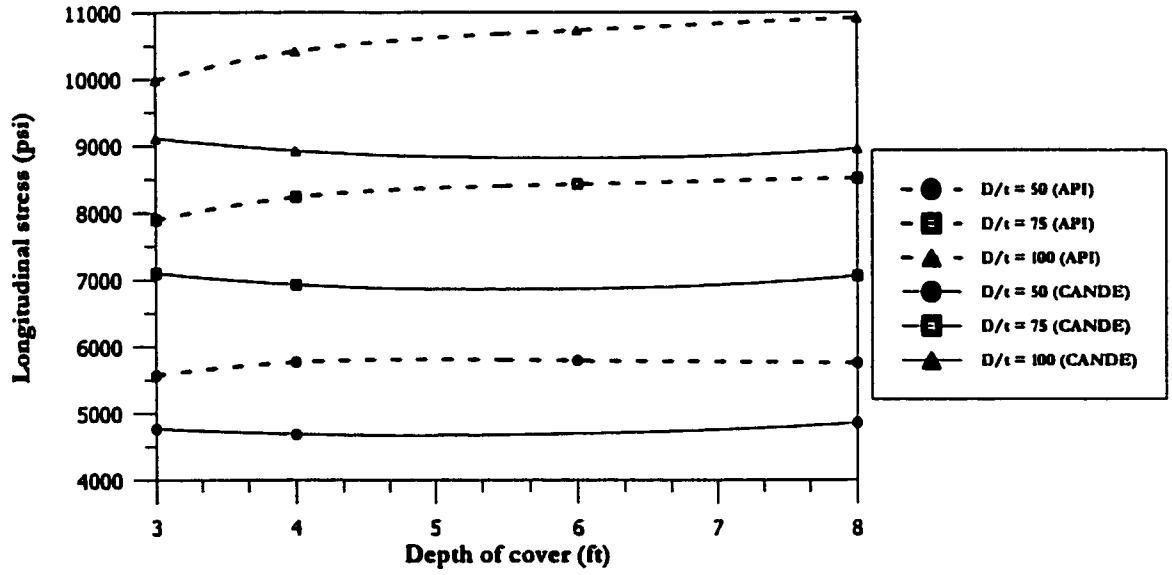

(b) Resilient modulus 10 ksi

Fig. 7.101: Longitudinal stresses for 36 inches pipe diameter and soil resilient modulus values of 5 and 10 ksi without temperature stresses

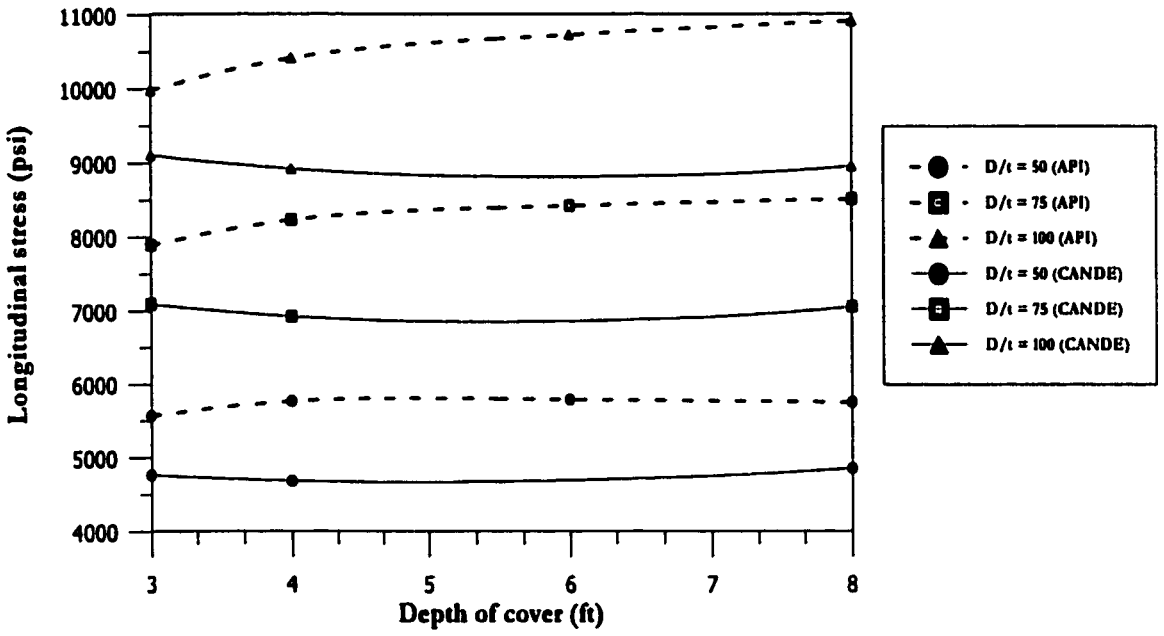

Fig. 7.102: Longitudinal stresses for 36 inches pipe diameter and soil resilient modulus value of 20 ksi without temperature stresses

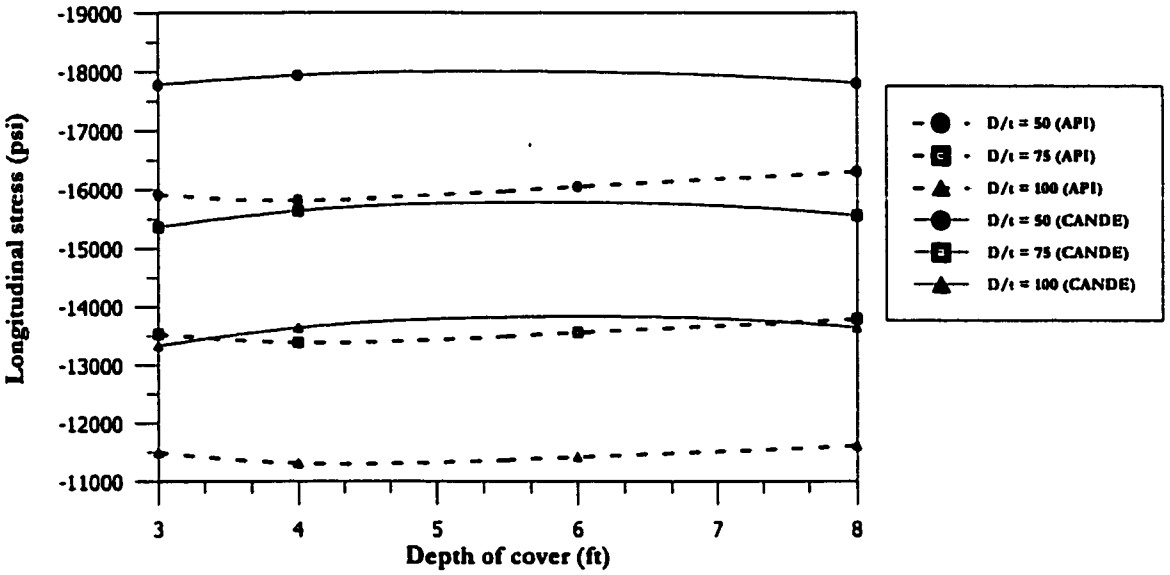

(a) Resilient modulus 5 ksi

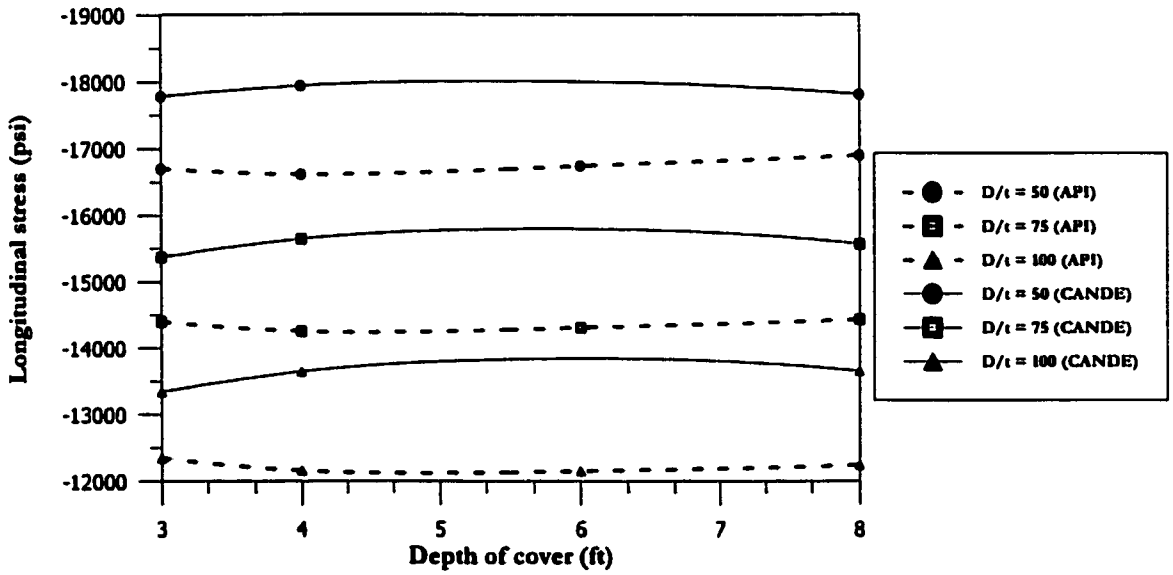

(b) Resilient modulus 10 ksi

Fig. 7.103: Longitudinal stresses for 12 inches pipe diameter and soil resilient modulus values of 5 and 10 ksi with temperature stresses

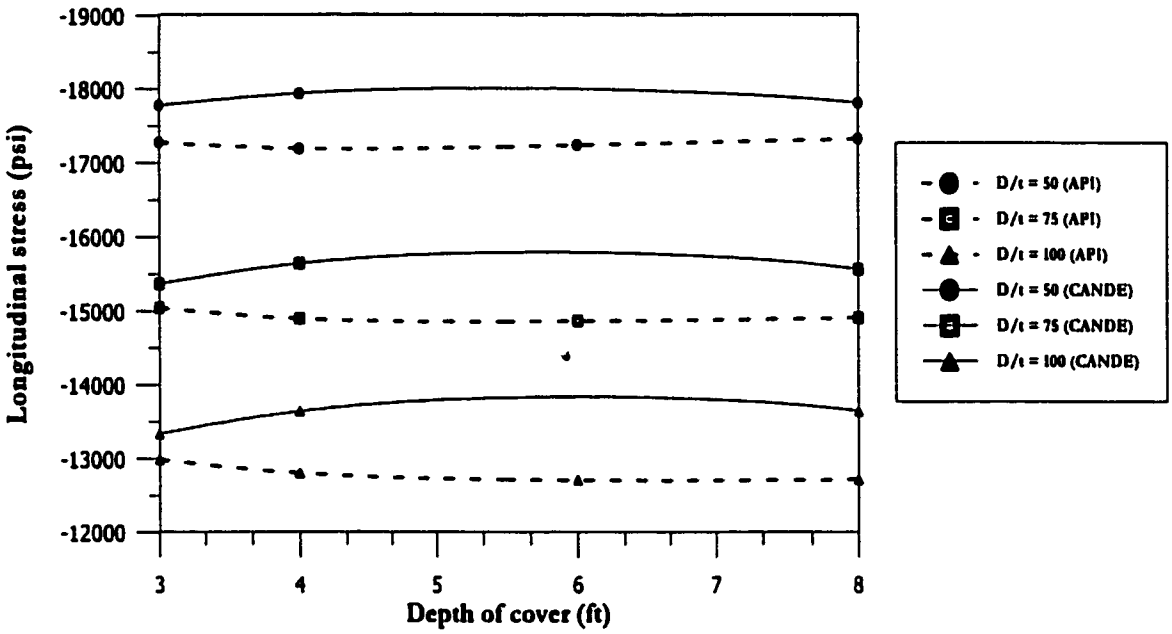

Fig. 7.104: Longitudinal stresses for 12 inches pipe diameter and soil resilient modulus value of 20 ksi with temperature stresses

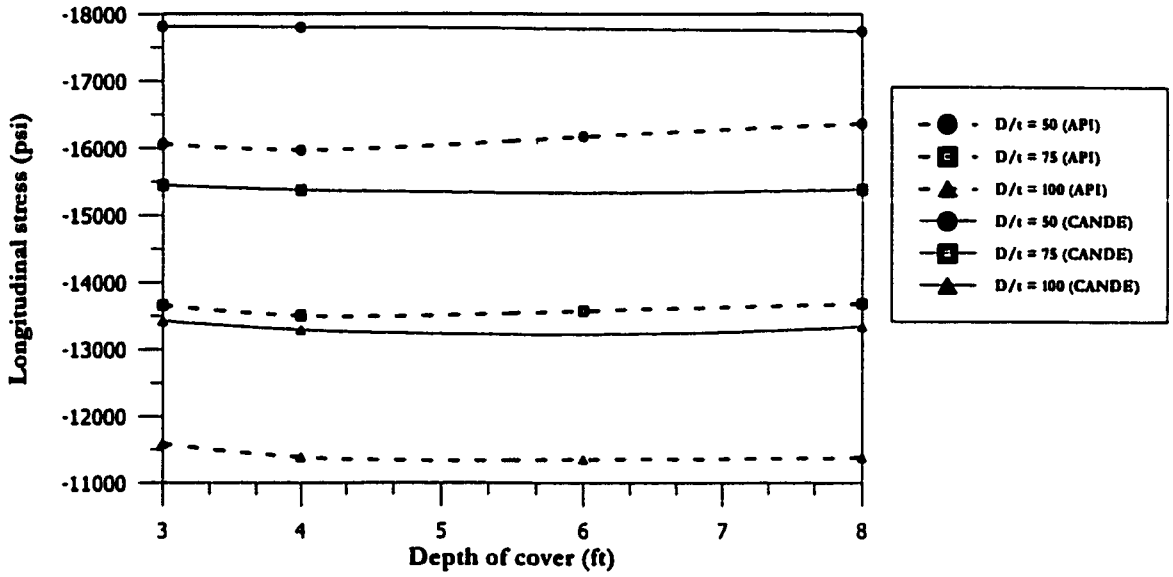

(a) Resilient modulus 5 ksi

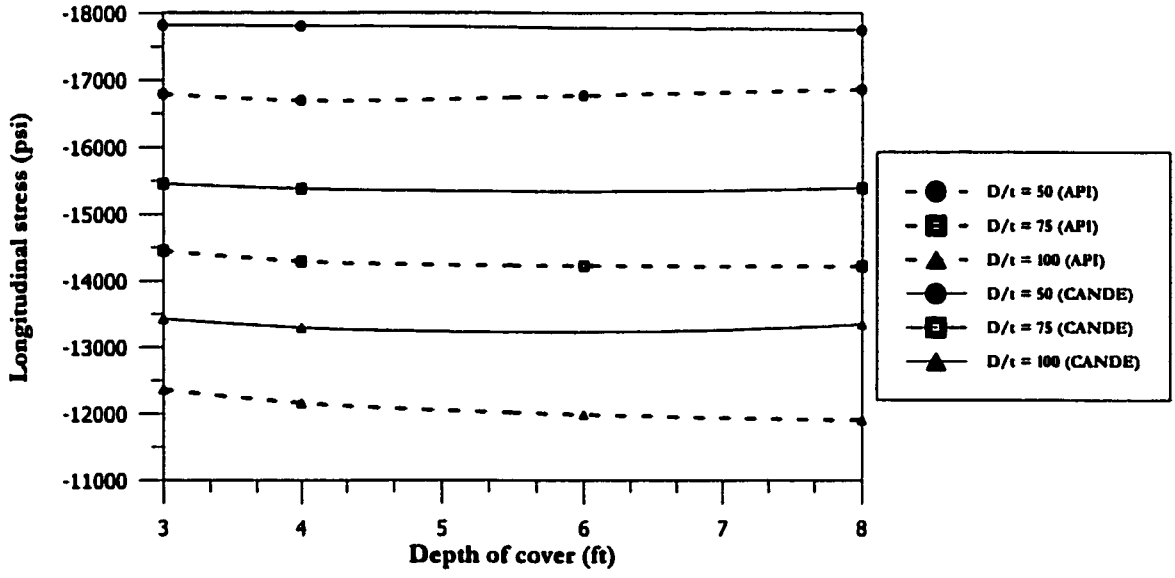

(b) Resilient modulus 10 ksi

Fig. 7.105: Longitudinal stresses for 24 inches pipe diameter and soil resilient modulus values of 5 and 10 ksi with temperature stresses

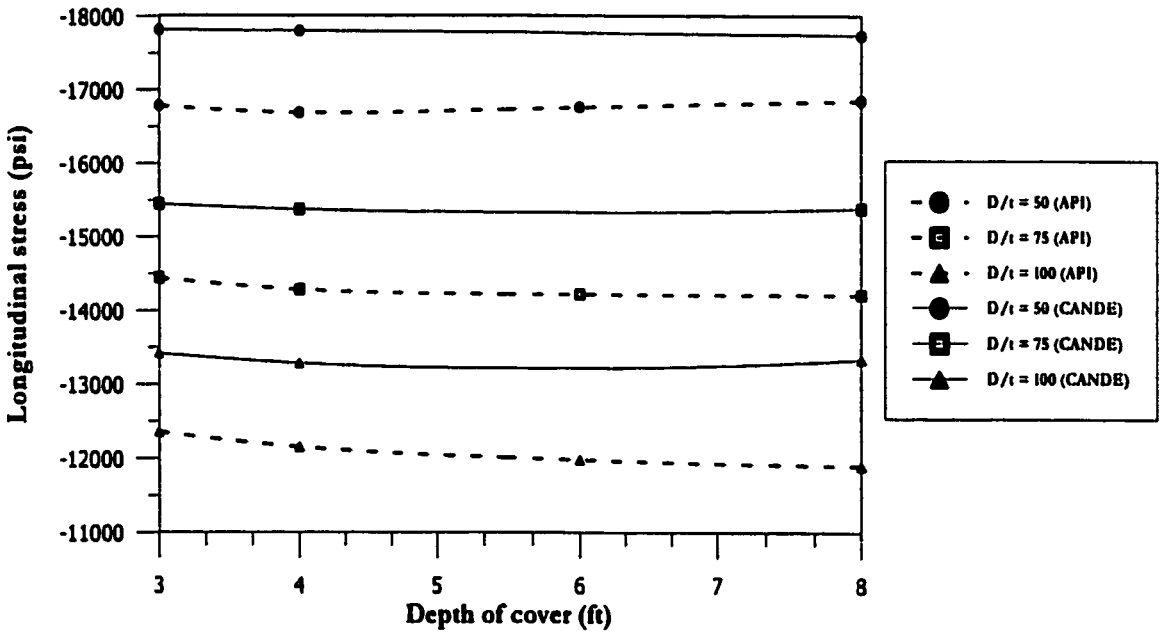

Fig. 7.106: Longitudinal stresses for 24 inches pipe diameter and soil resilient modulus value of 20 ksi with temperature stresses

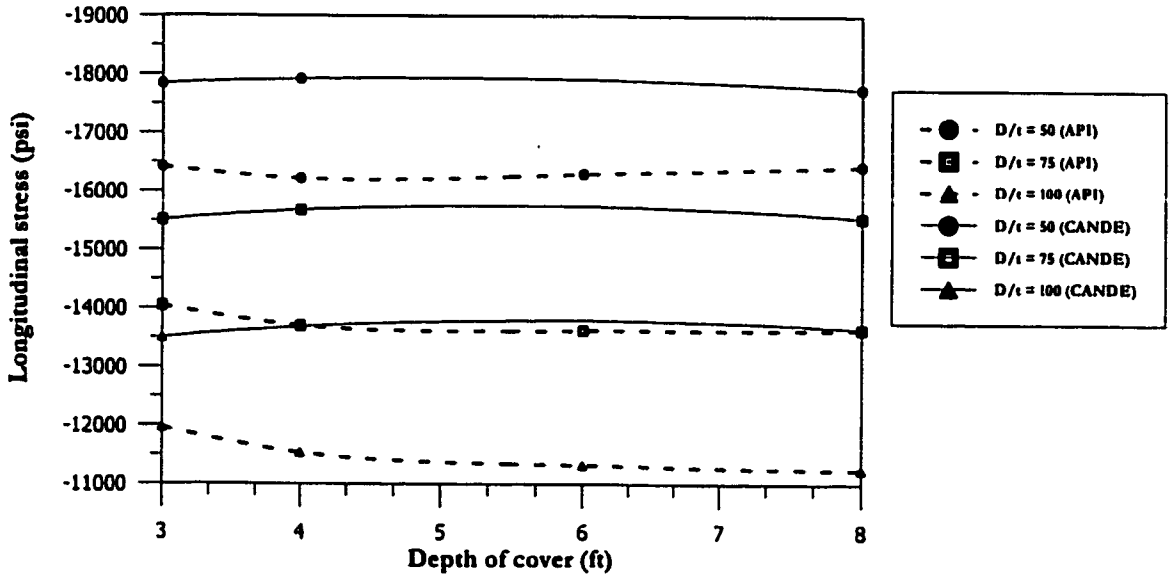

(a) Resilient modulus 5 ksi

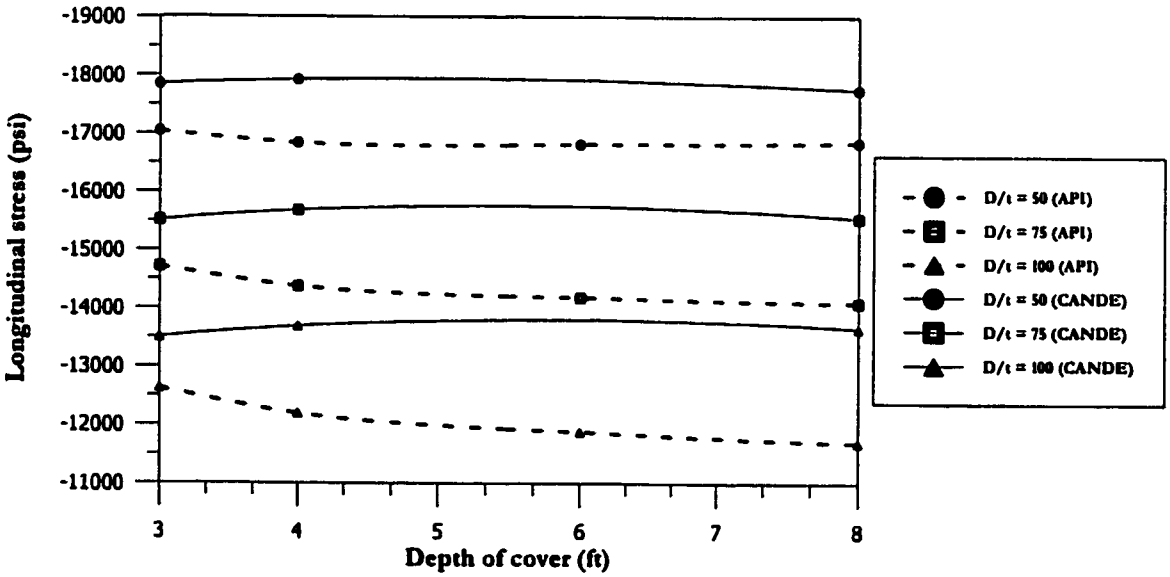

(b) Resilient modulus 10 ksi

Fig. 7.107: Longitudinal stresses for 36 inches pipe diameter and soil resilient modulus values of 5 and 10 ksi with temperature stresses

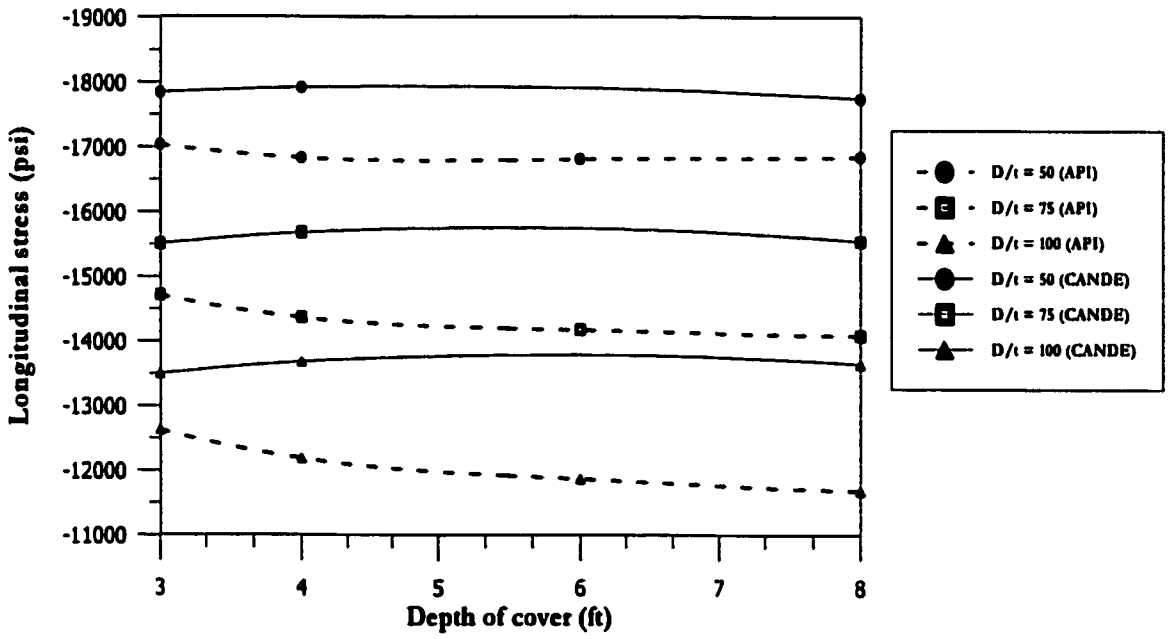

Fig. 7.108: Longitudinal stresses for 36 inches pipe diameter and soil resilient modulus value of 20 ksi with temperature stresses

to dead, live, and internal pressure of 500 psi. This will cause a net longitudinal stresses acting in the opposite direction. This clearly indicates that the longitudinal stresses due to temperature gradient of $120^{o}F$ dominate the combined longitudinal stresses due to other types of loading. Moreover, the stresses for API RP 1102 are less conservative than the CANDE results in contrast to longitudinal stresses without the temperature.

7.9.4 Comparison of Effective Stresses

In this section the effective stresses due to various loadings are calculated using the methodology recommended by [73] and [34] as presented in Subsection 3.14.5. The effective stresses are calculated for both API recommended practice 1102 and CANDE results. A first set of effective stress values are calculated making the assumption that the difference between the maximum temperature encountered in the field and the installation temperature is negligible. The second set of effective stress values are determined with the assumption that the maximum temperature encountered in the field is $120^{o}F$ more than the installation temperature.

The results without the temperature effect are shown in Figs. 7.109 to 7.114. It can be seen that the effective stresses predicted from CANDE are always less conservative than the API RP 1102 predictions except for 12 inches pipe diameter, in small depths of cover and soil resilient modulus of 20 ksi. Another important observation is that the difference between CANDE and API results is more for large diameter pipes and large depths of cover. This is because API RP 1102 is more conservative in predicting stresses due to dead load for large diameter pipes and high cover depths. The prediction of the two is quite

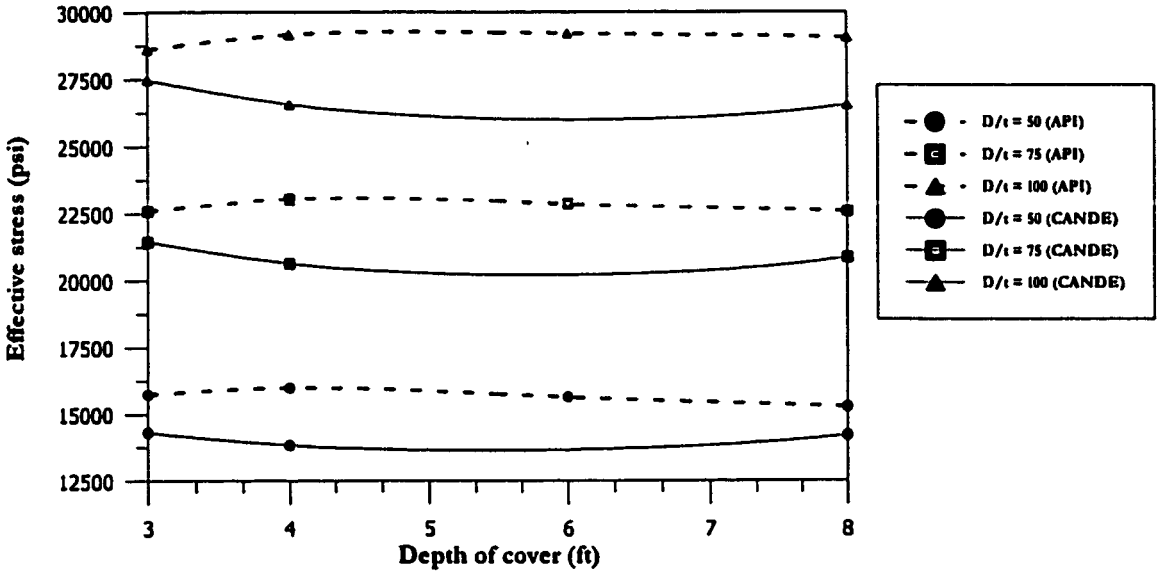

(a) Resilient modulus 5 ksi

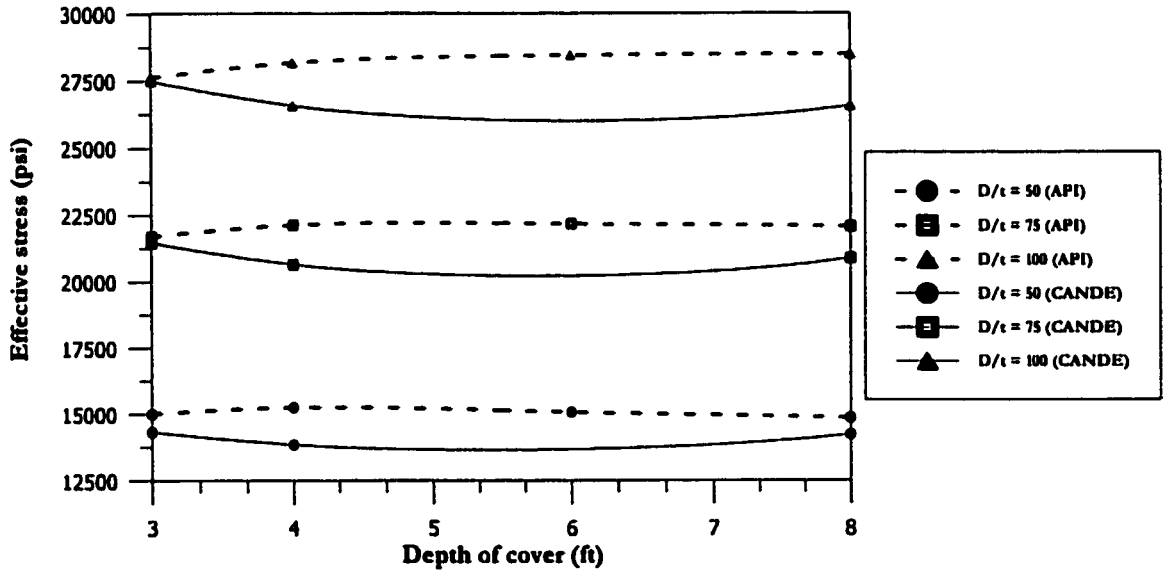

(b) Resilient modulus 10 ksi

Fig. 7.109: Effective stresses for 12 inches pipe diameter and soil resilient modulus values of 5 and 10 ksi without temperature stresses

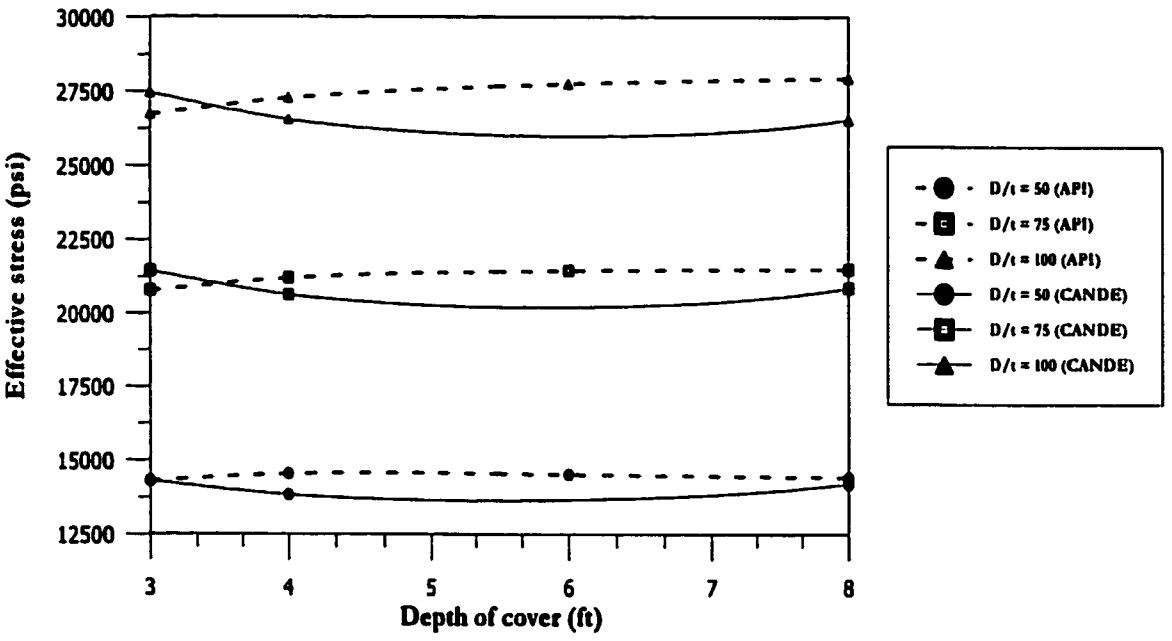

Fig. 7.110: Effective stresses for 12 inches pipe diameter and soil resilient modulus value of 20 ksi without temperature stresses

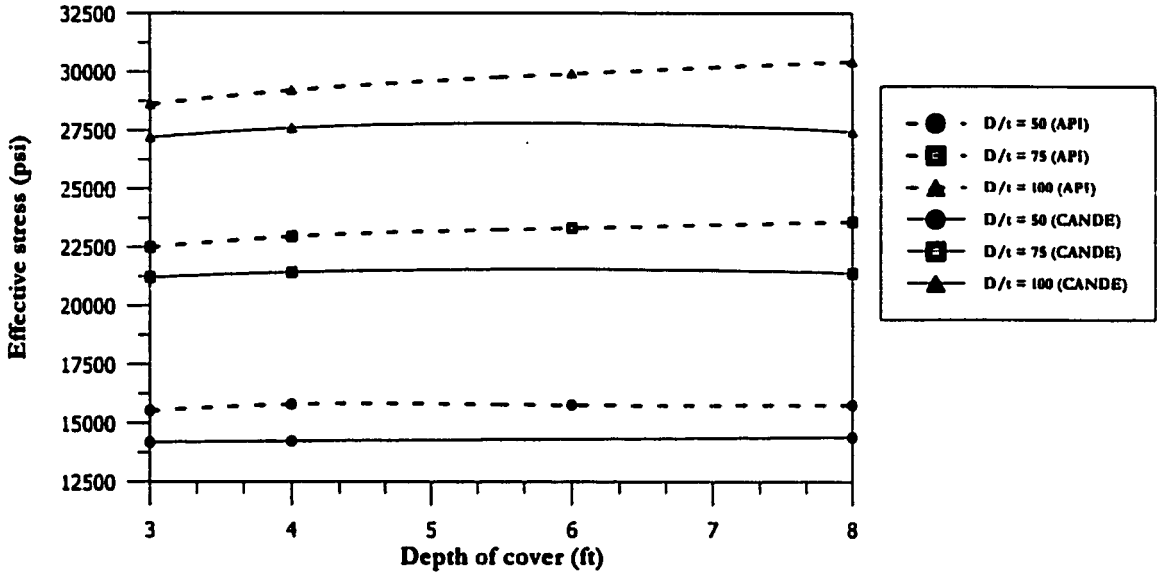

(a) Resilient modulus 5 ksi

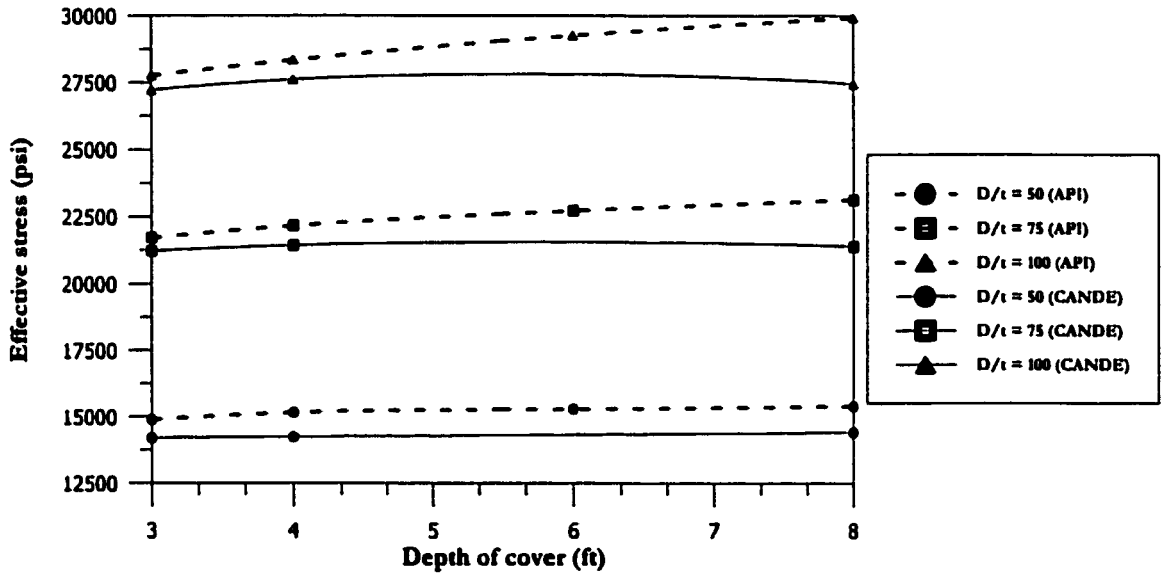

(b) Resilient modulus 10 ksi

Fig. 7.111: Effective stresses for 24 inches pipe diameter and soil resilient modulus values of 5 and 10 ksi without temperature stresses

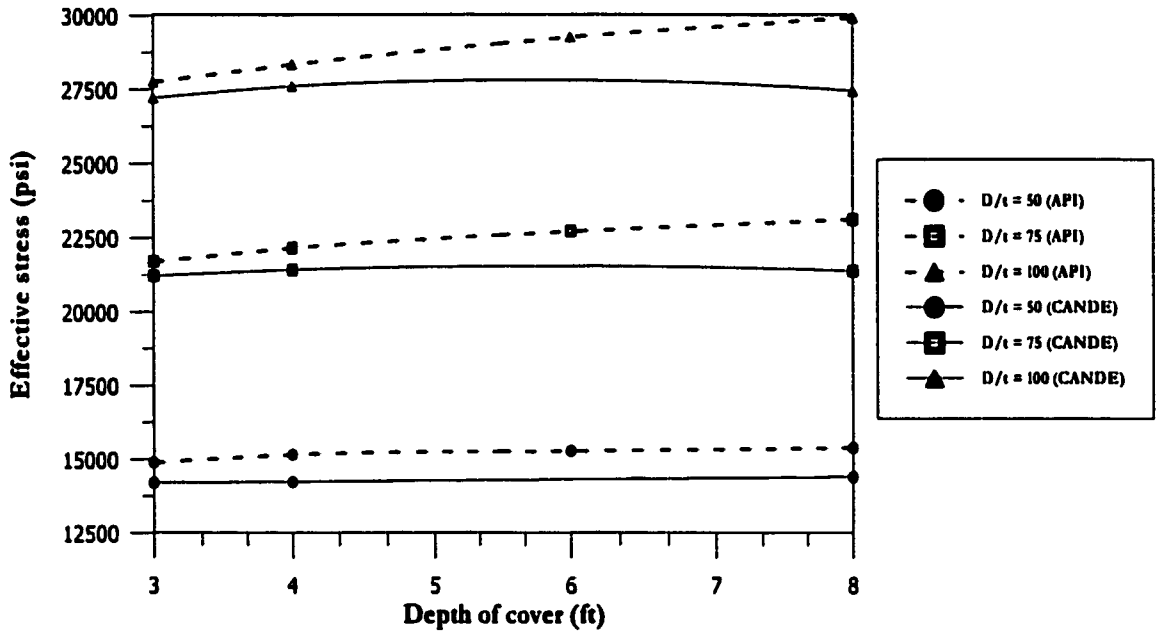

Fig. 7.112: Effective stresses for 24 inches pipe diameter and soil resilient modulus value of 20 ksi without temperature stresses

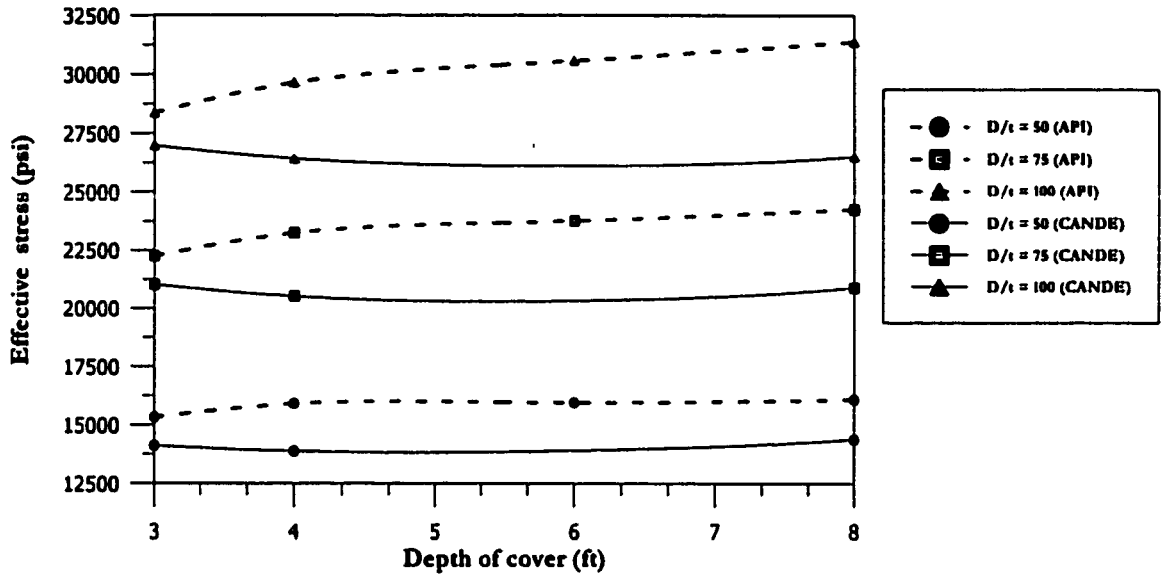

(a) Resilient modulus 5 ksi

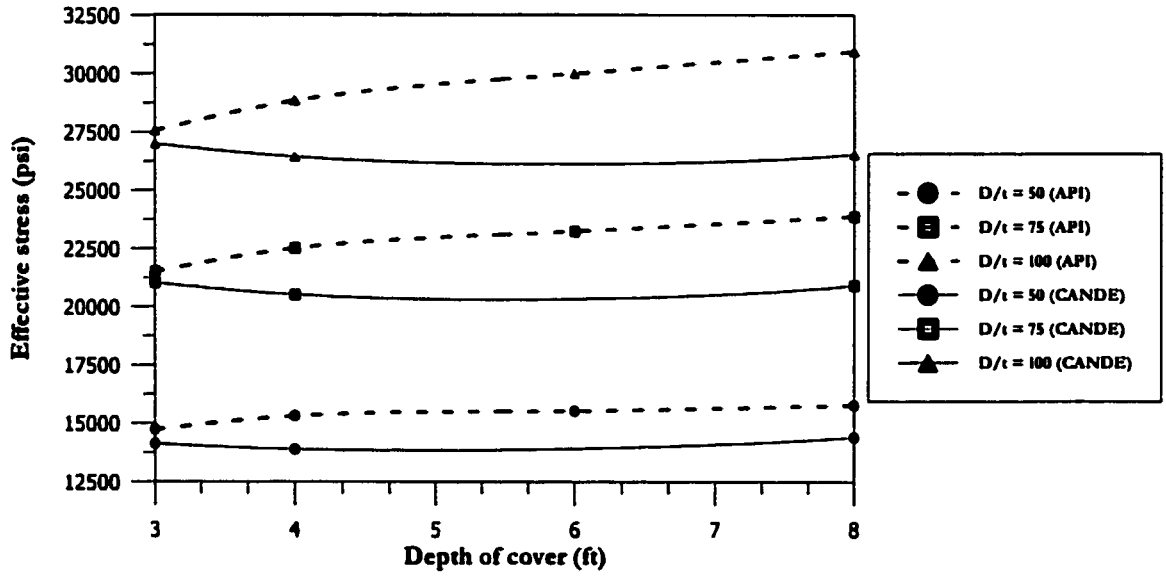

(b) Resilient modulus 10 ksi

Fig. 7.113: Effective stresses for 36 inches pipe diameter and soil resilient modulus values of 5 and 10 ksi without temperature stresses

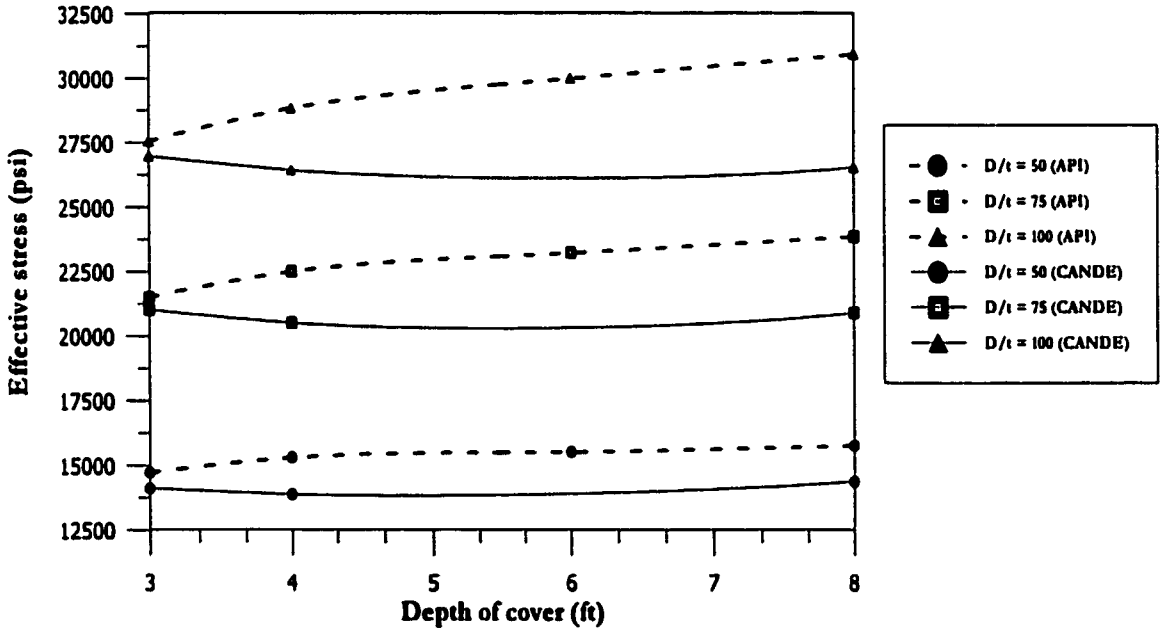

Fig. 7.114: Effective stresses for 36 inches pipe diameter and soil resilient modulus value of 20 ksi without temperature stresses

similar for small cover depths.

The comparison with the temperature effect is shown in Figs. 7.115 to 7.120. The results are quite different from those without the temperature stresses. The effective stresses calculated with the temperature are more than those without the temperature effect. This clearly indicates the domination of the temperature on the effective stresses. Also, the difference between CANDE and API results reduces drastically. This is because the longitudinal stresses obtained from CANDE after the inclusion of temperature become more than those obtained form API RP 1102 as shown in Subsection 7.9.3. The CANDE results are still less conservative than the API RP 1102 at large D/t ratios and diameters. It is important to notice that CANDE makes a good estimate of stresses for large diameters and D/t ratios taking into account the arching and mobilization of passive resistance around the sides of the pipe.

A comparison between the total circumferential stresses and effective stresses with and without temperature effect are shown in Figs. 7.121 to 7.123. An internal pressure of 500 psi is considered for the Barlow stress and a temperature gradient of $90^{o}F$ for the effect of temperature. It can be seen that the circumferential stresses are dominant if the effect of temperature is not taken into account however if the effect of temperature is considered the effective stresses exceed the circumferential stresses.

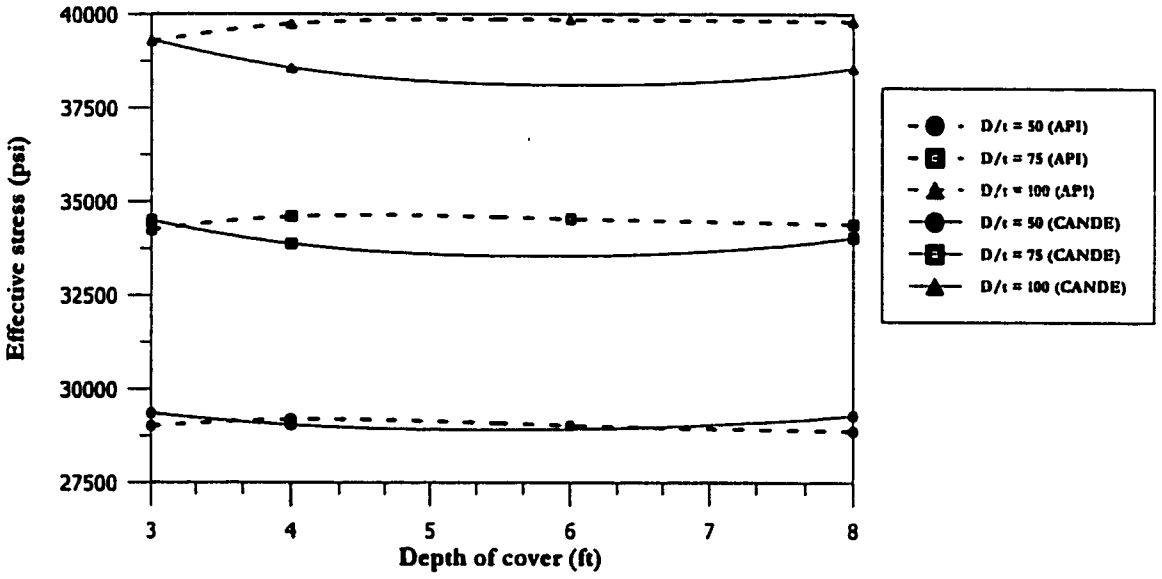

(a) Resilient modulus 5 ksi

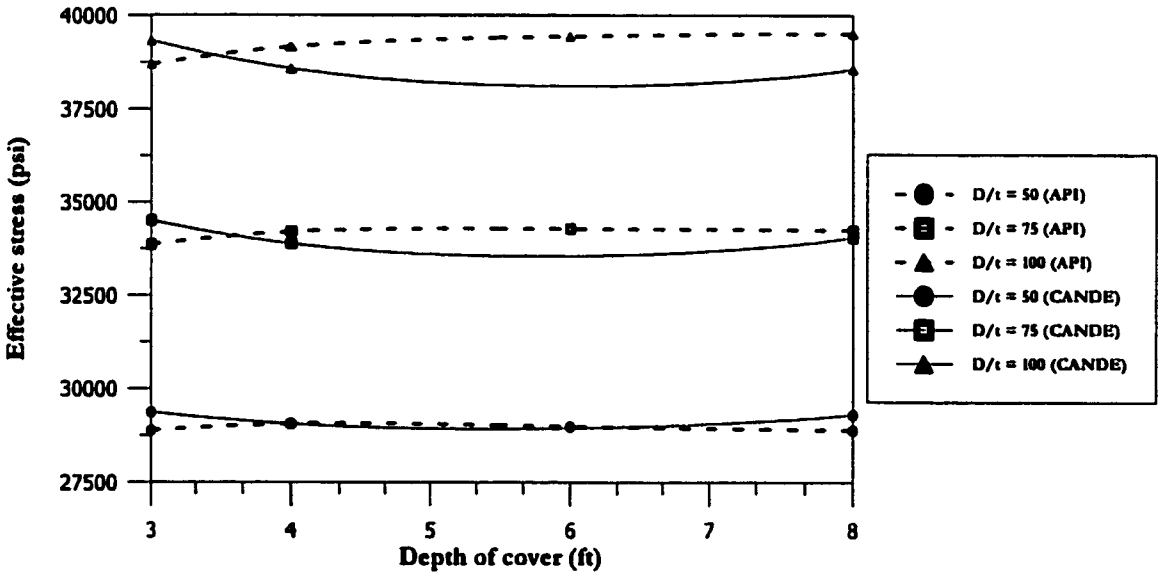

(b) Resilient modulus 10 ksi

Fig. 7.115: Effective stresses for 12 inches pipe diameter and soil resilient modulus values of 5 and 10 ksi with temperature stresses

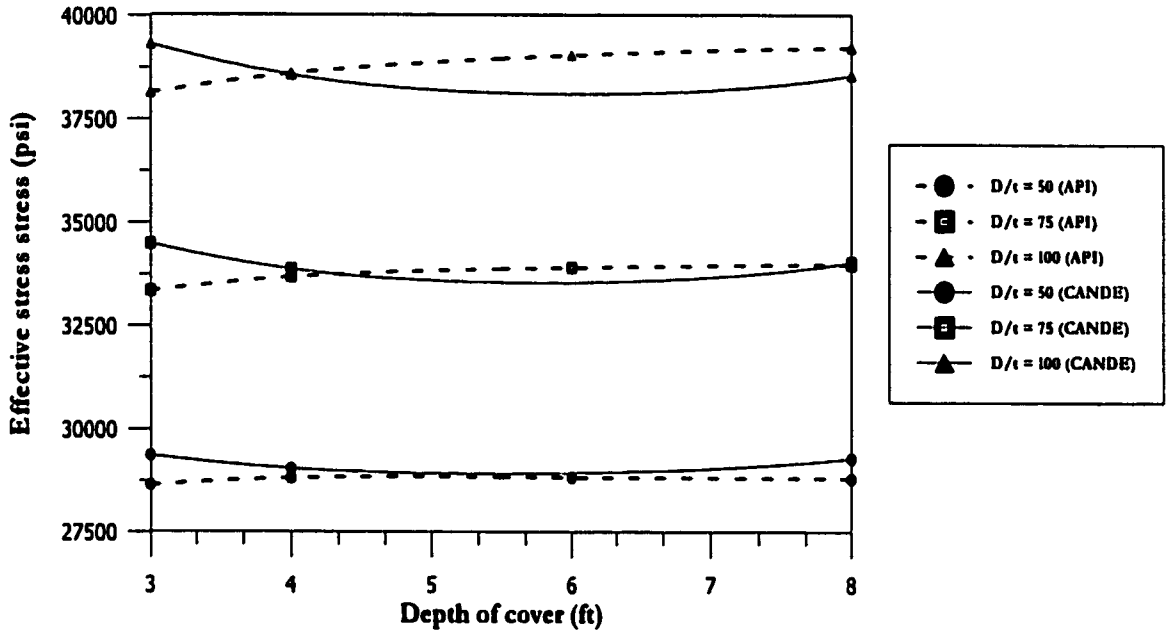

Fig. 7.116: Effective stresses for 12 inches pipe diameter and soil resilient modulus value of 20 ksi with temperature stresses

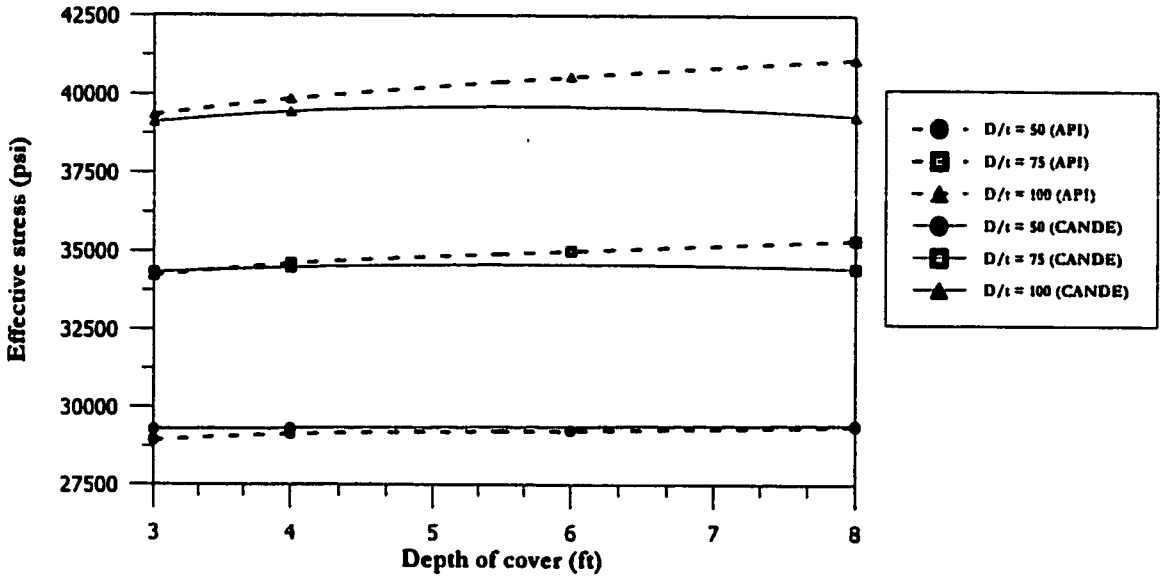

(a) Resilient modulus 5 ksi

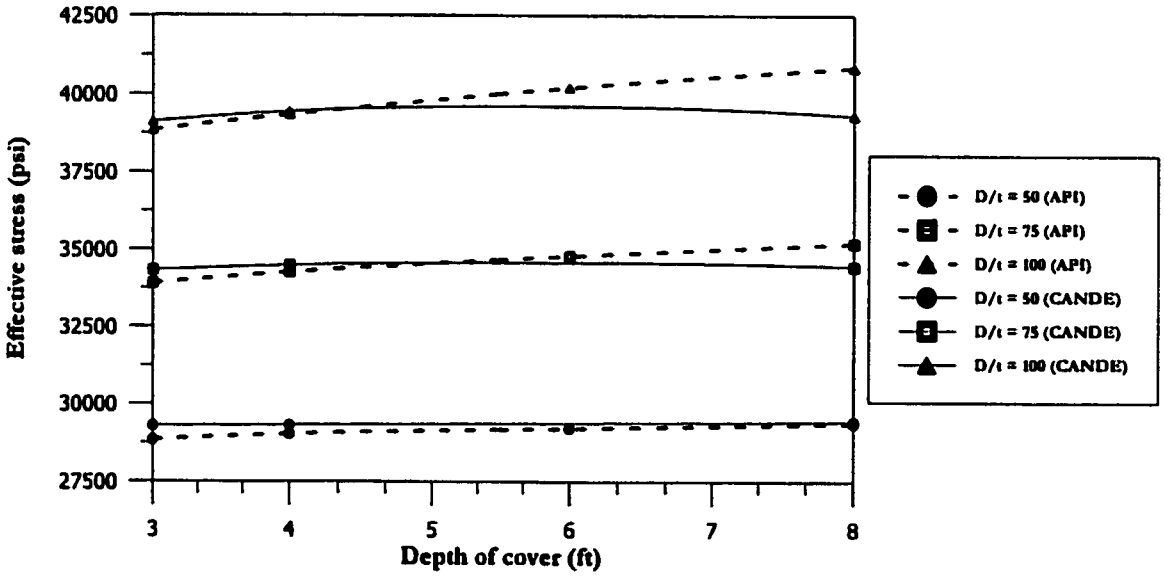

(b) Resilient modulus 10 ksi

Fig. 7.117: Effective stresses for 24 inches pipe diameter and soil resilient modulus values of 5 and 10 ksi with temperature stresses

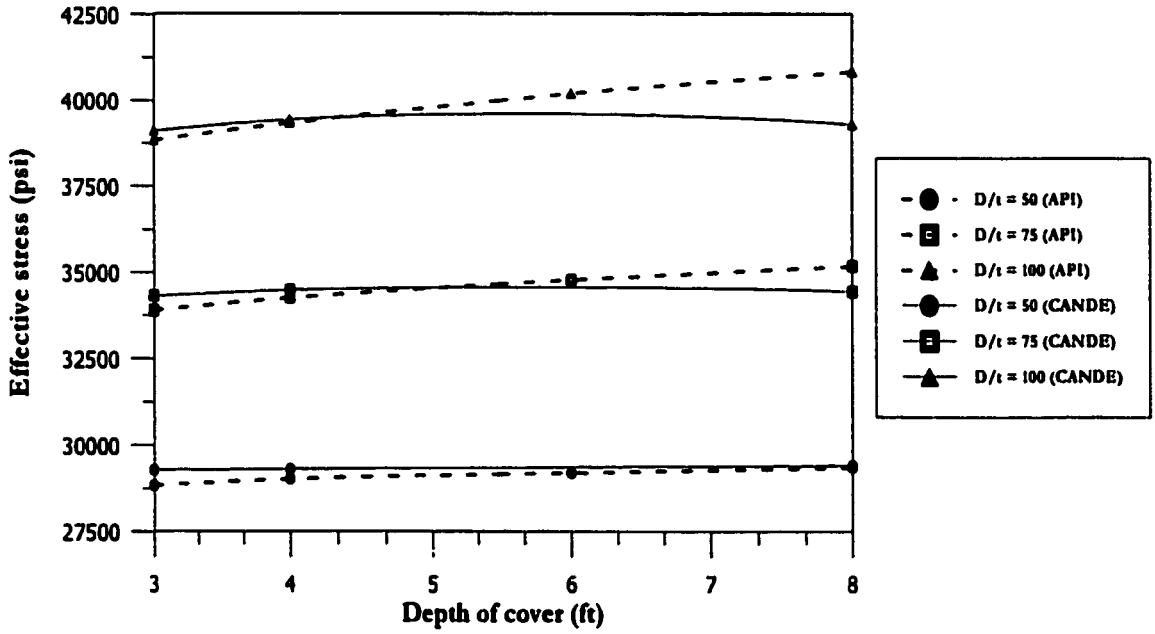

Fig. 7.118: Effective stresses for 24 inches pipe diameter and soil resilient modulus value of 20 ksi with temperature stresses

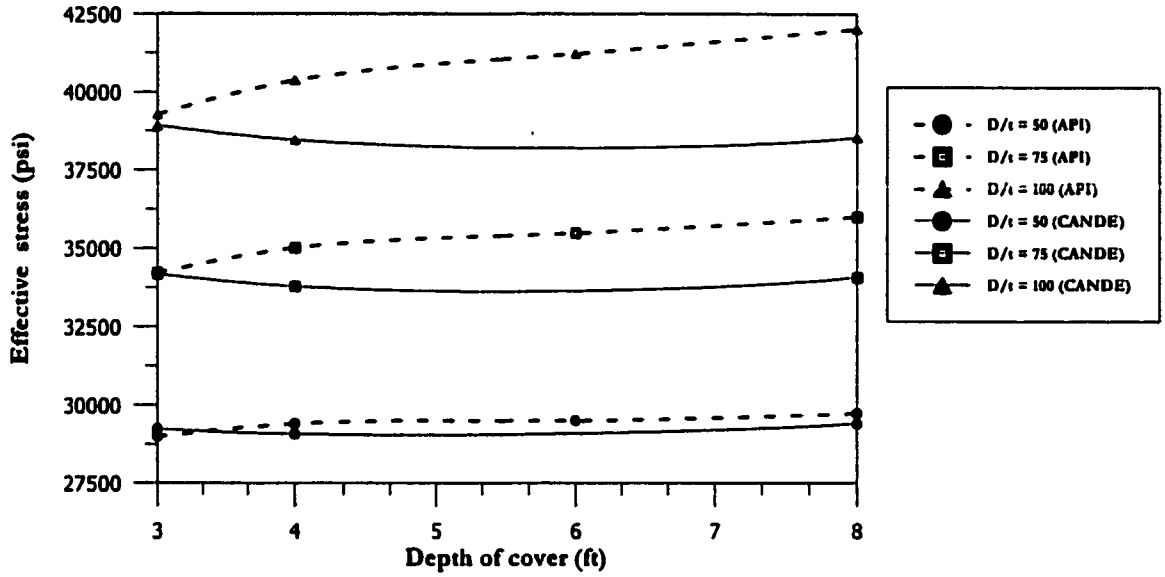

(a) Resilient modulus 5 ksi

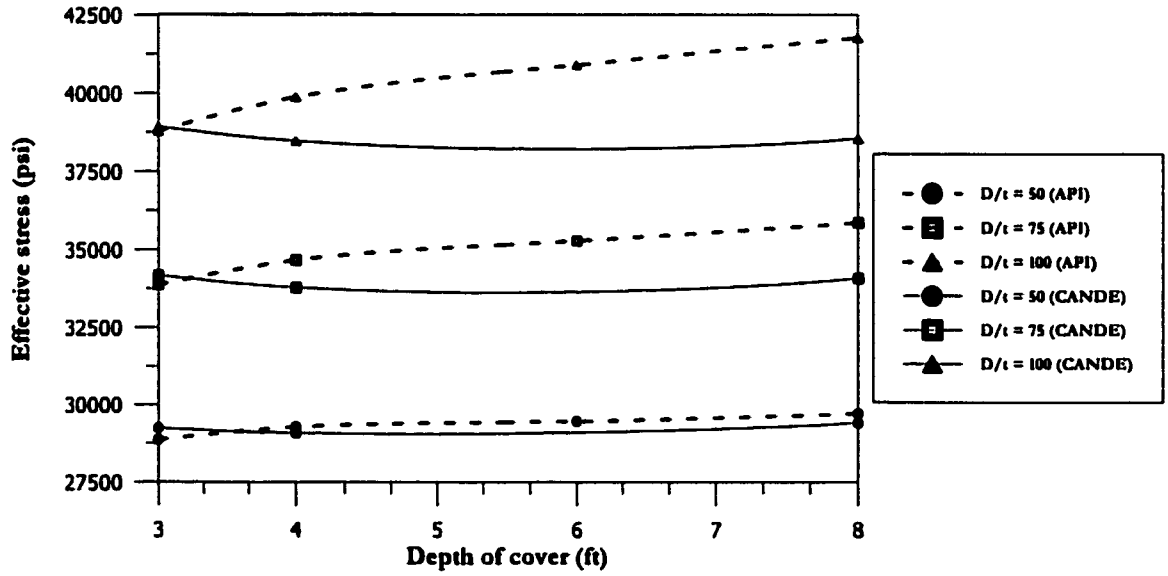

(b) Resilient modulus 10 ksi

Fig. 7.119: Effective stresses for 36 inches pipe diameter and soil resilient modulus values of 5 and 10 ksi with temperature stresses

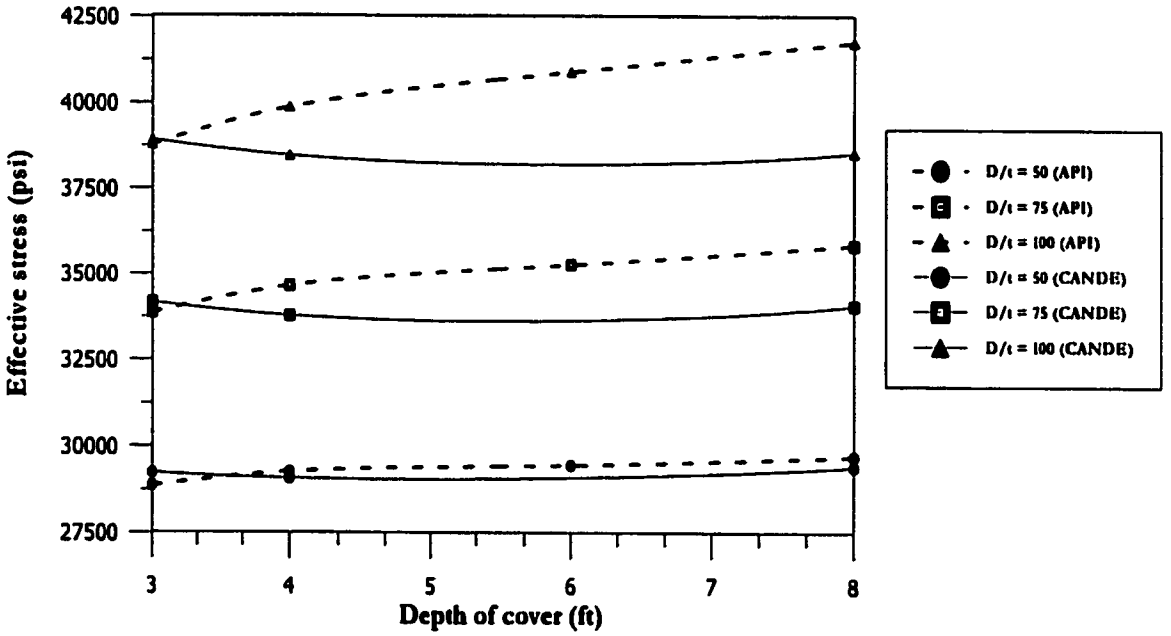

Fig. 7.120: Effective stresses for 36 inches pipe diameter and soil resilient modulus value of 20 ksi with temperature stresses

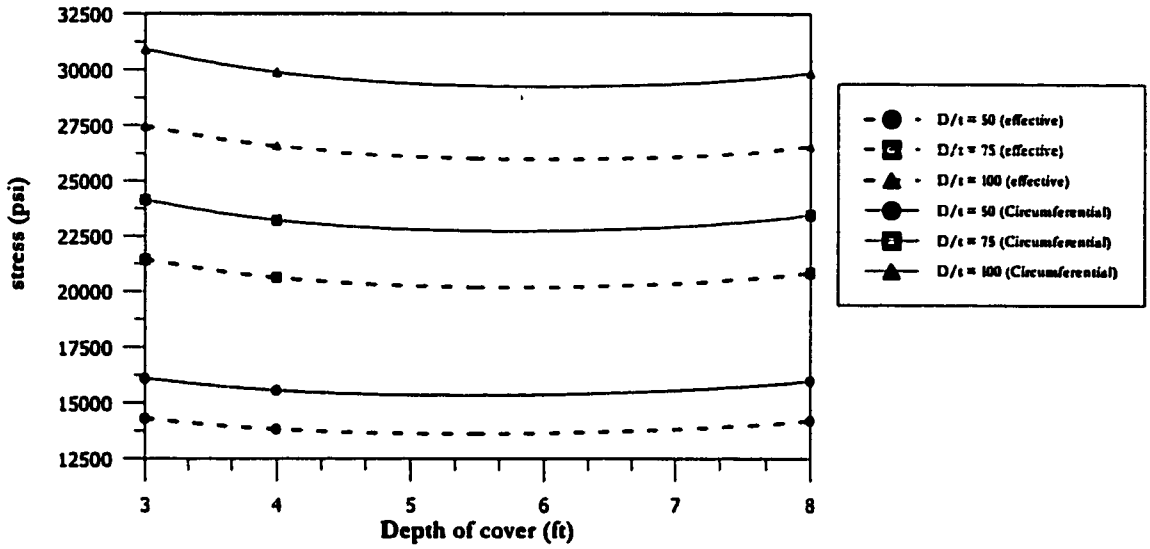

(a) Without temperature effect

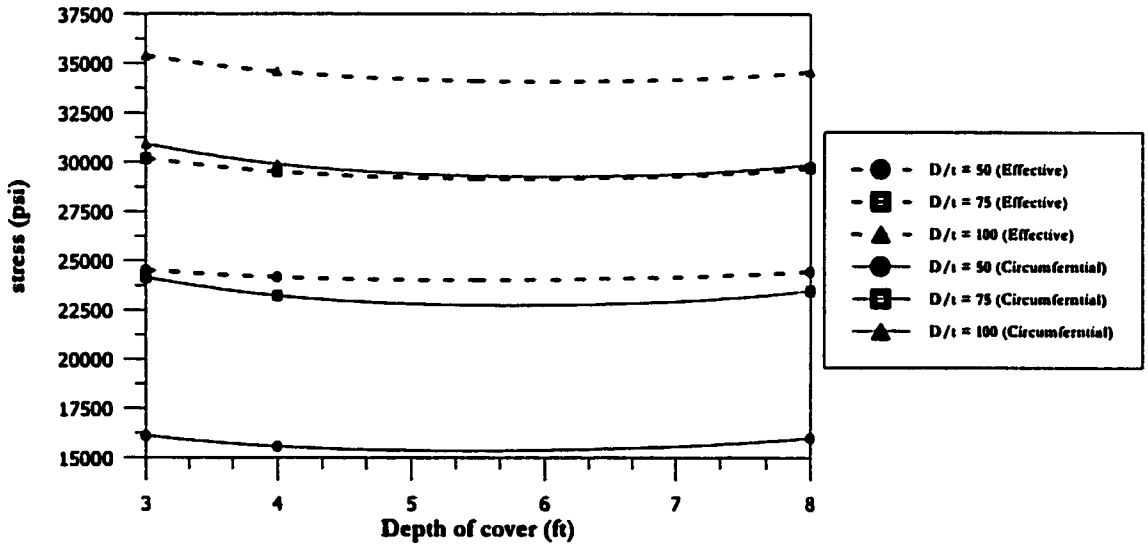

(b) With temperature effect

Fig. 7.121: Comparison of total circumferential stress and effective stresses for 12 inch diameter pipe

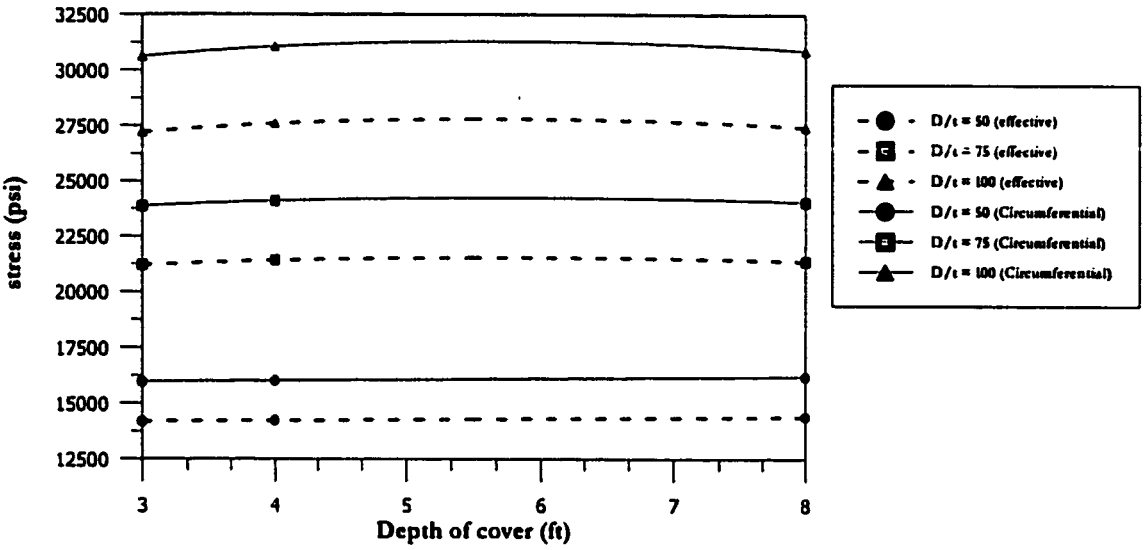

(a) Without temperature effect

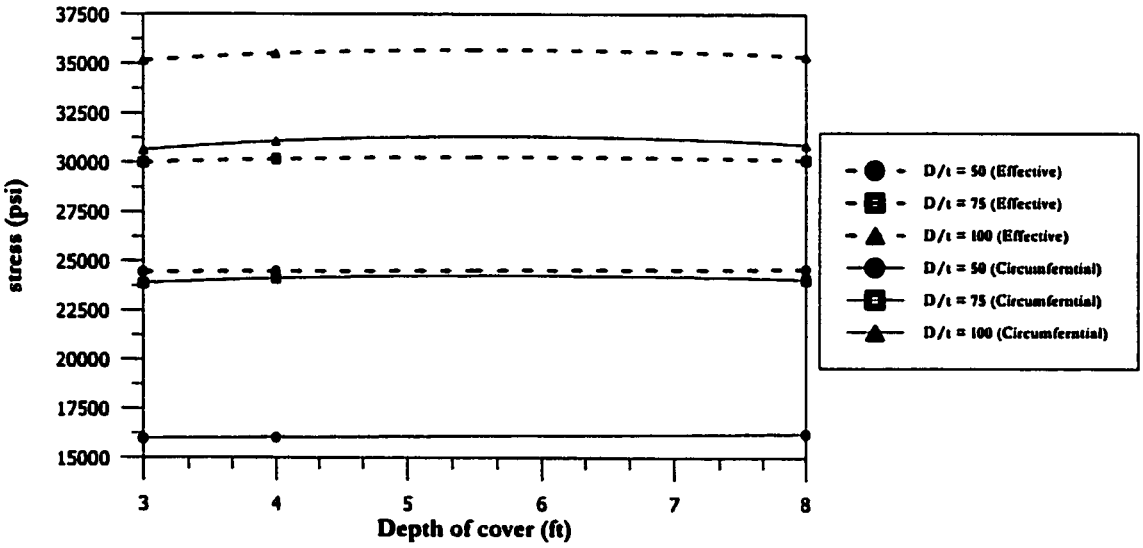

(b) With temperature effect

Fig. 7.122: Comparison of total circumferential stress and effective stresses for 24 inch diameter pipe

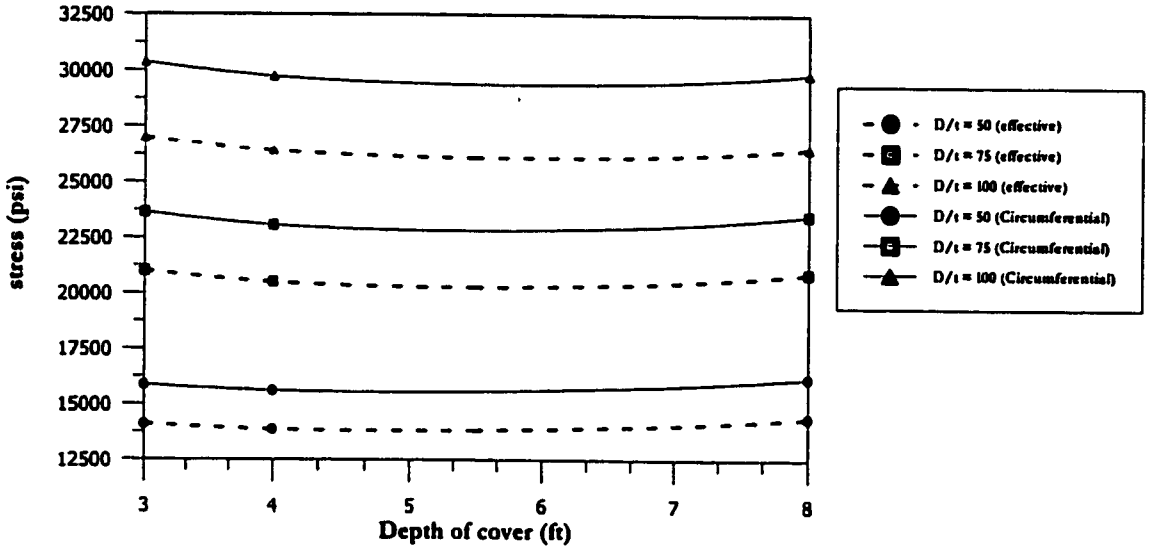

(a) Without temperature effect

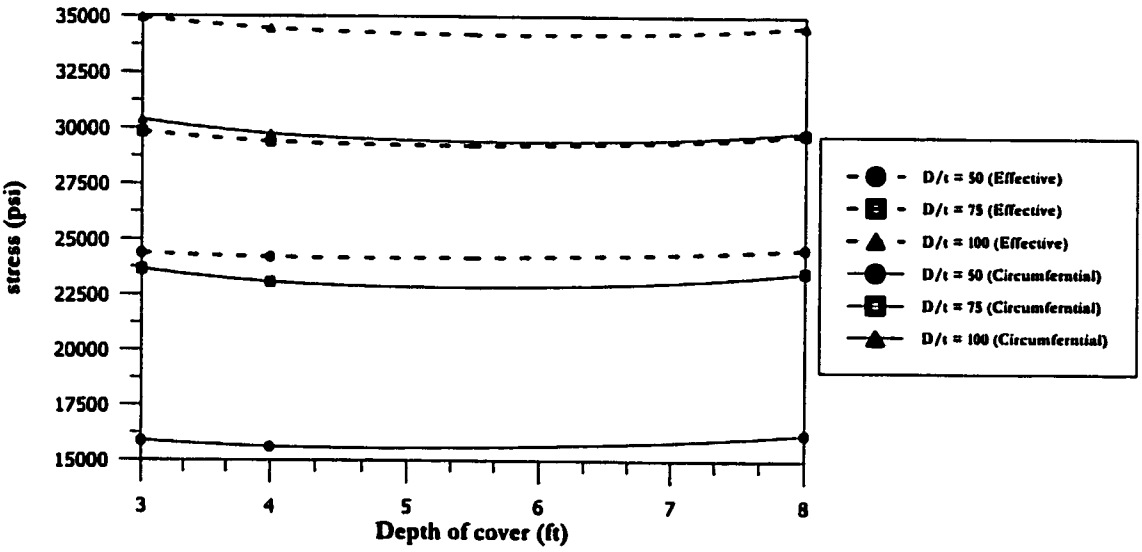

(b) With temperature effect

Fig. 7.123: Comparison of total circumferential stress and effective stresses for 36 inch diameter pipe

CHAPTER 8

DEVELOPMENT OF REGRESSION MODELS

8.1 Introduction

In order to develop design methods for pipelines under sand overburden and crossing highways it is decided to develop regression models from the finite element results presented in Chapter 7. Separate regression models are developed for the pipelines subjected to sand overburden and crossing highways. These models are capable of predicting pipe stresses and diameter changes in the buried pipelines.

8.2 Development Of Regression Equations For The Pipe Under Sand Overburden

8.2.1 Selection of Design Variables

This section explains the approach taken to formulate the design equations for the sand overburden problem. The parameters used in the development of the regression equations

are discussed in details in Section 7.3. CANDE software is used to calculate the different stresses in addition to the change in the pipe diameter for the four types of native soils considered in this study. A total of 100 finite element runs are made, in which the sand overfill is varied from 1 to 60 ft. for each of the soil types. In each of the finite element runs, the one foot depth of cover is activated in a separate construction increment, which enables getting the circumferential stress and the change in diameter for depths of cover from 1 to 60 ft. in an increment of 1 ft. from a single finite element simulation. The total number of analysis cases for each soil type is 1,500. The outputs of the finite element runs are summarized in tabular forms that include the absolute maximum stress and the change in the diameter.

From the generated data of the finite element runs, it is decided to build models that can predict the absolute maximum stress and the change in the pipe's diameter for the four types of the soils used in this research.

Linear multiple regression is used to build the relationships between the independent and the dependent variables. The independent variables are the pipe's diameter, wall's thickness, and depth of cover. The dependent variables are the absolute maximum stress and the change in the pipe's diameter.

The general purpose of the multiple regression is to assess statistical relationship between several independent or predictor variables and a dependent or criterion variable and to build models that enable the prediction of the dependent variables from the values of the independent variables. The principles of multiple linear regression are outlined in refrences

[90, 91]. The general form of the linear multiple regression model is:

$$Y = \beta_o + \beta_1 x_1 + \beta_2 x_2 + \ldots\ldots\ldots\ldots\ldots\ldots + \beta_k x_k + \varepsilon \qquad (8.1)$$

where,

Y = dependent variable,

β_i = regression coeiffecient,

x_i = independent variables, and

ε = random error with mean equals zero and variance equals σ^2.

The least squares method, which aims at decreasing the error term, is used to predict the regression coefficients.

8.2.2 Selection of Cases for Models Validation

To test the validity of the developed models in correctly predicting both the values of absolute maximum stress and diameter change, 39 cases out of the 1500 cases for each soil are selected randomly. These runs are not used in developing the models, but are used in to test the acuracy of the generated models in predicting the dependent variables. Tables 8.1 and 8.2 show the selected validation runs for the different soils.

8.2.3 Correlation Matrices of the Variables

To check the relationships between the variables used in the models, correlation matrices are obtained. The correlation matrices are obtained using the state of the art statistical software STATISTICA [92]. Table 8.3 shows the correlation matrices for the variables

TABLE 8.1: Selected validation runs for low and high density sand as native soils for pipe subjected to sand overburden

Observation number	Pipe Diameter (in)	Thickness of Pipe Wall (in)	Depth of Cover (ft)	Types of underlying soil			
				Sand at low density		Sand at high density	
				Abs. Max. Stress (psi)	Diameter Change (in)	Abs. Max. Stress (psi)	Diameter Change (in)
16	12	0.24	16	6165	-0.036	5671	-0.033
54	12	0.24	54	16167	-0.092	15319	-0.088
68	12	0.16	8	4666	-0.041	4260	-0.036
90	12	0.16	30	13403	-0.11	11870	-0.099
107	12	0.16	47	17795	-0.141	15948	-0.131
139	12	0.12	19	10130	-0.106	8705	-0.093
172	12	0.12	52	18920	-0.183	16840	-0.166
249	12	0.08	9	5369	-0.08	4543	-0.069
298	12	0.08	58	18080	-0.222	15950	-0.202
321	24	0.48	21	7749	-0.094	7464	-0.087
361	24	0.32	1	1290	-0.022	1052.5	-0.0159
393	24	0.32	33	14147	-0.239	12524	-0.211
414	24	0.32	54	19003	-0.31	17141	-0.282
427	24	0.24	7	4639	-0.109	4134	-0.093
448	24	0.24	28	13248	-0.28	11142	-0.237
471	24	0.24	51	18780	-0.376	16140	-0.329
494	24	0.192	14	8003	-0.21	6566	-0.173
531	24	0.192	51	18290	-0.419	15340	-0.362
562	24	0.16	22	10611	-0.3	8596	-0.245
593	24	0.16	53	17780	-0.456	14810	-0.388
612	36	0.72	12	4833	-0.086	4890	-0.083
632	36	0.72	32	10847	-0.198	10726	-0.186
670	36	0.48	10	5705	-0.153	5301	-0.135
703	36	0.48	43	16621	-0.41	14590	-0.363
752	36	0.36	32	14346	-0.445	11947	-0.373
812	36	0.288	32	14053	-0.507	11553	-0.413
853	36	0.24	13	7272	-0.324	5794	-0.26
911	48	0.96	11	5208	-0.123	4696	-0.103
940	48	0.96	40	13602	-0.32	12903	-0.293
988	48	0.64	28	14556	-0.476	11070	-0.372
1067	48	0.48	47	21370	-0.81	15480	-0.611
1114	48	0.384	34	18291	-0.821	12220	-0.567
1188	48	0.32	48	20990	-1.01	14300	-0.716
1213	60	1.2	13	4446	-0.12	5530	-0.152
1260	60	1.2	60	15843	-0.44	17096	-0.476
1293	60	0.8	33	14850	-0.63	12165	-0.514
1332	60	0.6	12	12471	-0.68	5825	-0.328
1396	60	0.48	16	14348	-0.93	7061	-0.448
1459	60	0.4	19	14938	-1.1	7600	-0.533

TABLE 8.2: Selected validation runs for marl and sabkha as native soils for pipe subjected to sand overburden

				Types of underlying soil			
				Marl		Sabkha	
Observation number	Pipe Diameter (in)	Thickness of Pipe Wall (in)	Depth of Cover (ft)	Abs. Max. Stress (psi)	Diameter Change (in)	Abs. Max. Stress (psi)	Diameter Change (in)
16	12	0.24	16	6751	-0.04	8370	-0.049
54	12	0.24	54	19870	-0.116	23683	-0.139
68	12	0.16	8	5305.7	-0.0456	6643	-0.059
90	12	0.16	30	15757	-0.131	19273	-0.166
107	12	0.16	47	21783	-0.178	26098	-0.222
139	12	0.12	19	11775	-0.125	14605	-0.161
172	12	0.12	52	23620	-0.237	28050	-0.297
249	12	0.08	9	6185	-0.0927	7713	-0.122
298	12	0.08	58	22520	-0.295	26390	-0.369
321	24	0.48	21	9148	-0.111	10854	-0.13
361	24	0.32	1	1465	-0.0229	1822.9	-0.029
393	24	0.32	33	17203	-0.298	20518	-0.364
414	24	0.32	54	24305	-0.405	28114	-0.48
427	24	0.24	7	5688	-0.131	6995	-0.167
448	24	0.24	28	16184	-0.348	19403	-0.435
471	24	0.24	51	23570	-0.502	27400	-0.61
494	24	0.192	14	9780	-0.256	11876	-0.329
531	24	0.192	51	22790	-0.557	26430	-0.69
562	24	0.16	22	12904	-0.372	15640	-0.48
593	24	0.16	53	22090	-0.612	25440	-0.748
612	36	0.72	12	6204.1	-0.111	6914	-0.124
632	36	0.72	32	13209	-0.238	15613	-0.27
670	36	0.48	10	7309	-0.196	8568	-0.233
703	36	0.48	43	20809	-0.53	23916	-0.63
752	36	0.36	32	17896	-0.572	21012	-0.71
812	36	0.288	32	17594	-0.652	20718	-0.8
853	36	0.24	13	9358	-0.413	11243	-0.53
911	48	0.96	11	6109.2	-0.142	6592	-0.15
940	48	0.96	40	15804	-0.37	18287	-0.43
988	48	0.64	28	15924	-0.55	18345	-0.65
1067	48	0.48	47	23280	-0.99	26500	-1.17
1114	48	0.384	34	18964	-0.94	22086	-1.15
1188	48	0.32	48	22010	-1.23	25060	-1.46
1213	60	1.2	13	7044	-0.204	7509	-0.23
1260	60	1.2	60	21410	-0.63	24260	-0.71
1293	60	0.8	33	17835	-0.78	20122	-0.9
1332	60	0.6	12	9617	-0.538	11155	-0.65
1396	60	0.48	16	11839	-0.763	13952	-0.94
1459	60	0.4	19	12945	-0.924	15264	-1.15

TABLE 8.3: Correlation matrix for the variables used in the sand overburden problem for all the soiltypes

	Correlation Coefficient					
	Variables	Diameter	Thickness	Cover	ABS. Max. Stress	Diamter change
Sand at low density	Diameter	1.00	.719378	.001991	.221941	-.685786
	Thickness	0.71937	1.0000	.001741	-.049532	-.137090
	Cover	.001991	.001741	1.0000	.891289	-.403152
	ABS. Max.Stress	.221941	-.049532	.891289	1.000	-.710081
	Diameter change	-.68578	-.137090	-.403152	-.710081	1.0000
Sand at high density	Diameter	1.000	-.71378	.001991	.000277	-.654334
	Thickness	.719378	1.000	.001741	-.011038	-.189229
	Cover	.001991	.001741	1.0000	.982145	-.562026
	ABS. Max.Stress	.000277	-.011038	.982145	1.0000	-.564447
	Diameter change	-.654334	-.189229	-.562026	-.564447	1.00000
Marl	Diameter	1.000	.719387	.001991	.073684	-.647110
	Thickness	.719378	1.000	.001741	-.064804	-.141440
	Cover	.001991	.001741	1.0000	.961040	-.517870
	ABS. Max.Stress	.073684	-.064804	.961040	1.0000	-.633637
	Diameter change	-.647110	-.141440	-.517870	-.633637	1.00000
Sabkha	Diameter	1.0000	.719378	.001991	.023456	-.635546
	Thickness	.719378	1.0000	.001741	-.108722	-.111348
	Cover	.001991	.001741	1.0000	.957165	-.506231
	ABS. Max.Stress	.023456	-.108722	.957165	1.0000	-.597971
	Diameter change	-.635546	-.111348	-.506231	-.597971	1.0000

used for all types of soils. Correlation coefficients provide a normalized and scale-free measure of the association between two variables. The correlation coefficient value ranges between -1 and +1. A positive correlation coefficient indicates that the variables vary in the same direction, while a negative coefficient indicates that the variables vary in the opposite direction. Statistically independent variables have an expected correlation coefficient of zero.

In Table 8.3, the correlation matrices include both the dependent variables (DV) and the independent variables (IV). The following can be concluded from the generated correlation matrices:

- The soil type does not affect the relation between the IV's, i.e., the correlation coefficients of the IV's don't change with the change in the type of native soil.
- Since the depth of cover is varied from 1 to 60 ft. for all pipe diameters and pipe wall thicknesses, there is no correlation between the depth of cover and those two variables (0.001991 and 0.001741, respectively).
- There is a positive correlation between the pipe's diameter and the absolute maximum stress.
- The highest correlation coefficient between the pipe's diameter and the maximum absolute stress is for sand at low density (0.221941), then marl at low density (0.073684), then sabkha at high density (0.023456), followed by sand at high density (0.000277). As the density of sand increases, the correlation between the pipe's diameter and the absolute maximum stress is lost (the correlation coefficient reduced from 0.221941 to 0.000277 due to the increase in sand density).

- There is a negative correlation between the thickness of the pipe's wall and the absolute maximum stress indicating more stresses in pipes with smaller thickness.
- There is a strong positive correlation between the height of the sand overfill and the maximum absolute stress (correlation coefficient values range between 0.891289 and 0.982145 for the different native soils).
- The relation among all the IV's with a diameter change is negative and relatively strong.
- The diameter change has the highest correlation coefficient with the pipe's diameter (correlation coefficient values range between -0.635546 and -0.685786 for the different native soils).

8.2.4 Linearization of the Relationships

To view the shape of the relation between the IV's and the DV's, a set of values from the data of the pipe with low density sand as native soil is selected and drawn in Figs. 8.1 to 8.6. Fig. 8.1 shows the effect of pipe's diameter on the absolute maximum stress for a pipe having 0.48 inch wall thickness under 10 ft. depth of cover. Fig. 8.2 shows the effect of pipe's wall thickness on the absolute maximum stress for a pipe with 12 inch diameter under 10 ft. depth of cover, while Fig. 8.3 shows the effect of the depth of the cover on the absolute maximum stress for a pipe with 12 inches diameter and 0.48 inch wall thickness. Figs. 8.4 to 8.6 show the effects of pipe's diameter, pipe's wall thickness, and depth of cover on the amount of change in the pipe's diameter, respectively.

It can be seen from Figs. 8.1 to 8.6 that the relationships between the IV's and DV's are not linear. To build linear models that relate the IV's and DV's, it is required to find

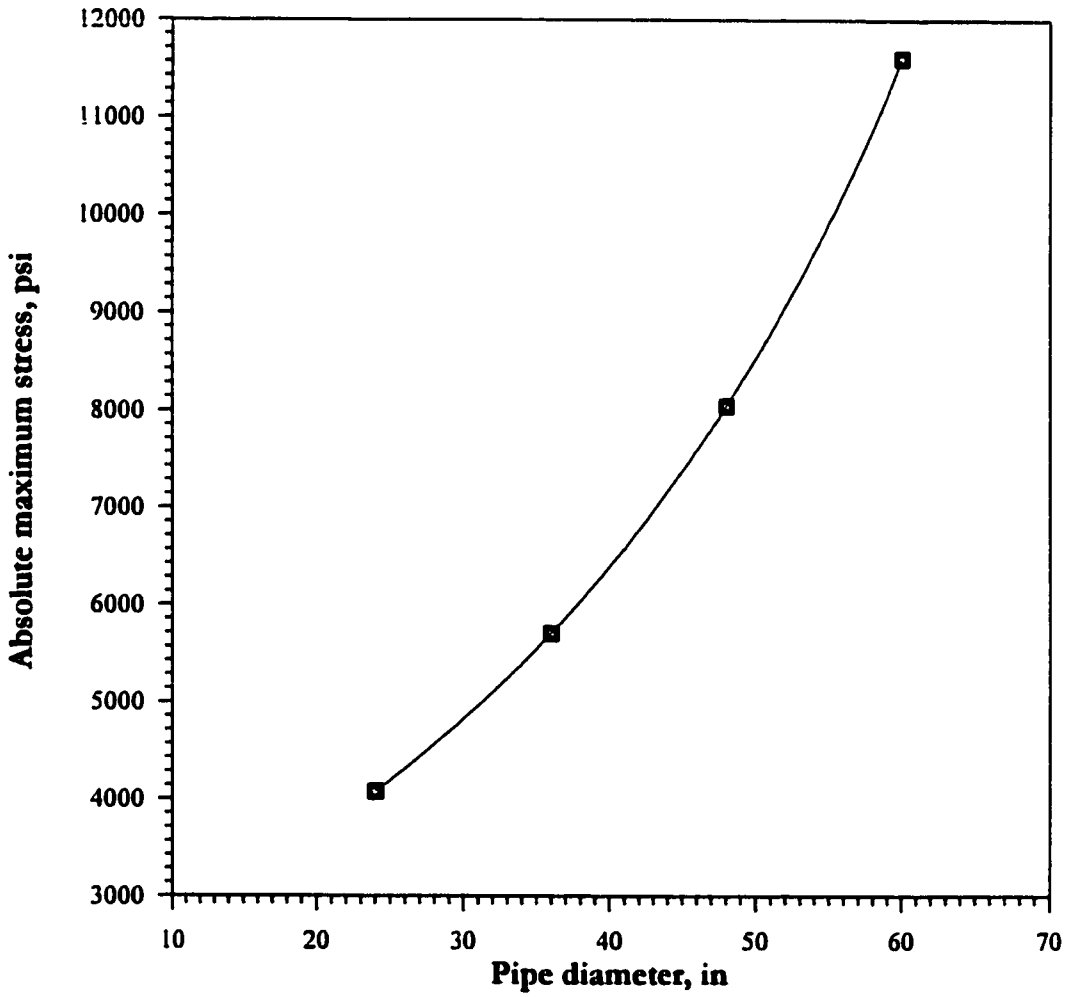

Fig. 8.1: Effect of changing the pipe diameter on absolute maximum stress for a pipe with t = 0.48 inch and H = 10 ft

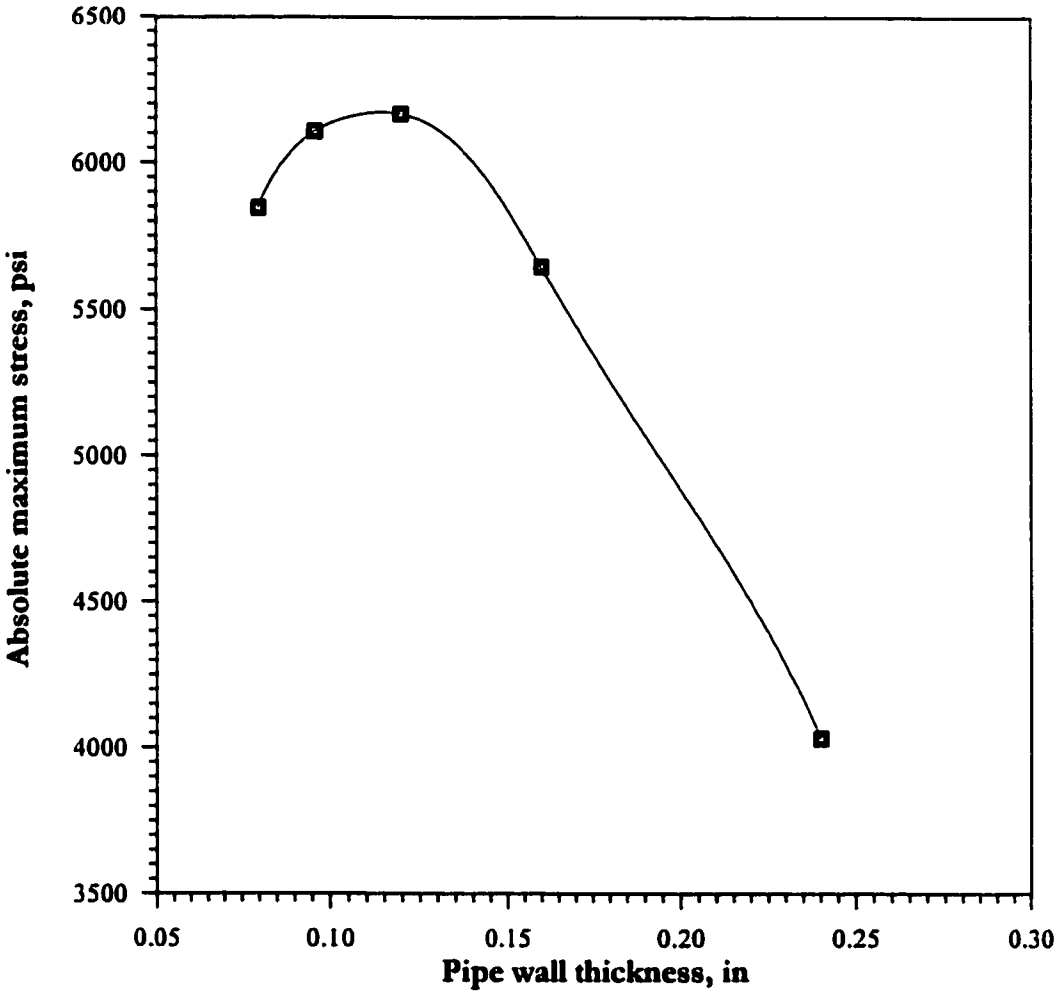

Fig. 8.2: Effect of changing the pipe wall thickness on the absolute maximum stress for a pipe with D = 12 inch and H = 10 ft.

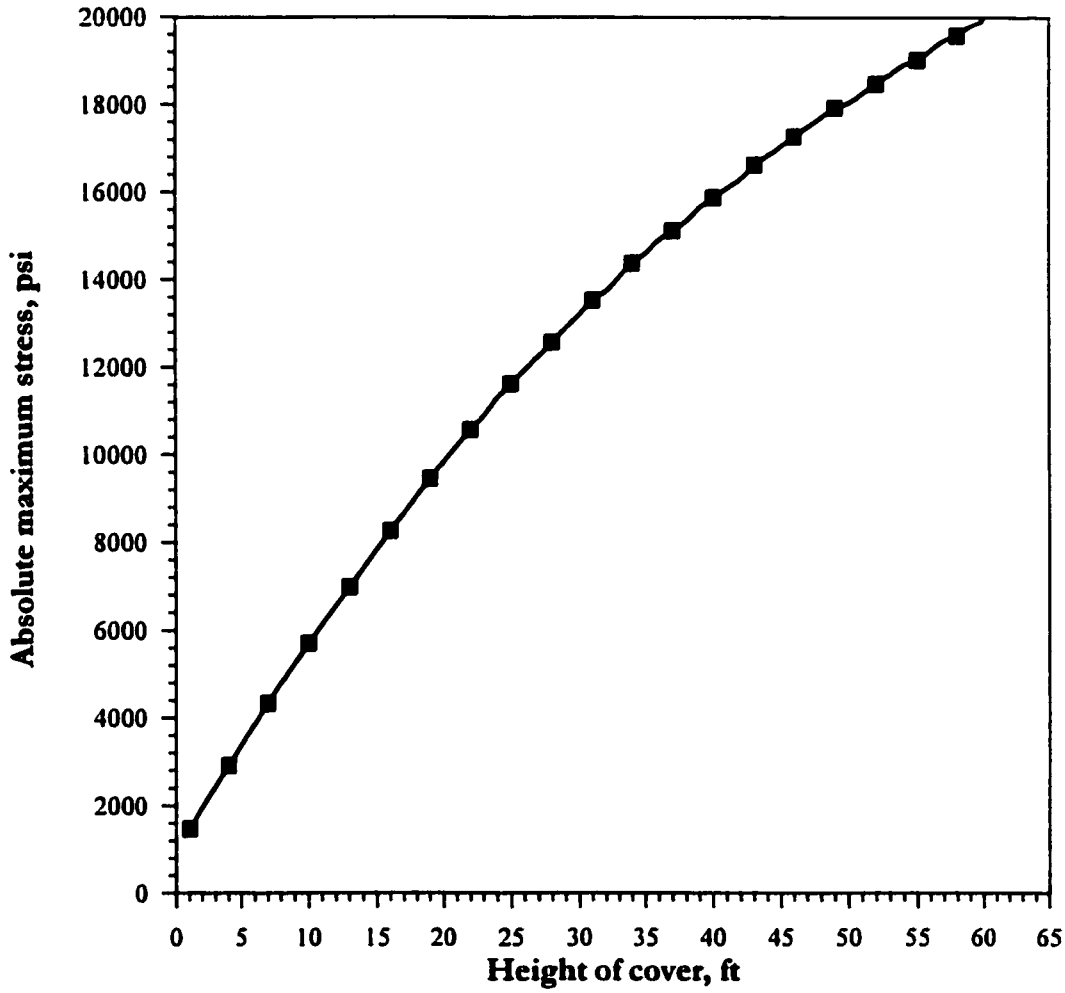

Fig. 8.3: Effect of changing the depth of cover on the absolute maximum stress for a pipe with D = 36 inch and t = 0.48 inch

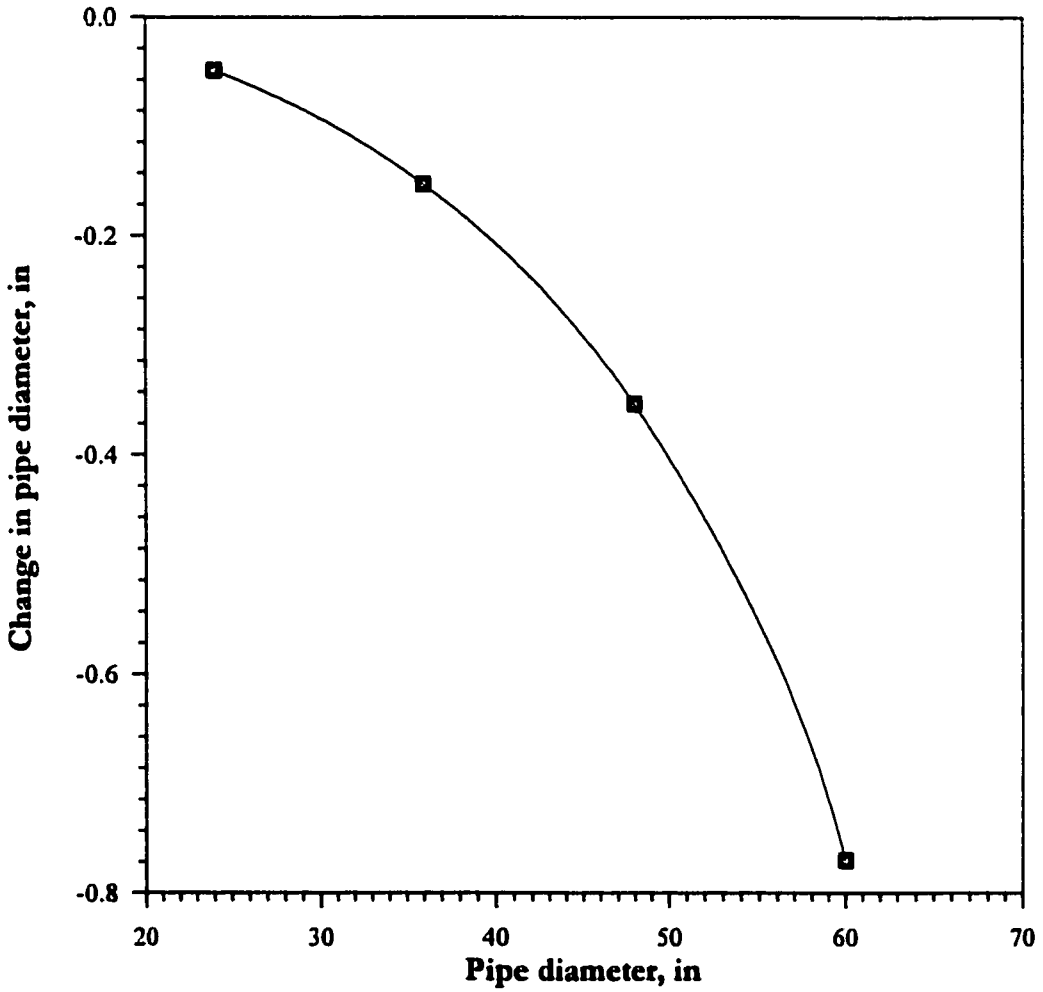

Fig. 8.4: Effect of changing the diameter of the pipe on the change in diameter of pipes having t = 0.48 inch and H = 10 ft.

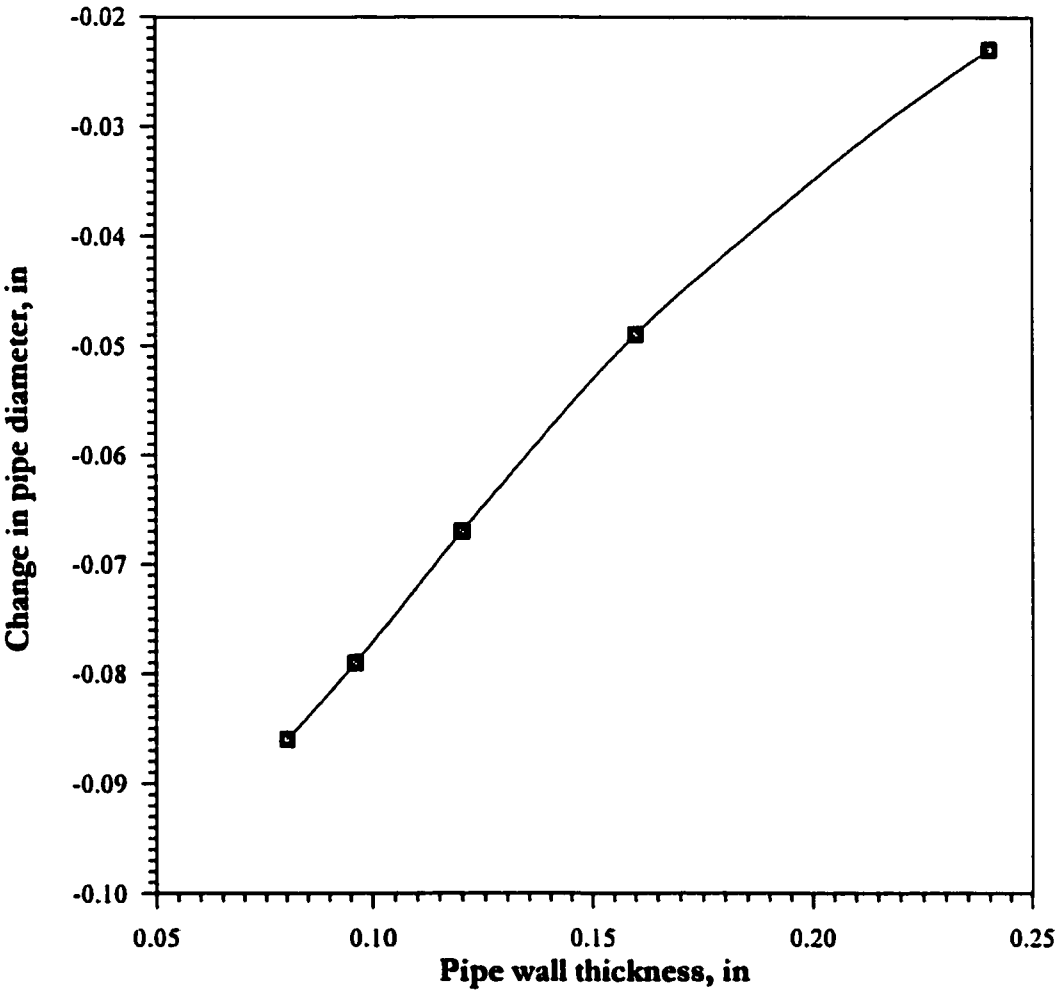

Fig. 8.5: Effect of changing the pipe wall thickness on the change in diameter of a pipe with D = 12 inch and H = 10 ft.

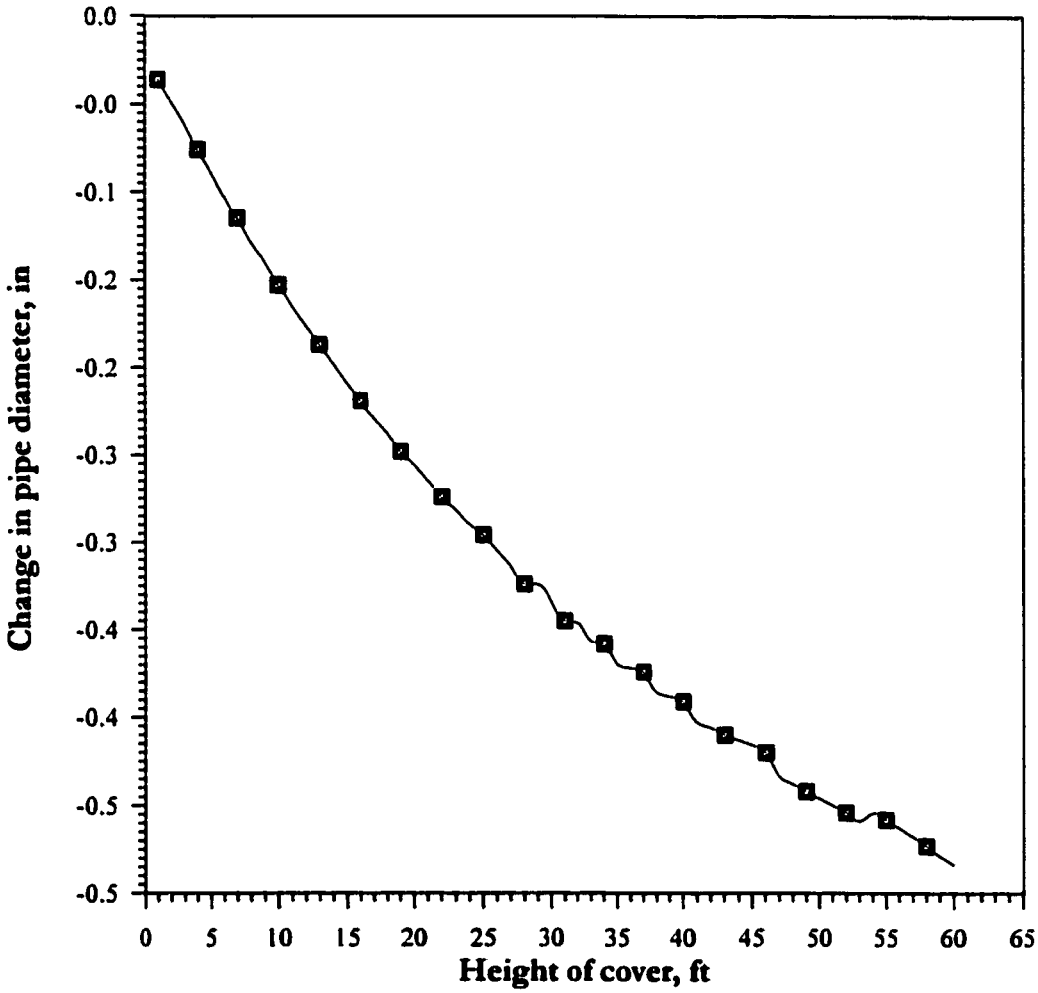

Fig. 8.6: Effect of changing the depth of cover on the change in diameter of the pipe with D = 36 inch and t = 0.48 inch

ways and means to linearize the relationships between each one of the IV's and each one of the DV's. Numerous trial and errors were implemented to find the best method to linearize the relationships. Figs. 8.7 to 8.9 show the linearized relations between the IV's and the absolute maximum stress. The square values of the pipe's diameter versus the square root values of the absolute maximum stress are used to linearize their relationship (Fig. 8.7). Fig. 8.8 shows that squaring the values of the pipe's wall thickness is the best method to linearize the relationship with the square root values of the absolute maximum stress, whereas, using the square roots of the height of cover values is the optimal procedure to linearize the relation with the square root values of the absolute maximum stress (Fig. 8.9). Squaring the values of the pipe's diameters and taking the square roots of the pipe's wall thickness and height of covers are used to linearize the relation with the exponential values of the change in the pipe's diameter (Figs. 8.10 to 8.12).

8.2.5 Developed Equations

A linear multiple regression procedure, included in STATISTICA personal computer software, is used to generate the required prediction models that relate the IV's (pipe's diameter, pipe's wall thickness and depth of cover) with the DV's (absolute maximum stress and change in diameter). Since more than one IV are used in each prediction model and some relation is present between these IV's, a number of trials are performed to increase the goodness of fit (R^2) of the prediction equations by using different combinations of transformed independent and dependent variables. The models that have the highest R^2 values are selected. R^2 is an indication of the percent of variance in the dependent variable

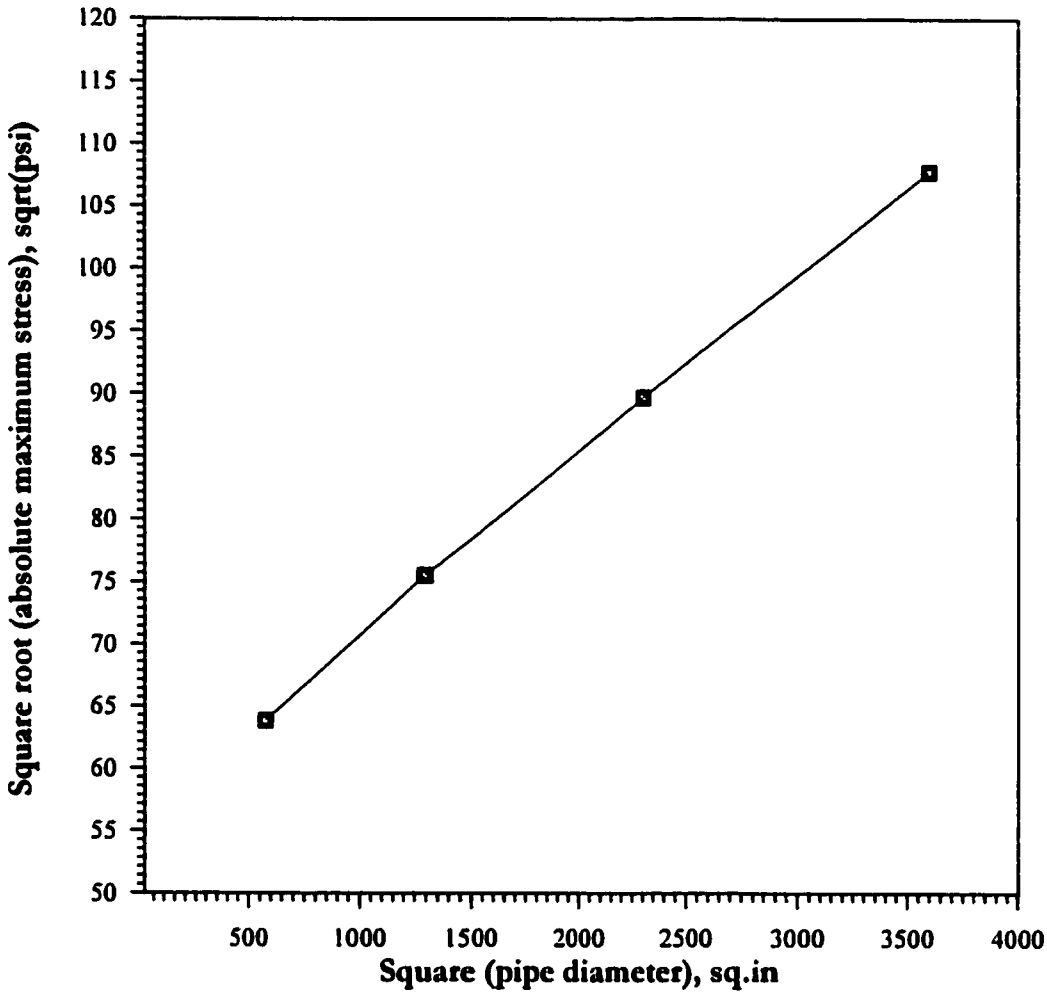

Fig. 8.7: Linearization of the change in pipe diameter vs. absolute maximum stress relation for a pipe with t = 0.48 inch and H = 10 ft.

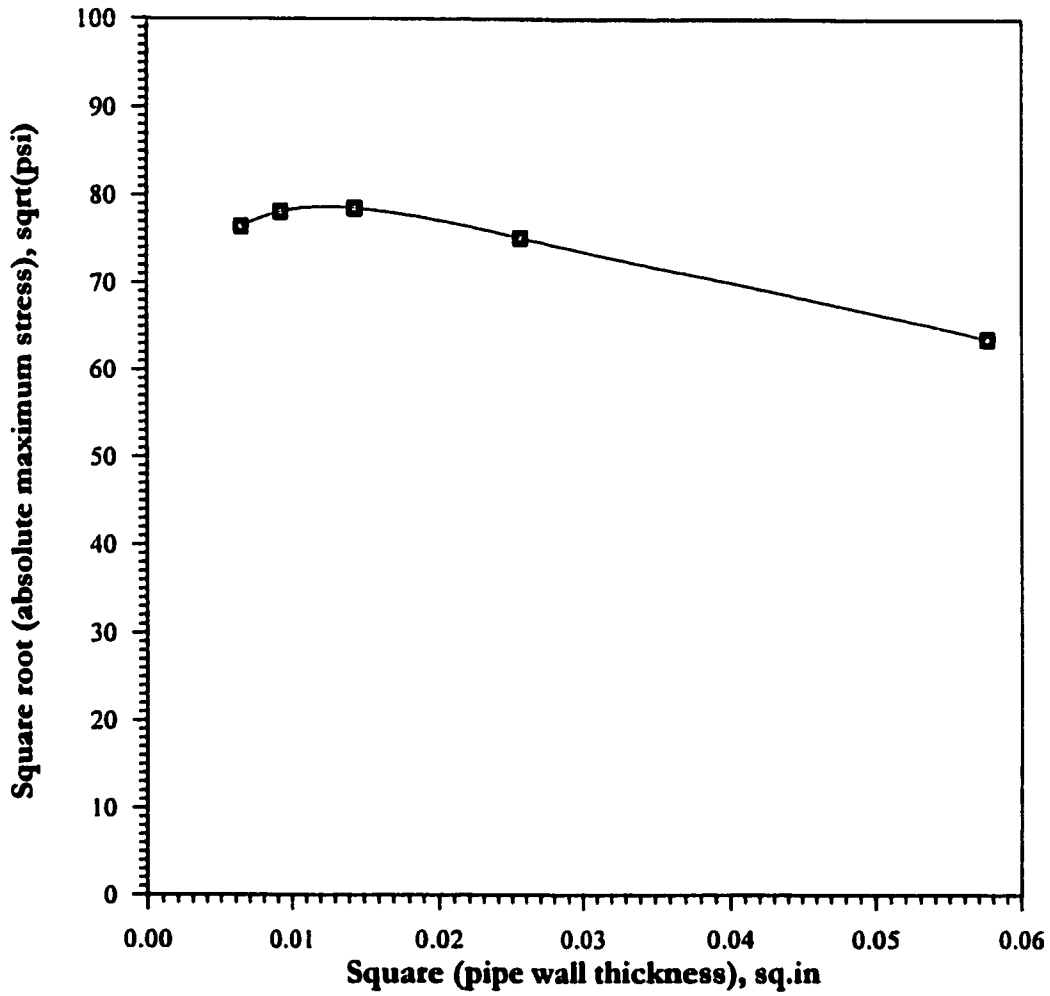

Fig. 8.8: Linearization of the change in pipe wall thickness vs. absolute maximum stress for a pipe with D = 12 inch and H = 10 ft.

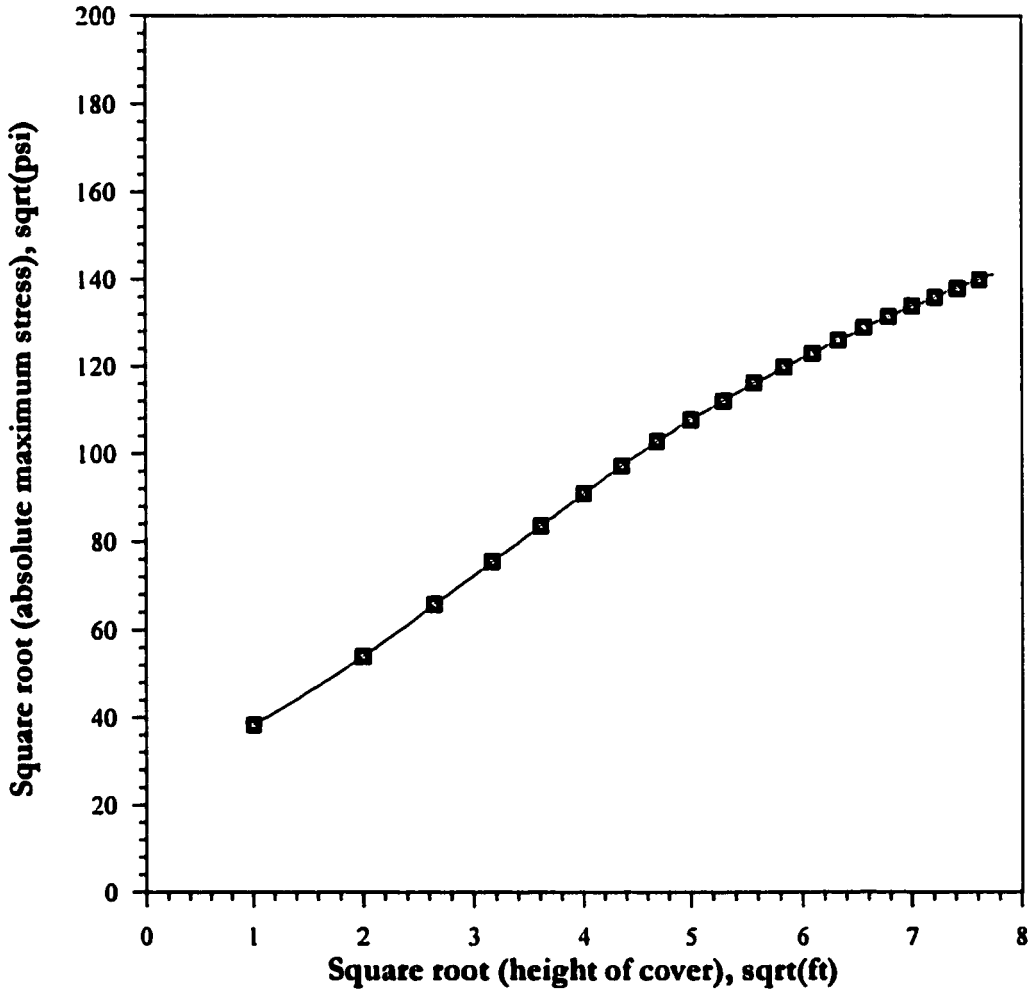

Fig. 8.9: Linearization of change in depth of cover vs. the absolute maximum stress for a pipe with D = 36 inch and t = 0.48 inch

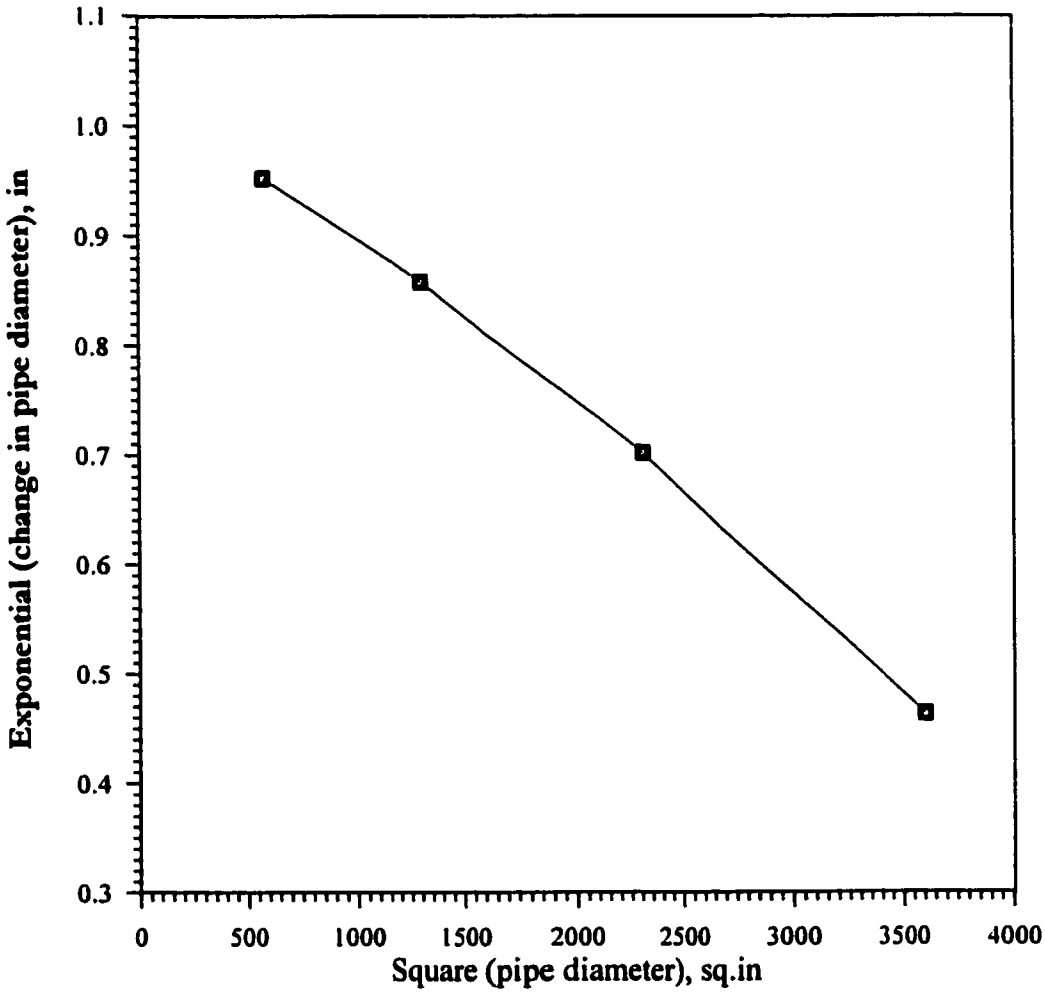

Fig. 8.10: Linearization of the change in pipe diameter vs. diameter deflection relation for a pipe with t = 0.48 inch and H = 10 ft.

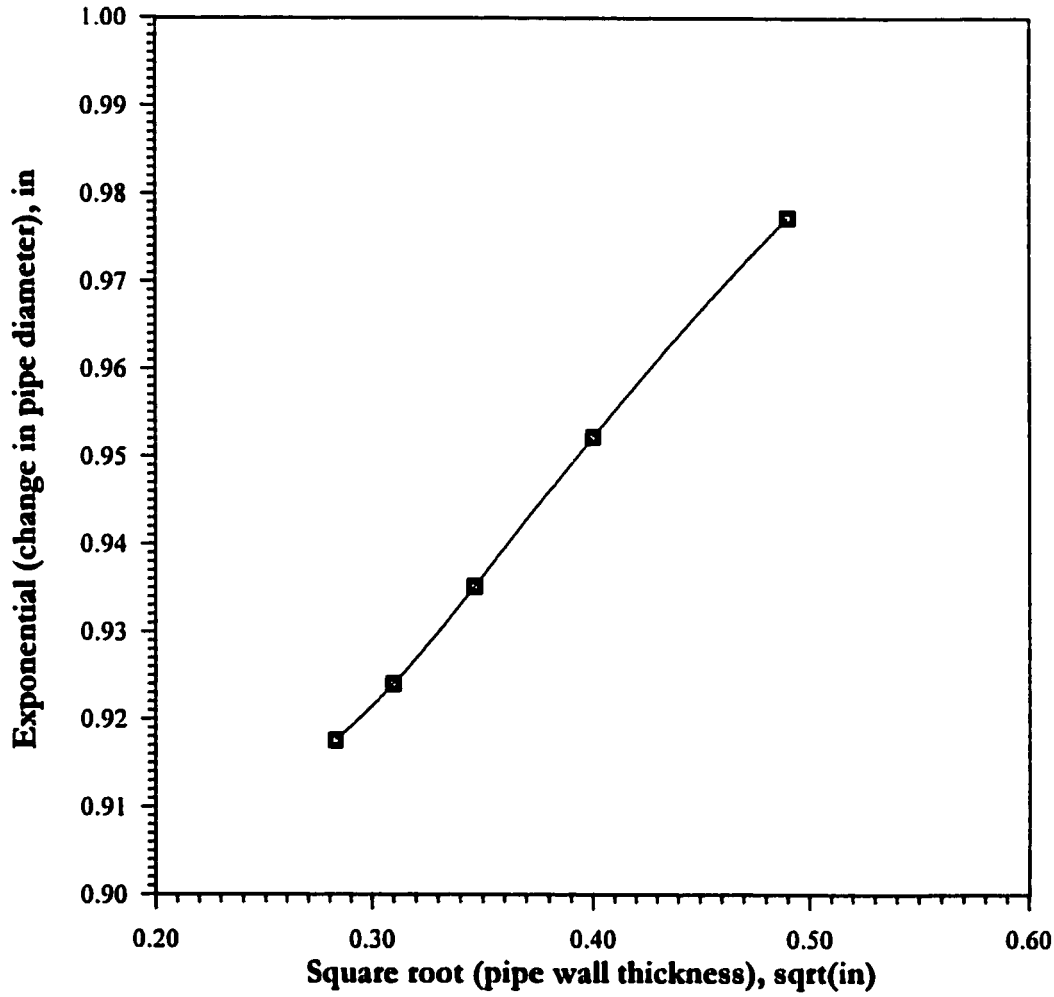

Fig. 8.11: Linearization of change in pipe wall thickness vs. change of diameter for a pipe with D = 12 inch and H = 10 ft.

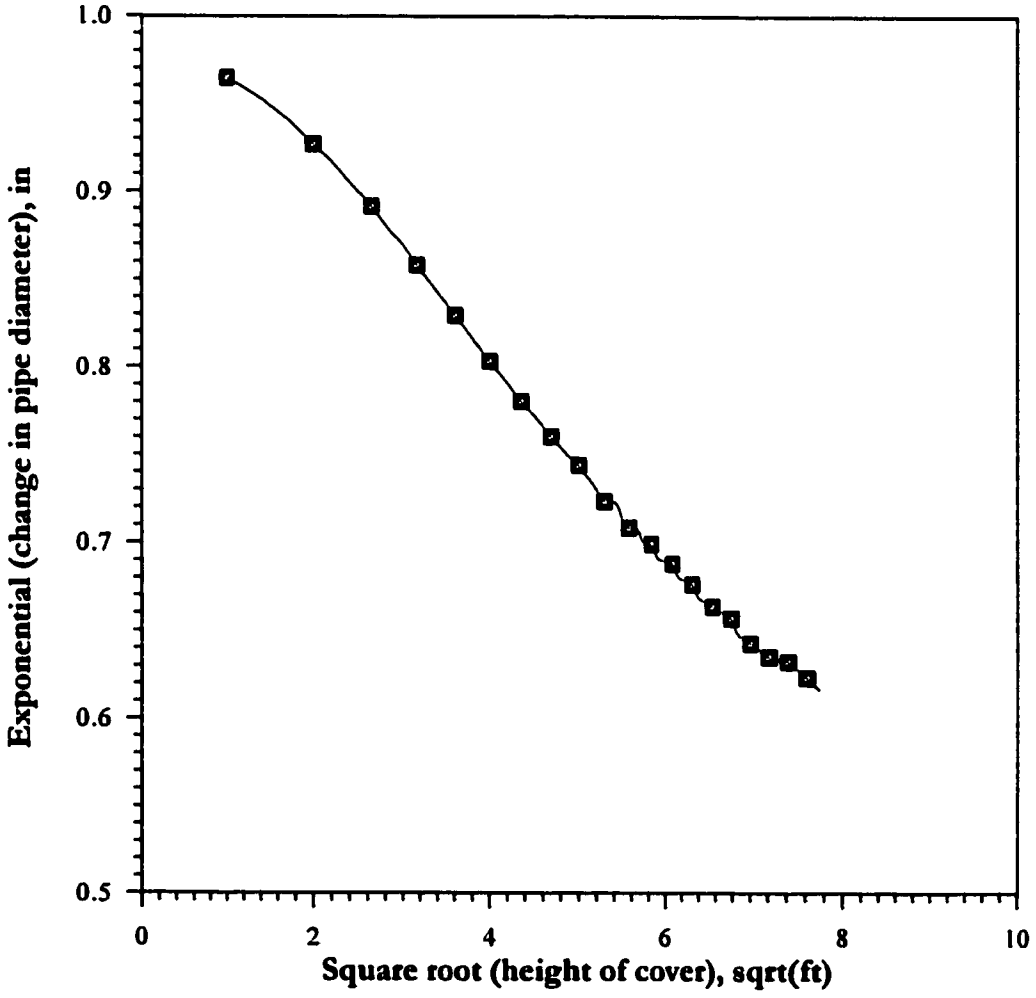

Fig. 8.12: Linearization of change in depth of cover vs. change in diameter for a pipe with D = 36 inch and t = 0.48 inch

explained by the model. Table 8.4 shows the developed transformed prediction models for both the absolute maximum stress and the diameter change for all types of native soils. In addition, the coefficient of determination (R^2) and the significance levels of the models are shown in that table. R^2 values for the developed models are higher than 0.94. In addition, the confidence levels for all the models are higher than 99.99%. Tables 8.5 to 8.12 give the model fitting results and the analysis of the variance for each model.

In the model fitting results, the coefficients of all variables introduced in the model are given, in addition to their t-value statistics and significance levels. It is worth noting that all of the parameters used have a confidence level of 99.9%. It is also observed that when fitting the models, the transferred variables are used for both the DV's and IV's. In the analysis of variance tables, the confidence levels of all the fitted models are above 99.99%.

Figs. 8.13 to 8.20 show plots of the predicted values versus the originally calculated values for all the models. The figures show the distribution of the points around the 45° line. In these figures, all the points are located around the 45° lines with minor disturbance. This indicates the accuracy of the generated models in predicting the DV's.

8.2.6 Testing Of Models

8.2.6.1 Sign Testing

The sign test is performed to check if the variables' signs in the developed models are according to the expected relationships between the independent and dependent variables. The following observations about the obtained signs in the developed models can be noticed:

TABLE 8.4: Generated models for the absolute maximum stress and diameter change for the different types of soils

Native Soil	Generated Model	R^2	Significance
Low Density	Stress = $-4.13054 + 2.21 * (D)^2 - 7079.25 * (t)^2 + 2969.83 * (H)^{\frac{1}{2}}$	0.9697	0.000
Sand	$\Delta D = \ln[1.529 - 0.0145 * (D) + 0.533 * (t) - 0.0508 * (H)^{\frac{1}{2}}]$	0.9612	0.000
High Density	Stress = $-2822.30 + 0.060 * (D)^2 - 343.31 * (t)^2 + 2549.65 * (H)^{\frac{1}{2}}$	0.9786	0.000
Sand	$\Delta D = \ln[1.221 - 0.095 * (D) + 0.3122 * (t) - 0.0498 * (H)^{\frac{1}{2}}]$	0.9406	0.000
Marl	Stress = $[26.081 + 0.438 * (D) - 26.211 * (t) + 16.835 * (H)^{\frac{1}{2}}]^2$	0.9734	0.000
	$\Delta D = \ln[1.283 - 0.0138 * (D) + 0.4935 * (t) - 0.0643 * (H)^{\frac{1}{2}}]$	0.9502	0.000
Sabkha	Stress = $[33.815 + 0.4045 * (D) - 30.181 * (t) + 17.735 * (H)^{\frac{1}{2}}]^2$	0.9688	0.000
	$\Delta D = \ln[1.270 - 0.0150 * (D) + 0.5626 * (t) - 0.0685 * (H)^{\frac{1}{2}}]$	0.9491	0.000

Stress = Absolute maximum stress (psi)
ΔD = Change in pipe's diameter (in.)
t = Pipe's wall thickness (in.)
D = Pipes's diameter (in.)
H = height of sand cover (ft)

TABLE 8.5: Model fitting results and analysis of variance for the prediction of the absolute maximum stress for the pipe with low density sand as native soil

Model fitting results for absolute maximum stress						
$N = 1461$	BETA	St. Err. of BETA	B	St. Err. of B	t(1457)	p-level
Intercept			-4130.54	89.5424	-46.1294	0.00
$(\text{Diameter})^2$	.476804	.005687	2.21	0.0269	82.2621	0.00
$(\text{Thickness})^2$	-.391523	.005687	-7079.25	102.8232	-68.8484	0.00
$(\text{Cover})^{\frac{1}{2}}$	.903376	.004557	2969.83	14.9823	198.2230	0.00
Analysis of Variance						
Effect	Sums of squares	df	Mean Squares	F	p-level	
Regress.	491051E5	3	163683E5	15563.43	00.00	
Residual	153236E4	1457	1051720			
Total	506374E5					

N = number of cases included for model devlopment

BETA = the value of Beta distribution of the parameter

St. Err. of Beta = the estimate of the standard error of the Beta distribution of the parameter

B = the estimate of the parameter value

St. Err. of B = the estimate of the standard deviation of the parameter estimate

df = degrees of freedom associated for the terms

$t(df)$ = the t test that the parameter is zero, calculated by dividing the value of the parameter by the standard error of the parameter

p-level = the probability of getting a greater t or F statistic than that observed if the hypothesis is true. It is the significance probability

Sums of Squres = sum of square of the terms

Mean of Squares = the sum of squares divided by the degrees of freedom

F = the F value for testing the hypothesis that all parametres are zero except for the intercept. It is formed by dividing the mean square for the regressors (model) by the mean square of residuals

TABLE 8.6: Model fitting results and analysis of variance for the prediction of change in diameter for the pipe with low denity sand as native soil

Model fitting results for change in diamter						
$N = 1461$	BETA	St. Err. of BETA	B	St. Err. of B	t(1457)	p-level
Intercept			1.259226	.003875	324.946	0.00
$(\text{Diameter})^2$	-1.22978	.007430	-.014527	.000088	-165.511	0.00
$(\text{Thickness})^2$	.72544	.007430	.533256	.005462	97.634	0.00
$(\text{Cover})^{\frac{1}{2}}$	-.45357	.005161	-.050782	.000578	-87.881	0.00
Analysis of Variance						
Effect	Sums of squares	df	Mean Squares	F	p-level	
Regress.	56.45381	3	18.81794	12028.01	0.00	
Residual	2.27949	1457	.00156			
Total	58.73330					

TABLE 8.7: Model fitting results and analysis of variance for the prediction of the absolute maximum stress for the pipe with high density sand as native soil

Model fitting results for absolute maximum stress						
$N = 1461$	BETA	St. Err. of BETA	B	St. Err. of B	t(1457)	p-level
Intercept			-2822.30	58.97681	-47.8543	0.00000
$(\text{Diameter})^2$	.015307	.004777	.06	.01770	3.2045	.001382
$(\text{Thickness})^2$	-.024214	.004777	-343.31	67.72456	-5.0692	0.0000
$(\text{Cover})^{\frac{1}{2}}$	.989069	.003828	2549.65	9.86803	258.3748	0.0000
Analysis of Variance						
Effect	Sums of squares	*df*	Mean Squares	F	p-level	
Regress.	$304706*10^5$	3	$101569*10^5$	22261.45	0.00	
Residual	$664761*10^3$	1457				
Total	$311353*10^5$					

TABLE 8.8: Model fitting results and analysis of variance for the prediction of change in diameter for the pipe with high density sand as native soil

Model fitting results for change in diamter						
$N = 1461$	BETA	St. Err. of BETA	B	St. Err. of B	t(1457)	p-level
Intercept			1.221069	.003602	338.988	0.00
$(\text{Diameter})^2$	-1.06693	.009190	-.009471	.000082	-116.090	0.00
$(\text{Thickness})^2$	.56521	.009190	.312228	.005077	61.500	0.00
$(\text{Cover})^{\frac{1}{2}}$	-.59153	.006384	-.049770	.000537	-92.659	0.00
Analysis of Variance						
Effect	Sums of squares	*df*	Mean Squares	F	p-level	
Regress.	31.19972	3	10.39991	7693.538	0.00	
Residual	1.96953	1457	.00135			
Total	33.16926					

TABLE 8.9: Model fitting results and analysis of variance for the prediction of the absolute maximum stress for the pipe with marl as native soil

Model fitting results for absolute maximum stress						
$N = 1461$	BETA	St. Err. of BETA	B	St. Err. of B	t(1457)	p-level
Intercept			26.0805	.496623	52.5157	0.00
$(\text{Diameter})^2$	.239428	.006148	.4381	.011248	38.9450	0.00
$(\text{Thickness})^2$	-.230218	.006148	-26.2110	.699953	-37.4468	0.00
$(\text{Cover})^{\frac{1}{2}}$	.970805	.004270	16.8350	.074054	227.3324	0.00
Analysis of Variance						
Effect	Sums of squares	*df*	Mean Squares	F	p-level	
Regress.	1371545	3	457181.7	17792.75	0.00	
Residual	37437	1427	25.7			
Total	1408982					

TABLE 8.10: Model fitting results and analysis of variance for the prediction of change in diameter for the pipe with marl as native soil

Model fitting results for change in diamter						
$N = 1461$	BETA	St. Err. of BETA	B	St. Err. of B	t(1457)	p-level
Intercept			1.283210	.004548	282.173	0.00
$(\text{Diameter})^2$	-1.12959	.008410	-.013835	.000103	-134.319	0.00
$(\text{Thickness})^2$	.64749	.008410	.493485	.006409	76.993	0.00
$(\text{Cover})^{\frac{1}{2}}$	-.55398	.005842	-.064308	.000678	-94.833	0.00
Analysis of Variance						
Effect	Sums of squares	*df*	Mean Squares	F	p-level	
Regress.	59.99928	3	19.99976	9282.584	0.00	
Residual	3.13917	1457	.00215			
Total	63.13846					

TABLE 8.11: Model fitting results and analysis of variance for the prediction of the absolute maximum stress for the pipe with sabkha as native soi

Model fitting results for absolute maximum stress						
$N = 1461$	BETA	St. Err. of BETA	B	St. Err. of B	t(1457)	p-level
Intercept			33.8149	.568805	59.4491	0.00
$(\text{Diameter})^2$	.20934	.006667	.4045	.012883	31.3939	0.00
$(\text{Thickness})^2$	-.250995	.006667	-30.1814	.801689	-37.6437	0.00
$(\text{Cover})^{\frac{1}{2}}$	.968349	.004631	17.7354	.084818	209.0998	0.00
Analysis of Variance						
Effect	Sums of squares	*df*	Mean Squares	F	p-level	
Regress.	1522567	3	507522.2	15056.90	0.00	
Residual	49111	1457	33.7			
Total	1571678					

TABLE 8.12: Model fitting results and analysis of variance for the prediction of change in diameter for the pipe with sabkha as native soil

Model fitting results for change in diamter						
$N = 1461$	BETA	St. Err. of BETA	B	St. Err. of B	t(1457)	p-level
Intercept			1.270458	.004931	257.635	0.00
$(\text{Diameter})^2$	-1.14104	.008509	-.014977	.000112	-134.093	0.00
$(\text{Thickness})^2$	.68878	.008509	.562584	.006950	80.945	0.00
$(\text{Cover})^{\frac{1}{2}}$	-.55049	.005911	-.068484	.000735	-93.134	0.00
Analysis of Variance						
Effect	Sums of squares	*df*	Mean Squares	F	p-level	
Regress.	68.82309	3	22.94103	9055.424	0.00	
Residual	3.69117	1457	.00253			
Total	72.51426					

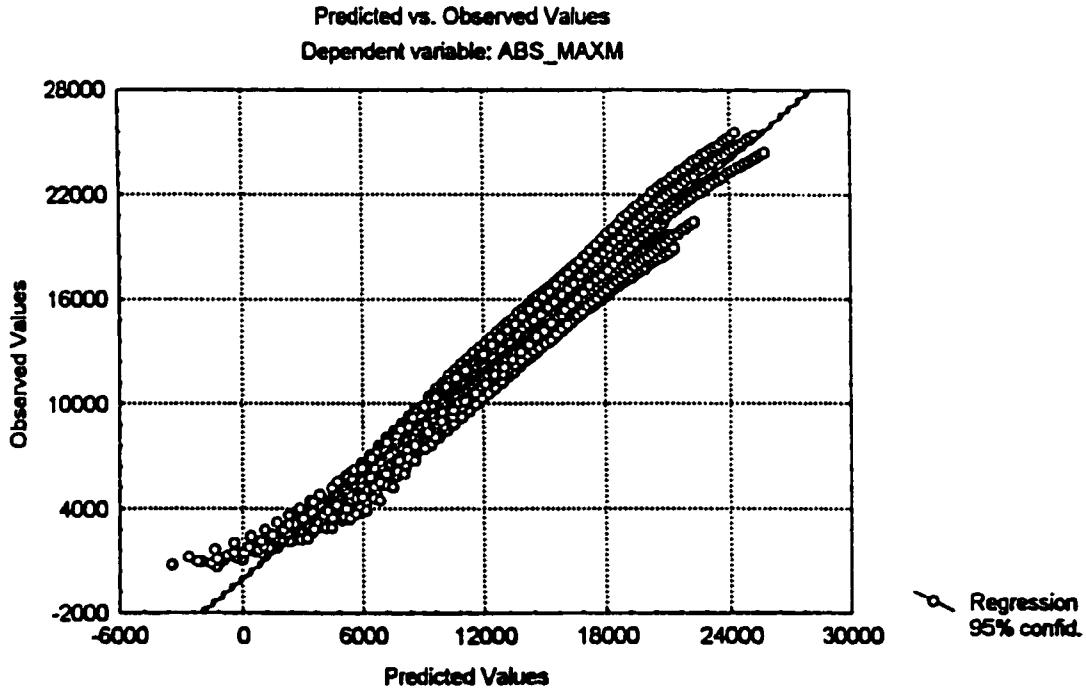

Fig. 8.13: Plot of predicted versus the measured values for absolute maximum stresses for the pipe with low density sand as native soil subjected to sand overburden

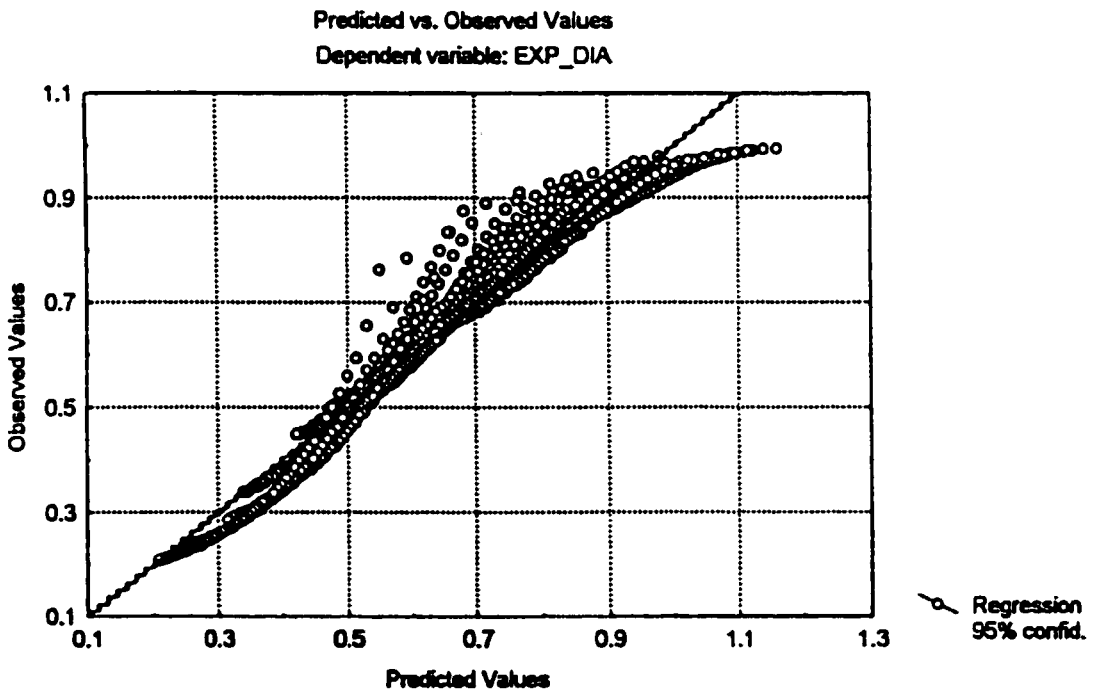

Fig. 8.14: Plot of predicted versus the measured values for the change in diameter for the pipe with low density sand as native soil subjected to sand overburden

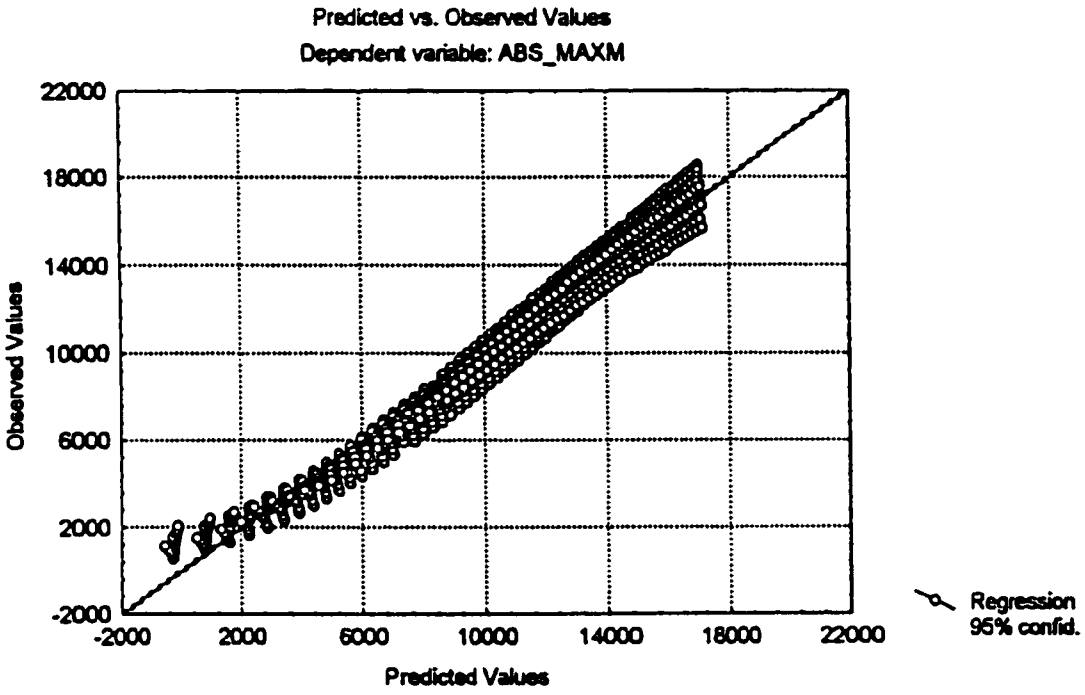

Fig. 8.15: Plot of predicted versus the measured values for absolute maximum stress for the pipe with high density sand as native soil subjected to sand overburden

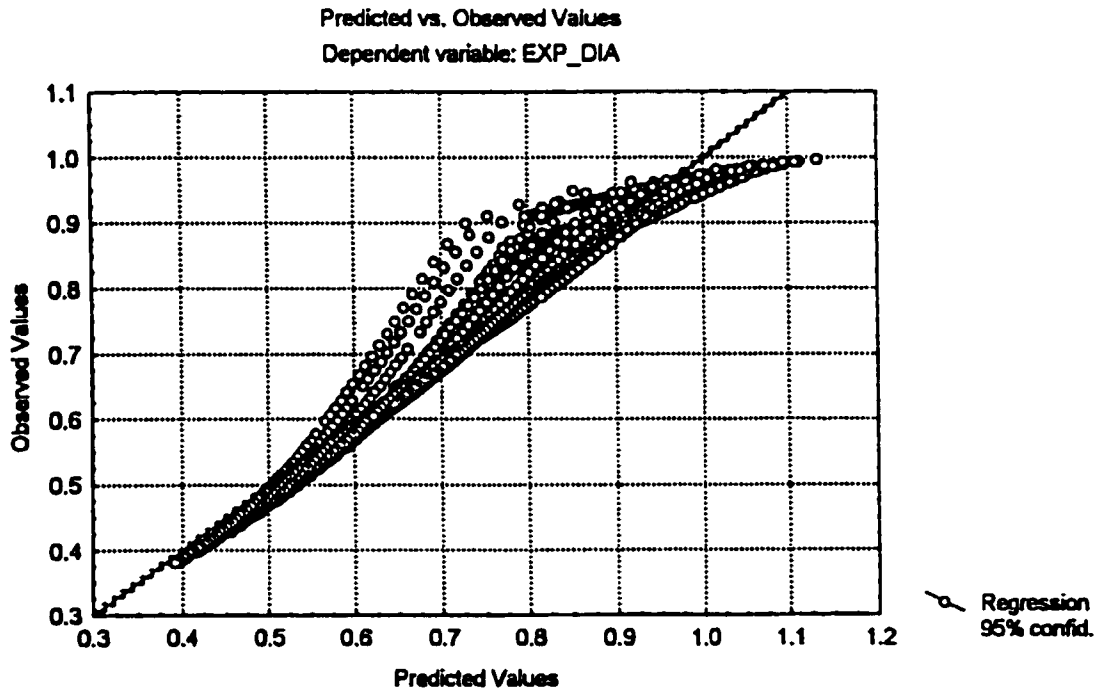

Fig. 8.16: Plot of predicted versus the measured values for the cahnge in diameter of pipe with high density sand as native soil subjected to sand overburden

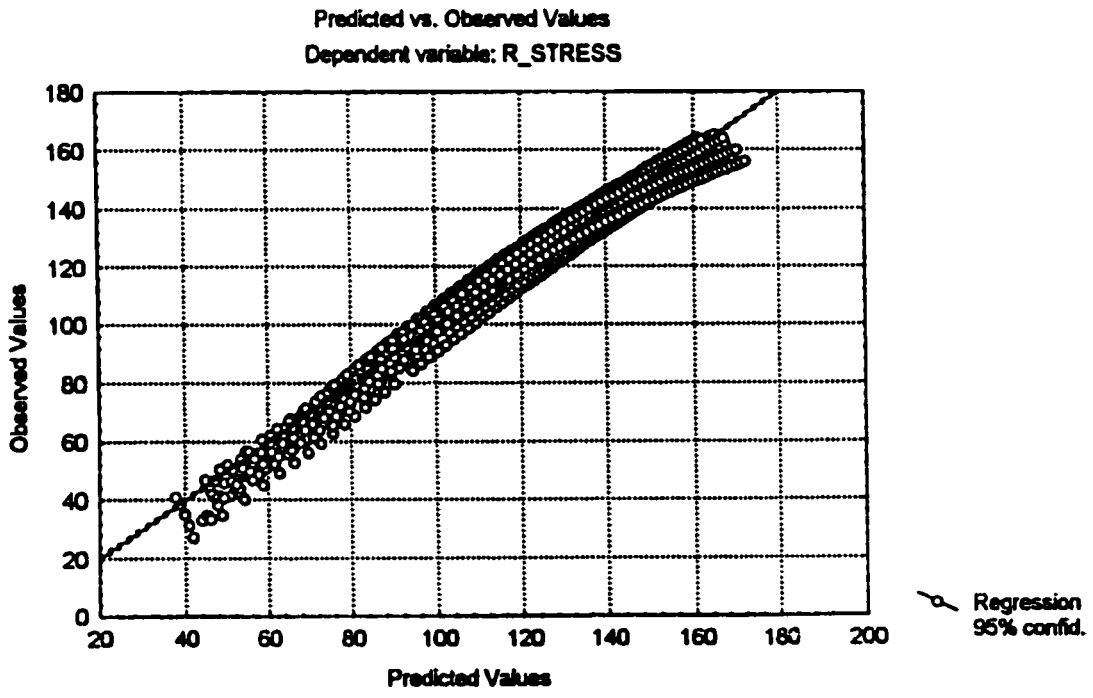

Fig. 8.17: Plot of predicted versus the measured values for absolute maximum stress in pipe with marl as native soil subjected to sand overburden

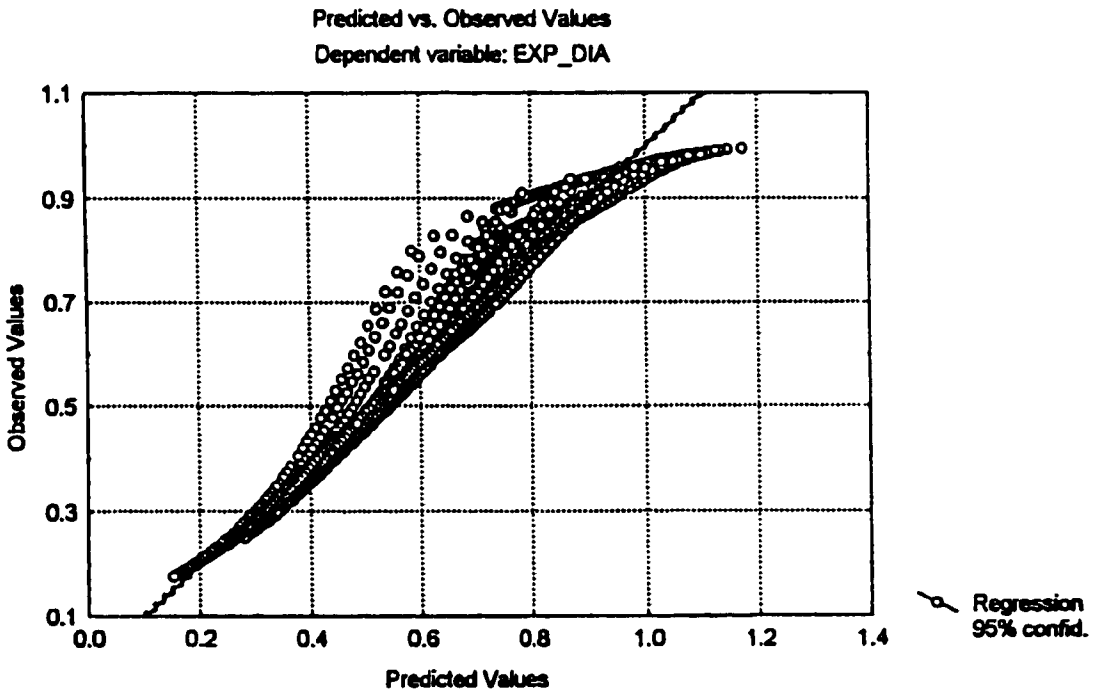

Fig. 8.18: Plot of predicted versus the measured values for the change in the diameter of pipe with marl as native soil subjected to sand overburden

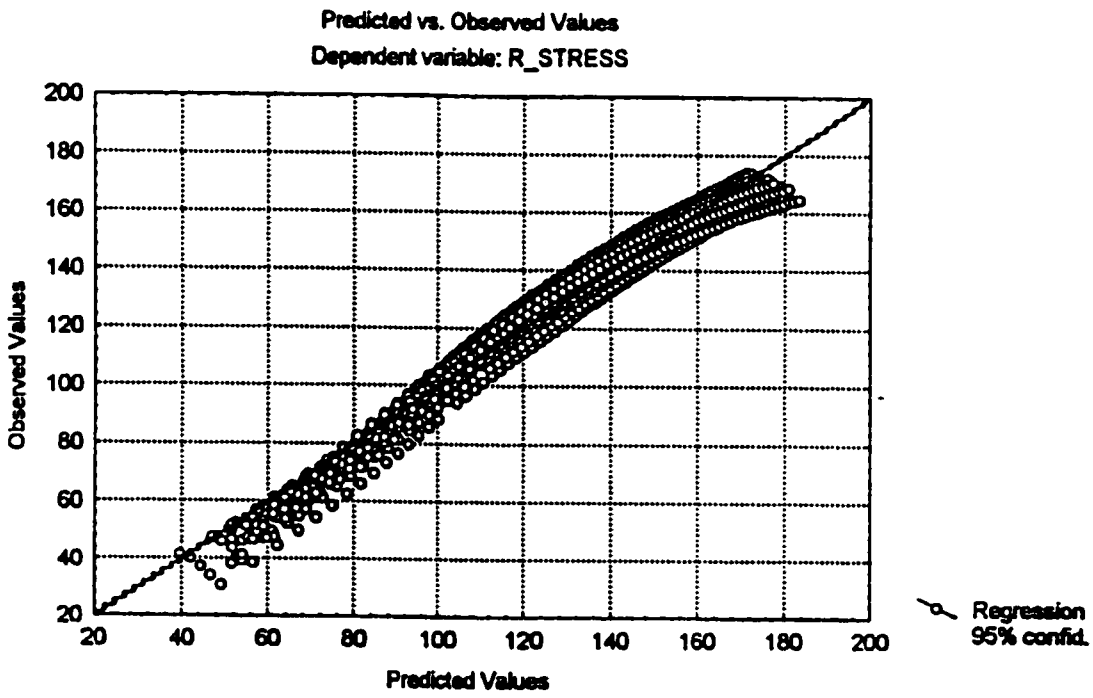

Fig. 8.19: Plot of predicted versus the measured values for absolute maximum stress in pipe with sabkha as native soil subjected to sand overburden

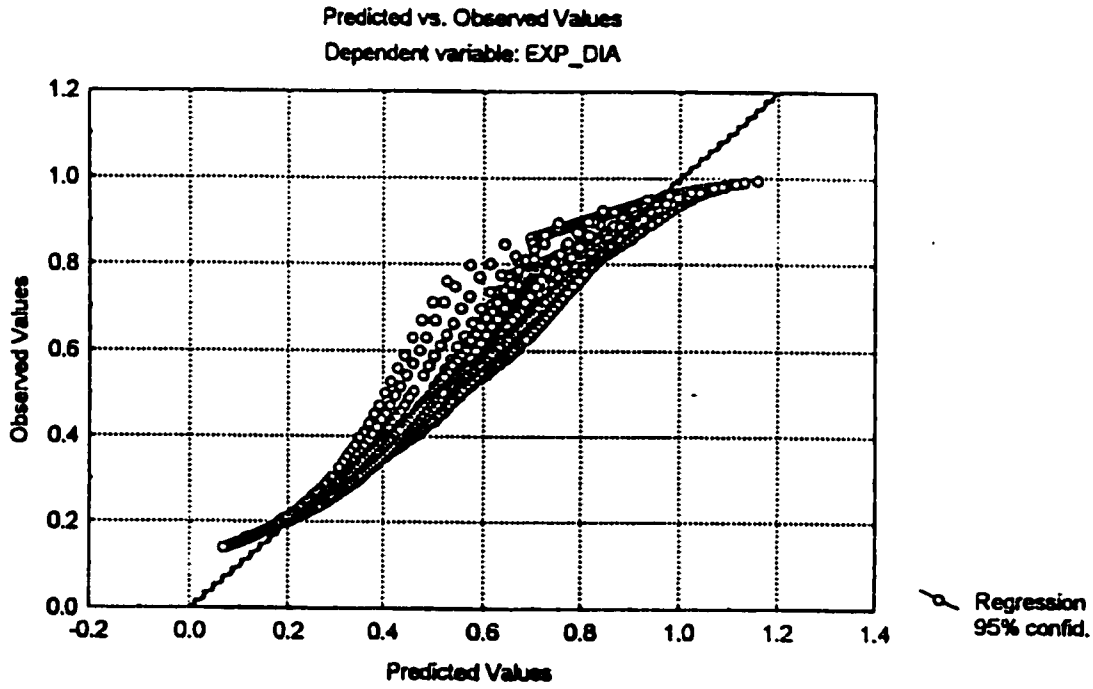

Fig. 8.20: Plot of predicted versus the measured values for change in the diameter of pipe with sabkha as native soil subjected to sand overburden

- The diameter of the pipe - This is positively related to the absolute maximum stress, i.e. the higher the pipe's diameter is, the higher the stresses.
- The thickness of the pipe's wall - This is negatively related to the absolute maximum stress, i.e., the higher the thickness of the pipe's wall is, the lower the stresses.
- The depth of the pipe cover - This is positively related to the absolute maximum stress.
- The diameter of the pipe - This is positively related to the amount of change in the pipe's diameter. Although the sign in the developed model is negative, the higher the value of the diameter change (in negative) is, the higher the amount of deformation.
- The thickness of the pipe's wall - This is negatively related to the amount of change in the pipe's diameter.
- The depth of the pipe cover - This is positively related to the amount of change in the pipe's diameter.
- The above-mentioned observations are all according to the expected relations between the IV's and DV's.

8.2.6.2 Homoscedasticity Testing

One of the main assumptions that must be satisfied when using the ordinary least squares method is that errors have a constant variance. This implies that there should be a scatter of errors around all points of the independent variables. This assumption is called homoscedasticity. To check for homoscedasticity of the variables used, plots of predicted values of DV against residuals (the difference between originally calculated and predicted values) reveal any violation of this assumption [91]. The plots of predicted values

versus residuals of estimation for all the developed models are shown in Figs. 8.21 to 8.28. From these figures, it can be said that the homoscedasticity conditions are met for all the developed models.

8.2.6.3 Normality Testing

In multiple regression, normality is part of the significance testing. Normal probability plots are drawn for the residuals to ensure that the errors are normally distributed. Figs. 8.29 to 8.36 are the normal probability plots for the residuals of the developed models. From a visual inspection of the normal lines and the distribution of the points around the lines, it appears that, except at the two extreme there is a normal distribution of the residuals. Therefore, the normality assumption of the error is met for all the models.

8.2.7 Model Validation for Sand Overburden Problem

39 cases for each soil type that were selected for validation of the developed models. The developed equations were used to calculate the absolute maximum stress and the diameter change for the different embedment soils for the validation data. Tables 8.13 to 8.16 compare the observed and the calculated values of the absolute maximum stresses and the diameter change for the validation data. Montgomery et al. [91] have suggested a procedure for validation testing by fitting the validation data for the developed models and calculating the coefficient of determination (R^2) for the newly fitted data, then comparing this value with the R^2 of the model with the original data. This test was performed for the developed models. Table 8.17 shows the coefficient of determination for both the original and validation data; in addition, it shows the accuracy of the developed models in predict-

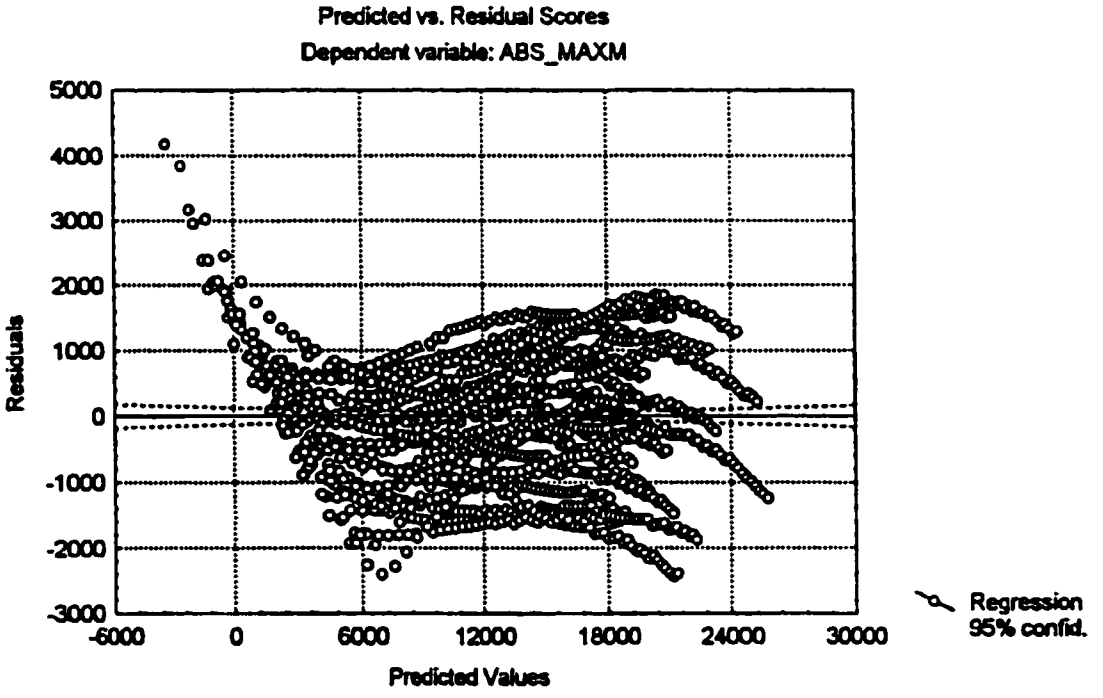

Fig. 8.21: Predicted values versus residuals of estimation for the absolute maximum stresses for the pipe with low density sand as native soil subjected to sand overburden

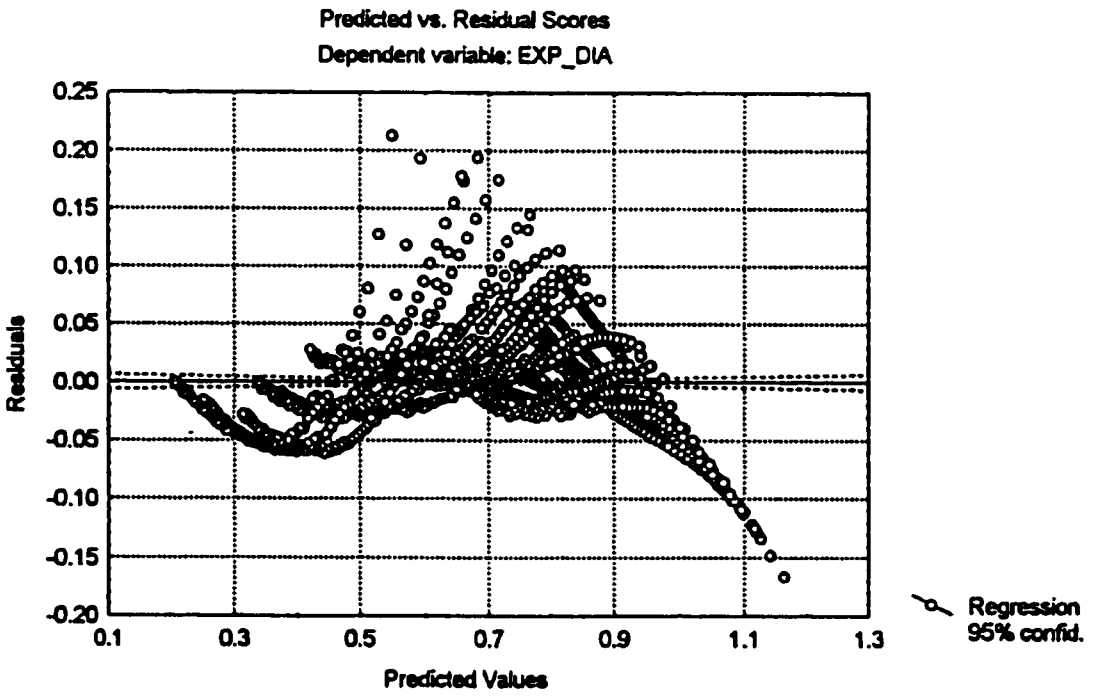

Fig. 8.22: Predicted values versus residuals of estimation for thechange in diameter of the pipe with low density sand as native soil subjected to sand overburden

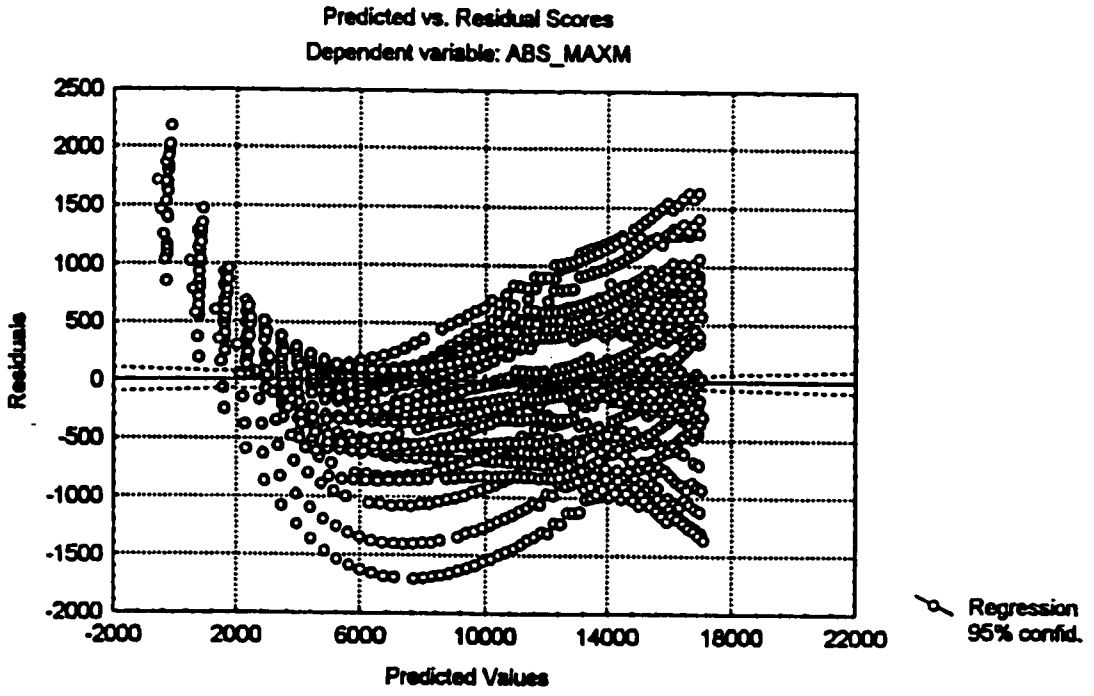

Fig. 8.23: Predicted values versus residuals of estimation for absolute maximum stresses for the pipe with high density sand as native soil subjected to sand overburden

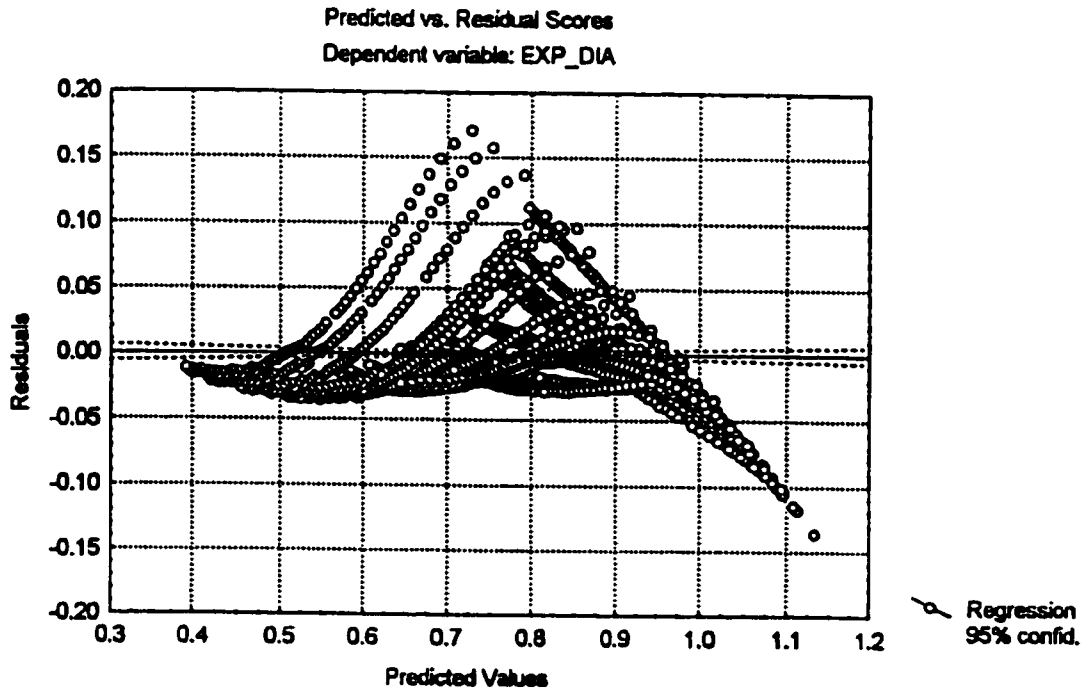

Fig. 8.24: Predicted values versus residuals of estimation for the change in diameter of the pipe with high density sand as native soil subjected to sand overburden

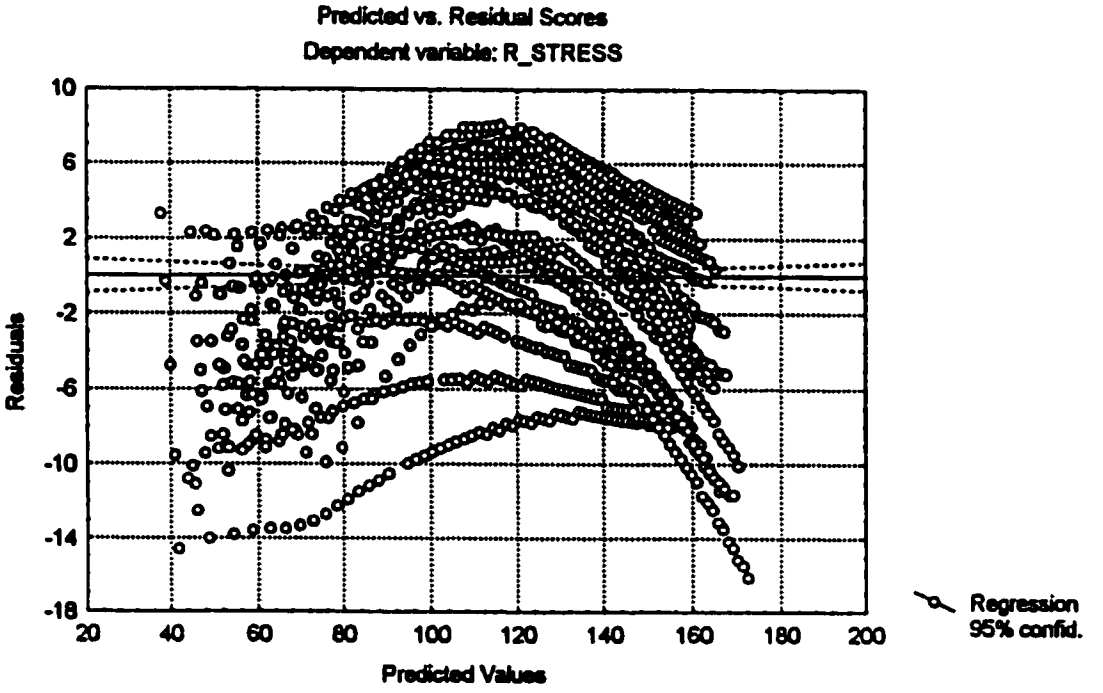

Fig. 8.25: Predicted values versus residuals of estimation for absolute maximum stresses for the pipe with marl as native soil subjected to sand overburden

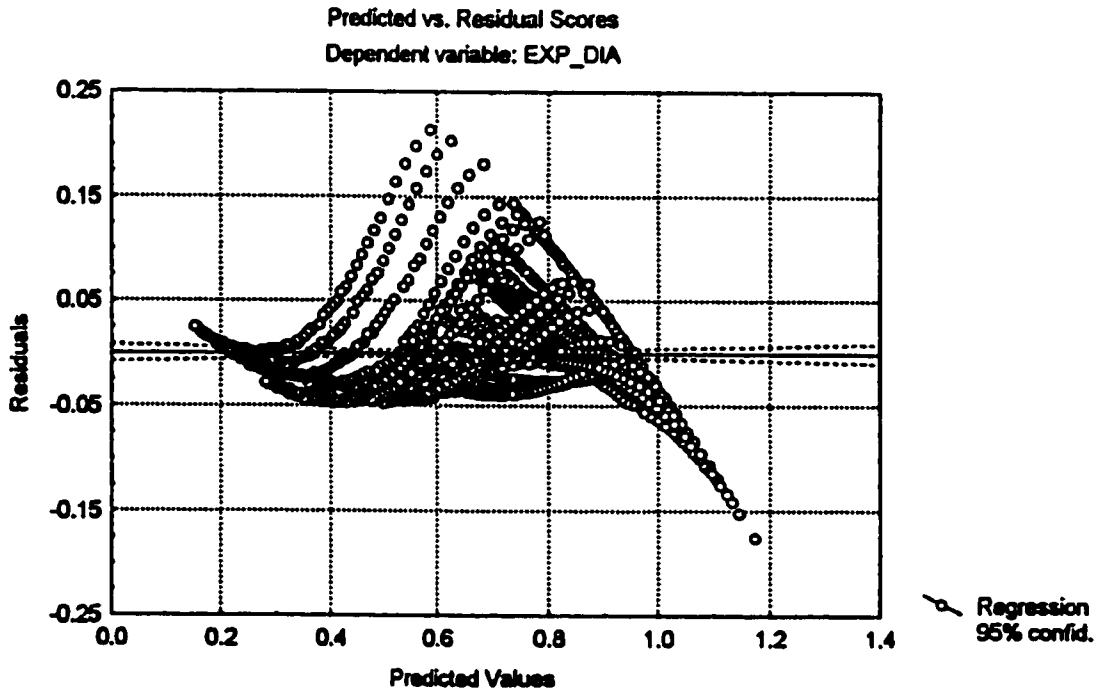

Fig. 8.26: Predicted values versus residuals of estimation for the change in diameter of the pipe with marl as native soil subjected to sand overburden

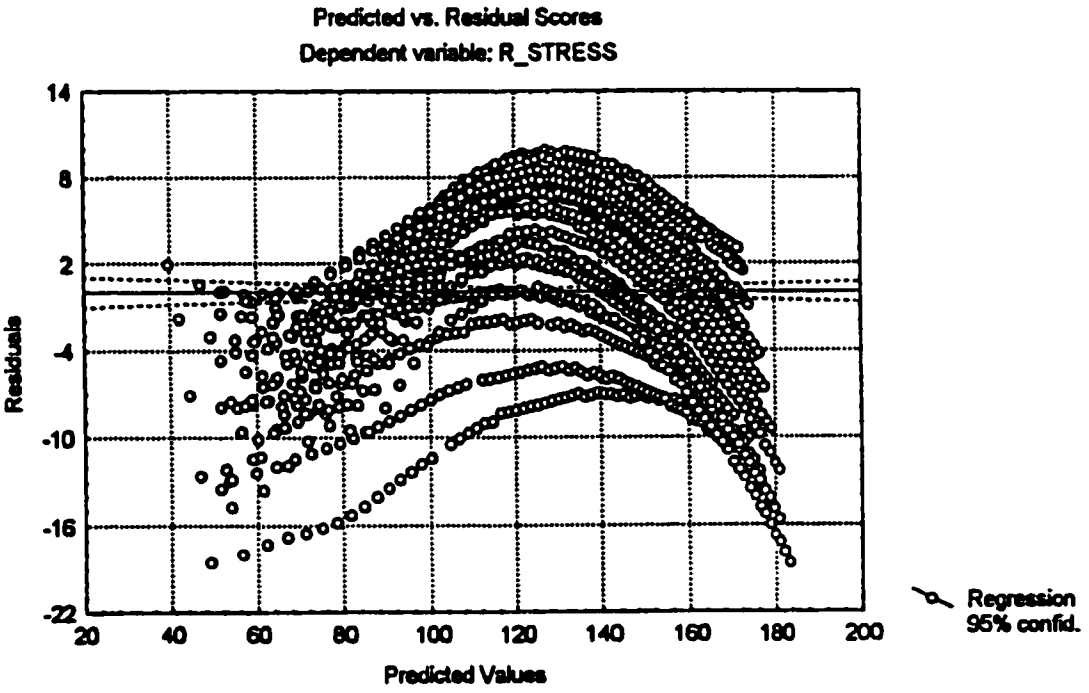

Fig. 8.27: Predicted values versus residuals of estimation for absolute maximum stresses for the pipe with sabkha as native soil subjected to sand overburden

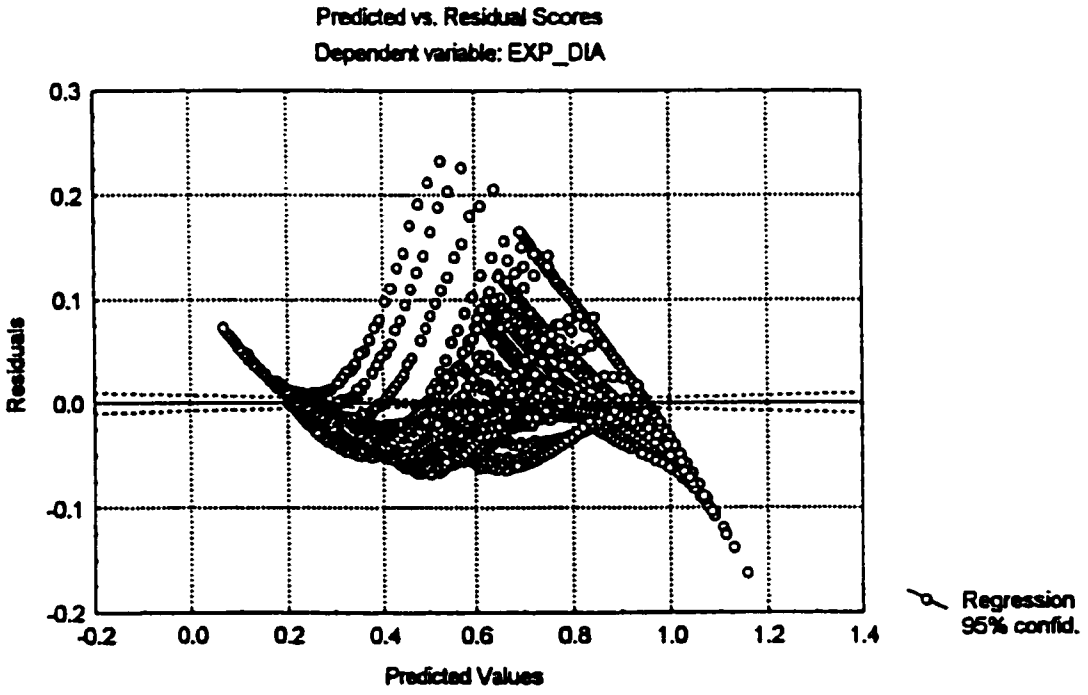

Fig. 8.28: Predicted values versus residuals of estimation for the change in diameter of the pipe with sabkha as native soil subjected to sand overburden

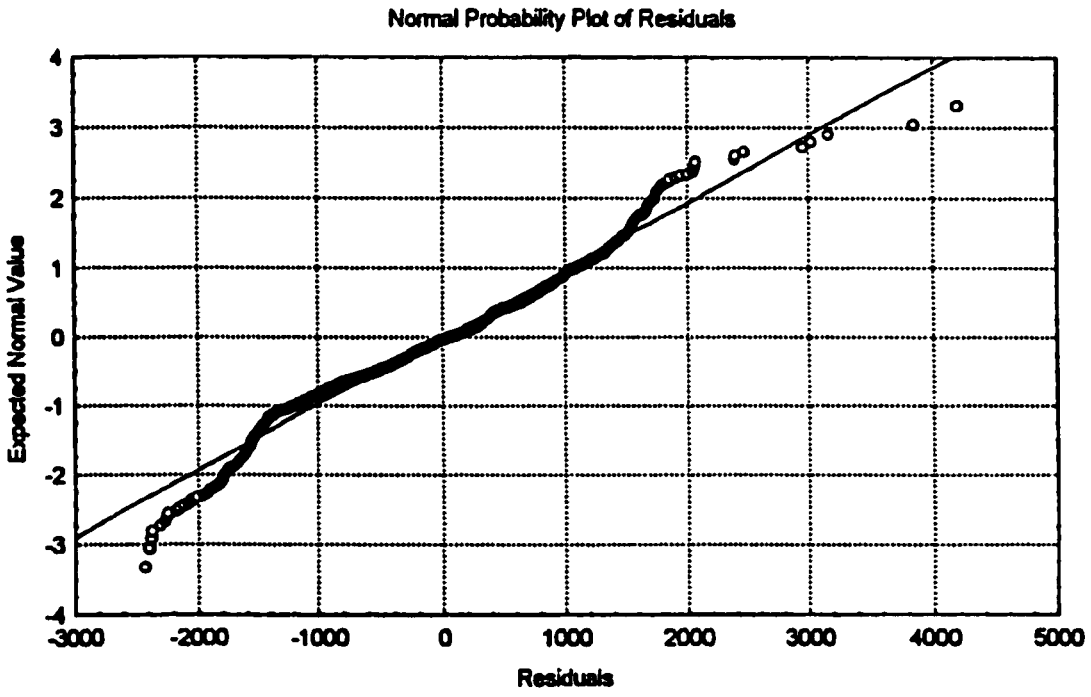

Fig. 8.29: Normal probability plot for the prediction of the absolute maximum stress for the pipe with low density sand as native soil subjected to sand overburden

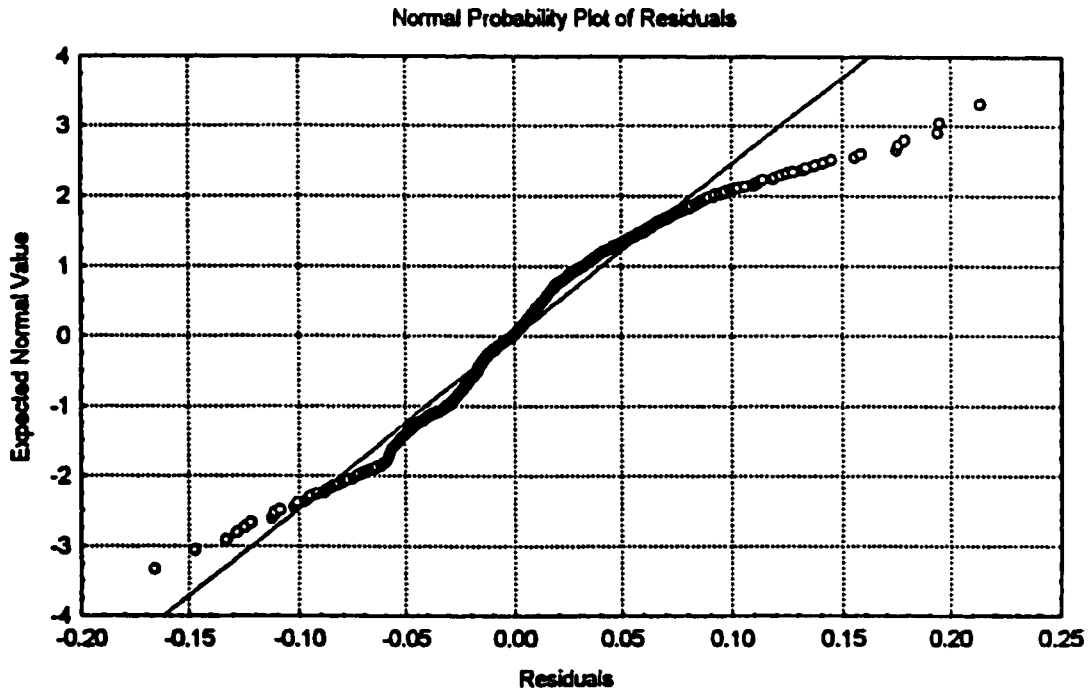

Fig. 8.30: Normal probability plot for the prediction of change in diameter for the pipe with low density sand as native soil subjected to sand overburden

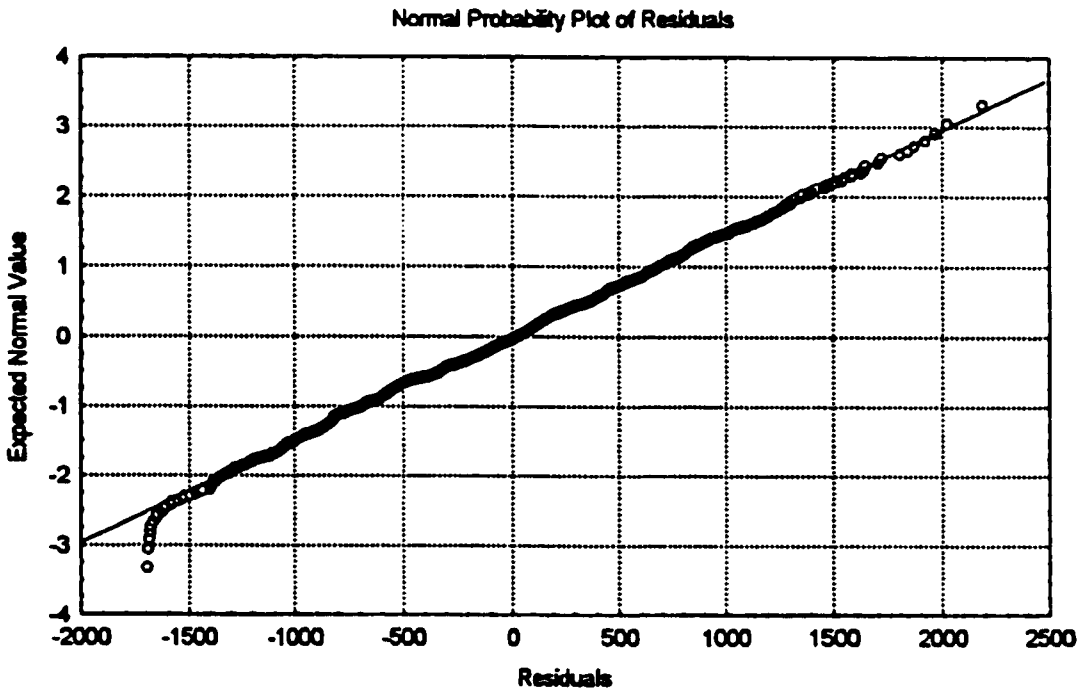

Fig. 8.31: Normal probability plot for the prediction of the absolute maximum stress for the pipe with high density sand as native soil subjected to sand overburden

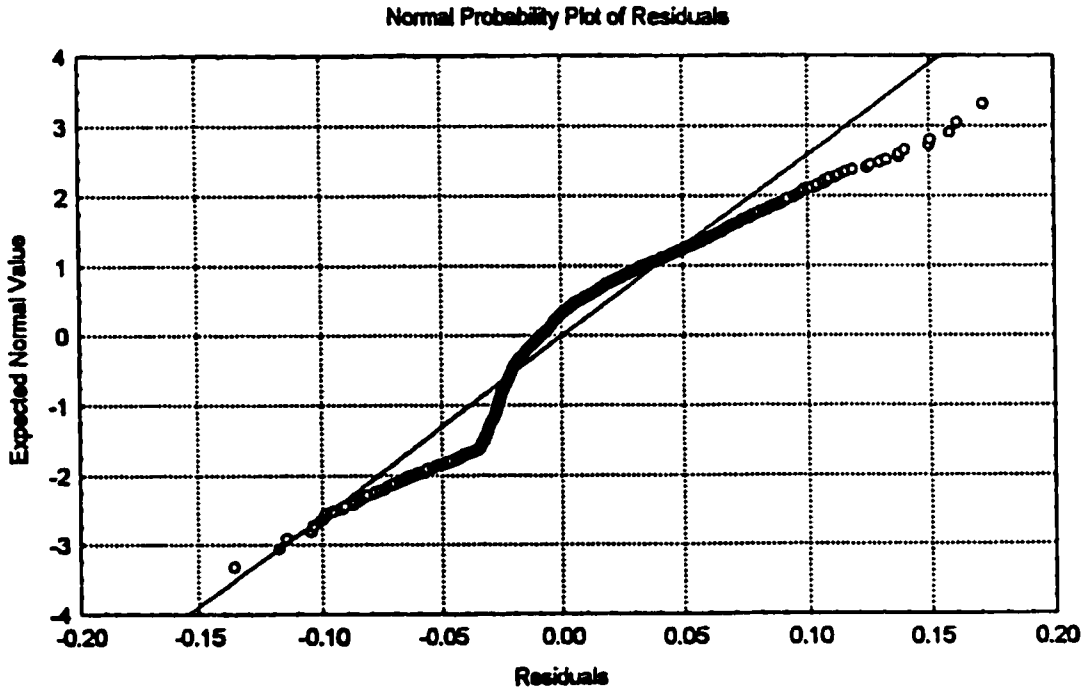

Fig. 8.32: Normal probability plot for the prediction of change in diameter for the pipe with high density sand as native soil subjected to sand overburden

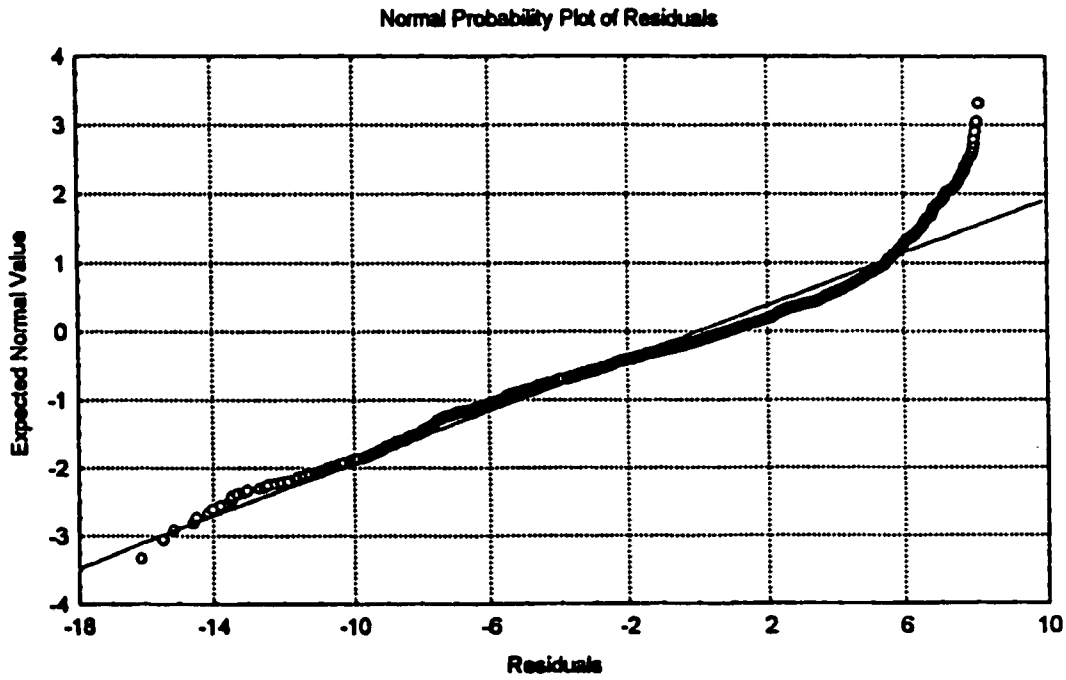

Fig. 8.33: Normal probability plot for the prediction of the absolute maximum stresses for the pipe with marl as native soil subjected to sand overburden

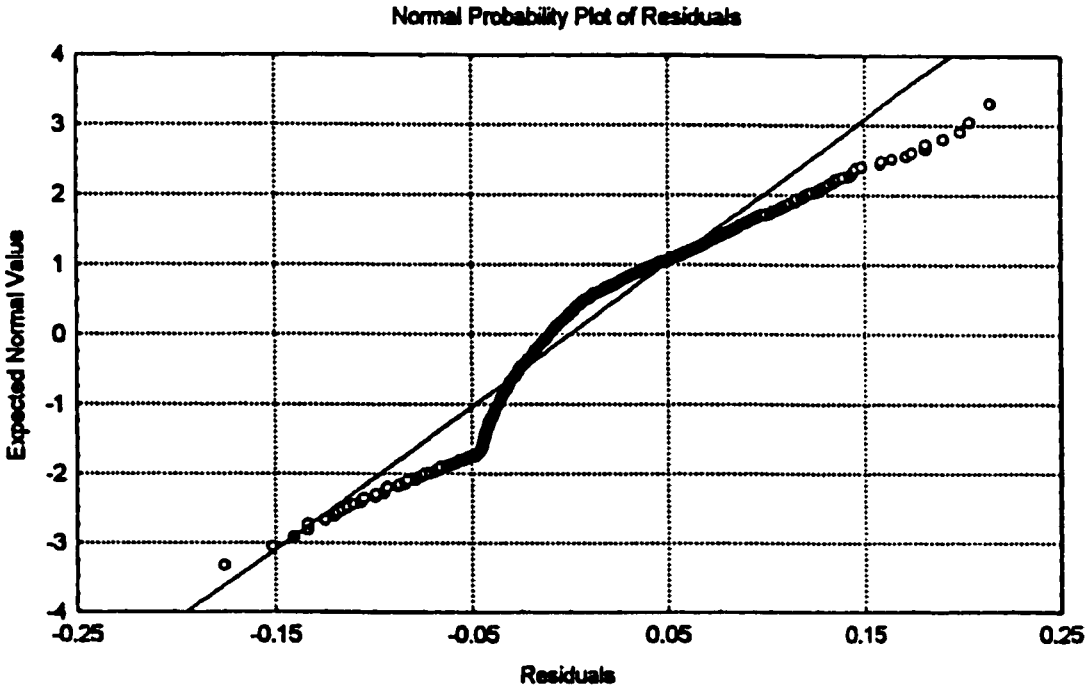

Fig. 8.34: Normal probability plot for the prediction of change in diameter for the pipe with marl as native soil subjected to sand overburden

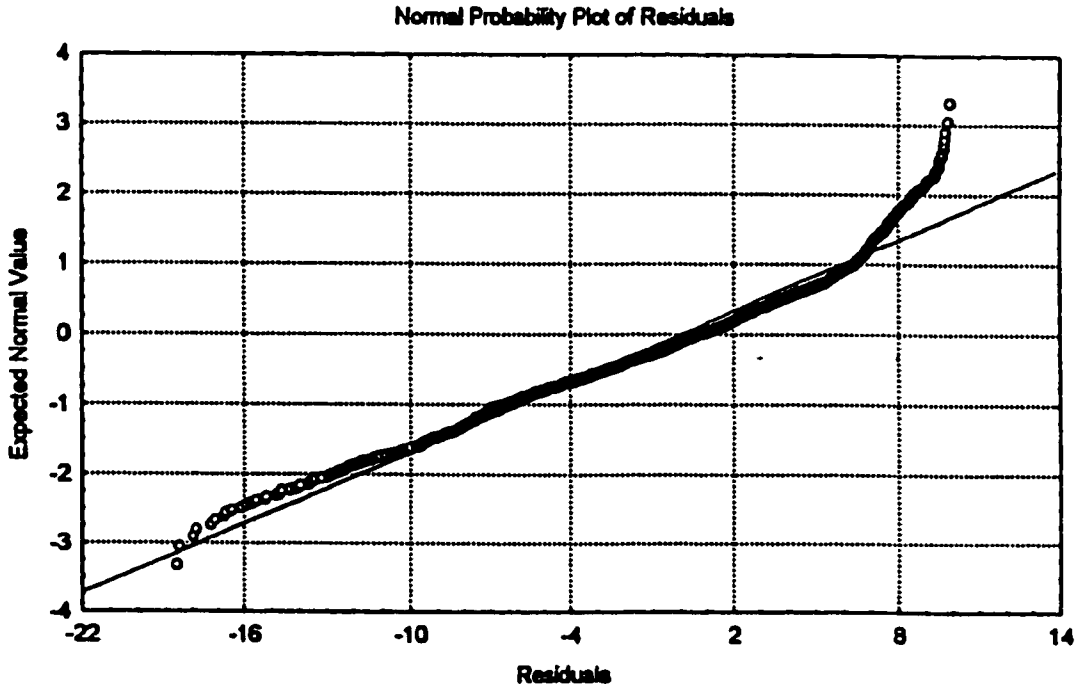

Fig. 8.35: Normal probabilty plot for the prediction of the absolute maximum stresses for the pipe with sabkha as native soil subjected to sand overburden

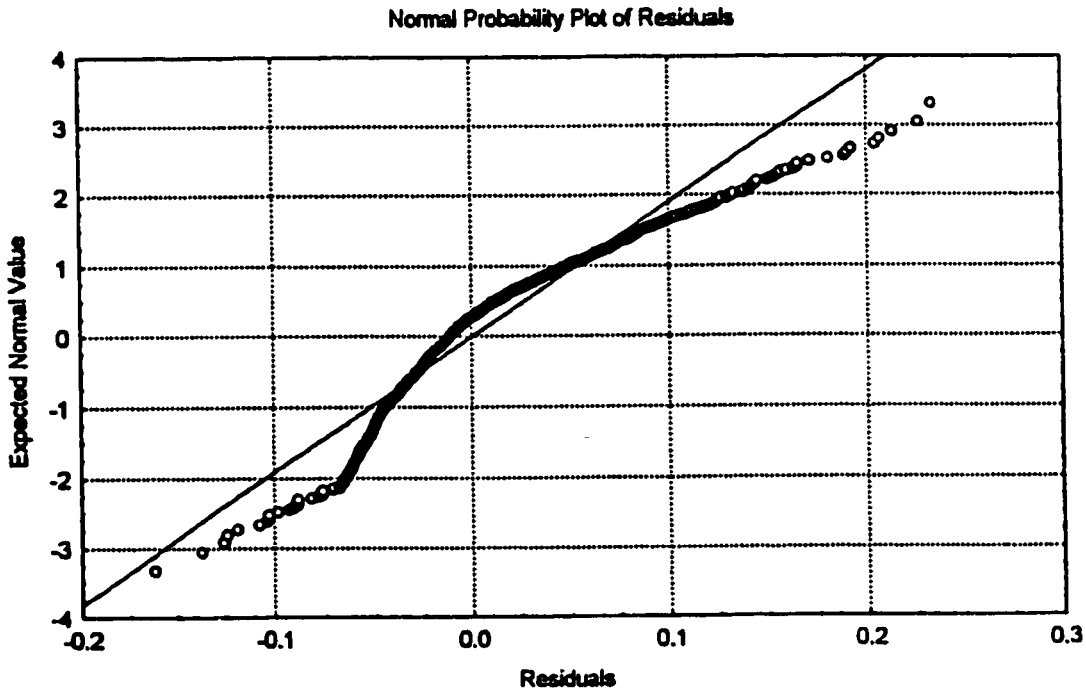

Fig. 8.36: Normal probabilty plot for the prediction of change in diameter for the pipe with sabkha as native soil subjected to sand overburden

TABLE 8.13: Comaprison of the observed and the calculated values of validation data for low density sand as native soil

Observation number	Pipe Diameter (in)	Thickness of Pipe Wall (in)	Depth of Cover (ft)	Abs. Max. Stress (psi) Observed	Abs. Max. Stress (psi) Calculted	Diameter Change (in) Observed	Diameter Change (in) Calculted
16	12	0.24	16	6165	7659.26	-0.04	0.01
54	12	0.24	54	16167	17603.64	-0.09	-0.17
68	12	0.16	8	4666	4406.42	-0.04	0.03
90	12	0.16	30	13403	12272.90	-0.11	-0.11
107	12	0.16	47	17795	16366.60	-0.14	-0.20
139	12	0.12	19	10130	9030.95	-0.11	-0.08
172	12	0.12	52	18920	17501.51	-0.18	-0.25
249	12	0.08	9	5369	5051.88	-0.08	-0.03
298	12	0.08	58	18080	18759.94	-0.22	-0.30
321	24	0.48	21	7749	9120.83	-0.09	-0.07
361	24	0.32	1	1290	-612.67	-0.02	0.03
393	24	0.32	33	14147	13477.88	-0.24	-0.24
414	24	0.32	54	19003	18241.21	-0.31	-0.34
427	24	0.24	7	4639	4592.09	-0.11	-0.10
448	24	0.24	28	13248	12449.52	-0.28	-0.26
471	24	0.24	51	18780	17943.48	-0.38	-0.39
494	24	0.192	14	8003	7993.54	-0.21	-0.19
531	24	0.192	51	18290	18090.28	-0.42	-0.43
562	24	0.16	22	10611	10890.93	-0.30	-0.28
593	24	0.16	53	17780	18581.88	-0.46	-0.47
612	36	0.72	12	4833	5351.53	-0.09	-0.06
632	36	0.72	32	10847	11863.63	-0.20	-0.18
670	36	0.48	10	5705	6493.99	-0.15	-0.18
703	36	0.48	43	16621	16577.04	-0.41	-0.42
752	36	0.36	32	14346	14616.04	-0.45	-0.44
812	36	0.288	32	14053	14946.33	-0.51	-0.51
853	36	0.24	13	7272	9033.73	-0.32	-0.38
911	48	0.96	11	5208	4286.88	-0.12	-0.10
940	48	0.96	40	13602	13219.92	-0.32	-0.28
988	48	0.64	28	14556	13776.50	-0.48	-0.45
1067	48	0.48	47	21370	19690.37	-0.81	-0.75
1114	48	0.384	34	18291	17234.36	-0.82	-0.75
1188	48	0.32	48	20990	20811.97	-1.01	-0.96
1213	60	1.2	13	4446	4339.21	-0.12	-0.17
1260	60	1.2	60	15843	16635.54	-0.44	-0.45
1293	60	0.8	33	14850	16355.11	-0.63	-0.65
1332	60	0.6	12	12471	11564.72	-0.68	-0.63
1396	60	0.48	16	14348	14073.72	-0.93	-0.82
1459	60	0.4	19	14938	15637.97	-1.10	-0.97

TABLE 8.14: Comaprison of the observed and the calculated values of validation data for high density sand as native soil

Observation number	Pipe Diameter (in)	Thickness of Pipe Wall (in)	Depth of Cover (ft)	Abs. Max. Stress (psi) Observed	Abs. Max. Stress (psi) Calculted	Diameter Change (in) Observed	Diameter Change (in) Calculted
16	12	0.24	16	5671	7365	-0.03	-0.02
54	12	0.24	54	15319	15903	-0.09	-0.20
68	12	0.16	8	4260	4389	-0.04	0.02
90	12	0.16	30	11870	11143	-0.10	-0.12
107	12	0.16	47	15948	14657	-0.13	-0.20
139	12	0.12	19	8705	8295	-0.09	-0.08
172	12	0.12	52	16840	15567	-0.17	-0.24
249	12	0.08	9	4543	4833	-0.07	-0.02
298	12	0.08	58	15950	16602	-0.20	-0.28
321	24	0.48	21	7464	8817	-0.09	-0.09
361	24	0.32	1	1053	-273	-0.02	0.04
393	24	0.32	33	12524	11824	-0.21	-0.21
414	24	0.32	54	17141	15913	-0.28	-0.32
427	24	0.24	7	4134	3938	-0.09	-0.07
448	24	0.24	28	11142	10684	-0.24	-0.22
471	24	0.24	51	16140	15401	-0.33	-0.34
494	24	0.192	14	6566	6740	-0.17	-0.14
531	24	0.192	51	15340	15408	-0.36	-0.36
562	24	0.16	22	8596	9162	-0.25	-0.21
593	24	0.16	53	14810	15765	-0.39	-0.39
612	36	0.72	12	4890	5910	-0.08	-0.07
632	36	0.72	32	10726	11500	-0.19	-0.20
670	36	0.48	10	5301	5239	-0.14	-0.14
703	36	0.48	43	14590	13896	-0.36	-0.35
752	36	0.36	32	11947	11634	-0.37	-0.34
812	36	0.288	32	11553	11650	-0.41	-0.38
853	36	0.24	13	5794	6429	-0.26	-0.26
911	48	0.96	11	4696	5456	-0.10	-0.11
940	48	0.96	40	12903	13125	-0.29	-0.29
988	48	0.64	28	11070	10667	-0.37	-0.35
1067	48	0.48	47	15480	14716	-0.61	-0.56
1114	48	0.384	34	12220	12132	-0.57	-0.52
1188	48	0.32	48	14300	14945	-0.72	-0.65
1213	60	1.2	13	5530	6092	-0.15	-0.17
1260	60	1.2	60	17096	16649	-0.48	-0.45
1293	60	0.8	33	12165	11821	-0.51	-0.49
1332	60	0.6	12	5825	6102	-0.33	-0.41
1396	60	0.48	16	7061	7513	-0.45	-0.51
1459	60	0.4	19	7600	8452	-0.53	-0.58

TABLE 8.15: Comaprison of the observed and the calculated values of validation data for marl as native soil

Observation number	Pipe Diameter (in)	Thickness of Pipe Wall (in)	Depth of Cover (ft)	Abs. Max. Stress (psi) Observed	Abs. Max. Stress (psi) Calculted	Diameter Change (in) Observed	Diameter Change (in) Calculted
16	12	0.24	16	6751	8535	-0.04	-0.02
54	12	0.24	54	19870	22129	-0.12	-0.27
68	12	0.16	8	5306	5589	-0.05	0.01
90	12	0.16	30	15757	14245	-0.13	-0.17
107	12	0.16	47	21783	20323	-0.18	-0.28
139	12	0.12	19	11775	10317	-0.13	-0.11
172	12	0.12	52	23620	22377	-0.24	-0.34
249	12	0.08	9	6185	6359	-0.09	-0.04
298	12	0.08	58	22520	24791	-0.30	-0.40
321	24	0.48	21	9148	10233	-0.11	-0.11
361	24	0.32	1	1465	2029	-0.02	0.04
393	24	0.32	33	17203	15604	-0.30	-0.30
414	24	0.32	54	24305	23079	-0.41	-0.45
427	24	0.24	7	5688	5602	-0.13	-0.11
448	24	0.24	28	16184	14253	-0.35	-0.31
471	24	0.24	51	23570	22659	-0.50	-0.49
494	24	0.192	14	9780	8940	-0.26	-0.22
531	24	0.192	51	22790	23039	-0.56	-0.53
562	24	0.16	22	12904	12402	-0.37	-0.32
593	24	0.16	53	22090	24013	-0.61	-0.58
612	36	0.72	12	6204	6609	-0.11	-0.08
632	36	0.72	32	13209	13974	-0.24	-0.25
670	36	0.48	10	7309	6807	-0.20	-0.20
703	36	0.48	43	20809	19506	-0.53	-0.51
752	36	0.36	32	17896	16294	-0.57	-0.51
812	36	0.288	32	17594	16779	-0.65	-0.57
853	36	0.24	13	9358	9266	-0.41	-0.40
911	48	0.96	11	6109	6049	-0.14	-0.13
940	48	0.96	40	15804	16491	-0.37	-0.37
988	48	0.64	28	15924	14259	-0.55	-0.52
1067	48	0.48	47	23280	22482	-0.99	-0.88
1114	48	0.384	34	18964	18280	-0.94	-0.83
1188	48	0.32	48	22010	24135	-1.23	-1.10
1213	60	1.2	13	7044	6660	-0.20	-0.20
1260	60	1.2	60	21410	22895	-0.63	-0.60
1293	60	0.8	33	17835	16410	-0.78	-0.73
1332	60	0.6	12	9617	9016	-0.54	-0.64
1396	60	0.48	16	11839	11475	-0.76	-0.83
1459	60	0.4	19	12945	13285	-0.92	-0.99

TABLE 8.16: Comaprison of the observed and the calculated values of validation data for sabkha as native soil

Observation number	Pipe Diameter (in)	Thickness of Pipe Wall (in)	Depth of Cover (ft)	Abs. Max. Stress (psi) Observed	Abs. Max. Stress (psi) Calculted	Diameter Change (in) Observed	Diameter Change (in) Calculted
16	12	0.24	16	8370	10479	-0.05	-0.05
54	12	0.24	54	23683	26163	-0.14	-0.33
68	12	0.16	8	6643	7056	-0.06	-0.01
90	12	0.16	30	19273	17155	-0.17	-0.22
107	12	0.16	47	26098	24157	-0.22	-0.34
139	12	0.12	19	14605	12623	-0.16	-0.15
172	12	0.12	52	28050	26548	-0.30	-0.41
249	12	0.08	9	7713	8003	-0.12	-0.07
298	12	0.08	58	26390	29351	-0.37	-0.49
321	24	0.48	21	10854	12168	-0.13	-0.14
361	24	0.32	1	1823	2663	-0.03	0.02
393	24	0.32	33	20518	18427	-0.36	-0.36
414	24	0.32	54	28114	26958	-0.48	-0.53
427	24	0.24	7	6995	6923	-0.17	-0.15
448	24	0.24	28	19403	16932	-0.44	-0.38
471	24	0.24	51	27400	26547	-0.61	-0.59
494	24	0.192	14	11876	10834	-0.33	-0.27
531	24	0.192	51	26430	27021	-0.69	-0.64
562	24	0.16	22	15640	14854	-0.48	-0.39
593	24	0.16	53	25440	28159	-0.75	-0.69
612	36	0.72	12	6914	7759	-0.12	-0.11
632	36	0.72	32	15613	16122	-0.27	-0.29
670	36	0.48	10	8568	8095	-0.23	-0.24
703	36	0.48	43	23916	22556	-0.63	-0.60
752	36	0.36	32	21012	18999	-0.71	-0.61
812	36	0.288	32	20718	19603	-0.80	-0.68
853	36	0.24	13	11243	11041	-0.53	-0.48
911	48	0.96	11	6592	6902	-0.15	-0.15
940	48	0.96	40	18287	18611	-0.43	-0.42
988	48	0.64	28	18345	16323	-0.65	-0.60
1067	48	0.48	47	26500	25705	-1.17	-1.05
1114	48	0.384	34	22086	21040	-1.15	-1.00
1188	48	0.32	48	25060	27704	-1.46	-1.36
1213	60	1.2	13	7509	7364	-0.23	-0.23
1260	60	1.2	60	24260	25358	-0.71	-0.66
1293	60	0.8	33	20122	18447	-0.90	-0.85
1332	60	0.6	12	11155	10284	-0.63	-0.75
1396	60	0.48	16	13952	13119	-0.94	-1.00
1459	60	0.4	19	15264	15207	-1.15	-1.22

TABLE 8.17: Coefficient of determination for both original and validation data for sand overburden problem

		R^2	
Type of embedment soil	Variable	Original data	Validiation data
Sand at low density	Absolute. Maximum Stress	0.9697	0.9689
	Diameter Change	0.9612	0.9747
Sand at high density	Absolute. Maximum Stress	0.9786	0.9747
	Diameter Change	0.9406	0.9410
Marl	Absolute. Maximum Stress	0.9734	0.9669
	Diameter Change	0.9502	0.9554
Sabkha	Absolute. Maximum Stress	0.9688	0.9625
	Diameter Change	0.9491	0.9597

ing both the absolute maximum stresses and the diameter change for all the embedment soils included in the study.

8.3 Development of Regression Equations for the Pipe Crossing Highways

8.3.1 Selection of Design Variables

The design variables taken into account to develop regression equations for the design of pipelines crossing highways are the diameter of the pipe, the thickness of the pipe, and the depth of cover. These variables are varied in the finite element runs to generate a database of stresses and deformation for each type of native soil. The complete details were provided in Section 7.7. For each type of the native soils two regression equation are developed. One of the developed equations is for the prediction of the absolute maximum stress while the other one is for the prediction of the diameter change in the pipe. Each regression equation is developed from 125 data points.

8.3.2 Selection of Cases for Model Validation for Pipelines Crossing Highways

In order to check the validity of the developed regression models for pipelines crossing highways 13 cases are selected randomly for each type of native soil. These runs are not used in the development of the regression equations but are used to test the accuracy of the developed equations. The cases are shown in Tables 8.18 and 8.19 and are selected on the principle of random sampling.

TABLE 8.18: Selected runs from the database for sand at low and high density as native soils

Observation number	Pipe Diameter (in)	Thickness of Pipe Wall (in)	Depth of Cover (ft)	Types of underlying soil: Sand at low density — Abs. Max. Stress (psi)	Sand at low density — Diameter Change (in)	Sand at high density — Abs. Max. Stress (psi)	Sand at high density — Diameter Change (in)
10	12	0.16	12	237	-0.002	187	-0.002
21	12	0.08	2	7942.4	-0.11	5981.8	-0.0755
28	24	0.48	4	1797.2	-0.022	1409.1	-0.019
36	24	0.24	2	7055	-0.156	5647.9	-0.1163
53	36	0.72	4	1607.7	-0.031	1284.4	-0.026
61	36	0.36	2	6008	-0.195	4968.6	-0.1502
68	36	0.288	4	2851	-0.104	2152	-0.074
76	48	0.96	2	3194.7	-0.074	2833.6	-0.068
92	48	0.384	3	3820	-0.177	2925	-0.124
99	48	0.32	8	933	-0.041	726	-0.025
111	60	0.6	2	3470.8	-0.22	3682	-0.172
116	60	0.48	2	3900	-0.28	3498	-0.192
124	60	0.4	8	510	-0.06	743	-0.031

TABLE 8.19: Selected runs from the database for marl and sabkha as native soils

Observation number	Pipe Diameter (in)	Thickness of Pipe Wall (in)	Depth of Cover (ft)	Types of underlying soil: Marl — Abs. Max. Stress (psi)	Marl — Diameter Change (in)	Sabkha — Abs. Max. Stress (psi)	Sabkha — Diameter Change (in)
10	12	0.16	12	432	-0.003	523	-0.004
21	12	0.08	2	5083.6	-0.0683	6883.1	-0.0958
28	24	0.48	4	1551.4	-0.02	1698.9	-0.022
36	24	0.24	2	4759.9	-0.106	6896.1	-0.164
53	36	0.72	4	1509.1	-0.029	1647.4	-0.033
61	36	0.36	2	4462.1	-0.155	5951.5	-0.214
68	36	0.288	4	2527	-0.094	2983	-0.127
76	48	0.96	2	2548.2	-0.066	3119.1	-0.074
92	48	0.384	3	2875.6	-0.143	3671	-0.198
99	48	0.32	8	962	-0.044	1181	-0.05
111	60	0.6	2	3027.6	-0.18	4196.9	-0.25
116	60	0.48	2	3058	-0.202	4146.2	-0.27
124	60	0.4	8	951	-0.056	1170	-0.07

8.3.3 Correlation Matrices of the Variables Used in Development of Pipelines Crossing Highways

To check the relationships among the variables used in the development of the models for the pipelines crossing highways, correlation matrices are obtained. Table 8.20 shows the correlation matrices for the variables used for all types of native soils. In Table 8.20, the correlation matrices include both the dependent variables and the independent variables. The following can be concluded from the generated correlation matrices:

- The native soil type does not affect the relation between the IV's, i.e., the correlation coefficients of the IV's don't change with the change in the type of native soil.
- There is a positive correlation between the pipe's diameter and the thickness of the wall (0.7396), i.e., the greater the value of the pipe's diameter the greater the thickness of the pipe wall.
- The depth of cover is varied from 2 ft. to 12 ft., and the pipe diameter is varied from 12 inches to 60 inches; however, there is no correlation between the two variables as the correlation coefficient is 0.0252.
- There is a negative correlation between the pipe's diameter and the absolute maximum stress. This is in support to the fact that larger diameter pipes have less absolute maximum stress.
- The highest correlation coefficient between the pipe's diameter and the absolute maximum stress is for sand at low density as native soil (−0.2768), then sand at high density (−0.2288), then marl at low density (−0.2176) and then for sabkha (−0.2111)
- There is a negative correlation between the thickness of the pipe wall and absolute

TABLE 8.20: Correlation matrices for the used variables for pipelines crossing highways for different soil types

	Correlation Coefficient					
	Variables	Diameter	Thickness	Cover	ABS. Max. Stress	Diamter change
Sand at low density	Diameter	1.00	.7390	.0252	-0.2768	-0.3187
	Thickness	0.7390	1.0000	.0258	-0.3128	-.0396
	Cover	.0252	.0258	1.0000	-0.8187	0.6986
	Absolute maximum stress	-0.2768	-.3128	-0.8187	1.000	-0.6441
	Diameter change	-.3187	-.0396	0.6968	-0.6441	1.0000
Sand at high density	Diameter	1.00	.7390	.0252	-0.2768	-0.3115
	Thickness	0.7390	1.0000	.0258	-0.3128	0.0059
	Cover	.0252	.0258	1.0000	-0.8389	0.7314
	Absolute maximum stress	-0.2288	-0.2584	-0.8389	1.000	-.6959
	Diameter change	-.3115	0.0059	0.7314	-0.6959	1.0000
Marl	Diameter	1.00	.7390	.0252	-0.2176	-0.3763
	Thickness	0.7390	1.0000	.0258	-0.2779	0.0059
	Cover	.0252	.0258	1.0000	-0.8851	0.7007
	Absolute maximum stress	-0.2176	-0.2779	-0.8851	1.000	-.6652
	Diameter change	-.3736	-0.0059	0.7007	-0.6652	1.0000
Sabkha	Diameter	1.00	.7390	.0252	-0.2111	-0.3512
	Thickness	0.7390	1.0000	.0258	-0.2840	0.0220
	Cover	.0252	.0258	1.0000	-0.8587	0.6809
	Absolute maximum stress	-0.2111	-0.2840	-0.8587	1.000	-.6781
	Diameter change	-.3512	-0.0220	0.6809	-0.6781	1.000

maximum stress.

- There is a strong negative correlation between the depth of cover and the absolute maximum stress. The correlation coefficients values range from −0.8187 to −0.8851.
- The depth of cover has the highest correlation coefficient with the diameter change. The correlation coefficient values range from .6809 and 0.7314 for the different native soils.
- The relations among all the IV's with the diameter change is negative and relatively strong.
- There is a negative and relatively strong correlation between the DV's.

8.3.4 Linearization of the Relationships

In order to get an idea about the relationships between the IV's and the DV's, a representative data set from the data of the pipe with low density sand as native soil is selected and is plotted in Figs. 8.37 to 8.42. Fig 8.37 shows the effect of the pipe's diameter on the absolute maximum stress values for a D/t ratio of 50 and a cover depth of 4 ft. Fig. 8.38 shows the effect of the pipe wall thickness on the absolute maximum stress for a pipe with 24 inches diameter and 4 ft. depth of cover. The effect of the depth of cover on the absolute maximum stress for a pipe with 24 inches diameter and 0.32 inch thickness is shown in Fig. 8.39. Fig. 8.40 shows the effect of the change in the pipe diameter for different diameters for a pipe having a wall thickness of 0.48 inch and a cover depth 4 feet, and Fig. 8.41 shows the effect of changing the pipe wall thickness on the change in the diameter for a pipe with 24 inches diameter and 4ft. depth of cover. The effect of the depth of cover on the change in the pipe diameter for a pipe with 0.32 inches wall thickness and 24 inch

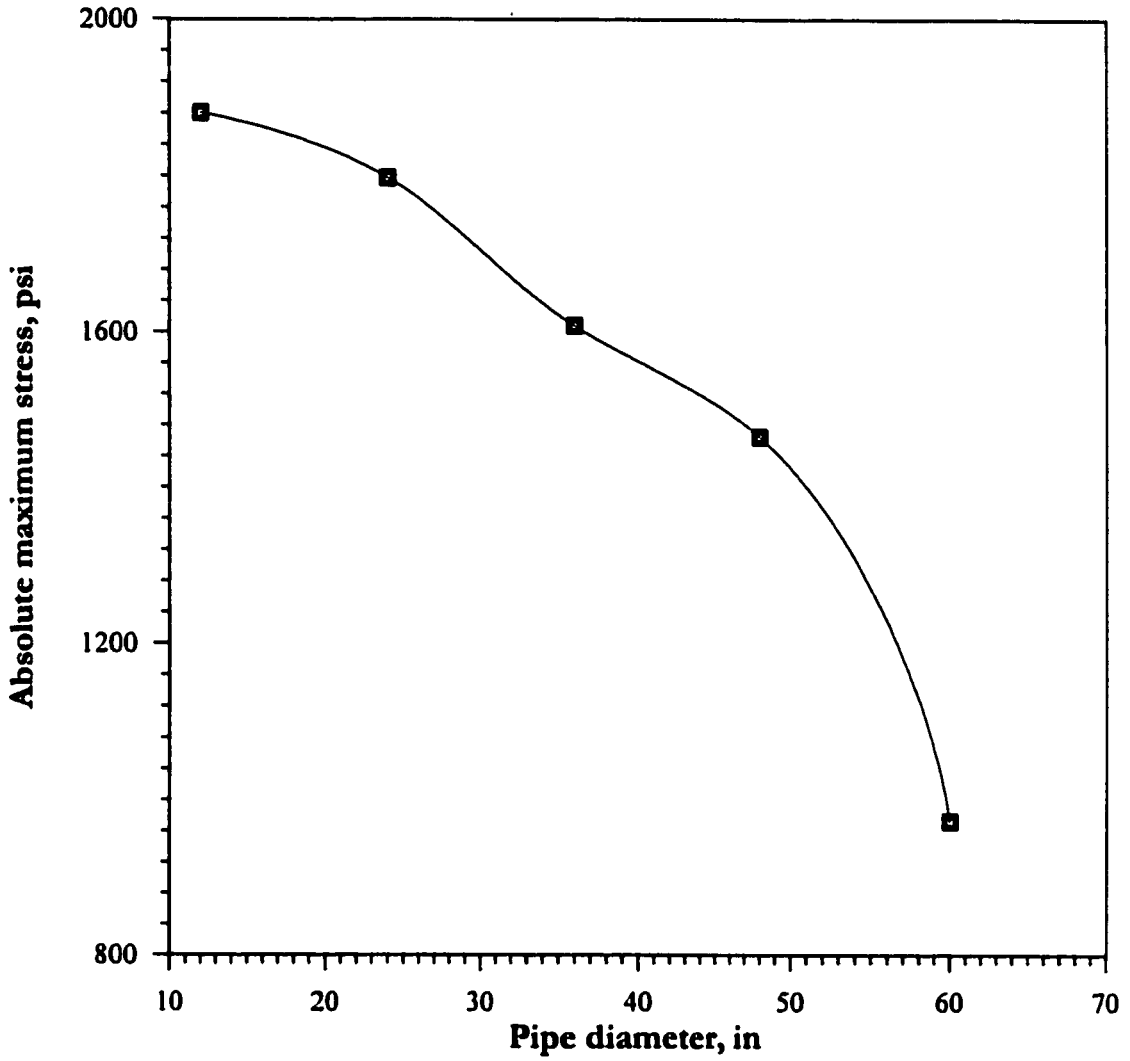

Fig. 8.37: Effect of changing the pipe diameter on the absolute maximum stress for a pipe with D/t = 50 H = 4 ft. subjected to live load conditions

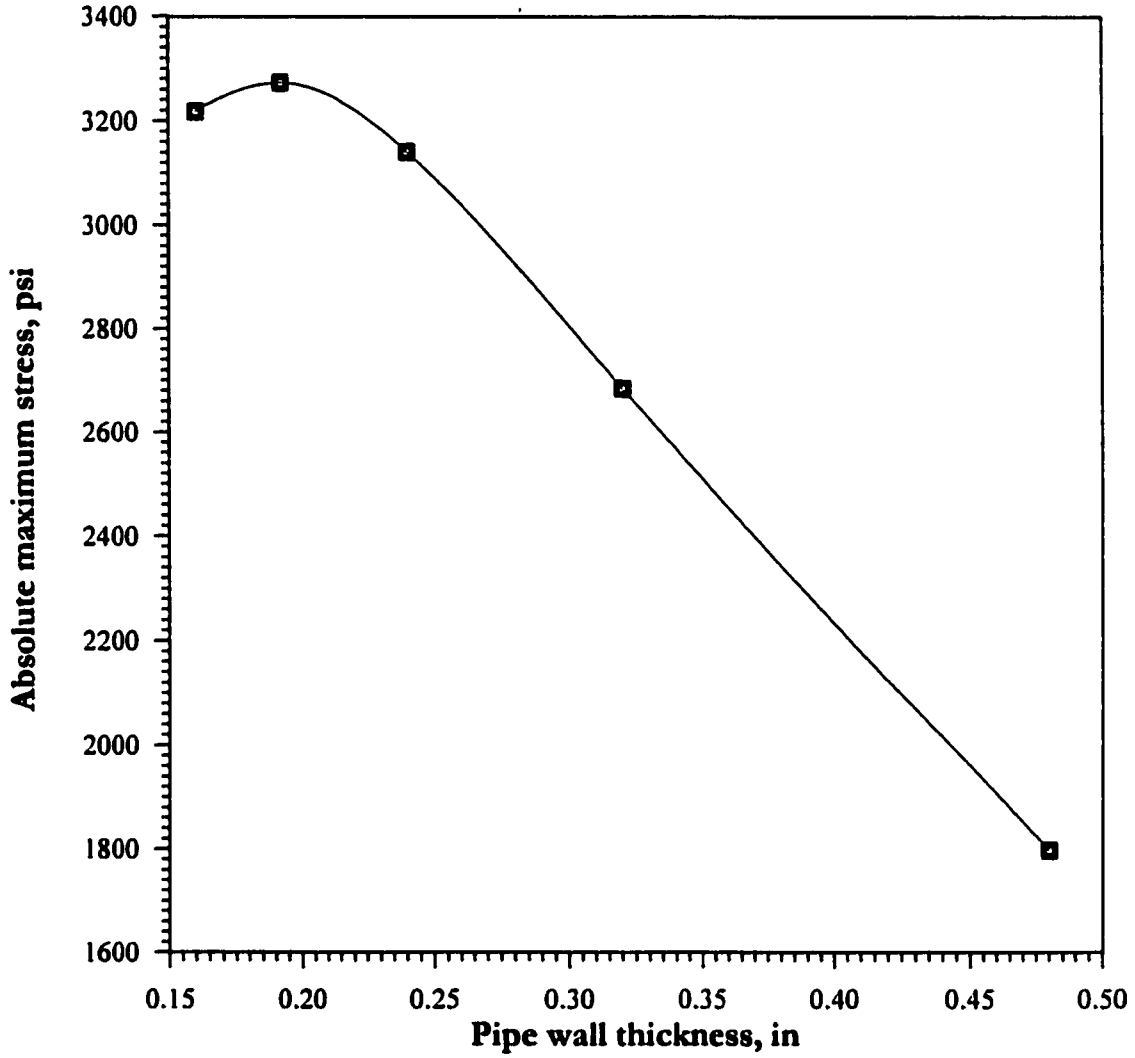

Fig. 8.38: Effect of changing the pipe wall thickness on the absolute maximum stress for a pipe with D =24 inch, H = 4 ft. subjected to live load conditions

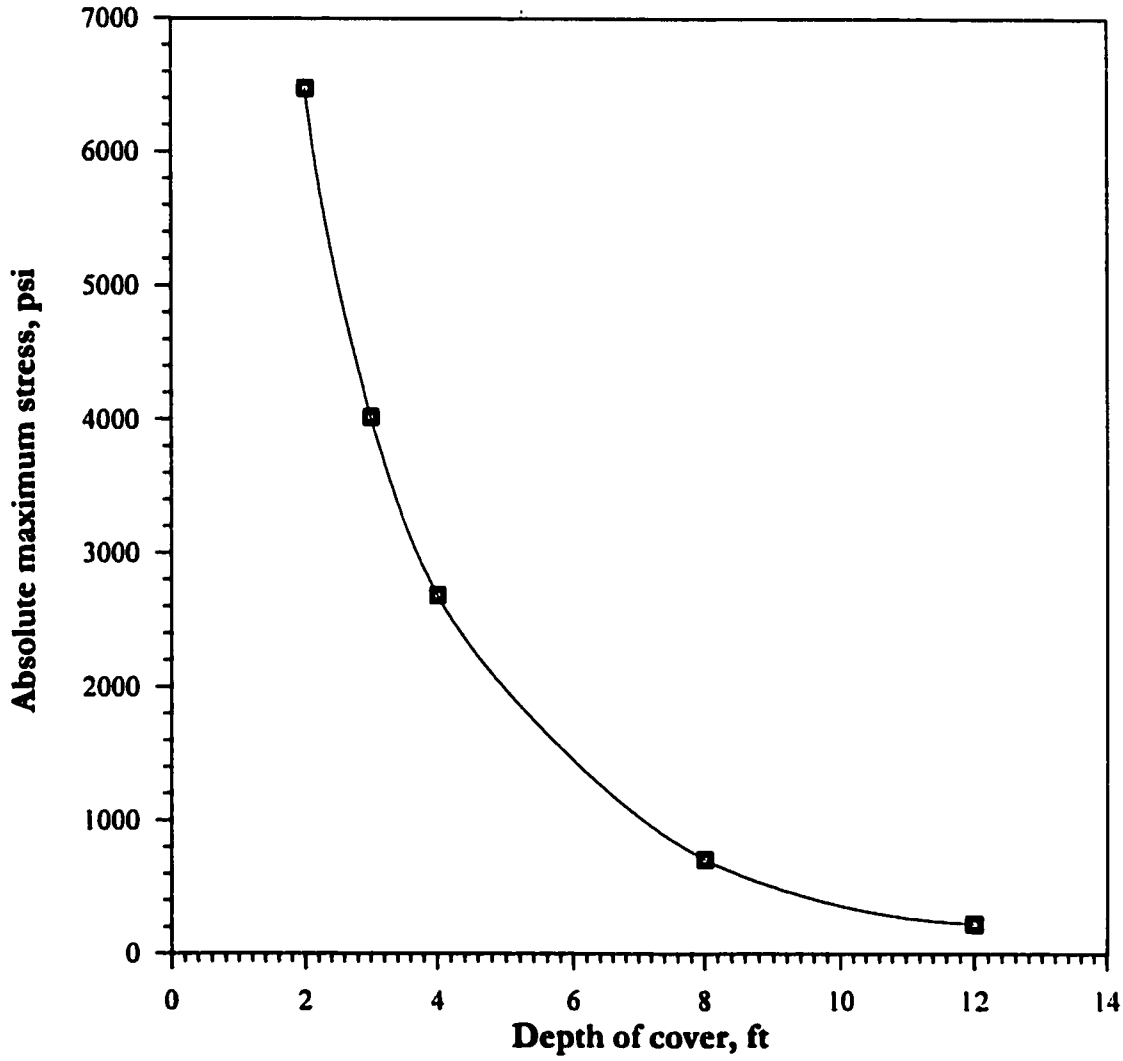

Fig. 8.39: Effect of changing the depth of cover on absolute maximum stress for a pipe with D = 24 inch, t = 0.32 inch subjected to live load conditions

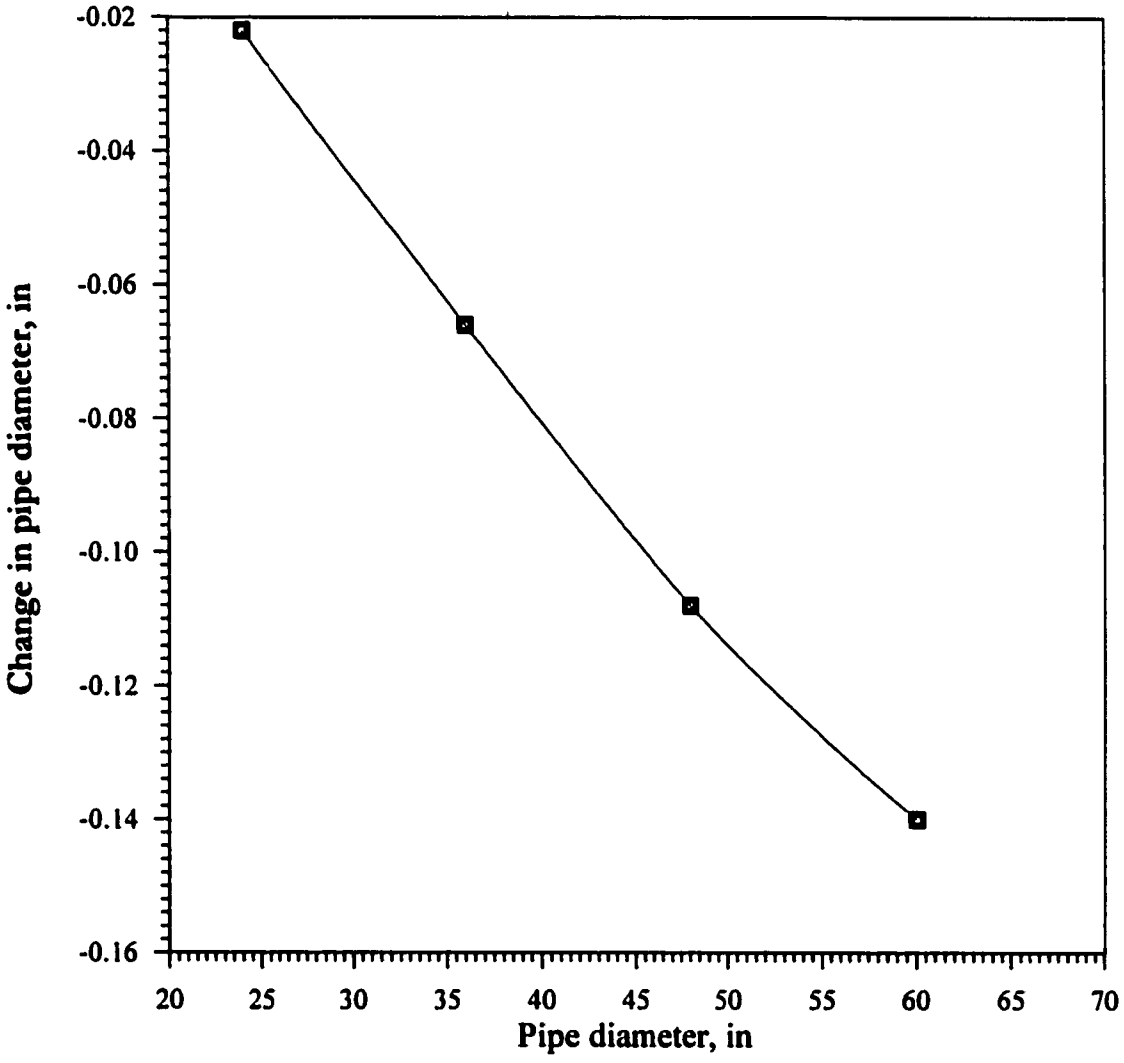

Fig. 8.40: Effect of changing the pipe diameter on the change of diameter for a pipe with t = 0.48 inch, H = 4 ft. subjected to live load conditions

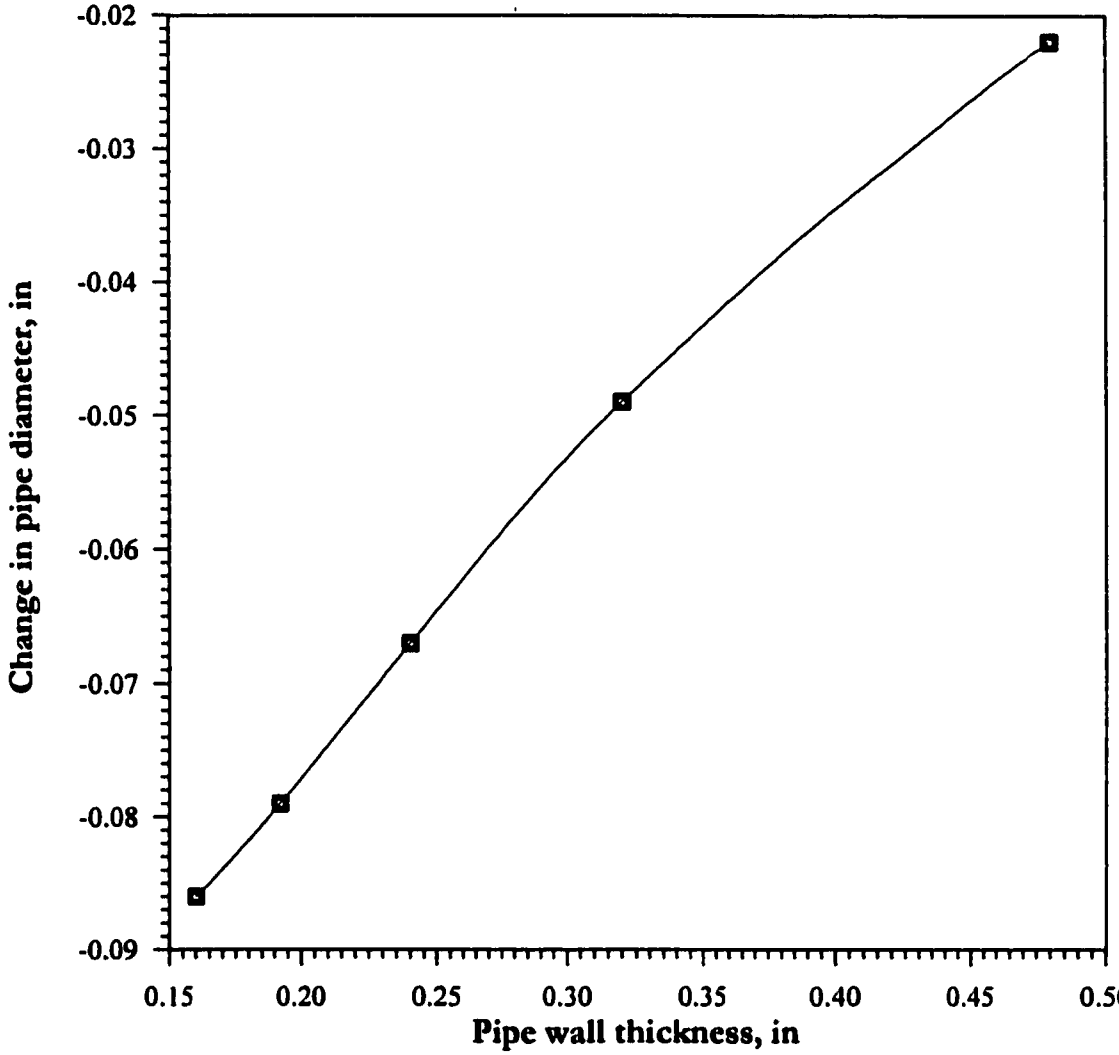

Fig. 8.41: Effect of changing the pipe wall thickness on the change in diameter for a pipe with D = 24 inch, H = 4 ft. subjected to live load conditions

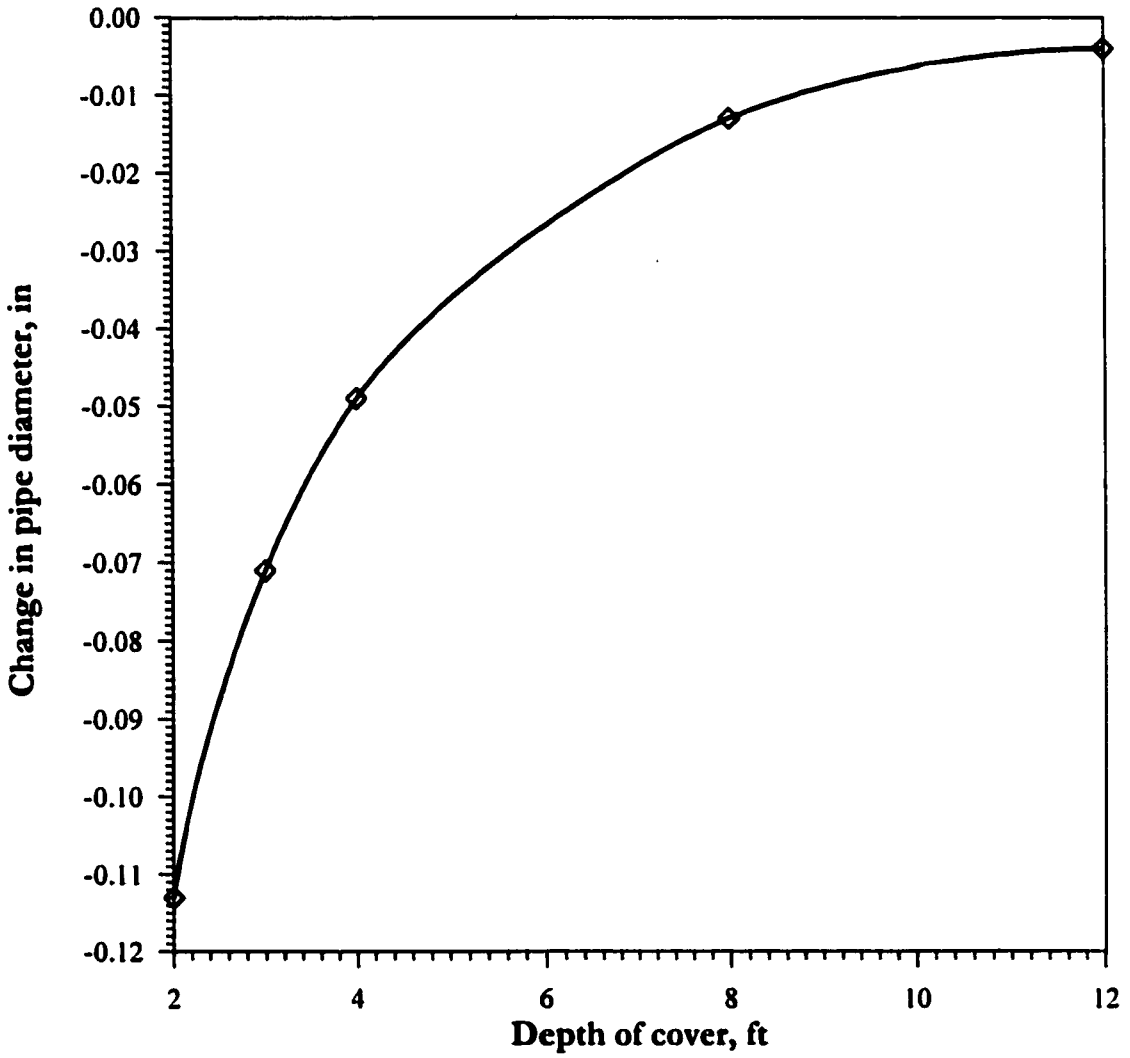

Fig. 8.42: Effect of changing the depth of cover on the change of diameter for a pipe with D = 24 inch, t = 0.32 inch subjected to live load conditions

diameter is shown in Fig. 8.42.

It can be seen from Figs. 8.37 to 8.42 that the relationships among the IV's and DV's are not linear. In order to develop models using multiple linear regression technique, it is essential to find ways to linearize these relationships. After numerous trials to find the best method to linearize the relationships, the linearized version of the relationships among the variables are shown in Figs. 8.43 to 8.48. Figs. 8.43 to 8.45 show the linearized relations between the IV's and the absolute maximum stress. The square values of the pipe's diameter versus the absolute maximum stress are used to linearize the relationship (Fig. 8.43). Fig. 8.44 shows that squaring the values of the pipe's wall thickness is the best method to linearize the relationship with the square root values of the absolute maximum stress, whereas using the log of the height of cover values is the optimal procedure to linearize the relation with the square root values of the absolute maximum stress (Fig. 8.45). Taking the log of the negative change in the pipe diameter is found to be suitable for linearizing the relationship between the pipe diameter and the change in diameter (Fig. 8.46). Taking the square root of the pipe wall thickness and the exponential of the change in the diameter is the way to linearize the relationship between the wall thickness and change in the diameter (Fig. 8.47). The log of the change in the pipe diameter and the cover depth is found to be adequate for linearizing the relationship between the change in the diameter and the height of cover (Fig. 8.48)

8.3.5 Developed Equations for Pipelines Crossing Highways

A multiple linear regression analysis is performed using the STATISTICA facility [92].

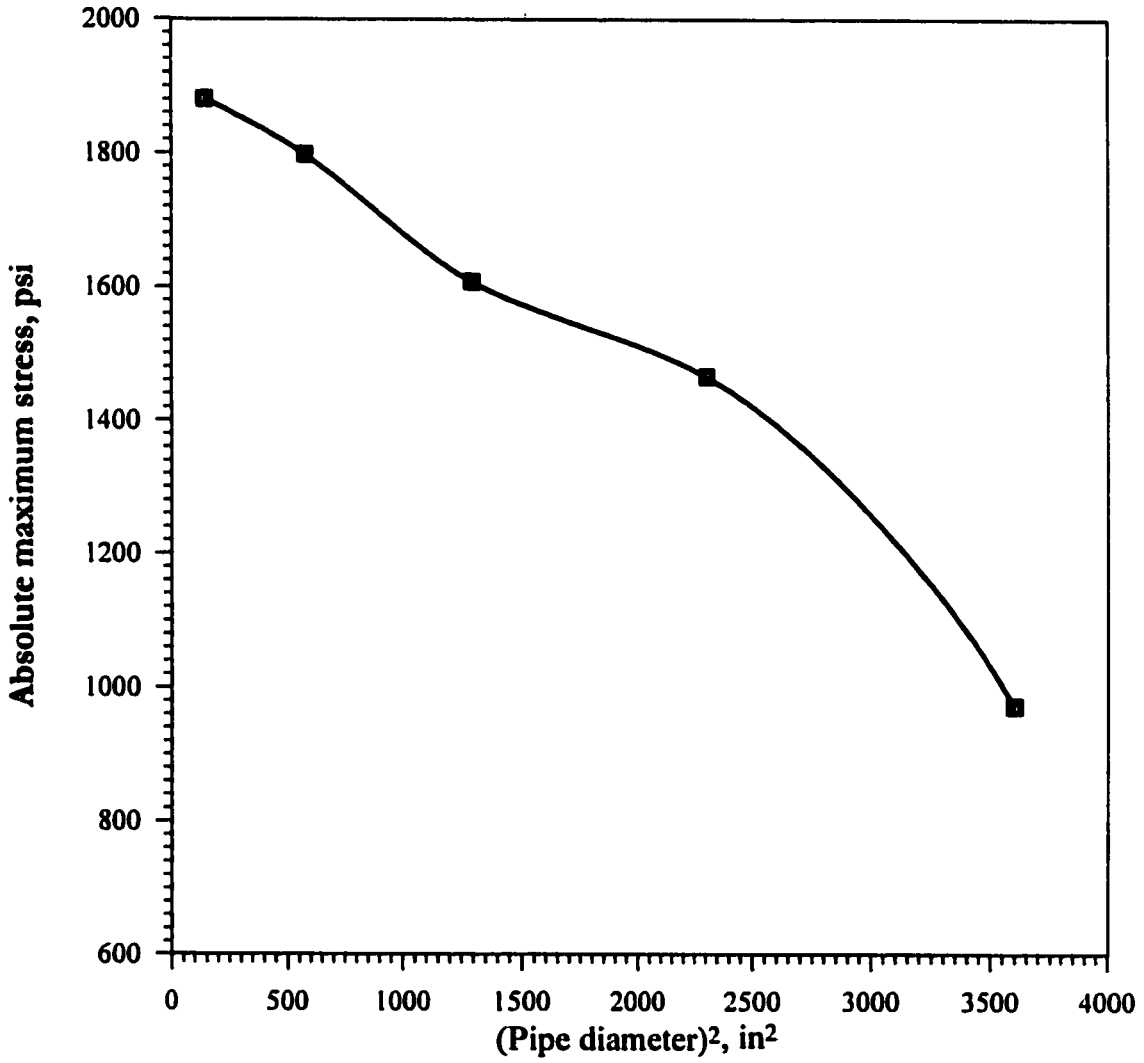

Fig. 8.43: Linearization of the change in pipe diameter vs. absolute value of the maximum stress relation for a pipe with D/t = 50, H = 4 ft. under live load condition

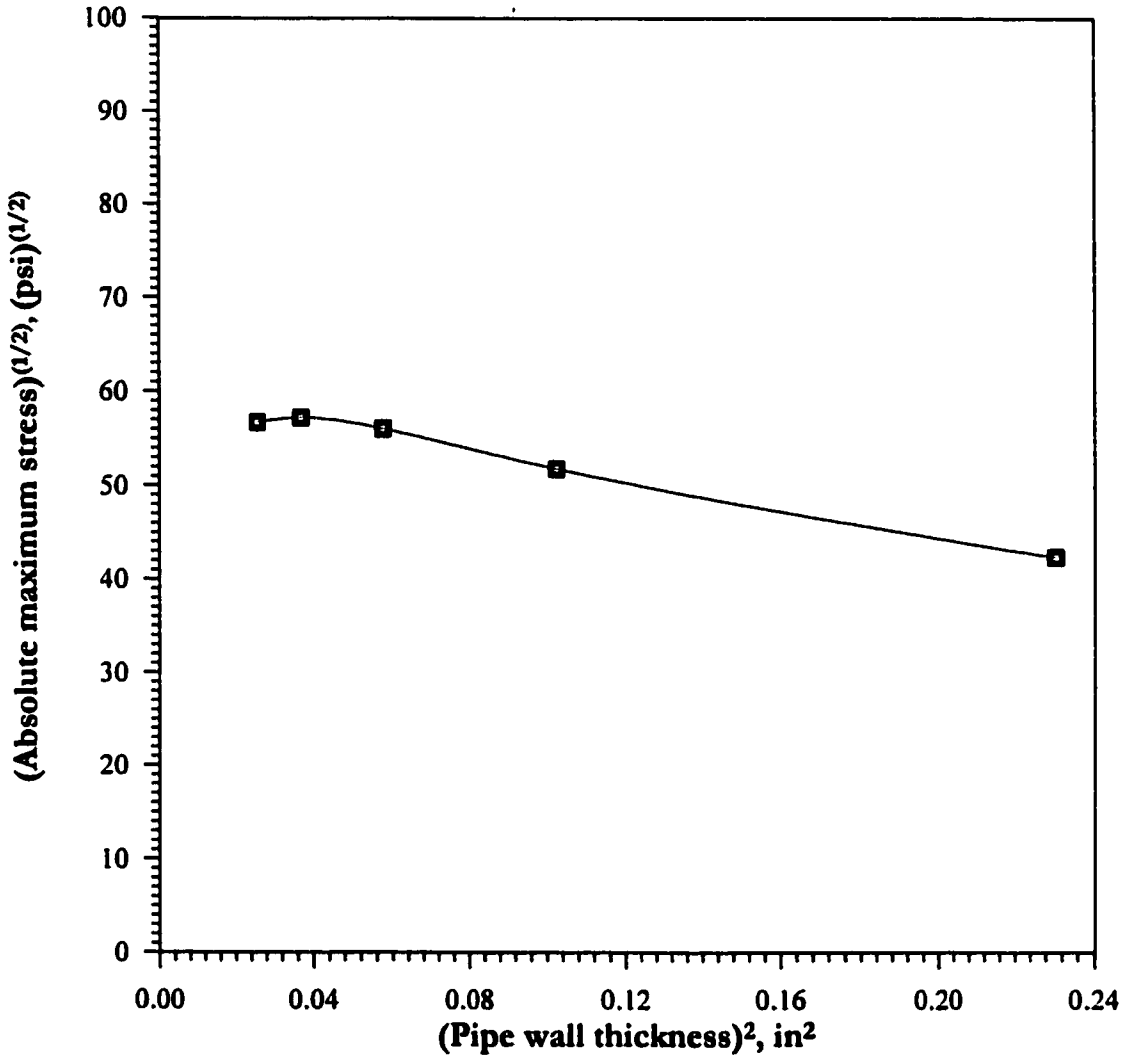

Fig. 8.44: Linearization of the change in pipe wall thickness vs. absolute value of the maximum stress relation for a pipe with D = 24 inch, H = 4 ft. under live load condition

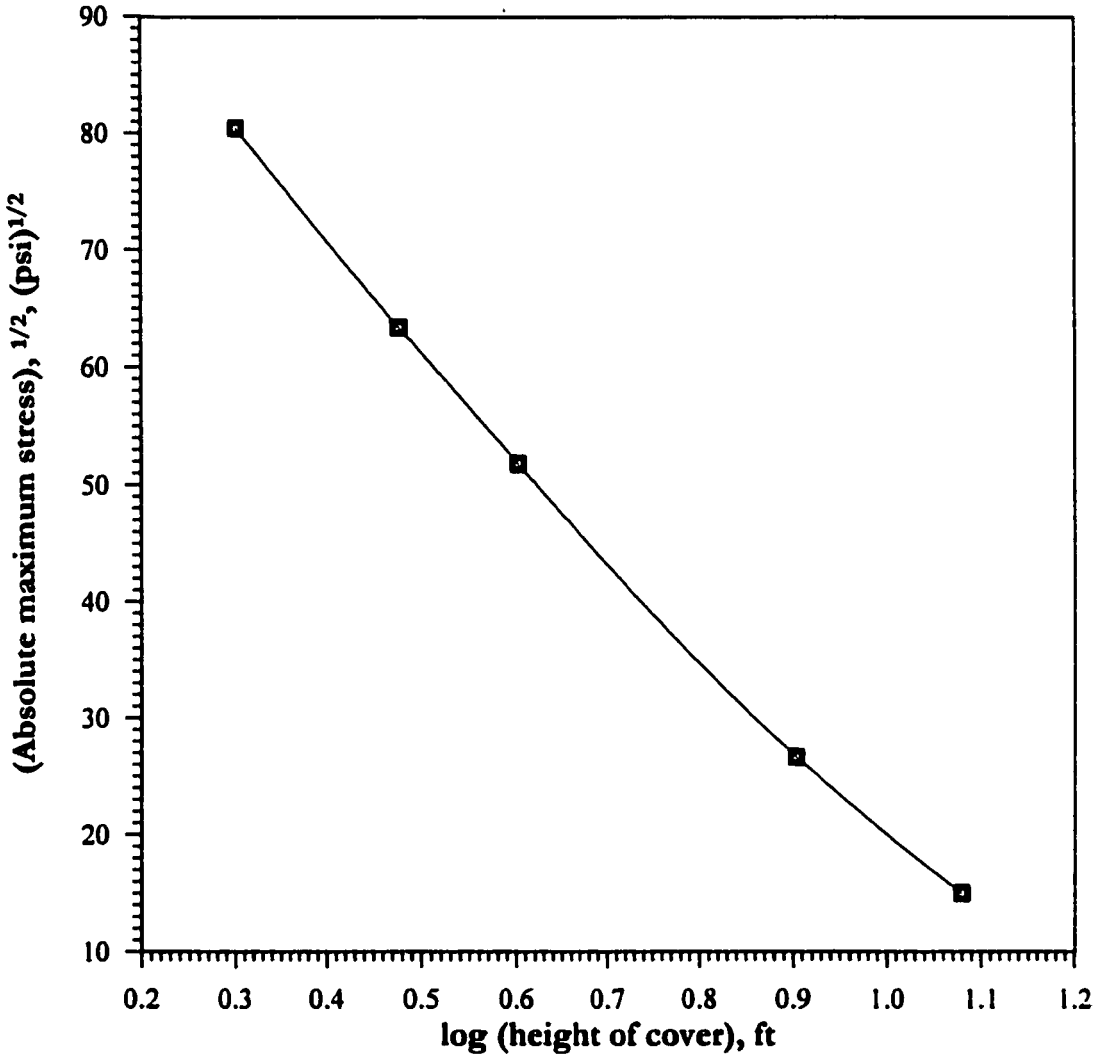

Fig. 8.45: Linearization of the change in cover height vs. the absolute value of the maximum stress relation for a pipe with t = 0.32 inch, D = 24 inch under live load conditions

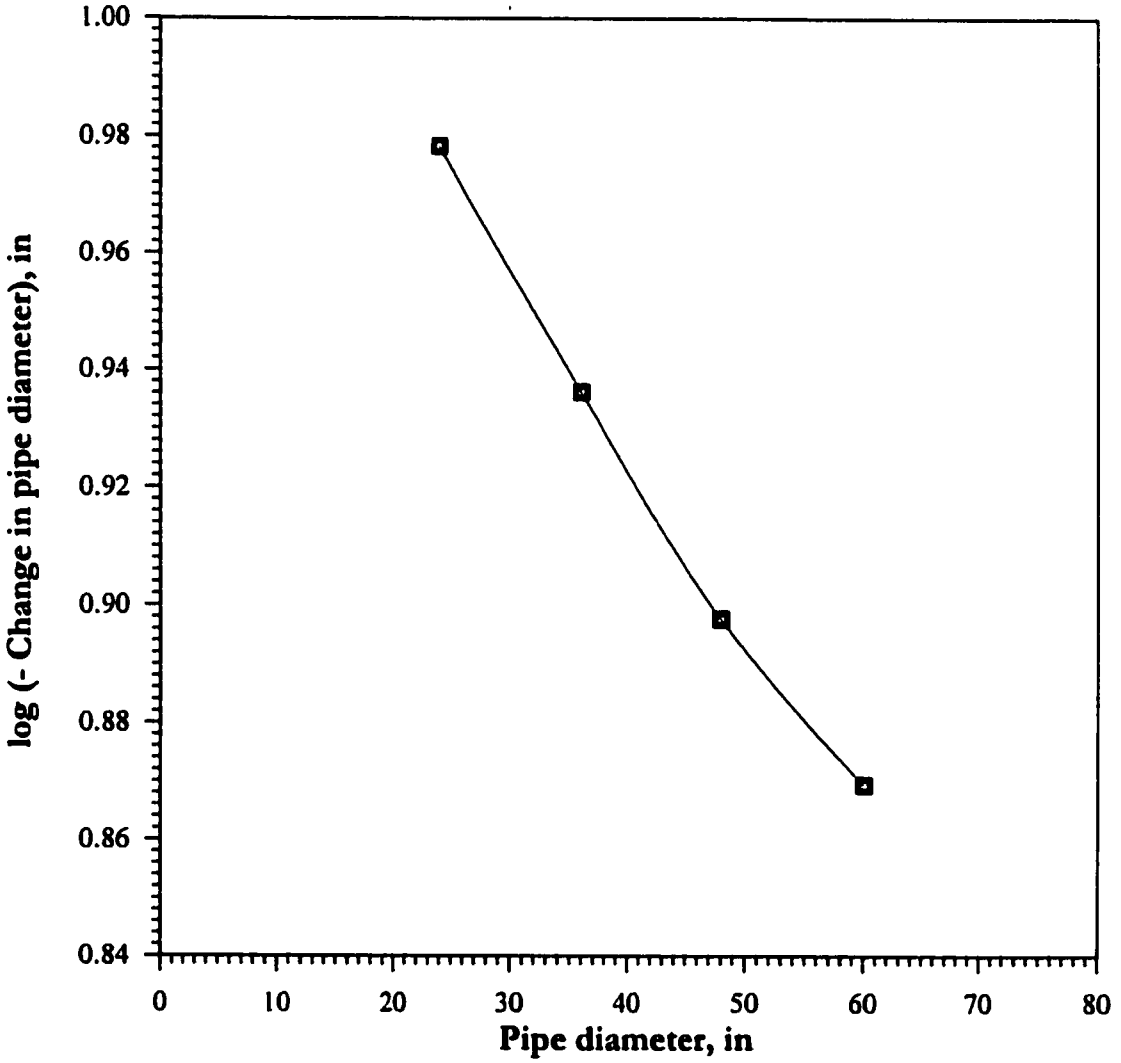

Fig. 8.46: Linearization of the change in pipe diameter vs. the change in diameter in a pipe with t = 0.48 inch, H = 4 ft. under live load condition

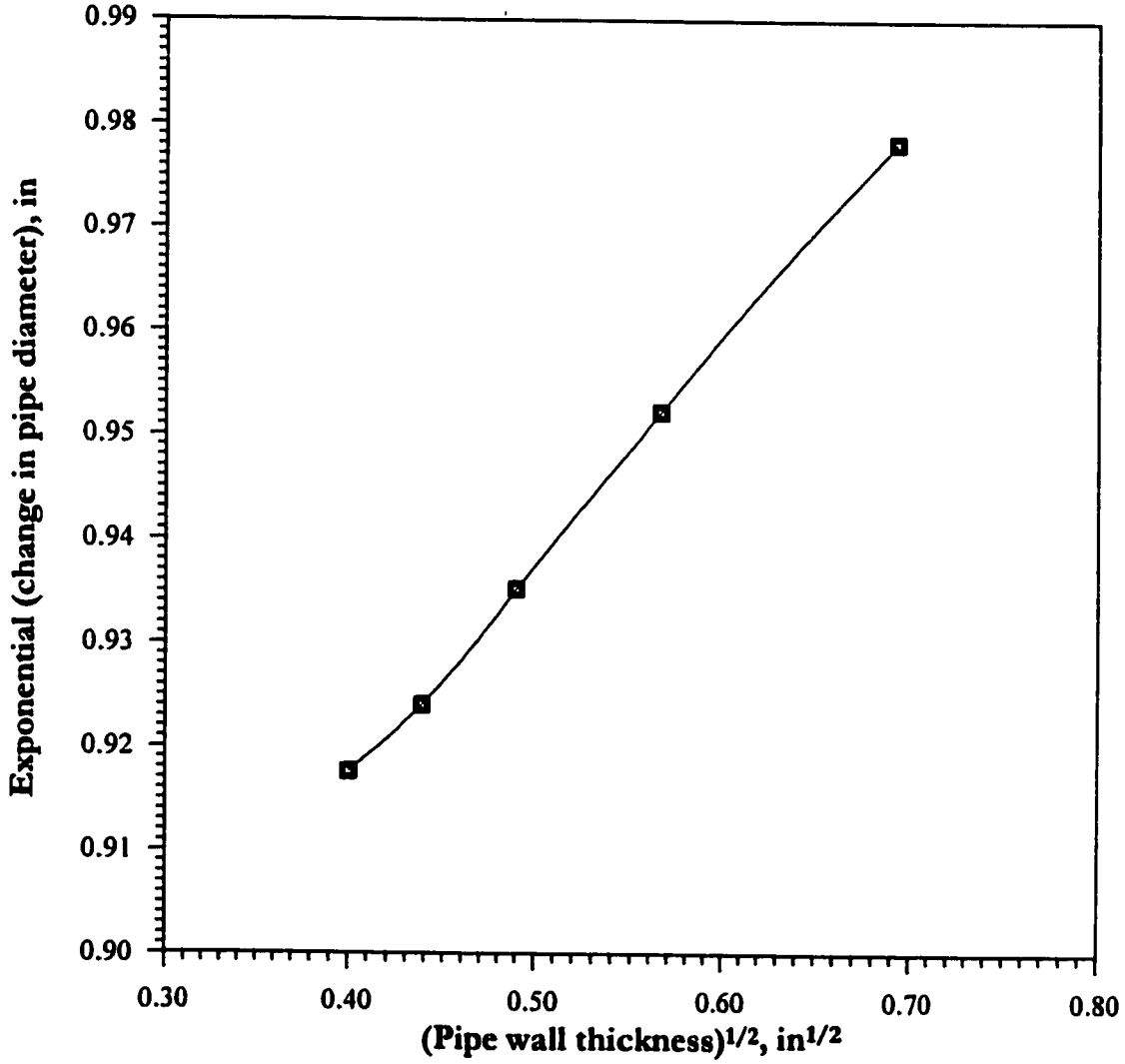

Fig. 8.47: Linearization of the change in pipe wall thickness vs. the change in diameter relation for a pipe with D = 24 inch, H = 4 ft. under live load conditions

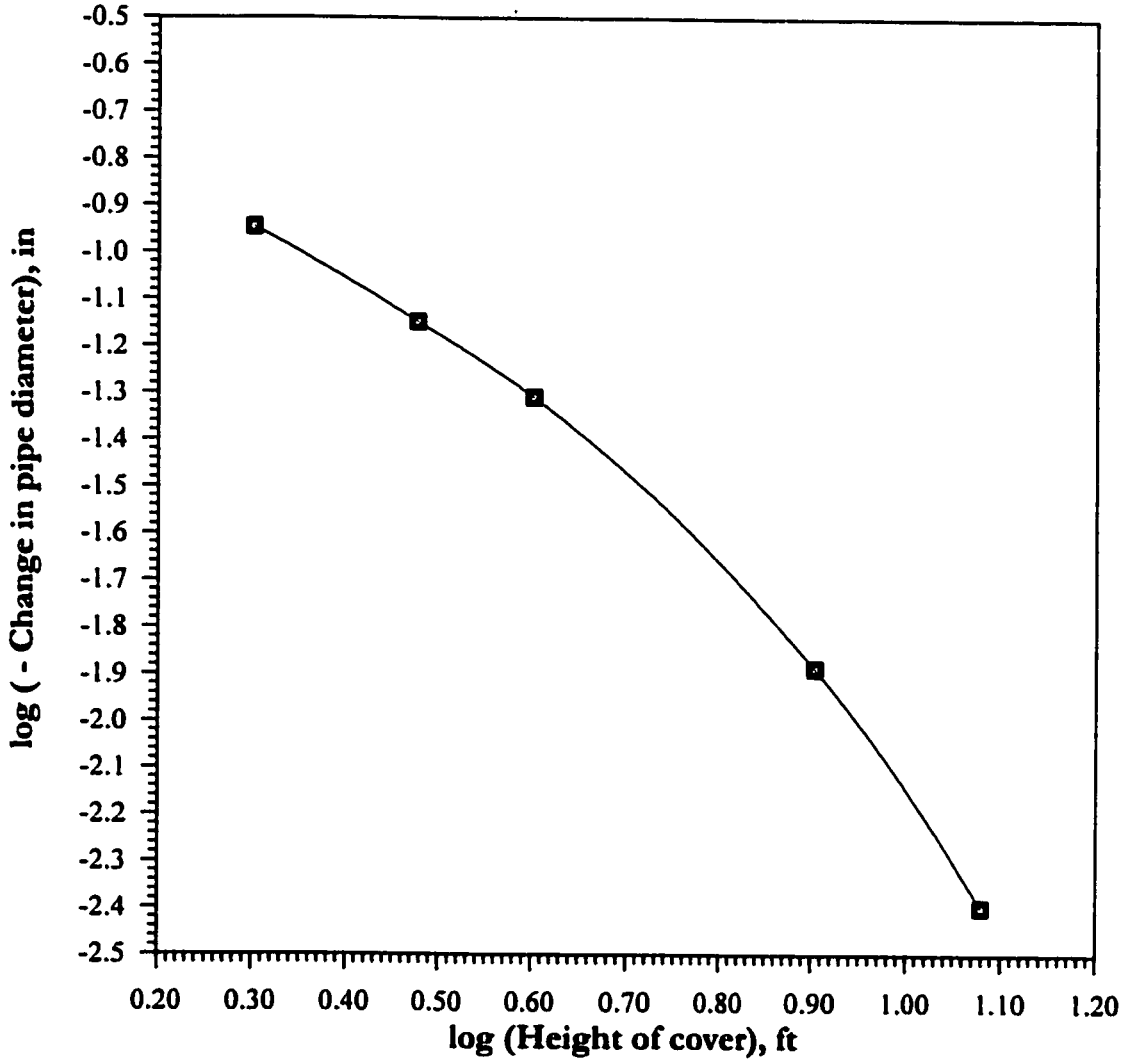

Fig. 8.48: Linearization of the change in cover height vs. the change in diameter relation for a pipe with t = 0.32 inch, D = 24 inch under live load condition

The resulting regression models relate the absolute maximum stress and diameter change to the pipe's diameter, pipe's wall thickness and depth of cover. A number of trials are performed to insure a good value for the goodness of fit (R^2).

Table 8.21 shows the developed transformed prediction models for both the absolute maximum stress and the diameter change for all types of native soils. In addition, the coefficient of determination (R^2) and the significance levels of the models are shown in the table. R^2 values for the developed models are higher than 0.94. In addition, the confidence levels for all the models are higher than 99.99%. Tables 8.22 to 8.29 give the model fitting results and the analysis of variance for each model.

In Tables 8.22 to 8.29, the coefficients of all variables in the model are given, in addition to their t-value statistics and F statistics. For all the parameters used in the model the confidence level is 99.9%, and also in analysis of variance tables, the confidence levels of all the fitted models are above 99.99%.

Figs. 8.49 to 8.56 show plots of the predicted values versus the original values for all the models. The figures show the distribution of the points around the 45° line. In these figures, all the points are located around the 45° lines without any major statistical outliers. This indicates the accuracy of the generated models in predicting the DV's.

8.4 TESTING OF MODELS

8.4.1 Sign Testing

The sign test is performed to check if the variables' signs in the developed models

TABLE 8.21: Generated models for the absolute maximum stress and diameter change for different native soils subjected to live load

Native Soil	Generated Model	R^2	Significance
Low Density	Stress = $[-102.45 - 0.0011 * (D)^2 - 16.5448(t) - 32.0902 * \ln(H)]^2$	0.9697	0.000
Sand	$\Delta D = -\exp[-5.73847 - 1.81359 * \ln(1/D) - 3.19599(t)^{1/2} - 0.31301(H)]$	0.9612	0.000
High Density	Stress = $[96.19028 - 0.6315 * \ln(1/D) - 20.9539(t)^{1/2} - 29.5689 * \ln(H)]^2$	0.9786	0.000
Sand	$\Delta D = \exp[-5.3445 - 1.52097 * \ln(1/D) - 2.63276 * (t)^{1/2} - 0.31591(H)]$	0.9406	0.000
Marl	Stress = $[88.18952 - 2.0459 * \ln(1/D) - 23.6648(t)^{1/2} - 25.3808 * \ln(H)]^2$	0.9734	0.000
	$\Delta D = -\exp[-5.75629 - 1.7346 * \ln(1/D) - 23.6648(t)^{1/2} - 0.27296(H)]$	0.9502	0.000
Sabkha	Stress = $[99.71828 - 3.12348 * \ln(1/D) - 30.5039(t)^{1/2} - 29.6722(H)]$	0.9688	0.000
	$\Delta D = -\exp[-5.51985 - 1.7171 * \ln(1/D) - 3.12495(t)^{1/2} - 0.26879(H)]$	0.9491	0.000

Stress = Absolute maximum stress (psi)
ΔD = Change in pipe's diameter (in.)
t = Pipe's wall thickness (in.)
D = Pipes's diameter (in.)
H = height of sand cover (ft)

TABLE 8.22: Model fitting results and analysis of variance for the prediction of the absolute maximum stress for pipe with sand at low density as native soil under live load connditions

Model fitting results for absolute maximum stress						
$N = 1461$	BETA	St. Err. of BETA	B	St. Err. of B	t(1457)	p-level
Intercept			102.447	1.47968	69.23592	0.00
ln(Diameter)	-0.06171	.032299	-0.0011	0.000576	-1.9107	0.058695
(Thickness)$^{1/2}$	-.20713	.032303	-16.5448	2.580239	-6.41213	3.88E-09
ln(Cover)	-.9328	.022034	-32.0902	0.758017	-42.3344	0.00
Analysis of Variance; DV: (Stress)$^{(1/2)}$						
Effect	Sums of squares	df	Mean Squares	F	p-level	
Regress.	52393.18	3	117464.39	651.0194	00.00	
Residual	2897.232	108	26.82623			
Total	55290.94					

N = number of cases included for model devlopment

BETA = the value of Beta distribution of the parameter

St. Err. of Beta = the estimate of the standard error of the Beta distribution of the parameter

B = the estimate of the parameter value

St. Err. of B = the estimate of the standard deviation of the parameter estimate

df = degrees of freedom associated for the terms

$t(df)$ = the t test that the parameter is zero, calculated by dividing the value of the parameter by the standard error of the parameter

p-level = the probability of getting a greater t or F statistic than that observed if the hypothesis is true. It is the significance probability

Sums of Squres = sum of square of the terms

Mean of Squares = the sum of squares divided by the degrees of freedom

F = the F value for testing the hypothesis that all parametres are zero except for the intercept. It is formed by dividing the mean square for the regressors (model) by the mean square of residuals

TABLE 8.23: Model fitting results and analysis of variance for the prediction of the change in diameter for pipe with sand at low density as native soil under live load condition

Model fitting results for change in diamter						
$N = 1461$	BETA	St. Err. of BETA	B	St. Err. of B	t(108)	p-level
Intercept			-5.7384	.003875	-33.7778	0.00
ln(1/Diameter)	-7642	.029453	-1.81359	.000088	-25.9466	0.00
(Thickness)$^{(1/2)}$	-.48744	.02945	-3.19599	.19309	-16.5518	2.14E-31
Cover	-.86319	0.018265	-.31301	.0066223	-47.2603	0.00
Analysis of Variance; DV: ln($-\Delta D$)						
Effect	Sums of squares	df	Mean Squares	F	p-level	
Regress.	37.39154	3	12.46385	964.2214	0.00	
Residual	1.396044	108	.012926			
Total	38.78759					

TABLE 8.24: Model fitting results and analysis of variance for the prediction of the absolute maximum stress for pipe with sand at high density as native soil under live load conditiont6.7.7

Model fitting results for absolute maximum stress						
$N = 1461$	BETA	St. Err. of BETA	B	St. Err. of B	t(108)	p-level
Intercept			96.119028	2.560052	37.57357	0.00
ln(1/Diameter)	-0.01805	.029104	-0.6315	1.018156	-0.62024	0.536408
(Thickness)$^{(1/2)}$	-.216779	.029102	-20.9539	2.812834	-7.44939	2.44E-11
ln(Cover)	-.95604	0.018047	-29.5689	0.558165	-52.9751	0.00
Analysis of Variance						
Effect	Sums of squares	df	Mean Squares	F	p-level	
Regress.	43117.77	3	14372.59	988.2515	0.00	
Residual	1570.693	108	14.54345			
Total	44688.47					

TABLE 8.25: Model fitting results and analysis of variance for the prediction of the change in diameter for pipe with sand at high density as native soil under live load condition

Model fitting results for change in diamter						
$N = 1461$	BETA	St. Err. of BETA	B	St. Err. of B	t(108)	p-level
Intercept			-5.3445	0.122717	-43.5516	0.00
ln(1/Diameter)	-0.66451	0.022059	-1.52097	0.050489	-30.1249	0.00
(Thickness)$^{(1/2)}$	-0.41634	0.022056	-2.63276	0.139475	-18.8762	5.47E-36
Cover	-0.90328	0.013679	-0.31591	0.004784	-66.0333	0.00
Analysis of Variance: DV:Ln(-ΔD)						
Effect	Sums of squares	df	Mean Squares	F	p-level	
Regress.	35.5316		11.78387	1747.175	0.00	
Residual	0.728409	3	0.006745		0.00	
Total	36.08001	108			0.00	

TABLE 8.26: Model fitting results and analysis of variance for the prediction of the absolute maximum stress for pipe with marl native soil under live load condition

Model fitting results for absolute maximum stress						
$N = 1461$	BETA	St. Err. of BETA	B	St. Err. of B	t(108)	p-level
Intercept			88.18952	2.15404	40.93263	0
ln(1/Diameter)	-0.06767	0.028341	-2.04597	0.856886	-2.38774	0.018689
(Thickness)$^{(1/2)}$	0-28331	0.02834	-23.6648	2.367242	-9.99679	4.74E-17
ln(Cover)	-0.94956	0.017574	-25.3808	0.469744	-54.0311	0
Analysis of Variance; DV: (Stress)$^{(1/2)}$						
Effect	Sums of squares	*df*	Mean Squares	F	p-level	
Regress.	32264.56		10754.85	1044.094	0.00	
Residual	1112.471	3	10.30065		0.00	
Total	33377.03	108			0.00	

TABLE 8.27: Model fitting results and analysis of variance for the prediction of the change in diameter for pipe with marl as native soil under live load condition

Model fitting results for change in diamter						
$N = 1461$	BETA	St. Err. of BETA	B	St. Err. of B	t(108)	p-level
Intercept			-5.75620	-32.2841	-32.2841	0.00
ln(1/Diameter)	-0.81508	0.034471	-1.7346	-23.6456	-23.6564	1.68E-44
(Thickness)$^{(1/2)}$	-0.5493	0.034467	-3.22962	-15.9369	-15.9369	3.94E-30
ln(Cover)	-0.83944	0.201376	-0.27296	-39.2693	-39.2693	0.00
Analysis of Variance: DV:Ln(-ΔD)						
Effect	Sums of squares	*df*	Mean Squares	F	p-level	
Regress.	29.6527	3	9.884234	694.2058	0.00	
Residual	1.537725	108	0.014238		0.00	
Total	31.19043				0.00	

TABLE 8.28: Model fitting results and analysis of variance for the prediction of the absolute maximum stress for pipe with sabkha as native soil under live load condition

Model fitting results for absolute maximum stress						
$N = 1461$	BETA	St. Err. of BETA	B	St. Err. of B	t(108)	p-level
Intercept			99.71852	2.419852	41.20842	0.00
ln(1/Diameter)	-0.08815	0.027159	-3.12348	0.962398	-3.24552	0.001561
(Thickness)$^{(1/2)}$	-0.31158	0.027158	-30.5039	2.658791	-11.4728	2.09E-20
ln(Cover)	-0.94716	0.016841	-29.6722	0.527597	-56.2403	0.00
Analysis of Variance; DV: (Stress)$^{(1/2)}$						
Effect	Sums of squares	*df*	Mean Squares	F	p-level	
Regress.	44446.73	3	14815.58	1140.173	0.00	
Residual	1403.368	108	12.99415		0.00	
Total	4580.1				0.00	

TABLE 8.29: Model fitting results and analysis of variance for the prediction of the change in diameter for pipe with sabkha as native soil under live load condition

Model fitting results for change in diamter						
$N = 1461$	BETA	St. Err. of BETA	B	St. Err. of B	t(108)	p-level
Intercept			-5.51985	0.164448	-33.566	0.00
ln(1/Diameter)	-0.82	0.03231	-1.7171	0.067658	-25.379	0.00
(Thickness)$^{(1/2)}$	-0.54015	0.032307	-3.12495	0.186905	-16.7195	9.76E-32
Cover	-0.84008	0.020037	-0.26879	0.006411	-41.2971	0.00
Analysis of Variance: DV:Ln(-ΔD)						
Effect	Sums of squares	*df*	Mean Squares	F	p-level	
Regress.	28.89073	3	9.630245	795.1265	0.00	
Residual	1.308052	108	0.012112		0.00	
Total	30.19879				0.00	

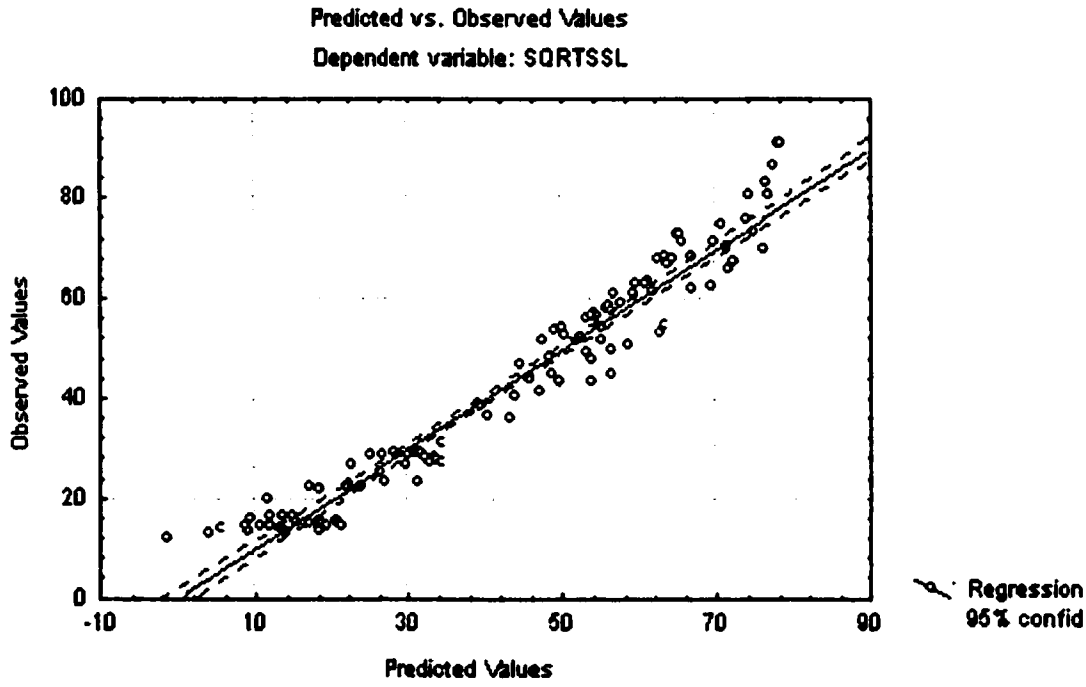

Fig. 8.49: Plot of predicted values versus the measured values for the absolute maximum stress for the pipe with low density sand as native soil under live load conditions

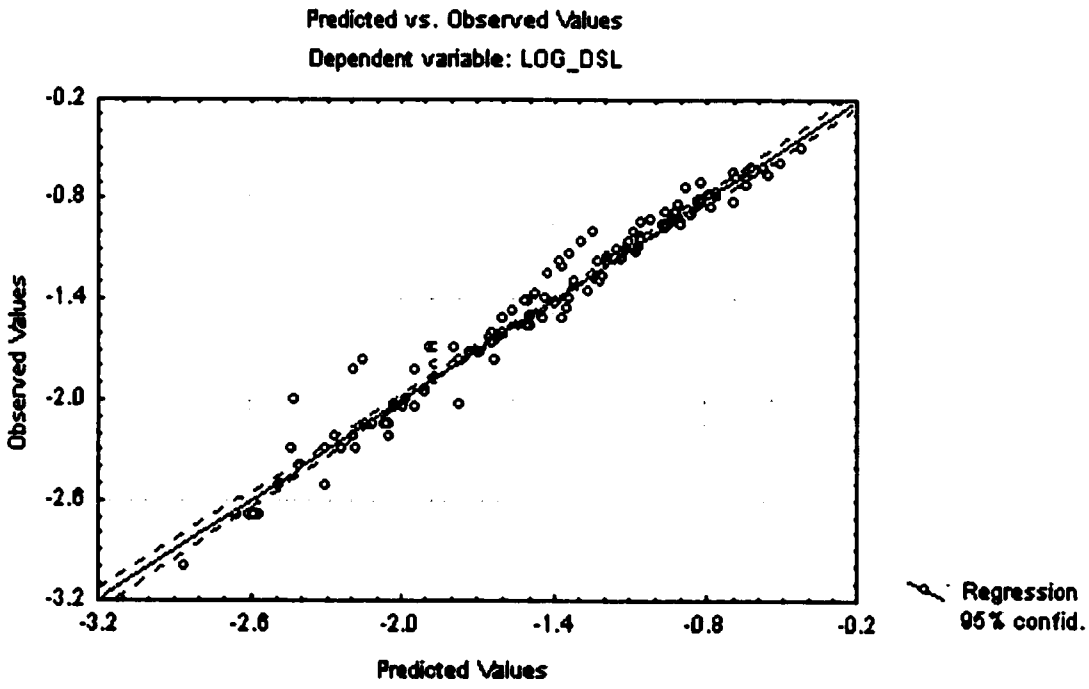

Fig. 8.50: Plot of predicted values versus the measured values for the change in pipe diameter for the pipe with low density sand as native soil under live load conditions

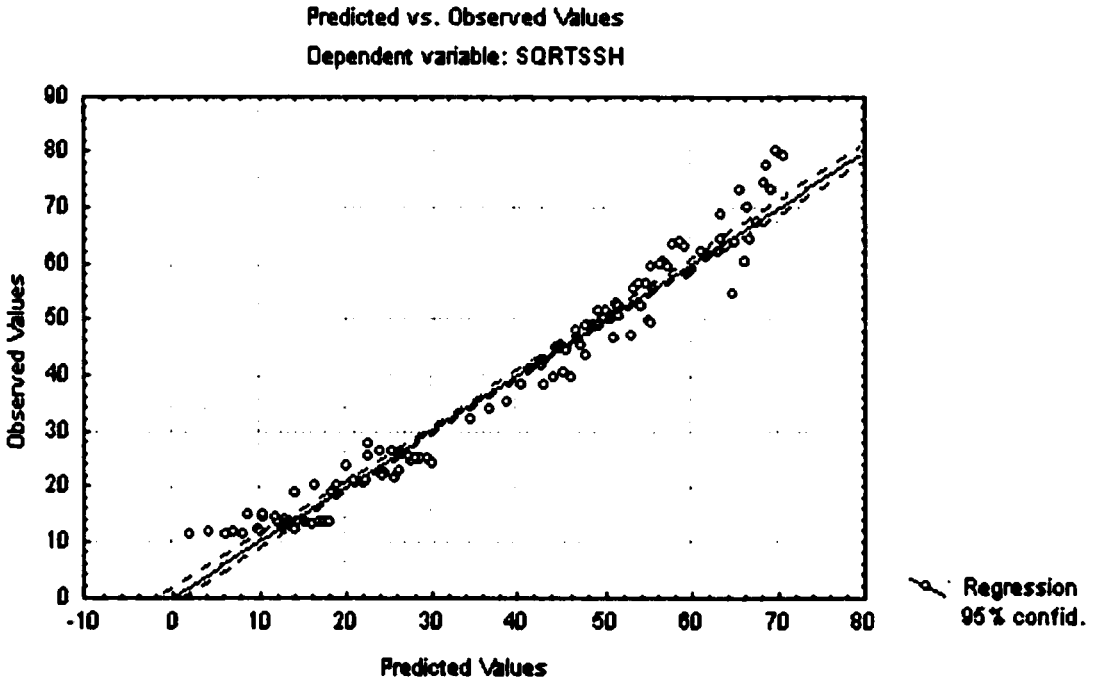

Fig. 8.51: Plot of predicted values versus the measured values for the absolute maximum stress for the pipe with high density as native soil under live load conditions

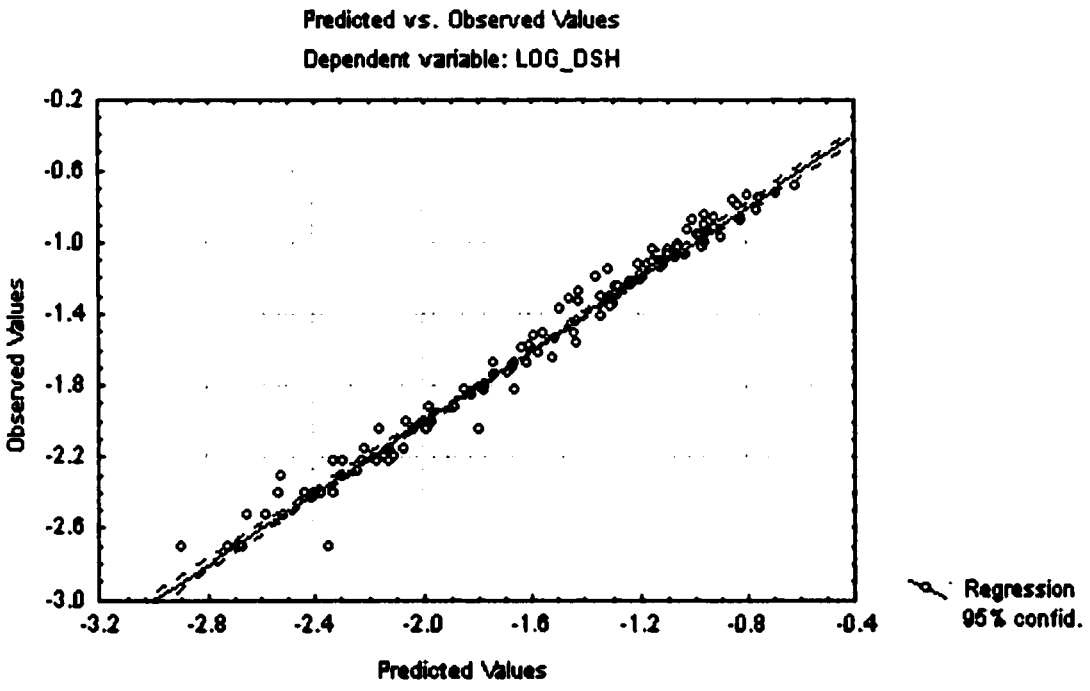

Fig. 8.52: Plot of predicted values versus the measured values for the change in pipe diameter for the pipe with high density sand as native soil under live load conditions

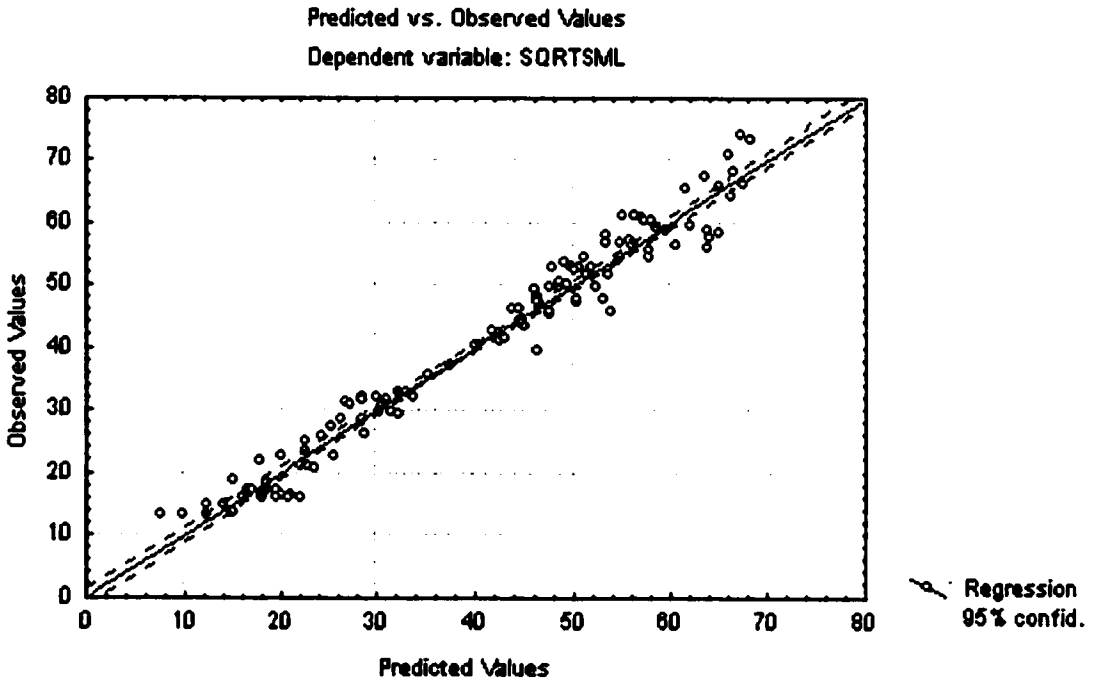

Fig. 8.53: Plot of predicted values versus the measured values for the absolute maximum stress for the pipe with marl as native soil under live load conditions

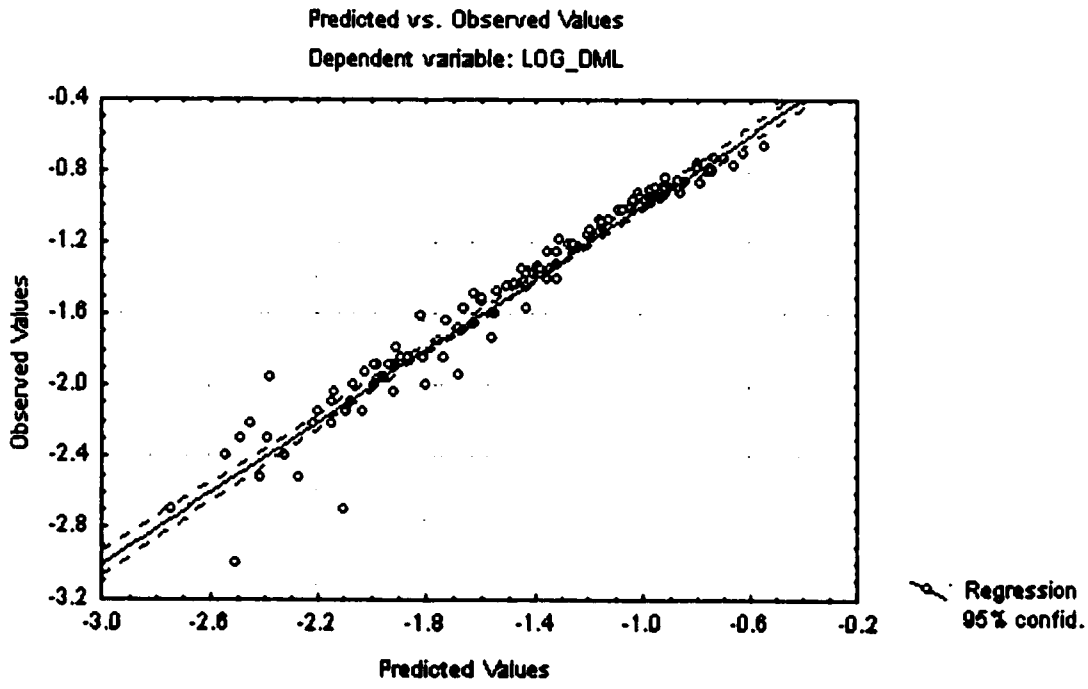

Fig. 8.54: Plot of predicted values versus the measured values for the change in pipe diameter for the pipe with marl as native soil under live load conditions

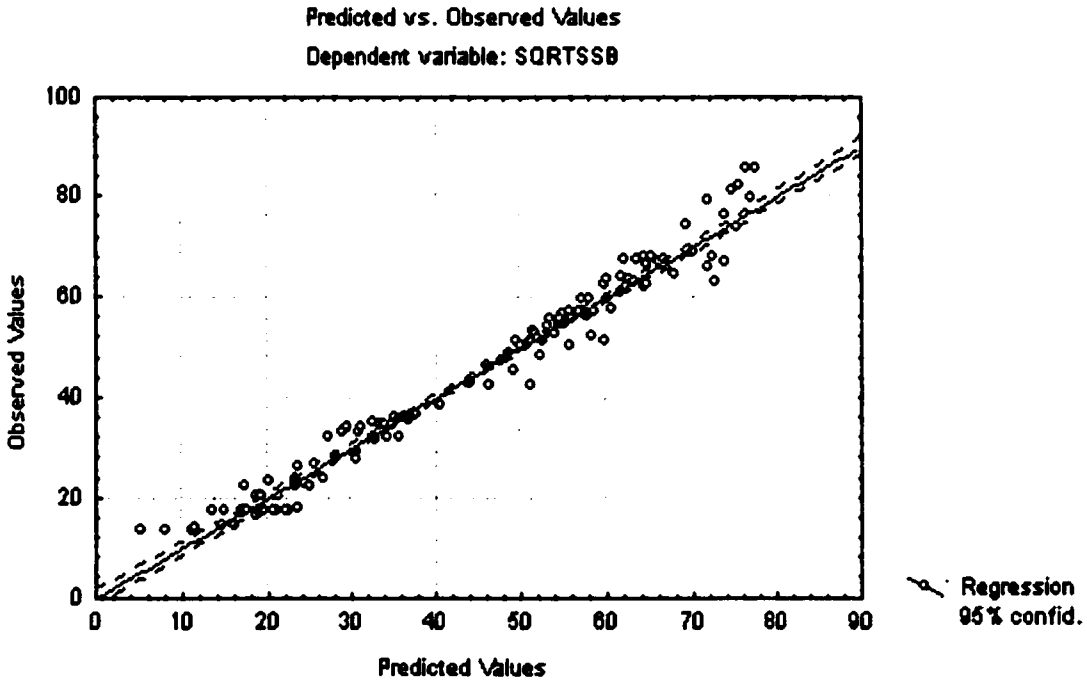

Fig. 8.55: Plot of predicted values versus the measured values for the absolute maximum stress for the pipe with sabkha as native soil under live load conditions

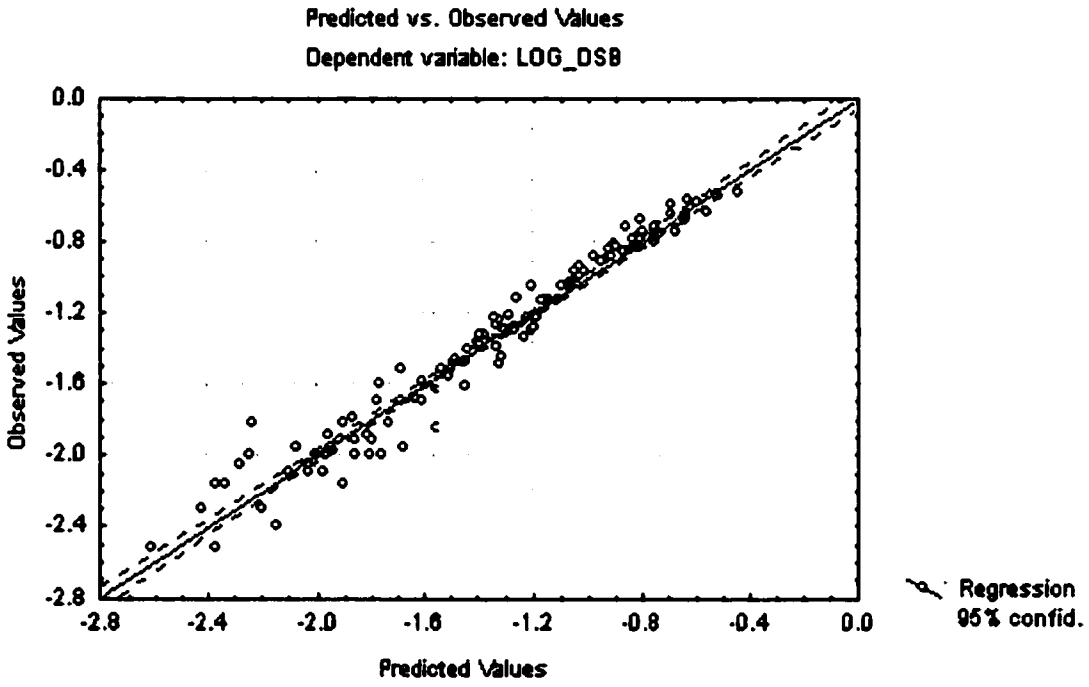

Fig. 8.56: Plot of predicted values versus the measured values for the change in pipe diameter for the pipe with sabkha as native soil under live load conditions

are according to the expected relationships between the independent and dependent variables. The following observations about the obtained signs in the developed models can be noticed:

- The diameter of the pipe is negatively related to the absolute maximum stress, i.e., the higher the pipe's diameter is, the lesser the stresses.
- The thickness of the pipe's wall is negatively related to the absolute maximum stress, i.e., the higher the thickness of the pipe's wall is, the lower will be the circumferential stresses.
- The depth of the pipe cover is negatively related to the absolute maximum stress, i.e., the more the depth of cover less the stress.
- The diameter of the pipe is positively related to the change in pipe diameter, i.e., the more the pipe diameter more will be the change in diameter.
- The thickness of the pipe's wall is negatively related to the amount of change in the pipe's diameter, i.e., the more the thickness of the pipe less the change in diameter.
- The depth cover is negatively related to the amount of the change in the pipe's diameter, i.e. the more the depth of cover less the change in diameter.

The above-mentioned observations are all according to the expected relations among the IV's and DV's.

8.4.2 Homoscedasticity Testing

Since the ordinary least squares method is used in the development of the regression models, the scatter of errors around all points of the independent variables must be checked

to satisfy the condition of homoscedasticity.

The condition of homoscedasticity is checked by plotting the values of the DV against the residuals. The plots of predicted values versus residuals of estimation for all the developed models are shown in Figs. 8.57 to 8.64. From these figures, it can be said that the homoscedasticity conditions are met for all the developed models.

8.4.3 Normality Testing

In multiple linear regression models, it is essential to check that the errors from the residual are distributed normally. Figs. 8.65 to 8.72 show the normal probability plots for the residuals of the developed models. From a visual inspection of the distribution of the points around the normal lines, it appears that, except at the two extremes there is a normal distribution of the residuals. Therefore, the normality assumption of the error is met for all the models.

8.5 Model Validation

For the 13 cases of different soil types that were not used in the model development. The developed equations are used to predict the stresses and the diameter change for these selected runs. Tables 8.30 to 8.33 compare the observed and calculated values of the absolute maximum stresses and the diameter change for the selected validation runs. The R^2 values are calculated for the original and the validation data and are shown in Table 8.34.

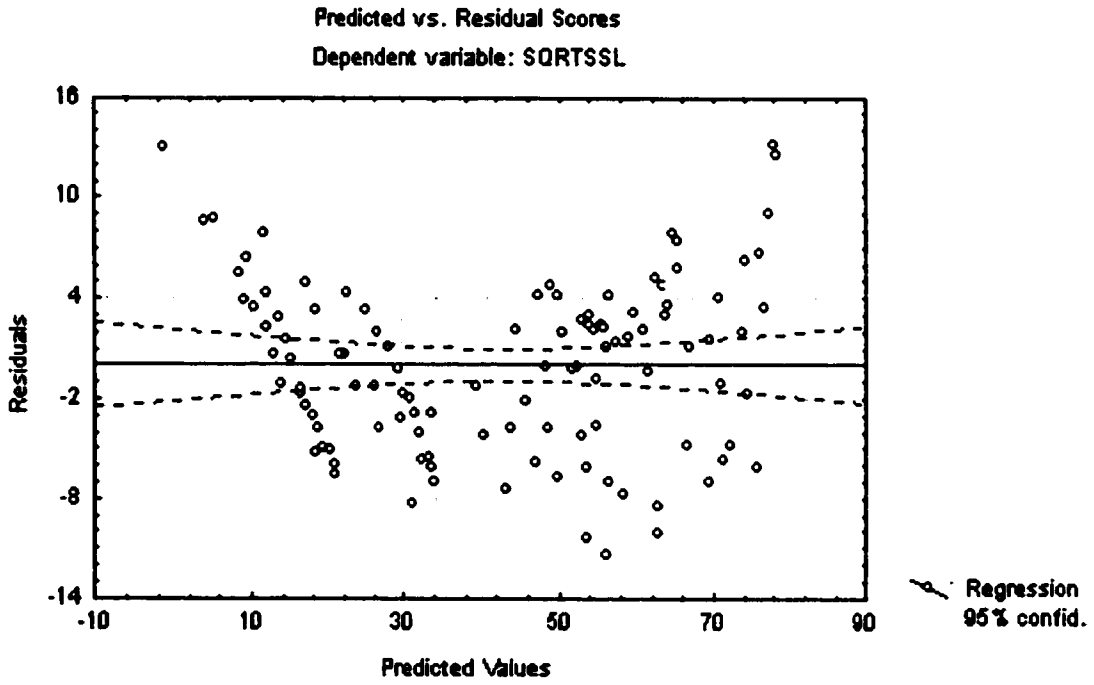

Fig. 8.57: Predicted values versus residuals of estimation for the prediction of the absolute maximum stresses for the pipe with loe denisty as native soil under live load conditions

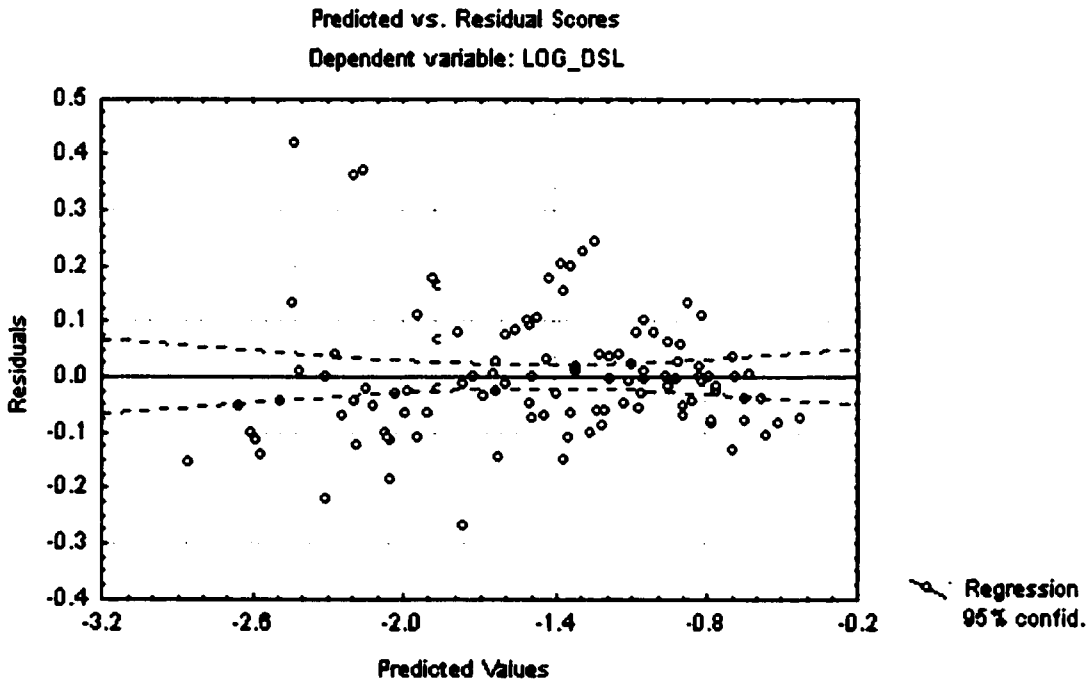

Fig. 8.58: Predicted values versus residuals of estimation for the prediction of the change in diameter for the pipe with loe density sand as native soil under live load conditions

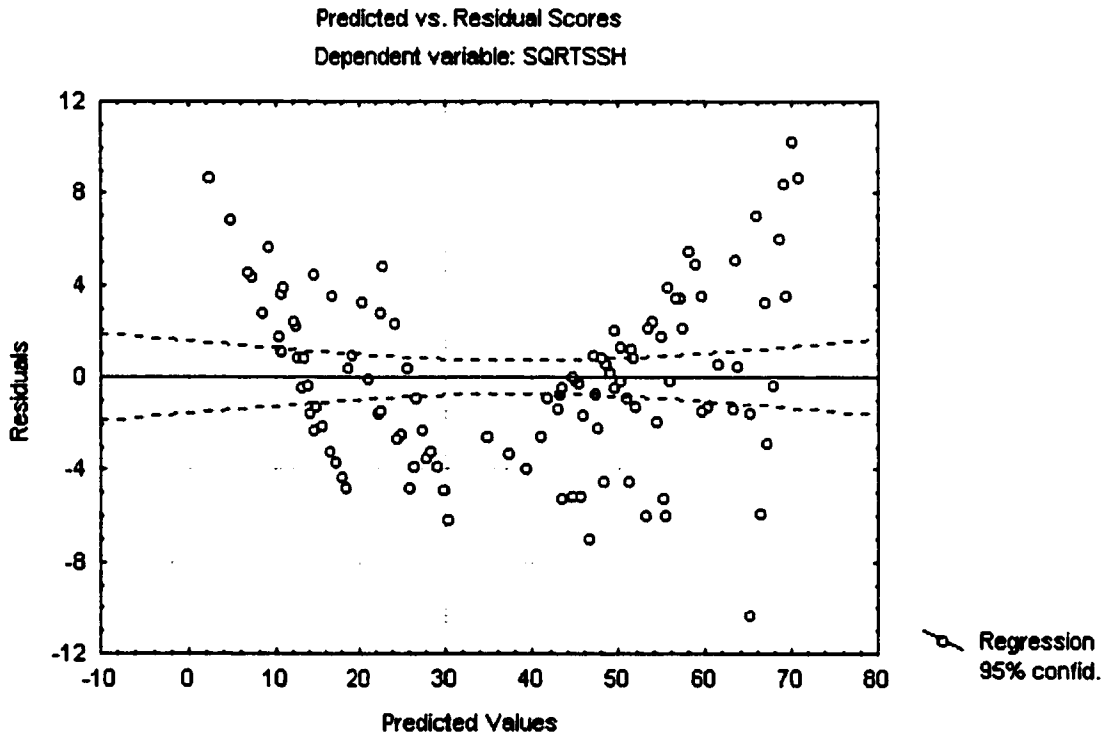

Fig. 8.59: Predicted values versus residuals of estimation for the prediction of the absolute maximum stresses for the pipe with high density sand as native soil under live load conditions

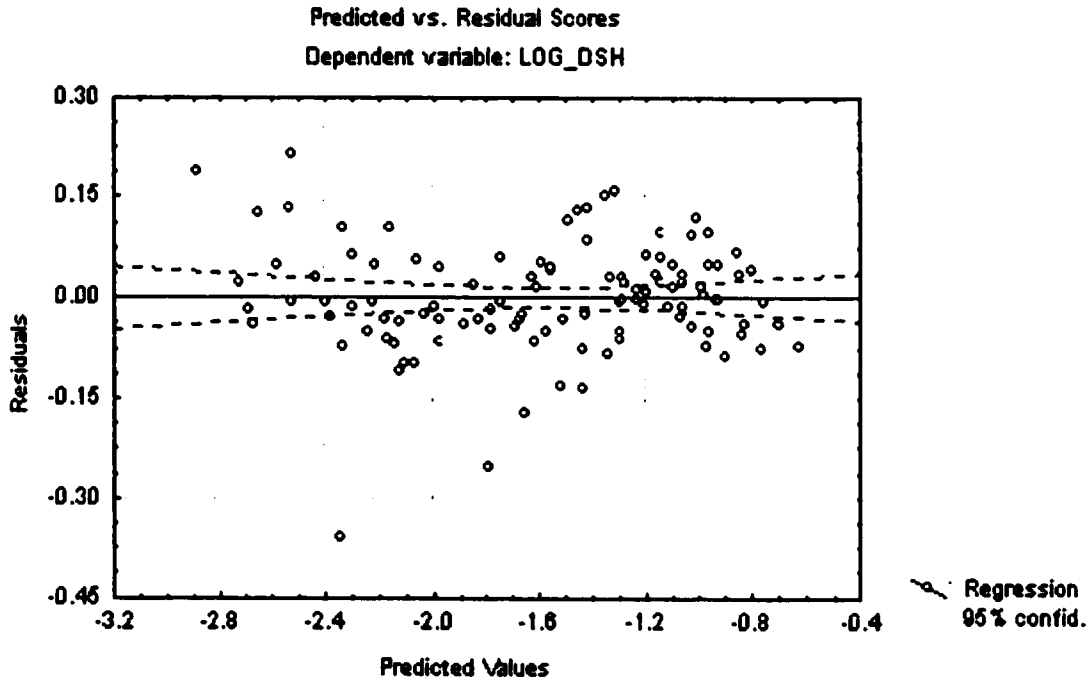

Fig. 8.60: Predicted values versus residuals of estimation for the prediction of the change in diameter for the pipe with high density sand as native soil under live load conditions

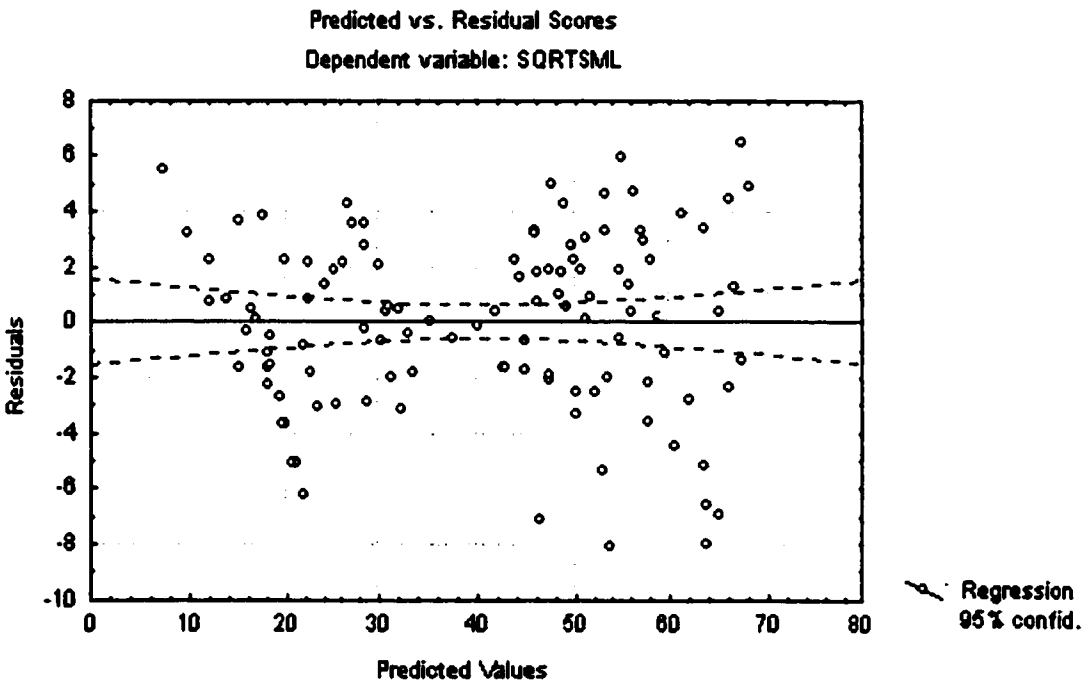

Fig. 8.61: Predicted values versus residuals of estimation for the prediction of the absolute maximum stresses for the pipe with marl as native soil under live load conditions

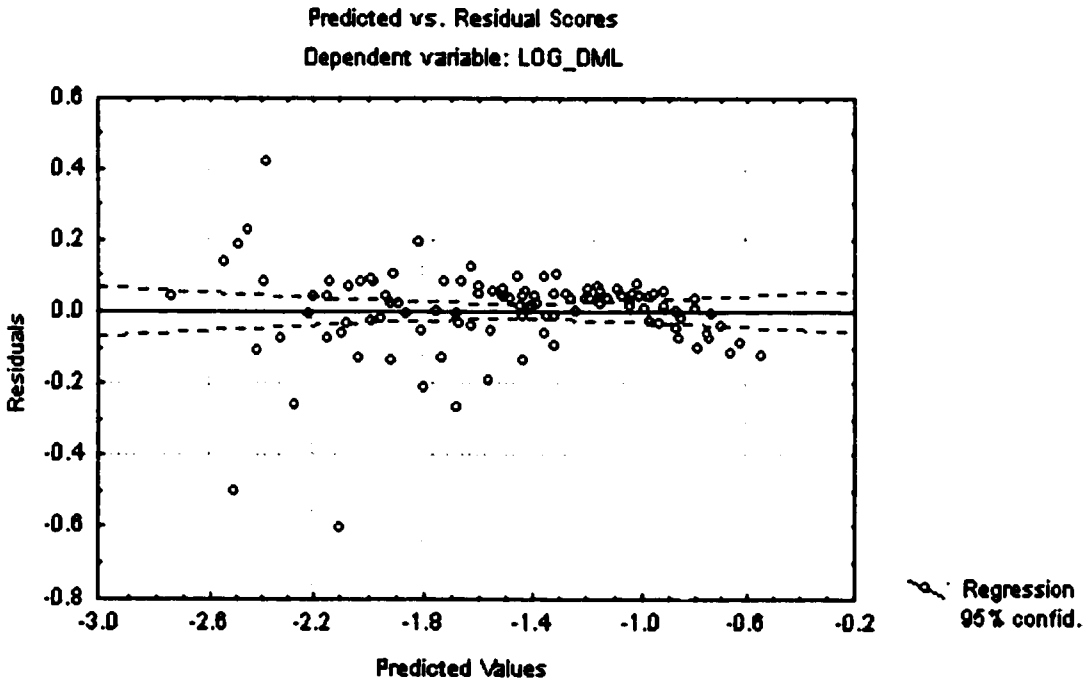

Fig. 8.62: Predicted values versus residuals of estimation for the prediction of the change in diameter for the pipe with marl as native soil under live load conditions

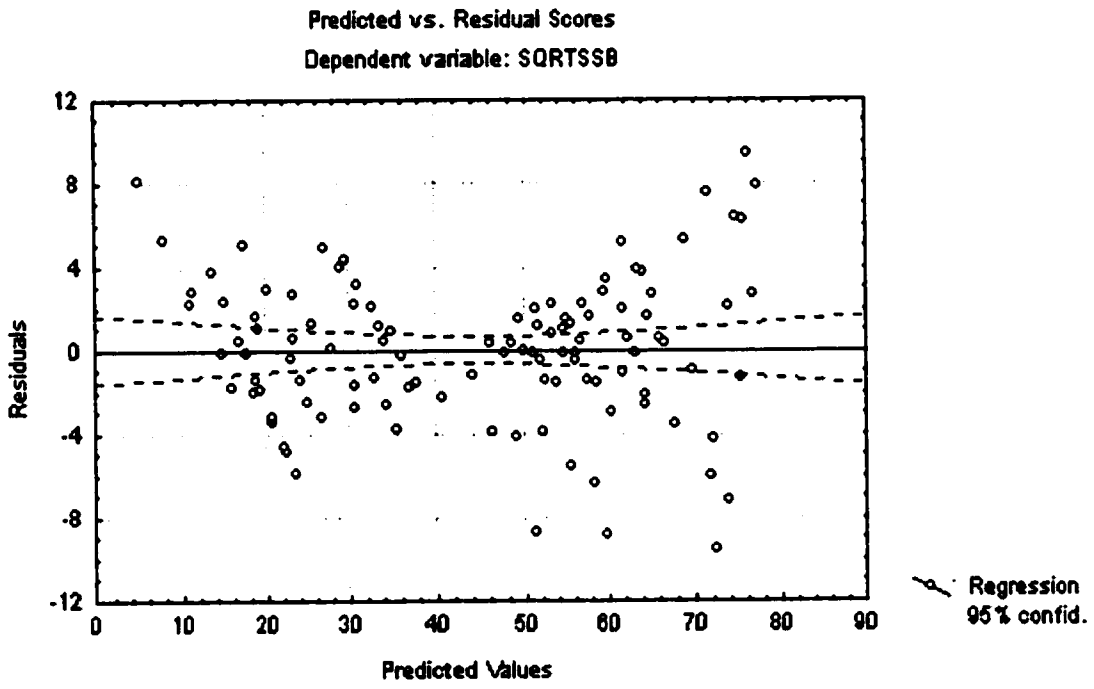

Fig. 8.63: Predicted values versus residuals of estimation for the prediction of the absolute maximum stresses for the pipe with sabkha as native soil under live load conditions

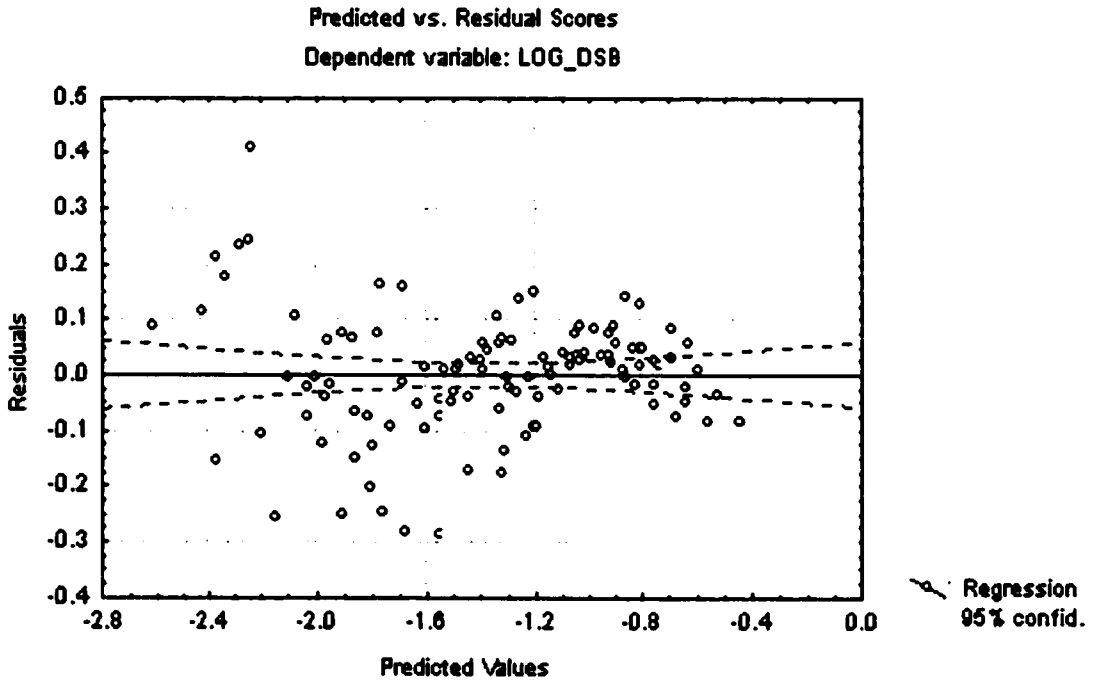

Fig. 8.64: Predicted values versus residuals of estimation for the prediction of the change in diameter for the pipe with sabkha as native soil under live load conditions

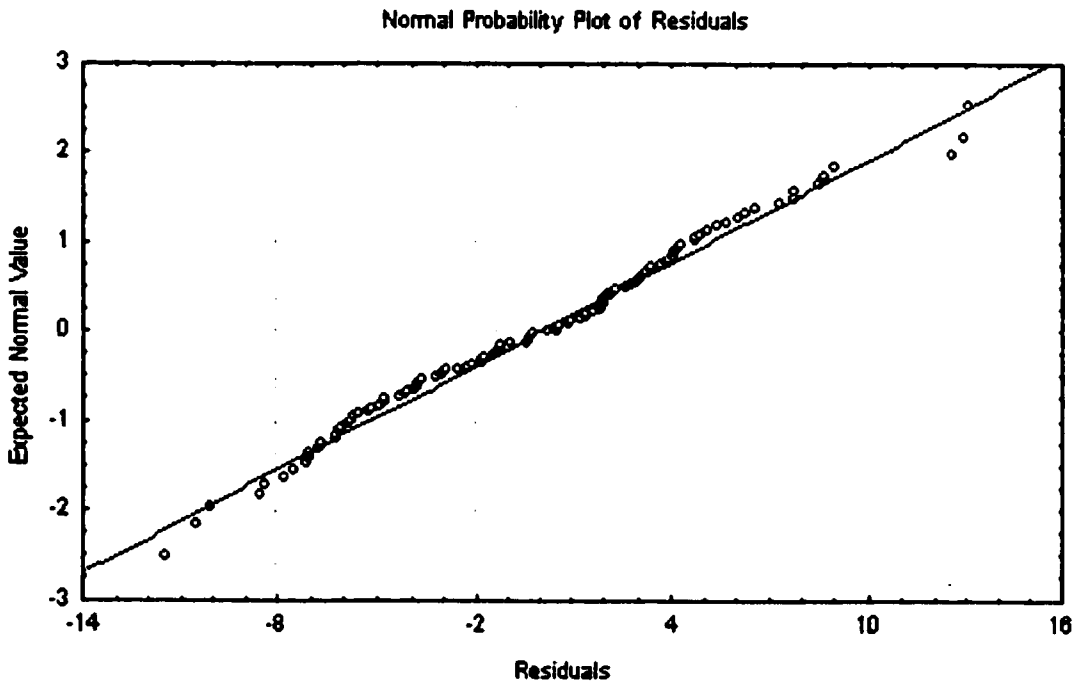

Fig. 8.65: Normal probability plot for the prediction of the absolute maximum stress for the pipe with low density sand as native soil under live load condition

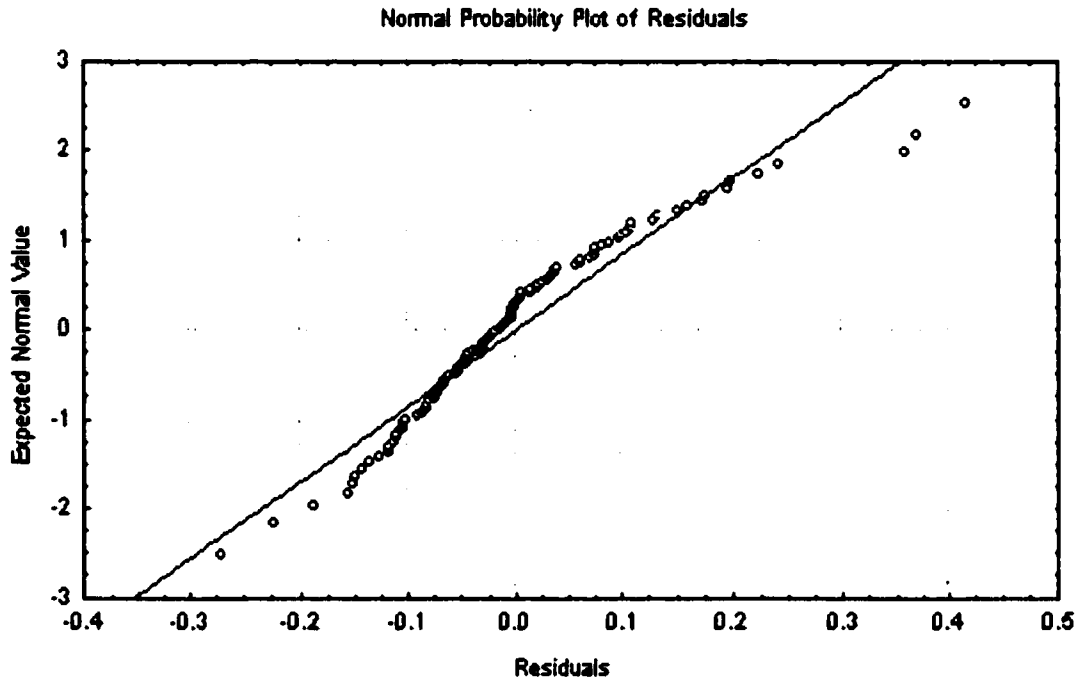

Fig. 8.66: Normal probability plot for the prediction of the change in diameter for the pipe with low density sand as native soil under live load condition

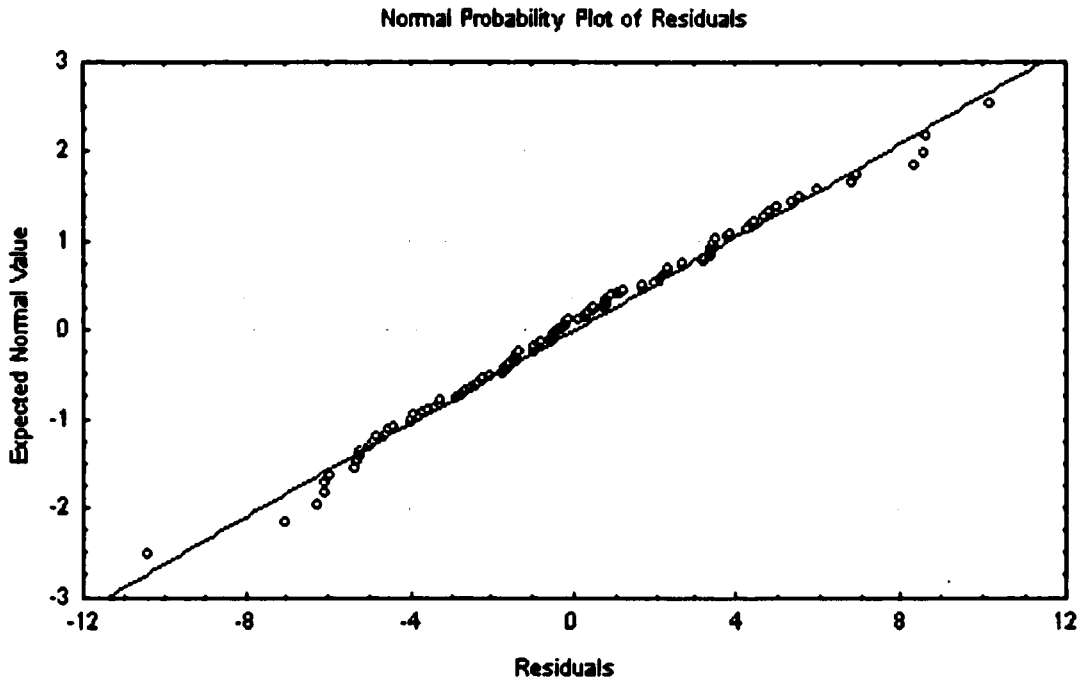

Fig. 8.67: Normal probability plot for the prediction of the absolute maximum stress for the pipe with high density sand as native soil under live load condition

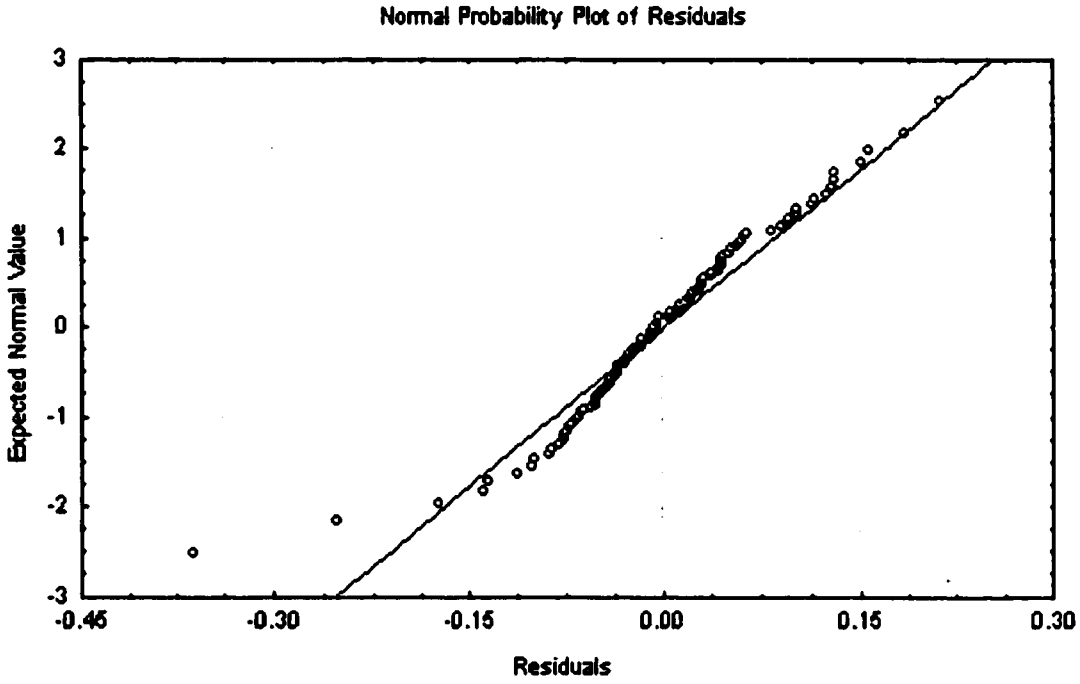

Fig. 8.68: Normal probability plot for the prediction of the change in diameter for the pipe with high density sand as native soil under live load condition

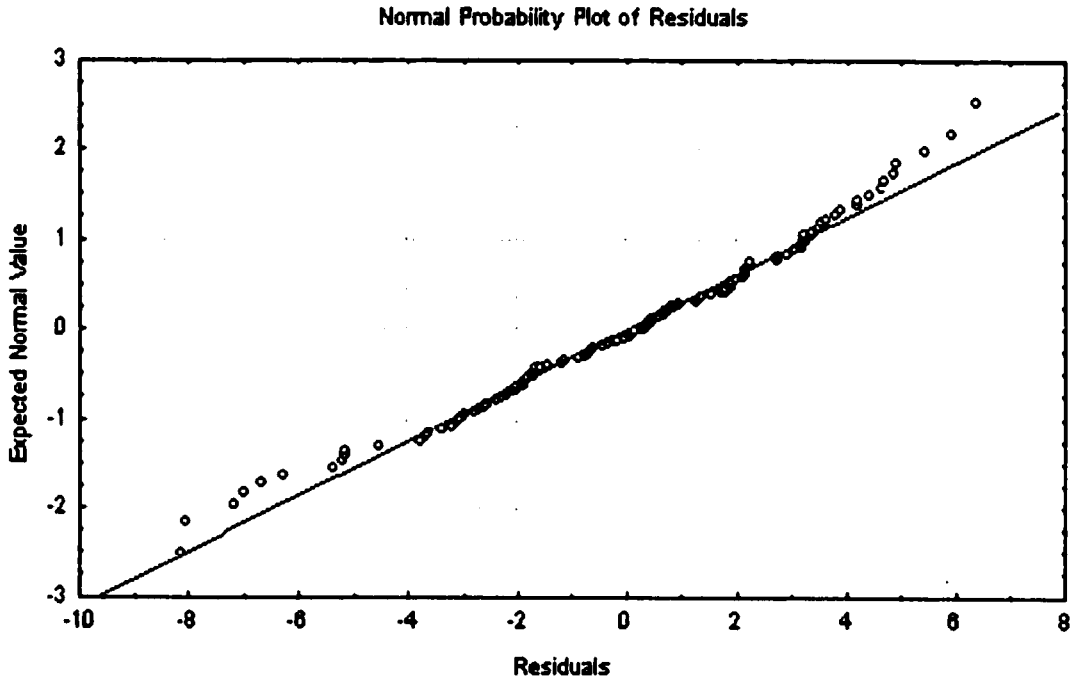

Fig. 8.69: Normal probability plot for the prediction of the absolute maximum stress for the pipe with marl as native soil under live load condition

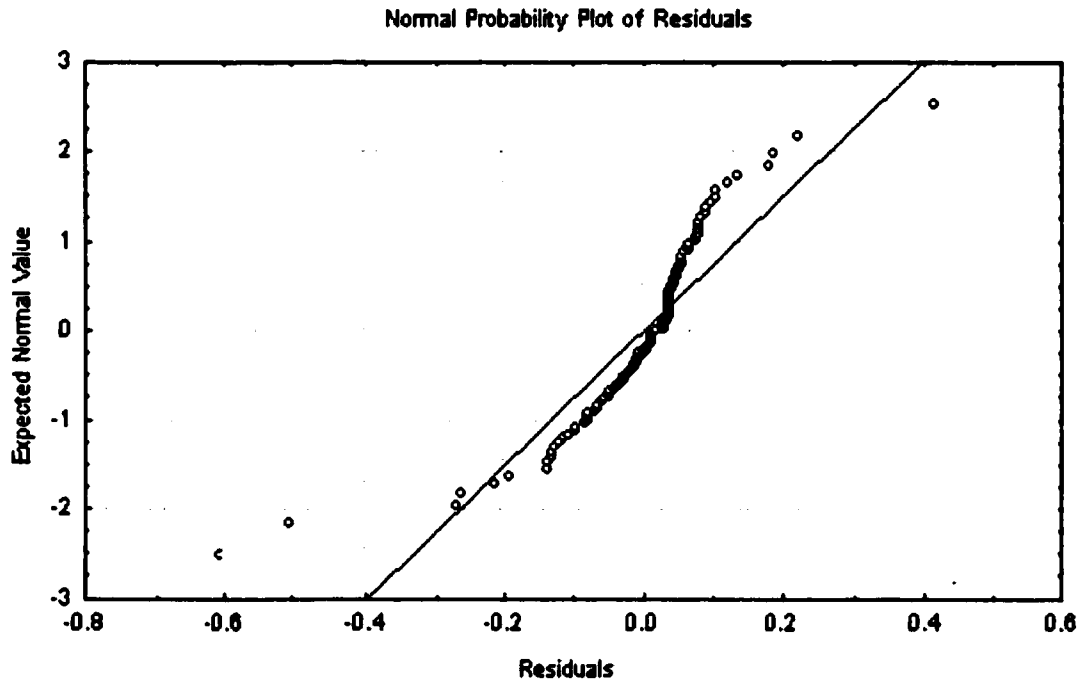

Fig. 8.70: Normal probability plot for the prediction of the change in diameter for the pipe with marl as native soil under live load condition

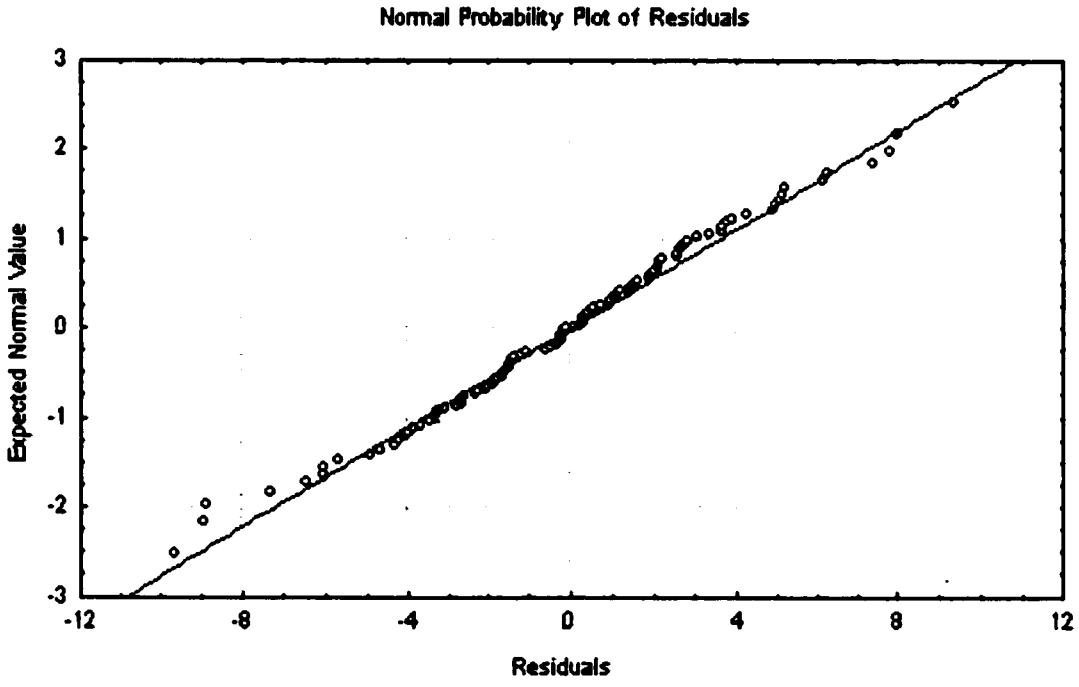

Fig. 8.71: Normal probability plot for the prediction of the absolute maximum stress for the pipe with sabkha as native soil under live load condition

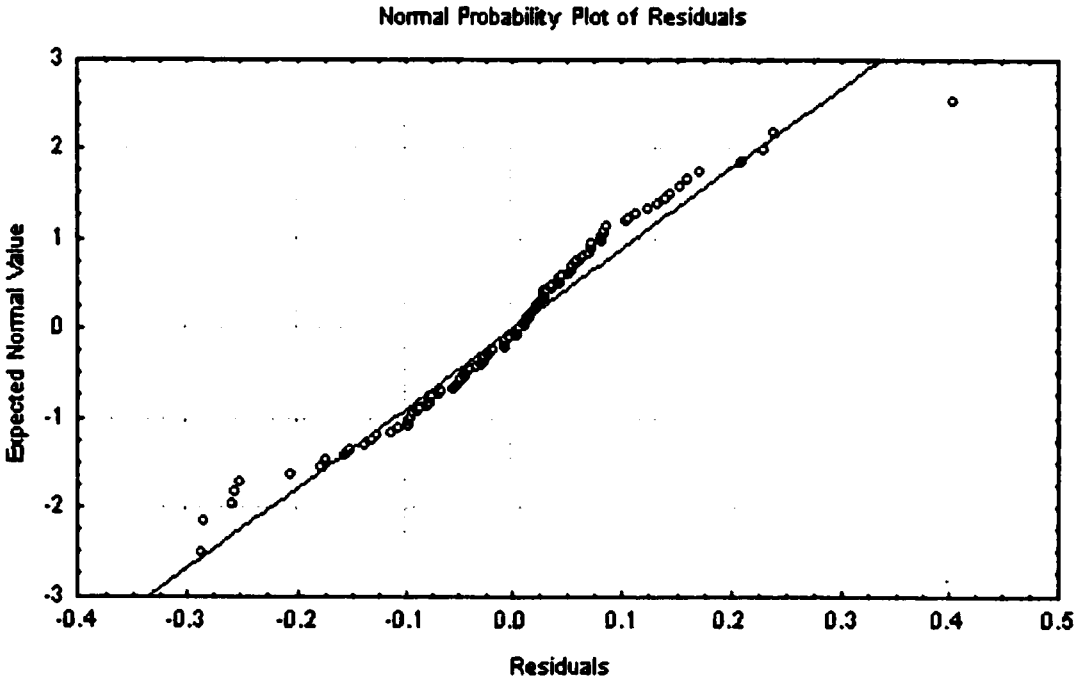

Fig. 8.72: Normal probability plot for the prediction of the change in diameter for the pipe with sabkha as native soil under live load condition

TABLE 8.30: Observed and calculated stresses and diameter change for the selected validation runs for low density sand as native soil and pipe subjected to live load

Observation number	Pipe Diameter (in)	Thickness of Pipe Wall (in)	Depth of Cover (ft)	Abs. Max. Stress (psi) Observed	Abs. Max. Stress (psi) Calculated	Diameter Change (in) Observed	Diameter Change (in) Calculated
10	12	0.16	12	237	396	0.00	0.00
21	12	0.08	2	7942.4	6198	-0.11	-0.06
28	24	0.48	4	1797.2	2439	-0.02	-0.03
36	24	0.24	2	7055	5716	-0.16	-0.11
53	36	0.72	4	1607.7	1991	-0.03	-0.04
61	36	0.36	2	6008	5303	-0.20	-0.17
68	36	0.288	4	2851	2680	-0.10	-0.11
76	48	0.96	2	3194.7	3818	-0.07	-0.08
92	48	0.384	3	3820	3400	-0.18	-0.19
99	48	0.32	8	933	778	-0.04	-0.05
111	60	0.6	2	3470.8	4398	-0.22	-0.24
116	60	0.48	2	3900	4666	-0.28	-0.32
124	60	0.4	8	510	632	-0.06	-0.06

TABLE 8.31: Observed and calculated stresses and diameter change for the selected validation runs for high density sand as native soil and pipe subjected to live load

Observation number	Pipe Diameter (in)	Thickness of Pipe Wall (in)	Depth of Cover (ft)	Abs. Max. Stress (psi) Observed	Abs. Max. Stress (psi) Calculated	Diameter Change (in) Observed	Diameter Change (in) Calculated
10	12	0.16	12	187	253	0.00	0.00
21	12	0.08	2	5981.8	5089	-0.08	-0.05
28	24	0.48	4	1409.1	1822	-0.02	-0.03
36	24	0.24	2	5647.9	4548	-0.12	-0.09
53	36	0.72	4	1284.4	1575	-0.03	-0.03
61	36	0.36	2	4968.6	4275	-0.15	-0.12
68	36	0.288	4	2152	2136	-0.07	-0.08
76	48	0.96	2	2833.6	3319	-0.07	-0.07
92	48	0.384	3	2925	2827	-0.12	-0.13
99	48	0.32	8	726	640	-0.03	-0.03
111	60	0.6	2	3682	3850	-0.17	-0.17
116	60	0.48	2	3498	4066	-0.19	-0.21
124	60	0.4	8	743	578	-0.03	-0.04

TABLE 8.32: Observed and calculated stresses and diameter change for the selected validation runs for marl as native soil and pipe subjected to live load

Observation number	Pipe Diameter (in)	Thickness of Pipe Wall (in)	Depth of Cover (ft)	Abs. Max. Stress (psi) Observed	Abs. Max. Stress (psi) Calculated	Diameter Change (in) Observed	Diameter Change (in) Calculated
10	12	0.16	12	432	430	0.00	0.00
21	12	0.08	2	5083.6	4759	-0.07	-0.05
28	24	0.48	4	1551.4	1859	-0.02	-0.03
36	24	0.24	2	4759.9	4291	-0.11	-0.09
53	36	0.72	4	1509.1	1621	-0.03	-0.03
61	36	0.36	2	4462.1	4061	-0.16	-0.13
68	36	0.288	4	2527	2269	-0.09	-0.09
76	48	0.96	2	2548.2	3061	-0.07	-0.06
92	48	0.384	3	2875.6	2869	-0.14	-0.16
99	48	0.32	8	962	897	-0.04	-0.05
111	60	0.6	2	3027.6	3678	-0.18	-0.18
116	60	0.48	2	3058	3916	-0.20	-0.24
124	60	0.4	8	951	831	-0.06	-0.06

TABLE 8.33: Observed and calculated stresses and diameter change for the selected validation runs for sabkha as native soil and pipe subjected to live load

Observation number	Pipe Diameter (in)	Thickness of Pipe Wall (in)	Depth of Cover (ft)	Abs. Max. Stress (psi) Observed	Abs. Max. Stress (psi) Calculated	Diameter Change (in) Observed	Diameter Change (in) Calculated
10	12	0.16	12	523	464	0.00	0.00
21	12	0.08	2	6883.1	6129	-0.10	-0.07
28	24	0.48	4	1698.9	2245	-0.02	-0.04
36	24	0.24	2	6896.1	5496	-0.16	-0.12
53	36	0.72	4	1647.4	1927	-0.03	-0.05
61	36	0.36	2	5951.5	5190	-0.21	-0.17
68	36	0.288	4	2983	2852	-0.13	-0.12
76	48	0.96	2	3119.1	3764	-0.07	-0.08
92	48	0.384	3	3671	3637	-0.20	-0.20
99	48	0.32	8	1181	1079	-0.05	-0.06
111	60	0.6	2	4196.9	4666	-0.25	-0.24
116	60	0.48	2	4146.2	5013	-0.27	-0.30
124	60	0.4	8	1170	993	-0.07	-0.07

TABLE 8.34: Coefficient of determination for both original and validation data for pipelines crossing highways

		R^2	
Type of embedment soil	Variable	Original data	Validiation data
Sand at low density	Absolute maximum stress	0.9476	0.9124
	Diameter change	0.964	0.9314
Sand at high density	Absolute maximum stress	0.9649	0.9387
	Diameter change	0.9798	0.9459
Marl	Absolute maximum stress	0.9667	0.9245
	Diameter change	0.9507	0.9598
Sabkha	Absolute maximum stress	0.9694	0.9208
	Diameter change	0.9567	0.9318

8.6 Procedure for the Analysis and Design of Buried Pipelines

The Follwing section outlines the steps for the analysis and design of buried pipelines based on the regression equations devloped in this chapter and the rationale of the current reserach. Fig. 8.73 shows the flowchart of the recommended design procedure.

Step 1. Check the pipe for stresses due to the internal pressure. The modified Barlow formula is used to calculate the internal stresses due to internal pressurization:

$$S_{Hi} = \frac{p(D-t)}{2t} \tag{8.2}$$

Using the allowable maximum stress ($\sigma_{allowable}$) of 43200 psi, the maximum allowable pressures mentioned in Table 8.35 can be found for the D/t range considered in this research.

TABLE 8.35: Maximum allowable pressure in the pipe for the D/t range 50-150

D/t	P_{max} (psi)
50	1763.26
75	1167.56
100	864
125	696.74
150	579.86

Step 2. Find the circumferential stress and the diameter change due to earth load. The regression equations stated in Table 8.4 should be used.

Step 3. Find the circumferential stress and the diameter change due to the live load. The regression equations for the calculation of live load stresses and diameter change are given in Table 8.21. A point to be noted here is that the live load equations are for a loading of 39-ton MOC vehicle.

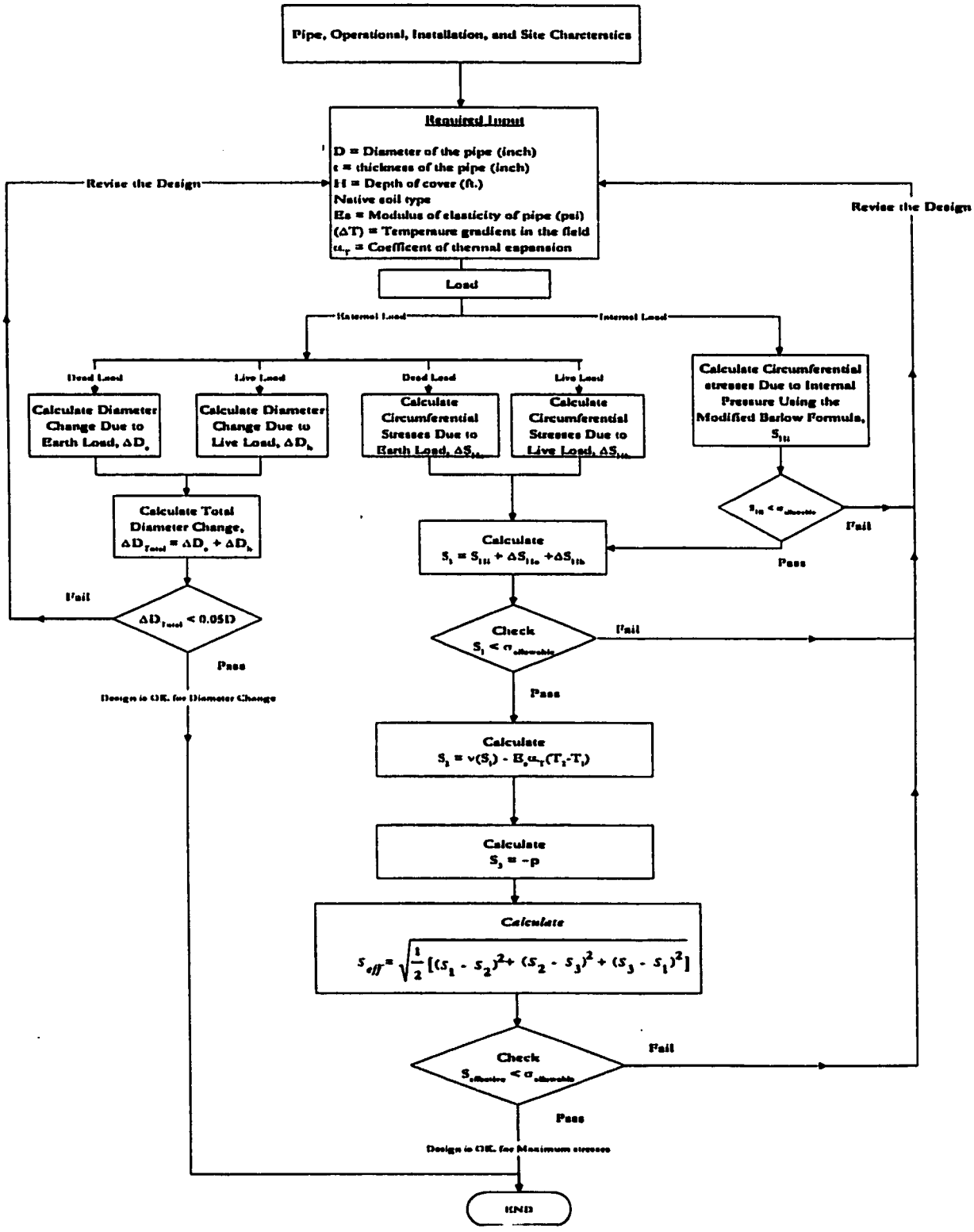

Fig. 8.73: Flow chart of the design procedure recommended by this research

Step 4. Calculate the total circumferential stresses and total diameter change.

$$S_1 = S_{Hi} + \Delta S_{He} + \Delta S_{Hh} \tag{8.3}$$

$$\Delta D_{Total} = \Delta D_e + \Delta D_h \tag{8.4}$$

Step 5. Find the total longitudinal stresses using the following equation

$$S_2 = v(S_1) - E_s \alpha_T (T_2 - T_1) \tag{8.5}$$

Step 6. Calculate the radial stresses in the pipe.

$$S_3 = -p \tag{8.6}$$

Step 7. Calculate the effective stresses.

$$S_{eff} = \sqrt{\frac{1}{2}\left[(S_1 - S_2)^2 + (S_2 - S_3)^2 + (S_3 - S_1)^2\right]} \tag{8.7}$$

Step 8. Calculate the factors of safety.

$$FOS_{(circumferential)} = \frac{\sigma_{allowable}}{S_1} \tag{8.8}$$

$$FOS_{(eff)} = \frac{\sigma_{allowable}}{S_{eff}} \tag{8.9}$$

$$FOS_{(diameter)} = \frac{0.05 * D}{\Delta D_{Total}} \tag{8.10}$$

where

$FOS_{(circumferential)}$ = factor of safety for circumferential stresses,

$FOS_{(eff)}$ = factor of safety for effective stresses,

$FOS_{(diameter)}$ = factor of safety for diameter change,and

$$\sigma_{allowable} = 43200\,psi.$$

CHAPTER 9

SUMMARY, CONCLUSIONS, AND RECOMMENDATIONS FOR FURTHER RESEARCH

9.1 Summary

The prediction of stresses and deformation for buried pipelines subjected to a variety of loading conditions is a problem of soil structure interaction. A number of finite element analyses have been carried for buried pipelines under a sand overburden up to a 60 ft. and for highway crossing, with and without internal pressure and temperature loading. CANDE finite element program was used for the finite element analyses and the variables varied in the analyses are pipe diameter, thickness of the pipe, and depth of cover. The analyses are carried out for four different soils identified earlier. The results of the finite element analyses are used to develop regression models to predict the stresses and diameter changes in the pipe.

9.2 Conclusions

General conclusions include:

1. The modified Duncan and Selig model represent very well the stresses and deformations for buried pipelines under a variety of loading conditions.
2. The inclination of the sides of the trench has an influence on the calculated stresses and deformations depending upon D/t ratio of the pipe, and type of the native soil.
3. The Finite element code CANDE is capable of modeling the behavior of buried pipelines under various loading conditions.

Conclusions from the sand overburden problem are as follows:

1. The type of native soil plays an important role in the calculated stresses and deformations produced in the buried pipe.
2. The D/t ratio has a major influence on the stiffness of the buried pipe. For the D/t ratios of 50 and 75 for the steel pipelines and the soils considered in this research the pipe is acting as a rigid pipe while for D/t ratio of 100 the pipe is intermediated between the flexible and rigid pipe. For D/t ratios of 125 and 150 the pipe is acting as a flexible pipe. This was reflected in the arching phenomenon, where for D/t ratios of 50 and 75 a negative arching is pronounced. While for D/t ratios of 125 and 150 the phenomenon of positive arching is dominant and a considerable amount of passive resistance at the pipe springline was noted.
3. The internal pressure dominates the values of circumferential stresses calculated for the

sand overburden. In particularly for the internal pressure values of 500 psi and above.

4. The degree of compaction of the fill soil influences the stresses and deformation produced in the buried pipelines. An increase in the density of the soil usually results in a decrease in stresses and deformations produced in the pipe.
5. The stresses predicted from finite element program CANDE are always less conservative than those predicted from API recommended practice 1102 provided that value for modulus of soil reaction used in API RP 1102 is less than or equal to 0.5 ksi.

Conclusions from the pipeline crossings problem are as follows:

1. There is a very small variation in the circumferential stresses due to live loads for the D/t range from 100 to 150. However the diameter change is always increasing with the increasing D/t ratio.
2. The live load stresses in the pipelines subjected to highway loads decrease exponentially with increase in depth of cover and after depth of cover of 12 feet the stresses are almost negligible.
3. The diameter change in the pipelines subjected to highway loads decrease exponentially with increase in depth of cover. For a depth of cover of 12 feet .and above there is no significant change in the pipe diameter.
4. The absolute maximum circumferential stresses for the pipeline crossing problem is higher for small diameter pipes than for the large diameter pipes however the diameter change follows an opposite behavior.
5. Pavement modulus plays an important role in the values of stresses and diameter change

of pipelines crossing highways.

6. The total longitudinal stresses in the pipeline due to dead load, live load and internal pressure are always dominated by the temperature stresses, which are acting in the opposite direction of the other stresses.
7. The total circumferential stresses are always greater than the effective stresses calculated using the Von Mises yield criteria provided that the field temperature is same as the installation temperature.
8. The computer program PC-PISCESL is not suitable for predicting stresses for trenched construction according to the specifications laid down in API recommended practice 1102.

9.3 Recommendations for Further Research

1. A geometric nonlinear analysis of the pipe soil system can be carried to model the buckling phenomenon for large D/t ratios.
2. A three dimensional finite element analysis of pipeline crossing highways can be carried out to give a better understanding of the three dimensional distribution of live load stresses and deformations.
3. A full scale loading test for the pipeline crossing highways under various depths of cover subjected to different loading conditions can provide excellent means for calibrating numerical models.
4. The effect of temperature on the stresses and deformation can be studied by simulating

temperature gradient in the finite element analysis.

5. Artificial neural networks can be used to develop models from the database generated for a better prediction of stresses and deformation of pipelines than ones obtained from multiple linear regression analysis.

REFERENCES

1. Watkins R. K. "Structural Design of Buried Circular Conduits". *Highway Reseach Record, No. 145*, Paper sponsered by Committe on Buried Structures and presented at 45th Annual Meeting, 1966.

2. Marston, A. and A.O. Andreson. *Bulliton no. 31.* Iowa Engineering Experiment Station, Ames, Iowa, 1913.

3. Marston, A. *Bulliton no. 96.* Iowa Engineering Experiment Station, Ames, Iowa, 1930.

4. Spangler, M. G. "Structural Design of Flexible Pipe Culverts". *Bulletin No. 153.* Iowa Engineering Experiment Station, Ames, Iowa, 1941.

5. American Railway Engineering Association. "Culvert Load Deformation". *Bulletin No 284.* 1926.

6. Spangler, M.G. "Underground Conduits-An Appraisal of Modern Research". *Transactions ASCE*, 113:316, 1948.

7. White, H. L. and P. J. Layer. "The Corrugated Metal Conduit as a Compression Ring". In *Proceedings, Highway Research Board vol 39*, Washington, D.C, 1960.

8. Lucher, U. "Buckling of Soil-Surrounded Tubes". *Journal of Soil Mechanics and Foundations Division ASCE*, SM6(92):211, November 1966.

9. Dar, S. M. and R. C. Bates. "Stress Analysis of Hollow Cylindrical Inclusions". *Journal of Geotechnical Engineering Division ASCE*, GT2(100):123–138, February 1974.

10. Allgood, J. R. "Structures in Soil Under High Loads". *Journal of the Soil Mechanics and Foundation Division ASCE*, SM3:565–579, 1971.

11. Burns, J. Q. and R. M. Richard. "Attenuation of Stresses for Buried Cylinders". In *Proceedings, Symposium on Soil Structure Interaction*, pages 378–392. University of Arizona, 1964.

12. Hoëg, K. "Stresses Against Underground Structural Cylinders". *Journal of Soil Mechanics and Foundations Division, ASCE*, SM4(94):833–857, July 1968.

13. Gerbault, M. *"Cacul des canalisations circulaires semi-rigides"*. Number 439. Annales des l'Institut du Batimentet des Travaux, Série Théories et Méthodes de Calcul 278, Paris, France., 1985.

14. Regelwerk-Abwasser-Arbeitsblatt A 127 Richtlinien fur die statische Berechnung von Entwasserung-Skanalen und leitungen,. "Abwassertechnische Vereinigung e. V". Germany, 1988.

15. Gerbault, M. "Soil-Structure Interaction Model". In *Proceedings of the 2nd International Conference on Advances in Underground Pipeline Engineering*, pages 42–53. ASCE, 1995.

16. Einstein, H. H. and C. W. Schwartz. "Simplified Analysis for Tunnel Supports". *Journal of the Geotechnical Engineering Division, ASCE*, 105(4):499–518, April 1979.

17. Duncan, J. M. . "Behavior and Design of Long-Span Metal Culverts". *Journal of the Geotechnical Engineering Division, ASCE*, 105(3):399–418, March 1979.

18. Moore, I. D. and J. R Booker. "Ground Failure Around Buried Tubes". *Journal of Rock Mechanics and Rock Engineering*, 20:243–260, 1987.

19. Moore, I. D. "Review of Buried Plastic Pipe Design". Technical Report 039.05.89, The University of Newcastle, Newcastle, Australia, 1989.

20. Jeyapalan, J. K. "Advances in Pipeline Material and Design in Europe and North America". In *Proceedings of the International Conference on Pipeline Design and Installation*, pages 1–16. ASCE, March 1990.

21. Spangler, M. G. "Pipeline Crossings Under Railroads and Highways". *Journal of American Water Works Association*, 56(8):1029–1046, August 1964.

22. Gerald F. Mouser. "Basic Pipe Stress Evaluation Summary ". *Transportation Engineering Journal, ASCE*, 105:349–359, July/August 1979.

23. API Recommended Practice 1102 (1981). *"Steel Pipelines Crossing Railroads and Highways"*. American Petroleum Institute, Washington, D.C., 1981.

24. Baidar Bakht. "Soil-Steel Structure Response to Live Loads ". *Journal of the Geotechnical Engineering Division, ASCE*, 107(6):779–798, June 1981.

25. Pierce, R.N., O. Lucas, P. Rogers and C.L. Rankin. "A Design Procedure for Uncased Natural Gas Pipeline Crossings of Roads and Highways". In *1977 American Gas Association Transmission Conference*, St. Louis, MO, 1977.

26. Oey, H. S., L. Vernon, Greggerson Jr. and Womack David P. "Buried Gas Pipelines Under Vehicul'r Crossings". *Journal of Transportation Engineering, ASCE*, 110(2):203–22, March/April 1984.

27. Timoshenko, S.P. and J.N. Goddier. *"Theory of Elasticity"*. Mc-Graw Hill Book Company, 3rd edition, 1970.

28. Poulos, H. G. and H. E. Davis. *"Elastic Solutions for Soil and Rock Mechanics"*. John Wiley, New York, 1980.

29. Daines R. W. "Stress on Buried Pipelines". In *1991 Operation Section Proceedings of American Gas Association*, Arlington, VA. USA, 1991.

30. Portland Cement Association. "Vertical Pressure on Culverts Under Wheel Loads in Concrete Pavement Slabs ". Pub No ST65.

31. O'Rourke, T.D. and S. L. El-Gharbawy and H. E. Stewart. "Soil Loads at Pipeline Crossings". In *Proceedings of a Specialty Conference on Pipeline Crossings*, pages 235–247. ASCE, March 1991.

32. Stewart, H. E. and T. D. O'Rourke. "Live Loads for Pipeline Design at Railroads and Highways". In *Proceedings of a Specialty Conference on Pipeline Crossings*, pages 317–329. ASCE, March 1991.

33. Ingraffea, A. R., T. D. O'Rourke, H. Stewart, A. Barry and C. Crossley. "Guidelines for Uncased Crossings of Highways and Railroads". In *Proceedings of The Specialty Conference on Pipeline Crossings*, pages 34–46. ASCE, March 1991.

34. API Recommended Practice 1102 (1993). *"Steel Pipelines Crossing Railroads and Highways"*. American Petroleum Institute, Washington, D.C., 1993.

35. Stewart, H. E. and T. D. O'Rourke. "Live Loads for Pipeline Design at Railroads and Highways". In *A Specialty Conference on Pipeline Crossing*. ASCE, Colorado Section, March 25-27 1991.

36. Potter, J.C. "Effects of Vehicles on Buried, High-Pressure Pipe". *Journal of Transportation Engineering, ASCE*, 111(3):224–236, May/June 1985.

37. Antaki, G. "A Review of Methods for the Analysis of Buried Pressure Piping". WRC Bulletin 425, Welding Research Council, Inc, 1997.

38. Chua, K. M. *"Time-Dependent Interaction of Soil and Flexible Pipe"*. PhD thesis, Texas A and M University, College Station, TX, May 1986.

39. Musser, S. C. "CANDE-89 Culvert ANalysis and DEsign computer program User's Manual". Technical report, Federal Highway Administration, Federal Highway Administration, 1990.

40. Seed, R. B. and J. M. Duncan. "Earth Pressure and Surface Load Effects on Buried Pipelines". In *Proceedings of the International Conference on Advances in Underground Pipeline Engineering*, pages 320–329. ASCE, 1985.

41. Duncan. J. M. and Chin-Yung Chang. "Nonlinear Analysis of Stress and Strain in Soils". *Journal of the Soil Mechanics and Foundation Divison, ASCE*, 96(SM5):1629–1653, March 1970.

42. Frank, S., W. H. Robert, C. B. Michael and H. A. Todres. "Influence of Depth-of-Cover on Pipe-Soil Interaction". In *Advances in Underground Pipeline Engineering*, pages 32–45. ASCE, ASCE, 1985.

43. Singh, S. and N. Pal. "Analysis of Ovalization of Buried Steel Pipe Due To Earth-Fill". *Journal of Performance of Constructed facilities, ASCE*, 4(2):111–123, May 1990.

44. Taylor, R. L. *Finite Element Analysis Program (FEAP)*. Univ. of California Berkely, Berkeley, Calif., 1988.

45. Leonards, G.A. and C.H. Juang and T.H. Wu and R.E. Stetkar. "Predicting Performance of Buried Metal conduits". *Transportation Research Record, TRB*, (1008):15–21, 1985.

46. Sharma, S. and H.H. James. "Evaluation of Culvert Deformations Using The Finite Element Method". *Transportation Research Record, TRB*, (1415):32–39, 1993.

47. Leonards, G.A. and C.H. Juang. "Predicting Performance of Buried Metal Pipe Arches". *Transportation Research Record, TRB*, (1008):53–57, 1985.

48. Sharp, K. D., L. R. Anderson, A.P. Moser and Ronald R. Bishop. "Finite-Element Analysis Applied to the Response of Buried FRP Pipe under Various Installation Conditions". *Transportation Research Record, TRB*, (1008):63–71, 1985.

49. Selig, E. T., C. M. Samuel. "Performance Evaluation of a Rib-Reinforced Culvert". *Transportation Research Record , TRB*, (1008):117–122, 1985.

50. Jeyapalan, J. K., T. Michael, W. E. Saleira and B. A. Magid. "Analysis and Design of RPM and Other Composite Underground Pipelines". *Journal of Transportation Engineering, ASCE*, 115(3):219–231, May/June 1989.

51. Tzong H. Wu and G. A. Leonards. "Characterization of Soil Arching Above Buried Conduits". In *Advances in Underground Pipeline Engineering*, pages 396–407. ASCE, 1985.

52. Yoshiyuki Mohri, Yujiro Tsurumaru and Isamu Asano. "Measured performance and Analysis of Buried Pipe". In *International Conference on Pipeline Design and Installation*, pages 535–545. ASCE, ASCE, March 1990.

53. Duane, J., R. Rees and C. A. Moore . "Culvert-Soil Interaction Finite Element Analysis". *Journal of Transportation Engineering, ASCE*, 112:250–263, May/june 1986.

54. Fernando, N. S. M. and J. P. Carter. "Elastic Analysis of Buried Pipes under Surface Patch Loadings". *Journal of Geotechnical and Geoenvironmental Engineering, ASCE*, 124(8):720–728, August 1998.

55. Abdel-Sayed,George, and Baidar Bakht. "Analysis of Live-Load Effects in Soil-Steel Structures". *Transportation Research Record , TRB*, pages 49–55, 1982.

56. Abduljauwad, S.N. "Interaction of Buried Pipeline with Surrounding Soil". In *Fifth Saudi Engineering Conference, "Engineering and its Role in the Preservation of National Assets"*, pages 259–269, Makkah, Kingdom of Saudi Arabia, March 1999.

57. Katona, M. G. and J. M. Smith and R. S. Odello and J. R. Allgood. "CANDE - A Modern Approach for the Structural Design and Analysis of Buried Culverts". Technical Report FHWA-RD-77-5, Federal Highway Administration, Washington, D.C., October 1976.

58. R.B. Seed and J.M. Duncan. Earth pressure and surface load effects on buried pipelines. In *International Conference on Advances in Underground Pipeline Engineering*, pages 320–329. ASCE, 1985.

59. Katona, M. G. "Allowable Fill Heights for Corrugated Polyethylene Pipe". *Transportation Research Record, TRB*, (1191):30–38, 1988.

60. Ko, H.-Y. and R. M. Masson. "Nonlinear Chracterization and Analysis of Sand". In *2nd International Conferenceon Numerical Methods in Geomechanics*, June 1976.

61. Desai, C. S. "Overview, Trends, Projections: Theory and Applications of the Finite Element Method in Geotechnical Engineering". In *Syposium on Application of Finite Element Method in Geotechnical Engineering*. U.S. Army Engrg. Waterway Experiment Station, 1972.

62. Truesdell, C. "Hypoelasticity". *Journal of Rational Mechanics and Analysis*, 4:83–133, 1955.

63. Coon, M. D. and R. J. Evans. "Recoverable Deformation of Cohesionless Soils". *Journal of Soil Mechanics and Foundations Division, ASCE*, 97(SM2):375–391, 1971.

64. Corotis, R. B., M. H. Farzin and R. J. Krizek. "Non linear Stress-Strain Formulation for Soils". *Journal of the Geotechnical Engineering Division, ASCE*, 10(GT9):993–1008, 1974.

65. Selig, E.T. "Soil Parameters for Design of Buried Pipelines". In *Conference Proceedings of Pipeline Infrastructure*, pages 99–116. ASCE, 1988.

66. Duncan, J.M., P. Byrne, K.S. Wong and P. Mabry. "Strength, Stress-strain and Bulk Modulus Parameters for Finite Element Analysis of Stresses and Movements in Soil Masses". Technical Report UCB/GT/80-01, University of California, College of Engineering, Berkeley, California, 1980 August.

67. Yang, G-R. Hyperbolic Young's Modulus Parameters for Compacted Soil. Project Report ACP87-342P for M.S. Degree, University of Massachusetts, Amherst, Massachusetts, May 1987.

68. Krizek, R. J. and D. K. Atmatzidis. Assesment of Soil Constitutive Models for Numerical Analysis of Buried Concrete Pipe Systems. In *Symposium on Concrete Pipe and The Soil-Structure System*, pages 76–90, Philadelphia, Pa, June 1976.

69. Leonards, G. A., T. Wu and C. Juang. "Predicting Performnace of Buried Conduits". Report PB831948, Purdue University, Lafayette, Indiana, 27 Jun 1982.

70. Spangler, M. G. *"Strucrural Design of Flexible Culverts"*. Iowa State College Bulletin No. 29, Ames, Iowa, December 1954.

71. Spangler, M. G. "Stresses in Pressure Pipelines and Protective Casing Pipes". *Journal of Structural Engineering, ASCE*, 82(ST5):33, September 1956.

72. Spangler, M.G. "Strucrural Design of Pipelines Casing Pipes". *Journal of the Pipeline Divison, ASCE*, 94(PL1):137–154, October 1968.

73. Ingraffea, A. R. ,T. D. O'Rourke, H. E. Stewart, M. T. Behn, A. Barry, C. W. Crossley and S. L. El-Gharbawy. "Technical Summary and Database for Guidelines for Pipelines Crossing Railroads and Highways". Final Report GRI-91/0285, Gas Research Institute, December 1991.

74. Stewart, H. E. , T. D. O'Rourke, A. R. Ingraffea, M. T. Behn, A. Barry, C. W. Crossley, and S. L. El-Gharbawy. "Guidelines for Pipelines Crossing Highways". Technical Report GRI-91/0284, Gas Research Institute,, Chicago, IL, December 1991b.

75. 49 Code of Fedearl Regulations Part 192. Department of Transportation, U.S. Government Printing Office, Washington, D.C.

76. 49 Code of Fedearl Regulations Part 195. Department of Transportation, U.S. Government Printing Office, Washington, D.C.

77. Belwitt, J. R., A. R. Ingraffea, T. D. O' Rourke, and H. E. Stewart. "Analytical Study of Stresses in Transmission and Distribution Piping Beneath Railroads". Technical Report GRI-87/0234, Gas Research Institute, Chicago, IL, September 1987.

78. ASME B31.4. *"Liquid Transportation Systems for Hydrocarbons, Liquid Petroleum Gas, Anhydrous Ammonia, and Alcohals"*. American Society of Mechanical Engineers, New York, 1992.

79. Lee, I. K., W. White and O. G. Ingles. *Geotechnical Engineering*. Pitman Publishing, Inc., Boston, 1983.

80. Bowles, J. E. *"Engineering Properties of Soils and their Measurement"*. The McGraw-Hill Comapnies, Inc., 5th edition, 1992.

81. Roy, M. B. and G. A. Leonards. "Predicting Performance of Pipe Culverts Buried in Soil". Technical Report JHRP-76-24, Joint Highway Research Project, Purdue University, 1976.

82. Duncan, et al. User's Guide for SSTIP, Unnumbered Research Report, University of California, Berkely, Januray 1979.

83. Pilkey, W. et al. Sturctural Mechanics Computer Programs. University Press of Virginia, 1974.

84. FEMAP User's Manual. Version 4.5 for Windows, Enterprise Software Products, Inc., 1996.

85. Goodman, L.E. and C.B. Brown. "Dead Load Stresses and the Instability of Slopes". *Journal of Soil Mechanics and Foundations Division, ASCE*, 89(SM3), March.

86. American Concrete Institute. Building Code Requirements for Reinforced Concrete, ACI 318-83. ACI, Michigan, 1992.

87. Witczak, M.W. "Design of Full-Depth Asphalt Airfield Pavements". In *Third International Conference on the Structural Design of Asphalt Pavements*, pages 500–567, London, 1972.

88. Bissada, A.F., S.K. Hamdani, and H.R. Guirguis. "Design Criteria of Asphalt Pavement Structures at High Service Temperatures". In *Fifth International Conference on the Structural Design of Asphalt Pavements*, pages 142–155, Delft University of Technology, Netherlands, 1982.

89. Fatani, M. N., H. I. Al-Abdul Wahhab, F. A., Balghunaim, A. Bubshait., and I. Al-Dhubeeb. "Evaluation of Permanent Deformation of Asphalt Concrete Pavement in Saudi Arabia". Final report, National Research Project, King Abdulaziz City for Science and Technology. (KACST), Saudi Arabia, June 1990.

90. Blank, L. *"Statistical Procedures for Engineering, Management, and Sciences"*. Industrial Engineering and Mangement Sicence. McGraw-Hill Book Company, New York, 1980.

91. Montomery, D. C. and G. C. Runger. *"Applied statistics and Probability for Engineers"*. John Wiley and Sons, Inc., New York, 1994.

92. STATISTICA for Windows [Computer Program Manual]. StatSoft, Inc., 2300 East 14th Street, Tulsa, OK 74104, 1997.